

Advanced Performance Simulation of Gas Turbine Components
and Fluid Thermodynamic Properties

Cranfield
UNIVERSITY

School Of Engineering
Department Of Power and Propulsion

PhD THESIS

Vishal Sethi

**Advanced Performance Simulation of Gas Turbine
Components and Fluid Thermodynamic Properties**

Supervisor: Prof. P. Pilidis

April 2008

© Cranfield University 2008. All rights reserved. No part of this publication may be reproduced without the written permission of the copyright owner.

PROJECT ABSTRACT

The VIVACE European Cycle Program (“VIVACE-ECP”) was part of the virtual engine sub-project of VIVACE and was worth 6.63 million Euros. The main outcome of the “VIVACE-ECP” was the development of a cost effective gas turbine simulation environment called PROOSIS. PROOSIS, which is the Greek word for “propulsion”, is an acronym for “**PR**opulsion **O**bject **O**riented **S**imulation **S**oftware”. PROOSIS was developed by facilitating optimal use of multi-partner gas turbine performance simulation research and development resources and expertise. PROOSIS is a single framework which provides shared standards and methodologies for the European Union (EU) gas turbine community, including original equipment manufacturers (OEMs), industrial companies, universities and research centres.

The primary objective of this doctoral thesis is to present advanced performance simulation models of gas turbine components and advanced fluid modelling capabilities developed by the author for the PROOSIS standard components library (SCLib). The main aims of this research are to provide a detailed insight into the effects of dissociation on fluid thermodynamic properties and subsequently on gas turbine performance. Detailed descriptions of the development of an advanced fluid model and a robust flow continuity model, which are the foundation of the PROOSIS standard component library, are provided. The effects of dissociation on isolated Burner and Afterburner components as well as overall engine performance are discussed with the aid of several case studies. Additionally, advanced performance simulation models of Burner and Afterburner components are presented. The development of an extended parametric representation of compressor characteristics is also analysed. Several advanced capabilities of PROOSIS (including test analysis, customer deck generation, 3D compressor zooming and distributed computing) are also introduced. The “evolution of PROOSIS” is presented with an in-depth analysis of the collaborative structure and project management of the VIVACE-ECP, as well as the channels of communication, technology transfer and quality control. A clear emphasis is placed on the contribution of the author to each of these tasks and subsequently the “VIVACE-ECP” as a whole.

The main outcome of this work is the development of an advanced fluid model which comprises multi-dimensional fluid property tables for several fuels. The advanced fluid model also caters for “levels of dissociation” ranging from “no dissociation” to chemical equilibrium. This advanced fluid model is complimented by a robust flow continuity model, also developed by the author, which calculates the unknown local flow properties at any point in an engine model. These robust, advanced fluid and flow continuity models facilitate improved accuracy thereby providing a solid foundation for several advanced gas turbine performance simulation capabilities.

ACKNOWLEDGEMENTS

“You don't choose your family. They are God's gift to you, as you are to them.”

I dedicate this work to the most important people in my life, my family: my mother Mrs. Sheesham Sethi, my brother Dr. Vikas Sethi and my sister Shivani. Their unconditional love as well as financial and moral support has enabled me conquer all obstacles and reach for the sky. For this I will always be sincerely appreciative and indebted to them. I am extremely grateful to Vikas for proof reading this thesis from cover to cover.

I would like to extend my deepest gratitude to my dearest friend Alima for her endless love and moral support.

Several individuals have provided invaluable assistance and guidance to me while I have been at Cranfield University, most notably Prof. P. Pilidis my project supervisor and mentor. I would like to express my sincere gratitude to him for his guidance and willingness time and time again to allow me to draw on his extensive knowledge not only for the project but also for all walks of life. I would also like to sincerely thank Mr. A. Jackson and Mr. R. Hales for their invaluable technical support, leadership and expertise throughout the project.

I am extremely grateful for the overwhelming support of the entire academic and administrative staff of the Cranfield University Department of Power and Propulsion particularly to Dr. K. W. Ramsden, Dr. V. Pachidis, Mr. A. Haslam, Ms. G. Hargreaves, Ms. R. Smith, Ms. M. Negus and Ms. C. Bellis.

This project provided me with an opportunity to liaise internationally both academically and socially with several individuals with a wealth of technical knowledge and extensive experience. I would like to sincerely thank all the “VIVACE-ECP” partners particularly M. Doussinault (Snecma), P. Cobas (Empresarios Agrupados Internacional), A. Rueda (EA), B. Garcia (EA), H. Gonser (MTU), K. Mathioudakis (NTUA), A. Alexiou (NTUA) and B. Banzhaf (USTUTT). The collaborative support of Airbus France, IberEspacio, ITP, Avio, Volvo Aero Corporation, Techspace Aero, Turbomeca, NLR and Cenaero is also much appreciated.

I would also like to extend my sincere gratitude to Prof. H. Saravanamuttoo, Dr. J. Kurzke, Dr. C. Morley and the late Dr. B. McBride for their technical advice and support.

Finally I would like to say a big “thank you” to all my friends and colleagues, past and present, in the Cranfield University Department of Power and Propulsion for their support and advice, particularly to A. Bala, F. Diara, S. Atabak, M. Katsourou, D. Laurans, E. Lo Gatto, R. Khan, G. Doulgeris, K. Psarra, K. Kyprianidis, F. Noppel, P. Zachos, M. Mucino, J. Janikovic, H. Hanumanthan, A. Orsini, V. Kyritsis, A. Duncombe and P. Bellocq.

The financial support of Cranfield University and the European Union is gratefully acknowledged.

I submit this thesis in the name of God.

ॐ Jai Mata Di ॐ

TABLE OF CONTENTS

PROJECT ABSTRACT	2
ACKNOWLEDGEMENTS	3
Chapter 1:	
General Introduction, Project Objectives and Thesis Structure	8
1.1: General Introduction and Project Objectives	9
1.2: Thesis Structure.....	11
Chapter 2:	
Advanced Modelling of Gas Turbine Fluid Thermodynamic Properties	13
Chapter 2: Nomenclature	14
2.1: PROOSIS Fluid Model	16
2.1.1: Introduction and General Description	16
2.1.2: Working Fluids	17
2.1.3: Fluid Model Types: No Dissociation & Chemical Equilibrium Models.....	19
2.1.4: Fluid Model Tables: Specific Enthalpy	23
2.1.5: Fluid Model Tables: Entropy Function	25
2.1.6: Fluid Model Tables: Isentropic Coefficient (Gamma)	27
2.1.7: Fluid Model Tables: Gas Constant.....	28
2.1.8: Fluid Model Tables: Dynamic Viscosity	29
2.1.9: Analysis of Fluid Model Tables: Effects of Temperature	31
2.1.10: Analysis of Fluid Model Tables: Effects of FARB and WAR.....	34
2.1.11: Fluid Model Validation and CEA Justification.....	35
2.1.12: PROOSIS Fluid Model Limitations.....	38
2.2: The CEA Software	43
2.2.1: Introduction	43
2.2.2: The CEA Input Files	43
2.2.3: The CEA Simulation and Output Files	45
2.3: PROOSIS Flow Continuity Model.....	46
2.3.1: Introduction	46
2.3.2: Auxiliary Thermodynamic Functions.....	46
2.3.3: Main Thermodynamic Functions.....	49
2.3.4: Example of a Main Thermodynamic Function Call.....	56
2.3.5: Importance of the Interpolation Method used for ϕ Fluid Tables.....	57
2.3.6: Intelligent Means of Implementing the Flow Continuity Model.....	59
Chapter 2: Figures	62
Chapter 2: Appendix 1	99
Chapter 2: References	103

Chapter 3:	
Advanced Performance Simulation of Gas Turbine Burners	105
Chapter 3: Nomenclature	106
3.1: PROOSIS Burner Component Modelling.....	109
3.1.1: Introduction	109
3.1.2: Burner Component Hierarchy and Ports.....	109
3.1.3: Burner Component Pressure Loss Model.....	110
3.1.4: Burner Component Efficiency Model	112
3.1.5: Burner Component Combustion Model.....	113
3.1.6: Variables Required for Global Engine Performance Calculations	116
3.2: PROOSIS Burner_Emissions Component Modelling.....	118
3.2.1: Introduction	118
3.2.2: Correlations for Oxides of Nitrogen (NO _x)	119
3.2.3: Carbon Monoxide (CO) Correlation	123
3.2.4: Unburned Hydrocarbons (UHC) Correlation	123
3.2.5: Smoke / Soot Correlation	124
3.3: Effects of Fuel Sensible Enthalpy.....	126
3.3.1: Introduction	126
3.3.2: Sources of Liquid Fuel Temperature Rise.....	126
3.3.3: Generating and Implementing Liquid Fuel Enthalpy Tables	129
3.3.4: Effects of Fuel Sensible Enthalpy – (Isolated Burner & Afterburner)	130
3.4: Burner Component Testing and Validation	134
3.4.1: Introduction	134
3.4.2: Isolated Burner Component Testing	134
3.5: Effects of Dissociation on Burner Component Performance	136
3.5.1: Introduction	136
3.5.2: Burner Component Case Study:.....	136
3.5.3: Afterburner Component Case Study:.....	137
3.6: Burner_Emissions Component Testing and Limitations	138
3.6.1: Introduction	138
3.6.2: Burner_Emissions Component Case Study:.....	138
Chapter 3: Figures	141
Chapter 3: References.....	156
Chapter 4:	
Engine Model Performance Simulations	160
Chapter 4: Nomenclature	161
4.1: Engine Model Generation and Performance Simulations	164
4.1.1: Introduction	164
4.1.2: CUTSTJR Engine Model: Schematic Generation	164
4.1.3: The “Inverse Design” Calculation Concept	166

Advanced Performance Simulation of Gas Turbine Components
and Fluid Thermodynamic Properties

4.1.4: CUTSTJR Engine Model: Off-Design Performance Simulation.....	168
4.1.5: CUTSTJR Engine Model: The Effects of Dissociation	171
4.2: Advanced Capabilities of PROOSIS.....	176
4.2.1: Introduction	176
4.2.2: Test Analysis.....	176
4.2.3: Customer Deck Generation	178
4.2.4: Integrated Aerodynamic Component Zooming	179
Chapter 4: Figures	181
Chapter 4: Appendix 1	198
Chapter 4: Appendix 2	201
Chapter 4: References	204
Chapter 5:	
Extended Parametric Representation of Compressor Characteristics	207
Chapter 5: Nomenclature	208
5.1: PROOSIS CompressorMFT Component Modelling.....	214
5.1.1: Introduction	214
5.1.2: BETA Line Compressor Maps	214
5.1.3: NASA and General Electric Representation of Compressor Maps.....	215
5.1.4: CompressorMFT Component Hierarchy.....	217
5.2: PROOSIS CompressorMFT Component Calculations.....	218
5.2.1: Introduction	218
5.2.2: Definition of W_c	218
5.2.3: Calculation of N_{cRdes}	219
5.2.4: Obtaining Alpha.....	219
5.2.5: Calculation of the Scalars for Gamma and Reynolds Correction	220
5.2.6: Calculation of $N_{cRdesMap}$	223
5.2.7: Calculation of $ghMap$	225
5.2.8: Calculation of $effMap$	225
5.2.9: Calculation of the Off-Design Isentropic Efficiency	229
5.2.10: Calculation of $PRmap$	231
5.2.11: Calculation of the Off-Design Pressure Ratio	232
5.2.12: Calculation of W_{cml}	232
5.2.13: Calculation of W_{cMap}	234
5.2.14: Calculation of the Off-Design Corrected Mass Flow Rate	235
5.2.15: Calculation of the Off-Design Compressor Percentage Surge Margin	237
Chapter 5: Figures	239
Chapter 5: Appendix 1	247
Chapter 5: References	253

Chapter 6:	
Project Management, Quality Control and Technology Transfer	254
Chapter 6: Nomenclature	255
6.1: "VIVACE-ECP" Project Structure.....	257
6.1.1: Introduction	257
6.1.2: The VIVACE Project.....	257
6.1.3: The "VIVACE-ECP" Work Package - PROOSIS	258
6.1.4: "VIVACE-ECP": Main Project Objectives and Deliverables	260
6.1.5: "VIVACE-ECP": Project Structure and Communication.....	265
6.1.6: "VIVACE-ECP": Quality Control.....	267
6.1.7: "VIVACE-ECP": Technology Transfer.....	271
6.1.8: Technology Transfer: The Author's Contribution to Dissemination	276
Chapter 6: Figures	278
Chapter 6: Appendix 1	287
Chapter 6: Appendix 2.....	288
Chapter 6: Appendix 3.....	289
Chapter 6: Appendix 4.....	290
Chapter 6: Appendix 5.....	294
Chapter 6: Appendix 6.....	296
Chapter 6: Appendix 7.....	299
Chapter 6: Appendix 8.....	300
Chapter 6: Appendix 9.....	300
Chapter 6: Appendix 10.....	301
Chapter 6: Appendix 11	302
Chapter 6: Appendix 12.....	303
Chapter 6: Appendix 13.....	304
Chapter 6: Appendix 14.....	305
Chapter 6: Appendix 15.....	306
Chapter 6: References	308
Chapter 7:	
General Conclusions and Recommendations for Further Work	313
7.1: Introduction	314
7.1.1: Chapter 2 Conclusions	314
7.1.2: Chapter 3 Conclusions	319
7.1.3: Chapter 4 Conclusions	324
7.1.4: Chapter 5 Conclusions	327
7.1.5: Chapter 6 Conclusions	328
GLOSSARY	329

Chapter 1: General Introduction, Project Objectives and Thesis Structure

1.1: General Introduction and Project Objectives

The “Value Improvement through a Virtual Aeronautical Collaborative Enterprise” (VIVACE) project was a European Union integrated project within Framework Package 6 (FP-6). The project began in January 2004 and concluded in December 2007. VIVACE set out to address several of the “Vision 2020” objectives that were formulated by the Advisory Council for Aeronautics Research in Europe (ACARE). The main objectives of VIVACE were to achieve a 5% cost reduction in aircraft development and a 5% reduction in the development phase of a new aircraft design combined with a contribution to a 30% reduction in the lead time and 50% reduction in development costs for a new or a derivative gas turbine.

The VIVACE European Cycle Program (“VIVACE-ECP”) was part of the virtual engine sub-project of VIVACE and was worth 6.63 million Euros. The main outcome of the “VIVACE-ECP” was the development of a cost effective gas turbine simulation environment called PROOSIS. PROOSIS, which is the Greek word for “propulsion”, is an acronym for “**PR**opulsion **O**bject **O**riented **S**imulation **S**oftware”. PROOSIS was developed by facilitating optimal use of multi-partner gas turbine performance simulation research and development resources and expertise. PROOSIS is a single framework which provides shared standards and methodologies for the European Union (EU) gas turbine community, including original equipment manufacturers (OEMs), industrial companies, universities and research centres.

Advanced gas turbine performance simulation software is becoming increasingly important in design studies, mission analysis, life cycle analysis, performance prediction and diagnostics. The international gas turbine community is worth thirty billion pounds annually. The EU gas turbine community are major contributors to research and development (R&D) of advanced gas turbine engines and cycles for aircraft propulsion as well as land and sea based applications. Currently the USA is Europe’s biggest gas turbine technology competitor. US engine manufacturers and research institutes including NASA, General Electric, Pratt and Whitney, Georgia Institute of Technology and Massachusetts Institute of Technology amongst others, have collaboratively developed NPSS (Numerical Propulsion System Simulation) as part of the EDS (Environmental Design Space) project. NPSS is a powerful gas turbine simulation tool with several advanced capabilities. Unfortunately, NPSS and the related technologies are broadly unavailable to the European gas turbine community. PROOSIS is effectively the EU’s equivalent to NPSS. PROOSIS encompasses advanced gas turbine simulation technology which provides significant competitive advantages for EU partners in this highly competitive industry.

The primary objective of this doctoral thesis is to present advanced performance simulation models of gas turbine components and advanced fluid modelling capabilities developed by the author for the PROOSIS standard components library (SCLib). The main aims of this research are to provide a detailed insight into the effects of dissociation on fluid thermodynamic properties and subsequently on gas turbine performance. Detailed descriptions of the development of an advanced fluid model and a robust flow continuity model, which are the foundation of the PROOSIS standard component library, are provided. The effects of dissociation on isolated Burner and Afterburner components as

Advanced Performance Simulation of Gas Turbine Components and Fluid Thermodynamic Properties

well as overall engine performance are discussed with the aid of several case studies. Additionally, advanced performance simulation models of Burner and Afterburner components are presented as well as the development of an extended parametric representation of compressor characteristics. Several advanced capabilities of PROOSIS (including test analysis, customer deck generation, 3D compressor zooming and distributed computing) are also introduced. The “evolution of PROOSIS” is presented with an in-depth analysis of the collaborative structure and project management of the VIVACE-ECP, as well as the channels of communication, technology transfer and quality control. A clear emphasis is placed on the contribution of the author to each of these tasks and subsequently the “VIVACE-ECP” as a whole.

1.2: Thesis Structure

This thesis adopts a “modular” structure. Each chapter is self contained with chapter specific brief abstracts, nomenclature guides, introductions, literature reviews, technical analyses, results, conclusions, appendices and references. The modular structure of this thesis reflects the object oriented nature of PROOSIS.

The work presented in Chapter 2 is the outcome of a collaborative effort between the author, two Cranfield University MSc course members and an exchange student. The extensive research into advanced modelling of fluid thermodynamic properties for gas turbine performance simulations has yielded the following reports which have already been published:

1. “Implementation of Accurate Gas Properties on Gas Turbine Simulations”
2. “Development of Accurate Fluid Models for Gas Turbine Performance Calculations”
3. “Advanced Modelling of Fluid and Thermodynamic Functions for Gas Turbine Mixers and Nozzles”

Chapter 2 presents the major contribution made by the author to the development of an advanced fluid model with densely populated multi-dimensional fluid model tables, catering for several fuels and accounting for different levels of dissociation. Additionally the evolution of a robust flow continuity model which was conceived and developed by the author is presented. The fluid model and flow continuity model developed by the author are the foundation of the PROOSIS standard components library (SCLib).

Chapter 3 presents several advanced considerations which are important for accurate performance simulations of gas turbine combustion systems. The performance simulation model of the PROOSIS Burner component is presented with detailed descriptions of the pressure loss, efficiency and energy balance models. A component which calculates Burner emissions (inheriting from the main Burner component) is also introduced. The effects of liquid fuel sensible enthalpy on isolated Burner and Afterburner performance are discussed. The results of the validation of the PROOSIS Burner component against well established (industry standard approved) gas turbine performance simulation software are presented. The chapter concludes with several isolated Burner and Afterburner simulation case studies which analyse:

1. The effects of dissociation on isolated Burner and Afterburner performance.
2. The limitations of the Burner_Emissions component.

The PROOSIS SCLib components, fluid functions and thermodynamic functions can be used to simulate a wide range of engine model configurations ranging from a simple single spool turbojet model to a complex mixed exhaust, multi-spool turbofan with several secondary air systems.

The first part of Chapter 4 describes the generation of a conceptual engine model of a twin spool turbojet with reheat. The design point performance calculation procedure is discussed. Important considerations that are required during the off-design performance simulation for engines with afterburners are also discussed. The effects of dissociation on overall engine performance are also analysed. This analysis is one of the major novel contributions to knowledge presented in this thesis.

The second part of Chapter 4 introduces some of the advanced capabilities of PROOSIS, which the author played a key role in developing including:

1. Test analysis and adaptation
2. “Stand alone” customer deck generation
3. High fidelity component zooming

Chapter 5 describes the structure and the implementation in PROOSIS of an extended parametric representation of compressor characteristics. The work presented in Chapter 5 is the outcome of a collaborative effort between M. Doussinault (Snecma) and the author. Snecma have introduced “Map Fitting Tool” (MFT) maps to model the off-design performance of all the turbomachinery components (Fans, Compressors and Turbines) within Janus (the in-house gas turbine performance simulation tool developed and used by Snecma). The MFT map methodology, which is based on a concept developed collaboratively by General Electric (GE) and NASA, is presented. The development and implementation of Compressor MFT maps in PROOSIS is discussed. The integration of Compressor_BETA and Compressor_MFT components, with respect to the overall hierarchy structure of the PROOSIS Compressor components is also highlighted. The implementation of MFT maps in PROOSIS while considering the object oriented modelling implications is the author’s contribution to extended parametric representation of compressor characteristics.

Chapter 6 (the penultimate chapter) provides a useful insight into the “evolution of PROOSIS” from the early stages of development until the final delivery of the gas turbine performance simulation software. The structure of the “VIVACE-ECP” collaboration is presented. Additionally a detailed time-line highlighting the evolution of the project is provided, emphasising the author’s contribution to the project. The importance of quality control for the “VIVACE-ECP” and the various tasks performed to maintain it are described. Technology transfer is a fundamental deliverable of a project such as the “VIVACE-ECP” and the chapter concludes with an analysis of the various channels of technology transfer with an emphasis on the author’s contribution. The author’s project responsibilities included project management. The author was an ambassador for the Cranfield University gas turbine group and the focal point of communication between Cranfield University and the “VIVACE-ECP” partners. This chapter provides an insight into the challenges faced by a PhD researcher, with respect to technical project management, for a typical modern EU collaborative project.

The final chapter of the thesis provides a general, collective conclusion of the work presented in each of the chapters highlighted above. The author’s main contributions to the development of knowledge in the field of advanced gas turbine performance simulation are presented. The limitations with the various analyses are highlighted and recommendations are made for further work.

Chapter 2: Advanced Modelling of Gas Turbine Fluid Thermodynamic Properties

Abstract

The work presented in this chapter is the outcome of a collaborative effort between the author, two Cranfield University MSc course members and an exchange student. The extensive research into advanced modelling of fluid thermodynamic properties for gas turbine performance simulations has yielded the following reports which have already been published:

1. "Implementation of Accurate Gas Properties on Gas Turbine Simulations"^[1]
2. "Development of Accurate Fluid Models for Gas Turbine Performance Calculations"^[2]
3. "Advanced Modelling of Fluid and Thermodynamic Functions for Gas Turbine Mixers and Nozzles"^[3]

This chapter presents the major contribution made by the author to the development of an advanced fluid model with densely populated multi-dimensional fluid model tables, catering for several fuels and accounting for different levels of dissociation. Additionally the evolution of a robust flow continuity model which was conceived and developed by the author is presented. The fluid model and flow continuity model developed by the author are the foundation of the PROOSIS standard components library (SCLib).

Chapter 2: Nomenclature

Symbols

Name	Description	Unit
$\%_{\text{diss}}$	Dissociation Percentage	-
Ae	Effective Area	m ²
Ang	Flow Angle	°
Ar	Atomic Weight (depending on context)	kg/(kg-mol)
Ar	Argon (depending on context)	-
CO	Carbon Monoxide	-
CO ₂	Carbon Dioxide	-
Cp	Specific Heat at Constant Pressure	J/(kg*K)
Cv	Specific Heat at Constant Volume	-
dPqP	Duct Component Fractional Pressure Loss	-
FARB	Burned Fuel to Air Ratio	-
FARr	Total Reactant Fuel to Air Ratio	-
FARU	Unburned Fuel to Air Ratio	-
flow	Flow Case (Subsonic, Sonic or Supersonic)	-
H ₂ O	Water	-
hs	Specific Enthalpy based on Static Conditions	J/kg
ht	Specific Enthalpy based on Total Conditions	J/kg
LHV	Lower Heating Value (Net Calorific Value)	J/kg
MN	Mach Number	-
Mr	Molecular Mass	kg/(kg-mol)
N ₂	Nitrogen Molecule	-
O ₂	Oxygen Molecule	-
Ps	Static Pressure	Pa
Pt	Total Pressure	Pa
R	Gas Constant	J/(kg*K)
Re	Reynolds Number	-
S	Specific Entropy	J/(kg*K)
Ts	Static Temperature	K
Tt	Total Temperature	K
V	Velocity	m/s
W	Mass Flow Rate	kg/s
WAR	Water to Air Ratio	-

Advanced Performance Simulation of Gas Turbine Components
and Fluid Thermodynamic Properties

Greek Symbols

Name	Description	Unit
ϕ	Equivalence Ratio (depending on context) $\left[\phi = \frac{FARr}{FARr_{Stoich}} \right]$	-
ϕ_s	Entropy Function based on Static Conditions	J/(kg*K)
ϕ_t	Entropy Function based on Total Conditions	J/(kg*K)
γ	Isentropic Coefficient (Gamma)	-
λ	Duct Component Pressure Loss Coefficient	-
μ	Dynamic Viscosity	(Pa*s)
ρ	Density	kg/m ³

Abbreviations

Name	Description	Unit
GUI	Graphical User Interface	-
NLR	National Aerospace Laboratory	-
SCLib	Standard Components Library	-
W&F	Walsh and Fletcher	-

Suffixes

The suffix “in” corresponds to a property at the inlet of the Duct component.
The suffix “crit” corresponds to a critical thermodynamic property (corresponding to MN=1).

Sub-Scripts

The sub-script “_{ref}” or “_{Ref}” corresponds to reference parameters.
The sub-script “_{Stoich}” corresponds to Stoichiometric values.

2.1: PROOSIS Fluid Model

2.1.1: Introduction and General Description

An accurate and reliable fluid model is essential for gas turbine performance simulation software as it provides a robust foundation for several advanced modelling capabilities. The fluid model, developed by the author, for the PROOSIS standard component library (SCLib), comprises a series of functions to obtain the following fluid properties from 3 – Dimensional, linearly interpolated tables, which were generated using the CEA ^[5] & ^[6] software developed by NASA:

1. Specific Enthalpy (h)
2. Entropy Function (ϕ)
3. Isentropic Coefficient (Gamma) (γ)
4. Gas Constant (R)
5. Dynamic Viscosity (μ)

The structure of the PROOSIS SCLib fluid model is shown in Fig: 2.1.1. The fluid model tables are in XML table format and stored in the SCLib “maps” folder. An example of an XML chemical equilibrium fluid model file for Jet-A is presented in Appendix 1.

NB: The nomenclature used in Appendix 1 is the PROOSIS object oriented nomenclature, which is slightly different from conventional engineering nomenclature.

Additionally, the fluid model also comprises “inverse functions” which are used to calculate the temperature (T), when the gas composition is known and either h or ϕ is provided as an additional input. If either of the two “inverse functions” (T_h or T_ϕ , highlighted in *Section 2.1.4* and *Section 2.1.5* respectively) is called, an iterative procedure to determine the temperature is required. The iterative procedure is given a limit of four loops, beyond which an error message indicating non-convergence is displayed.

There are conventionally two approaches for implementing fluid models in gas turbine performance simulation software. Fluid properties can either be obtained from linearly interpolated fluid tables or from polynomial functions. Although generating fluid model tables, either from polynomial relationships (such as those described in [4], [7], [8] & [9]) or chemical equilibrium software, (such as CEA ^[5] & ^[6], Gaseq ^[10] and CEC ^[11]) is far more laborious and time consuming than directly implementing polynomial functions, fluid tabulations offer several key advantages including^[12]:

1. Substitution of fluid models is numerically safer if only tabulations are changed.
2. The introduction of alternative function calls for different fluid models may lead to convergence problems due to the internal iterations of the functions.
3. The calculation speed is noticeably faster without these iterations.
4. The constraints of polynomials, with respect to range limits and precision, can be overcome by using high resolution tabulations over a wide range.
5. The required storage space for such dense tables is not a problem for modern computing systems.
6. The use of proprietary fluid models is safer with tabulations because even if keyed tabulations are decoded they just reveal heaps of numbers and not the model itself. This is particularly important for gas turbine performance simulation software (such as PROOSIS) which has been developed and will be used collaboratively by competitors.

7. A reduction of precision, for example to veil the quality of the gas turbine model to a competitor, can easily be obtained by using simplified gas property tables.
8. In cases where the effects of water to air ratio, unburned fuel to air ratio and dissociation, for each of the fluid properties outlined above, need to be considered, it is not easy to find polynomial relationships, which account for these effects, in the open literature. Tabulated fluid model tables, generated using chemical equilibrium software such as those described above, provide the ability to express any fluid property as a function of as many parameters as required. The only drawback is densely populated multi-dimensional tables which, as described above, are not a problem for modern computing systems.

The sections which follow describe the structure, validation and limitations of this fluid model (Fig: 2.1.1).

2.1.2: Working Fluids

The fluid model of a gas turbine simulation software typically comprises three types of fluids namely, the initial working fluid (typically air), the fuel and the products of combustion. As shown in Fig: 2.1.1, fluid model tables have been generated for four fuels, namely Jet-A, Diesel, Sample Natural Gas and Hydrogen (which for the purposes of this thesis will be referred to as the “PROOSIS fuels”). The chemical composition of atmospheric dry air (used for generating the PROOSIS SCLib fluid model) is highlighted in Fig: 2.1.2. The chemical compositions of the PROOSIS fuels are provided in Fig: 2.1.3 and the atomic weights (Ar) or molecular masses (Mr) of all the constituents (of the fuel and atmospheric dry air) are shown in Fig: 2.1.4. The data in Fig: 2.1.2 – Fig: 2.1.4 was obtained using the NASA ThermoBuild package ^[13], which is an online interactive tool which provides data subsets used in all NASA thermodynamic software including CEA ^[5] & ^[6]. A brief description of the atmospheric dry air (used in the PROOSIS fluid model) as well as the PROOSIS fuels is provided below.

Atmospheric Dry Air:

Fig: 2.1.2 shows the composition of dry air for the PROOSIS SCLib fluid model. Atmospheric dry air also comprises several other minor constituents (e.g. Neon, Helium, Methane, Krypton, Nitrogen Dioxide, Hydrogen, Xenon and Ozone) which constitute less than 0.003% of atmospheric dry air and are therefore generally ignored for gas turbine performance simulations. The composition of atmospheric dry air also varies significantly with geographical location with respect to weather, industrial activities and other factors. The water vapour and unburned hydrocarbons content of the air are accounted for by specifying the water to air ratio (WAR) and unburned fuel to air ratio (FARU) respectively. As a standard, the composition of air in Fig: 2.1.2 is used for the PROOSIS SCLib fluid model. However, users do have the option to employ user defined fluid models (for all working fluids).

Jet-A:

Kerosene is a fraction of crude oil which primarily comprises a band of hydrocarbons. Jet-A is just one of a number of commercial grades of kerosene. Aero-engines almost exclusively use kerosene as it has a relatively high lower heating value (LHV) (which minimises fuel weight – as there is a greater amount of energy released per unit mass)

and because it does not contain corrosive elements such as sulphur.”^[4] (Refer to *Section 3.1.5* for further details relating to fuel LHV).

Diesel:

“Diesel is a heavier fraction of crude oil than kerosene. It is less refined and contains small elements of corrosive substances such as sulphur and therefore costs less. For cost considerations, diesel is almost exclusively used for marine engines. The corrosive sulphur content is less of an issue since marine engines must be designed to withstand a highly corrosive sea water environment. Diesel is also used as a back up fuel for land based power generation engines. It is also utilised in military applications where it presents a lower risk of explosion than kerosene.”^[4]

Sample Natural Gas:

The composition (and consequently the properties) of natural gas vary significantly depending on the geographic location from where it is extracted. For the purposes of the PROOSIS SCLib fluid model, a “typical” natural gas (which will be referred to as sample natural gas) is used. The composition of sample natural gas (according to **[4]**) is shown in Fig: 2.1.5. Although sample natural gas is not one of the predefined species in CEA ^{[5] & [6]}, the CEA software is extremely flexible and allows the user to specify new species simply by specifying the chemical composition and relative amount (either mass fractions or mole fractions) of each constituent.

Hydrogen:

Although still not in commercial use, hydrogen is probably the most promising fuel for aero engines due to its high LHV (which implies a greater amount of heat energy released per unit mass of fuel burned as compared to kerosene). From an emissions perspective hydrogen is considered a “clean” fuel as water vapour is the only product of combustion. Additionally, hydrogen is characterised by high flame speeds, wide burning limits and easy ignition. Based on all the aforementioned properties, hydrogen is often considered as the nearest thing to an “ideal” fuel. The main drawbacks of hydrogen are its very low density and low boiling point which require the installation of heavily insulated storage tanks on the aircraft for practical and safety reasons. It is also quite costly to produce, however studies have revealed that these costs are easily offset (for aero engine applications) due to hydrogen’s high LHV. “In spite of formidable design and logistics problems, liquid hydrogen could still emerge as the commercial transport aircraft fuel of the future (driven by stringent emissions regulations). However, crippling capital investment would be required and high operating costs would be involved until there were enough new aircraft available to use the fuel and enough airports capable of supplying it.”^[14]

While the PROOSIS fluid model Jet-A tables were generated, tested and validated by the author, the fluid models for the other PROOSIS fuels were developed by D. Laurans ^[2], using the same modelling procedures and assumptions made by the author for the development of the Jet-A fluid model tables. Consequently some of the charts presented in *Section 2.1.4 – Section 2.1.8* are directly taken from **[2]** and referenced accordingly.

2.1.3: Fluid Model Types: No Dissociation & Chemical Equilibrium Models

The PROOSIS SCLib fluid model broadly comprises the following two models (for each fuel), as shown in Fig: 2.1.1.

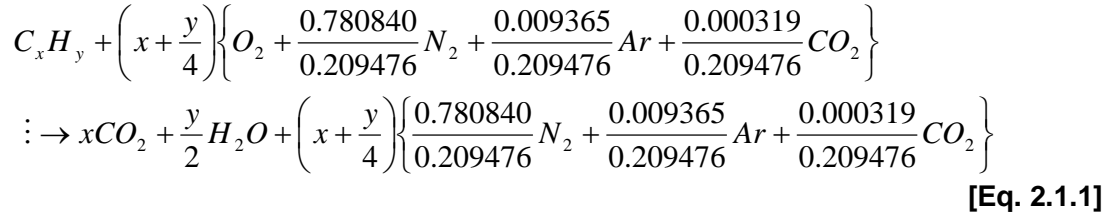
1. Assuming constant gaseous composition of the products of combustion (or air) (which will interchangeably be referred to as the “no dissociation” model).
2. Assuming Chemical Equilibrium

Fluid Model 1 (No dissociation model):

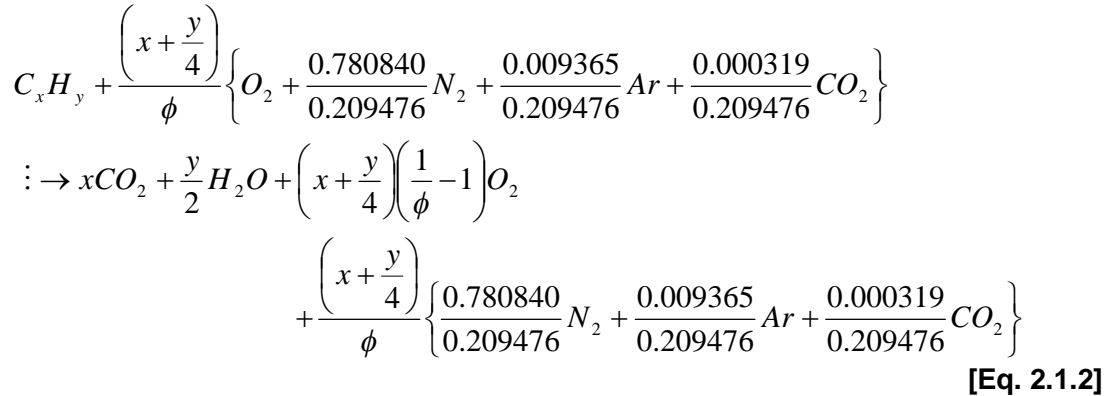
The tables generated for this fluid model are based on a constant gaseous composition of the products of combustion (or air). No allowances for dissociation have been made. The products of combustion comprise **only** water vapour ($H_2O_{(g)}$), carbon dioxide ($CO_{2(g)}$), argon ($Ar_{(g)}$), nitrogen ($N_{2(g)}$) and oxygen ($O_{2(g)}$) (if the reaction is fuel lean). Since there is no dissociation, the composition of the products does not change even with changes in temperature as the distributions of moles and consequently mole fractions remain the same at any temperature. This implies that the mean molecular weight of the gases in the products of combustion remains constant regardless of the temperature or pressure. Tables have only been generated for fuel lean and Stoichiometric reactions. [Eq. 2.1.1], [Eq. 2.1.2] and [Eq. 2.1.3] are generic, fully balanced equations for the combustion of any hydrocarbon with the structure C_xH_y for Stoichiometric, fuel lean and fuel rich combustion respectively.

NB: [Eq. 2.1.1], [Eq. 2.1.2] & [Eq. 2.1.3] are also valid for hydrogen where $x = 0$ and $y = 2$.

For Stoichiometric combustion ($\phi=1$):



For fuel lean combustion ($\phi < 1$):



For fuel rich combustion ($\phi > 1$):

$$\begin{aligned}
 & C_x H_y + \frac{\left(x + \frac{y}{4}\right)}{\phi} \left\{ O_2 + \frac{0.780840}{0.209476} N_2 + \frac{0.009365}{0.209476} Ar + \frac{0.000319}{0.209476} CO_2 \right\} \\
 & \therefore \rightarrow \frac{x}{\phi} CO_2 + \frac{y}{2\phi} H_2O + \left(1 - \frac{1}{\phi}\right) C_x H_y \\
 & \quad + \frac{\left(x + \frac{y}{4}\right)}{\phi} \left\{ \frac{0.780840}{0.209476} N_2 + \frac{0.009365}{0.209476} Ar + \frac{0.000319}{0.209476} CO_2 \right\}
 \end{aligned}
 \tag{Eq. 2.1.3}$$

Where the equivalence ratio (ϕ) is defined as shown in [Eq. 2.1.4]. $\phi = 1$ implies the combustion is Stoichiometric. In a Stoichiometric combustion reaction of a hydrocarbon, all the carbon is ideally converted to carbon dioxide and all the hydrogen to water. $\phi < 1$ implies the reactant mixture has excess air or is “fuel lean” while $\phi > 1$ implies the mixture has excess fuel or is “fuel rich”.

$$\phi = \frac{FARr}{FARr_{Stoich}}
 \tag{Eq. 2.1.4}$$

Where: FARr is the total reactant fuel to air ratio (Refer to Section 3.2 – [Eq. 3.2.2]).
FARr_{Stoich} is the Stoichiometric total reactant fuel to air ratio.

FARr_{Stoich} is defined as the ratio of the mass of fuel to the mass of air in the reactant mixture for a Stoichiometric combustion reaction [Eq. 2.1.5].

$$FARr_{Stoich} = \left(\frac{\text{mass of fuel}}{\text{mass of air in reactant mixture}} \right)_{Stoich}
 \tag{Eq. 2.1.5}$$

[Eq. 2.1.6] is a generic equation, which is used to calculate FARr_{Stoich} for any hydrocarbon with the structure C_xH_y as well as hydrogen (where $x = 0$ and $y = 2$). [Eq. 2.1.6] is obtained by substituting the values from [Eq. 2.1.1] and the appropriate atomic or molecular weights from Fig: 2.1.4, in [Eq. 2.1.5].

$$FARr_{Stoich} = \frac{12.01115x + 1.00794y}{138.27415 \left(x + \frac{y}{4}\right)}
 \tag{Eq. 2.1.6}$$

[Eq. 2.1.6] is used to calculate the Stoichiometric reactant total fuel to air ratios of all the PROOSIS fuels except sample natural gas as it is not a hydrocarbon with the structure C_xH_y. The Stoichiometric combustion of sample natural gas is more complex as

there are several secondary reactions that may occur. FAR_{Stoich} values for the various PROOSIS fuels are presented in Fig: 2.1.6.

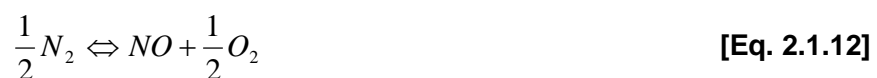
NB: The Stoichiometric combustion of sample natural gas is more complex as there are several secondary reactions that may occur. However for the purposes of the PROOSIS SCLib fluid model, it is assumed that the nitrogen and oxygen present in sample natural gas are inert during combustion. This assumption is justified as the effects of these trace elements are negligible for performance purposes.

For the “no dissociation” fluid model, it is assumed that all the working fluids are ideal gases and consequently the fluid properties are functions of temperature (T), burned fuel to air ratio (FARB) and water to air ratio (WAR) only (except for the Gas Constant (R) which is a function of FARB and WAR only). This assumption is based on Joule’s second law which states that the internal energy of an ideal gas is independent of its volume and pressure and is a function of temperature only.

Fluid Model 2 (Chemical Equilibrium):

The tables generated for this fluid model are based on chemical equilibrium and account for dissociation of the products of combustion. The combustion reactions highlighted in [Eq. 2.1.1] – [Eq. 2.1.3] are not based on chemical equilibrium and would therefore not be realised in practice. The description of chemical equilibrium and dissociation which follows is based on the literature in [15] & [16].

The combustion process involves a more complex series of reaction steps than suggested by the reactions highlighted in [Eq. 2.1.1] – [Eq. 2.1.3]. While the hydrogen content of a hydrocarbon burns fairly directly to $H_2O_{(g)}$, the released carbon goes through an intermediate state of carbon monoxide (CO) before complete oxidation to $CO_{2(g)}$. At relatively high temperatures (>1800K), characteristic of combustion, the otherwise stable products of combustion acquire sufficient energy to break down into non-zero concentrations of the intermediate atomic species e.g. H_2 , CO, H, OH and O. Furthermore N_2 (the nitrogen content in the air) also acquires sufficient energy to break down into N atoms and combine with the O atoms to produce NO atoms. This phenomenon is known as dissociation. The corresponding individual chemical equilibrium combustion reactions are defined in [Eq. 2.1.7] – [Eq. 2.1.12].



The level of dissociation is highly influenced by both temperature and pressure. LeChatelier's principle states: "If the external constraints under which an equilibrium is established are changed, the equilibrium will shift in such a way as to moderate the effect on the change". Using LeChatelier's principle, the following can be deduced:

1. Since the dissociation (forward) reactions highlighted in [Eq. 2.1.7] – [Eq. 2.1.12] are endothermic (absorb heat for bond breaking), an increase in temperature of the products of combustion will favour the forward reaction (so heat can be "removed" from the system) thereby yielding higher levels of dissociated species. Therefore the higher the temperature, the higher the level of dissociation.
2. In each of the equations highlighted above ([Eq. 2.1.7] – [Eq. 2.1.12]), it can be seen that the **total** number of moles (the sum of the number of moles of each species) on the "left" are less than the **total** number of moles on the right. For example, in [Eq. 2.1.7] there is a total of only 1 mole on the "left" (one mole of CO₂) but a total of 1.5 moles on the "right" (one mole of CO and half a mole of O₂). Pressure is proportional to the number of moles so effectively the pressure on the "left" is also less than that on the "right". Consequently an increase in pressure will favour the reverse reaction (so the pressure of the system can be reduced) thereby yielding higher levels of the non-dissociated species. Therefore the lower the pressure, the higher the level of dissociation.

This is just a qualitative analysis of the dissociation phenomenon. For an accurate, quantitative analysis of the concentration of the various species, suitable equilibrium constants need to be calculated. Detailed descriptions of the definition of equilibrium constants as well as the calculation procedures are highlighted in [1], [15] and [16].

Following dissociation, recombination of the various atomic species may subsequently result in a great host of additional intermediate constituents e.g. CH₄, CH, C₂, HCN, NH₂, NH₃, NO₂, CH₃, CN etc. The fluid model based on chemical equilibrium is based on the chemical equilibrium of all the species that may be present in the products of combustion as a consequence of dissociation and recombination.

The fluid model of the PROOSIS SCLib has two main limitations:

Limitation 1:

Theoretically, dissociation should cease, following subsequent cooling of the products of combustion which should consequently return to the non-dissociated species. In practice however, due to local chilling of the reactions due to turbulence and/or contact with the cooler walls of the Burner, as well as insufficient residence times of the working fluid in components downstream of the Burner, some dissociated species may still be present, in components downstream of the Burner (e.g. Turbines, Core Nozzle etc). This gives rise to the need of a third fluid model which is an intermediate fluid model that lies between the two extreme cases (no dissociation and chemical equilibrium) and is effectively a function of the "dissociation percentage" (%_{diss}). Generating an accurate fluid model of this type is not easy as the compositions of the species present in the products of combustion will need to be determined experimentally using techniques such as chemical absorption or adsorption, infrared radiation or paramagnetism^[16]. Although this third fluid model has not been implemented in PROOSIS, a simple model (external to PROOSIS) has been developed to determine the effects of %_{diss} on fluid properties and consequently isolated Burner component and overall engine performance. The results are presented in *Section 3.5* and *Section 4.1.5* respectively.

Limitation 2:

Currently, PROOSIS only supports a maximum of 3D tables (T, FARB and WAR) and therefore the fluid model tables do not account for the effects of pressure. This is acceptable for the “no dissociation” model. However, as mentioned above, pressure heavily influences the level of dissociation. As shown in Fig: 2.1.1, the chemical equilibrium fluid model has been generated for only one pressure (50atm). Currently the chemical equilibrium fluid model is only used for Burner and Afterburner simulations while the “no dissociation” model is used for all other components. Based on the limitation, this model is fairly accurate for Burner and Afterburner component simulations as Burner pressures of >50atm are unlikely to be encountered even for modern and conceptual high pressure ratio engines. Although the default chemical equilibrium fluid model is based on a pressure of 50atm, it can easily be replaced by different user defined models which have been generated for more appropriate pressures. Although not implemented in PROOSIS, the effects of pressure on dissociation (with respect to fluid properties) and isolated component performance are discussed in *Section 2.1.12*.

2.1.4: Fluid Model Tables: Specific Enthalpy

Specific enthalpy is a measure of the thermodynamic potential of a system. It is used to calculate the “useful” work obtainable, under constant pressure, from a thermodynamic system. According to Joule’s first and second laws, specific enthalpy (h) at any temperature (T) is defined as shown [Eq. 2.1.13].

$$h(T) = h_{T_{ref}} + \int_{T_{ref}}^T C_p(T) dT \quad \text{[Eq. 2.1.13]}$$

Where: Tref is a stipulated reference temperature

C_p(T) is the specific heat capacity at constant pressure as a function of temperature

For gas turbine performance calculations, it is changes in specific enthalpy, rather than absolute values, which are important [4]. The CEA software [5] & [6] calculates specific enthalpy based on a reference temperature (Tref) of 298.15K. For the fluid model of the PROOSIS SCLib, specific enthalpy (h) is a function of temperature (T), burned fuel to air ratio (FARB) and water to air ratio (WAR).

Specific Enthalpy Fluid Tables Description (at a glance)

Function call required: h_T

Function arguments (required inputs): fluid, T, FARB & WAR

Output: h

Inverse function call required: T_h

Function arguments (required inputs): fluid, h, FARB & WAR

Output: T

NB: The argument "fluid" gives users the flexibility to select the fluid model they wish to use. For a given fuel, the user can choose either the "no dissociation" model, the

"complete dissociation model" or can use company specific user defined fluid model tables based on a fluid model selector switch which is present in the attributes editor of each PROOSIS SCLib component. The switch is set to the "no dissociation" model by default. One of the main aims of PROOSIS is to allow the several industrial partners of the consortium to develop collaborative engine models. The flexibility of the fluid model selection allows an industrial partner e.g. Snecma to simulate their individual component (which would have been designed based on their company specific fluid model), using their confidential fluid model, whilst using the Default fluid model to simulate the rest of the engine. (As an example, refer to Fig: 3.1.3, which shows the fluid model selection switch for the Burner component in the component's attributes editor.

Temperature (T) range: 200K – 3000K (with tabulations at 50K intervals)

Tabulated burned fuel to air ratios (FARB):

Jet-A: 0.00, 0.02, 0.04, 0.06 & 0.06817 ($FAR_{rStoich}$)

Diesel: 0.00, 0.02, 0.04, 0.06 & 0.68956 ($FAR_{rStoich}$)

Sample Natural Gas: 0.00, 0.02, 0.04, 0.06 & 0.60644 ($FAR_{rStoich}$)

Hydrogen: 0.00, 0.01, 0.02 & 0.02916 ($FAR_{rStoich}$)

Tabulated water to air ratios (WAR): 0.00 & 0.10

NB: For all the fluid property tables, only values of $WAR \leq 0.10$ are considered because for values of $WAR > 0.10$ the mixture cannot be treated as a perfect gas.

Interpolation method for T, FARB and WAR: Linear Interpolation

(This has been justified. The validation process and results are presented in [2].)

Fig: 2.1.7 shows the variation of specific enthalpy as a function of temperature, burned fuel to air ratio and water to air ratio for Jet-A_(g), assuming a constant gaseous composition of the products of combustion (no dissociation).

Fig: 2.1.8 shows the variation of specific enthalpy as a function of temperature, burned fuel to air ratio and water to air ratio for Jet-A_(g), assuming chemical equilibrium (at 50atm).

Fig: 2.1.9 shows the Jet-A_(g) specific enthalpy discrepancy (%) between the two fluid models (no dissociation and chemical equilibrium) as a function of temperature for:

a.) FARB = 0.00 & WAR = 0.00 (Dry Air)

b.) FARB = 0.06 & WAR = 0.10

NB: For the purpose of this analysis, for given values of T, FARB and WAR, the % discrepancy is defined as shown in [Eq. 2.1.14].

$$\% \text{ discrepancy} = \frac{h(\text{chemical equilibrium}) - h(\text{no dissociation})}{h(\text{chemical equilibrium})} \times 100 \quad [\text{Eq. 2.1.14}]$$

Fig: 2.1.10^[2] shows a comparison of the chemical equilibrium (at 2atm*) specific enthalpy variation for the various PROOSIS fuels as a function of temperature for:

a.) FARB = 0.00 & WAR = 0.00 (Dry Air)

b.) FARB = 0.02 & WAR = 0.10

*NB: The effects of pressure on the chemical equilibrium specific enthalpy are discussed in *Section 2.1.12*.

2.1.5: Fluid Model Tables: Entropy Function

During compression or expansion, the increase in specific entropy (S) is a measure of the thermal energy lost to friction, which becomes unavailable as useful work. As with specific enthalpy, it is changes in specific entropy, rather than absolute values, which are important. The change in specific entropy at any condition (where $P = P_2$ and $T = T_2$) and a stipulated reference datum point (where $P = P_{Ref}$ and $T = T_{Ref}$) can be represented as shown in [Eq. 2.1.15].

NB: For CEA ^[5] & ^[6] $P_{Ref} = 1$ bar and $T_{Ref} = 288.15$ K

$$S(T_2, P_2) - S(T_{Ref}, P_{Ref}) = \int_{T_{Ref}}^{T_2} \frac{C_p}{T} dT - R \times \ln\left(\frac{P_2}{P_{Ref}}\right) \quad [\text{Eq. 2.1.15}]$$

Where: The term $\int_{T_{Ref}}^{T_2} \frac{C_p}{T} dT$ is defined as the entropy function (ϕ).

For an adiabatic, isentropic process, it is assumed that there is no change in entropy, so [Eq. 2.1.5] can be rewritten as shown in [Eq. 2.1.16].

$$\int_{T_{Ref}}^{T_2} \frac{C_p}{T} dT = R \times \ln\left(\frac{P_2}{P_{Ref}}\right) \quad [\text{Eq. 2.1.16}]$$

A detailed account of how to use this relationship within the CEA code to obtain values of entropy function (ϕ) is highlighted in **[3]**. Together with specific enthalpy, entropy function is used extensively in gas turbine performance simulation calculations as is presented in later sections. For the fluid model of the PROOSIS SCLib, entropy function (ϕ) is a function of temperature (T), burned fuel to air ratio (FARB) and water to air ratio (WAR).

Entropy Function Fluid Tables Description (at a glance)

Function call required: ϕ_T

Function arguments (required inputs): fluid, T, FARB & WAR

Output: ϕ

Inverse function call required: T_phi

Function arguments (required inputs): fluid, ϕ , FARB & WAR

Output: T

NB: Although the required function arguments for ϕ_T are fluid, T, FARB and WAR, the entropy function is calculated via a 3D linear interpolation of the natural log of temperature ($\ln(T)$), FARB and WAR. Investigations have revealed that inaccurate interpolations of entropy function with respect to temperature adversely affects the results and convergence (especially close to sonic conditions) of the thermodynamic

functions. A detailed account of these investigations is presented in *Section 2.3.5*. The variation of entropy function with respect to temperature is not linear (as shown in Fig: 2.1.11 and Fig: 2.1.13). However, the variation of entropy function with respect to the natural logarithm of temperature is almost linear (as shown in Fig: 2.1.12 and Fig: 2.1.14). Consequently interpolating with $\ln(T)$ is more accurate and yields improved results and convergence (especially close to sonic conditions) for the thermodynamic functions.

Temperature (T) range: 200K – 3000K (with tabulations at 50K intervals)

Tabulated burned fuel to air ratios (FARB):

Jet-A: 0.00, 0.02, 0.04, 0.06 & 0.06817 ($FAR_{rStoich}$)

Diesel: 0.00, 0.02, 0.04, 0.06 & 0.68956 ($FAR_{rStoich}$)

Sample Natural Gas: 0.00, 0.02, 0.04, 0.06 & 0.60644 ($FAR_{rStoich}$)

Hydrogen: 0.00, 0.01, 0.02 & 0.02916 ($FAR_{rStoich}$)

Tabulated water to air ratios (WAR): 0.00 & 0.10

Interpolation method for T, FARB and WAR: Linear Interpolation

(This has been justified. The validation process and results are presented in [2].)

Fig: 2.1.11 shows the variation of entropy function as a function of temperature, burned fuel to air ratio and water to air ratio for Jet-A_(g), assuming a constant gaseous composition of the products of combustion (no dissociation).

Fig: 2.1.12 shows the variation of entropy function as a function of the natural logarithm of temperature, burned fuel to air ratio and water to air ratio for Jet-A_(g), assuming a constant gaseous composition of the products of combustion (no dissociation).

Fig: 2.1.13 shows the variation of entropy function as a function of temperature, burned fuel to air ratio and water to air ratio for Jet-A_(g), assuming chemical equilibrium (at 50atm).

Fig: 2.1.14 shows the variation of entropy function as a function of the natural logarithm of temperature, burned fuel to air ratio and water to air ratio for Jet-A_(g), assuming chemical equilibrium (at 50atm).

Fig: 2.1.15 shows the Jet-A_(g) entropy function discrepancy (%) between the two fluid models (no dissociation and chemical equilibrium) as a function of temperature for:

a.) FARB = 0.00 & WAR = 0.00 (Dry Air)

b.) FARB = 0.06 & WAR = 0.10

NB: For the purpose of this analysis, for given values of T, FARB and WAR, the % discrepancy is defined as shown in [Eq. 2.1.17].

$$\% \text{ discrepancy} = \frac{\phi(\text{chemical equilibrium}) - \phi(\text{no dissociation})}{\phi(\text{chemical equilibrium})} \times 100 \quad \text{[Eq. 2.1.17]}$$

Fig: 2.1.16^[2] shows a comparison of the chemical equilibrium (at 2atm*) entropy function variation for the various PROOSIS fuels as a function of temperature for:

a.) FARB = 0.00 & WAR = 0.00 (Dry Air)

b.) FARB = 0.02 & WAR = 0.10

*NB: The effects of pressure on the chemical equilibrium entropy function are discussed in *Section 2.1.12*.

2.1.6: Fluid Model Tables: Isentropic Coefficient (Gamma)

The isentropic coefficient (γ) is defined as the ratio of specific heat at constant pressure to the specific heat at constant volume as shown in [Eq. 2.1.18].

$$\gamma = \frac{C_p(T)}{C_v(T)} = \frac{C_p}{C_p - R} \quad \text{[Eq. 2.1.18]}$$

For the fluid model of the PROOSIS SCLib, the isentropic coefficient (γ) is a function of temperature (T), burned fuel to air ratio (FARB) and water to air ratio (WAR).

Isentropic Coefficient Fluid Tables Description (at a glance)

Function call required: γ_T

Function arguments (required inputs): fluid, T, FARB & WAR

Output: γ

Temperature (T) range: 200K – 3000K (with tabulations at 50K intervals)

Tabulated burned fuel to air ratios (FARB):

Jet-A: 0.00, 0.02, 0.04, 0.06 & 0.06817 ($\text{FAR}_{\text{Stoich}}$)

Diesel: 0.00, 0.02, 0.04, 0.06 & 0.68956 ($\text{FAR}_{\text{Stoich}}$)

Sample Natural Gas: 0.00, 0.02, 0.04, 0.06 & 0.60644 ($\text{FAR}_{\text{Stoich}}$)

Hydrogen: 0.00, 0.01, 0.02 & 0.02916 ($\text{FAR}_{\text{Stoich}}$)

Tabulated water to air ratios (WAR): 0.00 & 0.10

Interpolation method for T, FARB and WAR: Linear Interpolation

(This has been justified. The validation process and results are presented in [2].)

Fig: 2.1.17 shows the variation of the isentropic coefficient as a function of temperature, burned fuel to air ratio and water to air ratio for Jet-A_(g), assuming a constant gaseous composition of the products of combustion (no dissociation).

Fig: 2.1.18 shows the variation of the isentropic coefficient as a function of temperature, burned fuel to air ratio and water to air ratio for Jet-A_(g), assuming chemical equilibrium (at 50atm).

Fig: 2.1.19 shows the Jet-A_(g) isentropic coefficient discrepancy (%) between the two fluid models (no dissociation and chemical equilibrium) as a function of temperature for:

a.) FARB = 0.00 & WAR = 0.00 (Dry Air)

b.) FARB = 0.06 & WAR = 0.10

NB: For the purpose of this analysis, for given values of T, FARB and WAR, the % discrepancy is defined as shown in [Eq. 2.1.19].

$$\% \text{ discrepancy} = \frac{\gamma(\text{chemical equilibrium}) - \gamma(\text{no dissociation})}{\gamma(\text{chemical equilibrium})} \times 100 \quad [\text{Eq. 2.1.19}]$$

Fig: 2.1.20^[2] shows a comparison of the chemical equilibrium (at 2atm*) isentropic coefficient variation for the various PROOSIS fuels as a function of temperature for:

- a.) FARB = 0.00 & WAR = 0.00 (Dry Air)
- b.) FARB = 0.02 & WAR = 0.10

*NB: The effects of pressure on the chemical equilibrium isentropic coefficient are discussed in *Section 2.1.12*.

2.1.7: Fluid Model Tables: Gas Constant

The gas constant (R) is defined as the ratio of the universal gas constant ($R_{\text{universal}} = 8.314.3 \text{ J}/(\text{mol} \cdot \text{K})$) to the molecular mass as shown in [Eq. 2.1.20].

$$R = \frac{R_{\text{universal}}}{Mr} \quad [\text{Eq. 2.1.20}]$$

For the “no dissociation” fluid model, the molecular weight of the products does not change (as there is a constant gaseous composition of the products of combustion). Consequently R does not vary with T but does vary with FARB and WAR. However, for the chemical equilibrium fluid model the level of dissociation is strongly influenced by temperature (>1800K). There is a change in the composition and consequently the molecular weight of the products of combustion. R is therefore a function of FARB, WAR and T for the chemical equilibrium fluid model. However, to avoid having two different functions to obtain R (with a different set of arguments) for the “no dissociation” and chemical equilibrium fluid models, the same function call is used, with the same arguments. When obtaining R using the “no dissociation” model, the user can input any value of T (e.g. T_{Std}) as it is still required (even though it is obsolete).

Gas Constant Fluid Tables Description (at a glance)

Function call required: R_FARB

Function arguments (required inputs): fluid, T, FARB & WAR

Output: R

Temperature (T) range: 200K – 3000K (with tabulations at 50K intervals)

Tabulated burned fuel to air ratios (FARB):

Jet-A: 0.00, 0.02, 0.04, 0.06 & 0.06817 ($\text{FAR}_{\text{Stoich}}$)

Diesel: 0.00, 0.02, 0.04, 0.06 & 0.68956 ($\text{FAR}_{\text{Stoich}}$)

Sample Natural Gas: 0.00, 0.02, 0.04, 0.06 & 0.60644 ($\text{FAR}_{\text{Stoich}}$)

Hydrogen: 0.00, 0.01, 0.02 & 0.02916 ($\text{FAR}_{\text{Stoich}}$)

Tabulated water to air ratios (WAR): 0.00 & 0.10

Interpolation method for T, FARB and WAR: Linear Interpolation

(This has been justified. The validation process and results are presented in [2].)

Fig: 2.1.21 shows the variation of the gas constant as a function of temperature, burned fuel to air ratio and water to air ratio for Jet-A_(g), assuming a constant gaseous composition of the products of combustion (no dissociation).

Fig: 2.1.22 shows the variation of the gas constant as a function of temperature, burned fuel to air ratio and water to air ratio for Jet-A_(g), assuming chemical equilibrium (at 50atm).

Fig: 2.1.23 shows the Jet-A_(g) gas constant discrepancy (%) between the two fluid models (no dissociation and chemical equilibrium) as a function of temperature for:

- a.) FARB = 0.00 & WAR = 0.00 (Dry Air)
- b.) FARB = 0.06 & WAR = 0.10

NB: For the purpose of this analysis, for given values of T, FARB and WAR, the % discrepancy is defined as shown in [Eq. 2.1.21].

$$\% \text{ discrepancy} = \frac{R(\text{chemical equilibrium}) - R(\text{no dissociation})}{R(\text{chemical equilibrium})} \times 100 \quad [\text{Eq. 2.1.21}]$$

Fig: 2.1.24^[2] shows a comparison of the chemical equilibrium (at 2atm*) gas constant variation for the various PROOSIS fuels as a function of temperature for:

- a.) FARB = 0.00 & WAR = 0.00 (Dry Air)
- b.) FARB = 0.02 & WAR = 0.10

*NB: The effects of pressure on the chemical equilibrium gas constant are discussed in Section 2.1.12.

2.1.8: Fluid Model Tables: Dynamic Viscosity

Dynamic viscosity (μ) is used to calculate the Reynolds number, which reflects the ratio of momentum forces to viscous forces present in a fluid. Dynamic viscosity is defined as shown in [Eq. 2.1.22] and is used to calculate the Reynolds number as shown in [Eq. 2.1.23].

$$\mu = \frac{F_{\text{shear}}}{\left(\frac{dV_{\text{shear}}}{dy} \right)} \quad [\text{Eq. 2.1.22}]$$

Where: F_{shear} is the shear stress in the fluid

V_{shear} is the velocity in the direction of the shear stress

dv/dy is the velocity gradient perpendicular to the shear stress

$$\text{Re} = \rho \times D \times \frac{V}{\mu} \quad [\text{Eq. 2.1.23}]$$

Where: Re is the Reynolds number

ρ is the fluid density

D is a representative dimension

V is a representative velocity

For the fluid model of the PROOSIS SCLib, the dynamic viscosity (μ) is a function of temperature (T), burned fuel to air ratio (FARB) and water to air ratio (WAR). However, as illustrated in the charts which follow, the effects of FARB and WAR are negligible for practical purposes.

Dynamic Viscosity Fluid Tables Description (at a glance)

Function call required: μ_T

Function arguments (required inputs): fluid, T, FARB & WAR

Output: μ

Temperature (T) range: 200K – 3000K (with tabulations at 50K intervals)

Tabulated burned fuel to air ratios (FARB):

Jet-A: 0.00, 0.02, 0.04, 0.06 & 0.06817 ($FAR_{rStoich}$)

Diesel: 0.00, 0.02, 0.04, 0.06 & 0.68956 ($FAR_{rStoich}$)

Sample Natural Gas: 0.00, 0.02, 0.04, 0.06 & 0.60644 ($FAR_{rStoich}$)

Hydrogen: 0.00, 0.01, 0.02 & 0.02916 ($FAR_{rStoich}$)

Tabulated water to air ratios (WAR): 0.00 & 0.10

Interpolation method for T, FARB and WAR: Linear Interpolation

(This has been justified. The validation process and results are presented in [2].)

Fig: 2.1.25 shows the variation of dynamic viscosity as a function of temperature, burned fuel to air ratio and water to air ratio for Jet-A_(g), assuming a constant gaseous composition of the products of combustion (no dissociation).

Fig: 2.1.26 shows the variation of dynamic viscosity as a function of temperature, burned fuel to air ratio and water to air ratio for Jet-A_(g), assuming chemical equilibrium (at 50atm).

Fig: 2.1.27 shows the Jet-A_(g) dynamic viscosity discrepancy (%) between the two fluid models (no dissociation and chemical equilibrium) as a function of temperature for:

a.) FARB = 0.00 & WAR = 0.00 (Dry Air)

b.) FARB = 0.06 & WAR = 0.10

NB: For the purpose of this analysis, for given values of T, FARB and WAR, the % discrepancy is defined as shown in [Eq. 2.1.24].

$$\% \text{discrepancy} = \frac{\mu(\text{chemical equilibrium}) - \mu(\text{no dissociation})}{\mu(\text{chemical equilibrium})} \times 100 \quad \text{[Eq. 2.1.24]}$$

Fig: 2.1.28^[2] shows a comparison of the chemical equilibrium (at 2atm*) dynamic viscosity variation for the various PROOSIS fuels as a function of temperature for:

a.) FARB = 0.00 & WAR = 0.00 (Dry Air)

b.) FARB = 0.02 & WAR = 0.10

*NB: The effects of pressure on the chemical equilibrium dynamic viscosity are discussed in Section 2.1.12.

2.1.9: Analysis of Fluid Model Tables: Effects of Temperature

Following a thorough investigation, linear interpolation of temperature for the all the fluid properties (both for the “no dissociation” and chemical equilibrium fluid models), except entropy function, was deemed acceptable for tabulated intervals of 50K. Despite the fact that the variation of majority of the fluid properties with temperature is far from linear (as shown in Fig: 2.1.7, Fig: 2.1.8, Fig: 2.1.11, Fig: 2.1.13, Fig: 2.1.17, Fig: 2.1.18, Fig: 2.1.22, Fig: 2.1.25 and Fig: 2.1.26) an interpolation interval of 50K is small enough to minimise errors to an acceptable level. However, linear interpolation of the natural logarithm of temperature is required for the entropy function tables as discussed in *Section 2.1.5*. Although reducing the tabulated temperature intervals (i.e. from 50K to 10K or even 1K) would increase the accuracy of the fluid model tables, the time it would take to generate these dense tables would overwhelm the improved accuracy that could be achieved.

“No Dissociation” Fluid Model:

As shown in Fig: 2.1.7, Fig: 2.1.11 and Fig: 2.1.25, for a fixed WAR and FARB, specific enthalpy, entropy function and dynamic viscosity increase with an increase in temperature respectively. Specific enthalpy is a measure of the thermodynamic potential of a system, the higher the temperature, the higher the energy level and therefore the higher the specific enthalpy relative to a stipulated reference. The higher the energy level, the higher the entropy of the system and therefore entropy function also increases with temperature. The higher the energy level, the higher the friction and sheer stresses between the molecules and therefore the higher the dynamic viscosity with an increase in temperature.

For a fixed WAR and FARB, the value of the gas constant does not change with an increase in temperature as shown in Fig. 2.1.21. The gas constant is calculated as shown in [Eq. 2.2.20]. Since for the “no dissociation” fluid model it is assumed that there is a constant composition of the products of combustion (or air), the molecular weight of the products of combustion (or air) remains unchanged as the temperature changes and consequently the gas constant does not vary with temperature. Fig: 2.1.29 is a graph which shows the variation in composition of dry air as a function of temperature for the “no dissociation” fluid model as obtained from the CEA ^[5] & ^[6] output file. It is evident that the composition does not change with temperature, both in terms of the constituents present (only N₂, O₂, CO₂ and Ar) as well as the mole fractions of each constituent (0.78084, 0.20948, 0.00032 and 0.00936 respectively). Similarly, Fig: 2.1.30 is a graph which shows the variation in composition of the products of combustion of Jet-A_(g) as function of temperature for FARB = 0.06 and WAR = 0.10 for the “no dissociation” fluid model as obtained from the CEA ^[5] & ^[6] output file. As with the previous case, it can be observed that the composition of the products of combustion does not change with temperature, both in terms of the constituents present (only N₂, O₂, CO₂, H₂O and Ar) as well as the mole fractions of each constituent (0.73683, 0.02369, 0.11792, 0.11272 and 0.00884 respectively).

For a fixed WAR and FARB, the isentropic coefficient (γ), decreases as the temperature increases as shown in Fig: 2.1.17. C_v is defined as the difference between C_p

and the gas constant (R) as shown in [Eq. 2.1.25].

$$C_v = C_p - R \quad \text{[Eq. 2.1.25]}$$

Substituting [Eq. 2.1.25] (for C_v) in [Eq. 2.1.18] yields [Eq. 2.1.26].

$$\gamma = \frac{C_p}{C_p - R} \quad \text{[Eq. 2.1.26]}$$

For the “no dissociation” fluid model, for a given FARB and WAR, R remains constant and C_p increases with temperature. Consequently γ decreases with an increase in temperature. The variation of γ with temperature is effectively similar to the “inverse” of the variation of C_p with temperature.

Chemical equilibrium Fluid Model:

In order to examine the differences in the fluid properties (h , ϕ , γ , R and μ) between the “no dissociation” and chemical equilibrium fluid models, it is important to understand how the composition of the products of combustion (or air) varies with temperature.

Fig: 2.1.31 is a graph which shows the variation in composition of dry air as a function of temperature for the chemical equilibrium fluid model ($P = 50\text{atm}$) as obtained from the CEA ^[5] & ^[6] output file. It is evident that the composition changes with temperature, both in terms of the constituents present, as well as the mole fractions of each constituent. Fig: 2.1.32 shows the composition of each constituent, in terms of mole fractions, for five temperatures (200K, 1500K, 2000K, 2500K and 3000K). Between 200K – 1500K the changes in composition are broadly negligible and the composition is consistent with that of the “no dissociation” model (Fig: 2.1.29). However, as the temperature increases further (beyond 1500K), dissociation begins to take its toll and the concentrations of the dissociated species (CO, NO_2 , N_2O , O and especially NO) increase rapidly.

NB: In addition to the species highlighted in Fig: 2.1.31 and Fig: 2.1.32, the following species are also considered as they are present in the chemical equilibrium composition. However, the mole fraction of each of these species is less than 0.000005.

Minor constituents: C, CN, CNN, C_2 , CCN, CNC, OCCN, C_2N_2 , C_2O , C_3 , CNCOCN, C_3O_2 , C_4 , C_4N_2 , C_5 , N, NCO, NO_3 , NCN, N_2O_3 , N_2O_4 , N_2O_5 , N_3 and O_3 .

Fig: 2.1.33 is a graph which shows the variation in composition of the products of combustion of Jet-A as a function of temperature for FARB = 0.06 and WAR = 0.10, for the chemical equilibrium fluid model ($P = 50\text{atm}$) as obtained from the CEA ^[5] & ^[6] output file. It is evident that the composition of the products of combustion changes with temperature, both in terms of the constituents present, as well as the mole fractions of each constituent. Fig: 2.1.34 shows the composition of each combustion product constituent, in terms of mole fractions, for the same five temperatures as the case above. Between 200K – 1500K the changes in composition are broadly negligible and the composition is consistent with

that of the “no dissociation” model (Fig: 2.1.30). However, as the temperature increases further (beyond 1500K), dissociation once again begins to take its toll and the concentrations of the dissociated species (H, HO₂, H₂, NO₂, N₂O, O and especially CO, NO and OH) increase rapidly.

NB: In addition to the species highlighted in Fig: 2.1.33 and Fig: 2.1.34, the following species are also considered as they are present in the chemical equilibrium composition of the products of combustion of Jet-A. However, the mole fraction of each of these species is less than 0.000005.

Minor constituents: C₂H₂, CH₂CO, O(CH)₂O, HO(CO)₂OH, C₂H₃, CH₃CN, CH₃CO, C₂H₄, C₂H₄O, CH₃CHO, CH₃COOH, OHCH₂COOH, C₂H₅, C₂H₆, CH₃N₂CH₃, C₂H₅OH, CH₃OCH₃, CH₃O₂CH₃, CCN, CNC, OCCN, C₂N₂, C₂O, C₃, C₃H₃, C₃H₄, C₃H₅, C₃H₆, C₃H₆O, C₃H₇, C₃H₈, CNCOCN, C₃O₂, C₄, C₄H₂, C₄H₄, C₄H₆, C₄H₈, (CH₃COOH)₂, C₄H₉, C₄H₁₀, C₄N₂, C₅, C₅H₆, C₅H₈, C₅H₁₀, C₅H₁₁, C₅H₁₂, CH₃C(CH₃)₂CH₃, C₆H₂, C₆H₅, C₆H₅O, C₆H₆, C₆H₅OH, C₆H₁₀, C₆H₁₂, C₆H₁₃, C₆H₁₄, C₇H₇, C₇H₈, C₇H₈O, C₇H₁₄, C₇H₁₅, C₇H₁₆, C₈H₈, C₈H₁₀, C₈H₁₆, C₈H₁₇, C₈H₁₈, C₉H₁₉, C₁₀H₈, C₁₀H₂₁, C₁₂H₉, C₁₂H₁₀, HCN, HCO, HCCN, HCCO, HNC, HNCO, HNO, HNO₂, HNO₃, HCHO, HCOOH, H₂O₂, (HCOOH)₂, N, NCO, NH, NH₂, NH₃, NH₂OH, NO₃, NCN, N₂H₂, NH₂NO₂, N₂H₄, N₂O₃, N₂O₄, N₂O₅, N₃, N₃H and O₃.

The analysis above clearly highlights that chemical equilibrium fluid composition begins to change significantly, due to dissociation, as the temperature increases beyond 1500K. This is consistent with the literature presented in *Section 2.1.3*. Referring to Fig: 2.1.9, Fig: 2.1.15, Fig: 2.1.19, Fig: 2.1.23 and Fig: 2.1.27 it is evident why discrepancies of h , ϕ , γ , R and μ respectively, between the “no dissociation” and the chemical equilibrium fluid models begin to exist (and increase significantly) at temperatures above 1500K.

The analyses below are only valid for temperatures above 1500K.

For a given temperature, FARB and WAR the specific enthalpy and entropy function of the dissociated products of combustion are higher than that of the non dissociated products as the dissociation process is endothermic (as highlighted in *Section 2.1.3*) and therefore heat is absorbed by the dissociated species.

For a given temperature, FARB and WAR, the chemical equilibrium gas constant is also higher because the molecular weight of the dissociated species is lower than that of the non dissociated species. (Refer to [Eq. 2.1.20]). Due to conservation of mass, the total mass of the products of combustion (dissociated or non-dissociated) is constant. However, the total number of moles of dissociated species is higher than that of non dissociated species, which is why the molecular weight of the chemical equilibrium products of combustion is less.

For a given temperature, FARB and WAR, the chemical equilibrium isentropic coefficient is lower than that of the “no dissociation” model. Referring to [Eq. 2.1.26], although the chemical equilibrium C_p is higher, the chemical equilibrium gas constant is proportionally even higher so the term $(C_p - R)$ dominates and γ is therefore lower.

For a given temperature, FARB and WAR, the discrepancy between the chemical equilibrium and “no dissociation” dynamic viscosity is relatively significantly lower than that for the other fluid properties. The chemical equilibrium dynamic viscosity is slightly lower than the “no dissociation” dynamic viscosity.

2.1.10: Analysis of Fluid Model Tables: Effects of FARB and WAR

Fig: 2.1.35 is a graph which shows the variation of Jet-A specific enthalpy as a function of FARB for a selection of temperatures (500K, 1000K, 1500K, 2000K, 2500K and 3000K) and a fixed WAR (0.00), both for the “no dissociation” and chemical equilibrium ($P = 50\text{atm}$) fluid models. Fig: 2.1.35 clearly justifies the use of linear interpolation for FARB for specific enthalpy for both fluid tables (“no dissociation” and chemical equilibrium). Although not presented similar trends were observed for all the other fluid properties (ϕ , γ , R and μ) as well as for the other PROOSIS fuels. Consequently linear interpolation of all the fluid tables with respect to FARB was deemed acceptable.

Fig: 2.1.36 is a graph which shows the variation of Jet-A specific enthalpy as a function of WAR for a selection of temperatures (500K, 1000K, 1500K, 2000K, 2500K and 3000K) and a fixed FARB (0.06), both for the “no dissociation” and chemical equilibrium fluid models. Although for the PROOSIS fluid model tables the tabulated values of WAR are only 0.00 and 0.10, Fig: 2.1.36 includes values of WAR = 0.025, WAR = 0.05 and WAR = 0.075 to justify the use of linear interpolation for WAR. As shown in Fig: 2.1.36, linear interpolation for WAR for specific enthalpy for both fluid tables (“no dissociation” and chemical equilibrium) is clearly justified. Although not presented similar trends were observed for all the other fluid properties (ϕ , γ , R and μ) as well as for the other PROOSIS fuels. Consequently linear interpolation of all the fluid tables with respect to WAR was deemed acceptable.

Effects of FARB:

As shown in Fig: 2.1.7, Fig: 2.1.8, Fig: 2.1.11 and Fig: 2.1.13, for a fixed temperature and WAR, specific enthalpy and entropy function increase with an increase in FARB (as the products of combustion have a higher specific enthalpy than air). This increase is greater for the chemical equilibrium fluid model compared to the “no dissociation” fluid model (for $T > 1500\text{K}$).

As shown in Fig: 2.1.21, for the “no dissociation” fluid model, for a given temperature as FARB increases, the molecular weight of the products of combustion increase and therefore the gas constant decreases. (Refer to [Eq. 2.1.20]). This is also true for the chemical equilibrium fluid model until a temperature limit after which the increase in molecular weight due to an increased FARB is overwhelmed by the decrease in molecular weight due to dissociation. As shown in Fig: 2.1.22, for temperatures greater than this limit, the gas constant increases with FARB.

NB: Like specific enthalpy, C_p also increases with an increase in FARB (for a fixed temperature and WAR). This variation of C_p and the variation of R (discussed above) explains the variation of the isentropic coefficient (shown in Fig: 2.1.17 and 2.1.18 for the “no dissociation” and chemical equilibrium fluid models respectively), as a function of FARB for a fixed temperature and WAR.

Fig: 2.1.25 and Fig: 2.1.26 clearly illustrate that the effects of FARB on dynamic viscosity are extremely small and could therefore be neglected, both for the “no dissociation” model and the chemical equilibrium model.

Effects of WAR:

As shown in Fig: 2.1.7, Fig: 2.1.8, Fig: 2.1.11, Fig: 2.1.13, Fig: 2.1.21 and Fig: 2.1.22, for a fixed temperature and FARB, specific enthalpy, entropy function as well as the gas constant increase with an increase with an increase in WAR. This increase is greater for the chemical equilibrium fluid model compared to the “no dissociation” fluid model (for $T > 1500\text{K}$).

NB: Like specific enthalpy, C_p also increases with an increase in WAR for a given temperature and FARB.

Based on the variations of C_p and R as functions of WAR it is evident that the isentropic coefficient decreases with a decrease in WAR for a fixed temperature and FARB for both the “no dissociation” and chemical equilibrium fluid models as shown in Fig: 2.1.17 and Fig: 2.1.18 respectively.

As discussed for FARB above, Fig: 2.1.25 and Fig: 2.1.26 also highlight that the effects of WAR on dynamic viscosity are extremely small and could therefore be neglected, both for the “no dissociation” and chemical equilibrium models.

2.1.11: Fluid Model Validation and CEA Justification

CEA ^[5] & ^[6] is an industrially accepted chemical equilibrium software, which has been used to develop the fluid models of well established gas turbine simulation software (e.g. GasTurb ^[18] and GSP ^[17]). However, the PROOSIS fluid model (which was generated using the CEA ^[5] & ^[6] software), still underwent the following validation tests before being implemented in the PROOSIS SCLib.

1. Comparison with the “Walsh and Fletcher” (W&F) polynomials defined in **[4]**.
2. Comparison with the tables generated using Gaseq ^[10].
3. Rigorous testing by the National Aerospace Laboratory (NLR), which involved comparing the PROOSIS fluid model to the fluid model developed by NLR for GSP ^[17] (NLR’s in-house gas turbine performance simulation software).

NB: NLR were the ECP industrial partners responsible for testing the fluid model developed by the author for the PROOSIS SCLib.

This section presents the results available from the validation and testing of the PROOSIS SCLib fluid model. The use of CEA ^[5] & ^[6] is also justified based on the limitations of:

1. The W&F polynomials ^[4]
2. Gaseq ^[10]

Testing and Validation using the W&F Polynomials ^[4].

The main limitations of the W&F polynomials are as follows:

Advanced Performance Simulation of Gas Turbine Components and Fluid Thermodynamic Properties

1. They do not cater for chemical equilibrium (i.e. they do not account for dissociation) and assume a constant gaseous composition for the products of combustion (or air).
2. Since the polynomials do not cater for dissociation, they do not account for the effects of pressure on fluid properties.
3. They are only valid for a temperature range of 200K – 2000K (for temperatures > 2000K the values obtained from the polynomials are meaningless).
4. The W&F basic polynomials are a function of temperature and FARB only. The effects of water to air ratio on the fluid properties are incorporated via “correction equations”, which although acceptable are not entirely accurate. This is not the case for the CEA software, which accurately accounts for the effects of water in all calculations.
5. The same polynomials are used for both Diesel and Jet-A, and although the discrepancies in the fluid properties of the two fuels are quite small, discrepancies do exist (as shown in Fig: 2.1.10, Fig: 2.1.16, Fig: 2.1.20, Fig: 2.1.24 and Fig: 2.1.28).
6. The polynomials are limited to only a small selection of fuels (Jet-A, Diesel and Sample Natural Gas). Some fuels e.g. hydrogen are not catered for.

Within the constraints of these limitations however, the W&F polynomials are highly accurate and have therefore been established as an industrial standard. Consequently they were used (as a first approach) to validate the “no dissociation” fluid model generated using CEA.

Fig: 2.1.37 shows a comparison of the variation of C_p (as a function of T and FARB, for WAR=0) between the W&F polynomials and the “no dissociation” fluid model generated using the CEA software. The curves shown are for dry air (FARB=0, WAR=0) and the products of combustion of Jet-A (assuming a constant gaseous composition of the products of combustion).

Fig: 2.1.38 shows a comparison of the variation of specific enthalpy (as a function of T and FARB, for WAR=0) between the W&F polynomials and the “no dissociation” fluid model generated using the CEA software. The curves shown are for dry air (FARB=0, WAR=0) and the products of combustion of Jet-A (assuming a constant gaseous composition of the products of combustion).

NB: The specific enthalpy values obtained directly from the W&F polynomials are not the values which have been plotted in Fig: 2.1.38. In order to compare the two fluid models, it was necessary to ensure that the reference temperature used for both models was the same ($T_{ref} = 298.15K$). Consequently the specific enthalpy values obtained from the W&F polynomials were corrected such that at 298.15K (the reference temperature), the specific enthalpy was set to zero (this correction effectively shifts the whole characteristic vertically). This correction is valid as it is changes in specific enthalpy rather than absolute values which are important for gas turbine performance calculations.

Fig: 2.1.39 shows a comparison of the variation of entropy function (as a function of T and FARB, for WAR=0) between the W&F polynomials and the “no dissociation” fluid model generated using the CEA software. The curves shown are for dry air (FARB=0, WAR=0) and the products of combustion of Jet-A (assuming a constant gaseous composition of the products of combustion).

NB: The entropy function values obtained directly from the W&F polynomials are not the values which have been plotted in Fig: 2.1.38. In order to compare the two fluid

models, it was necessary to ensure that the reference temperature used for both models was the same ($T_{ref} = 298.15K$). Consequently the characteristics obtained using the W&F polynomials were shifted vertically until the entropy function values (at 298.15K) were superimposed on the CEA values (for a given temperature and FARB). As with specific enthalpy, this correction is valid as it is changes in entropy function rather than absolute values which are important for gas turbine performance calculations.

Although the W&F polynomials are only valid for a temperature range of 200K-2000K, (as mentioned above) Fig: 2.1.37, Fig: 2.1.38 and Fig: 2.1.39 clearly show that the two fluid models are consistent for this temperature range. At no point does the percentage discrepancy between the two fluid models exceed 0.1% (for a given T and FARB). Although the comparison graphs for R , γ and μ are not presented, they show a similar trend i.e. the discrepancy between the two fluid models is negligible.

Testing and Validation using Gaseq [10]:

Detailed results of the comparison between the CEA [5] & [6] generated fluid model and a Gaseq generated fluid model is presented in [1]. The results for the “no dissociation” models are very consistent (which is not surprising because Gaseq uses the same polynomials, with the same coefficients, as CEA). [1] also presents, in detail, the limitations of Gaseq and consequently the reasons for deciding to use the CEA software. The two major limitations of Gaseq are summarised below.

1. The main limitation of Gaseq is the inaccuracy of the chemical equilibrium models.
2. Additionally the library of species in Gaseq is significantly smaller than that of CEA (typical fuels like Jet-A and Diesel are not catered for in the default library). Gaseq however, does allow the user to define new fuels (e.g. Jet-A or Diesel) either by [10]:
 - a. Specifying the elemental composition, the heat of formation and the entropy of the fuel at 298K and its specific heat at, at least one, and preferably more, temperatures.
 - b. Entering its elemental composition (as weight percent) and its heat of combustion.

However, Gaseq was often found to “crash” when trying to enter new polynomials. (The author reported this to C. Morley (the developer of Gaseq) and believes this problem has now been rectified).

NLR Rigorous Testing and Validation:

Despite some limitations, (which are discussed in *Section 2.1.12*), the PROOSIS SCLib fluid model (comprising both the “no dissociation” and chemical equilibrium (for $P = 50\text{atm}$) models) was approved by NLR following the successful outcome of their internal rigorous testing. The results of the validation tests performed by NLR are not presented due to confidentiality constraints.

2.1.12: PROOSIS Fluid Model Limitations

As discussed in *Section 2.1.3*, the two main limitations of the fluid model of the SCLib are:

1. PROOSIS only supports a maximum of 3D tables (T, FARB and WAR) and therefore the fluid model tables do not account for the effects of pressure. Although the “no dissociation” model is independent of pressure, the chemical equilibrium fluid model is heavily dependent on pressure (the reasons are presented in *Section 2.1.3*). Based on the limitation discussed above, the chemical equilibrium fluid model tables were generated for only one pressure (50atm) (the reasons for choosing 50atm are justified in *Section 2.1.3*). This section presents the effects of pressure on all the chemical equilibrium fluid properties.
2. Only two types of fluid models have been generated. One assuming chemical equilibrium and the other assuming no dissociation. These two fluid models are based on two extreme scenarios and reality lies somewhere in between. As mentioned in *Section 2.1.3*, a third fluid model has been developed and tested (though not yet implemented in PROOSIS). This third fluid model lies between the two extreme cases and is effectively a function of the “dissociation percentage” ($\%_{\text{diss}}$). This section presents the “ $\%_{\text{diss}}$ ” fluid model.

Effects of Pressure on Chemical Equilibrium Fluid Properties:

Fig: 2.1.40 shows the variation of chemical equilibrium specific enthalpy as a function of temperature and pressure for dry air.

Fig: 2.1.41 shows the variation of chemical equilibrium specific enthalpy as a function of temperature and pressure for the products of combustion of Jet-A (FARB = 0.02, WAR = 0.00).

Fig: 2.1.42 shows the variation of chemical equilibrium entropy function as a function of temperature and pressure for dry air.

Fig: 2.1.43 shows the variation of chemical equilibrium entropy function as a function of temperature and pressure for the products of combustion of Jet-A (FARB = 0.02, WAR = 0.00).

Fig: 2.1.44 shows the variation of the chemical equilibrium isentropic coefficient as a function of temperature and pressure for dry air.

Fig: 2.1.45 shows the variation of the chemical equilibrium isentropic coefficient as a function of temperature and pressure for the products of combustion of Jet-A (FARB = 0.02, WAR = 0.00).

Fig: 2.1.46 shows the variation of the chemical equilibrium gas constant as a function of temperature and pressure for dry air.

Fig: 2.1.47 shows the variation of the chemical equilibrium gas constant as a function of temperature and pressure for the products of combustion of Jet-A (FARB = 0.02, WAR = 0.00).

Fig: 2.1.48 shows the variation of the chemical equilibrium dynamic viscosity as a function of temperature and pressure for dry air.

Fig: 2.1.49 shows the variation of the chemical equilibrium dynamic viscosity as a function of temperature and pressure for the products of combustion of Jet-A (FARB = 0.02, WAR = 0.00).

Based on these charts it is evident that for temperatures above 1500K, (the temperature at which dissociation starts to become significant) pressure begins to strongly influence the chemical equilibrium fluid properties of both dry air and the products of combustion of Jet-A. All the results shown in the various charts presented above are consistent with the literature discussed in *Section 2.1.3* and *Section 2.1.9*.

The analyses below are only valid for temperatures above 1500K.

For a given temperature, FARB and WAR, the chemical equilibrium specific enthalpy and entropy function increase as the pressure reduces. As discussed in *Section 2.1.3*, the total number of moles of the dissociated species is more than the total number of moles of the non-dissociated species. Since pressure is proportional to the number of moles, LeChatelier's principle dictates that a reduction in pressure will favour dissociation (the "forward" reactions outlined in [Eq. 2.1.7] – [Eq. 2.1.12]) to maintain chemical equilibrium. Since the dissociated species have a higher specific enthalpy and entropy function than the non-dissociated species (as discussed in *Section 2.1.9*), it is fair to deduce that the lower the pressure, the greater the level of dissociation, therefore the higher the concentration of the dissociated species and consequently the higher the specific enthalpy and entropy function of the products of combustion (or air). From Fig: 2.1.40 and Fig: 2.1.41 it can be observed that for a temperature of 3000K the maximum discrepancies between the "no dissociation" and chemical equilibrium (at P=0.02atm) specific enthalpies are approximately 40% and 48% for dry air and the products of combustion of Jet-A (FARB=0.02) respectively. From Fig: 2.1.42 and Fig: 2.1.43 it can be observed that for a temperature of 3000K the maximum discrepancies between the "no dissociation" and chemical equilibrium (at P=0.02atm) entropy functions are approximately 8% and 11% for dry air and the products of combustion of Jet-A (FARB=0.02) respectively.

For a given temperature, FARB and WAR, the chemical equilibrium gas constant increases as the pressure reduces. Since lower pressures favour dissociation, at lower pressures the molecular weight of dissociated products of combustion (or air) is lower (as discussed in *Section 2.1.9*) and therefore the gas constant is higher. (Refer to [Eq. 2.1.20]). From Fig: 2.1.46 and Fig: 2.1.47 it can be observed that for a temperature of 3000K the maximum discrepancies between the "no dissociation" and chemical equilibrium (at P=0.02atm) gas constant are approximately 10% and 15% for dry air and the products of combustion of Jet-A (FARB=0.02) respectively.

For a given temperature, FARB and WAR, the chemical equilibrium isentropic coefficient reduces as the pressure reduces. Referring to [Eq. 2.1.26] as the pressure reduces (consequently increasing the level of dissociation), although C_p increases, the gas constant is proportionally even higher so the term $(C_p - R)$ dominates and γ is therefore lower. This is the general trend. Referring to Fig: 2.1.44 and Fig: 2.1.45) it can be

observed that for $P=0.02\text{atm}$, γ actually begins to increase for temperatures greater than approximately 2600K. For these temperatures (for $P=0.02\text{atm}$) it can therefore be deduced that the increase in C_p is proportionally higher than the increase in R therefore γ increases. From Fig: 2.1.44 and Fig: 2.1.45 it can be observed that for a temperature of 3000K the maximum discrepancies between the “no dissociation” and chemical equilibrium (at $P=0.02\text{atm}$) isentropic coefficients are approximately (-)12% and (-)11% for dry air and the products of combustion of Jet-A ($\text{FARB}=0.02$) respectively.

For a given temperature, FARB and WAR , the chemical equilibrium dynamic viscosity increases as the pressure reduces. The discrepancy however is negligible as highlighted in Fig: 2.1.48 and Fig: 2.1.49.

From Fig: 2.1.40 – Fig: 2.1.49 it can clearly be deduced that for higher temperatures ($>1500\text{K}$), the effects of pressure on all the fluid properties (except dynamic viscosity) cannot be ignored. Similar results were obtained and therefore the same conclusions can be drawn for different values of FARB and WAR (for Jet-A) as well as for all the other PROOSIS fuels. The results are presented in [2].

The %_{diss} Fluid Model:

As discussed in *Section 2.1.3*, a “%_{diss}” fluid model, which lies between the two extreme fluid models, (i.e. “no dissociation” and chemical equilibrium) is needed for a more realistic representation of fluid properties especially for components downstream of the Burner where dissociation should have ceased. However, due to local chilling of the reactions due to turbulence and/or contact with the cooler walls of the Burner, as well as insufficient residence times of the working fluid in components downstream of the Burner, some dissociated species may still be present. As mentioned in *Section 2.1.3*, determining the exact concentration of the various species present in the products of combustion is not trivial and requires complex analytical techniques. However, a very simple method to obtain the fluid properties corresponding to two intermediate levels of dissociation (33% and 66%) is described below. The model presented is based on the collaborative research between M. Katsourou [1] and the author.

Fig: 2.1.50 shows how the value of a fluid property (gas constant is used for the example but the methodology applies for all the fluid properties) corresponding to a particular value of %_{diss} is determined for a particular temperature, FARB and WAR . Assuming that chemical equilibrium corresponds to %_{diss} = 100% and “no dissociation” corresponds to %_{diss} = 0%, intermediate levels of %_{diss} (e.g. 33% and 66%) are obtained using a simple linear interpolation between the two extremes. Fig: 2.1.51 – Fig: 2.1.55 are respectively graphs of h , ϕ , γ , R and μ as a function of T and %_{diss} for dry air and the products of combustion of Jet-A ($P = 50\text{atm}$, $\text{FARB}=0.06$ and $\text{WAR}=0.10$). These graphs are shown as an example but provide a good indication of the structure of the “%_{diss}” fluid model. The effects of %_{diss} on isolated Burner component and overall engine performance are discussed in *Section 3.5* and *Section 4.1.5* respectively.

The Effects of Unburned Fuel to Air Ratio (FARU):

In addition to the two main limitations highlighted above, the PROOSIS SCLib fluid model does not account for the effects of unburned fuel on the fluid properties. As discussed in *Section 3.1.4*, due to the stringent constraints associated with gas turbine pollutants, Burner efficiencies of less than 90%, anywhere in the operational envelope, are unlikely to be tolerated. Consequently the relative unburned fuel to air ratio is highly unlikely to exceed 0.01 and this limitation is therefore not a fundamental limitation unlike the two limitations described above. Although the effects of unburned fuel are almost negligible (except for engines with afterburners), this section presents the development of a fluid model to cater for the unburned fuel to air ratio (FARU). In particular the assumptions made and the effects on fluid properties are presented. Although the presented “FARU” model was developed, it has not been implemented in the PROOSIS SCLib due to the limitation of not being able to implement tables greater than 3D in PROOSIS.

NB: The work involving modelling the effects of FARU on fluid thermodynamic properties was a collaborative effort between the author and D. Laurans [2]. A detailed description of the assumptions made, the modelling approach and the effects of FARU on fluid properties and consequently gas turbine performance is presented in [2]. A brief summary is provided below.

Modelling the effects of FARU using the CEA [5] & [6] software proved to be difficult for the following reasons:

1. The CEA software is a chemical equilibrium software which only allows the user to specify reactants. The software then calculates the products of combustion and consequently the fluid properties of these products of combustion. Unburned fuel is a constituent of the products, so a value of FARU cannot be specified as an input.
2. As mentioned above (for the %_{diss} model), determining the concentration of the products of combustion is not trivial and therefore it is difficult to determine what exactly constitutes “unburned fuel”. Unburned fuel could range from carbon monoxide to hydrogen to a whole host of small hydrocarbon chains.

In order to model the effects of FARU, two approaches were investigated.

FARU Modelling - Simple Approach (Less Accurate):

As a first approach, the simple method described below, was investigated following a discussion with Dr. J. Kurzke, the author of the gas turbine simulation software “GasTurb” [18]. The main constituent of the unburned fuel of a hydrocarbon is carbon monoxide (for hydrogen it is OH). The fluid properties of carbon monoxide are similar to those of air. Consequently, as a first approach, unburned fuel was simply modelled as excess air. A detailed description of how this was implemented using the CEA software is described in [2]. Although this approach proved slightly less accurate than the approach described below, it was relatively easier to implement as all the calculations are performed internally by the CEA software.

FARU Modelling - Complex Approach (More Rigorous):

The second, more rigorous approach, involved applying mixture rules to determine the effects of FARU on the fluid properties. Once again it was assumed that the main constituent of unburned fuel is carbon monoxide. The CEA software was then run twice. The first simulation yielded the fluid properties of the products of combustion while the

second simulation yielded the fluid properties of carbon monoxide only. Mixture algorithms (which are outlined in detail in [2]) were then applied (externally to the CEA software) to the two sets of fluid properties to determine the fluid properties of the products of combustion and carbon monoxide mixture. Although this method was more rigorous than the simple approach described above, there was still one fundamental limitation. The exact composition of the unburned fuel was not used and only carbon monoxide was considered. However, if the exact composition of the products of combustion could be determined, using one of the complex analytical techniques described in *Section 2.1.3*, then the mixture laws could easily be extended to cater for a more accurate representation of the unburned fuel.

The results obtained (the effects of FARU on fluid properties and consequently gas turbine performance simulation) using each of these two approaches are presented in [2]. The main observation that can be drawn is that for engine model simulations for engines without afterburners the effects of FARU are so small that they can be neglected. However for extremely rigorous engine model simulations for engines with afterburners the effects of FARU can be modelled using one of the two approaches described above. Although the second approach is far more complex, the discrepancies between the results obtained for the two approaches are negligible. Considering the trade-off between complexity and accuracy, it's the author's view that the first approach is more practical for gas turbine performance simulations.

2.2: The CEA Software

2.2.1: Introduction

Detailed descriptions of how the CEA [5] & [6] software works and how it can be used to generate fluid property tables for air and the products of combustion of any fuel are highlighted in [6] and [2] respectively. A brief summary is provided in this section with an emphasis on the specific considerations which were made for the development of the PROOSIS SCLib fluid model presented in *Section 2.1*. The examples shown will be based on the fluid model tables generated for Jet-A. However, the same procedure applies for all the other PROOSIS fuels.

2.2.2: The CEA Input Files

CEA simulations can be performed by using either “CEA_GUI” (which is the CEA software with a graphical user interface (GUI)) or by using “FCEA2” (which is a Fortran executable version of CEA without a GUI). The calculation procedure of both methods is fundamentally the same. Although CEA_GUI automatically generates the CEA input files, its main flaw is that the number of simulations that can be performed simultaneously is more limited than those that can be performed using FCEA2. For generating densely populated fluid property tables (such as those generated for the PROOSIS SCLib), it is desirable to run as many simulations as possible simultaneously, to generate the tables as quickly and efficiently as possible. Consequently the FCEA2 version was used. However, based on the author’s experience, it is advisable for first time users of CEA to familiarise themselves with CEA_GUI before using FCEA2.

CEA_GUI Case Study:

The following case study is used as an example to illustrate how a typical input file (to create the fluid model of the PROOSIS SCLib) was generated using CEA_GUI. The limitations of CEA_GUI (relative to FCEA2) will also be addressed. The presented case study provides a step by step guide to creating an input file to obtain the fluid properties of the products of combustion of Jet-A (for FARB = 0.02 and WAR = 0.00) for:

1. The “no dissociation” fluid model
2. The chemical equilibrium fluid model

The CEA_GUI platform (Fig: 2.2.1) comprises the following six tabs which assist the user in generating specific CEA input files:

- “Problem” tab
- “Reactant” tab
- “Only” tab
- “Omit” tab
- “Insert” tab
- “Output” tab

The CEA software is a chemical equilibrium software capable of solving the nine problem types highlighted in Fig: 2.2.1. The “Assigned Temperature and Pressure” (TP) problem (selected from the “Problem” tab) was used to generate the fluid model of the

PROOSIS SCLib. Once the problem type is specified, the temperatures and pressures are specified in the “TP” tab which is a sub-tab of the “Problem” tab as shown in Fig: 2.2.2. The main limitation of CEA_GUI (relative to FCEA2) is that it only allows the user to specify a maximum of 16 temperatures per simulation. However for FCEA2 the input file (Fig: 2.2.3) can comprise up to a maximum of 50 temperatures per simulation and therefore is more efficient with respect to time. The “Problem” tab is also where the fuel to air ratio is specified. As shown in Fig: 2.2.1, the fuel to air ratio can be specified using one of four options. For the purposes of generating the PROOSIS SCLib fluid model, the “Oxide-to-fuel” weight ratio input option (which is effectively the reciprocal of the fuel to air ratio) was used e.g. for a fuel to air ratio of 0.02 an oxide-to-fuel weight ratio of 50 was specified.

The “Reactant” tab (Fig: 2.2.4) is where the reactants (fuel and oxidiser) are defined. The CEA database comprises a comprehensive number of species from which a required fuel and oxidiser can be selected. Jet-A, Diesel, Hydrogen and Air are all readily available from this database (the composition of air and the compositions of each of these fuels are described in *Section 2.1.2*). The user must also specify the relative amounts of each species as well as the reference temperature ($T_{ref} = 298.15K$).

NB: The relative amount specified for the fuel and oxidiser is the amount relative to the total fuel and total oxidiser and should not be confused with the fuel to air ratio which is specified in the “Problem” tab. For Jet-A there is only one fuel and one oxidiser per fluid model, consequently the relative amounts of the fuel and oxidiser are set to unity. If the user wishes to simulate “multi-fuels” or “multi-oxidisers” the user can specify the relative amount of each fuel or oxidiser as a fraction (either moles or weight) of the total fuel or oxidiser. This approach was used to define sample natural gas using the composition (fuel species) and relative mole fractions defined in Fig: 2.1.5.

The “Only” tab and “Omit” tab are mutually exclusive (i.e. data can only be selected using one of the two tabs). The “Only” tab is used to select the species which are the only ones to be considered in the problem while the “Omit” tab is used to select the species which are to be omitted as possible products. For practical reasons, the “Only” tab was used for generating the CEA input files (to create the PROOSIS SCLib fluid model tables). The “Only” tab is essential for creating different input files for the “no dissociation” and chemical equilibrium models. For generating the input file for the “no dissociation” model, the only (hydrocarbon) combustion product species that need to be considered, as mentioned in *Section 2.1.3*, are H_2O , CO_2 , Ar, N_2 and O_2 as shown in Fig: 2.2.5. For generating the input files for the chemical equilibrium model, no species are selected either in the “Only” tab or the “Omit” tab so that all the species (highlighted in *Section 2.1.9*) are considered thereby providing a true chemical equilibrium calculation.

Initially some CEA chemical equilibrium simulations (particularly at lower temperatures and pressures) did not converge. After a detailed investigation it was deduced that the problem was attributed to a high presence of “condensed species” for these conditions. Consequently for all CEA chemical equilibrium simulations all the “condensed species” ($C_{(gr)}$, $H_2O_{(cr)}$ and $H_2O_{(l)}$) were omitted via the “Omit” tab. This ensured convergence of all cases whilst not compromising the accuracy of the results. A detailed analysis of the problem associated with the condensed species is provided in [2].

NB: The condensed species did not need to be omitted for the “no dissociation” simulations because as mentioned in the paragraph above, the “Only” tab and “Omit” tab are mutually exclusive. For the “no dissociation” simulations the “condensed species” are automatically omitted as they are not specified as the “Only Species” (H₂O, CO₂, Ar, N₂ and O₂).

The “Insert” tab is used to specify the set of condensed species to be included with gaseous species for initial equilibrium iterations. This tab was not used as condensed species were not considered.

The final tab is the “Output” tab (Fig: 2.2.6) which allows the user to select the specific variables (with specific units) to be automatically written to a plot file. The plot file can then be easily opened in software like Microsoft Excel for further analysis (e.g. producing graphs such as those presented in *Section 2.1*).

Once all the CEA_GUI tabs have been appropriately edited, the case is saved and this automatically generates an input file (with an extension “.inp”). The structure of the “.inp” file is as shown in Fig: 2.2.3.

2.2.3: The CEA Simulation and Output Files

Once the CEA input file has been generated, the simulation can be performed using one of the following two options:

1. For CEA_GUI, the simulation is performed by simply selecting the “Execute CEA2” command from the “Activity” tab located in the main toolbar.
2. For FCEA2, the simulation is performed simply by entering the “.inp” filename at the prompt.

The simulation yields the following two sets of results:

1. A comprehensive report file which provides a detailed set of results for each iteration.
2. A plot file with the variables defined by the user in the “Output” tab.

Following several simulations, the dense fluid model tables can be populated and the XML format fluid model input files (an example is shown in Appendix 1) can be generated.

2.3: PROOSIS Flow Continuity Model

2.3.1: Introduction

The flow continuity model of the PROOSIS SCLib comprises twelve thermodynamic functions to calculate the unknown local flow properties, at any point (inlet, outlet or intermediate) of any component provided one of a set of twelve compatible input options is satisfied. Additionally the flow continuity model comprises three auxiliary functions which are required for the calculations contained within the twelve main thermodynamic functions. The presented flow continuity model is valid for all the PROOSIS fuels, provided robust fluid models for dry air and the products of combustion of each of these fuels are available. An accurate and robust flow continuity model, such as that developed for the PROOSIS SCLib, is particularly important to ensure global convergence of isolated component as well as engine model simulations.

Some thermodynamic functions (both main and auxiliary) require iterations. These iterations are solved using a Newton Raphson (NR) routine, known as the “root function” [19] & [20], which has been specifically developed for PROOSIS by the software developers (Empresarios Agrupados – (EA)). The tolerance of the “root function” (thermTol) is defined as a global variable by the user. The default value for thermTol is 1e-12.

2.3.2: Auxiliary Thermodynamic Functions

The auxiliary thermodynamic functions described in this section are a fundamental part of the flow continuity model and are used extensively within the calculations of the main thermodynamic functions. For the PROOSIS SCLib, the order of the inputs and outputs for the following function calls are important and should not be changed.

Function Name: VS_Ts

Purpose: To obtain the local velocity of sound (VS) when the static temperature (Ts) is known.

Output: VS

Required Inputs: fluid, Ts, FARB and WAR

NB: The argument “fluid” is needed for all the thermodynamic functions (both main and auxiliary) as all the functions within the flow continuity model obtain fluid properties from the fluid model. The argument “fluid” defines which fluid model is used for the function. (Refer to *Section 2.1.4* for more details regarding the argument “fluid”).

For a given fluid, static temperature (Ts), burnt fuel to air ratio (FARB) and water to air ratio (WAR), the local velocity of sound (VS) is calculated using [Eq. 2.3.1]

$$VS = \sqrt{\gamma_s \times R \times Ts} \quad \text{[Eq. 2.3.1]}$$

Where: The isentropic coefficient based on static conditions (γ_s) and the gas constant (R) are obtained from the fluid model as shown in [Eq. 2.3.2] and [Eq. 2.3.3] respectively.

$$\gamma_s = \gamma_T(\text{fluid}, T_s, \text{FARB}, \text{WAR}) \quad [\text{Eq. 2.3.2}]$$

$$R = R_ \text{FARB}(\text{fluid}, T_s, \text{FARB}, \text{WAR}) \quad [\text{Eq. 2.3.3}]$$

Function Name: CritTsVS_Tt

Purpose: To obtain the critical static temperature (Tscrit) and the critical velocity of sound (VScrit), for a given total temperature (Tt).

Outputs: Tscrit and VScrit

Required Inputs: fluid, Tt, FARB and WAR

An iterative procedure is required to obtain the values of the critical static temperature and the critical local velocity of sound (i.e. the values of these variables which correspond to $MN = 1$) when the fluid, total temperature (Tt), burnt fuel to air ratio (FARB) and water to air ratio (WAR) are known.

The relationship between total specific enthalpy (ht), static specific enthalpy (hs) and velocity (V) is highlighted in [Eq. 2.3.4].

$$ht = hs + \frac{V^2}{2} \quad [\text{Eq. 2.3.4}]$$

[Eq. 2.3.5] shows the relationship between V, VS and Mach Number (MN)

$$V = MN \times VS \quad [\text{Eq. 2.3.5}]$$

Where: VS is defined as shown in [Eq. 2.3.1].

The properties of a fluid at the location where the Mach number is unity (i.e. the throat, where the flow is choked) are called critical properties.

Thus for critical conditions: $MN = 1 \Rightarrow V = VScrit$ where VScrit is obtained using the function VS_Ts as shown in [Eq. 2.3.6].

$$VScrit = VS_Ts(\text{fluid}, Tscrit, \text{FARB}, \text{WAR}) \quad [\text{Eq. 2.3.6}]$$

Where: Tscrit is the critical static temperature.

Therefore for critical conditions, [Eq. 2.3.4] can be written as [Eq. 2.3.7].

$$ht = hscrit + \frac{VScrit^2}{2} \quad [\text{Eq. 2.3.7}]$$

Where: The critical static specific enthalpy (hscrit) and the total specific enthalpy (ht) are obtained from the fluid model as shown in [Eq. 2.3.8] and [Eq. 2.3.9] respectively.

$$h_{scrit} = h_T(\text{fluid}, T_{scrit}, \text{FARB}, \text{WAR}) \quad [\text{Eq. 2.3.8}]$$

$$h_t = h_T(\text{fluid}, T_t, \text{FARB}, \text{WAR}) \quad [\text{Eq. 2.3.9}]$$

[Eq. 2.3.7] is solved iteratively to obtain the value of T_{scrit} (and consequently V_{Scrit}). In order to increase the iterative speed, the range of T_{scrit} specified in [Eq. 2.3.10] is used for the iteration.

$$(0.6 \times T_{scrit_{fg}}) < T_{scrit} < T_t \quad [\text{Eq. 2.3.10}]$$

Where: $T_{scrit_{fg}}$ is the first guess of T_{scrit} and is obtained as shown below.

A reasonable assumption to make for the first guess of T_{scrit} ($T_{scrit_{fg}}$) is that the static isentropic coefficient is equal to the total isentropic coefficient ($\gamma_t = \gamma_s = \gamma$). The relationship between total temperature (T_t), static temperature (T_s) and Mach Number (MN) is highlighted in [Eq. 2.3.11] (based on the assumption that the gas has constant isentropic coefficients).

$$\frac{T_t}{T_s} = 1 + \left(\frac{\gamma - 1}{2} \right) MN^2 \quad [\text{Eq. 2.3.11}]$$

For critical conditions ($MN = 1$) and assuming $\gamma = 1.4$ (for air), $T_{scrit_{fg}}$ can be expressed as a function of T_t as shown in [Eq. 2.3.12].

$$T_{scrit_{fg}} = T_t \times 0.83333333 \quad [\text{Eq. 2.3.12}]$$

If [Eq. 2.3.7] does not converge, the following error message is displayed:

"FUNCTION CritTsVS_Tt does not converge"

Function Name: CritPs_TtPt

Purpose: To obtain the critical static pressure (P_{scrit}) for a given total temperature (T_t) and total pressure (P_t).

Outputs: P_{scrit}

Required Inputs: fluid, T_t , P_t , FARB, WAR

In order to obtain the value of the critical static pressure (P_{scrit}) given the total temperature (T_t) and total pressure (P_t), the value of T_{scrit} is first obtained using the function call shown in [Eq. 2.3.13].

$$\text{CritTsVS_Tt}(\text{fluid}, T_t, \text{FARB}, \text{WAR}, T_{scrit}, V_{Scrit}) \quad [\text{Eq. 2.3.13}]$$

NB: This function also calculates V_{Scrit} even though it is not used for the calculations of the function CritPs_TtPt .

The value of P_{scrit} is then obtained using [Eq. 2.3.14].

$$P_{scrit} = \frac{P_t}{\exp\left\{\frac{(\phi_t - \phi_{scrit})}{R_{crit}}\right\}} \quad [\text{Eq. 2.3.14}]$$

Where: The critical static entropy function (ϕ_{scrit}), the total entropy function (ϕ_t) and the critical gas constant (R_{crit}) are obtained from the fluid model as shown in [Eq. 2.3.15], [Eq. 2.3.16] and [Eq. 2.3.17] respectively.

$$\phi_{scrit} = \phi_T(\text{fluid}, T_{scrit}, FARB, WAR) \quad [\text{Eq. 2.3.15}]$$

$$\phi_t = \phi_T(\text{fluid}, T_t, FARB, WAR) \quad [\text{Eq. 2.3.16}]$$

$$R_{crit} = R_FARB(\text{fluid}, T_{scrit}, FARB, WAR) \quad [\text{Eq. 2.3.17}]$$

2.3.3: Main Thermodynamic Functions

The flow continuity model comprises the following twelve main thermodynamic functions which are used to calculate the unknown local flow properties at any point of the engine performance model.

NB: For the flow continuity model of the PROOSIS SCLib, the order of the variables for all the main thermodynamic functions should not be altered regardless of whether the variables are input or output variables. For all twelve functions the order of the variables is as follows:

1. "fluid"
2. Mass flow rate (W)
3. Total Temperature (T_t)
4. Total Pressure (P_t)
5. Burned fuel to air ratio ($FARB$)
6. Water to Air Ratio (WAR)
7. Effective Area (A_e)
8. Mach Number (MN)
9. Velocity (V)
10. Static Temperature (T_s)
11. Static Pressure (P_s)
12. Flow Case (flow)

NB: The term Flow Case (flow) corresponds to the state of the flow, which is either Subsonic, Sonic or Supersonic. This term should not be confused with the mass flow rate (W). For some functions (e.g. therm_WTtPtAe), two solutions may exist (one supersonic solution and one subsonic solution). The user must therefore choose which solution is required by specifying the Flow Case (flow) as an additional input. For the functions where the Flow Case (flow) is not needed as there is a unique solution (e.g. therm_WTtPtMN) the Flow Case (flow) is given as an output of the function.

Function Name: `therm_WTtPtAe`

Outputs: MN, V, Ts and Ps

Required Inputs: fluid, W, Tt, Pt, FARB, WAR, Ae and flow

Mass flow rate is defined as the product of the density (ρ), the effective area (Ae) and the velocity (V) as shown in [Eq. 2.3.18].

$$W = \rho \times Ae \times V \quad [\text{Eq. 2.3.18}]$$

[Eq. 2.3.18] can be rewritten as [Eq. 2.3.19]

$$W = \left(\frac{Ps}{R \times Ts} \right) \times Ae \times V \quad [\text{Eq. 2.3.19}]$$

Where: The static pressure (Ps), is calculated using [Eq. 2.3.20]

$$Ps = \frac{Pt}{\exp\left\{\frac{(\phi t - \phi s)}{R}\right\}} \quad [\text{Eq. 2.3.20}]$$

The values of R, ϕt and ϕs are obtained from the fluid model as shown in [Eq. 2.3.3], [Eq. 2.3.16] and [Eq. 2.3.21] respectively.

$$\phi s = \phi_T(\text{fluid}, Ts, FARB, WAR) \quad [\text{Eq. 2.3.21}]$$

Velocity (V) is calculated using [Eq. 2.3.4].

Where: The values of ht and hs are obtained from the fluid model as shown in [Eq. 2.3.9] and [Eq. 2.3.22] respectively.

$$hs = h_T(\text{fluid}, Ts, FARB, WAR) \quad [\text{Eq. 2.3.22}]$$

[Eq. 2.3.19] is solved iteratively based on the following conditions:

If the Flow Case (flow) is Subsonic, $(T_{scrit} - 0.001) < Ts < Tt$ is imposed.

If the Flow Case (flow) is Supersonic, $200K < Ts < (T_{scrit} + 0.001)$ is imposed.

If the Flow Case (flow) is Sonic, $(T_{scrit} - 0.001) < Ts < (T_{scrit} + 0.001)$ is imposed.

NB: The factors of 0.001 have been introduced to improve convergence very close to or at Sonic conditions.

The converged solution provides the values of Ts, Ps and V.

MN is then obtained using [Eq. 2.3.23].

$$MN = \frac{V}{\sqrt{\gamma s \times R \times Ts}} \quad [\text{Eq. 2.3.23}]$$

Where: The value of γ_s is obtained from the fluid model as shown in [Eq. 2.3.2]

If the solution does not converge, the following error message is displayed:

"FUNCTION therm_WTtPtAe does not converge"

If therm_WTtPtAe does not converge the following conditions [Eq. 2.3.24] – [Eq. 2.3.27] are imposed, despite the error message being displayed. This ensures the outputs of therm_WTtPtAe are physical solutions (despite being wrong) as opposed to non-physical solutions (e.g. a negative Mach Number) which may seriously affect global convergence and adversely affect the troubleshooting process.

$$MN = 1 \quad \text{[Eq. 2.3.24]}$$

$$T_s = T_{scrit} \quad \text{[Eq. 2.3.25]}$$

$$P_s = P_{scrit} \quad \text{[Eq. 2.3.26]}$$

$$V = V_{scrit} \quad \text{[Eq. 2.3.27]}$$

Function Name: therm_WTtPtMN
Outputs: Ae, V, Ts, Ps and flow
Required Inputs: fluid, W, Tt, Pt, FARB, WAR and MN

Mach Number (MN) is defined as shown in [Eq. 2.3.23]. V, γ_s and R are obtained in the same way as highlighted for therm_WTtPtAe.

[Eq. 2.3.23] is solved iteratively based on the following conditions:

If the Flow Case (flow) is Subsonic, $(T_{scrit} - 0.001) < T_s < T_t$ is imposed.

If the Flow Case (flow) is Supersonic, $200K < T_s < (T_{scrit} + 0.001)$ is imposed.

If the Flow Case (flow) is Sonic, $(T_{scrit} - 0.001) < T_s < (T_{scrit} + 0.001)$ is imposed.

NB: The factors of 0.001 have been introduced to improve convergence very close to or at Sonic conditions.

The converged solution yields the values of Ts and V.

Ps is obtained using [Eq. 2.3.20]. ϕ_t , ϕ_s and R are obtained in the same way as highlighted for therm_WTtPtAe.

Ae is obtained by rearranging [Eq. 2.3.19].

If the solution does not converge, the following error message is displayed:

"FUNCTION therm_WTtPtMN does not converge"

Function Name: **therm_WTtPtV**
Outputs: Ae, MN, Ts, Ps and flow
Required Inputs: fluid, W, Tt, Pt, FARB, WAR and V

Velocity (V) is defined using [Eq. 2.3.4]. ht and hs are obtained in the same way as highlighted for therm_WTtPtAe.

[Eq. 2.3.4] is solved iteratively based on the following conditions:

If the Flow Case (flow) is Subsonic, $(T_{scrit} - 0.001) < T_s < T_t$ is imposed.

If the Flow Case (flow) is Supersonic, $200K < T_s < (T_{scrit} + 0.001)$ is imposed.

If the Flow Case (flow) is Sonic, $(T_{scrit} - 0.001) < T_s < (T_{scrit} + 0.001)$ is imposed.

NB: The factors of 0.001 have been introduced to improve convergence very close to or at Sonic conditions.

The converged solution yields the value of Ts.

Ps is obtained using [Eq. 2.3.20]. ϕ_t , ϕ_s and R are obtained in the same way as highlighted for therm_WTtPtAe.

Ae is obtained by rearranging [Eq. 2.3.19].

MN is obtained using [Eq. 2.3.23].

If the solution does not converge, the following error message is displayed:

"FUNCTION therm_WTtPtV does not converge"

Function Name: **therm_WTsPsAe**
Outputs: Tt, Pt, MN, V and flow
Required Inputs: fluid, W, FARB, WAR, Ae, Ts, and Ps

V is obtained by rearranging [Eq. 2.3.19].

Where: R is obtained from the fluid model as shown in [Eq. 2.3.3].

Tt is calculated using the reverse fluid model function T_h as shown in [Eq. 2.3.28]

$$T_t = T_h(\text{fluid}, ht, FARB, WAR) \quad \text{[Eq. 2.3.28]}$$

Where: The value of ht is calculated by rearranging [Eq. 2.3.4]. hs is obtained from the fluid model as shown in [Eq. 2.3.22].

Pt is calculated by rearranging [Eq. 2.3.20].

Where: The values of ϕ_t and ϕ_s are obtained from the fluid model as shown in [Eq.16] and [Eq.21] respectively.

MN is calculated by rearranging [Eq. 2.3.5].

Where: The value of VS is obtained using the function VS_Ts as shown in [Eq. 2.3.29].

$$VS = VS_Ts(\text{fluid}, Ts, FARB, WAR) \quad \text{[Eq. 2.3.29]}$$

Function Name: therm_WTsPsMN

Outputs: Tt, Pt, Ae, V and flow

Required Inputs: fluid, W, FARB, WAR, MN, Ts, and Ps

V is calculated by rearranging [Eq. 2.3.5].

Where: The value of VS is obtained using the function VS_Ts as shown in [Eq. 2.3.29].

Ae is obtained by rearranging [Eq.19]

Where: R is obtained from the fluid model as shown in [Eq. 2.3.3].

Tt and Pt are obtained in the same way as highlighted for therm_WTsPsAe.

Function Name: therm_WTsPsV

Outputs: Tt, Pt, Ae, MN and flow

Required Inputs: fluid, W, FARB, WAR, V, Ts, and Ps

Ae is obtained in the same way as highlighted for therm_WTsPsMN.

Tt, Pt and MN are obtained in the same way as highlighted for therm_WTsPsAe.

Function Name: therm_WTtPtTs

Outputs: Ae, MN, V, Ps and flow

Required Inputs: fluid, W, Tt, Pt, FARB, WAR and Ts

V is obtained by rearranging [Eq. 2.3.4].

Where: The values of ht and hs are obtained from the fluid model as shown in [Eq. 2.3.9] and [Eq. 2.3.22] respectively.

Ae is obtained in the same way as highlighted for therm_WTsPsMN.

Ps is obtained in the same way as highlighted for therm_WTtPtAe.

MN is obtained in the same way as highlighted for therm_WTsPsAe.

Function Name: therm_WTtPtPs

Outputs: Ae, MN, V, Ts and flow

Required Inputs: fluid, W, Tt, Pt, FARB, WAR and Ps

Ts is calculated using the reverse fluid model function T_φ as shown in [Eq. 2.3.30].

$$T_s = T_{-}\phi(\text{fluid}, \phi_s, \text{FARB}, \text{WAR}) \quad \text{[Eq. 2.3.30]}$$

Where: The value of ϕ_s is calculated by rearranging [Eq. 2.3.20]. ϕ_t and R are obtained from the fluid model as shown in [Eq. 2.3.16] and [Eq. 2.3.3] respectively.

V is obtained in the same way as highlighted for therm_WTtPtTs.

Ae is obtained in the same way as highlighted for therm_WTsPsMN.

MN is obtained in the same way as highlighted for therm_WTsPsAe.

Function Name: therm_TtPtAeMN

Outputs: W, V, Ts, Ps and flow

Required Inputs: fluid, Tt, Pt, FARB, WAR, Ae and MN

The calculations for therm_TtPtAeMN are almost identical to the calculations for therm_WTtPtMN.

The only two differences between the two functions are, for therm_TtPtAeMN:

1. [Eq. 2.3.19] is rearranged to obtain the value of W.
2. If the solution does not converge, the following error message is displayed:

"FUNCTION therm_TtPtAeMN does not converge"

Function Name: therm_TtPtPsAe

Outputs: W, MN, V, Ts and flow

Required Inputs: fluid, Tt, Pt, FARB, WAR, Ae and Ps

Ts is obtained in the same way as highlighted for therm_WTtPtPs.

V is obtained in the same way as highlighted for therm_WTtPtTs.

W is obtained by rearranging [Eq. 2.3.19].

Where: R is obtained from the fluid model as shown in [Eq. 2.3.3].

MN is obtained in the same way as highlighted for therm_WTsPsAe.

Function Name: therm_WTtPsAe

Outputs: Pt, MN, V, Ts

Required Inputs: fluid, W, Tt, FARB, WAR, Ae, Ps and flow

The calculations for therm_WTtPsAe are almost identical to the calculations for therm_WTtPtAe.

The only two differences between the two functions are, for therm_WTtPsAe:

1. [Eq. 2.3.20] is rearranged to obtain the value of Pt.
2. If the solution does not converge, the following error message is displayed:

"FUNCTION therm_WTtPsAe does not converge"

Function Name: therm_WTtPsV
Outputs: Pt, Ae, MN, Ts and flow
Required Inputs: fluid, W, Tt, FARB, WAR, V and Ps

The calculations for therm_WTtPsV are almost identical to the calculations for therm_WTtPtV.

The only two differences between the two functions are, for therm_WTtPsV:

1. [Eq. 2.3.20] is rearranged to obtain the value of Pt.
2. If the solution does not converge, the following error message is displayed:

"FUNCTION therm_WTtPsV does not converge"

The twelve main thermodynamic functions described above, cover all the calculations that may arise in gas turbine performance simulation. However, using a similar philosophy, a PROOSIS user can easily define additional thermodynamic functions provided the function inputs are compatible. However, this is only recommended for level 1 users of PROOSIS as the source file of the thermodynamic functions will need to be modified.

The calculations of the twelve main thermodynamic functions presented in this section, are deemed to be fully rigorous as the calculations are done based on fundamental thermodynamic definitions, using changes in specific enthalpy and entropy function between total and static properties. Conventionally, [Eq. 2.3.31] and [Eq. 2.3.32] are used to calculate static properties from total properties and vice versa.

$$\frac{Pt}{Ps} = \left\{ 1 + \left[\left(\frac{\gamma - 1}{2} \right) \times MN^2 \right] \right\}^{\left(\frac{\gamma}{\gamma - 1} \right)} \quad \text{[Eq. 2.3.31]}$$

$$\frac{Tt}{Ts} = 1 + \left[\left(\frac{\gamma - 1}{2} \right) \times MN^2 \right] \quad \text{[Eq. 2.3.32]}$$

These equations are derivatives which arise from the fundamental definition of specific enthalpy ([Eq. 2.1.13]). These equations however, are only true provided constant (mean) values of C_p and γ are assumed. These assumptions are valid for fairly accurate calculations. However, for fully rigorous calculations, especially for cases where there are large differences between Pt and Ps (and also between Tt and Ts) i.e. at higher values of

MN, the “changes in specific enthalpy and entropy function between static properties” method, although relatively tedious is far more accurate.

2.3.4: Example of a Main Thermodynamic Function Call

A simple example (using the PROOSIS SCLib Duct component) of how the thermodynamic functions are called within the PROOSIS SCLib is illustrated below.

Duct Component Example:

One of the options to determine the Duct fractional pressure loss (dPqP) (typically during off design) is to calculate the value based on a pressure loss coefficient (λ) as shown in [Eq. 2.3.33].

$$dPqP = \lambda \times \left[1 - \frac{1}{(P_{tin} / P_{sin})} \right] \quad \text{[Eq. 2.3.33]}$$

Where: P_{tin} and P_{sin} are the Duct inlet total pressure and static pressure respectively.

For the Duct component the main inlet flow port variables are obtained from the immediate upstream component. The main inlet flow port variables of the Duct component comprise the following:

Mass flow rate	(Win)
Total temperature	(Ttin)
Total pressure	(Ptin)
Burnt fuel to air ratio	(FARBin)
Unburnt fuel to air ratio	(FARUin)
Water to air ratio	(WARin)
Flow angle	(Angin)

Assuming that the pressure loss coefficient (λ) and all the main inlet flow port variables are known, in order to calculate dPqP, the value of the Duct inlet static pressure (P_{s_in}) is still required.

For a user specified Flow Case (flow) (subsonic for this example) and Duct inlet effective area (A_{ein}) the value of P_{sin} is obtained using the function therm_WTtPtAe as shown below.

therm_WTtPtAe (fluid, Win, Ttin, Ptin, FARBin, WARin, Aein, MNin, Vin, Tsin, Psin, Subsonic)

NB: The values of the Duct inlet Mach Number (MNin), the Duct inlet velocity (Vin) and the Duct inlet static temperature (Tsin) are also calculated in addition to P_{sin} even though these variables are not used.

Once the value of P_{sin} is obtained, dPqP is calculated using [Eq. 2.3.33].

2.3.5: Importance of the Interpolation Method used for ϕ Fluid Tables

The work presented in this section is based on the collaborative research between F. Diara ^[3] and the author. As discussed in Section 2.1.5, although the required function arguments for ϕ_T are fluid, T, FARB and WAR, the entropy function (ϕ) is calculated via a 3D linear interpolation of the natural log of temperature ($\ln(T)$), FARB and WAR. This section justifies the decision to use linear interpolation of the natural log of temperature as opposed to linear interpolation of temperature for entropy function fluid tables.

Initially, entropy function was obtained via linear interpolation of temperature, FARB and WAR (this model will be referred to as the “Old PROOSIS Fluid Model” for the analyses which follow). However, rigorous internal testing (by the author and his team) as well as external testing by the PROOSIS industrial partners revealed that the main thermodynamic functions were experiencing convergence problems for sonic and close to sonic conditions. The work presented in this section is a brief summary of the work. A detailed account of the trouble shooting process is presented in [3].

NB: Although the trouble shooting process, described in this section, was performed using a large variety of boundary conditions, this section highlights the results obtained using the boundary conditions shown in Fig: 2.3.1.

The Problem:

When using the “Old PROOSIS Fluid Model”, it was observed that when the area approaches the critical value (i.e. the value corresponding to $MN=1$), the main thermodynamic function $therm_WTtPtAe$ did not converge as shown in Fig: 2.3.2. Closer inspection of all the other main thermodynamic functions revealed that the critical area (which is the minimum area and should correspond to $MN=1$) was not obtained at $MN=1$ as shown in Fig: 2.3.3 (using $therm_WTtPtMN$ as an example). Similar trends were observed for different boundary conditions, i.e. the critical area did not correspond to $MN=1$. For some cases, the critical area was obtained at $MN>1$ and in other cases at $MN<1$.

The Initial Analysis:

The first step of the lengthy trouble shooting process which followed, involved investigating the effects of using a different fluid model for the analysis. The “Old PROOSIS Fluid Model” was replaced with the fluid property W&F polynomials ^[4]. (Refer to Section 2.1.11). Fig: 2.3.4 shows a comparison of the results obtained for $therm_WTtPtTs$ between the two fluid models. At a glance it seems that the results obtained are consistent. However zooming into the results, (Fig: 2.3.4a) clearly revealed discrepancies (close to sonic conditions) between the two models. The problem seemed to have been eliminated when using the W&F polynomials ^[4]. The main fluid properties used in the main thermodynamic functions are specific enthalpy (h) and entropy function (ϕ). Consequently, in an effort to establish which of these properties was the root of the problem (when using the “Old PROOSIS Fluid Model”), some hybrid fluid models were developed and tested. These hybrid fluid models were a “cocktail” of the “Old PROOSIS Fluid Model” and the W&F polynomials ^[4].

The “Cocktail” of Fluid Models:

Hybrid Model 1:

Description: This fluid model used the “Old PROOSIS Fluid Model” for all the fluid properties except specific enthalpy (h). Specific enthalpy was calculated using the W&F polynomials [4].

Results: Fig: 2.3.5 shows a comparison of the results obtained for therm_WTtPtTs when using Hybrid Model 1.

Conclusion: Hybrid Model 1 does not solve the problem. This implies that the poor results, obtained close to MN=1, are not related to the values of specific enthalpy being obtained from the “Old PROOSIS Fluid Model”.

Hybrid Model 2:

Description: This fluid model used the “Old PROOSIS Fluid Model” for all the fluid properties except entropy function (ϕ). Entropy function was calculated using the W&F polynomials [4].

Results: Fig: 2.3.6 shows a comparison of the results obtained for therm_WTtPtTs when using Hybrid Model 2.

Conclusion: Hybrid Model 2 clearly solves the problem. This implies that the source of the problem is related to the values entropy function obtained from the “Old PROOSIS Fluid Model”.

Entropy Function – The Source of the Problem:

The “cocktail of fluid models” analysis described above clearly suggested that the entropy function tables of the “Old PROOSIS Fluid Model” needed to be studied more carefully. The variation of entropy function (for dry air and the products of combustion of Jet-A) as a function of temperature, FARB and WAR is shown in Fig: 2.1.11 and Fig: 2.1.13 (for the “no dissociation” and chemical equilibrium fluid models respectively). As mentioned above, for the “Old PROOSIS Fluid Model”, linear interpolation of T, FARB and WAR was used to obtain the value of entropy function from the ϕ fluid tables. Since the variation of entropy function with temperature is not linear (as shown in Fig: 2.1.11 and Fig: 2.1.13), it was likely that the errors arose due to inaccurate entropy function values interpolated from the ϕ fluid tables. Two obvious methods which could yield improved results were investigated.

Method 1: Reducing the temperature intervals for the ϕ fluid tables

Description: The tabulated temperature intervals for the ϕ fluid tables of the “Old PROOSIS Fluid Model” were reduced to 25K and then to 10K. Linear interpolation was still used for T, FARB and WAR. The main thermodynamic functions therm_WTtPtAe and thermWTtPtMN were retested with these new ϕ fluid tables.

Results: Fig: 2.3.7 shows the effects, on therm_WTtPtAe, of using ϕ fluid tables with smaller tabulated temperature intervals (25K and 10K), while still using linear interpolation for T, FARB and WAR.

Fig: 2.3.8 shows the effects, on therm_WTtPtMN, of using ϕ fluid tables with smaller tabulated temperature intervals (25K and 10K), while still using linear interpolation for T, FARB and WAR.

Conclusion: Fig: 2.3.7 and Fig 2.3.8 suggest that reducing the tabulated temperature intervals for the ϕ fluid tables clearly results in significantly improved solutions. However, the solution is still not perfect very close to sonic conditions (MN=1) and there is still a small region on non-convergence for some of the main thermodynamic functions. Of course the tabulated temperature intervals could be reduced even further (1K). This however is not practical in terms of the time it would take to generate these extremely densely populated tables using CEA ^[5] & ^[6]. Additionally, although the solution may improve even further, it is unlikely that the problem will be completely eliminated.

Following a discussion with J. Kurzke (the developer of GasTurb ^[18]), it was decided to try an alternative method to solve the problem i.e. using an improved interpolation method while still maintaining 50K tabulated temperature intervals rather than reducing the tabulated temperature intervals and using linear interpolation for the ϕ fluid tables.

Method 2: Using “logarithmic interpolation” for temperature for the ϕ fluid tables

Description: The variation of entropy function (ϕ) as a function of the natural logarithm of temperature ($\ln(T)$) is (approximately) linear as shown in Fig: 2.1.12 and Fig: 2.1.14. Therefore linear interpolation of the natural logarithm ($\ln(T)$) rather than linear interpolation of T is more suitable for the ϕ fluid tables. For the purposes of the analyses which follow, linear interpolation of the natural logarithm of T ($\ln(T)$) will be referred to as “logarithmic interpolation”.

Results: Fig: 2.3.9 shows the effects, on therm_WTtPtAe, of using “logarithmic interpolation” for T for the ϕ fluid tables.

Fig: 2.3.10 shows the effects, on therm_WTtPtMN, of using “logarithmic interpolation” for T for the ϕ fluid tables.

Conclusion: Fig: 2.3.9 and Fig 2.3.10 clearly suggest that the problem is eliminated as a consequence of using “logarithmic interpolation” instead of linear interpolation of T for the ϕ fluid tables. Although the presented results are only for the set of boundary conditions highlighted in Fig: 2.3.1, and only cover a few of the main thermodynamic functions, all the main thermodynamic functions (highlighted in *Section 2.3.4*) were tested over a wide range of boundary conditions, both by the author and his team as well as the PROOSIS industrial partners. Similar results, as those presented were obtained and consequently the current fluid model of the PROOSIS SCLib uses linear interpolation of $\ln(T)$ as opposed to linear interpolation of T for the ϕ fluid tables, as discussed in *Section 2.1.5*.

2.3.6: Intelligent Means of Implementing the Flow Continuity Model

The approach used to model the thermodynamic functions of the flow continuity model of the PROOSIS SCLib is based on the conventional approach whereby a different main thermodynamic function call is required depending on which of the twelve sets of

compatible inputs is available. However, during the early development phase of the PROOSIS SCLib flow continuity model, an “intelligent” means of implementing the thermodynamic functions was investigated. The main objective was to develop a model which would:

1. Automatically detect which inputs are available.
2. Check to see if at least one of the twelve compatible input sets is satisfied.
3. Automatically perform all the relevant series of calculations corresponding to the compatible input option to obtain all the local thermodynamic properties.

After exploring several options to implement the “intelligent” flow continuity model and following the advice from the software developers (Empresarios Agrupados – (EA), Abstract Component THERM was developed. The intention was that every component of the PROOSIS SCLib would inherit from Abstract Component THERM. Consequently, any flow property required at the inlet or outlet of any component would be readily available. In addition to fulfilling the three main objectives highlighted above, Abstract Component THERM seemed to offer another significant advantage arising from the object oriented nature of the PROOSIS software. As opposed to the conventional means of implementing the main thermodynamic functions (described in *Section 2.3.3*), within Abstract Component THERM, all the equations could just be listed once for the input of the component and once for the output and in a random order. The equations would then be automatically rearranged based on the known variables (as opposed to the relatively more sequential programming that is required for the conventional approach). Abstract Component THERM consequently introduces an element of intelligence which serves to minimise the need for skilled user resource. A detailed description of the structure of Abstract Component THERM and the calculations contained within it are presented in [21]. NB: The thermodynamic equations used in Abstract Component THERM are identical to those outlined for the main thermodynamic functions in *Section 2.3.3*.

Despite the several foreseeable advantages, implementing Abstract Component THERM in PROOSIS proved to be unsuccessful mainly due to limitations of the solver and the object oriented programming approach of PROOSIS. The main limitations associated with the implementation of Abstract Component THERM are highlighted below:

1. Abstract Component THERM relied on the effective area (A_e) being a main flow port variable. The inlet and outlet effective areas of components are not always known. Furthermore defining effective area as a port variable can lead to modelling complications especially for components like the Mixer. Consequently, A_e was removed from the main flow port variables.
2. Not all the components may necessarily have sufficient information for Abstract Component THERM. A possible solution could be to introduce several abstract components with different levels of inheritance. However, this directly translates to increased modelling complexity.
3. Abstract Component THERM should have allowed the calculations of the “non static” to continue even if insufficient information was available for the calculations of the “static” properties.
4. Abstract Component THERM introduced at least three non-linear algebraic loops for each component. For an engine with 20 components, there were as many as 60 non-linear algebraic loops just for solving thermodynamic functions. Not only did this adversely effect simulation time but it also was extremely cumbersome for the user to

Advanced Performance Simulation of Gas Turbine Components and Fluid Thermodynamic Properties

select all the appropriate tearing variables. Additionally the presence of so many non-linear algebraic loops resulted in a less robust continuity model.

5. Abstract Component THERM assumed that all the data was received and transmitted via the main flow inlet port and the main flow outlet port of the component respectively. A problem arose when trying to obtain the thermodynamic properties at a point in the flow where there was no main flow port (e.g. a bleed). Additionally, problems arose for components with one or more inlet or outlet ports e.g. the Mixer and Flow Splitter components.

Based on the problems highlighted above and due to time constraints, the PROOSIS partners collaboratively decided to abandon the idea of developing an “intelligent” means to implement the thermodynamic functions and decided to stick to the conventional, more robust approach (outlined in *Section 2.3.3*). However, research into an intelligent means for implementing the thermodynamic functions with a view to minimise skilled user resource whilst minimizing modelling complexity and retaining robustness of the flow continuity model is definitely a thought for future developments.

Chapter 2: Figures

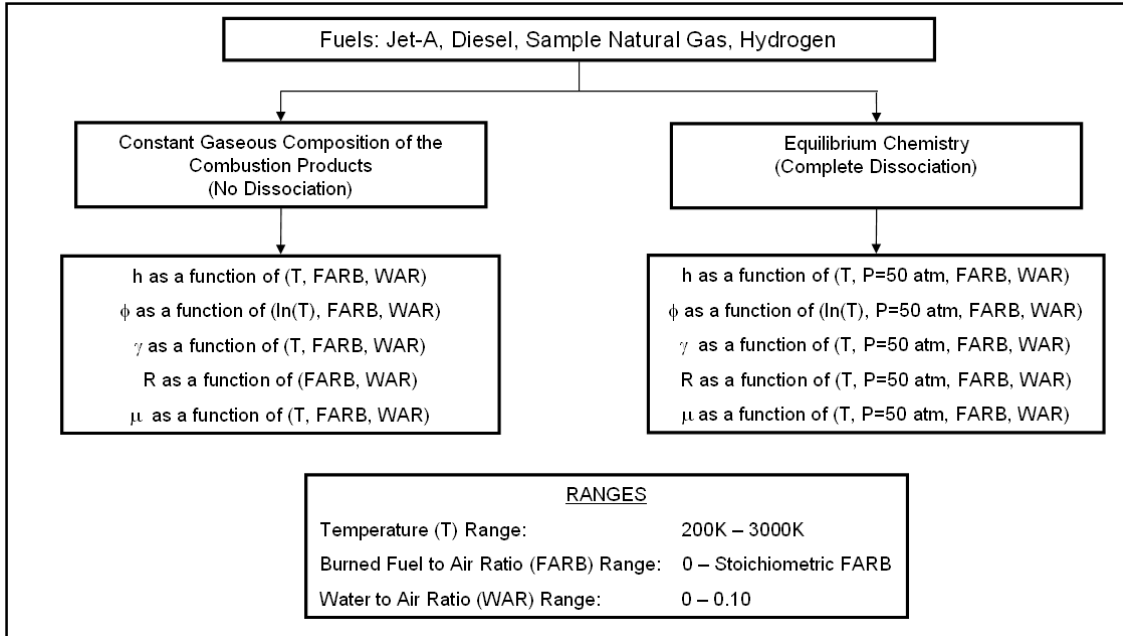


Fig: 2.1.1 Structure of the PROOSIS SCLib Fluid Model

<u>Constituent</u>	<u>Chemical Formula</u>	<u>Mole Fractions</u>	<u>Mass Fractions</u>
Nitrogen	N ₂	0.780840	0.755184
Oxygen	O ₂	0.209476	0.231416
Argon	Ar	0.009365	0.012916
Carbon Dioxide	CO ₂	0.000319	0.000485

Fig: 2.1.2 Chemical Composition of Atmospheric Dry Air ^[13]

<u>Fuel</u>	<u>Formula</u>	<u>Mole Fractions</u>			
		C	H	O	N
Jet-A _(g)	C ₁₂ H _{23.5}	0.342857	0.657143	0.000000	0.000000
Diesel _(g)	C _{12.9} H _{23.22}	0.357143	0.642857	0.000000	0.000000
Sample Natural Gas _(g)	C _{1.02} H _{3.97} O _{0.01} N _{0.03}	0.202783	0.789264	0.001988	0.005964
Hydrogen _(g)	H ₂	0.000000	1.000000	0.000000	0.000000

Fig: 2.1.3 Chemical Composition of PROOSIS Fuels ^[13]

Advanced Performance Simulation of Gas Turbine Components
and Fluid Thermodynamic Properties

<u>Constituent</u>	<u>Chemical Symbol</u>	<u>Ar or Mr (kg/(kg-mol))</u>
Argon	Ar	39.94800
Carbon	C	12.01115
Carbon Dioxide	CO ₂	44.00950 (Mr)
Hydrogen	H	1.00794
Nitrogen	N	14.00670
Oxygen	O	15.99940

Fig: 2.1.4 Atomic Weights (Ar) or Molecular Masses (Mr) of Fuel and Atmospheric Dry Air Constituents ^[13]

<u>Constituent</u>	<u>Chemical Formula</u>	<u>Mole Fractions</u>
Methane	CH ₄	0.9021
Ethane	C ₂ H ₆	0.0445
Propane	C ₃ H ₈	0.0052
I-Butane	C ₄ H _{10,i}	0.001
N-Butane	C ₄ H _{10,n}	0.001
I-Pentane	C ₅ H _{12,i}	0.0004
N-Pentane	C ₅ H _{12,n}	0.0004
Hexane	C ₆ H ₁₄	0.0005
Nitrogen	N ₂	0.0266
Carbon Dioxide	CO ₂	0.0183

Fig: 2.1.5 Chemical Composition of Sample Natural Gas ^[4]

<u>Fuel</u>	<u>FAR_{rStoich}</u>
Jet – A _(g)	0.06817
Diesel _(g)	0.68956
Sample Natural Gas _(g)	0.60644 ^[4]
Hydrogen _(g)	0.02916

Fig: 2.1.6 Stoichiometric Reactant Total Fuel to Air Ratios of PROOSIS Fuels

Advanced Performance Simulation of Gas Turbine Components
and Fluid Thermodynamic Properties

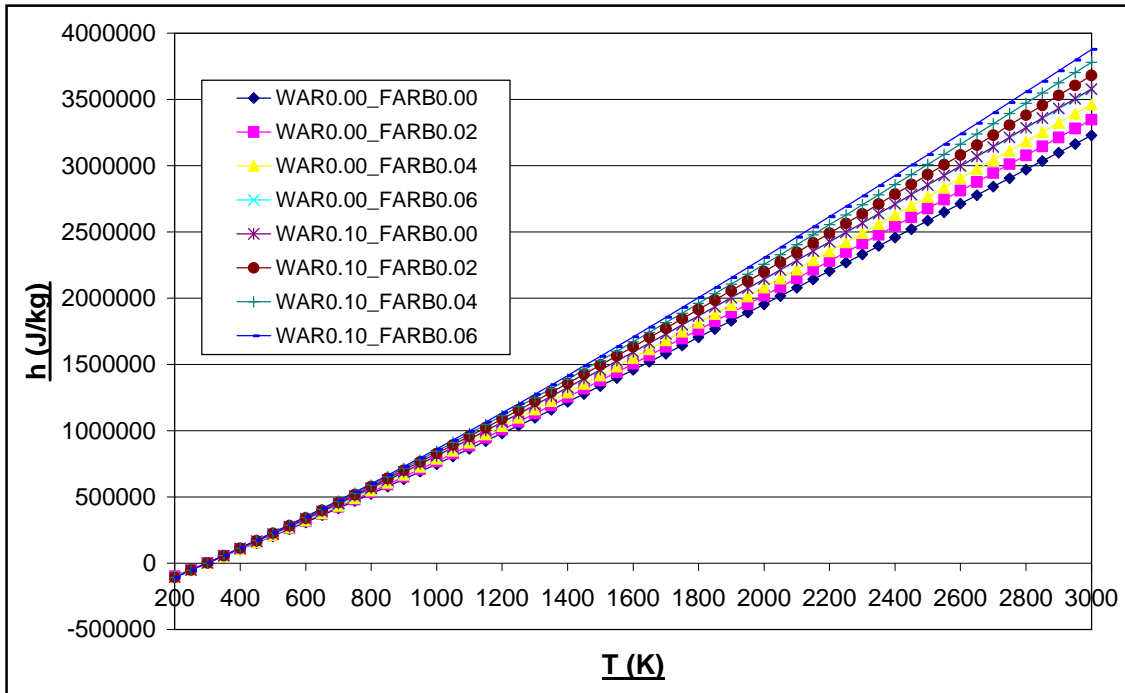


Fig: 2.1.7 Graph of h as a function of T , FARB & WAR (No dissociation)

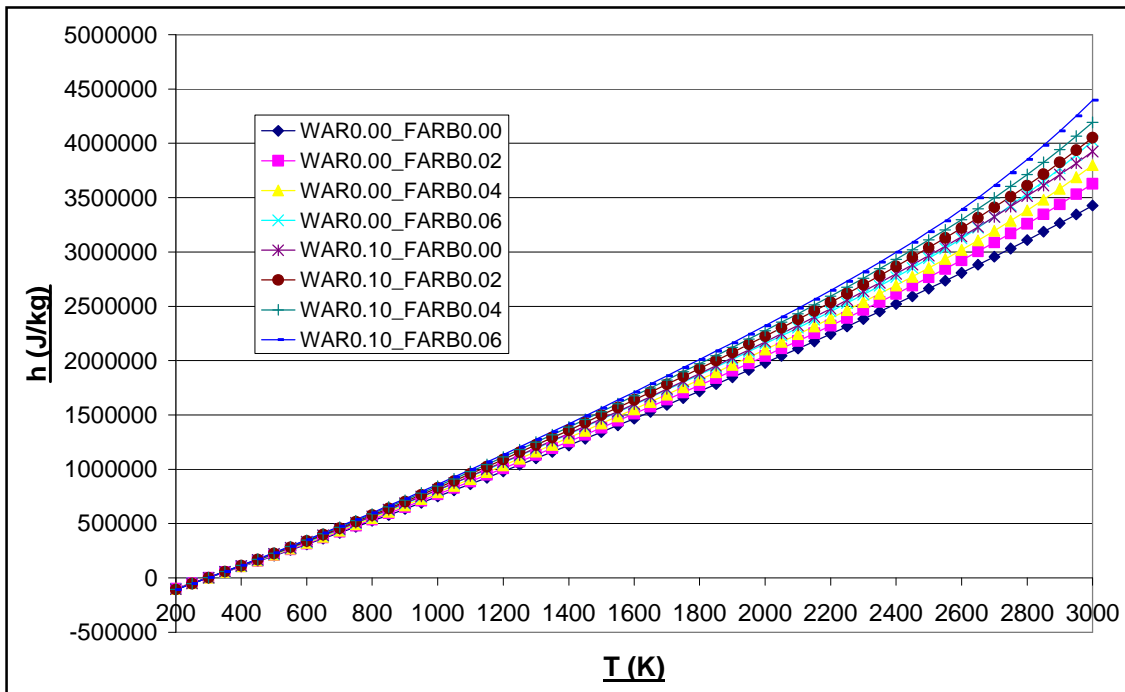


Fig: 2.1.8 Graph of h as a function of T , FARB & WAR (Chemical Equilibrium)

Advanced Performance Simulation of Gas Turbine Components
and Fluid Thermodynamic Properties

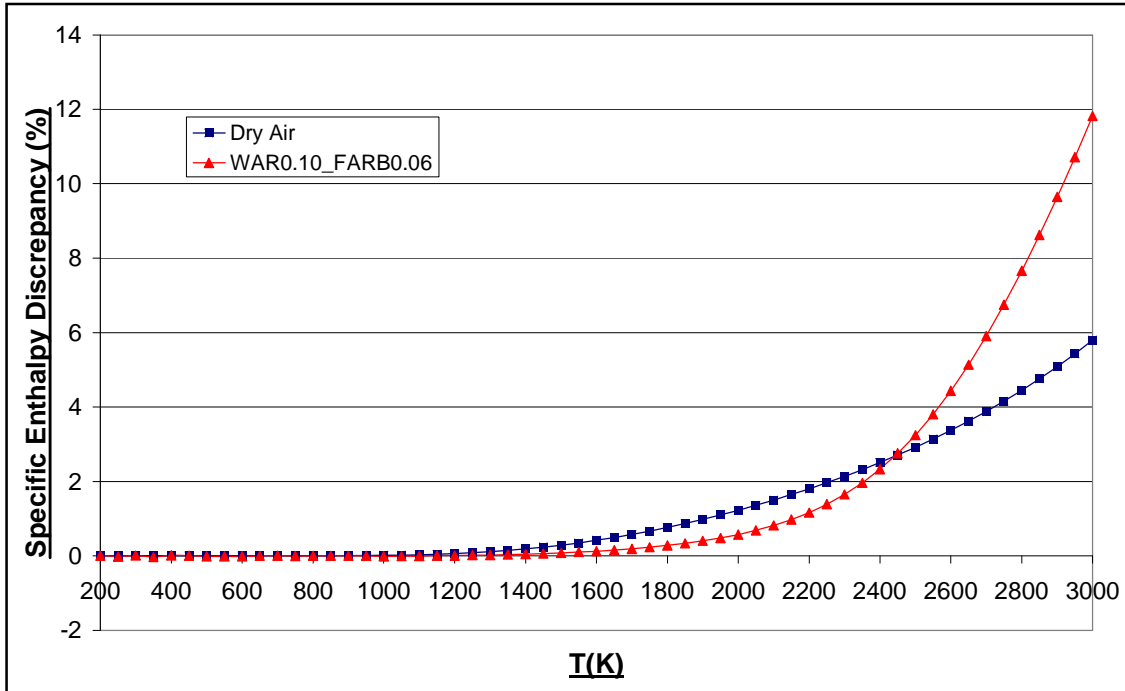


Fig: 2.1.9 Graph of h Discrepancy (%) between No Dissociation and Chemical Equilibrium Fluid Models as a function of T for:
a.) FARB = 0.00 & WAR = 0.00 (Dry Air)
b.) FARB = 0.06 & WAR = 0.10

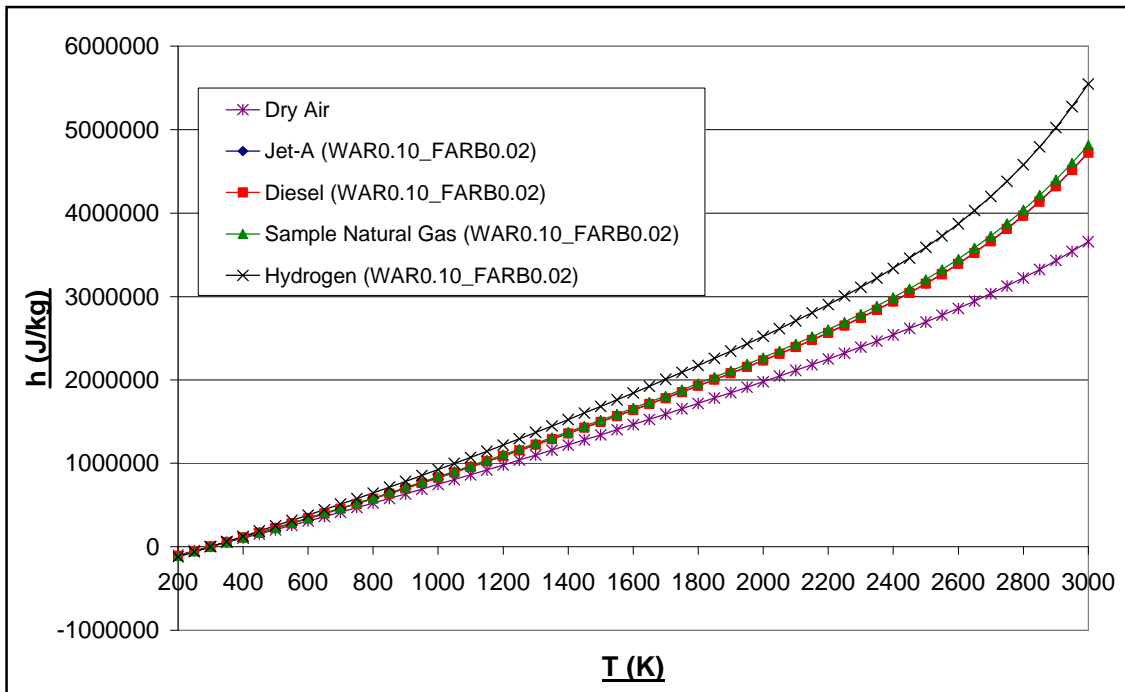


Fig: 2.1.10^[2] Comparison of Chemical Equilibrium h as a function of T for the Various PROOSIS Fuels for FARB = 0.02 & WAR = 0.10 ($P = 2\text{atm}$).

Advanced Performance Simulation of Gas Turbine Components
and Fluid Thermodynamic Properties

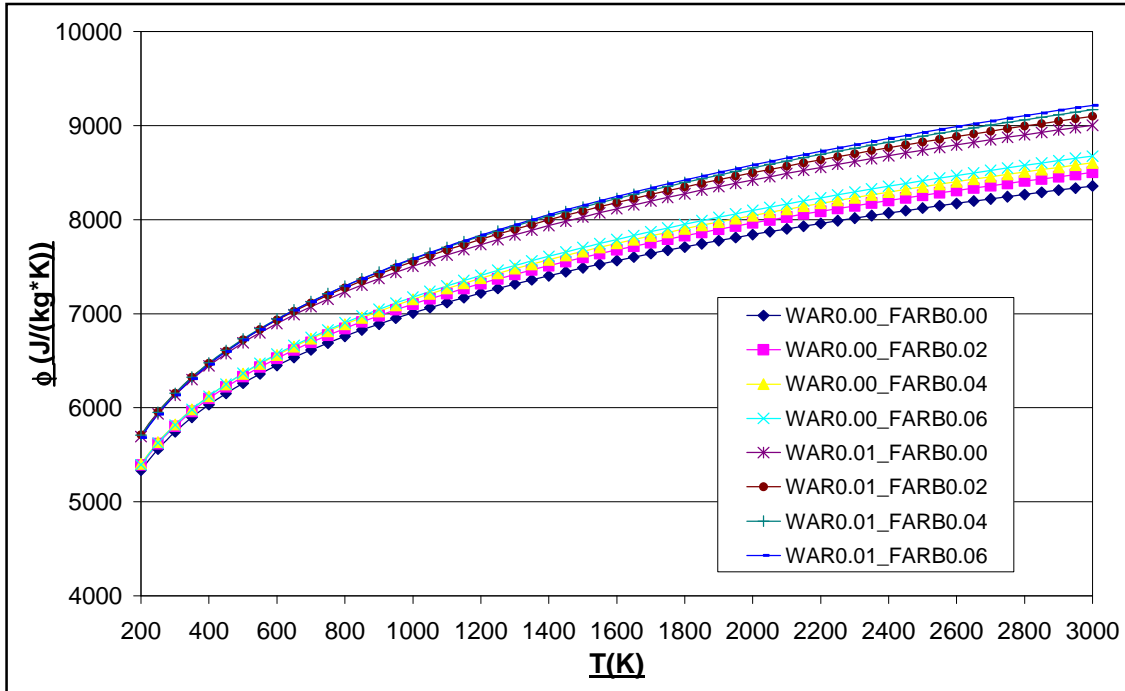


Fig: 2.1.11 Graph of ϕ as a function of T , FARB & WAR (No dissociation)

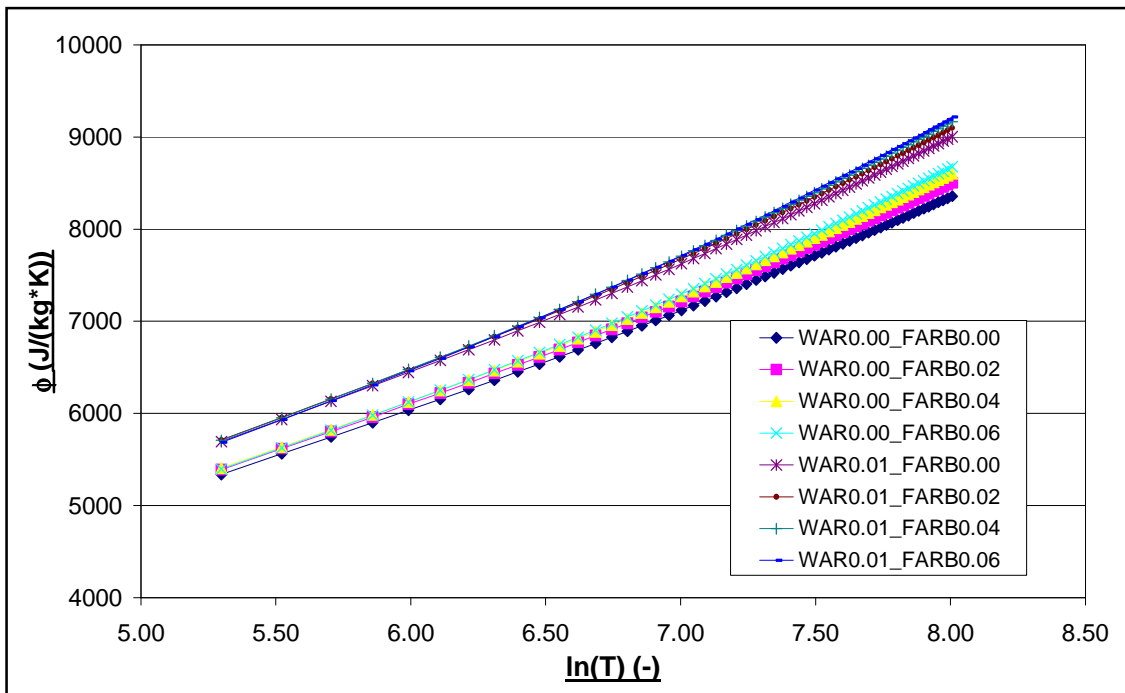


Fig: 2.1.12 Graph of ϕ as a function of $\ln(T)$, FARB & WAR (No dissociation)

Advanced Performance Simulation of Gas Turbine Components
and Fluid Thermodynamic Properties

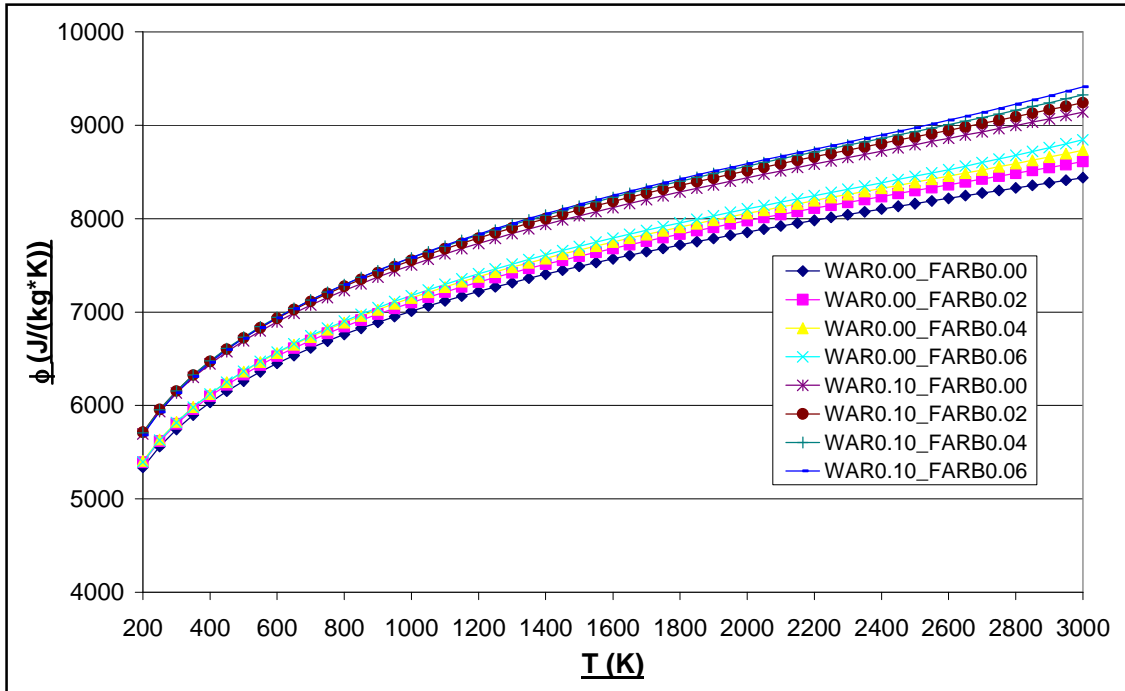


Fig: 2.1.13 Graph of ϕ as a function of T , FARB & WAR (Chemical Equilibrium)

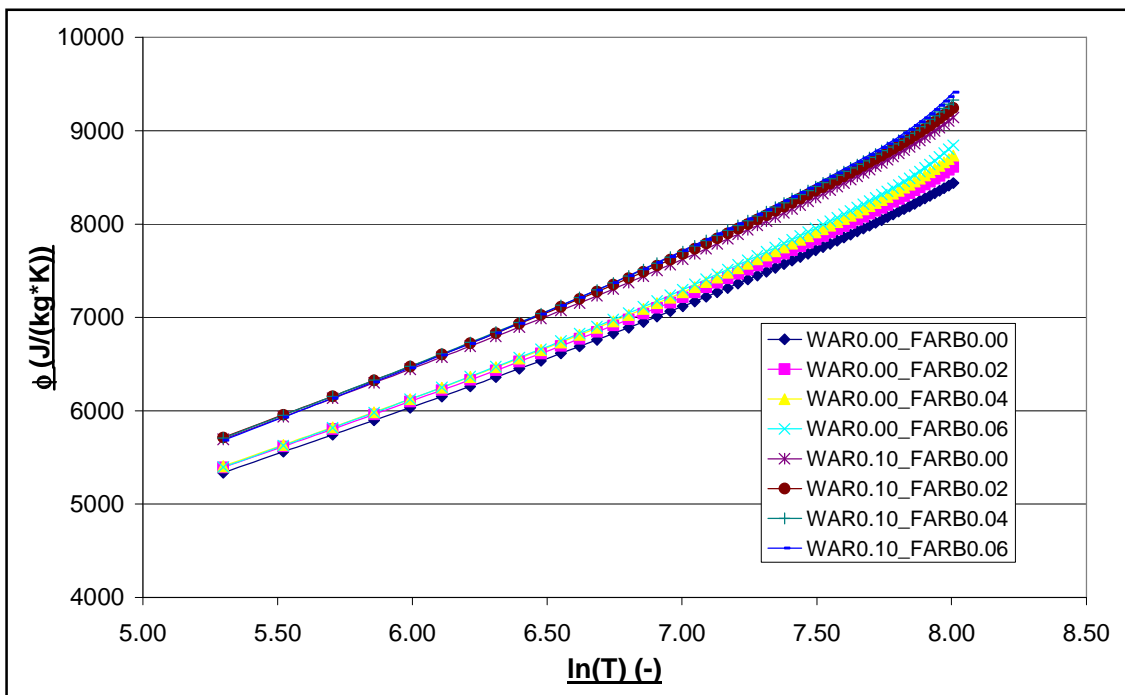


Fig: 2.1.14 Graph of ϕ as a function of $\ln(T)$, FARB & WAR (Chemical Equilibrium)

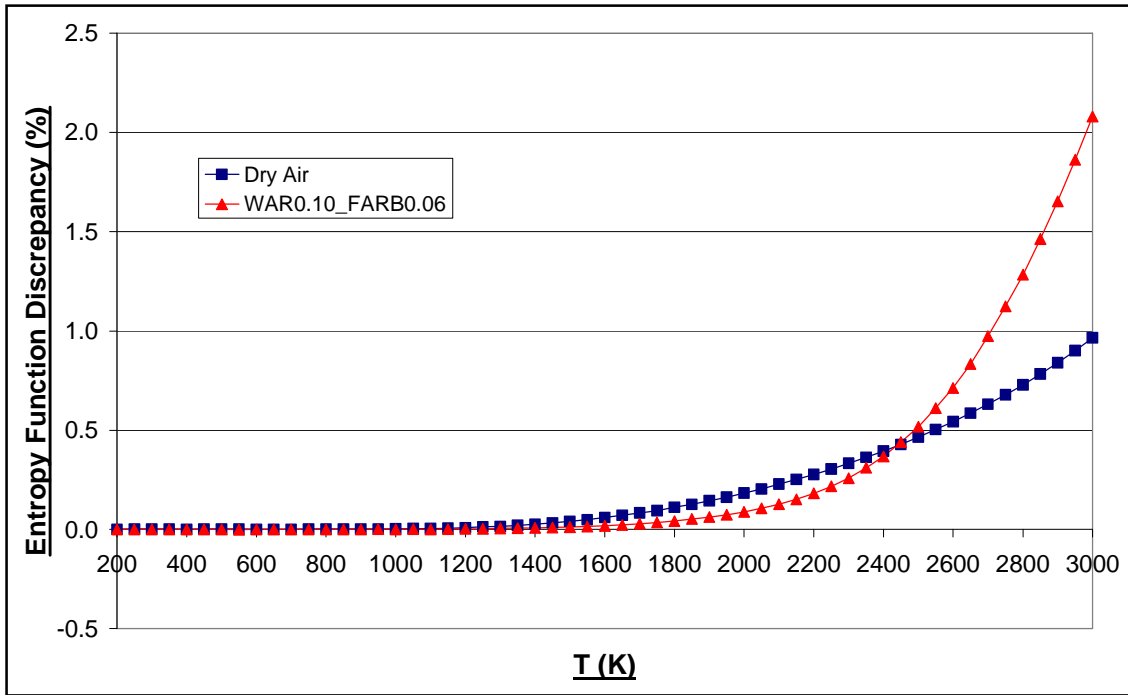


Fig: 2.1.15 Graph of ϕ Discrepancy (%) between No Dissociation and Chemical Equilibrium Fluid Models as a function of T for:
a.) FARB = 0.00 & WAR = 0.00 (Dry Air)
b.) FARB = 0.06 & WAR = 0.10

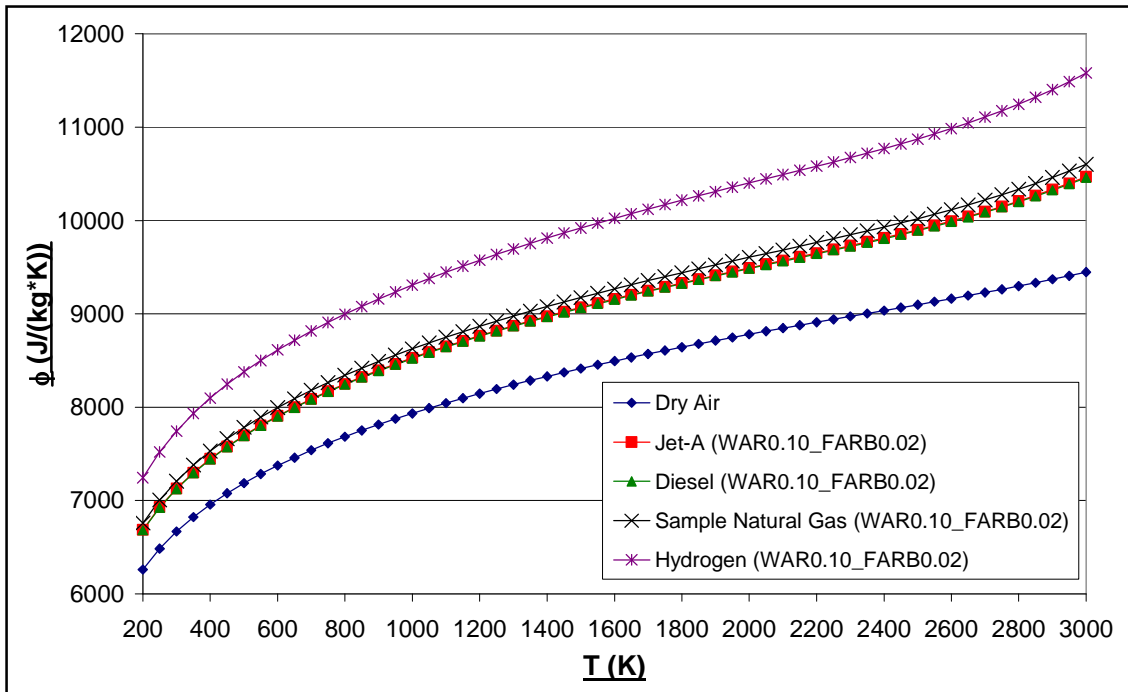


Fig: 2.1.16^[2] Comparison of Chemical Equilibrium ϕ as a function of T for the Various PROOSIS Fuels for FARB = 0.02 & WAR = 0.10 (P = 2atm).

Advanced Performance Simulation of Gas Turbine Components and Fluid Thermodynamic Properties

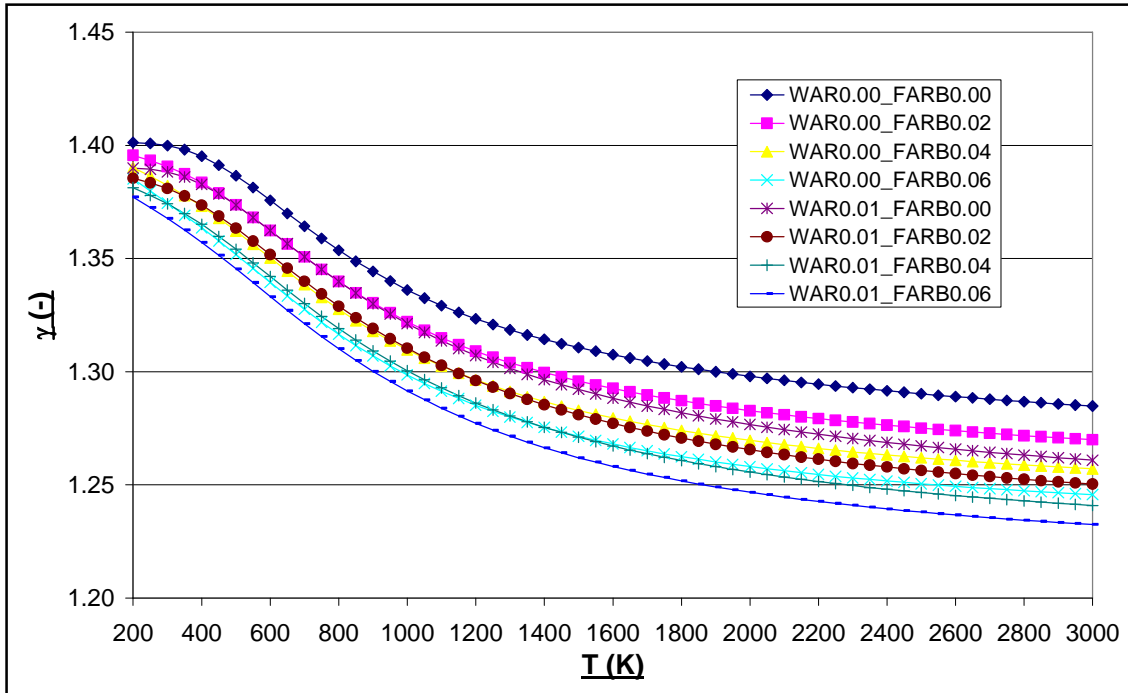


Fig: 2.1.17 Graph of γ as a function of T , FARB & WAR (No dissociation)

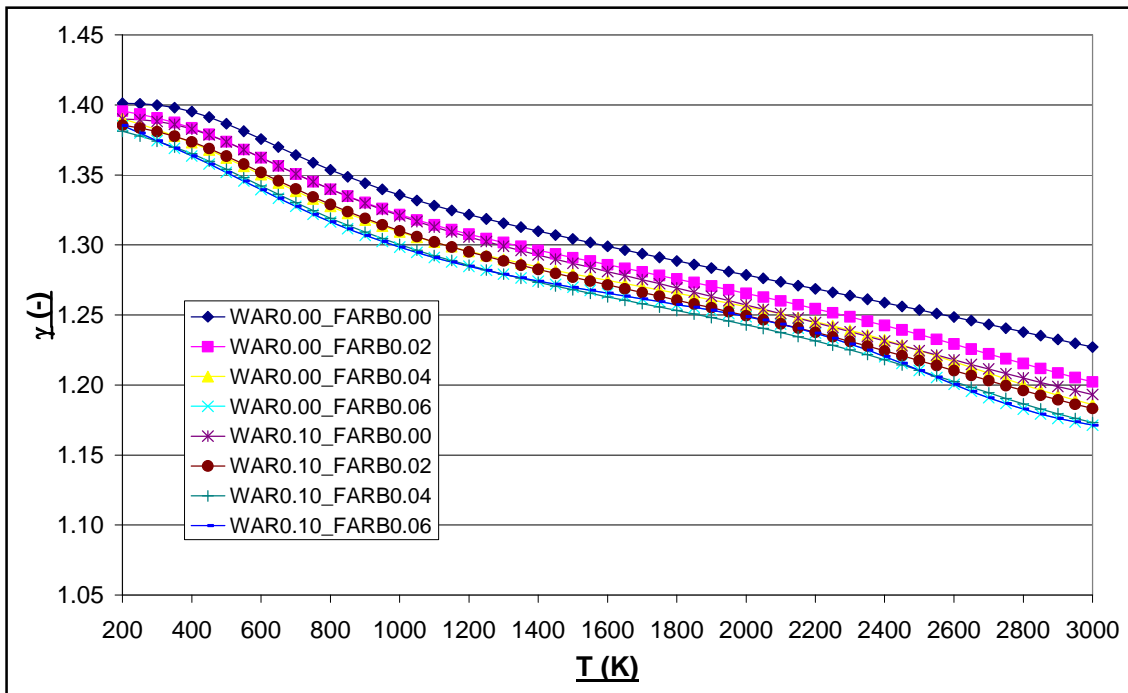


Fig: 2.1.18 Graph of γ as a function of T , FARB & WAR (Chemical Equilibrium)

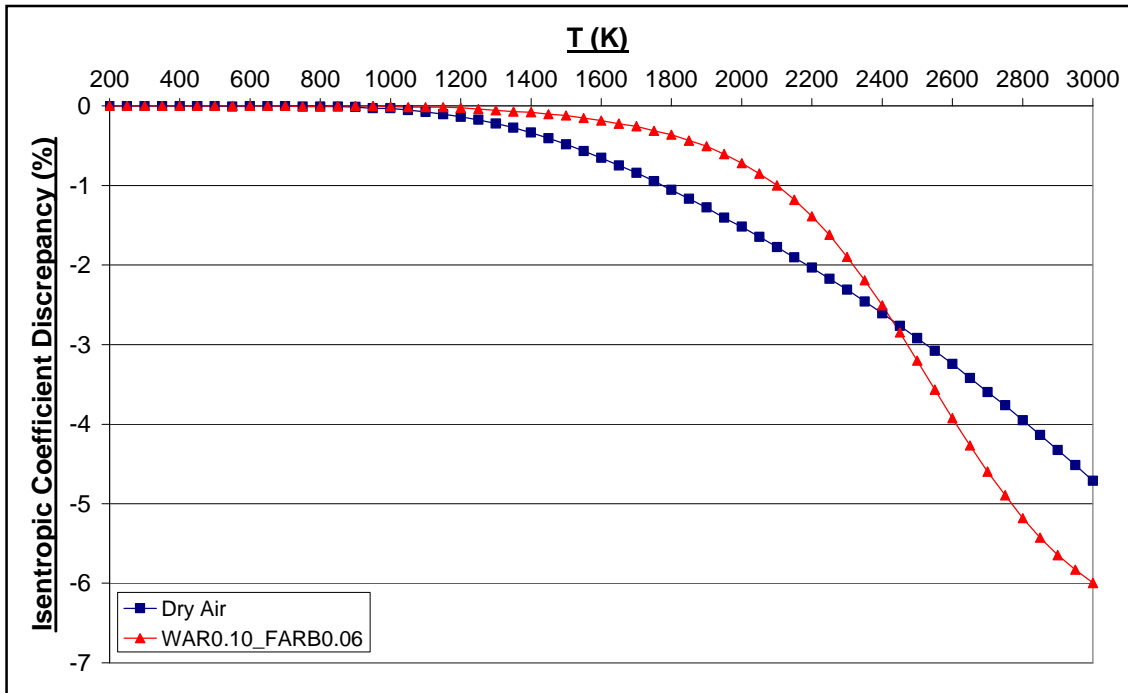


Fig. 2.1.19 Graph of γ Discrepancy (%) between No Dissociation and Chemical Equilibrium Fluid Models as a function of T for:
a.) FARB = 0.00 & WAR = 0.00 (Dry Air)
b.) FARB = 0.06 & WAR = 0.10

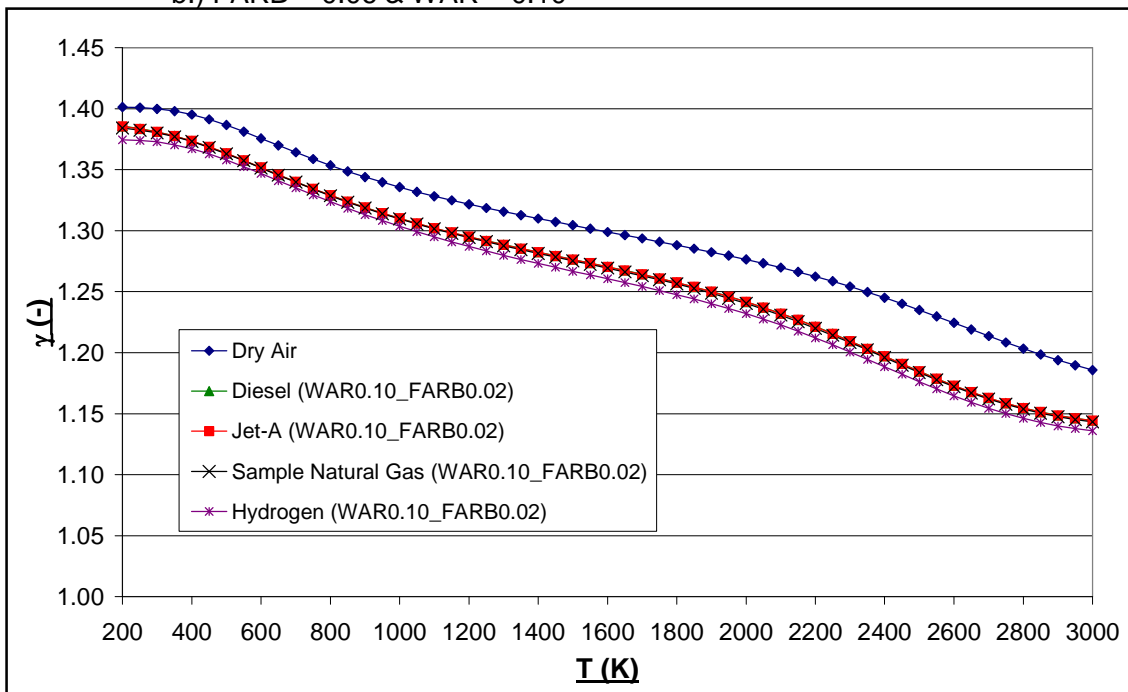


Fig. 2.1.20^[2] Comparison of Chemical Equilibrium γ as a function of T for the Various PROOSIS Fuels for FARB = 0.02 & WAR = 0.10 (P = 2atm).

Advanced Performance Simulation of Gas Turbine Components
and Fluid Thermodynamic Properties

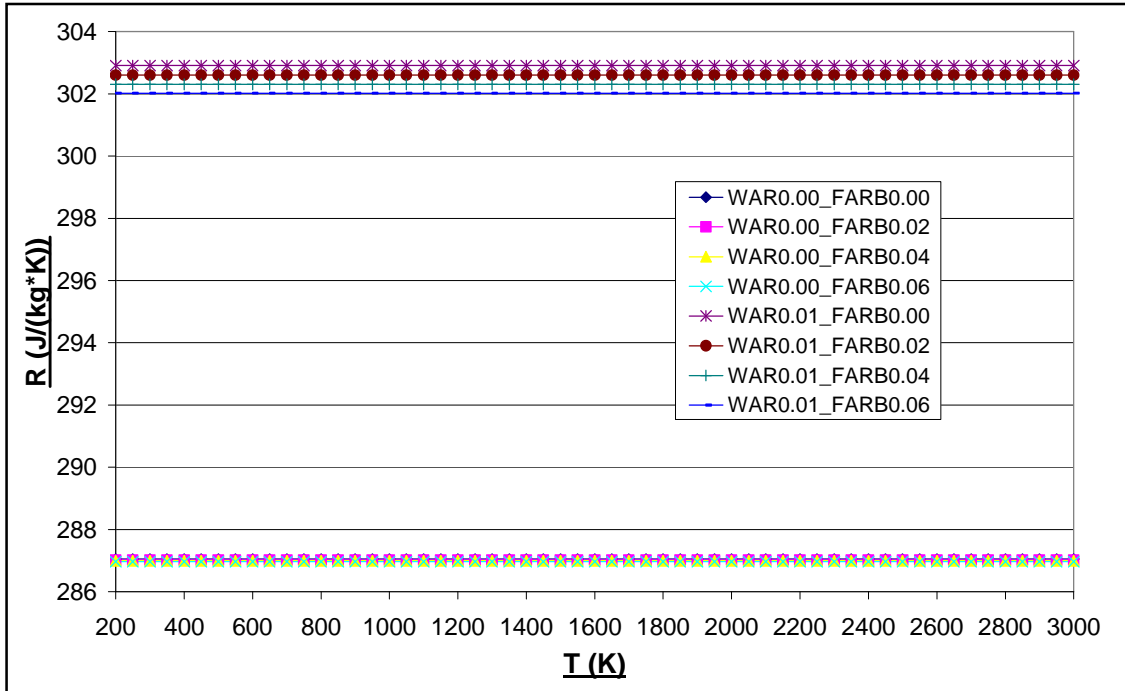


Fig: 2.1.21 Graph of R as a function of T, FARB & WAR (No dissociation)

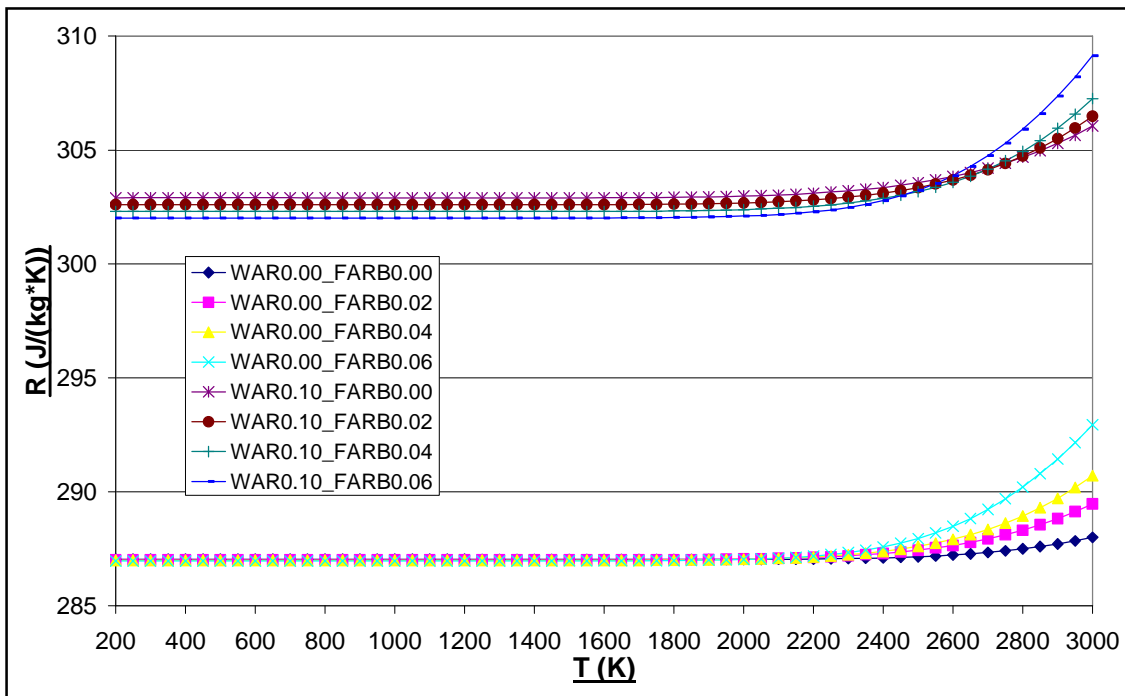


Fig: 2.1.22 Graph of R as a function of T, FARB & WAR (Chemical Equilibrium)

Advanced Performance Simulation of Gas Turbine Components
and Fluid Thermodynamic Properties

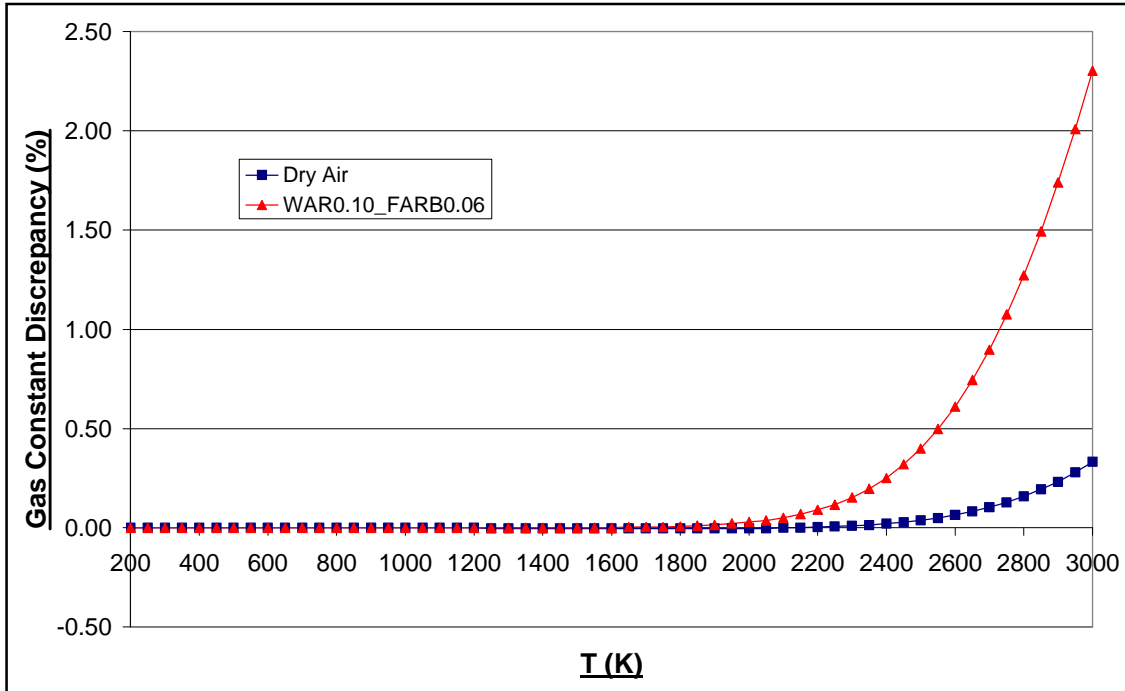


Fig: 2.1.23 Graph of R Discrepancy (%) between No Dissociation and Chemical Equilibrium Fluid Models as a function of T for:
a.) FARB = 0.00 & WAR = 0.00 (Dry Air)
b.) FARB = 0.06 & WAR = 0.10

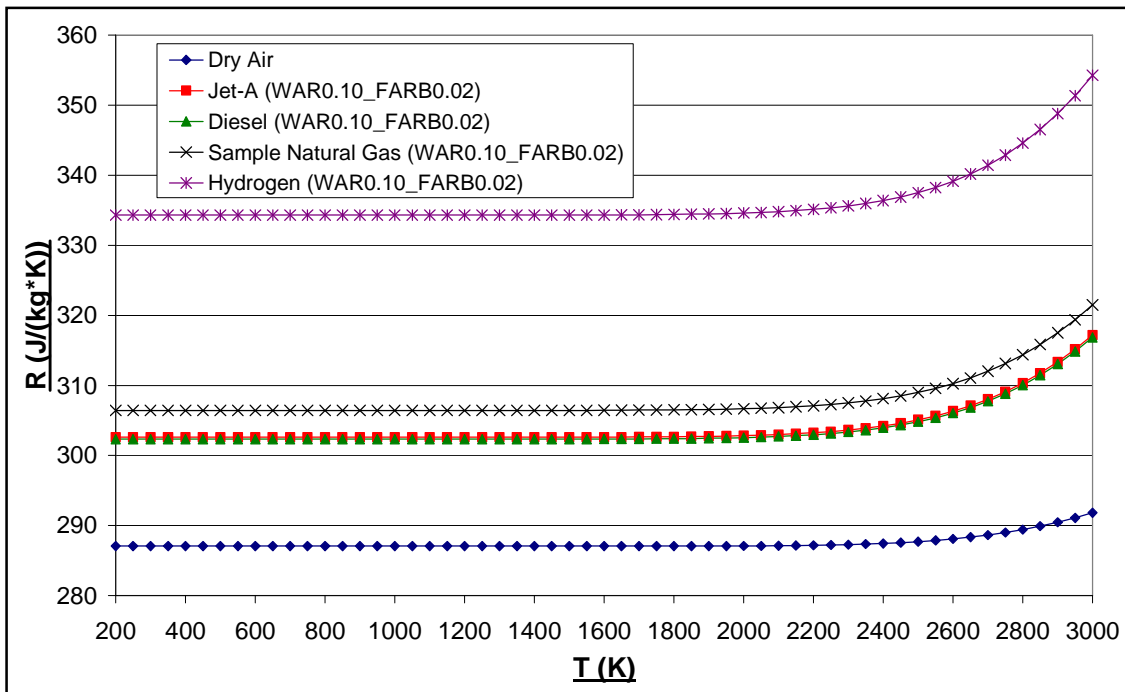


Fig: 2.1.24^[2] Comparison of Chemical Equilibrium R as a function of T for the Various PROOSIS Fuels for FARB = 0.02 & WAR = 0.10 (P = 2atm).

Advanced Performance Simulation of Gas Turbine Components
and Fluid Thermodynamic Properties

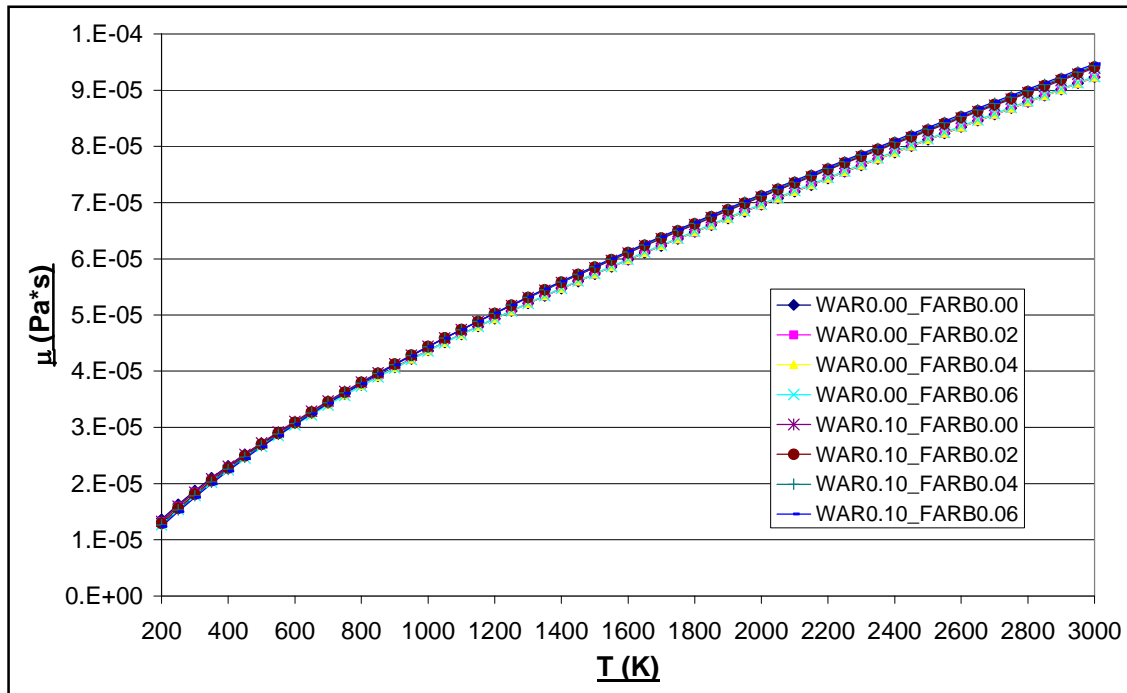


Fig: 2.1.25 Graph of μ as a function of T , FARB & WAR (No dissociation)

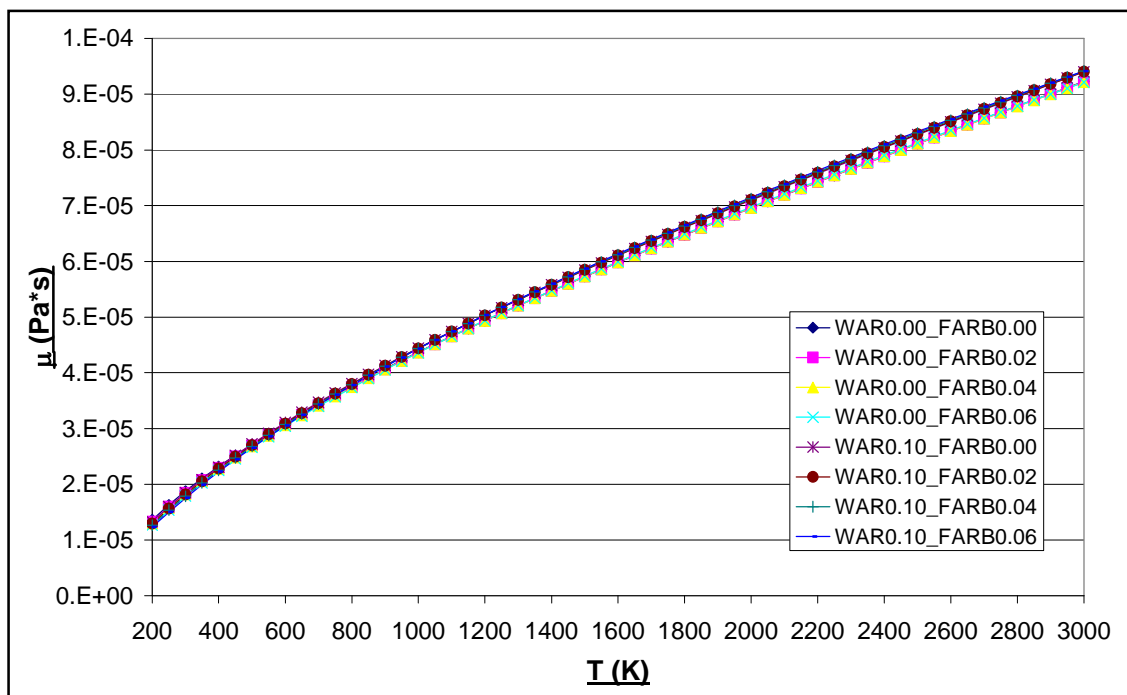


Fig: 2.1.26 Graph of μ as a function of T , FARB & WAR (Chemical Equilibrium)

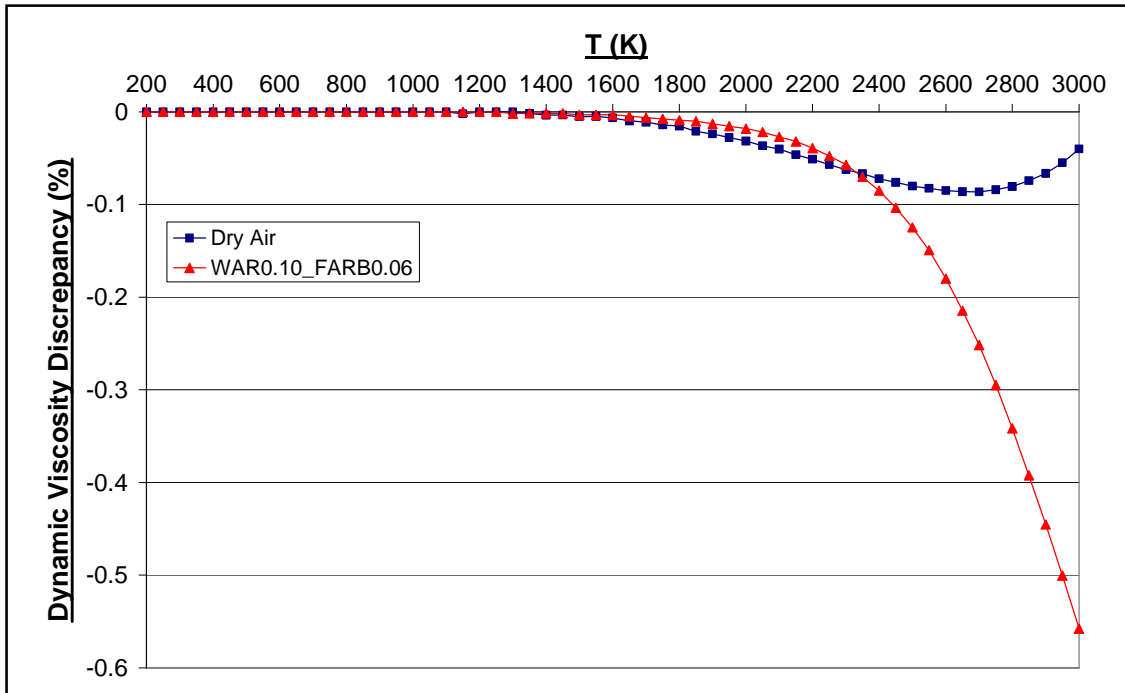


Fig: 2.1.27 Graph of μ Discrepancy (%) between No Dissociation and Chemical Equilibrium Fluid Models as a function of T for:
a.) FARB = 0.00 & WAR = 0.00 (Dry Air)
b.) FARB = 0.06 & WAR = 0.10

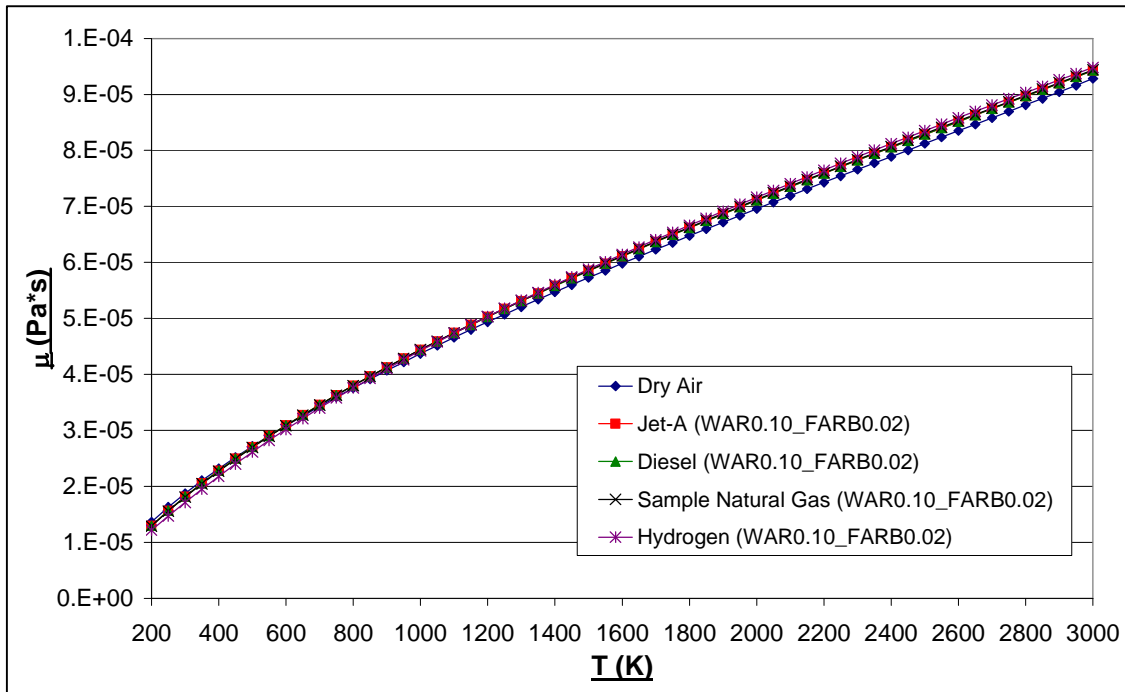


Fig: 2.1.28^[2] Comparison of Chemical Equilibrium μ as a function of T for the Various PROOSIS Fuels for FARB = 0.02 & WAR = 0.10 (P = 2atm).

Advanced Performance Simulation of Gas Turbine Components and Fluid Thermodynamic Properties

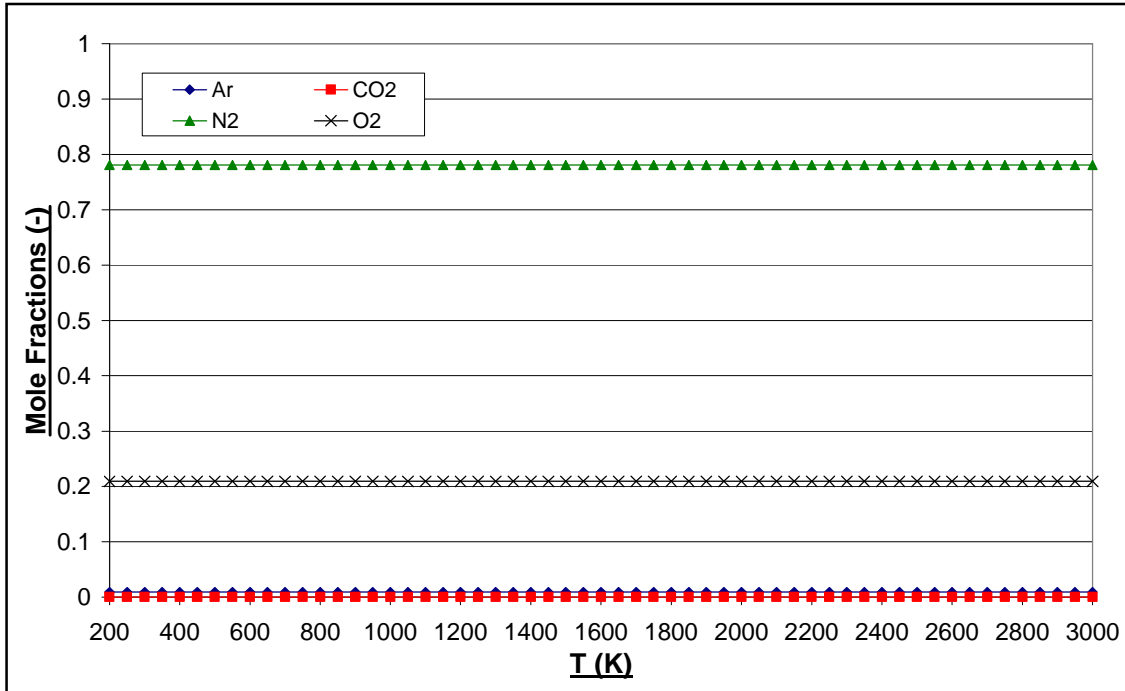


Fig: 2.1.29 Graph to show the Variation in Composition of Dry Air as a Function of Temperature for the "No Dissociation" Fluid Model

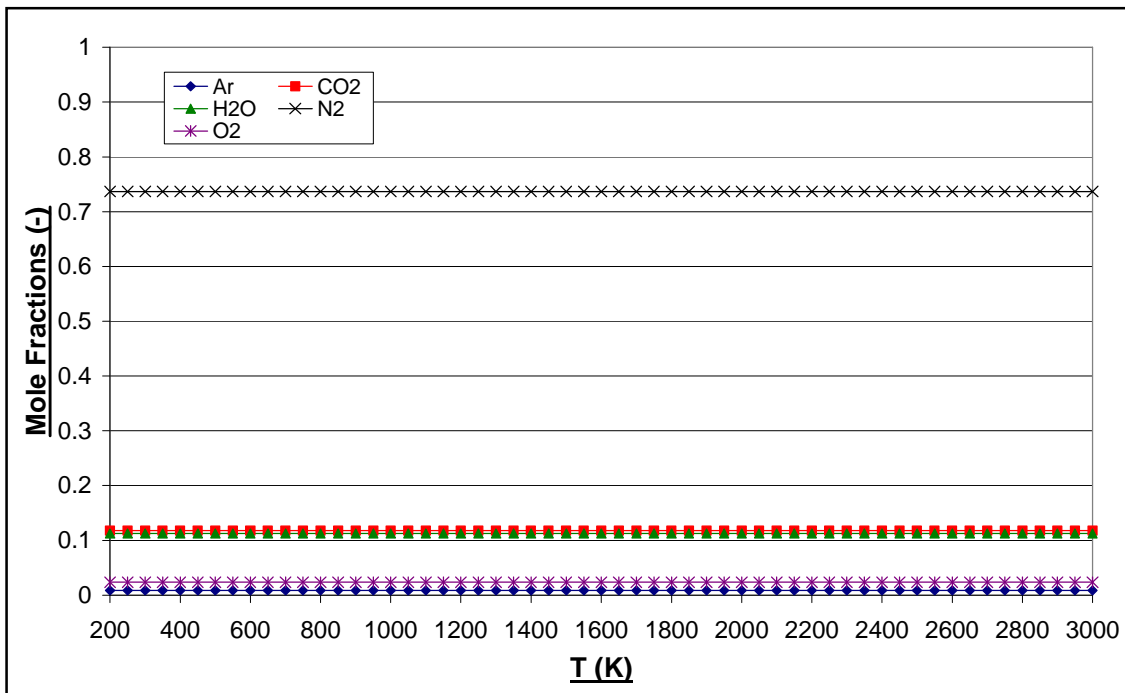


Fig: 2.1.30 Graph to show the Variation in Composition of the Products of Combustion of Jet-A as a Function Temperature for the "No Dissociation" Fluid Model for FARB = 0.06 & WAR = 0.10.

Advanced Performance Simulation of Gas Turbine Components
and Fluid Thermodynamic Properties

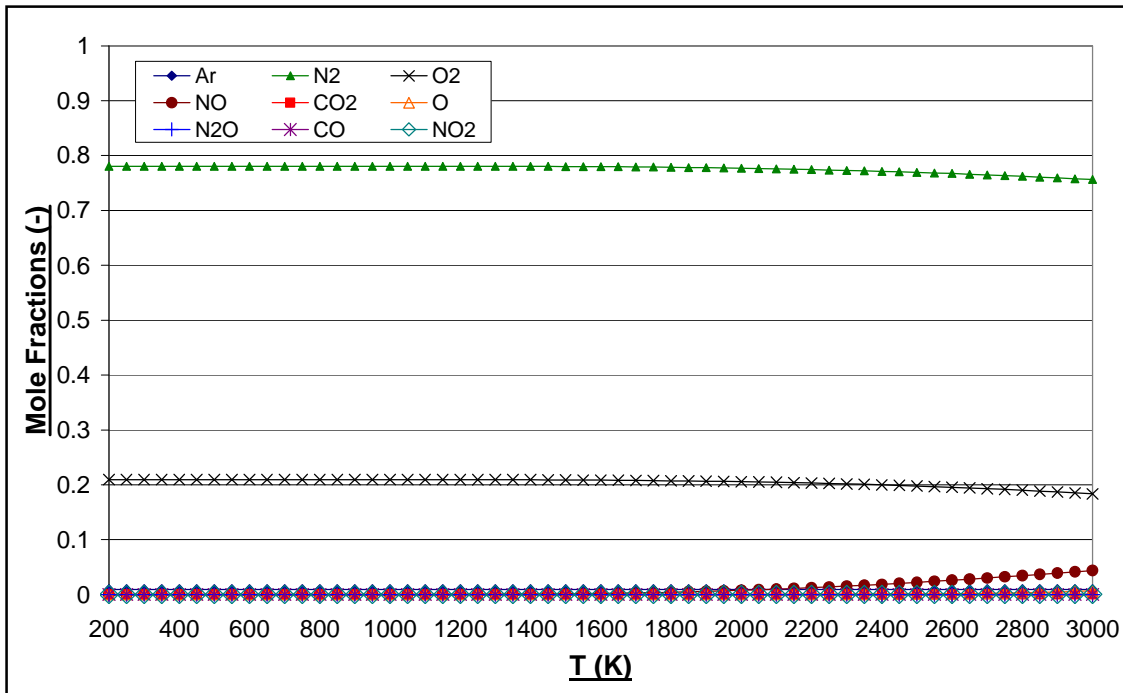


Fig: 2.1.31 Graph to show the Variation in Composition of Dry Air as a Function of Temperature for the Chemical Equilibrium Fluid Model (P = 50atm).

<u>Constituent</u>	<u>Mole Fraction (-) at Specified Temperature</u>				
	200K	1500K	2000K	2500K	3000K
Ar	0.00936	0.00937	0.00937	0.00936	0.00933
CO	0.00000	0.00000	0.00000	0.00000	0.00003
CO ₂	0.00032	0.00032	0.00032	0.00032	0.00029
NO	0.00000	0.00121	0.00753	0.02205	0.04371
NO ₂	0.00000	0.00005	0.00009	0.00014	0.00017
N ₂	0.78084	0.78023	0.77705	0.76944	0.75629
N ₂ O	0.00000	0.00000	0.00000	0.00001	0.00002
O	0.00000	0.00000	0.00004	0.00090	0.00681
O ₂	0.20948	0.20883	0.20560	0.19778	0.18336

Fig: 2.1.32 Composition of Dry Air for a Range of Temperatures for the Chemical Equilibrium Fluid Model (P = 50atm).

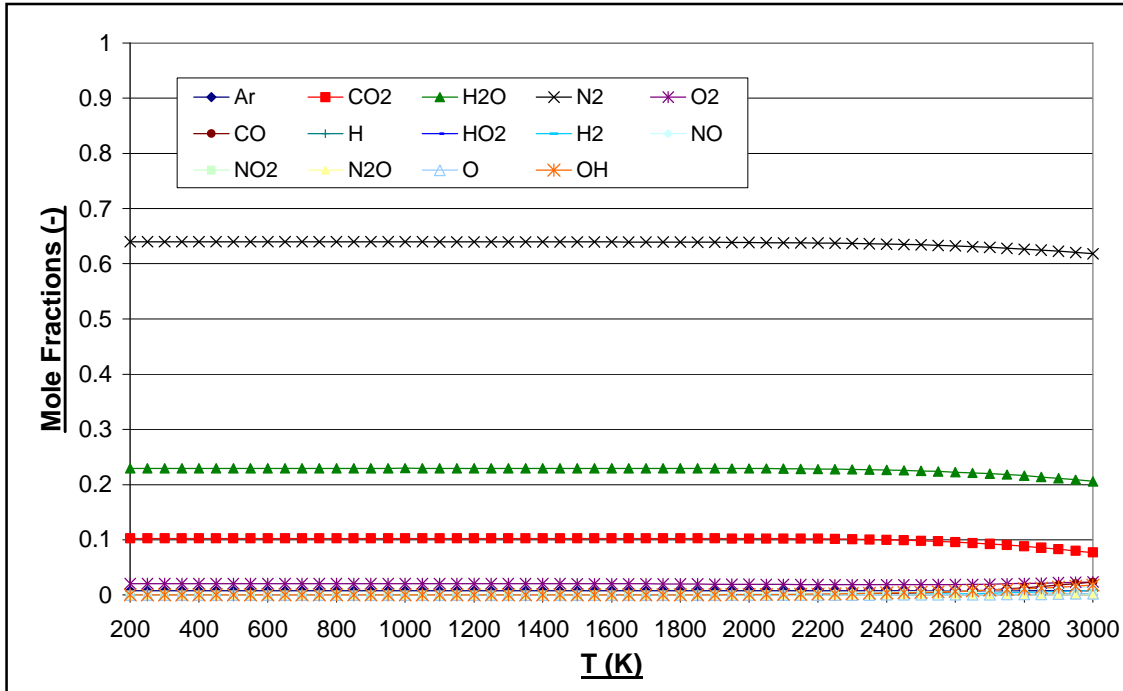


Fig: 2.1.33 Graph to show the Variation in Composition of the Products of Combustion of Jet-A as a Function Temperature for the Chemical Equilibrium Fluid Model for FARB = 0.06 & WAR = 0.10 (P = 50atm).

Constituent	Mole Fraction (-) at Specified Temperature				
	200K	1500K	2000K	2500K	3000K
Ar	0.00767	0.00767	0.00767	0.00764	0.00750
CO2	0.10239	0.10239	0.10222	0.09826	0.07677
H2O	0.22960	0.22959	0.22911	0.22479	0.20588
N2	0.63977	0.63959	0.63853	0.63413	0.61791
O2	0.02057	0.02038	0.01942	0.01861	0.02360
CO	0.00000	0.00000	0.00014	0.00372	0.02325
H	0.00000	0.00000	0.00000	0.00013	0.00204
HO2	0.00000	0.00000	0.00000	0.00001	0.00003
H2	0.00000	0.00000	0.00007	0.00137	0.00842
NO	0.00000	0.00034	0.00210	0.00614	0.01417
NO2	0.00000	0.00000	0.00001	0.00001	0.00002
N2O	0.00000	0.00000	0.00000	0.00000	0.00001
O	0.00000	0.00000	0.00001	0.00028	0.00244
OH	0.00000	0.00003	0.00072	0.00490	0.01793

Fig: 2.1.34 Composition of the Products of Combustion of Jet-A for a Range of Temperatures for the Chemical Equilibrium Fluid Model (P = 50atm) for FARB = 0.06 and WAR = 0.10.

Advanced Performance Simulation of Gas Turbine Components and Fluid Thermodynamic Properties

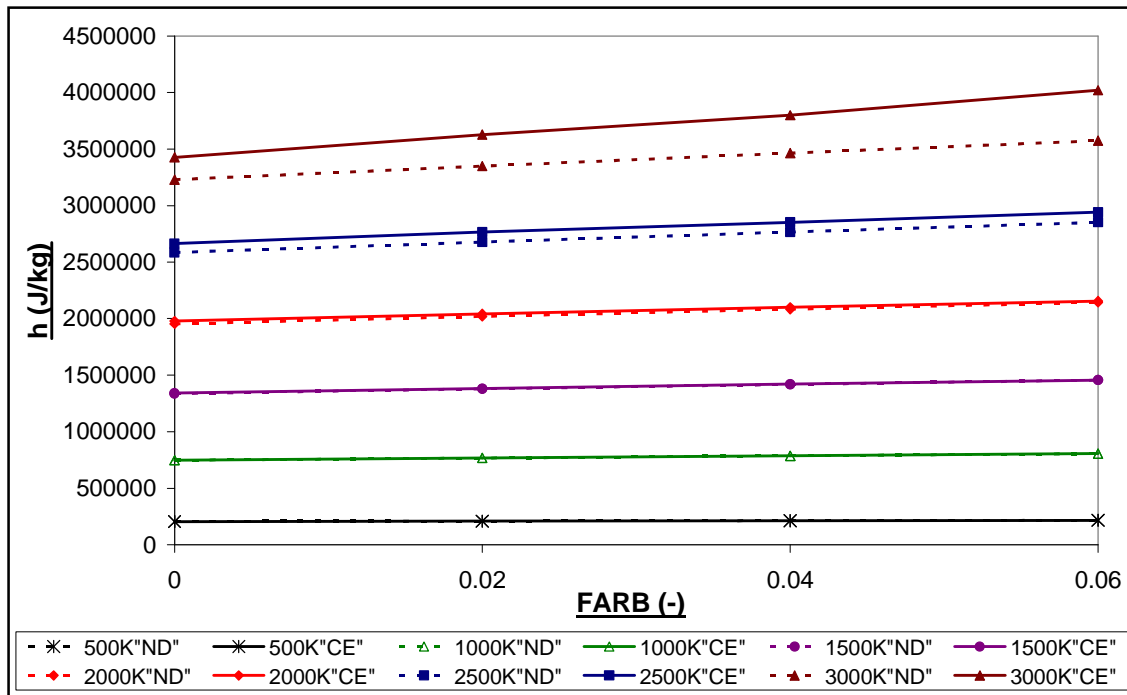


Fig: 2.1.35 Graph of Jet-A Specific Enthalpy (“No Dissociation” (“ND”) and Chemical Equilibrium (“CE”)) as a Function of FARB, for a Range of Temperatures (WAR = 0.00).

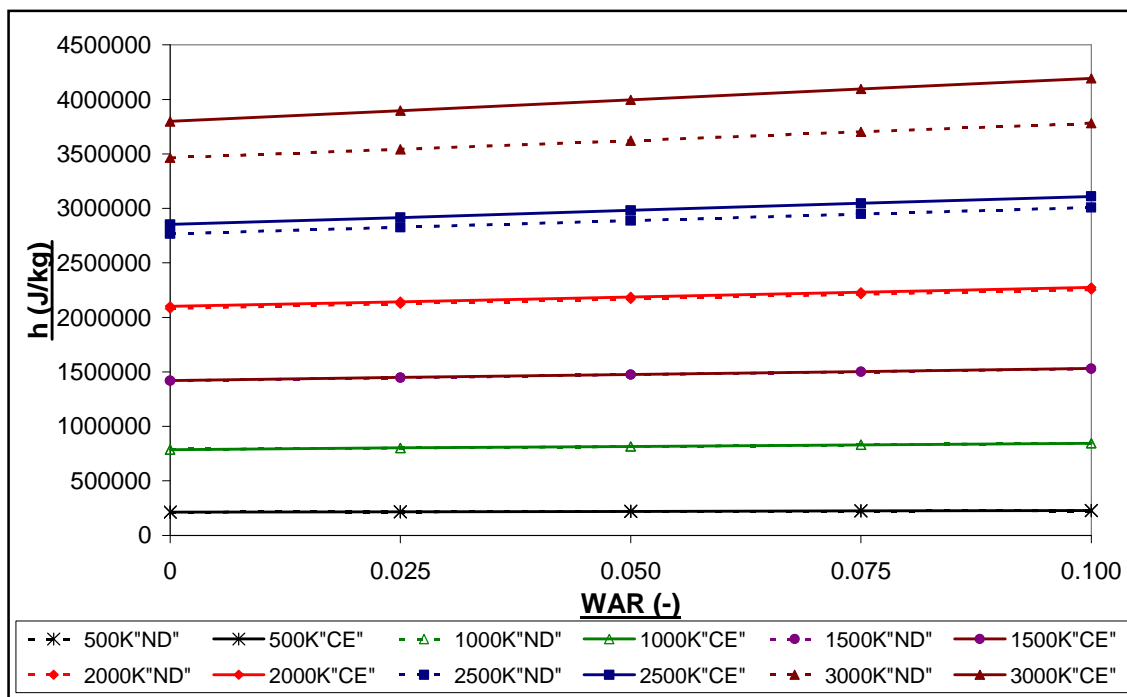


Fig: 2.1.36 Graph of Jet-A Specific Enthalpy (“No Dissociation” (“ND”) and Chemical Equilibrium (“CE”)) as a Function of WAR, for a Range of Temperatures (FARB = 0.04).

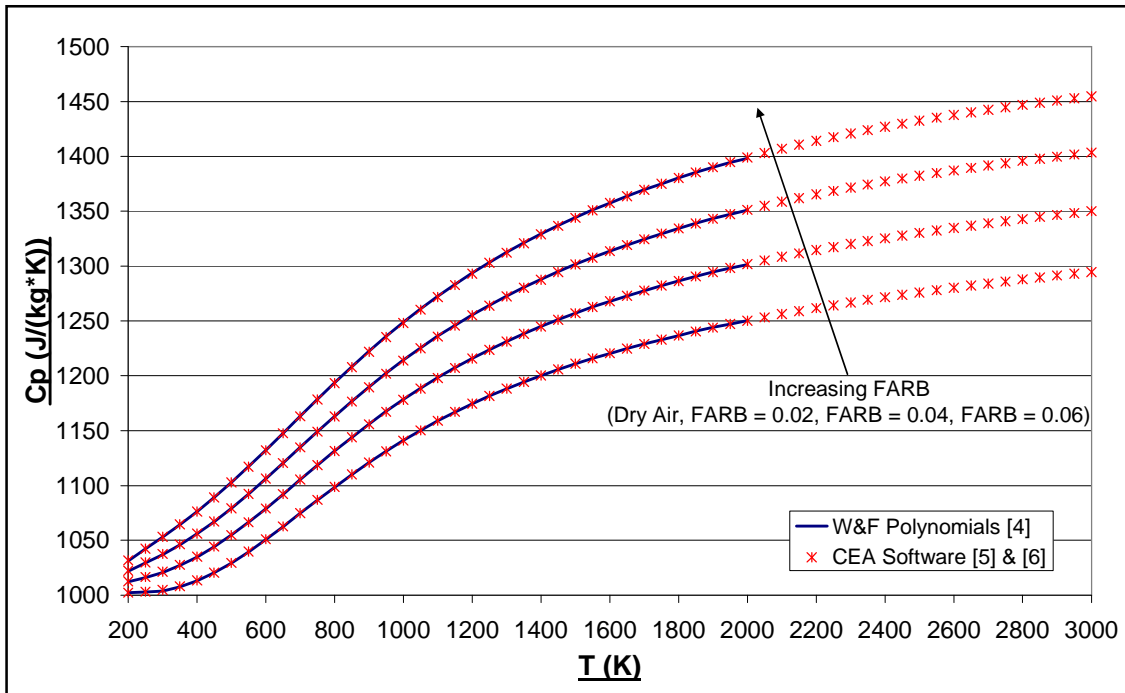


Fig: 2.1.37 Comparison of the variation of C_p (of Dry Air and the Products of Combustion of Jet-A) Between the W&F Polynomials [4] and the PROOSIS “No Dissociation” Fluid Model (Generated Using the CEA [5] & [6] software).

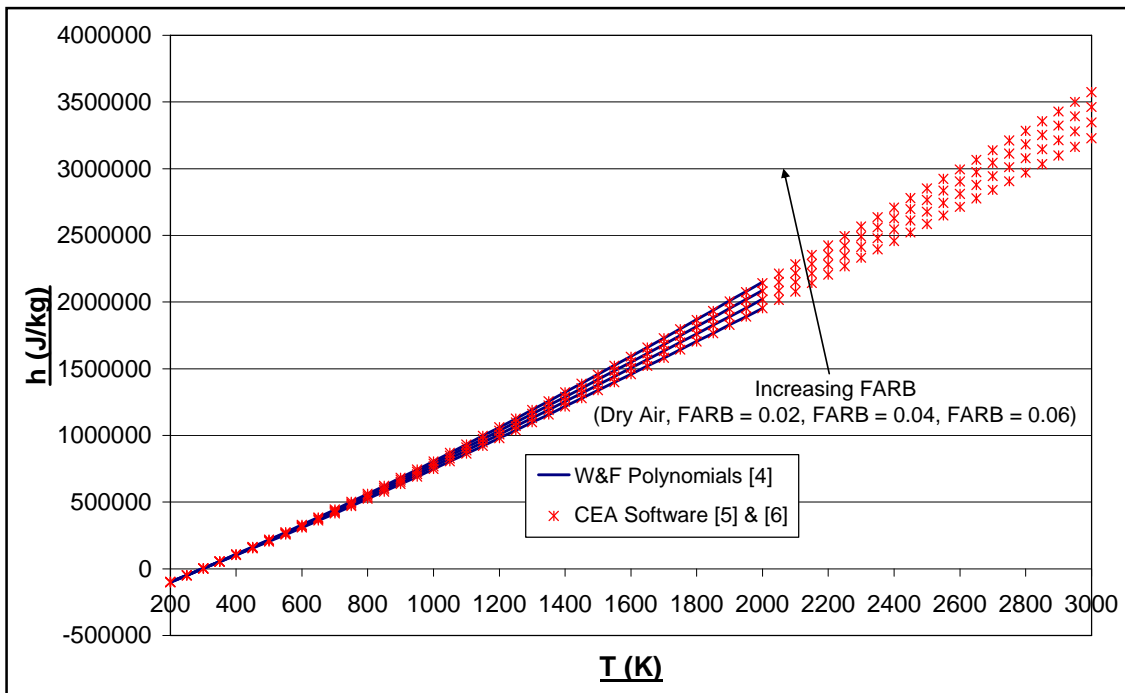


Fig: 2.1.38 Comparison of the variation of Specific Enthalpy (of Dry Air and the Products of Combustion of Jet-A) Between the W&F Polynomials [4] and the PROOSIS “No Dissociation” Fluid Model (Generated Using the CEA [5] & [6] software).

Advanced Performance Simulation of Gas Turbine Components
and Fluid Thermodynamic Properties

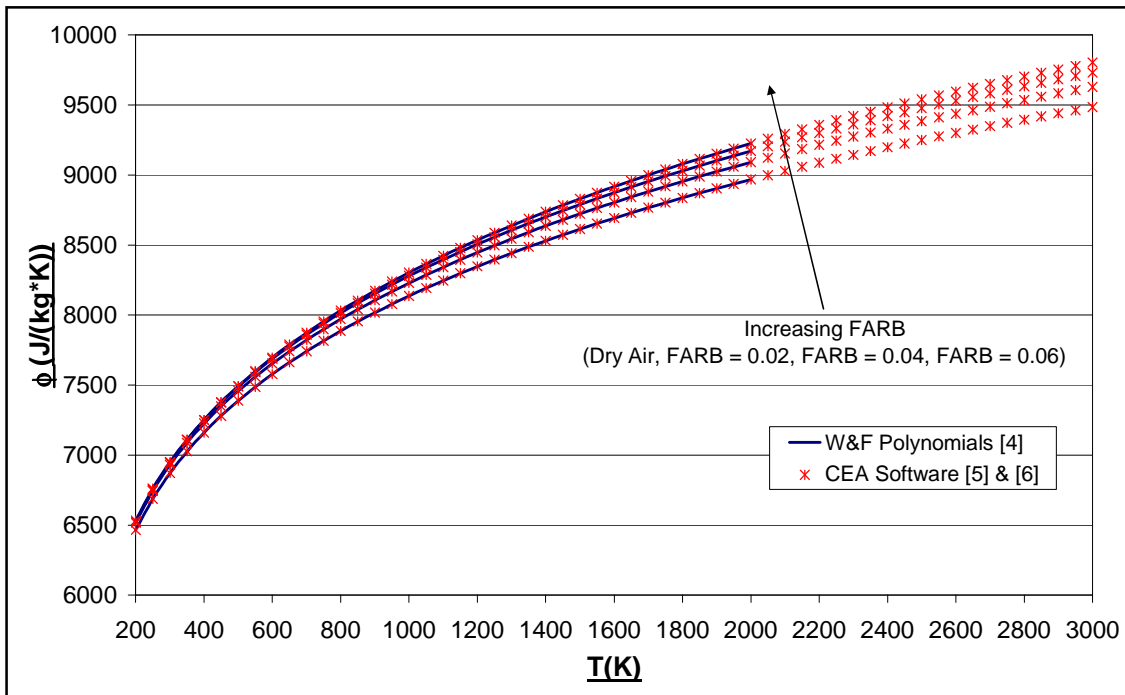


Fig: 2.1.39 Comparison of the variation of Entropy Function (of Dry Air and the Products of Combustion of Jet-A) Between the W&F Polynomials ^[4] and the PROOSIS “No Dissociation” Fluid Model (Generated Using the CEA ^[5] & ^[6] software).

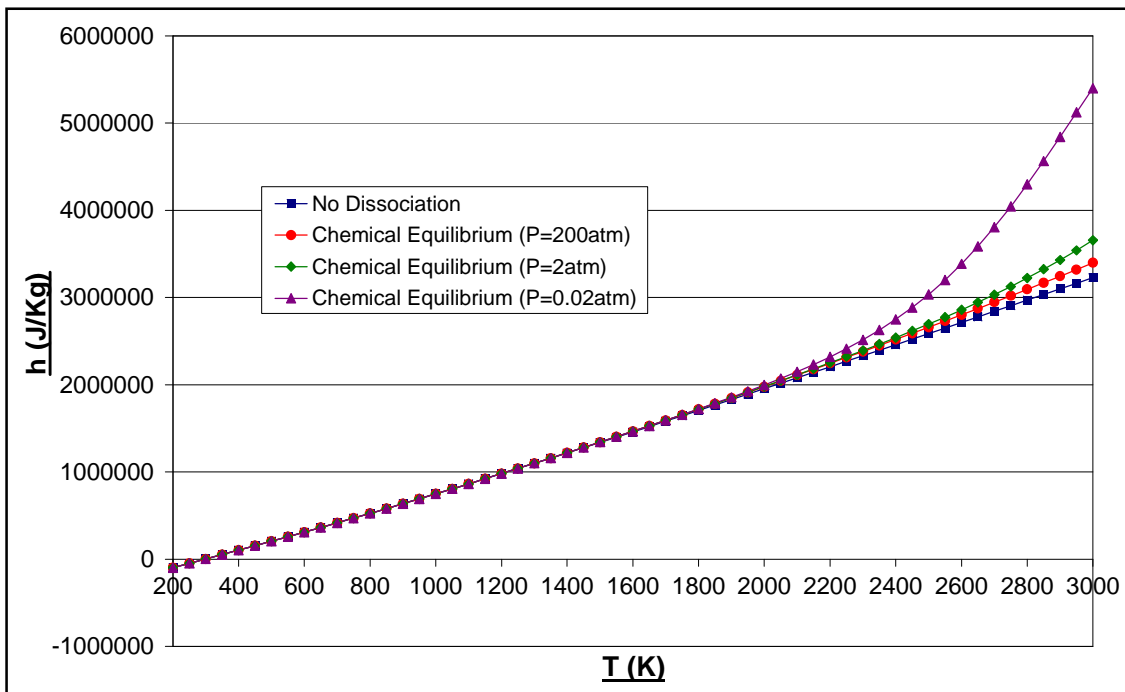


Fig: 2.1.40 Graph of Chemical Equilibrium h as a function of T and P for Dry Air

Advanced Performance Simulation of Gas Turbine Components
and Fluid Thermodynamic Properties

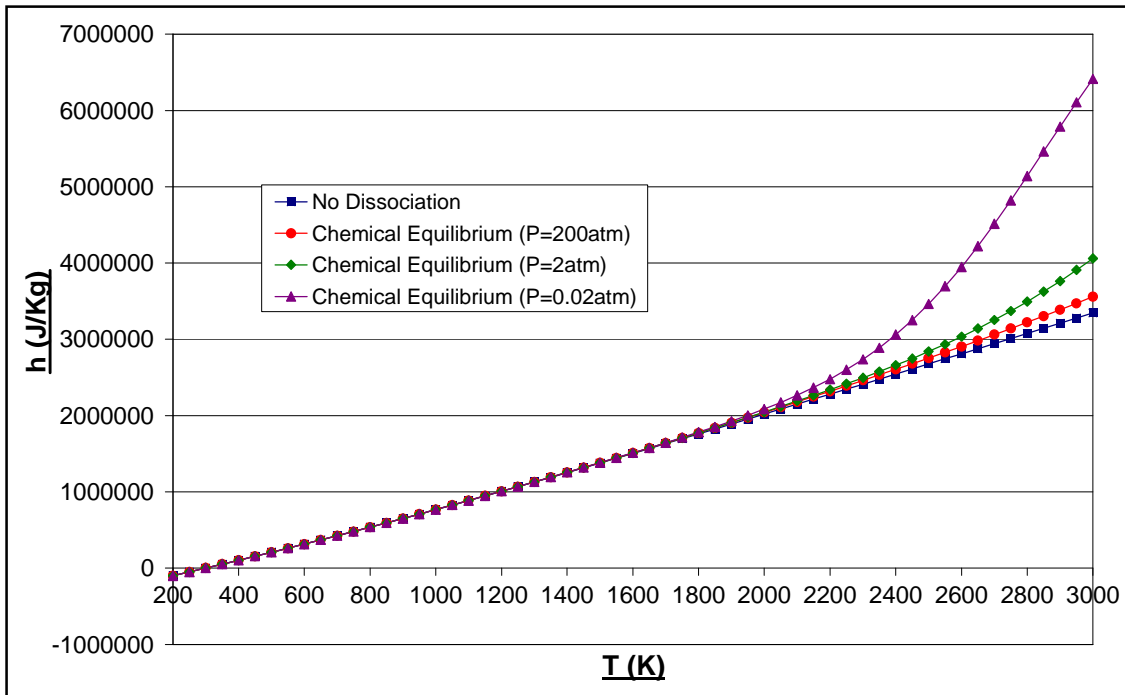


Fig: 2.1.41 Graph of Chemical Equilibrium h as a function of T and P for the Products of Combustion of Jet-A (FARB = 0.02, WAR = 0.00)

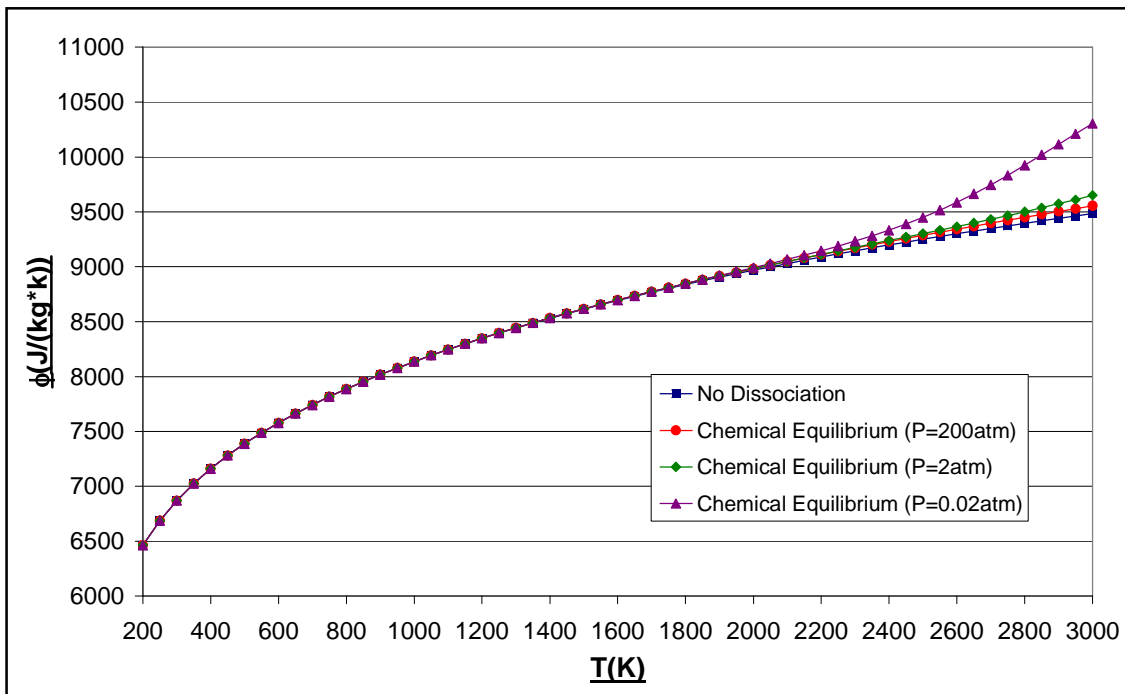


Fig: 2.1.42 Graph of Chemical Equilibrium ϕ as a function of T and P for Dry Air

Advanced Performance Simulation of Gas Turbine Components
and Fluid Thermodynamic Properties

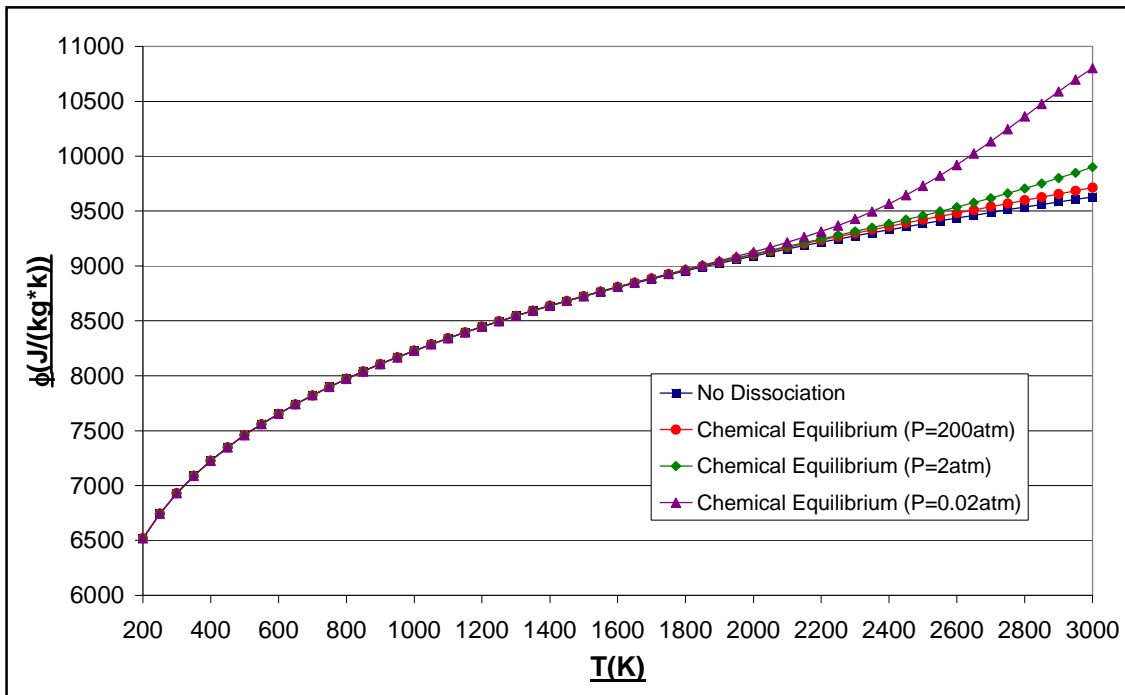


Fig: 2.1.43 Graph of Chemical Equilibrium ϕ as a function of T and P for the Products of Combustion of Jet-A (FARB = 0.02, WAR = 0.00)

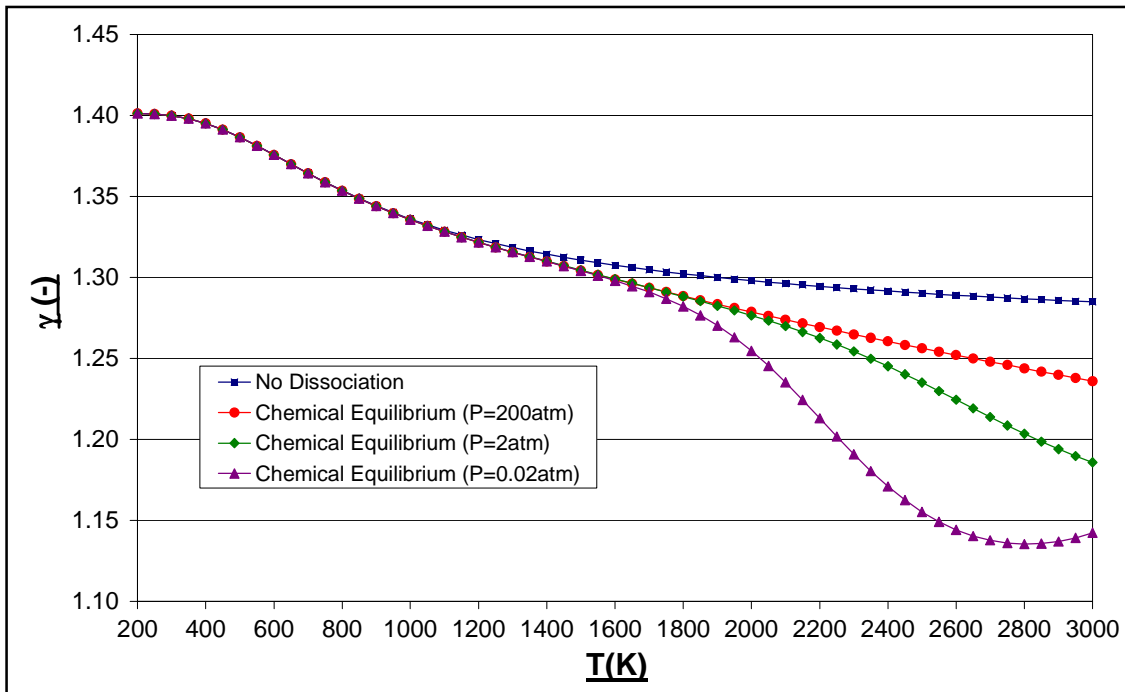


Fig: 2.1.44 Graph of Chemical Equilibrium γ as a function of T and P for Dry Air

Advanced Performance Simulation of Gas Turbine Components
and Fluid Thermodynamic Properties

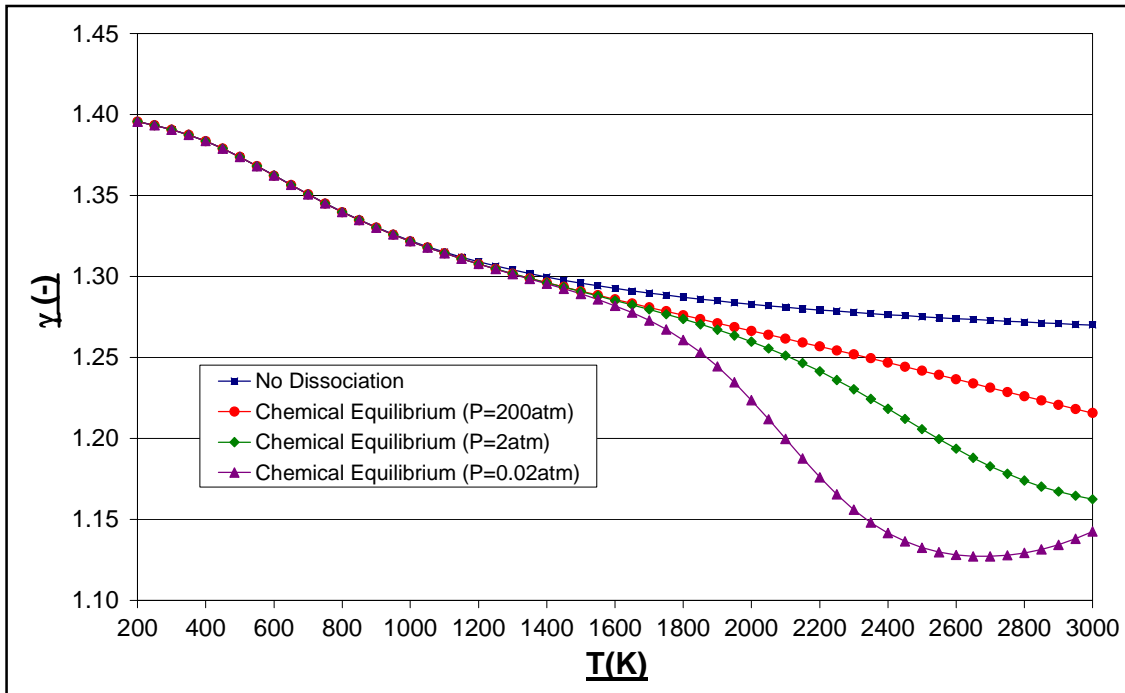


Fig: 2.1.45 Graph of Chemical Equilibrium γ as a function of T and P for the Products of Combustion of Jet-A (FARB = 0.02, WAR = 0.00)

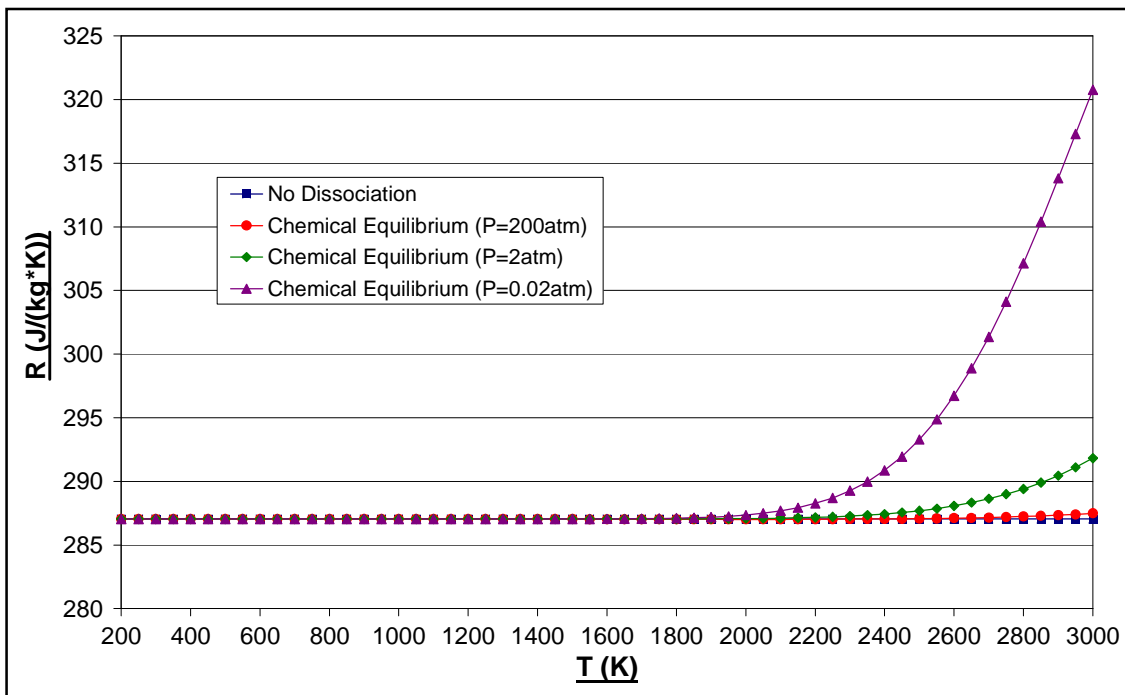


Fig: 2.1.46 Graph of Chemical Equilibrium R as a function of T and P for Dry Air

Advanced Performance Simulation of Gas Turbine Components
and Fluid Thermodynamic Properties

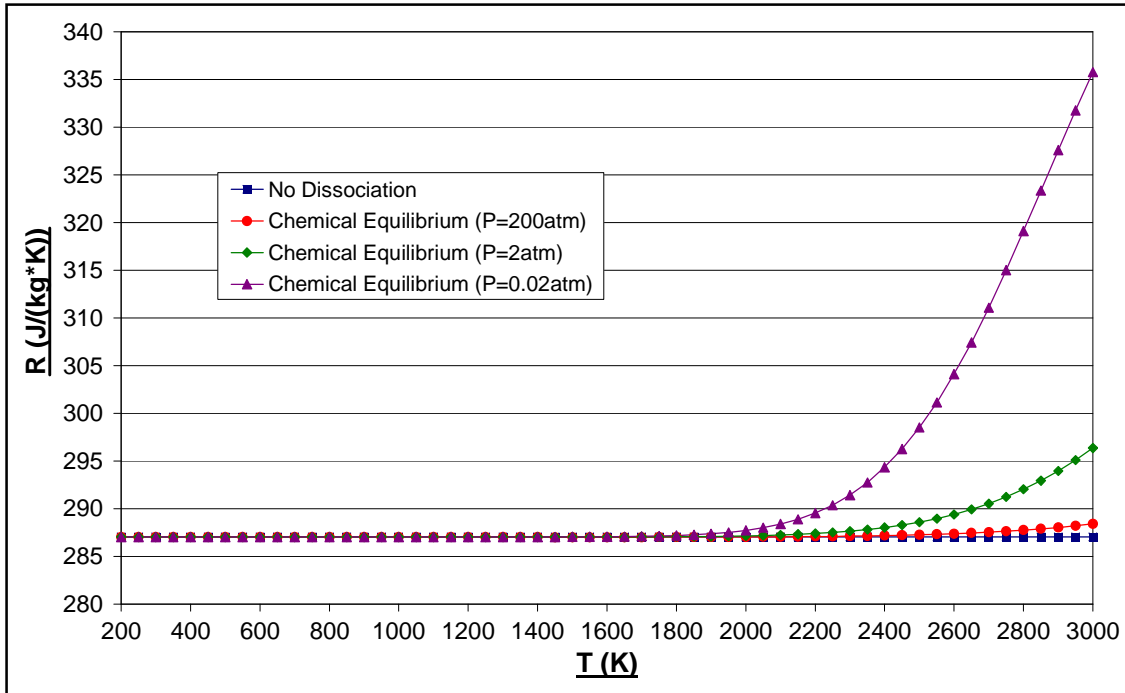


Fig: 2.1.47 Graph of Chemical Equilibrium R as a function of T and P for the Products of Combustion of Jet-A (FARB = 0.02, WAR = 0.00)

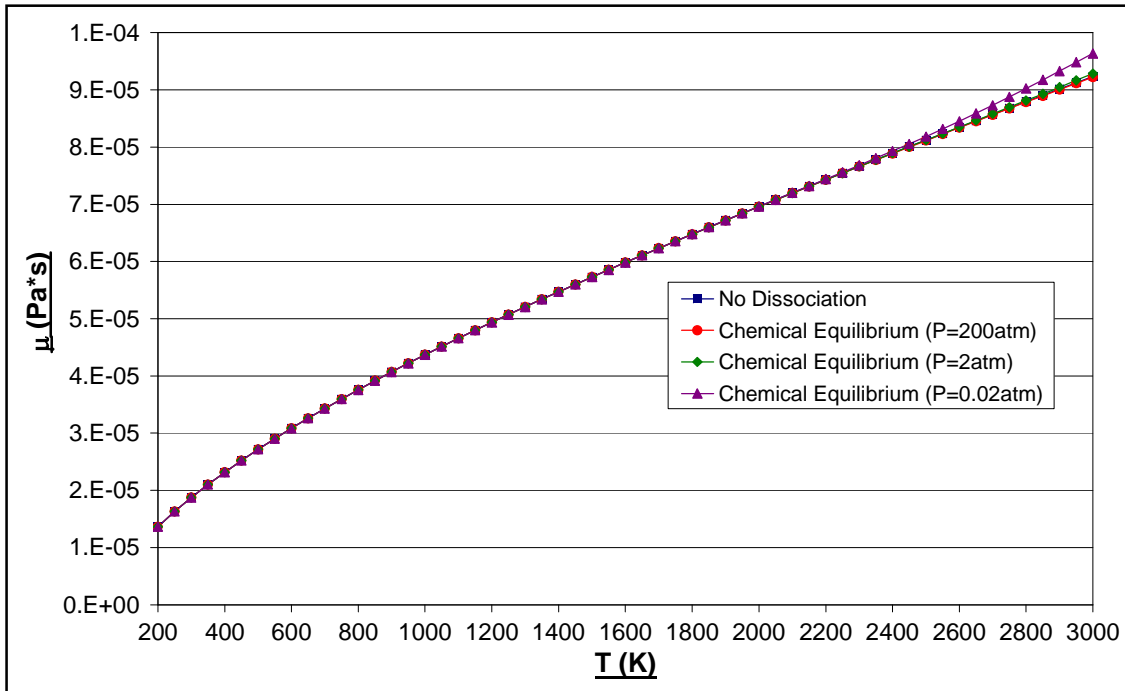


Fig: 2.1.48 Graph of Chemical Equilibrium μ as a function of T and P for Dry Air

Advanced Performance Simulation of Gas Turbine Components
and Fluid Thermodynamic Properties

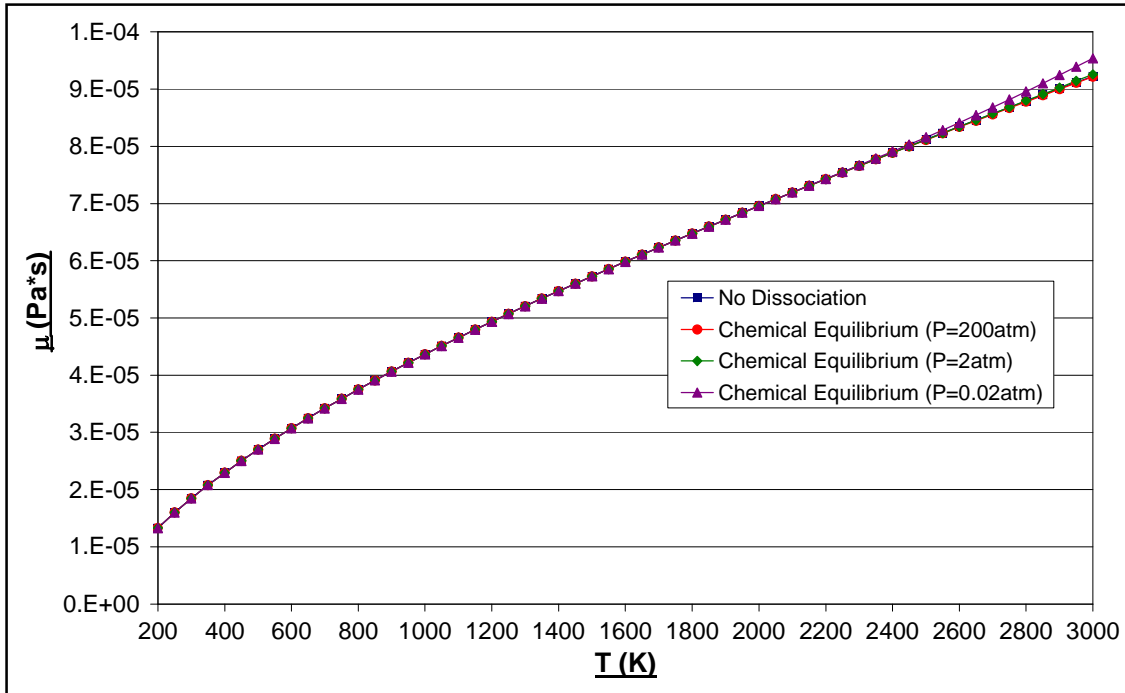


Fig: 2.1.49 Graph of Chemical Equilibrium μ as a function of T and P for the Products of Combustion of Jet-A (FARB = 0.02, WAR = 0.00)

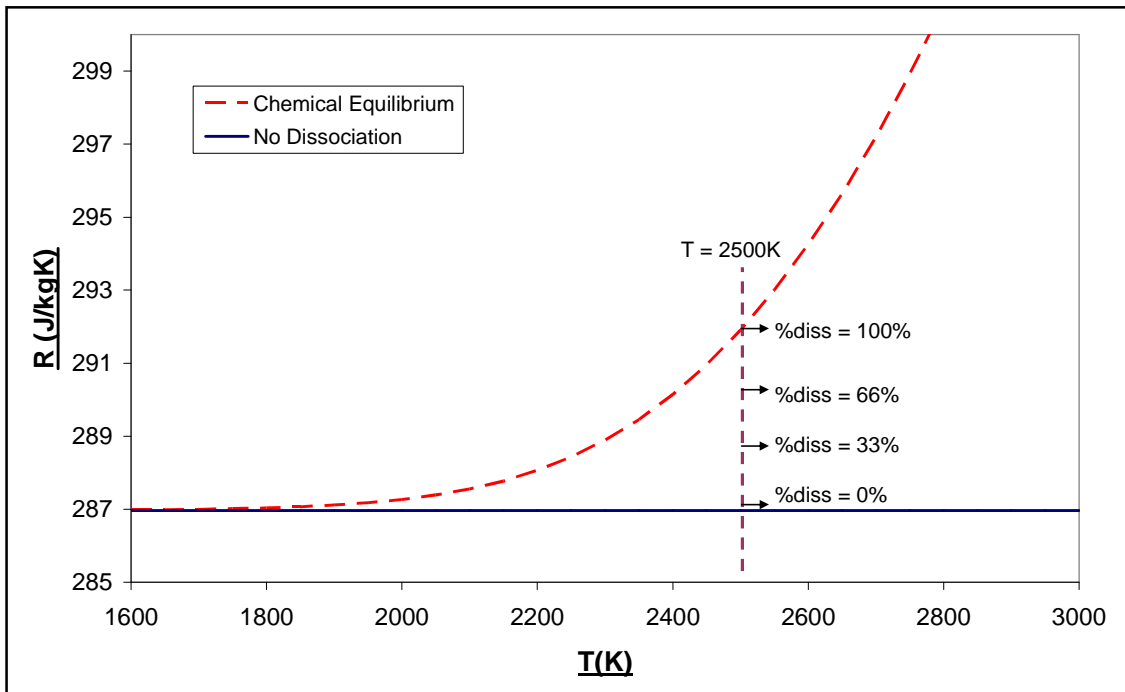


Fig: 2.1.50 Graph to Illustrate How Values of Fluid Properties Corresponding to Different Values of $\%_{diss}$ were Determined (FARB = 0.06, WAR = 0.00)

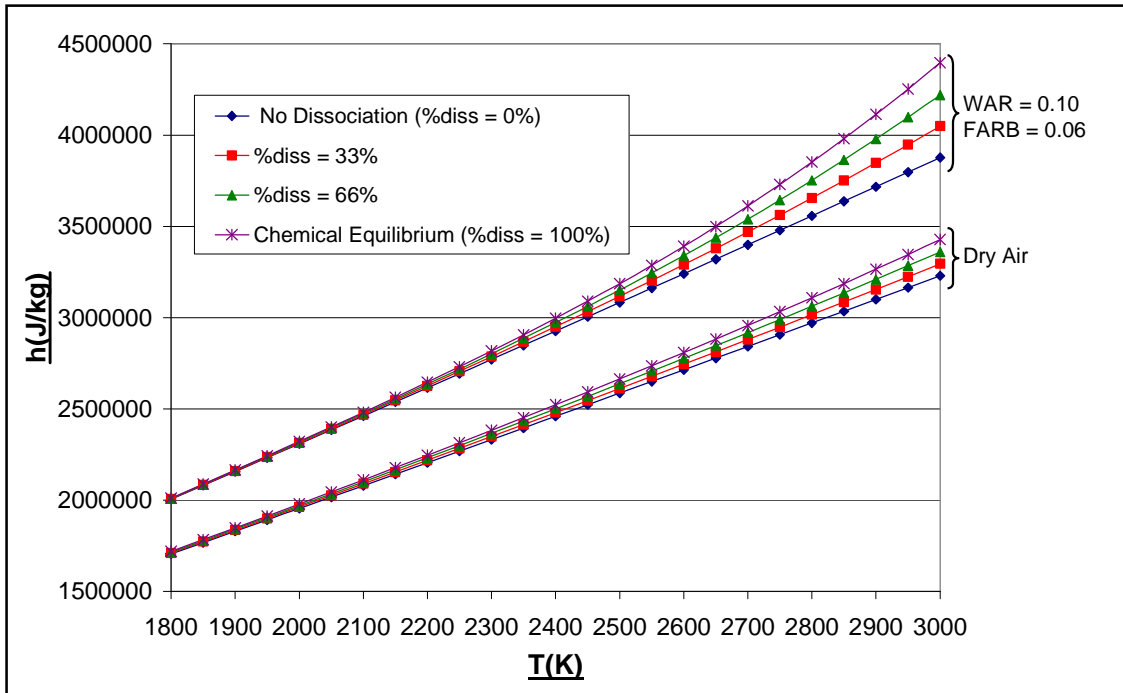


Fig: 2.1.51 Graph of h as a function of T and %diss ($P=50\text{atm}$) for:
a.) Dry Air (FARB = 0.00, WAR = 0.00)
b.) Products of Combustion of Jet-A (FARB = 0.06, WAR = 0.10)

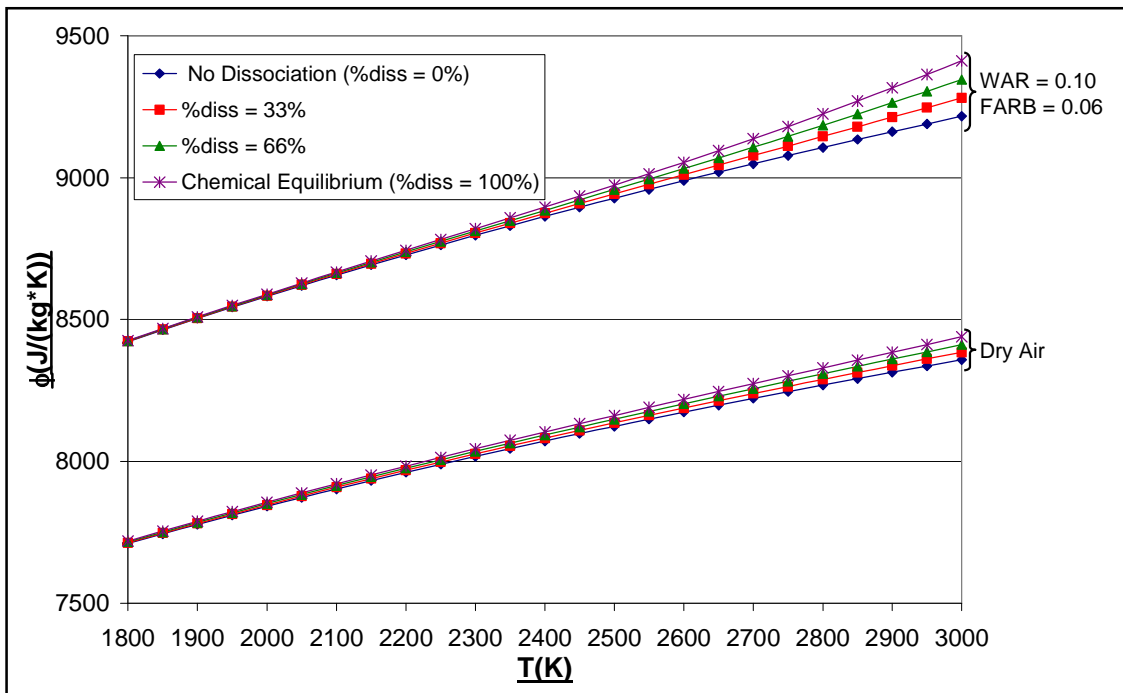


Fig: 2.1.52 Graph of ϕ as a function of T and %diss ($P=50\text{atm}$) for:
a.) Dry Air (FARB = 0.00, WAR = 0.00)
b.) Products of Combustion of Jet-A (FARB = 0.06, WAR = 0.10)

Advanced Performance Simulation of Gas Turbine Components and Fluid Thermodynamic Properties

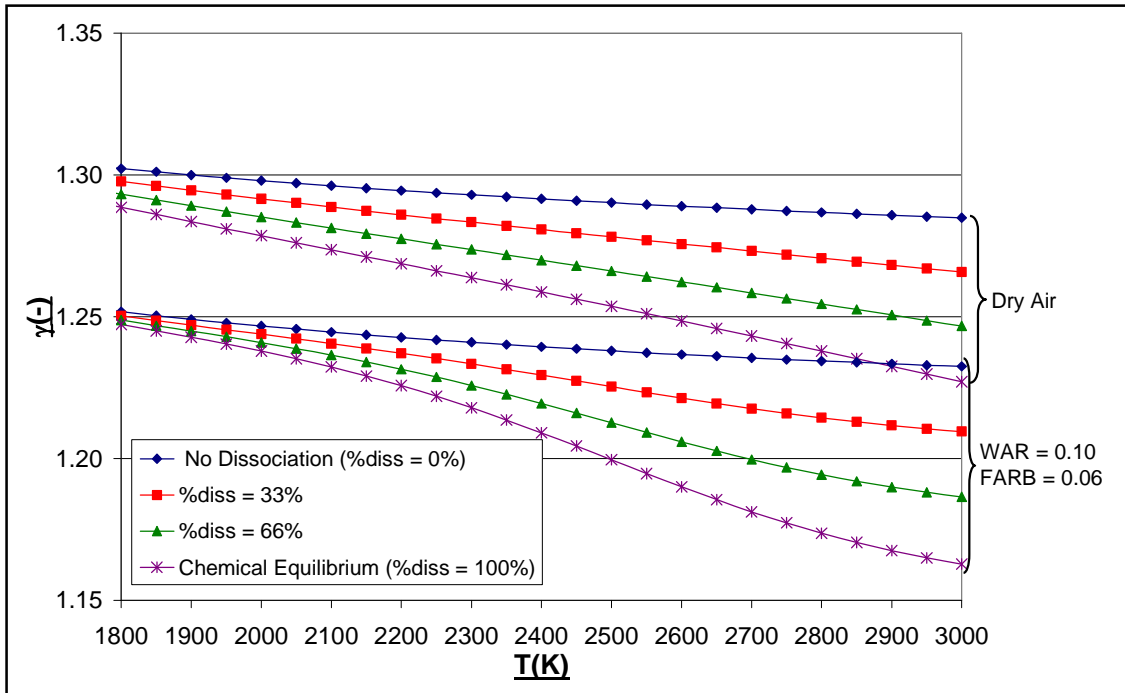


Fig: 2.1.53 Graph of γ as a function of T and %diss ($P=50\text{atm}$) for:
 a.) Dry Air ($\text{FARB} = 0.00$, $\text{WAR} = 0.00$)
 b.) Products of Combustion of Jet-A ($\text{FARB} = 0.06$, $\text{WAR} = 0.10$)

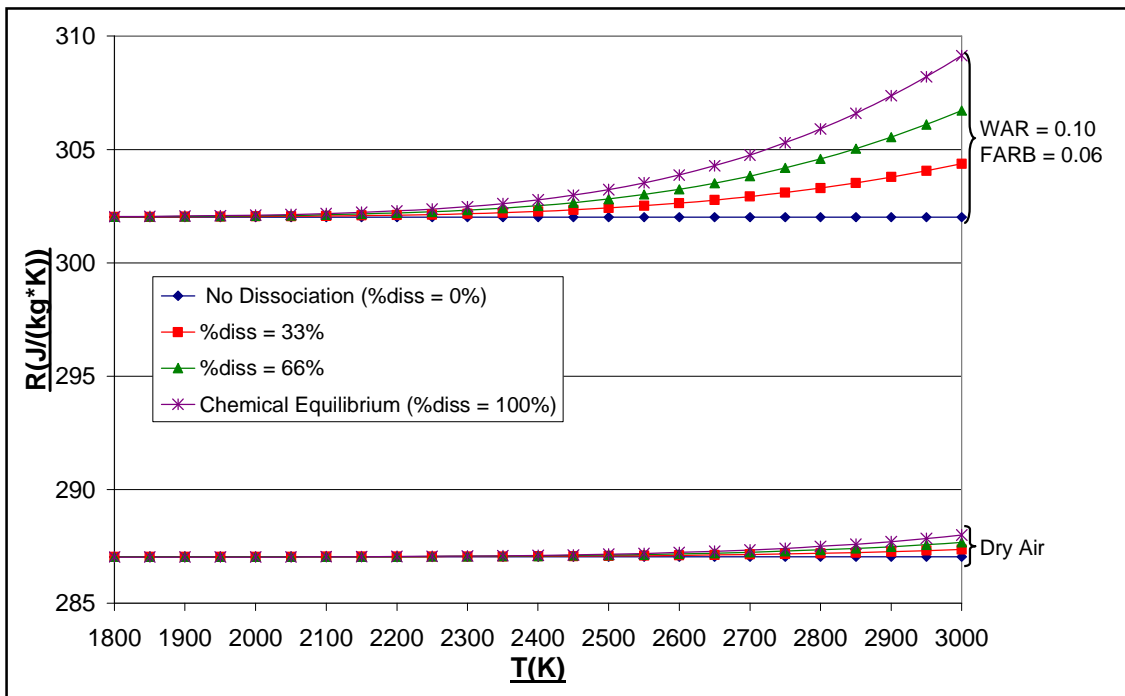


Fig: 2.1.54 Graph of R as a function of T and %diss ($P=50\text{atm}$) for:
 a.) Dry Air ($\text{FARB} = 0.00$, $\text{WAR} = 0.00$)
 b.) Products of Combustion of Jet-A ($\text{FARB} = 0.06$, $\text{WAR} = 0.10$)

Advanced Performance Simulation of Gas Turbine Components
and Fluid Thermodynamic Properties

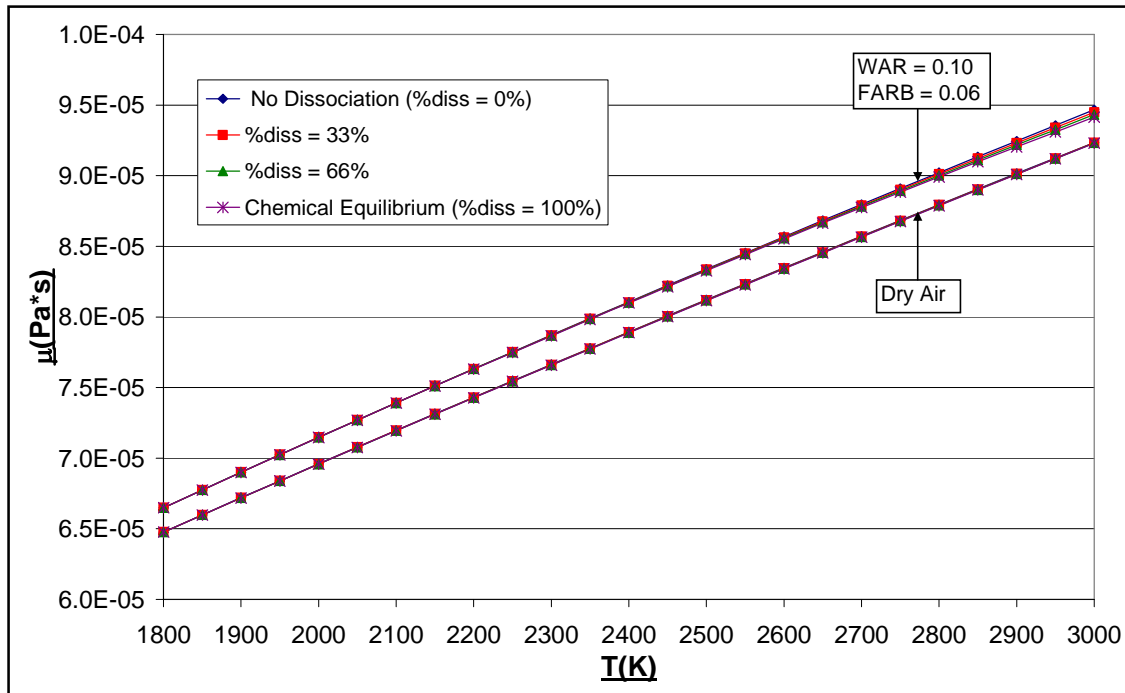


Fig: 2.1.55 Graph of μ as a function of T and %diss ($P = 50\text{atm}$) for:
a.) Dry Air (FARB = 0.00, WAR = 0.00)
b.) Products of Combustion of Jet-A (FARB = 0.06, WAR = 0.10)

Advanced Performance Simulation of Gas Turbine Components
and Fluid Thermodynamic Properties

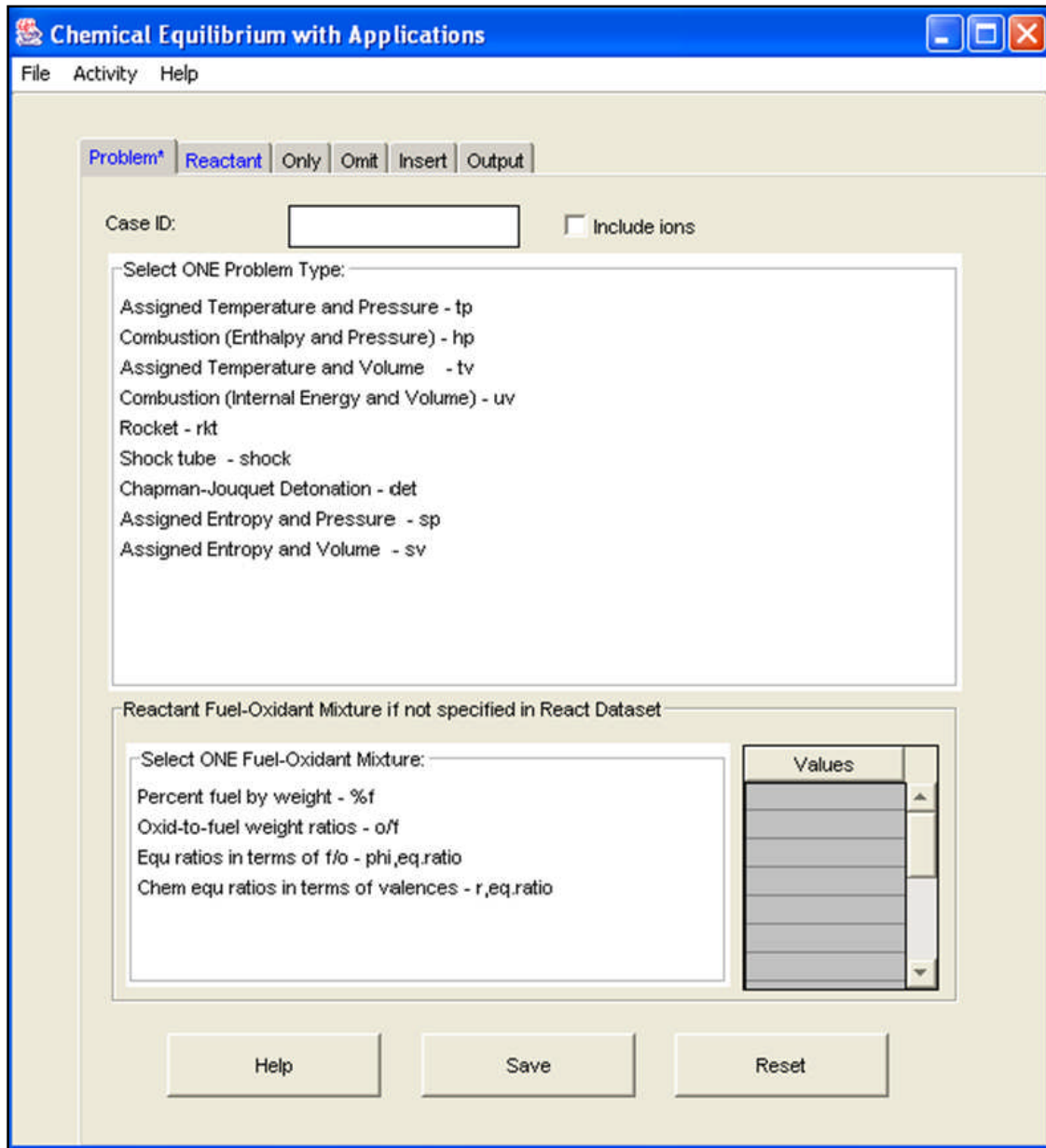


Fig: 2.2.1 The CEA_GUI Platform

Advanced Performance Simulation of Gas Turbine Components
and Fluid Thermodynamic Properties

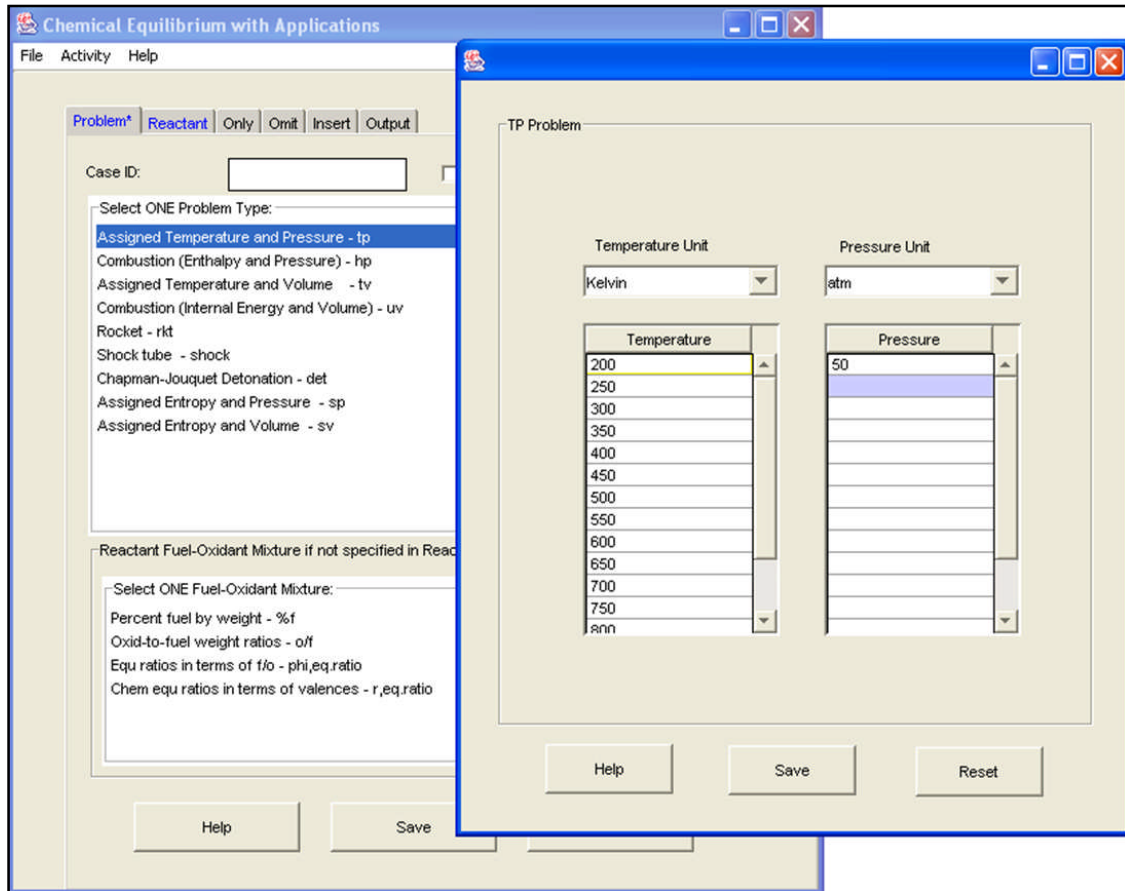


Fig: 2.2.2 CEA_GUI "TP" Sub-tab Temperature and Pressure Selection

```

problem  o/f=50,
tp t,k=200, 250, 300, 350, 400, 450, 500, 550, 600, 650, 700, 750, 800, 850,
900, 950, 1000,1050, 1100, 1150, 1200, 1250, 1300, 1350, 1400, 1450, 1500,
1550, 1600, 1650, 1700, 1750,1800,1850, 1900, 1950, 2000, 2050, 2100,
2150, 2200, 2250, 2300, 2350, 2400, 2450, 2500,
p,atm=50,
react
  oxid=Air wt=1 t,k=298.15
  fuel=Jet-A(g) wt=1 t,k=298.15
omit
  C(gr) H2O(cr) H2O(L)
output
  transport
plot
  t h s gam m vis
end
  
```

Fig: 2.2.3 Sample Input File for FCEA2

Advanced Performance Simulation of Gas Turbine Components
and Fluid Thermodynamic Properties

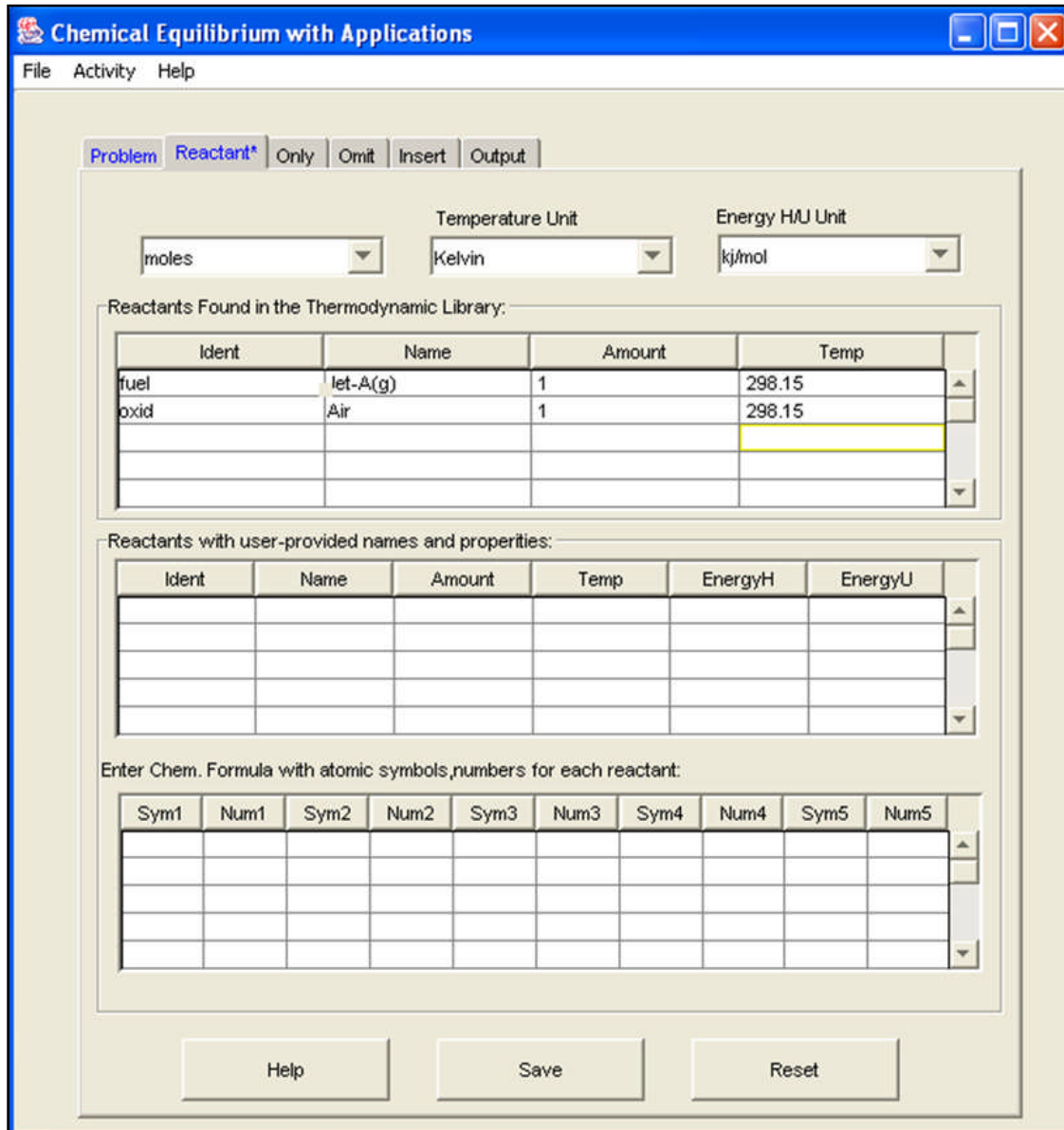


Fig: 2.2.4 CEA_GUI "Reactant" Tab

Advanced Performance Simulation of Gas Turbine Components
and Fluid Thermodynamic Properties

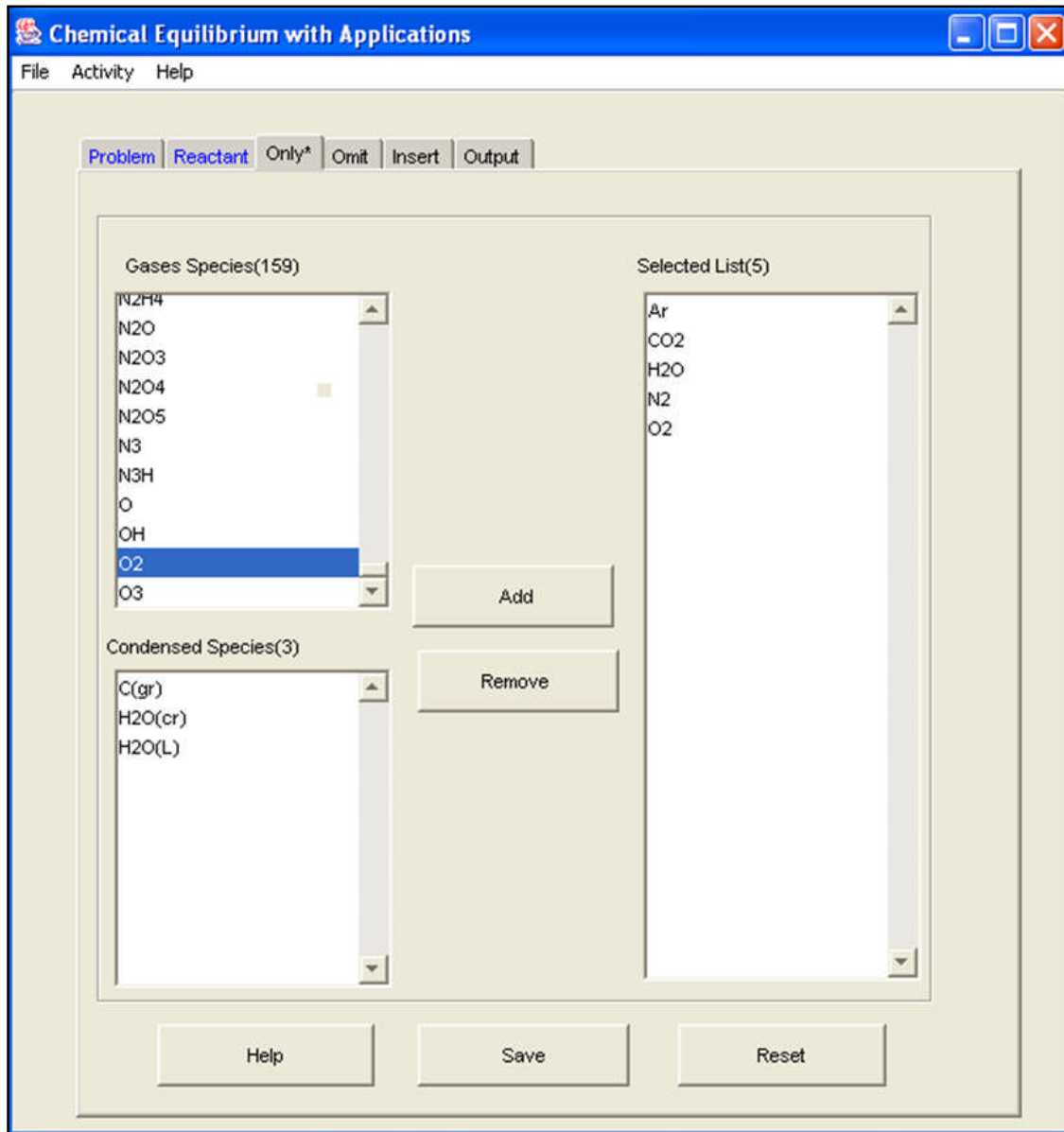


Fig: 2.2.5 CEA_GUI “Only” Tab (For the “No Dissociation” Fluid Model)

Advanced Performance Simulation of Gas Turbine Components
and Fluid Thermodynamic Properties

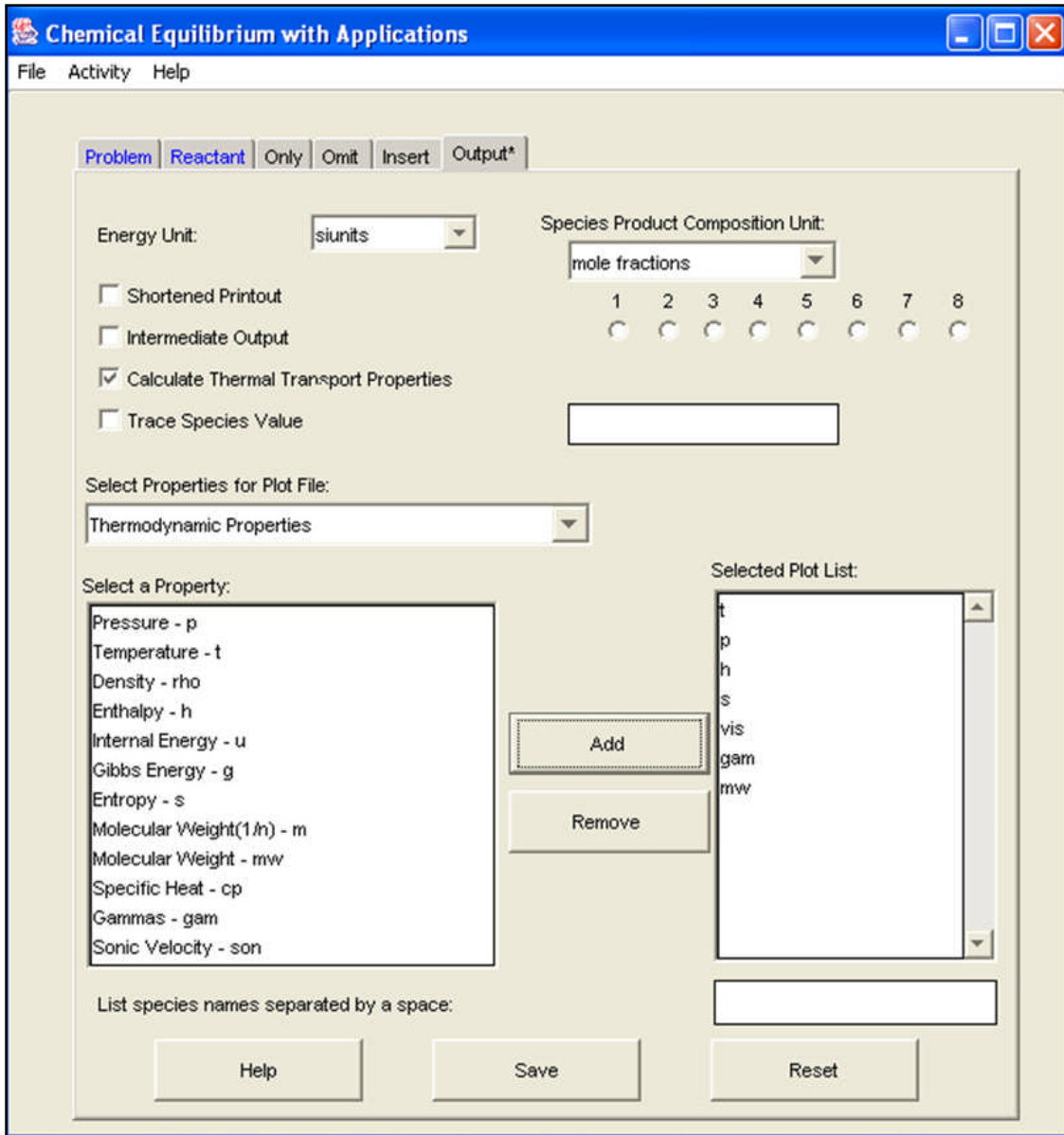


Fig: 2.2.6 CEA_GUI “Output” Tab

<u>Boundary Condition</u>	<u>Value</u>
W (kg/s)	77.20
Tt (K)	578.68
Pt (Pa)	891661
FARB (-)	0.00
WAR (-)	0.00

Fig: 2.3.1 Boundary Conditions for the Trouble Shooting process of the Thermodynamic Functions Convergence Problem

Advanced Performance Simulation of Gas Turbine Components
and Fluid Thermodynamic Properties

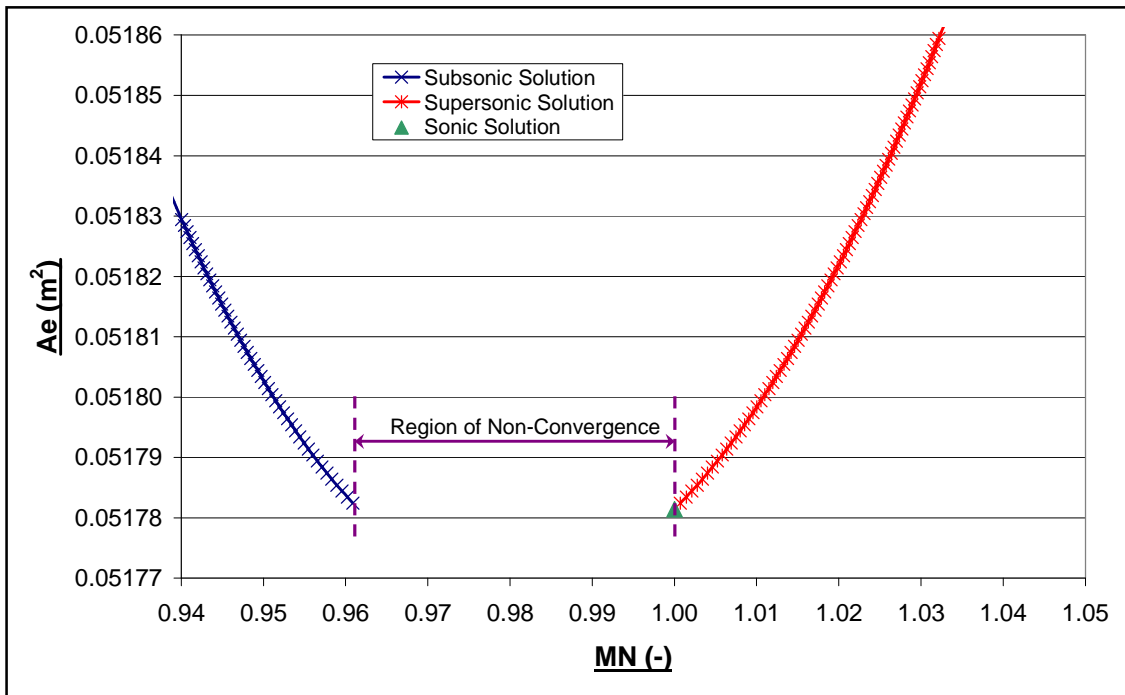


Fig: 2.3.2 Graph to Show Non-Convergence of therm_WTtPtAe Close to Sonic Conditions

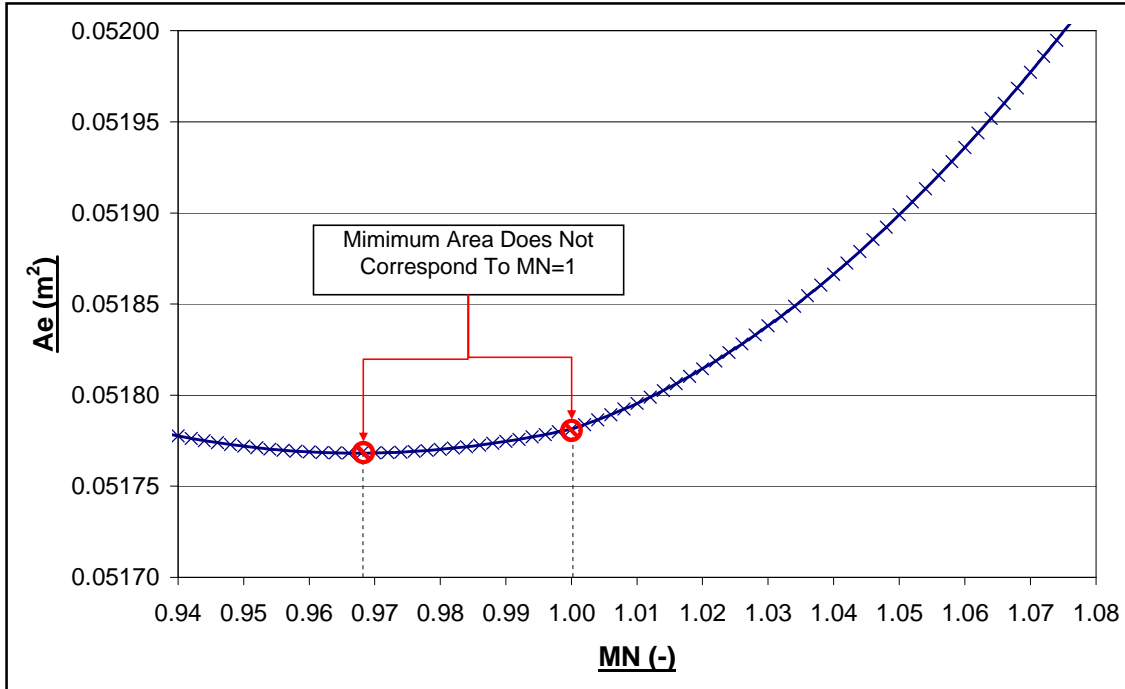


Fig: 2.3.3 Graph to Show Poor Result for therm_WTtPtMN at Sonic Condition

Advanced Performance Simulation of Gas Turbine Components
and Fluid Thermodynamic Properties

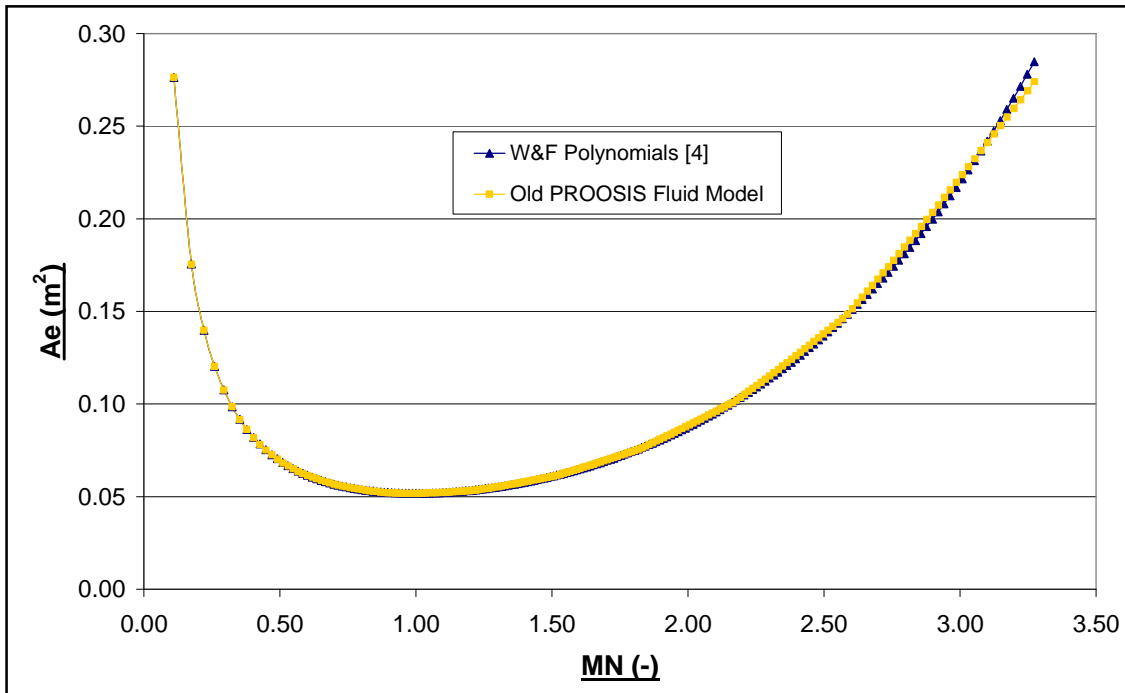


Fig: 2.3.4 Graph to Show Comparison of Results of therm_WTtPtTs Between the Two Fluid Models

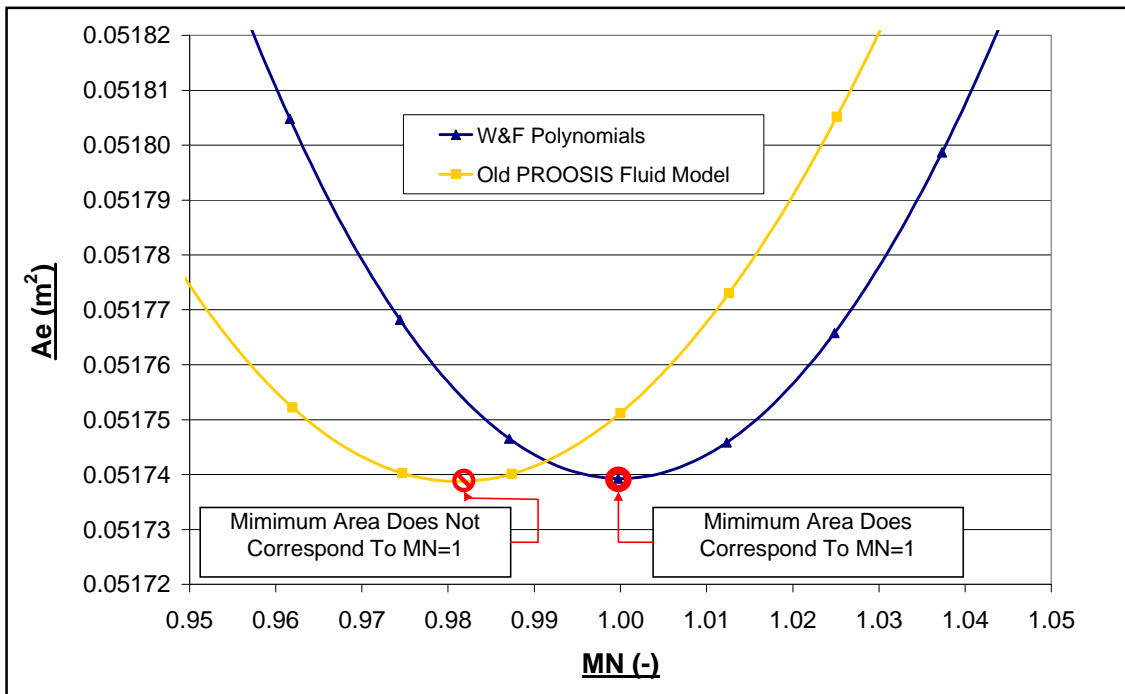


Fig: 2.3.4a Graph to Show Comparison of Results of therm_WTtPtTs Between the Two Fluid Models (Zoomed)

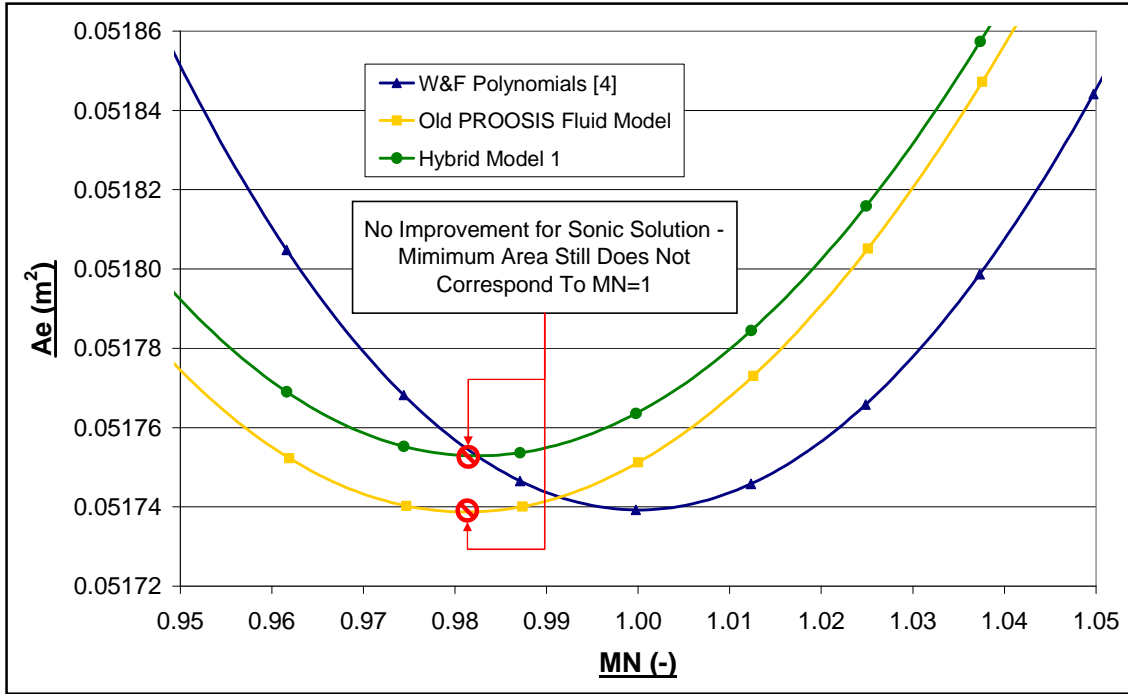


Fig: 2.3.5 Effect of Hybrid Model 1 on therm_WTtPtTs

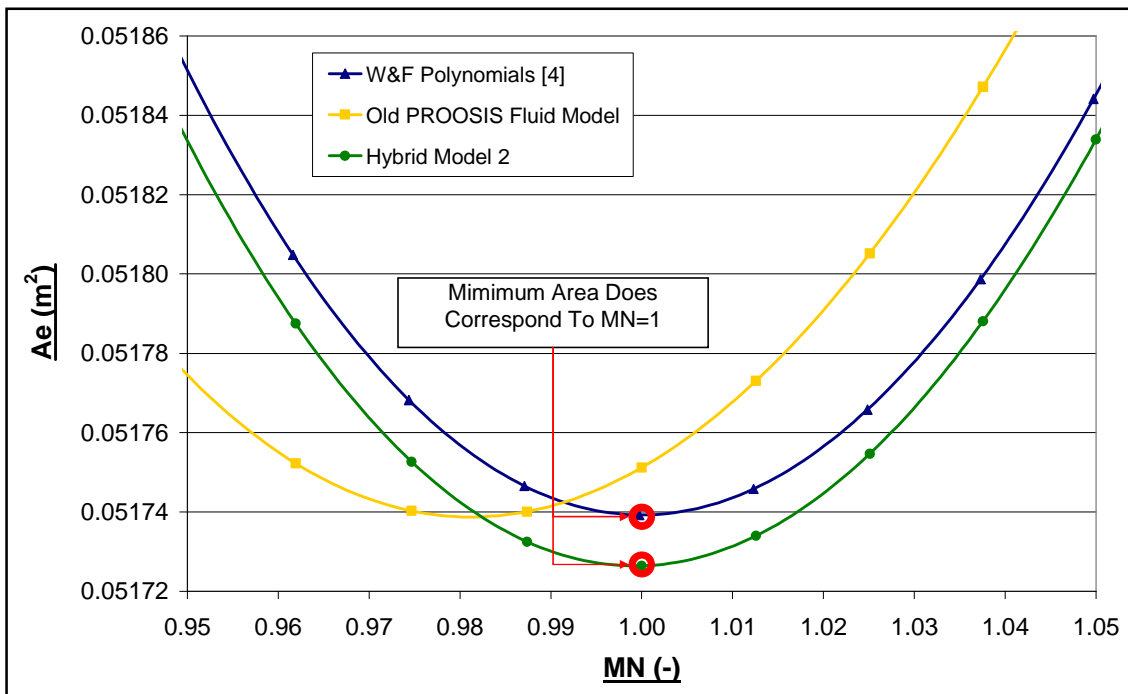


Fig: 2.3.6 Effect of Hybrid Model 2 on therm_WTtPtTs

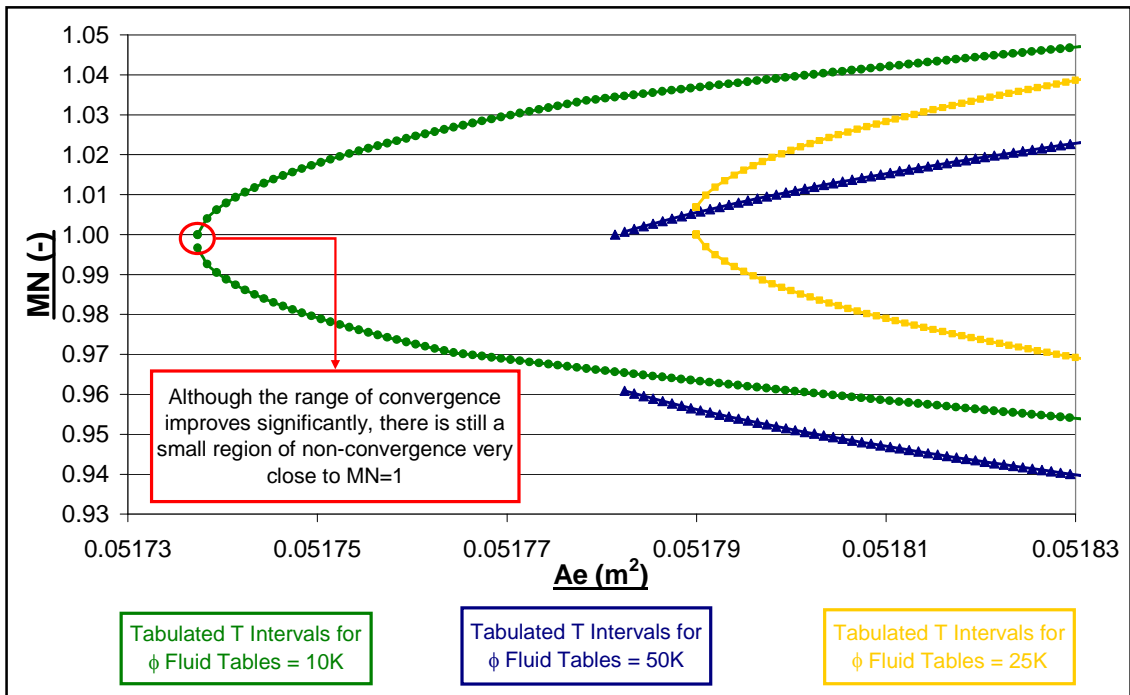


Fig: 2.3.7 Effects of Reducing the Tabulated Temperature Intervals of ϕ Fluid Tables on the Convergence Range of therm_WTtPtAe

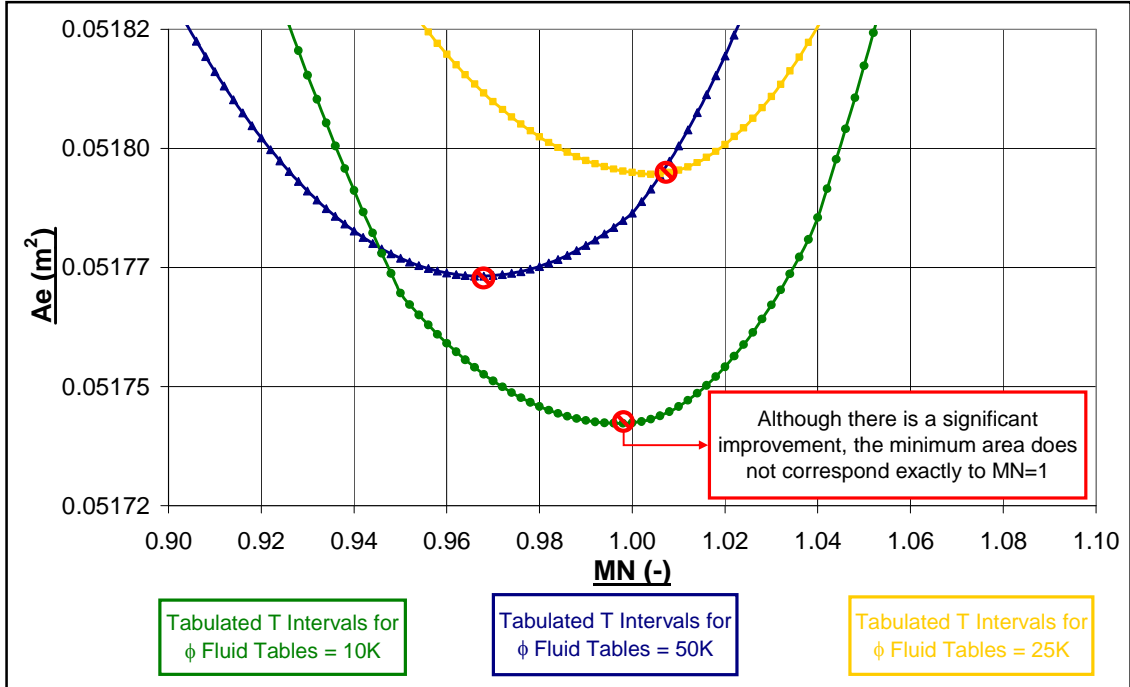


Fig: 2.3.8 Effects of Reducing the Tabulated Temperature Intervals of ϕ Fluid Tables on therm_WTtPtMN

Advanced Performance Simulation of Gas Turbine Components
and Fluid Thermodynamic Properties

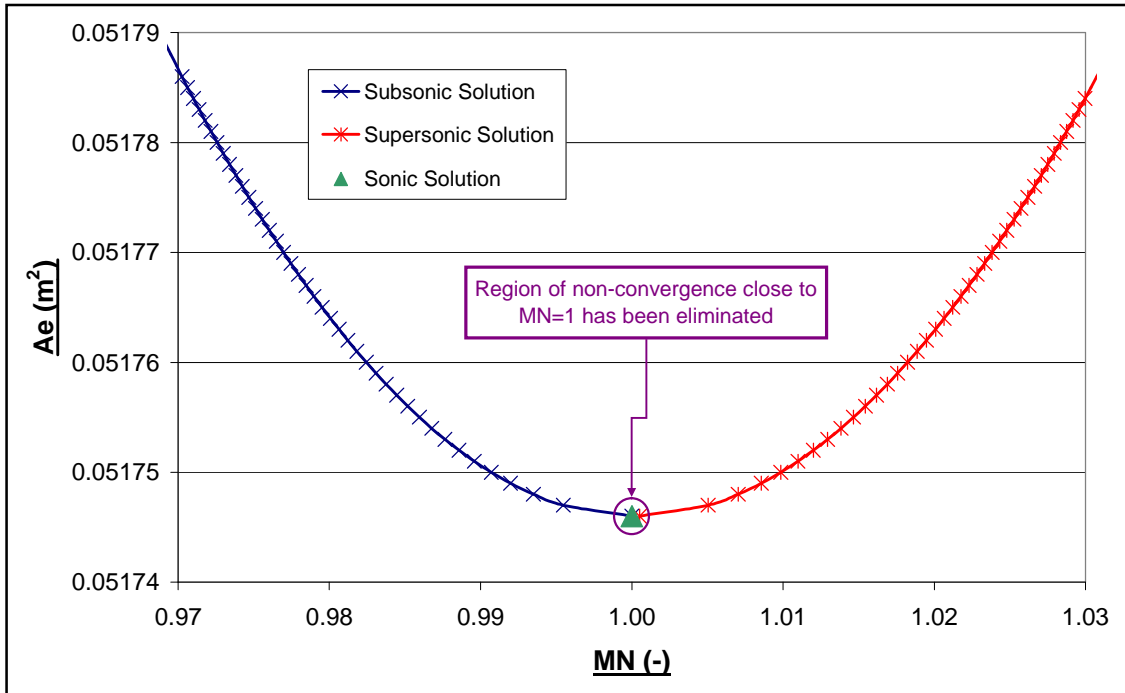


Fig: 2.3.9 Effects of using "Logarithmic Interpolation" for T for ϕ Fluid Tables on therm_WTtPtAe

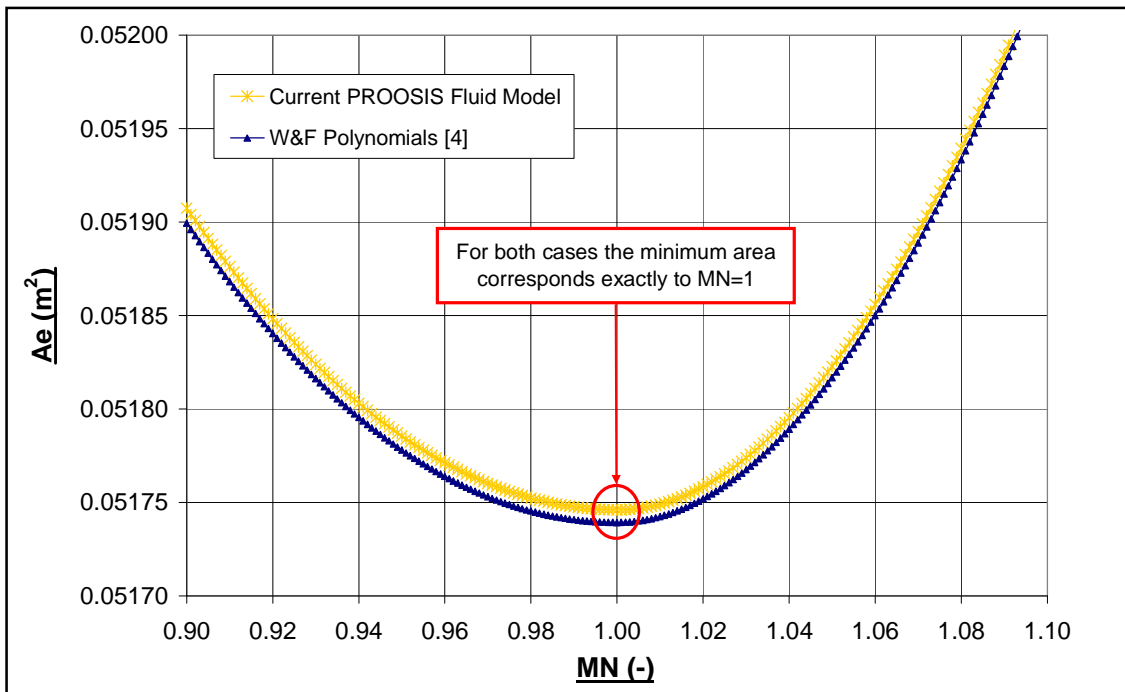


Fig: 2.3.10 Effects of using "Logarithmic Interpolation" for T for ϕ Fluid Tables (Current PROOSIS Fluid Model) on therm_WTtPtMN.

Chapter 2: Appendix 1

Sample PROOSIS Fluid Model XML Input File

Fuel: Jet-A

Fluid Model Type: Chemical Equilibrium (P=50atm)

```
<?xml version="1.0" encoding="UTF-8" standalone="no" ?>
<map version="1.0" type="Jet A Fluid Model With Complete Dissociation (50atm)" name="Dissociation50" description="Jet A Fluid Model With Complete
Dissociation (50atm)" cdate="11/05/2007" mdate="" revision="0.1">
<table type="3D" name="h_T" description="Enthalpy as a function of T, FARB and WAR">
<interp default="LINEAR" valid="{CONSTANT, LINEAR, SPLINE}" />
<extrap default="CONSTANT" valid="{FORBIDDEN, CONSTANT, LINEAR, SPLINE}" />
<axis1 id="WAR" description="Water to Air Ratio (-)" value="{0.00, 0.10}" />
<axis2 id="T" description="Temperature(K)" value="{200, 250, 300, 350, 400, 450, 500, 550, 600, 650, 700, 750, 800, 850, 900, 950, 1000, 1050, 1100, 1150,
1200, 1250, 1300, 1350, 1400, 1450, 1500, 1550, 1600, 1650, 1700, 1750,1800, 1850, 1900, 1950, 2000, 2050, 2100, 2150, 2200, 2250, 2300, 2350, 2400, 2450, 2500, 2550, 2600,
2650, 2700, 2750, 2800, 2850, 2900, 2950, 3000}" />
<axis3 id="FARB" description="Burnt Fuel to Air Ratio (-)" value="{0.00, 0.02, 0.04, 0.06}" />
<return id="h" description="Specific Enthalpy (J/kg)" value="{ {-98466.2, -99790, -101100, -102300}, {-48333.2, -49060, -49800, -50400}, {1858.8, 1890,
1900, 1900}, {52175.8, 53120, 54000, 54900}, {102707.8, 104680, 106600, 108400}, {153553.8, 156670, 159700, 162500}, {204803.8, 209140, 213300, 217300}, {256533.8,
262180, 267600, 272800}, {308793.8, 315820, 322600, 329100}, {361643.8, 370100, 378200, 386100}, {415083.8, 425040, 434600, 443800}, {469133.8, 480650, 491700,
502400}, {523783.8, 536910, 549500, 561700}, {579013.8, 593800, 608000, 621700}, {634813.8, 651310, 667200, 682400}, {691143.8, 709420, 727000, 743900}, {747993.8,
768090, 787420, 806000}, {805353.8, 827315, 848440, 868700}, {863193.8, 887066.3, 910020, 932100}, {921493.8, 947323, 972150, 996000}, {980243.8, 1008070, 1034800,
1060400}, {1039434, 1069280, 1097960, 1125400}, {1099034, 1130960, 1161600, 1190900}, {1159034, 1193090, 1225720, 1256900}, {1219534, 1255660, 1290300, 1323400},
{1280434, 1318680, 1355340, 1390300}, {1341634, 1382130, 1420820, 1457600}, {1403334, 1446030, 1486760, 1525400}, {1465534, 1510380, 1553140, 1593610}, {1528034,
1575180, 1619970, 1662230}, {1591034, 1640440, 1687253, 1731280}, {1654434, 1706170, 1755005, 1800770}, {1718334, 1772380, 1823236, 1870700}, {1782534, 1839090,
1891960, 1941110}, {1847334, 1906270, 1961210, 2012030}, {1912534, 1974070, 2031000, 2083490}, {1978134, 2042370, 2101380, 2155570}, {2044334, 2111370, 2172380,
2228350}, {2110934, 2180870, 2244070, 2301920}, {2178034, 2251070, 2316500, 2376430}, {2245634, 2322070, 2389750, 2452013}, {2313834, 2393770, 2463920, 2528876},
{2382534, 2466270, 2539100, 2607237}, {2451834, 2539770, 2615430, 2687350}, {2521834, 2614170, 2693050, 2769510}, {2592334, 2689670, 2772100, 2854030}, {2663634,
2766470, 2852800, 2941230}, {2735634, 2844470, 2935300, 3031440}, {2808434, 2923280, 3019900, 3125000}, {2882134, 3004870, 3106800, 3222200}, {2956634, 3087570,
3196100, 3323310}, {3032234, 3172070, 3288300, 3428550}, {3108834, 3258570, 3383400, 3538090}, {3186534, 3347270, 3481800, 3652000}, {3265534, 3438270, 3583700,
3770500}, {3345834, 3531670, 3689200, 3893400}, {3427534, 3627770, 3798500, 4020900}, { {-106100, -107100, -108200, -109200}, {-52100, -52700, -53300, -53800}, {2000,
2000, 2000, 2100}, {56200, 57000, 57800, 58500}, {110700, 112400, 114000, 115600}, {165700, 168300, 170800, 173300}, {221100, 224800, 228300, 231700}, {277060,
281900, 286500, 290900}, {333670, 339700, 345400, 350900}, {390950, 398200, 405100, 411800}, {448920, 457400, 465600, 473500}, {507590, 517400, 526900, 536000},
{566970, 578200, 589000, 599400}, {627030, 639700, 651800, 663600}, {687760, 701900, 715500, 728600}, {749150, 764800, 779800, 794400}, {811170, 828400, 844900,
860900}, {873810, 892600, 910700, 928200}, {937050, 957500, 977200, 996200}, {1000880, 1023030, 1044300, 1064900}, {1065280, 1089140, 1112100, 1134200}, {1130230,
1155840, 1180500, 1204200}, {1195732, 1223110, 1249400, 1274700}, {1261776, 1290950, 1319000, 1345900}, {1328360, 1359340, 1389100, 1417600}, {1395480, 1428280,
1459800, 1489900}, {1463150, 1497780, 1531000, 1562700}, {1531370, 1567840, 1602800, 1636100}, {1600150, 1638450, 1675100, 1709900}, {1669500, 1709640, 1748000,
1784300}, {1739440, 1781410, 1821470, 1859300}, {1809990, 1853780, 1895520, 1934800}, {1881170, 1926775, 1970170, 2010800}, {1953010, 2000415, 2045440, 2087400},
{2025530, 2074734, 2121370, 2164700}, {2098780, 2149770, 2197990, 2242600}, {2172790, 2225560, 2275360, 2321300}, {2247600, 2302150, 2353530, 2400900}, {2323300,
2379610, 2432580, 2481410}, {2399800, 2458000, 2512590, 2563090}, {2477400, 2537390, 2593670, 2646080}, {2555900, 2617870, 2675913, 2730600}, {2635600, 2699530,
2759475, 2816930}, {2716400, 2782480, 2844507, 2905330}, {2798500, 2866840, 2931190, 2996160}, {2882000, 2952760, 3019730, 3089760}, {2966900, 3040400, 3110350,
3186490}, {3053300, 3129800, 3203300, 3286750}, {3141500, 3221300, 3298850, 3390878}, {3231500, 3315100, 3397300, 3499231}, {3323300, 3411300, 3498950, 3612110},
{3417300, 3510100, 3604120, 3729790}, {3513500, 3611800, 3713130, 3852480}, {3612200, 3716700, 3826300, 3980370}, {3713300, 3824900, 3943900, 4113580}, {3817300,
3936800, 4066200, 4252220}, {3924100, 4052500, 4193500, 4396340}}" />
</table>
<table type="3D" name="phi_T" description="Entropy Function as a function of T, FARB and WAR">
```

Advanced Performance Simulation of Gas Turbine Components and Fluid Thermodynamic Properties

```

<interp default="LINEAR" valid="{CONSTANT, LINEAR, SPLINE}" />
<extrap default="CONSTANT" valid="{FORBIDDEN, CONSTANT, LINEAR, SPLINE}" />
<axis1 id="WAR" description="Water to Air Ratio (-)" value="{0.00, 0.10}" />
<axis2 id="ln(T)" description="Natural log of Temperature" value="{5.29831736654804, 5.52146091786225, 5.70378247465620, 5.85793315448346, 5.99146454710798, 6.10924758276437, 6.21460809842219, 6.30991827822652, 6.39692965521615, 6.47697236288968, 6.55108033504340, 6.62007320653036, 6.68461172766793, 6.74523634948436, 6.80239476332431, 6.85646198459459, 6.90775527898214, 6.95654544315157, 7.00306545878646, 7.04751722135730, 7.09007683577609, 7.13089883029635, 7.17011954344963, 7.20785987143248, 7.24422751560335, 7.27931883541462, 7.31322038709030, 7.34601020991329, 7.37775890822787, 7.40853056689463, 7.43838353004431, 7.46737106691756, 7.49554194388426, 7.52294091807237, 7.54960916515453, 7.57558465155779, 7.60090245954208, 7.62559507213245, 7.64969262371151, 7.67322312112171, 7.69621263934641, 7.71868549519847, 7.74066440191724, 7.76217060713820, 7.78322401633604, 7.80384330353877, 7.82404601085629, 7.84384863815247, 7.86326672400957, 7.88231491898027, 7.90100705199242, 7.91935619066062, 7.93737469616330, 7.95507427326270, 7.97246601597457, 7.98956044933387, 8.00636756765025}" />
<axis3 id="FARB" description="Burnt Fuel to Air Ratio (-)" value="{0.00, 0.02, 0.04, 0.06}" />
<return id="phi" description="Entropy Function(J/(kg*K))" value="{5336.9, 5391.4, 5405.9, 5395.4, 5560.7, 5617.8, 5634.9, 5626.8, 5743.7, 5803.6, 5823.3, 5817.8, 5898.8, 5961.5, 5983.9, 5981, 6033.7, 6099.2, 6124.3, 6123.9, 6153.5, 6221.6, 6249.3, 6251.4, 6261.5, 6332.2, 6362.4, 6366.9, 6360.1, 6433.3, 6465.8, 6472.7, 6451, 6526.6, 6561.5, 6570.5, 6535.6, 6613.5, 6650.6, 6661.7, 6614.8, 6694.9, 6734.1, 6747.4, 6689.4, 6771.7, 6812.9, 6828.1, 6760, 6844.3, 6887.5, 6904.7, 6826.9, 6913.3, 6958.5, 6977.4, 6890.7, 6979, 7026.1, 7046.9, 6951.6, 7041.8, 7090.7, 7113.3, 7009.9, 7102, 7152.7, 7177, 7065.9, 7159.8, 7212.3, 7238.2, 7119.7, 7215.4, 7269.6, 7297.2, 7171.5, 7269, 7324.8, 7354, 7221.5, 7320.7, 7378.1, 7408.9, 7269.9, 7370.6, 7429.7, 7461.9, 7316.6, 7419, 7479.6, 7513.3, 7361.9, 7465.9, 7528, 7563.1, 7405.9, 7511.4, 7575, 7611.4, 7448.6, 7555.7, 7620.6, 7658.4, 7490.2, 7598.7, 7665, 7704.1, 7530.6, 7640.6, 7708.3, 7748.5, 7570.1, 7681.4, 7750.4, 7791.8, 7608.6, 7721.3, 7791.5, 7834.1, 7646.2, 7760.3, 7831.7, 7875.3, 7682.9, 7798.4, 7871, 7915.6, 7718.9, 7835.7, 7909.4, 7955, 7754.1, 7872.3, 7947.1, 7993.5, 7788.7, 7908.1, 7984, 8031.4, 7822.5, 7943.3, 8020.3, 8068.5, 7855.8, 7977.9, 8055.9, 8105, 7888.4, 8011.9, 8091, 8140.9, 7920.6, 8045.5, 8125.5, 8176.4, 7952.1, 8078.5, 8159.6, 8211.4, 7983.2, 8111.1, 8193.3, 8246.2, 8013.9, 8143.4, 8226.6, 8280.7, 8044.1, 8175.2, 8259.7, 8315.2, 8073.9, 8206.8, 8292.5, 8349.7, 8103.3, 8238.2, 8325.2, 8384.2, 8132.4, 8269.3, 8357.8, 8419.1, 8161.2, 8300.3, 8390.4, 8454.3, 8189.8, 8331.2, 8423.1, 8490.1, 8218, 8362.1, 8455.9, 8526.4, 8246.1, 8392.9, 8489, 8563.4, 8274, 8423.8, 8522.4, 8601.2, 8301.7, 8454.8, 8556.2, 8639.8, 8329.3, 8486, 8590.5, 8679.3, 8356.8, 8517.4, 8625.4, 8719.6, 8384.3, 8549.1, 8660.8, 8760.8, 8411.7, 8581, 8696.9, 8802.9, 8439.2, 8613.3, 8733.6, 8845.7, 5694.4, 5712.8, 5707.8, 5684.2, 5935.4, 5955.9, 5953, 5931.3, 6132.6, 6155.3, 6154.6, 6135.1, 6299.9, 6324.9, 6326.5, 6309.1, 6445.5, 6472.9, 6476.7, 6461.4, 6574.9, 6604.5, 6610.5, 6597.4, 6691.6, 6723.5, 6731.6, 6720.5, 6798.3, 6832.3, 6842.4, 6833.3, 6896.8, 6932.8, 6944.9, 6937.8, 6988.5, 7026.5, 7040.5, 7035.2, 7074.4, 7114.3, 7130.2, 7126.6, 7155.4, 7197.1, 7214.7, 7212.9, 7232, 7275.5, 7294.9, 7294.7, 7304.8, 7350.1, 7371.1, 7372.5, 7374.3, 7421.2, 7443.8, 7446.8, 7440.6, 7489.2, 7513.4, 7518, 7504.3, 7554.4, 7580.2, 7586.2, 7565.4, 7617.1, 7644.4, 7651.9, 7624.2, 7677.5, 7706.3, 7715.1, 7681, 7735.7, 7765.9, 7776.2, 7735.8, 7792, 7823.6, 7835.2, 7788.8, 7846.5, 7879.4, 7892.3, 7840.2, 7899.2, 7933.5, 7947.7, 7890, 7950.4, 7986, 8001.4, 7938.5, 8000.2, 8037, 8053.5, 7985.6, 8048.6, 8086.6, 8104.3, 8031.5, 8095.7, 8134.9, 8153.6, 8076.2, 8141.6, 8182, 8201.7, 8119.9, 8186.5, 8227.9, 8248.6, 8162.5, 8230.3, 8272.8, 8294.4, 8204.3, 8273.1, 8316.6, 8339.2, 8245.2, 8315.1, 8359.6, 8382.9, 8285.3, 8356.2, 8401.6, 8425.8, 8324.7, 8396.5, 8442.9, 8467.8, 8363.4, 8436.2, 8483.4, 8509, 8401.4, 8475.2, 8523.2, 8549.4, 8438.9, 8513.5, 8562.3, 8589.3, 8475.8, 8551.4, 8601, 8628.6, 8512.3, 8588.7, 8639, 8667.4, 8548.3, 8625.6, 8676.7, 8705.8, 8584, 8662.1, 8714, 8744, 8619.3, 8698.3, 8750.9, 8782, 8654.3, 8734.2, 8787.7, 8819.9, 8689.1, 8769.8, 8824.2, 8858, 8723.6, 8805.4, 8860.7, 8896.2, 8758, 8840.8, 8897.3, 8934.8, 8792.3, 8876.2, 8933.9, 8973.9, 8826.6, 8911.6, 8970.7, 9013.6, 8860.8, 8947.1, 9007.8, 9054, 8895.1, 8982.9, 9045.3, 9095.3, 8929.4, 9018.8, 9083.3, 9137.5, 8963.9, 9055.1, 9121.9, 9180.7, 8998.6, 9091.7, 9161.2, 9224.9, 9033.5, 9128.9, 9201.2, 9270.2, 9068.7, 9166.5, 9242.1, 9316.5, 9104.2, 9204.7, 9283.9, 9363.9, 9140.2, 9243.6, 9326.7, 9412.3}" />
</table>
= <table type="3D" name="gam_T" description="Isentropic Coefficient (gam) as a function of T, FARB and WAR">
<interp default="LINEAR" valid="{CONSTANT, LINEAR, SPLINE}" />
<extrap default="CONSTANT" valid="{FORBIDDEN, CONSTANT, LINEAR, SPLINE}" />
<axis1 id="WAR" description="Water to Air Ratio (-)" value="{0.00, 0.10}" />
<axis2 id="T" description="Temperature(K)" value="{200, 250, 300, 350, 400, 450, 500, 550, 600, 650, 700, 750, 800, 850, 900, 950, 1000, 1050, 1100, 1150, 1200, 1250, 1300, 1350, 1400, 1450, 1500, 1550, 1600, 1650, 1700, 1750, 1800, 1850, 1900, 1950, 2000, 2050, 2100, 2150, 2200, 2250, 2300, 2350, 2400, 2450, 2500, 2550, 2600, 2650, 2700, 2750, 2800, 2850, 2900, 2950, 3000}" />
<axis3 id="FARB" description="Burnt Fuel to Air Ratio (-)" value="{0.00, 0.02, 0.04, 0.06}" />
<return id="gam" description="Isentropic Coefficient(-)" value="{1.4013, 1.3956, 1.3903, 1.3853, 1.4009, 1.3934, 1.3864, 1.3799, 1.3999, 1.3907, 1.3823, 1.3745, 1.3981, 1.3875, 1.3779, 1.3691, 1.3952, 1.3836, 1.3731, 1.3636, 1.3913, 1.379, 1.3679, 1.3578, 1.3866, 1.3738, 1.3622, 1.3518, 1.3813, 1.3682, 1.3563, 1.3457, 1.3757, 1.3623, 1.3503, 1.3395, 1.37, 1.3565, 1.3444, 1.3334, 1.3643, 1.3507, 1.3385, 1.3276, 1.3588, 1.3451, 1.3329, 1.3219, 1.3536, 1.3398, 1.3276, 1.3166,

```


Advanced Performance Simulation of Gas Turbine Components and Fluid Thermodynamic Properties

```
{1.3487, 1.3349, 1.3226, 1.3116}, {1.3441, 1.3302, 1.3179, 1.3069}, {1.3397, 1.3259, 1.3135, 1.3026}, {1.3357, 1.3218, 1.3094, 1.2985}, {1.3318, 1.3179, 1.3056, 1.2947},
{1.3282, 1.3143, 1.302, 1.2911}, {1.3248, 1.3109, 1.2987, 1.2878}, {1.3216, 1.3077, 1.2955, 1.2848}, {1.3186, 1.3047, 1.2925, 1.2819}, {1.3156, 1.3018, 1.2897, 1.2792},
{1.3127, 1.299, 1.287, 1.2766}, {1.3099, 1.2962, 1.2844, 1.2742}, {1.3071, 1.2936, 1.2819, 1.2719}, {1.3044, 1.2909, 1.2794, 1.2697}, {1.3017, 1.2884, 1.277, 1.2676}, {1.299,
1.2858, 1.2747, 1.2655}, {1.2964, 1.2833, 1.2724, 1.2635}, {1.2938, 1.2808, 1.2701, 1.2615}, {1.2912, 1.2782, 1.2678, 1.2595}, {1.2886, 1.2757, 1.2655, 1.2575}, {1.2861,
1.2732, 1.2632, 1.2555}, {1.2836, 1.2706, 1.2609, 1.2534}, {1.281, 1.2681, 1.2585, 1.2512}, {1.2786, 1.2654, 1.256, 1.2488}, {1.2761, 1.2628, 1.2535, 1.2463}, {1.2736, 1.2601,
1.2509, 1.2435}, {1.2711, 1.2573, 1.2481, 1.2404}, {1.2687, 1.2545, 1.2453, 1.2371}, {1.2662, 1.2516, 1.2423, 1.2334}, {1.2638, 1.2487, 1.2391, 1.2294}, {1.2613, 1.2456,
1.2357, 1.225}, {1.2588, 1.2425, 1.2322, 1.2203}, {1.2562, 1.2393, 1.2285, 1.2155}, {1.2537, 1.236, 1.2247, 1.2104}, {1.2511, 1.2326, 1.2207, 1.2054}, {1.2485, 1.2292, 1.2167,
1.2004}, {1.2459, 1.2257, 1.2125, 1.1955}, {1.2432, 1.2222, 1.2084, 1.1909}, {1.2406, 1.2187, 1.2043, 1.1867}, {1.2379, 1.2153, 1.2002, 1.1828}, {1.2352, 1.2118, 1.1963,
1.1793}, {1.2325, 1.2085, 1.1927, 1.1762}, {1.2298, 1.2053, 1.1892, 1.1736}, {1.2271, 1.2022, 1.1861, 1.1713}, {1.2245, 1.1991, 1.183, 1.1687}, {1.2219, 1.196, 1.18, 1.166,
1.3726}, {1.3883, 1.381, 1.3742, 1.3678}, {1.3861, 1.3777, 1.3699, 1.3627}, {1.3828, 1.3736, 1.3651, 1.3572}, {1.3786, 1.3688, 1.3598, 1.3515}, {1.3736, 1.3634, 1.3541,
1.3455}, {1.3681, 1.3577, 1.3481, 1.3394}, {1.3624, 1.3518, 1.3421, 1.3332}, {1.3566, 1.3458, 1.3361, 1.3271}, {1.3508, 1.34, 1.3302, 1.3212}, {1.3452, 1.3343, 1.3245, 1.3155},
{1.3398, 1.3289, 1.3191, 1.3101}, {1.3347, 1.3238, 1.314, 1.305}, {1.3298, 1.319, 1.3092, 1.3002}, {1.3253, 1.3144, 1.3046, 1.2957}, {1.3209, 1.3101, 1.3003, 1.2914}, {1.3168,
1.306, 1.2963, 1.2874}, {1.3129, 1.3022, 1.2924, 1.2837}, {1.3093, 1.2985, 1.2889, 1.2802}, {1.3057, 1.2951, 1.2855, 1.2769}, {1.3024, 1.2918, 1.2822, 1.2737}, {1.2991, 1.2886,
1.2792, 1.2708}, {1.296, 1.2856, 1.2763, 1.268}, {1.2929, 1.2826, 1.2734, 1.2654}, {1.2899, 1.2797, 1.2707, 1.2629}, {1.2869, 1.2769, 1.2681, 1.2605}, {1.284, 1.2742, 1.2655,
1.2582}, {1.281, 1.2714, 1.263, 1.2559}, {1.2781, 1.2687, 1.2605, 1.2537}, {1.2752, 1.266, 1.2581, 1.2516}, {1.2723, 1.2634, 1.2557, 1.2494}, {1.2693, 1.2606, 1.2532, 1.2473},
{1.2663, 1.2579, 1.2507, 1.245}, {1.2633, 1.2552, 1.2482, 1.2428}, {1.2603, 1.2524, 1.2457, 1.2404}, {1.2572, 1.2495, 1.243, 1.2379}, {1.2541, 1.2466, 1.2403, 1.2352}, {1.251,
1.2437, 1.2375, 1.2323}, {1.2478, 1.2407, 1.2346, 1.2291}, {1.2446, 1.2376, 1.2316, 1.2257}, {1.2413, 1.2344, 1.2284, 1.222}, {1.2381, 1.2312, 1.2251, 1.2179}, {1.2347, 1.2278,
1.2217, 1.2136}, {1.2314, 1.2244, 1.2181, 1.2091}, {1.2281, 1.221, 1.2143, 1.2044}, {1.2247, 1.2175, 1.2105, 1.1996}, {1.2214, 1.2139, 1.2065, 1.1947}, {1.218, 1.2103, 1.2025,
1.19}, {1.2147, 1.2067, 1.1984, 1.1855}, {1.2114, 1.2031, 1.1944, 1.1812}, {1.2082, 1.1995, 1.1904, 1.1773}, {1.205, 1.196, 1.1865, 1.1736}, {1.2019, 1.1926, 1.1828, 1.1704},
{1.1989, 1.1893, 1.1794, 1.1675}, {1.196, 1.1862, 1.1761, 1.165}, {1.1931, 1.1832, 1.1732, 1.1628}}" />
```

```
</table>
```

```
= <table type="3D" name="mu_T" description="Dynamic Viscosity as a function of T, FARB and WAR" >
```

```
<interp default="LINEAR" valid="{CONSTANT, LINEAR, SPLINE}" />
```

```
<extrap default="CONSTANT" valid="{FORBIDDEN, CONSTANT, LINEAR, SPLINE}" />
```

```
<axis1 id="WAR" description="Water to Air Ratio (-)" value="{0.00, 0.10}" />
```

```
<axis2 id="T" description="Temperature(K)" value="{200, 250, 300, 350, 400, 450, 500, 550, 600, 650, 700, 750, 800, 850, 900, 950, 1000, 1050, 1100, 1150,
1200, 1250, 1300, 1350, 1400, 1450, 1500, 1550, 1600, 1650, 1700, 1750,1800, 1850, 1900, 1950, 2000, 2050, 2100, 2150, 2200, 2250, 2300, 2350, 2400, 2450, 2500, 2550, 2600,
2650, 2700, 2750, 2800, 2850, 2900, 2950, 3000}" />
```

```
<axis3 id="FARB" description="Burnt Fuel to Air Ratio (-)" value="{0.00, 0.02, 0.04, 0.06}" />
```

```
<return id="mu" description="Dynamic Viscosity (Ns/m2)" value="{1.363E-05, 1.329E-05, 1.296E-05, 1.266E-05}, {1.630E-05, 1.600E-05, 1.569E-05, 1.538E-
05}, {1.875E-05, 1.847E-05, 1.819E-05, 1.790E-05}, {2.102E-05, 2.078E-05, 2.052E-05, 2.025E-05}, {2.316E-05, 2.295E-05, 2.272E-05, 2.247E-05}, {2.520E-05, 2.501E-05, 2.481E-
05, 2.459E-05}, {2.715E-05, 2.699E-05, 2.680E-05, 2.661E-05}, {2.902E-05, 2.888E-05, 2.872E-05, 2.855E-05}, {3.083E-05, 3.071E-05, 3.057E-05, 3.042E-05}, {3.259E-05, 3.248E-
05, 3.236E-05, 3.223E-05}, {3.429E-05, 3.419E-05, 3.409E-05, 3.399E-05}, {3.595E-05, 3.587E-05, 3.579E-05, 3.569E-05}, {3.756E-05, 3.749E-05, 3.742E-05, 3.735E-05}, {3.914E-
05, 3.908E-05, 3.902E-05, 3.897E-05}, {4.069E-05, 4.064E-05, 4.059E-05, 4.055E-05}, {4.220E-05, 4.216E-05, 4.212E-05, 4.209E-05}, {4.369E-05, 4.365E-05, 4.362E-05, 4.361E-
05}, {4.514E-05, 4.511E-05, 4.509E-05, 4.509E-05}, {4.657E-05, 4.655E-05, 4.654E-05, 4.654E-05}, {4.797E-05, 4.795E-05, 4.795E-05, 4.797E-05}, {4.936E-05, 4.934E-05, 4.934E-
05, 4.937E-05}, {5.072E-05, 5.070E-05, 5.071E-05, 5.074E-05}, {5.206E-05, 5.205E-05, 5.206E-05, 5.210E-05}, {5.339E-05, 5.338E-05, 5.340E-05, 5.345E-05}, {5.470E-05, 5.469E-
05, 5.471E-05, 5.477E-05}, {5.599E-05, 5.599E-05, 5.602E-05, 5.608E-05}, {5.728E-05, 5.727E-05, 5.731E-05, 5.738E-05}, {5.855E-05, 5.855E-05, 5.858E-05, 5.866E-05}, {5.981E-
05, 5.981E-05, 5.985E-05, 5.993E-05}, {6.107E-05, 6.106E-05, 6.110E-05, 6.119E-05}, {6.231E-05, 6.230E-05, 6.235E-05, 6.244E-05}, {6.354E-05, 6.353E-05, 6.358E-05, 6.368E-
05}, {6.476E-05, 6.476E-05, 6.481E-05, 6.491E-05}, {6.598E-05, 6.597E-05, 6.602E-05, 6.613E-05}, {6.718E-05, 6.718E-05, 6.723E-05, 6.734E-05}, {6.838E-05, 6.837E-05, 6.843E-
05, 6.855E-05}, {6.957E-05, 6.956E-05, 6.962E-05, 6.974E-05}, {7.076E-05, 7.075E-05, 7.081E-05, 7.093E-05}, {7.194E-05, 7.192E-05, 7.198E-05, 7.211E-05}, {7.311E-05, 7.309E-
05, 7.315E-05, 7.328E-05}, {7.427E-05, 7.426E-05, 7.432E-05, 7.445E-05}, {7.543E-05, 7.541E-05, 7.547E-05, 7.560E-05}, {7.658E-05, 7.656E-05, 7.662E-05, 7.673E-05}, {7.773E-
05, 7.771E-05, 7.777E-05, 7.790E-05}, {7.888E-05, 7.885E-05, 7.891E-05, 7.904E-05}, {8.001E-05, 7.998E-05, 8.004E-05, 8.017E-05}, {8.115E-05, 8.111E-05, 8.117E-05, 8.129E-
05}, {8.228E-05, 8.224E-05, 8.229E-05, 8.241E-05}, {8.340E-05, 8.336E-05, 8.340E-05, 8.351E-05}, {8.452E-05, 8.448E-05, 8.452E-05, 8.461E-05}, {8.564E-05, 8.559E-05, 8.562E-
05, 8.571E-05}, {8.676E-05, 8.670E-05, 8.672E-05, 8.680E-05}, {8.787E-05, 8.781E-05, 8.782E-05, 8.788E-05}, {8.898E-05, 8.891E-05, 8.891E-05, 8.895E-05}, {9.009E-05, 9.002E-
05, 9.000E-05, 9.002E-05}, {9.120E-05, 9.112E-05, 9.109E-05, 9.108E-05}, {9.231E-05, 9.221E-05, 9.217E-05, 9.213E-05}, {1.326E-05, 1.295E-05, 1.264E-05, 1.236E-05},
{1.598E-05, 1.565E-05, 1.533E-05, 1.501E-05}, {1.849E-05, 1.817E-05, 1.785E-05, 1.754E-05}, {2.084E-05, 2.054E-05, 2.024E-05, 1.994E-05}, {2.307E-05, 2.280E-05, 2.252E-05,
2.223E-05}, {2.520E-05, 2.495E-05, 2.469E-05, 2.443E-05}, {2.723E-05, 2.700E-05, 2.677E-05, 2.654E-05}, {2.919E-05, 2.899E-05, 2.878E-05, 2.857E-05}, {3.108E-05, 3.090E-05,
3.071E-05, 3.053E-05}, {3.290E-05, 3.275E-05, 3.258E-05, 3.242E-05}, {3.468E-05, 3.454E-05, 3.440E-05, 3.426E-05}, {3.640E-05, 3.628E-05, 3.616E-05, 3.605E-05}, {3.808E-05,
3.798E-05, 3.788E-05, 3.779E-05}, {3.972E-05, 3.964E-05, 3.956E-05, 3.948E-05}, {4.132E-05, 4.126E-05, 4.119E-05, 4.114E-05}, {4.289E-05, 4.284E-05, 4.279E-05, 4.275E-05},
{4.443E-05, 4.439E-05, 4.436E-05, 4.434E-05}, {4.593E-05, 4.591E-05, 4.589E-05, 4.589E-05}, {4.741E-05, 4.739E-05, 4.739E-05, 4.740E-05}, {4.886E-05, 4.885E-05, 4.887E-05,
4.889E-05}, {5.028E-05, 5.029E-05, 5.031E-05, 5.035E-05}, {5.176E-05, 5.174E-05, 5.179E-05, 5.179E-05}, {5.307E-05, 5.309E-05, 5.314E-05, 5.321E-05}, {5.443E-05, 5.447E-05,
5.453E-05, 5.460E-05}, {5.578E-05, 5.583E-05, 5.589E-05, 5.598E-05}, {5.711E-05, 5.717E-05, 5.724E-05, 5.734E-05}, {5.843E-05, 5.849E-05, 5.858E-05, 5.869E-05}, {5.974E-05,
```


Chapter 2: References

- [1] Katsourou, M., Sept. 2005, "Implementation of Accurate Gas Properties on Gas Turbine Simulations", MSc Thesis, School of Engineering, Department of Power and Propulsion, Cranfield University.
- [2] Laurans, D., Sept. 2006, "Development of Accurate Fluid Models for Gas Turbine Performance Calculations", Exchange Student Training Period Report, School of Engineering, Department of Power and Propulsion, Cranfield University.
- [3] Diara, F., Sept. 2007, "Advanced Performance Modelling of Fluid and Thermodynamic Functions for Gas Turbine Mixers and Nozzles", MSc Thesis, School of Engineering, Department of Power and Propulsion, Cranfield University.
- [4] Walsh. P.P. and Fletcher. P., 1998, "Gas Turbine Performance", 2nd Edition, Oxford: Blackwell Science.
- [5] Gordon, S. and McBride, B.J., Oct. 1994, "Computer Program for Calculation of Complex Chemical Equilibrium and Applications: Part I" NASA RP 1311.
- [6] Gordon, S. and McBride, B.J., Jun. 1996, "Computer Program for Calculation of Complex Chemical Equilibrium and Applications: Part II" NASA RP 1311.
- [7] Alvarez, Ulizar, J.I., Jan. 1998, "Simulation of Multi Fluid Gas Turbines", PhD Thesis, School of Engineering, Department of Power and Propulsion, Cranfield University.
- [8] Guha, A., 2001, "An Efficient Generic Method for Calculating the Properties of Combustion Products", Proceedings of the Institution of Mechanical Engineers, 215, 3; Wilson Applied Science & Technology Abstracts pp.375-387.
- [9] Bucker, D., Span, R. and Wagner, W., Jan. 2003, "Thermodynamic Property Models for Moist Air and Combustion Gases", ASME Journal of Engineering for Gas Turbines and Power, Vol.125, pp.374-384.
- [10] Morley, C., "Gaseq – A Chemical Equilibrium Program for Windows" Official Website, URL: <http://www.arcl02.dsl.pipex.com/>
- [11] Gordon, S. and McBride, B.J., 1992, "Computer Program for Calculation of Complex Chemical Equilibrium Compositions, Rocket Performance, Incident and Reflected Shocks and Chapman-Jouguet Detonations" NASA SP 273.
- [12] Sethi, V., Jackson, A. and Pilidis, P., (Cranfield University), 2007, "PROOSIS Standard Component Library: Fluid Model Specification" VIVACE 2.4.4/CU/T/076003.
- [13] ThermoBuild – NASA Online Interactive Tool to Obtain Thermodynamic Data used in NASA Thermodynamic Software, Official Website, URL: <http://cea.grc.nasa.gov>

- [14] Lefebvre, A. H., 1983, "Gas Turbine Combustion", 1st Edition, New York: Hemisphere Publishing Corporation.
- [15] Moss, J.B., 2003, "Combustion Thermodynamics and Thermochemistry", Fuels and Combustion Course Notes: School of Engineering – Cranfield University.
- [16] Goodger, E.M., 2000, "Transport Fuels Technology – Mobility for the Millennium", Norwich: Landfill Press.
- [17] National Aerospace Laboratory, 2007, "GSP v 10.0.1.6 – Gas Turbine Performance Simulation Program", GSP Official Website,
URL: <http://www.gspteam.com/main/main.shtml>
- [18] Kurzke, J., 2007, "GasTurb 11 – Gas Turbine Performance Simulation Software", GasTurb Official Website,
URL: <http://www.gasturb.de>
- [19] Empresarios Agrupados Internacional, 2006, "PROOSIS Users Manual", PROOSIS Official Website,
URL: <http://www.proosis.com>
- [20] Empresarios Agrupados Internacional, 2006, "PROOSIS User Language", PROOSIS Official Website,
URL: <http://www.proosis.com>
- [21] Sethi, V. and Pilidis, P., (Cranfield University), 2003, "PROOSIS Standard Component Library: Abstract Component THERM" VIVACE 2.4.4/CU/T/04XX.

Chapter 3: Advanced Performance Simulation of Gas Turbine Burners

Abstract

This chapter presents several advanced considerations which are important for accurate performance simulations of gas turbine combustion systems. The performance simulation model of the PROOSIS Burner component is presented with detailed descriptions of the pressure loss, efficiency and energy balance models. A component which calculates Burner emissions (inheriting from the main Burner component) is also introduced. The effects of liquid fuel sensible enthalpy on isolated Burner and Afterburner performance are discussed. The results of the validation of the PROOSIS Burner component against well established (industry standard approved) gas turbine performance simulation software are presented. The chapter concludes with several isolated Burner and Afterburner simulation case studies which analyse:

1. The effects of dissociation on isolated Burner and Afterburner performance.
2. The limitations of the Burner_Emissions component.

Chapter 3: Nomenclature

Symbols

Name	Description	Unit
Ae	Effective Area	m ²
Ang	Flow Angle	°
Ar	Argon (depending on context)	-
Ar	Atomic Weight (depending on context)	kg/(kg-mol)
CO	Carbon Monoxide	-
CO ₂	Carbon Dioxide	-
Csoot	Emitted Soot Concentration (Smoke Number)	-
dPqP	Fractional Pressure Loss	-
dPqPcold	Cold Fractional Pressure Loss	-
dPqP _{hot}	Hot Fractional Pressure Loss	-
EICO	Carbon Monoxide Emissions Index	g/kg
EINO _x	Emissions Index for Oxides of Nitrogen	g/Kg
EIUHC	Unburned Hydrocarbons Emissions Index	g/kg
F	Air Fraction	-
FAR	Reactant Total Fuel to Air Ratio (Burned + Unburned)	-
FARB	Burned Fuel to Air Ratio	-
FARBr	Reactant Burned Fuel to Burner Inlet Air Ratio	-
FARinj	Injected Fuel to Burner Inlet Air Ratio	-
FARr	Total Reactant Fuel to Air Ratio	-
FARU	Unburned Fuel to Air Ratio	-
FARUr	Reactant Unburned Fuel to Burner Inlet Air Ratio	-
GeoAm	Burner Geometric Maximum Cross Sectional Area	m ²
GeoAref	Burner Geometric Reference Area	m ²
GeoDref	Burner Geometric Reference Diameter	m
H ₂ O	Water	-
Hs	Sensible Enthalpy	J/kg
ht	Total Specific Enthalpy	J/kg
Kcold	Cold Loss Pressure Loss Factor	-
KEinlet	Power Associated with Inlet Flow Kinetic Energy	W
KEjet	Power Associated with Jet Kinetic Energy	W
Khot	Hot Loss Pressure Loss Factor	-
LHV	Lower Heating Value (Net Calorific Value)	J/kg
MCO	Mass of Carbon Monoxide	g
Mfuel	Fuel Mass	kg
MN	Mach Number	-
MNO _x	Mass of Oxides of Nitrogen	g
Mr	Molecular Mass	kg/(kg-mol)

Advanced Performance Simulation of Gas Turbine Components
and Fluid Thermodynamic Properties

Name	Description	Unit
MUHC	Mass of Unburned Hydrocarbons	g
N ₂	Nitrogen Molecule	-
NO _x	Oxides of Nitrogen	-
O ₂	Oxygen Molecule	-
P	Pressure	Pa
P _s	Static Pressure	Pa
P _t	Total Pressure	Pa
Q _{hyd}	Fuel Pump Hydraulic Power	W
Q _{loss}	Fuel Pump Mechanical Losses	W
Q _{out}	Fuel Pump Output Power	W
Q _{rate}	Heat Rate for Shaft Power Engines	J/(N*hr)
Q _{reject}	Fuel Pump Rejected Power	W
Q _{shaft}	Shaft Power	W
R	Gas Constant	J/(kg*K)
s ₁ ,s ₂s _n	Adaptive Scalars for Emissions Model	-
SFC	Specific Fuel Consumption	kg/(N*hr)
T	Temperature	K
tevap	Fuel Evaporation Time	s
T _{fl}	Flame Temperature	K
t _{res}	Burner Residence Time	s
T _s	Static Temperature	K
T _t	Total Temperature	K
UHC	Unburned Hydrocarbons	-
V	Velocity	m/s
V _b	Burner Volume	m ³
V _e	Burner Volume Occupied by the Evaporated Fuel	m ³
W	Mass Flow Rate	kg/s
W _{air}	Air Mass Flow Rate	kg/s
WAR	Water to Air Ratio	-
WCO	Rate of Carbon Monoxide Emissions	g/s
WUHC	Rate of Unburned Hydrocarbons Emissions	g/s
WNO _x	Rate of Oxides of Nitrogen Emissions	g/s

Greek Symbols

Name	Description	Unit
φ	Equivalence Ratio	-
η _b	Burner Efficiency	-
η _{th}	Thermal Efficiency	-
θ	Lefebvre's θ Parameter	-
ρ	Density	kg/m ³

Advanced Performance Simulation of Gas Turbine Components
and Fluid Thermodynamic Properties

Abbreviations

Name	Description	Unit
ACOC	Air Cooled Oil Cooler	-
CUHBR	Engine Model of a Three Spool High Bypass Ratio Turbofan Engine With Separate Exhausts (used for the isolated Burner Component Case Studies)	-
CULBR	Engine Model of a Two Spool Low Bypass Ratio Turbofan Engine With Mixed Exhausts & Reheat (used for the isolated Afterburner Component Case Studies)	-
CCD	Computational Combustor Dynamics	-
EEC	Electronic Engine Control	-
EU	European Union	-
FADEC	Full Authority Digital Control	-
FCOC	Fuel Cooled Oil Cooler	-
FlowCase	Either "Subsonic", "Sonic" or "Supersonic"	-
FMU	Fuel Metering Unit	-
FOHE	Fuel Oil Heat Exchanger	-
FP	Framework Package	-
HP	High Pressure	-
IATA	International Air Transport Association	-
ICAO	International Civil Aviation Authority	-
LP	Low Pressure	-
MTU	MTU Aero Engines	-
NTUA	National Technical University of Athens	-

Suffixes

The suffix "in" corresponds to a property at the Burner inlet.

The suffix "out" corresponds to a property at the Burner outlet.

The suffix "fuel" corresponds to a fuel property.

The suffix "_in" corresponds to a variable input as DATA by the user in the attributes editor of the Burner component.

The suffix "pz" corresponds to a property in the Burner primary zone.

Sub-Scripts

The sub-script "_{ref}" or "_{Ref}" corresponds to reference parameters.

The sub-script "_{Stoich}" corresponds to Stoichiometric values.

3.1: PROOSIS Burner Component Modelling

3.1.1: Introduction

This section describes the modelling of the Burner Component for the PROOSIS Standard Components Library (SCLib). The Burner component is used to simulate the performance of a range of combustion systems including the combustion chambers of gas turbine engines, reheat pipes of military aero engines and boiler burners.

The Burner component calculates the Burner outlet total pressure (P_{tout}) and either the Burner outlet total temperature (T_{tout}) (if the injected fuel mass flow rate (W_{fuel}) is provided) or the injected fuel mass flow rate (if the Burner outlet total temperature is provided) based on several data input options. Additionally, the values of the Burner outlet mass flow rate (W_{out}), burned fuel to air ratio (FAR_{Bout}), unburned fuel to air ratio (FAR_{Uout}), water to air ratio (WAR_{out}), and flow angle (Ang_{out}) are calculated.

3.1.2: Burner Component Hierarchy and Ports

Fig: 3.1.1 shows the PROOSIS icon, the ports and the port variables of the Burner component. The Burner component has one main flow inlet port, one main flow outlet port, a fuel inlet port and two outlet information ports.

NB: Fig: 3.1.1 highlights the Burner component port variables using both PROOSIS nomenclature (which is based on [1]) and conventional gas turbine engineering nomenclature (which is based on [2]).

The Burner component inlet mass flow rate (W_{in}), total temperature (T_{tin}), total pressure (P_{tin}), burned fuel to air ratio (FAR_{Bin}), unburned fuel to air ratio (FAR_{Uin}), water to air ratio (WAR_{in}) and flow angle (Ang_{in}) are main flow port variables and are obtained from the immediate upstream component (typically the high pressure compressor). The Burner fuel inlet port variables comprise the injected fuel mass flow rate (W_{fuel}) as well as the temperature (T_{fuel}) and pressure (P_{fuel}) of the injected fuel. The two information ports communicate the values of the fuel flow (W_{fuel}) and the fuel lower heating value (LHV) to the Performance Monitor component. These values are subsequently used by the Performance Monitor component to calculate some of the overall engine performance parameters e.g. specific fuel consumption and thermal efficiency. These calculations are discussed in *Section 3.1.6*.

The component hierarchy for the Burner component is illustrated in Fig: 3.1.2. The PROOSIS SCLib comprises the following Burner components:

1. Simple Burner component (which inherits from Abstract Component GasInGasOut).
2. Burner component with an emissions calculation model (which inherits from the simple Burner component).

In addition to all the Burner component calculations, the Burner_Emissions component calculates the emitted pollutants (NO_x, CO, UHC and smoke) using semi-empirical calculations. The exhaust gas composition is also calculated from the specified composition of air and fuel. The Burner_Emissions component is described in *Section 3.2*.

The fundamental station numbers for the Burner component in an engine depend on the Burner under consideration; for example in a simple turbojet without reheat, the stations are numbered 3 and 4 ^[2] for the Burner inlet and outlet respectively.

3.1.3: Burner Component Pressure Loss Model

In order to determine the Burner outlet total pressure (P_{tout}), the Burner fractional pressure loss ($dPqP$) is first determined. The Burner fractional pressure loss is defined as shown in [Eq. 3.1.1].

$$dPqP = \frac{(P_{tin} - P_{tout})}{P_{tin}} \quad \text{[Eq. 3.1.1]}$$

NB: $0 \leq dPqP < 1$ (For any other value an error message is displayed)

There are three options for obtaining the Burner fractional pressure loss. These options are discussed below. The user can select one of the three options outlined below via a switch in the attributes editor (refer to the “Glossary” section of the thesis) of the Burner component (Fig: 3.1.3 and Fig 3.1.4).

dPqP Calculation – Option 1:

Value of the Burner fractional pressure loss directly input by the user ($dPqP_{in}$)

If the value of the Burner fractional pressure loss is known, the user can directly input the value as DATA in the attributes editor of the Burner component (“Fig: 3.1.3” and “Fig 3.1.4”). The nomenclature for the variable representing the Burner fractional pressure loss directly input by the user is $dPqP_{in}$. However, the Burner outlet total pressure is calculated using $dPqP$ which is obtained as shown in [Eq. 3.1.2].

$$dPqP = dPqP_{in} \quad \text{[Eq. 3.1.2]}$$

NB: Option 1 is recommended for design point calculations.

dPqP Calculation – Option 2:

Calculating the value of the Burner fractional pressure loss ($dPqP$) based on pressure loss factors

If the Burner fractional pressure loss ($dPqP$) is not known, but the cold loss pressure loss factor (K_{cold_in}), the hot loss pressure loss factor (K_{hot_in}), the Burner inlet effective area (Ae_in), the FlowCase (Subsonic or Supersonic) and the Burner maximum cross sectional area ($GeoAm_in$) are known then $dPqP$ is calculated using [Eq. 3.1.3]. For this option the user must input the values of K_{cold_in} , K_{hot_in} , Ae_in and $GeoAm_in$ as DATA in the attributes editor of the Burner component (Fig: 3.1.3 and Fig 3.1.4).

$$dPqP = \left[\frac{Win^2}{2 \times \rho_{in} \times GeoAm_in^2 \times P_{tin}} \right] \times \left[K_{cold} + K_{hot} \left(\frac{T_{tout}}{T_{tin}} - 1 \right) \right] \quad \text{[Eq. 3.1.3]}$$

Where:

1. The value of the Burner inlet static density (ρ_{in}) is calculated using [Eq. 3.1.4].

$$\rho_{in} = \frac{P_{sin}}{R_{in} \times T_{sin}} \quad \text{[Eq. 3.1.4]}$$

Where:

- 1a. The Burner inlet Gas Constant (R_{in}) is obtained from the fluid model:

$$R_{in} = R_FARB(\text{fluid}, T_{sin}, FARBin, WARin)$$

- 1b. The Burner inlet static pressure (P_{sin}) and static temperature (T_{sin}) are obtained using the following thermodynamic function call:

$$\text{therm_WTtPtAe}(\text{fluid}, W_{in}, T_{tin}, P_{tin}, FARBin, WARin, Ae_{in}, MN_{in}, V_{in}, T_{sin}, P_{sin}, \text{FlowCase})$$

where: The FlowCase (either Subsonic or Supersonic) is defined by the user.

(Typically for Burner component calculations, it is highly unlikely that the inlet flow is Supersonic.)

2. The combustor cold loss is due to the dump of air, for cooling, being injected through the wall. Depending on geometric constraints of the combustor (including the diffuser) good designs typically have values of cold pressure loss between 2% and 4% of total pressure at design point. However, for high flight Mach number aero engines, the cold loss may be as high as 7%.

The value of the cold loss pressure loss factor (K_{cold}) is usually obtained from a cold run combustion chamber rig test using [Eq. 3.1.5].

$$K_{cold} = \frac{dPqP_{cold}}{\left(\frac{W1 \times \sqrt{Tt1}}{Pt1}\right)^2} \quad \text{[Eq. 3.1.5]}$$

NB: $dPqP_{cold}$ is the cold fractional pressure loss.

3. The combustor hot loss (fundamental loss) occurs in the combustion section of the flame tube. For Raleigh Flow, fundamental thermodynamics dictate that there is a pressure loss associated with heat release. The corresponding density increase results in an increased velocity which requires a pressure drop for the momentum change.

The value of the hot loss pressure loss factor (K_{hot}) is usually obtained from a hot run combustion chamber rig test using [Eq. 3.1.6].

$$K_{hot} = \frac{dPqP_{hot}}{\left(\frac{Tt2}{Tt1} - 1\right) \times \left(\frac{W1 \times \sqrt{Tt1}}{Pt1}\right)^2} \quad \text{[Eq. 3.1.6]}$$

NB: $dPqP_{hot}$ is the hot fractional pressure loss.

NB: Option 2 is recommended for off design calculations.

dPqP Calculation – Option 3:

Obtaining the value of the Burner fractional pressure loss (dPqP) from a user defined loss model

Alternatively, the Burner fractional pressure loss (dPqP) can be obtained from a user defined loss model (e.g. from a fractional pressure loss map of dPqP as a function of the Burner inlet non dimensional mass flow ^{[3] & [4]}).

NB: Option 3 is recommended for off design calculations and only for level 1 users of PROOSIS as the Burner source file will need to be modified.

Once the Burner fractional pressure loss is calculated using one of the three options described above, the Burner outlet total pressure (Ptout) is determined by rearranging [Eq. 3.1.1].

3.1.4: Burner Component Efficiency Model

There are several definitions which are used to describe the Burner efficiency (η_b). However, for the PROOSIS SCLib Burner component, the Burner efficiency is defined as shown in [Eq. 3.1.7].

$$\eta_b = \frac{FARBr}{FARinj} \quad \text{[Eq. 3.1.7]}$$

NB: $0 < \eta_b \leq 1$ (For any other value an error message is displayed)

Where: FARBr is the reactant burned fuel to Burner inlet air ratio
FARinj is the injected fuel to Burner inlet air ratio

There are three options for obtaining the Burner efficiency. These options are discussed below. The user can select one of the three options outlined below via a switch in the attributes editor of the Burner component (Fig: 3.1.3 and Fig 3.1.4).

η_b Calculation – Option 1:

Value of the Burner efficiency directly input by the user (η_b_in)

If the value of the Burner efficiency is known, the user can directly input the value as DATA in the attributes editor of the Burner component (Fig: 3.1.3 and Fig 3.1.4). The nomenclature for the variable representing the Burner efficiency directly input by the user is η_b_in . However, the Burner energy balance model requires η_b which is obtained as shown in [Eq. 3.1.8].

$$\eta_b = \eta_b_in \quad \text{[Eq. 3.1.8]}$$

η_b Calculation – Option 2:

Obtaining the value of the Burner efficiency (η_b) from a Burner efficiency map

Alternatively, the Burner efficiency (η_b) can be obtained from a Burner efficiency map where the Burner efficiency is expressed as a function of the theta parameter (θ). The θ parameter is defined as shown in [Eq. 3.1.9].

$$\theta = P_{tin}^{1.75} \times GeoAref \times GeoDref^{0.75} \times \left[\frac{\exp\left(\frac{T_{tin}}{300}\right)}{W_{airin}} \right] \quad [\text{Eq. 3.1.9}]$$

Where: GeoAref is the Burner reference area
GeoDref is the Burner reference diameter
Wairin is the Burner inlet air mass flow rate

The θ parameter for combustion performance, which was derived by Greenhough V. W. and Lefebvre A. H.^[5], is based on a burning – velocity model which envisages the combustion chamber as being similar in structure to the flame produced on a Bunsen burner under turbulent flow conditions. This parameter is a good means of correlating Burner efficiency to burner inlet pressure, temperature and mass flow rate as well as Burner geometric dimensions. These correlations (which have been obtained empirically) are extremely useful in the design and development of new combustors. Combustor dimensions and operation constraints can be scaled to common values. Consequently, any discrepancies in performance can be directly attributed to differences in design. A typical Burner efficiency map is shown in Fig: 3.1.5 for different chamber configurations. Due to the stringent constraints associated with gas turbine generated pollutants, efficiencies of less than 90% anywhere in the operational envelope are unlikely to be tolerated. Further details of the derivation and constraints of using the θ parameter can be found in [3] & [6].

η_b Calculation – Option 3:

Obtaining the value of the Burner efficiency (η_b) from a user defined efficiency model

Alternatively, the Burner efficiency (η_b) can be obtained from a user defined efficiency model.

NB: Option 3 is only recommended for level 1 users of PROOSIS as the Burner source file will need to be modified.

3.1.5: Burner Component Combustion Model

As discussed in *Section 3.1.1*, two different partitions (mathematical models) (refer to the “Glossary” section of the thesis) can be generated for the Burner component. For the default partition, the value of the injected fuel mass flow rate (W_{fuel}) is known and communicated to the Burner component via the fuel port. The Burner outlet temperature (T_{out}) is then calculated using the Burner component energy balance equations.

NB: This calculation method is rarely used except in engine test analysis and in some non-steady state calculations. It is also often used in iterations where a certain amount of fuel is injected to achieve a given thrust.

Alternatively the user can design a different partition where the Burner outlet total temperature (T_{out}) is known. In this case PROOSIS will simply rearrange the energy balance equations and calculate the value of the injected fuel mass flow rate (W_{fuel}).

NB: This calculation method is used in virtually all design point and off design steady state calculations.

In addition to the injected fuel mass flow rate (W_{fuel}) or the Burner outlet total temperature (T_{tout}) the following properties are also calculated:

1. Burner outlet total mass flow rate (W_{out})
2. Burner outlet burned fuel to air ratio (FAR_{Bout})
3. Burner outlet unburned fuel to air ratio (FAR_{Uout})
4. Burner outlet water to air ratio (WAR_{out})
5. Burner outlet flow angle (Ang_{out})

The combustion model of the Burner component has been designed to enable the Burner Component to also be used as an Afterburner component.

NB: The following calculation procedure is for the partition where the injected fuel mass flow rate (W_{fuel}) is known and all the main outlet flow port variables are calculated. For the partition where the Burner outlet total temperature (T_{tout}) is known, the equations are simply rearranged by PROOSIS to calculate the values of the remaining main outlet flow port variables and the injected fuel mass flow rate.

The Burner inlet air mass flow rate (W_{airin}) is calculated using [Eq. 3.1.10].

$$W_{airin} = \frac{W_{in}}{(1 + FAR_{Bin} + FAR_{Uin} + WAR_{in})} \quad [\text{Eq. 3.1.10}]$$

The injected fuel to inlet air ratio (FAR_{inj}) is calculated using [Eq. 3.1.11].

$$FAR_{inj} = \frac{W_{fuel}}{W_{airin}} \quad [\text{Eq. 3.1.11}]$$

Once the combustion process occurs it yields a certain amount of burned fuel and a certain amount of unburned fuel based on the Burner efficiency. Once the injected fuel to inlet air ratio is calculated (as shown in [Eq. 3.1.11]), the reactant burned fuel to air ratio (FAR_{Br}) is calculated based on the Burner efficiency definition shown in [Eq. 3.1.7] (the Burner efficiency (η_b) is obtained using one of the options highlighted in *Section 3.1.4*). The reactant unburned fuel to air ratio (FAR_{Ur}) is then calculated using [Eq. 3.1.12].

$$FAR_{Ur} = FAR_{inj} - FAR_{Br} \quad [\text{Eq. 3.1.12}]$$

NB: The reactant burned fuel to air ratio (FAR_{Br}) and the reactant unburned fuel to air ratio (FAR_{Ur}) do not take account of any burned or unburned fuel that may be present at the inlet of the Burner respectively.

The Burner outlet total mass flow rate (W_{out}) is calculated using [Eq. 3.1.13].

$$W_{out} = W_{in} + W_{fuel} \quad [\text{Eq. 3.1.13}]$$

The Burner outlet burned fuel to air ratio (FARBout) is the sum of the Burner inlet burned fuel to air ratio (FARBin) and the reactant burned fuel to air ratio (FARBr) as shown in [Eq. 3.1.14].

$$FARBout = FARBin + FARBr \quad \text{[Eq. 3.1.14]}$$

Similarly, the Burner outlet unburned fuel to air ratio (FARUout) is the sum of the Burner inlet unburned fuel to air ratio (FARUin) and the reactant unburned fuel to air ratio (FARUr) as shown in [Eq. 3.1.15].

$$FARUout = FARUin + FARUr \quad \text{[Eq. 3.1.15]}$$

The Burner outlet total specific enthalpy (htout) is then calculated by rearranging the energy balance equation - [Eq. 3.1.16].

$$(Wout \times htout) = (Win \times htin) + (Wfuel \times LHV \times \eta_b) + [(Wout \times ht'') - (Win \times ht')] + (Wfuel \times Hs) \quad \text{[Eq. 3.1.16]}$$

Where:

$(Wout \times htout)$ is the Burner outlet total power

$(Win \times htin)$ is the Burner inlet total power

$(Wfuel \times LHV \times \eta_b)$ is the power rise due to the combustion process

Calorific value is defined as the heat energy released per unit mass of fuel burned. The lower heating value or net calorific value of a fuel is defined as the heat released under pressure in a constant volume when the combustion products are cooled to an initial reference temperature (typically 288.15K). The lower heating value accounts for the latent heat of vaporisation of the products of combustion and is therefore the parameter most commonly used for gas turbine calculations (as opposed to the gross calorific value which is the total heat released making no allowance for the latent heat of vaporisation of the combustion products). For the PROOSIS Burner component, the LHV is chosen based on the fuel selection switch setting made by the user in the attributes editor of the Burner component (Fig: 3.1.3 and Fig 3.1.4). The default LHV values for the various fuels are shown in Fig: 3.1.6 however, the user does have the option to change these values if necessary. As PROOSIS is developed, it is likely that further fuels will be added and the Burner component coding ensures that this may be achieved with minimal disruption.

$[(Wout \times ht'') - (Win \times ht')]$ is the power of the injected fuel.

(Where: ht'' is the enthalpy corresponding to Tstd & FARBout and
 ht' is the enthalpy corresponding to Tstd & FARBin)

NB: This term allows the Burner component to be used as an Afterburner as it accounts for any products of combustion which may exist upstream of the Burner.

$(W_{fuel} \times H_s)$ is the power associated with the sensible enthalpy (H_s) of the liquid or gaseous fuel. The sensible enthalpy of the fuel is the change in enthalpy of the fuel corresponding to the difference in the temperature of the fuel in the fuel tank ($T_{Ref} = 288.15K$) (which is also the reference temperature at which the fuel LHV is defined) and the temperature of the fuel at the point of Burner injection (T_{fuel}). The Burner component comprises one dimensional fuel tables with sensible enthalpy as a function of temperature for the fuel. As with the main fluid model, these fuel enthalpy charts have been generated using the CEA ^[7] & ^[8] software developed by NASA. Based on the variation of fuel enthalpy with temperature, linear interpolation is used to obtain the value of fuel enthalpy corresponding to a particular temperature. The fuel enthalpy tables for the liquid fuels cover a temperature range of 288.15K – 450K. The effects of including (or neglecting) the sensible enthalpy of the liquid fuel for the energy balance of the Burner component is presented in detail in *Section 3.3*. In particular, the effects of this negligence with respect to both engine performance engineers and airframe engineers are discussed.

The PROOSIS Burner component does not currently account for the effects of water injection on performance. For the current version, the Burner outlet water to air ratio (WAR_{out}) is simply equal to the Burner inlet water to air ratio (WAR_{in}) as shown in [Eq. 3.1.17]. Water / steam injection is often employed in industrial gas turbine engine burners primarily to reduce NO_x emissions (by reducing peak combustion temperatures in the primary zone). This boosts power but adversely affects specific fuel consumption. Although the technology of water / steam injection to reduce emissions is being slowly phased out by the introduction of dry low emission combustion technology, the Burner component will be modified in the near future to account for water injection. A more detailed explanation of the effects of water injection on burner performance can be found in [6] and [40].

$$WAR_{out} = WAR_{in} \quad \text{[Eq. 3.1.17]}$$

Similarly the effects of combustion on the Burner outlet flow angle (Ang_{out}) have not been implemented. Consequently the Burner outlet flow angle (Ang_{out}) is simply equal to the Burner inlet flow angle (Ang_{in}) as shown in [Eq.3.1.18].

$$Ang_{out} = Ang_{in} \quad \text{[Eq. 3.1.18]}$$

3.1.6: Variables Required for Global Engine Performance Calculations

The following variables are communicated to the Performance Monitor component via information ports:

- The Injected Fuel Mass Flow Rate (W_{fuel})
- The Fuel Lower Heating Value (LHV)

These values are required for the following calculations in the Performance Monitor component.

NB: [Eq. 3.1.19] – [Eq. 3.1.23] are all contained within the Performance Monitor component and are not part of the Burner component calculations.

For the Performance Monitor of Thrust Power Engines:

[Eq. 3.1.19] and [Eq. 3.1.20] are used to calculate the engine thermal efficiency (η_{th}) and the engine specific fuel consumption (SFC) for thrust power engines respectively.

$$\eta_{th} = \frac{KE_{jet} - KE_{inlet}}{W_{fuel} \times LHV} \quad \text{[Eq. 3.1.19]}$$

$$SFC = \frac{3600 \times W_{fuel}}{F_n} \quad \text{[Eq. 3.1.20]}$$

Where: KE_{jet} is the power associated with the jet kinetic energy
 KE_{inlet} is the power associated with the inlet flow kinetic energy
 F_n is the total net thrust

For the Performance Monitor of Shaft Power Engines:

[Eq. 3.1.21], [Eq. 3.1.22] and [Eq. 3.1.23] are used to calculate the engine thermal efficiency (η_{th}), the specific fuel consumption (SFC) and the heat rate (Q_{rate}) for shaft power engines respectively.

$$\eta_{th} = \frac{Q_{shaft}}{W_{fuel} \times LHV} \quad \text{[Eq. 3.1.21]}$$

$$SFC = \frac{3600 \times W_{fuel}}{Q_{shaft}} \quad \text{[Eq. 3.1.22]}$$

$$Q_{rate} = SFC \times LHV \quad \text{[Eq. 3.1.23]}$$

Where: Q_{shaft} is the shaft power

3.2: PROOSIS Burner_Emissions Component Modelling

3.2.1: Introduction

With emission legislation becoming more stringent, low emissions of pollutants such as CO, NO_x, UHC and smoke are essential for existing and future gas turbine engines. Consequently a robust emissions prediction model is now a fundamental requirement for any gas turbine simulation software.

There are three basic types of methods employed for predicting gas turbine combustion emissions^[9]:

1. Empirical / Semi – Empirical correlations which are based on measurements of combustor emissions.^{[10], [24], [11], [12] & [13]}
2. Analytical methods using a stirred reactor assumption and simplified chemical reactions.^{[12] & [14]}
3. Detailed computational combustion dynamics (CCD) analyses.^{[13], [15] & [16]}

The PROOSIS Burner_Emissions component, developed collaboratively by Cranfield University and the National Technical University of Athens (NTUA), calculates the emitted pollutants (oxides of nitrogen (NO_x), carbon monoxide (CO), unburned hydrocarbons (UHC) and smoke) using semi-empirical calculations. Although CCD and analytical methods may yield more accurate results, the semi-empirical approach was chosen as CCD and analytical methods are numerically too expensive and more complicated than the semi-empirical approach respectively. The exhaust gas composition is also calculated from the specified composition of air and fuel. The Burner_Emissions component inherits from the Burner component (as shown in Fig: 3.1.2) and therefore (in addition to the emissions calculations) performs all the calculations of the Burner component highlighted in *Section 3.1*.

The description of the Burner_Emissions component provided below is based on [17]. A detailed analysis of gas turbine emissions is beyond the scope of the research work. ([18] & [19] provide a thorough introduction to gas turbine emissions, control of pollutant generation processes, control of pollutant emissions and emerging technology solutions). This section simply provides a brief description of the PROOSIS Burner_Emissions model.

The main factors which affect the level of emissions during the operation of a gas turbine engine are:

1. Burner design (directly related to η_b)
2. Ambient and burner inlet conditions
3. Fuel composition and LHV
4. Flame and combustor primary zone temperature
5. Residence time (directly related to air velocity and combustor volume)

Emission measurements for several engines and/or burners have yielded a number of semi-empirical correlations^{[10], [24], [11], [12] & [13]} which are available in the open literature (especially for NO_x which has the greatest environmental impact). These correlations are based on certain ambient and/or burner inlet conditions and there is consequently a lot of uncertainty when using them for different operating conditions. An extensive investigation

by NTUA (as part of the AEROTEST** project [28]), which involved testing several existing emissions predicting correlations, revealed that application of the correlations in their original form does not provide a reliable estimation of emissions. However, adaptation of these correlations via suitable optimization techniques demonstrated that improved predictions can be achieved [23]. The emissions calculation algorithms, for the PROOSIS Burner_Emission component have been therefore fitted with adaptive scalars so the correlations can be adjusted for different operating conditions based on user defined optimization techniques.

** The AEROTEST project is an EU project within FP6 which ran between March 2004 and October 2007. The main objective of this project was *“to achieve a high level of confidence in aircraft engine emission measurements with a view to using the technique for engine emissions certification.”* [28]

Although several correlations are presented in the sections which follow, they have all evolved from the correlations developed by the pioneer of advanced gas turbine combustor technology – the late A. LeFebvre.

3.2.2: Correlations for Oxides of Nitrogen (NOx)

The PROOSIS Burner_Emissions component currently comprises five correlations to determine the NOx emissions index (EINOx). The user can select one of the five options outlined below via a switch in the attributes editor of the Burner_Emissions component (Fig: 3.2.1), or incorporate a user defined model. The definition of EINOx is shown in [Eq. 3.2.1].

$$EINOx = \frac{MNOx}{Mfuel} \quad \text{[Eq. 3.2.1]}$$

Where: MNOx is the mass of NOx (in grams).
Mfuel is the mass of fuel used (in kilograms).

NOx Correlation – Option 1:

A. Lefebvre correlation [24]

The A. Lefebvre NOx correlation is presented in [Eq. 3.2.2]. The actual algorithm from [24] has been slightly modified to incorporate the adaptive scalars discussed in Section 3.2.1.

$$EINOx = \frac{0.8 \times s1 \times \left(\frac{Ptin}{1000}\right)^{1.25 \times s2} \times V_b \times e^{(0.004 \times Tfl \times s3)}}{Win \times Tfl} \quad \text{[Eq. 3.2.2]}$$

Where:

1. s1, s2 and s3 are the adaptive scalars.
2. Tfl is the flame temperature and is obtained as shown below:

Step 1: The total reactant fuel to air ratio (FARr), which is the sum of the reactant burned fuel to air ratio (FARBr) and the reactant unburned fuel to air ratio (FARUr) is obtained as shown in [Eq. 3.2.3].

$$FARr = FARBr + FARUr \quad \text{[Eq. 3.2.3]}$$

NB: For simplicity, unlike the Burner component, the Burner_Emissions component does not differentiate between burned fuel and unburned fuel and uses the total fuel (which is the sum of the burned fuel and unburned fuel) for the calculations. This generalization does not have a big impact on the results as modern gas turbine Burners have very high efficiencies (>0.99) and the amount of the unburned fuel and consequently the effects of the unburned fuel can be neglected. However, for an Afterburner_Emissions component, this generalization will yield slightly inaccurate results due to the relatively lower efficiencies (≈ 0.90) of gas turbine Afterburners.

Step 2: The primary zone reactant fuel to air ratio (FARpz) is then obtained using [Eq. 3.2.4].

$$FARpz = \frac{FARr}{Fpz} \quad \text{[Eq. 3.2.4]}$$

Where: Fpz is the air fraction in the primary zone. The value of Fpz is input as DATA by the user in the attributes editor of the Burner_Emissions component (Fig: 3.2.1). The default value of Fpz is 0.20 as about 20% of the air is introduced around the jet of fuel in the primary zone to provide Stoichiometric conditions which results in the greatest heat release ^[22]. However, with the development of modern and future “staged combustion” Burners (either “rich burn, rapid quench” or “lean pre-mix” concepts) ^[18] to combat NOx, it is unlikely that primary zones of future Burners will operate under Stoichiometric conditions.

Step 3: The primary zone reactant total specific enthalpy (htpz) is then calculated using a primary zone energy balance equation [Eq. 3.2.5] ^[17].

$$htpz = \frac{htin + (FARpz \times LHV \times \eta_b)}{1 + FARpz} \quad \text{[Eq. 3.2.5]}$$

Step 4: Finally the flame temperature (Tfl) is obtained from the fluid model using the reverse function T_h as shown in [Eq. 3.2.6].

$$\begin{aligned} \text{htpz} &= (\text{fluid}, T_{fl}, FARpz, WARpz) \\ \text{INVERSE}(T_{fl}) \quad T_{fl} &= T_h(\text{fluid}, \text{htpz}, FARpz, WARpz) \end{aligned} \quad \text{[Eq. 3.2.6]}$$

Where: The primary zone water to air ratio (WAR_{pz}) = WAR_{in} = WAR_{out}
(Refer to: [Eq. 3.1.17]).

3. V_b is the Burner primary zone volume.

NOx Correlation – Option 2:

Doppelheuer & Lecht correlation ^[20]

The NOx correlation below ([Eq. 3.2.7]) is based on [20] however the algorithm has been slightly modified to incorporate the adaptive scalars discussed in Section 3.2.1.

$$\frac{EINO_x}{EINO_{x,ref}} = s1 \times \left(\frac{P_{tin}}{P_{tin,ref}} \right)^{0.5 \times s2} \times \left(\frac{T_{tin,ref}}{T_{tin}} \right)^{0.5 \times s3} \times \left(\frac{T_{pz,ref}}{T_{pz}} \right)^{1.5 \times s4} \times e^{\left\{ 38000 \times s5 \times \left(\frac{1}{T_{fl,ref}} - \frac{1}{T_{fl}} \right) \right\}}$$

[Eq. 3.2.7]

Where:

1. The subscript “_{ref}” refers to reference values. These values could either be measured values (at certain operating conditions) or could be obtained from an existing databank (e.g. the International Civil Aviation Authority (ICAO) Engine Exhaust Emissions Data Bank) which provides comprehensive emissions data for a given engine at different operating conditions. [21] is a link to the ICAO website where the ICAO Engine Exhaust Emissions Data for the CFM56-5C2 engine is provided as an example. All the reference values in [Eq. 3.2.7] are entered as DATA by the user in the attributes editor of the Burner_Emissions component (Fig: 3.2.1).
2. s1, s2, s3, s4 and s5 are the adaptive scalars.
3. T_{fl} is calculated as outlined for the A. Lefebvre correlation presented above ([Eq. 3.2.3] – [Eq. 3.2.6]).
4. T_{pz} is the primary zone temperature and is the mean of the flame temperature (T_{fl}) and the Burner inlet total temperature (T_{tin}) as shown in [Eq. 3.2.8] ^[17].

$$T_{pz} = \frac{T_{fl} + T_{tin}}{2}$$

[Eq. 3.2.8]

NOx Correlation – Option 3:

Snecma correlation from the CYPRESS report ^[11]

The CYPRESS project was created to explore the relationships between emissions, engine architecture and other design parameters. One of the many (performance prediction) deliverables of this project was the development of emission prediction models, using semi-empirical correlations for several aero engines. This study yielded several correlations (which have undergone a thorough sensitivity analysis) some of which have been used for the emissions model of the Burner_Emissions component.

The Snecma NO_x correlation algorithm from the CYPRESS report is shown in [Eq. 3.2.9]. The actual algorithm from [11] has been slightly modified to incorporate the adaptive scalars in a similar fashion as outlined for option 1.

$$EINO_x = s1 \times 225.013 \times \tau^{(-0.82129 \times s4)} \quad [\text{Eq. 3.2.9}]$$

Where:

1. The coefficient (τ) is defined as shown in [Eq. 3.2.10].

$$\tau = \frac{Win \times Ttin^{0.5 \times s2} \times 10^5}{V_b \times Ptin \times e^{\frac{Ttin}{230 \times s3}}} \quad [\text{Eq. 3.2.10}]$$

Where: V_b is the Burner primary zone volume.

2. $s1$, $s2$, $s3$ and $s4$ are the adaptive scalars.

This correlation has been derived experimentally. The only difficulty with using this algorithm is that the user needs to know the Burner volume (V_b) which needs to be entered as DATA in the attributes editor of the Burner_Emissions component (Fig: 3.2.1).

NO_x Correlation – Option 4:

MTU correlation from the CYPRESS report [11]

The MTU NO_x correlation algorithm from the CYPRESS report is shown in [Eq. 3.2.11]. The actual algorithm from [11] has been slightly modified to incorporate the adaptive scalars in a similar fashion as outlined for option 1.

$$EINO_x = (s1 \times 3.7) + \left\{ s2 \times 26 \times \left(\frac{Ptin}{29.83 \times 10^5 \times s3} \right)^{0.4 \times s4} \times e^\mu \right\} \quad [\text{Eq. 3.2.11}]$$

Where:

1. The coefficient (μ) is defined as shown in [Eq. 3.2.11].

$$\mu = \frac{(1.8 \times Ttin \times s5) - (1487.27 \times s6)}{349.9 \times s7} \quad [\text{Eq. 3.2.12}]$$

2. $s1$, $s2$, $s3$, $s4$, $s5$, $s6$ and $s7$ are the adaptive scalars.

NO_x Correlation – Option 5:

NTUA generic correlation [23]

A common feature of the correlations found in the open literature (such as those described above) is that they are based on analysis of experimental data which refer to a specific

engine or Burner. NTUA successfully developed and tested a generic correlation [Eq. 3.2.13], as part of the AEROTEST project.

$$EINO_x = s_1 \times 10 \times \left(\frac{P_{tin}}{10^5} \right)^{(0.5 \times s_2)} \times e^{\left(\frac{T_{tin}}{s_3 \times 300} \right)} \times FARr^{s_4} \quad [\text{Eq. 3.2.13}]$$

Where:

1. FARr is the total reactant fuel to air ratio as defined in [Eq. 3.2.3].
2. s₁, s₂, s₃ and s₄ are the adaptive scalars.

3.2.3: Carbon Monoxide (CO) Correlation

The carbon monoxide emissions index (EICO) (defined in [Eq. 3.2.14]) is calculated using the correlation defined in [24] as shown in [Eq. 3.2.15].

NB: The actual algorithm from [24] has been slightly modified to incorporate the adaptive scalars in a similar fashion as outlined for the NO_x correlations.

$$EICO = \frac{MCO}{M_{fuel}} \quad [\text{Eq. 3.2.14}]$$

Where: MCO is the mass of CO (in grams).
M_{fuel} is the mass of fuel used (in kilograms).

$$EICO = \frac{s_1 \times 18.57 \times Win \times Tfl \times dPqPcold^{(-0.5 \times s_2)} \times \left(\frac{P_{tin}}{1000} \right)^{(-1.5 \times s_3)} \times e^{(-0.00345 \times Tfl \times s_4)}}{V_b - V_e} \quad [\text{Eq. 3.2.15}]$$

Where:

1. s₁, s₂, s₃, and s₄ are the adaptive scalars.
2. Tfl is calculated as outlined in Section 3.2.2.
3. V_b (the Burner primary zone volume), V_e (the Burner volume occupied by the evaporated fuel) and dPqPcold (the Burner cold fractional pressure loss) are input as DATA in the attributes editor of the Burner_Emissions component (Fig: 3.2.1).

3.2.4: Unburned Hydrocarbons (UHC) Correlation

The unburned hydrocarbons emissions index (EIUHC) (defined in [Eq. 3.2.16]) is calculated using the correlation defined in [24] as shown in [Eq. 3.2.17].

NB: The actual algorithm from [12] has been slightly modified to incorporate the adaptive scalars in a similar fashion as outlined for the NO_x correlations. This correlation is only recommended when UHC emissions are known to be low.

$$EIUHC = \frac{MUHC}{M_{fuel}} \quad [\text{Eq. 3.2.16}]$$

Where: MUHC is the mass of UHC (in grams).
M_{fuel} is the mass of fuel used (in kilograms).

$$EIUHC = \frac{s1 \times 910 \times Win \times Tfl \times dPqPcold^{(-1 \times s2)} \times \left(\frac{Ptin}{1000}\right)^{(-2.5 \times s3)} \times e^{(-0.00345 \times Tfl \times s4)}}{V_b - V_e} \quad [\text{Eq. 3.2.17}]$$

Where: Tfl, V_b, V_e, dPqPcold, s1, s2, s3 and s4 are obtained as described in Section 3.2.3.

3.2.5: Smoke / Soot Correlation

The emitted soot concentration (C_{soot}), which is also known as the Smoke Number, is a dimensionless term quantifying smoke emissions. Smoke Number is calculated from the reflectance of a filter paper measured before and after the passage of a known volume of a smoke bearing sample. The Smoke Number, is calculated using the correlation defined in [20] as shown in [Eq. 3.2.17].

NB: The actual algorithm from [20] has been slightly modified to incorporate the adaptive scalars in a similar fashion as outlined for the NO_x correlations.

$$C_{soot} = s1 \times C_{soot_{ref}} \times \left(\frac{\phi}{\phi_{ref}}\right)^{2.5 \times s2} \times \left(\frac{Ptin}{Ptin_{ref}}\right)^{1.35 \times s3} \times e^{\left\{s4 \times 20000 \times \left(\frac{1}{Tfl_{ref}} - \frac{1}{Tfl}\right)\right\}} \quad [\text{Eq. 3.2.17}]$$

Where:

1. The subscript “_{ref}” refers to reference values. C_{soot_{ref}} is the reference Smoke Number and is calculated using [Eq. 3.2.18]. The remaining reference parameters could either be measured values (at certain operating conditions) or could be obtained from an existing databank such as that outlined in Section 3.2.2. These reference parameters are entered as DATA by the user in the attributes editor of the Burner_Emissions component (Fig: 3.2.1).

$$C_{soot_{ref}} = 0.00459 \times e^{(0.0106 \times Ttin)} \quad [\text{Eq. 3.2.18}]$$

ϕ is the equivalence ratio and is defined as shown in [Eq. 2.1.4]. (Refer to Section 2.1.3)

Where:

- a. The total reactant fuel to air ratio (FARr) is calculated as shown in [Eq. 3.2.3].

Advanced Performance Simulation of Gas Turbine Components
and Fluid Thermodynamic Properties

- b. FAR_{Stoich} is the Stoichiometric total reactant fuel to air ratio and is calculated as highlighted in *Section 2.1.3*.
2. T_{fl} , s_1 , s_2 , s_3 and s_4 are as described in *Section 3.2.2*.

3.3: Effects of Fuel Sensible Enthalpy

3.3.1: Introduction

The work presented in this section is the outcome of a collaborative effort between the author and a Cranfield University MSc research student. The MSc research work entitled “Advanced Performance Simulation of Gas Turbine Burners and Afterburners” [27] has already been published. However, the author technically led the MSc research and provided significant intellectual input into the project. The work undertaken and results obtained are summarised in this section with references to [27] where necessary.

As a consequence of global fuel cost escalation and increased stringent engine emission regulations, fuel conservation is a high priority for engineers (airframe and engine) as well as Airline companies. Reliable fuel consumption estimations are fundamental in order to achieve the engine performance and emissions targets defined in a contractual agreement between Airline companies and engine manufacturers. The energy balance equation of the PROOSIS Burner component [Eq. 3.1.16], described in *Section 3.1.5*, was developed based on significant input from several industrial partners (including both airframe and engine manufacturers) from the VIVACE ECP consortium and includes a term which accounts for the sensible enthalpy of the fuel. The sensible enthalpy of the fuel is the change in enthalpy of the liquid fuel (Jet-A_(l) or Diesel_(l)) or the gaseous fuel (Sample Natural Gas_(g) or Hydrogen_(g)) corresponding to the difference in the temperature of the fuel in the fuel tank ($T_{\text{Ref}} = 288.15\text{K}$) (which is also the reference temperature at which the fuel LHV is defined) and the temperature of the fuel at the point of Burner injection (T_{fuel}). The sections below describe the following:

1. The sources of the liquid fuel temperature rise (between the fuel tank and the point of injection) with a brief description of an aero-engine fuel system. The analysis of fuel systems is limited to aero-engine fuel systems only. Several additional engine fuel system considerations need to be made when calculating the sensible enthalpy of gaseous fuels for power plants operating with gaseous fuels (i.e. Sample Natural Gas_(g) and Hydrogen_(g)). These considerations are beyond the scope of the research work.
2. The generation (using the CEA [7] & [8] software developed by NASA) and implementation (in the Burner component) of the fuel enthalpy tables.
3. Analyses (at isolated Burner component level and isolated Afterburner component level) of the effects of neglecting the sensible enthalpy term in the energy balance equation of the Burner and Afterburner components, with respect to both engine performance engineers and airframe engineers.

3.3.2: Sources of Liquid Fuel Temperature Rise

This section describes the main sources of the temperature rise (and subsequently the enthalpy rise) of the liquid fuel between the fuel tank and the point of Burner (or Afterburner) injection. A description of a typical aero-engine fuel system is provided with a brief analysis of each engine fuel system component.

A schematic of a typical engine fuel system is shown in Fig: 3.3.1 [29]. The engine fuel system broadly comprises the following three main sub-systems:

- The low pressure (LP) sub-system
- The high pressure (HP) sub-system
- The fuel metering unit (FMU)

Liquid fuel from the aircraft fuel tank is first fed to the LP sub-system (Fig: 3.3.2 [30] shows a typical, engine LP fuel system) and subsequently to the HP sub-system. All LP and some HP systems comprise a fuel pump, a fuel \leftrightarrow oil heat exchanger (FOHE) (which is sometimes referred to as a fuel cooled oil cooler (FCOC)), a fuel heater and a fuel filter. A brief description of each of these components is provided below (based on [30] and [31]) with particular emphasis on any sources of liquid fuel temperature rise.

Fuel pumps: [30] & [31] The LP fuel pump is required to increase the fuel pressure by about 1MPa to prevent vapour locking and fuel cavitation multi-phase flow as well as flow starvation to the HP fuel pump. The HP pump (where present) is necessary to ensure that the fuel pressure at the fuel injectors is kept at an optimal level. There are several kinds of fuel pumps including, axial piston pumps, vane pumps, twin pinion gear pumps and internal gear pumps. A detailed analysis of the performance of these various fuel pumps is beyond the scope of the research work. (Further information with respect to engine fuel pumps is presented in [31]). In addition to raising the fuel pressure, the fuel pumps are also one of the major sources of liquid fuel temperature rise. The temperature rise is calculated by applying a steady state energy balance to the control volume. The heat input to the fuel (via the fuel pump) is due to the pump rejected power (Q_{reject}), which is the sum of the pump hydraulic power (Q_{hyd}) and the mechanical losses (Q_{loss}) of the pump less the pump output power (Q_{out}), as defined in [Eq. 3.3.1].

$$Q_{reject} = Q_{hyd} + Q_{loss} - Q_{out} \quad \text{[Eq. 3.3.1]}$$

Where:

1. Q_{hyd} is a function of the (ideal) pump speed, the pump displacement and the pump pressure rise.
2. Q_{loss} is a function of the pump design, the pump speed and the pump pressure rise
3. Q_{out} is a function of the (actual) pump speed, the pump displacement and the pump pressure rise.

FOHE (or FCOC): [30] & [31] The FOHE / FCOC is also a major source of liquid fuel temperature rise. All engines transfer heat to the lubricating oil by friction of mechanical parts. It is therefore necessary to fit an oil cooler in recirculatory oil systems. The cooling medium may be either fuel (in a FOHE / FCOC) or air (in an air cooled oil cooler (ACOC)) or both. Oil to fuel heat transfer is more efficient than oil to air heat transfer. Consequently, for a given heat dissipation, a FOHE will be smaller and lighter than an ACOC and therefore fuel cooling of the oil is generally preferred. The fuel which passes through the FOHE is used as a heat sink to cool the engine lubricating oil. Cooling the lubricating oil is the primary purpose of the FOHE, however during cold operation the oil is used to heat the fuel to help prevent ice contamination of the fuel filter. During critical phases of a flight, such as descent, when the temperature across

the pump is very high, the temperature rise of the fuel in the LP FOHE must be limited to prevent the fuel temperature becoming too high at entry to the fuel metering unit (FMU). This is achieved by bypassing the hot lubricating oil from the LP FOHE to the HP FOHE (and possibly also the ACOC) thereby reducing the fuel temperature rise.

Fuel heaters: ^[30] As mentioned above, the lubricating oil in a FOHE is sometimes used to heat the fuel during cold operation to prevent ice contamination. However, when heat transfer by the FOHE is insufficient, the fuel is passed through a second heat exchanger where it absorbs heat from a thermostatically controlled airflow taken from the compressor.

Fuel filters: ^[31] Fuel filters are required to protect downstream components in the engine fuel system from solid contaminants and ice. The solid contaminants may enter the system from dirty fuel supplies or from dirt in the pipes or tanks. Fuels can contain both free and dissolved water and as the temperature falls dissolved water will come out of solution and form ice particles, as will free water in the fuel if the temperature falls below 273.15K. Ice particles may then contaminate downstream components. Since fuel filters are not a source of liquid fuel temperature rise, in the engine fuel system, they will not be discussed further. However, further information is available in **[30]** & **[31]**.

The fuel metering unit (FMU) is a fundamental part of an engine fuel system. The FMU is an electro-hydro-mechanical controller which is controlled by a redundant, dual channel full authority digital control (FADEC). The engine fuel system schematic shown in Fig. 3.3.1 is based on electronic engine control (EEC) but this technology has now been superseded by FADEC. FADEC takes over virtually all of the steady state and transient control intelligence of an engine including the operation of the FMU. The main functions of the FMU are:

1. To regulate the rate of fuel injection into the engine to ensure the engine operates within the limits of safe operation.
2. To pressurise the fuel system to provide servo-control of actuators and valves.
3. To help protect the engine by limiting any over-speed condition.
4. To shut down the engine on direct order of the pilot.

Engine fuel system control is beyond the scope of this research work. However, further information is available in **[30]** & **[32]**.

Based on the engine fuel system architecture described above, it is evident that the main sources of liquid fuel temperature rise between the fuel tank and the point of Burner injection are:

1. Heat rejection from the fuel pump(s).
2. Heat transfer from the lubricating oil in the FOHE(s).
3. Heat transfer from the compressor air in the fuel heater(s).

Fig: 3.3.3 ^[31] and Fig: 3.3.4 ^[31] highlight typical values of engine fuel system parameters, at various stations of the fuel system, for typical civil and military engines respectively. For a typical civil engine, it can be seen that the liquid fuel temperature typically varies from 218.15K (which occurs when the aircraft has been standing on the ground in cold weather) to 438.15K (which occurs during descent when there is considerable heat transfer to the fuel from cooling of the lubricating engine oil (from the FOHE) and from the heat rejection

from the second stage fuel pump). The station parameters for the engine fuel system of military engines are broadly similar to those for civil engines with liquid fuel temperatures ranging from a minimum of 243.15K to a maximum of 453.15K.

3.3.3: Generating and Implementing Liquid Fuel Enthalpy Tables

For the Burner component energy balance equation [Eq. 3.1.16], the term $W_{fuel} \times H_s$ is a measure of the power associated with the sensible enthalpy (H_s) of the fuel. The sensible enthalpy of the fuel (H_s) is the change in enthalpy of the fuel corresponding to the difference in the reference temperature and pressure of the fuel in the fuel tank ($T_{Ref} = 288.15K$ and $P_{Ref} = 101325Pa$) (which are also the reference temperature and pressure, respectively, at which the fuel LHV is defined) and the temperature and pressure of the fuel at the point of Burner injection (T_{fuel} and P_{fuel} respectively), as shown in [Eq. 3.3.2].

$$H_s = h_{fuel} - h_{fuel_{Ref}} \quad \text{[Eq. 3.3.2]}$$

Where: h_{fuel} is the enthalpy of the fuel at the point of Burner injection and is a function of T_{fuel} and P_{fuel}
 $h_{fuel_{Ref}}$ is the enthalpy of the fuel corresponding to the reference conditions at which the fuel LHV is specified and is a function of T_{Ref} and P_{Ref}

Fig: 3.3.5 shows the variation of fuel enthalpy as a function of temperature and pressure for Jet-A_(l). The enthalpy chart covers a temperature range of 288.15K (the reference value at which the fuel LHV is most commonly specified) to 450K (the maximum temperature at the point of Burner injection – Refer to: Fig: 3.3.4) and a pressure range of 1atm (the reference value at which the fuel LHV is most commonly specified) to 200atm. From Fig: 3.3.5 it can be deduced that temperature strongly influences the enthalpy of the liquid fuel, however the effects of pressure are almost negligible and have therefore been ignored when generating the liquid fuel enthalpy tables. Consequently for the sensible enthalpy term in the PROOSIS Burner component, h_{fuel} and $h_{T_{ref}}$ are functions of only temperature (T_{fuel} and T_{ref} respectively).

NB: Currently, for the PROOSIS Burner component, it is assumed that the gaseous fuels are ideal gases and consequently the enthalpies of these gaseous fuels (as with the liquid fuels) are functions of temperature only. (This assumption is based on Joule's second law which states that the internal energy of an ideal gas is independent of its volume and pressure and is a function of temperature only.)

The fuel enthalpy tables for all the fuels of the Burner component were generated using the CEA [7] & [8] software developed by NASA. A detailed description of how to use the CEA software to generate the liquid fuel enthalpy charts is presented in [27]. Fig: 3.3.6 shows the variation of fuel enthalpy, as a function of temperature (for a temperature range of 288.15K to 450K) for these fuels. Based on the variation of fuel enthalpy with temperature, linear interpolation is justifiably used to obtain the values of $h_{fuel_{Ref}}$ and h_{fuel} corresponding to the reference temperature ($T_{Ref}=288.15K$) and the Burner injection temperature (T_{fuel}) (which is a user defined fuel port boundary condition) as shown in [Eq. 3.3.3] and [Eq.3.3.4] respectively.

$$hfuel_{Ref} = linearInterp1D(Jet - A_{(l)} hfuel_T, T_{Ref}) \quad [Eq. 3.3.3]$$

$$hfuel = linearInterp1D(Jet - A_{(l)} hfuel_T, T_{fuel}) \quad [Eq. 3.3.4]$$

Where: linearInterp1D is the PROOSIS one dimensional table interpolation routine
Jet-A_(l)hfuel_T is the fuel enthalpy table for Jet-A_(l)

NB: [Eq. 3.3.3] and [Eq. 3.3.4] are examples of how the Jet-A_(l) fuel enthalpies are calculated. The fuel enthalpies of all the other fuels are calculated in a similar fashion i.e. by one – dimensional linear interpolation of the respective fuel enthalpy tables. The appropriate fuel enthalpy table and interpolation routine is selected based on the fuel enthalpy switch setting made by the user in the attributes editor of the Burner component (Fig: 3.1.3 and Fig: 3.1.4).

Once the values of hfuel_{Ref} and hfuel are known, Hs is calculated using [Eq. 3.3.2] and then applied to the Burner component energy balance equation [Eq. 3.1.16].

3.3.4: Effects of Fuel Sensible Enthalpy – (Isolated Burner & Afterburner)

This section analyses (at isolated Burner component level and isolated Afterburner component level) the effects of neglecting the sensible enthalpy term in the energy balance equation of the Burner and Afterburner components, with respect to both engine performance engineers and airframe engineers. These investigations were conceived following a discussion between Cranfield University, Airbus France and MTU Aero Engines regarding the Burner component energy balance equation. The initial Burner energy balance equation, proposed by the author (on the behalf of Cranfield University) and approved by an MTU engineer (MTU were the industrial partner responsible for the approval of the PROOSIS Burner component model) was as shown in [Eq. 3.3.5].

$$(W_{out} \times ht_{out}) = (W_{in} \times ht_{in}) + (W_{fuel} \times LHV \times \eta_b) + [(W_{out} \times ht'') - (W_{in} \times ht')] \quad [Eq. 3.3.5]$$

This Burner component energy balance equation is similar to [Eq. 3.1.16]. However, it does not include the term $W_{fuel} \times H_s$ (which is a measure of the fuel sensible enthalpy). The term $W_{fuel} \times H_s$ was neglected because it was perceived that:

1. This term is relatively significantly lower than the other terms in the Burner energy balance equation and could therefore be neglected (from the perspective of an engine performance engineer anyway).
2. Implementing this (relatively “insignificant”) term would involve a great deal of time and resources to generate and implement the fuel enthalpy tables.

However, based on the following correspondence from Airbus France, it was decided that this term could not be ignored.

“The liquid fuel enthalpy difference can be neglected on condition that the fuel injection temperature (T_{fuel}) is not very far from the temperature at which the LHV is given (usually T_{ref} = 288.15K). For the engines we know, the fuel temperature (at injection) is typically in the range of 348.15K to 388.15K in cruise conditions (let’s say an average value of 368.15K). When neglecting the liquid fuel sensible enthalpy, and when

considering that the fuel is injected at $T_{fuel}=T_{ref}=288.15K$, the fuel injection temperature is underestimated by 80K on average.

Using the following trade:

An increase of 20K in fuel injection temperature brings about +20 kJ per kg of fuel and reduces the fuel consumption by 0.1%, it can be considered that underestimating the fuel injection temperature by 80K overestimates the fuel flow by ~0.4%. Whilst this may be negligible for an engine performance engineer, it can certainly not be neglected from an airframe engineer's perspective due to the significant errors which would arise in fuel cost and weight calculations.^[33]

The case studies which follow, justify these claims and subsequently the need to account for the fuel sensible enthalpy in the Burner component energy balance equation.

Case Study 1:

Description: Investigation of the effects of Jet-A₍₀₎ sensible enthalpy on isolated Burner performance. The isolated Burner component used in this case study is based on the Burner component of an engine model of a typical three spool, high bypass turbofan engine (with separate exhausts).

Simulation Information:

DATA: $\eta_b_in = 0.998$ and $dPqP_in = 0.06$

Boundaries: $W_{in} = 104.8kg/sec$, $T_{tin} = 928.39K$, $P_{tin} = 4212kPa$, $FAR_{Bin} = 0$,
 $FAR_{Uin} = 0$, $WAR_{in} = 0$, $Angin = 0$, $P_{fuel} = P_{Std} = 101.325kPa$ and
 $T_{tout} = 1791.72K$

NB: The DATA values and boundary conditions of this isolated Burner component simulation were chosen from the results of the design point simulation of an existing TURBOMATCH^{[34] & [35]} engine model of a typical three spool, high bypass turbofan engine (with separate exhausts).

Fig: 3.3.7 shows the effects of varying the fuel injection temperature (T_{fuel}) on the required injected fuel mass flow rate (W_{fuel}) for a specified Burner outlet total temperature (T_{tout}) keeping all other variables (including the fuel injection pressure (P_{fuel}), the Burner efficiency (η_b), the Burner fractional pressure loss ($dPqP$) and all the Burner inlet main flow port variables (W_{in} , T_{tin} , P_{tin} , FAR_{Bin} , FAR_{Uin} , WAR_{in} , $Angin$)) constant.

NB: As part of an engine model configuration the values of the Burner component main flow port variables would be obtained from the immediate upstream component (typically the high pressure compressor). However for isolated Burner component simulations, the values of these variables need to be specified as boundary conditions.

Fig: 3.3.8 shows the injected fuel mass flow rate over / under estimation as a function of fuel injection temperature relative to:

1. $T_{fuel} = 368.15K$ (which, according to [33], is the average fuel injection temperature at cruise conditions for civil engines).
2. $T_{fuel} = 438.15K$ (which, according to [31], is the maximum fuel injection temperature for civil engines (which typically occurs during descent) – (Refer to Fig: 3.3.3).

For this particular case study, it can be observed that as a consequence of neglecting the fuel sensible enthalpy (i.e. by keeping $T_{fuel} = 288.15K$) the fuel flow is over estimated by $\approx 0.35\%$ and $\approx 0.70\%$ for cruise conditions and descent respectively. Several similar investigations (which included similar isolated Burner simulations for different civil engines) yielded similar results. These results are clearly consistent with the claims made by Airbus [33]. Additionally during descent (for larger values of T_{fuel}), the injected fuel mass flow rate over estimation is even greater.

Fig: 3.3.9 shows the effects of varying the fuel injection temperature (T_{fuel}) on the required injected fuel mass flow rate (W_{fuel}) and consequently fuel cost.

NB: For the purposes of these investigations, fuel cost was calculated as shown below:

The price of Jet-A_(l) was obtained from the IATA "Jet Fuel Price Monitor" [36]. At the time of the case study (January 2008), the fuel price was 108.4\$/barrel = 258.2cts/gal = 679.47\$/m³. The density of Jet-A_(l) varies from 775kg/m³ - 830 kg/m³ at 288.15K^[37]. Using a mean value of 802.5 kg/m³ the fuel cost is ≈ 0.847 \$/kg.

For this particular case study, using the fuel cost calculation procedure described above, it can be observed that as a consequence of neglecting the fuel sensible enthalpy (i.e. by keeping $T_{fuel} = 288.15K$) the fuel cost is over estimated by ≈ 29 \$/hr and ≈ 59 \$/hr for cruise conditions and descent respectively.

NB: Since the fuel cost is directly proportional to the injected fuel mass flow rate (as described above) the fuel cost is also over estimated by $\approx 0.35\%$ and $\approx 0.70\%$ for cruise conditions and descent respectively.

Case Study 2:

Description: Investigation of the effects of Jet-A_(l) sensible enthalpy on isolated Afterburner performance. The isolated Afterburner component used in this case study is based on the Afterburner component of an engine model of a two spool low by-pass turbofan engine (with mixed exhausts and reheat).

Simulation Information:

DATA: $\eta_{b_in} = 0.90$ and $dPqP_in = 0.05$

Boundaries: $W_{in} = 77.393kg/sec$, $T_{tin} = 986.23K$, $P_{tin} = 443.7kPa$,
 $FAR_{Bin} = 0.01828$, $FAR_{Uin} = 0.00004$, $WAR_{in} = 0$, $Angin = 0$,
 $P_{fuel} = P_{std} = 101.325kPa$ and $T_{tout} = 1990K$

NB: The DATA values and boundary conditions of this isolated Afterburner component simulation were chosen from the results of an off-design simulation of an existing TURBOMATCH [34] & [35] engine model of a typical two spool, low by-pass turbofan engine (with mixed exhausts and reheat).

Fig: 3.3.10 shows the effects of varying the fuel injection temperature (T_{fuel}) on the required injected fuel mass flow rate (W_{fuel}) and subsequently fuel cost for a specified Afterburner outlet total temperature (T_{tout}) keeping all other variables (including the fuel injection pressure (P_{fuel}), the Afterburner efficiency (η_b), the Afterburner fractional pressure loss ($dPqP$) and all the Afterburner inlet main flow port variables (W_{in} , T_{tin} , P_{tin} , FAR_{Bin} , FAR_{Uin} , WAR_{in} , $Angin$)) constant.

NB: As part of an engine model configuration the values of the Afterburner component main flow port variables would be obtained from the immediate upstream component (typically a mixer component). However for isolated Afterburner component simulations, the values of these variables need to be specified as boundary conditions.

For this particular case study, it can be observed that as a consequence of neglecting the fuel sensible enthalpy (i.e. by keeping $T_{fuel} = 288.15K$) the fuel flow and fuel cost are over estimated by a maximum of $\approx 91kg/hr$ and $\approx 77\$/hr$ respectively during descent ($T_{fuel} = 453.15$) (Refer to Fig: 3.3.4).

Fig: 3.3.11 shows the injected fuel mass flow rate and fuel cost over estimation relative to $T_{fuel} = 453.15K$. (which, according to [31], is the maximum fuel injection temperature for military engines (which typically occurs during descent) – (Refer to Fig: 3.3.4). As a consequence of neglecting the fuel sensible enthalpy the fuel flow (and subsequently the fuel cost) are over estimated by a maximum of $\approx 0.9\%$. Several similar investigations (which included similar isolated Afterburner simulations for different military engines) yielded similar results. It is evident that as a consequence of neglecting the liquid fuel sensible enthalpy, for an Afterburner component, the over estimation of fuel flow and subsequently fuel cost is even greater than that for a Burner component.

Based on the results of these two case studies (and several other case studies which have not been presented) it is evident that, over a complete flight envelope and for several long range flights, the cumulative effect of the weight and cost miscalculations cannot be ignored by an airframe engineer especially for aircraft with afterburners. Consequently the fuel sensible enthalpy has been accounted for in the energy balance of the Burner component [Eq. 3.1.16].

The effects of neglecting the fuel sensible enthalpy on the overall engine main performance parameters (thrust and SFC) are presented in [41], with the aid of a case study of a two spool, low bypass turbofan engine model with mixed exhausts and reheat. The engine model case study confirmed that including (or neglecting) the liquid fuel sensible enthalpy can be negligible for calculations of the main engine DP performance parameters (thrust and SFC). However, as suggested by the isolated component performance simulations, for several long range flights the cumulative effect of the fuel weight and subsequent cost penalty cannot be neglected by an airframe engineer especially for aircraft with afterburners for thrust augmentation.

3.4: Burner Component Testing and Validation

3.4.1: Introduction

This section highlights the results of the testing and validation of the PROOSIS SCLib Burner component (in isolation), which was developed by the author, against the following well established (industry standard approved) gas turbine performance simulation software.

1. TURBOMATCH^[34] & ^[35] (the Cranfield University, in-house gas turbine performance simulation software).
2. GasTurb^[39]

NB: A detailed account of PROOSIS component and function testing procedures (with respect to testing, validation and reliability) is presented in **[38]**.

In addition, to the tests described in this section, the Burner component was also rigorously tested by MTU using both GasTurb^[39] as well as the MTU in-house gas turbine performance simulation tool – MOPS. Due to confidentiality restrictions the results of these tests are not presented. However, MTU (the PROOSIS industrial partner responsible for the testing and validation of the SCLib Burner component) approved the PROOSIS Burner component following the successful outcome of their rigorous internal testing.

3.4.2: Isolated Burner Component Testing

Both partitions of the Burner component (Refer to: Section 3.1.1 and Section 3.1.5) were rigorously tested over a wide range of boundary conditions and DATA including:

- A range of Burner inlet conditions (W_{in} , T_{in} and P_{tin})
- A range of Burner fractional pressure losses (dP_{qP}) and efficiencies (η_b)
- A range of Burner fuel injection temperatures (T_{fuel})

In particular the Burner component pressure loss model and, more importantly, the Burner energy balance model were tested. The results were validated using GasTurb^[39] and TURBOMATCH^[34] & ^[35]. Although the testing process was extensive, the four case studies presented in this section are representative both of the testing process as well as the results obtained.

For the four presented case studies, the Burner outlet temperature (T_{tout}) was calculated based on the boundary conditions (W_{in} , T_{in} , P_{tin} , FAR_{Bin} , FAR_{Uin} , WAR_{in} , Ang_{in} , P_{fuel} , W_{fuel} , dP_{qP} and η_b) summarised in Fig: 3.4.1 (for a range of T_{fuel} values). Fig: 3.4.2 shows the relative discrepancies (for the calculated value of T_{tout}) obtained between PROOSIS (for different values of T_{fuel}) and GasTurb and between PROOSIS (for different values of T_{fuel}) and TURBOMATCH, for each of the case studies.

The validation tests highlighted in the case studies were performed within the following software constraints:

1. Unlike PROOSIS, both GasTurb and TURBOMATCH do not facilitate isolated component performance simulation. Consequently simple engine models (single shaft turbojets) were developed in GasTurb and TURBOMATCH. The engine models were

carefully designed such that for each of the case studies, the boundary conditions of the Burner component were identical to the values defined in Fig: 3.4.1.

2. Both GasTurb and TURBOMATCH do not allow the user to specify values of T_{fuel} without modifying the source codes. Therefore for each case study the default value of T_{fuel} (hard coded in the source file of the respective software) was used.
3. The validation tests did not account for dissociation as the results available from GasTurb and TURBOMATCH were based on simulations where dissociation was not accounted for.

The results obtained in Fig: 3.4.2 are highly representative of the results that were obtained for a wide range of boundary conditions. The main conclusions that can be drawn for the calculated value of T_{out} (regardless of the values of the boundary conditions (W_{in} , T_{in} , P_{in} , FAR_{in} , FAR_{Uin} , WAR_{in} , Ang_{in} , P_{fuel} , W_{fuel} , dP_{qP} and η_b)) are:

1. The maximum discrepancy between GasTurb and PROOSIS never exceeds a magnitude of 0.3% regardless of the value of T_{fuel} .
2. The discrepancy between GasTurb and PROOSIS for $T_{fuel} = 358.15K$ never exceeds 0.1%. Since the discrepancy between GasTurb and PROOSIS is negative for $T_{fuel} = 288.15K$ and positive for $T_{fuel} = 438.15$, it appears that GasTurb also accounts for the sensible enthalpy of the liquid fuel. Although GasTurb does not allow the user to change the value of T_{fuel} , it seems to use a default value of T_{fuel} very close to 358.15K. It can fairly be deduced that if GasTurb did allow the user to change the value of T_{fuel} , the results for all simulations would be very consistent with the results obtained for the PROOSIS Burner component.
3. The discrepancy between TURBOMATCH and PROOSIS is greater. The results obtained suggest that TURBOMATCH does not account for the sensible enthalpy of the liquid fuel. Consequently the discrepancy between TURBOMATCH and PROOSIS increases as T_{fuel} increases. Developing the TURBOMATCH Burner "brick" to cater for liquid fuel sensible enthalpy is a strong recommendation for the future.

Despite the relatively high discrepancies between TURBOMATCH and PROOSIS, the results obtained from the validation tests (over a wide range of boundary conditions) using GasTurb are sufficient to confirm that the PROOSIS Burner component combustion model is robust. The values of FAR_{out} , FAR_{Uout} , WAR_{out} , W_{out} and Ang_{out} between all three gas turbine performance simulation software were identical (for the partition where the Burner injected fuel mass flow rate is specified).

Additionally, for all the simulations GasTurb, PROOSIS and TURBOMATCH all yield identical results for P_{tout} for specified values of P_{tin} and dP_{qP} thereby validating the PROOSIS Burner component pressure loss model.

Although not presented the Afterburner validation tests proved equally successful, thereby suggesting that the PROOSIS Burner component can also be used to simulate a gas turbine Afterburner.

3.5: Effects of Dissociation on Burner Component Performance

3.5.1: Introduction

The effects of dissociation on isolated Burner and Afterburner component simulations are presented in this section, with the aid of two case studies. The isolated Burner component simulations are based on the Burner component of a typical three spool high bypass ratio turbofan engine with separate exhausts (CUHBR engine model) while the isolated Afterburner component simulations are based on the Afterburner component of a typical two spool low bypass ratio turbofan engine with mixed exhausts and reheat (CULBR engine model). The boundary conditions used for each case study were taken from existing TURBOMATCH [34] & [35] engine models, of the aforementioned configurations, and are summarised in Fig: 3.5.1.

3.5.2: Burner Component Case Study:

For the Burner component case study a range of $1600\text{K} \leq T_{\text{tout}} \leq 2200\text{K}$ was investigated. Although for the CUHBR engine the design point Burner outlet total temperature is $\approx 1800\text{K}$, it is highly likely that, with advances in turbine materials technology, Burner outlet temperatures of future military engines (for which emission regulations are not as stringent as for civil engines) may exceed 2200K . The presented case study therefore provides an insight into the effects of dissociation on the performance of not only an existing Burner component but also Burner components with higher Burner outlet temperatures which may be developed in the future.

Fig: 3.5.2 shows the effects of dissociation on the calculated values of W_{fuel} as a function of T_{tout} for the Burner component boundary conditions summarised in Fig: 3.5.1. At a glance it may seem that the effects of dissociation are negligible, particularly at lower temperatures. Fig: 3.5.3 shows the percentage discrepancies, for the calculated values of W_{fuel} as a function of T_{tout} , between the various fluid models ("no dissociation", " $\%_{\text{diss}} = 33\%$ " and " $\%_{\text{diss}} = 66\%$ ") and the chemical equilibrium fluid model. The main observations that can be made are as follows:

1. The design point ($T_{\text{tout}} = 1800\text{K}$) W_{fuel} discrepancy, between the "no dissociation" fluid model and chemical equilibrium fluid model simulations is approximately 1.1%. This is not negligible for gas turbine performance simulation calculations.
2. As expected, the W_{fuel} discrepancy between the "no dissociation" fluid model and the chemical equilibrium fluid model simulations increases significantly with an increase in T_{tout} . For $T_{\text{tout}} = 2200\text{K}$, this discrepancy is approximately 2.3% and is certainly not negligible.
3. For a given value of T_{tout} , the discrepancy between the chemical equilibrium fluid model ($\%_{\text{diss}} = 100\%$) increases as $\%_{\text{diss}}$ decreases. The results for the $\%_{\text{diss}} = 33\%$ and $\%_{\text{diss}} = 66\%$ fluid models have only been presented as references. In reality, the Burner combustion reaction reaches chemical equilibrium. The $\%_{\text{diss}} = 33\%$ and $\%_{\text{diss}} = 66\%$ fluid models are therefore only applicable for components downstream of the Burner as discussed in *Section 2.1.3* and *Section 2.1.12*.

3.5.3: Afterburner Component Case Study:

For the Afterburner component case study a range of $1900\text{K} \leq T_{\text{tout}} \leq 2400\text{K}$ was investigated. An upper temperature limit of 2400K was chosen for T_{tout} as this is the temperature which corresponds to a calculated value of W_{fuel} required for Stoichiometric combustion (for the presented case study). Beyond this temperature, the combustion reaction would be fuel rich and therefore the calculation would be inaccurate as the PROOSIS fluid models do not currently cater for fuel rich mixtures. (In reality, however, the maximum attainable temperature would be slightly lower as $\approx 10\%$ of the inlet gas mass flow would be used for Afterburner cooling.) As for the Burner component case study, existing material restrictions were ignored. For the CULBR engine model, the design point Afterburner T_{tout} is approximately 2000K (to achieve the rated “wet” thrust).

Fig: 3.5.4 shows the effects of dissociation on the calculated values of W_{fuel} as a function of T_{tout} for the Afterburner component boundary conditions summarised in Fig: 3.5.1. Fig: 3.5.5 shows the percentage discrepancies, for the calculated values of W_{fuel} as a function of T_{tout} , between the various fluid models (“no dissociation”, “ $\%_{\text{diss}} = 33\%$ ” and “ $\%_{\text{diss}} = 66\%$ ”) and the chemical equilibrium fluid model. The main observations are consistent with those obtained for the Burner component case study and are as follows:

1. The design point ($T_{\text{tout}} = 2000\text{K}$) W_{fuel} discrepancy, between the “no dissociation” fluid model and chemical equilibrium fluid model simulations is approximately 1.1% . This is not negligible for gas turbine performance simulation calculations.
2. As expected, the W_{fuel} discrepancy between the “no dissociation” fluid model and the chemical equilibrium fluid model simulations increases significantly with an increase in T_{tout} . For $T_{\text{tout}} = 2400\text{K}$, this discrepancy is approximately 3% and is certainly not negligible.
3. For a given value of T_{tout} , the discrepancy between the chemical equilibrium fluid model ($\%_{\text{diss}} = 100\%$) increases as $\%_{\text{diss}}$ decreases.

3.6: Burner Emissions Component Testing and Limitations

3.6.1: Introduction

A typical isolated Burner_Emissions component performance simulation is presented in this section with the aid of a case study. The presented case study reveals several limitations of emissions correlations available in the public domain. The isolated Burner_Emissions component simulations are based on the Burner component of the CUHBR engine model described in *Section 3.5*. The boundary conditions used for each case study are identical to the boundary conditions used for the case studies described in *Section 3.5* and are summarised in Fig: 3.5.1.

NB: A. Lefebvre's NO_x correlation ^[24] (refer to Section 3.2.2 – NO_x Correlation Option 1- [Eq. 3.2.2]), was used for the presented case study. However the results obtained and limitations presented below are valid for all the other correlations.

3.6.2: Burner Emissions Component Case Study:

It is important to note that only the chemical equilibrium fluid model is valid for the calculations of the Burner_Emissions component. Using the “no dissociation” model for this component is physically meaningless as the “no dissociation” model assumes that the products of combustion comprise only H₂O, CO₂, Ar, N₂ and O₂ (if the reaction is fuel lean), as discussed in *Section 2.1.3*.

In addition to the boundary conditions in Fig: 3.5.1, the following boundary conditions were specified as DATA in the attributes editor Burner_Emissions component:

1. $F_{pz} = 0.65$

Although the default value of F_{pz} in the attributes editor of the Burner_Emissions component is 0.2 (Refer to *Section 3.2.2*), the reasons for choosing $F_{pz} = 0.65$ (for this particular case study) are justified below.

Fig: 3.6.1 shows the effects of F_{pz} on FAR_{pz} and consequently T_{fl} for $T_{tout} = 1800K$ (the design point value of T_{tout}) and the boundary conditions specified in Fig: 3.5.1. It can be observed that F_{pz} cannot be reduced below 0.4 as this would result in fuel rich combustion in the primary zone. Since the PROOSIS fluid model tables have been accurately generated to cater for fuel lean to Stoichiometric combustion, the results obtained for $F_{pz} < 0.4$ would be questionable. In practice, gas turbine burners are designed to ensure that that $FAR_{pz} \approx FAR_{Stoich}$ to achieve the maximum temperature rise for a given fuel flow. For this case study however, a value of $F_{pz} = 0.65$ was chosen. Although using a value of $F_{pz} = 0.65$ at design point ($T_{tout} = 1800K$) results in lean primary zone combustion, it allows the off-design analysis (for this particular case study) to be extended to Burner outlet temperatures of 2200K whilst ensuring $FAR_{pz} \leq FAR_{Stoich}$.

NB: For $F_{pz} = 1$, $T_{fl} = T_{tout}$ and $FAR_{pz} = FAR_{Bout}$

2. $V_b = 0.03m^3$, $V_e = 0.00014 m^3$

Since combustor volume DATA is not easily available in the public domain, intelligent guesses were made for the values of V_b and V_e .

3. $s_1 = s_2 = s_3 = s_4 = 1$
The absolute values of the scalars (for the purposes of the presented case study) are not important and were therefore all set to unity (implying no scaling).
4. $dPqP_{cold} = 0.03$
As mentioned in *Section 3.1.3*, good Burner designs typically have values of cold pressure loss between 2% and 4%.

Fig: 3.6.2 shows the rate of NO_x emissions (WNO_x) as a function of T_{tout} . WNO_x is defined as shown in [Eq. 3.6.1].

$$WNO_x = EINO_x \times W_{fuel} \quad \text{[Eq. 3.6.1]}$$

Fig: 3.6.3 shows the rate of CO emissions (WCO) as a function of T_{tout} . WCO is defined as shown in [Eq. 3.6.2].

$$WCO = EICO \times W_{fuel} \quad \text{[Eq. 3.6.2]}$$

Fig: 3.6.4 shows the rate of UHC emissions ($WUHC$) as a function of T_{tout} . $WUHC$ is defined as shown in [Eq. 3.6.3].

$$WUHC = EIUHC \times W_{fuel} \quad \text{[Eq. 3.6.3]}$$

From Fig: 3.6.2 – Fig: 3.6.4 the main observations that can be made are as follows:

1. As expected, the rate of NO_x emissions (WNO_x) increases with an increase in T_{tout} . As discussed in *Section 2.1.9*, the higher the temperature, the higher the level of dissociation and therefore the higher the concentration of NO_x.
NB: With respect to A. Lefebvre's NO_x emissions model, as T_{tout} increases, W_{fuel} increases and therefore FAR_r also increases. Consequently, for a fixed value of F_{pz} , FAR_{pz} also increases ([Eq. 3.2.4]). For fixed values of all the Burner inlet port variables (W_{in} , P_{tin} , T_{tin} , FAR_{Bin} , FAR_{Uin} , WAR_{in} and Ang_{in}) and fixed values of η_b and LHV, an increase in FAR_{pz} implies an increase in h_{tpz} ([Eq. 3.2.5]) and consequently a higher value of T_{fl} ([Eq. 3.2.6]). A higher value of T_{fl} implies a higher value of $EINO_x$ and subsequently a higher value of WNO_x .
2. The rate of CO (WCO) and UHC ($WUHC$) emissions initially decrease with an increase in T_{tout} . As expected higher values of T_{tout} favour complete combustion and consequently less CO and UHC are present as T_{tout} increases. This however, is only true for temperatures where dissociation does not occur. At higher temperatures, which favour dissociation, an increase in T_{tout} should result in an increase in CO and UHC (as discussed in *Section 2.1.9*). Therefore, as T_{tout} increases, WCO and $WUHC$ should decrease (until $\approx 1900K$) and then increase. Fig: 3.6.3 and Fig: 3.6.4 clearly suggest that a limitation with the emissions correlations for CO and UHC is that they calculate $EICO$ and $EIUHC$ on the basis of combustion "completeness" only and do not account for the effects of dissociation. Therefore it can be deduced that the

correlations are only valid for temperatures less than 1900K where the effects of dissociation on CO and UHC emissions are negligible.

One approach to rectify this could be to directly connect a chemical equilibrium software (e.g. CEA) to PROOSIS so that at any point an accurate calculation of the exact chemical equilibrium composition corresponding to a specific T_{tout} , W_{out} and FAR_{out} (including the concentration of NO_x, CO and UHC) could be readily available. This would eliminate the need for emissions correlations. Fig: 3.6.5 shows how the chemical composition of the NO and CO content of the products of combustion of Jet-A varies with T_{tout} for a fixed FAR_{out} and WAR_{out} and can be used as a qualitative comparison to the results obtained in Fig: 3.6.2 – Fig: 3.6.4. Fig: 3.6.5 was generated from the output file of a CEA simulation. Although the NO characteristic is quite accurate, Fig: 3.6.6 seems to suggest that CO emissions at lower temperatures (200K – 1900K) are negligible. This is in contrast to results obtained in Fig: 3.6.4. It is therefore evident that the CEA chemical equilibrium calculations do not account for combustion “completeness” which is a function of several factors like Burner efficiency, primary zone residence time, inadequate mixing of fuel and air and quenching of post flame products of combustion. Clearly these factors cannot be implemented in chemical equilibrium software such as CEA as they are specific to gas turbine applications only. Therefore although the NO calculations of the CEA software are accurate, correction factors would need to be applied to the CO results.

Currently the emissions correlations available in the public domain only cater for relatively modest values of T_{tout} . It is the author’s view that engine rig tests should be extended to cater for higher values of T_{tout} so that the correlations account for the effects of dissociation thereby yielding accurate results for a broader range of T_{tout} .

NB: It is highly likely that such correlations have already been developed by industrial companies (for their in-house legacy gas turbine performance simulation software) but have not been published in the public domain.

Chapter 3: Figures

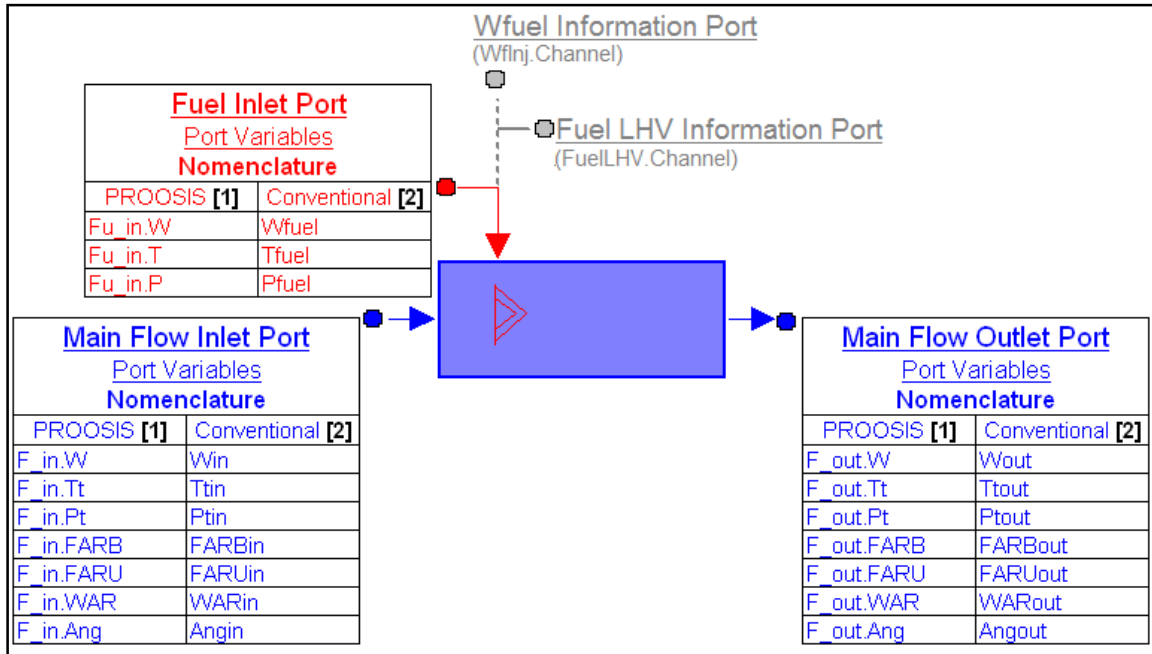


Fig: 3.1.1 Burner Component Icon, Ports and Port Variables

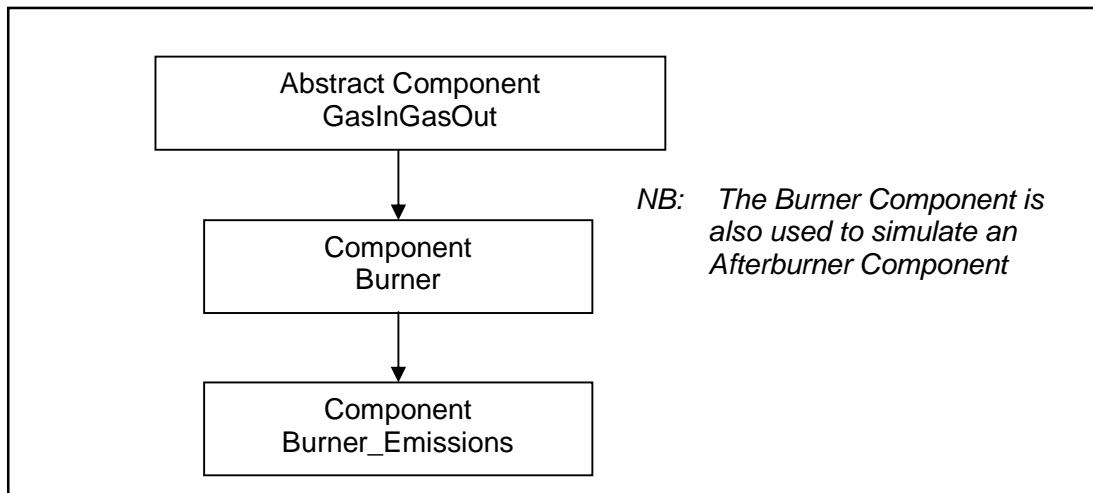


Fig: 3.1.2 Burner Component Hierarchy

Advanced Performance Simulation of Gas Turbine Components and Fluid Thermodynamic Properties

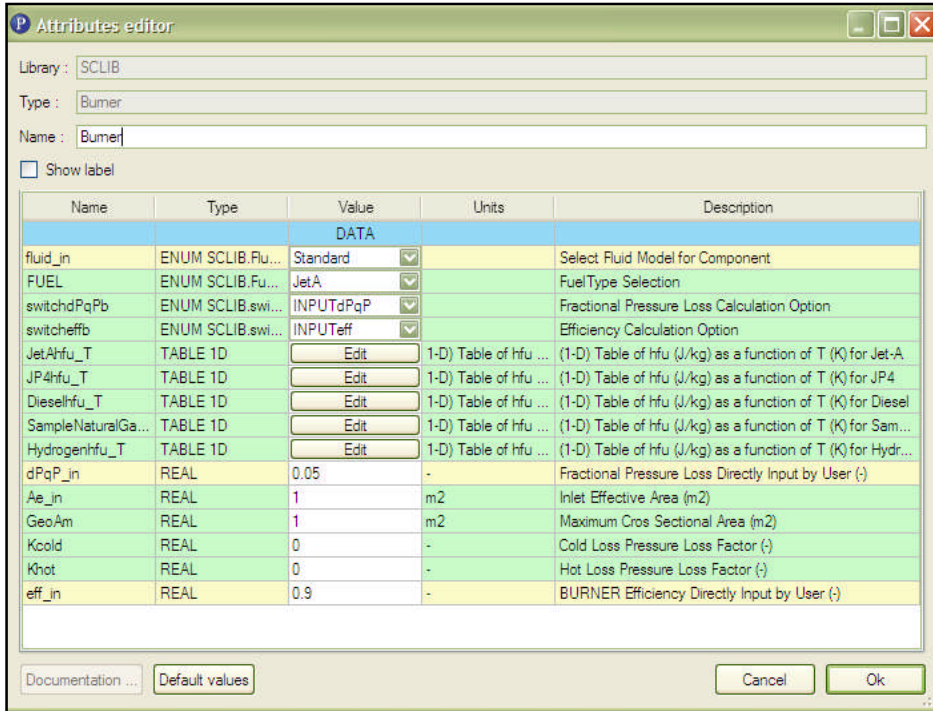


Fig. 3.1.3 Burner Component (Old) Attributes Editor

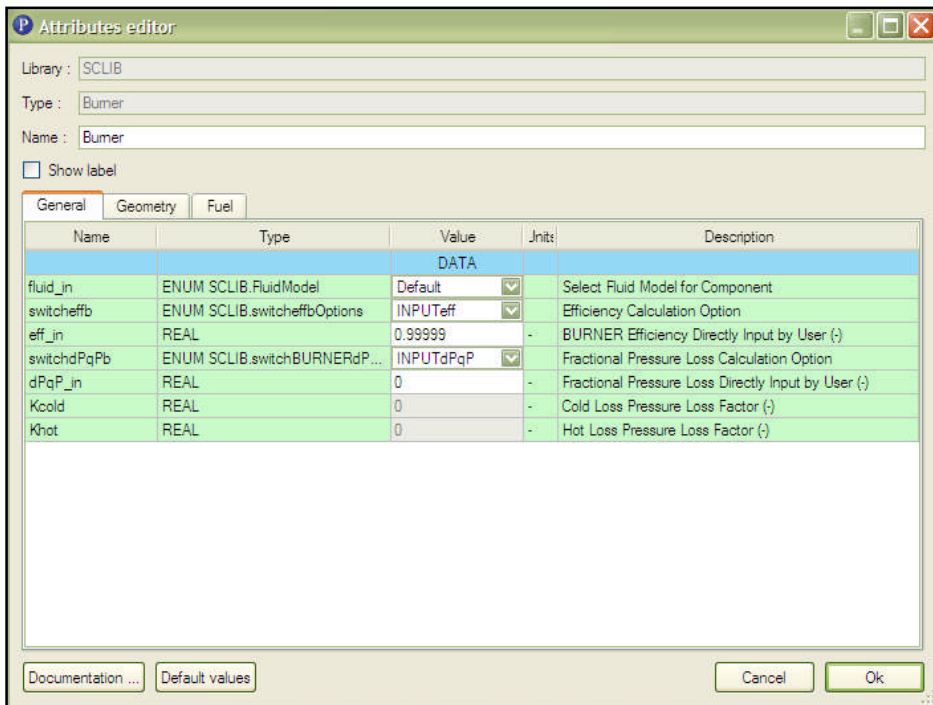


Fig. 3.1.4 Burner Component (New "Intelligent") Attributes Editor

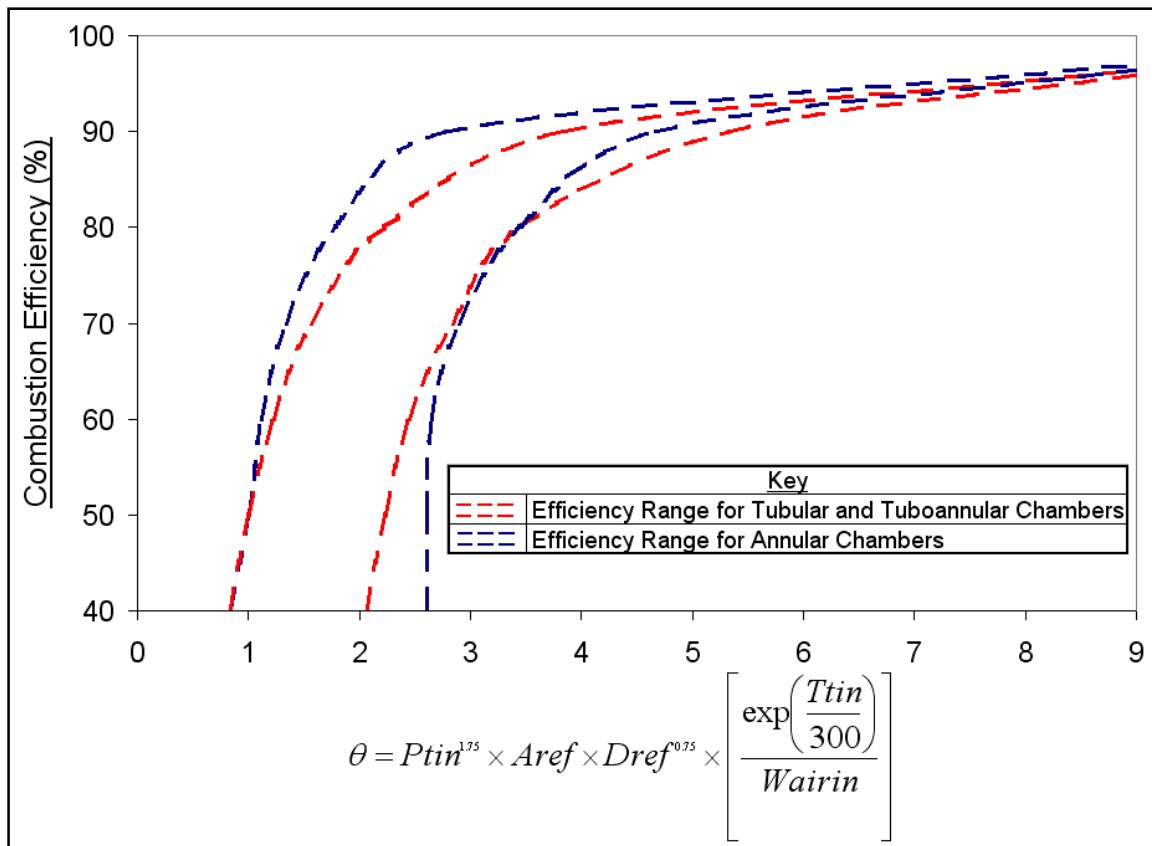


Fig: 3.1.5 Burner Efficiency Map for Different Chamber Configurations [4]

Fuel	LHV (x10⁷ J/kg)
Jet – A _(g)	4.3124
Diesel _(g)	4.2600
Sample Natural Gas _(g)	4.8120
Hydrogen _(g)	12.000

Fig: 3.1.6 Default Lower Heating Values for PROOSIS Fuels [6]

Advanced Performance Simulation of Gas Turbine Components and Fluid Thermodynamic Properties

Attributes editor

Library: SCLIB

Type: Burner_Emissions

Name: Bm_Emm

Show label

Name	Type	Value	Units	Description
DATA				
fluid_in	ENUM SCLIB.FluidModel	Standard		Select Fluid Model for Component
FUEL	ENUM SCLIB.FuelType	JetA		Fuel Type Selection
switchdPaPb	ENUM SCLIB.switchBURNERdPaPbOptions	INPUTdPaP		Fractional Pressure Loss Calculation Option
switcheffb	ENUM SCLIB.switcheffbOptions	INPUTeff		Efficiency Calculation Option
JetAfu_T	TABLE 1D			(1-D) Table of hfu (J/kg) as a f... (1-D) Table of hfu (J/kg) as a function of T (K) for Jet-A
JP4fu_T	TABLE 1D			(1-D) Table of hfu (J/kg) as a f... (1-D) Table of hfu (J/kg) as a function of T (K) for JP4
Dieselfu_T	TABLE 1D			(1-D) Table of hfu (J/kg) as a f... (1-D) Table of hfu (J/kg) as a function of T (K) for Diesel
SampleNaturalGasfu_T	TABLE 1D			(1-D) Table of hfu (J/kg) as a f... (1-D) Table of hfu (J/kg) as a function of T (K) for SampleNaturalGas
Hydrogenfu_T	TABLE 1D			(1-D) Table of hfu (J/kg) as a f... (1-D) Table of hfu (J/kg) as a function of T (K) for Hydrogen
dPaP_in	REAL	0	-	Fractional Pressure Loss Directly Input by User (-)
Ae_in	REAL	1	m2	Inlet Effective Area (m2)
GeoAm	REAL	1	m2	Maximum Cros Sectional Area (m2)
Kcold	REAL	0	-	Cold Loss Pressure Loss Factor (-)
Khot	REAL	0	-	Hot Loss Pressure Loss Factor (-)
eff_in	REAL	0.99999	-	BURNER Efficiency Directly Input by User (-)
XFuelCustom[FuelComp]	ARRAY REAL	{ 0.05,0.15,0.0,0 }	-	Custom Fuel Mass Fractions
NOxSwitch	ENUM SCLIB.NOxSwitchOptions	DOP		Select correlation for EINOx calculation
Fpz	REAL	0.6	-	Air/Fraction in Primary Zone in DOP
P3ref	REAL	1670000	Pa	Reference Burner Inlet Pressure in DOP
T3ref	REAL	683	K	Reference Burner Inlet Temperature in DOP
TpzRef	REAL	1553	K	Reference Burner Primary Zone Temperature in DOP
TfRef	REAL	2423	K	Reference Burner Flame Temperature in DOP
EINOxRef	REAL	45	gr/kg	Reference NOx Emissions Index in DOP
ERef	REAL	0.8	-	Reference Equivalence Ratio
Vb	REAL	0.07	m3	Burner volume in SNM
tEvap	REAL	0.002	sec	Fuel Evaporation time
s_NOx[7]	ARRAY REAL	{ 1,1,1,1,1,1,1 }	-	NOx correlation adaptation scalars
s_CO[5]	ARRAY REAL	{ 1,1,1,1,1 }	-	CO correlation adaptation scalars
s_UHC[4]	ARRAY REAL	{ 1,1,1,1 }	-	UHC correlation adaptation scalars
s_Soot[4]	ARRAY REAL	{ 1,1,1,1 }	-	Soot correlation adaptation scalars
c[4]	ARRAY REAL	{ 10,0.5,300,1 }	-	Default coefficients in GEN

Documentation | Default values | Cancel | Ok

Fig: 3.2.1 Burner_Emissions Component Attributes Editor

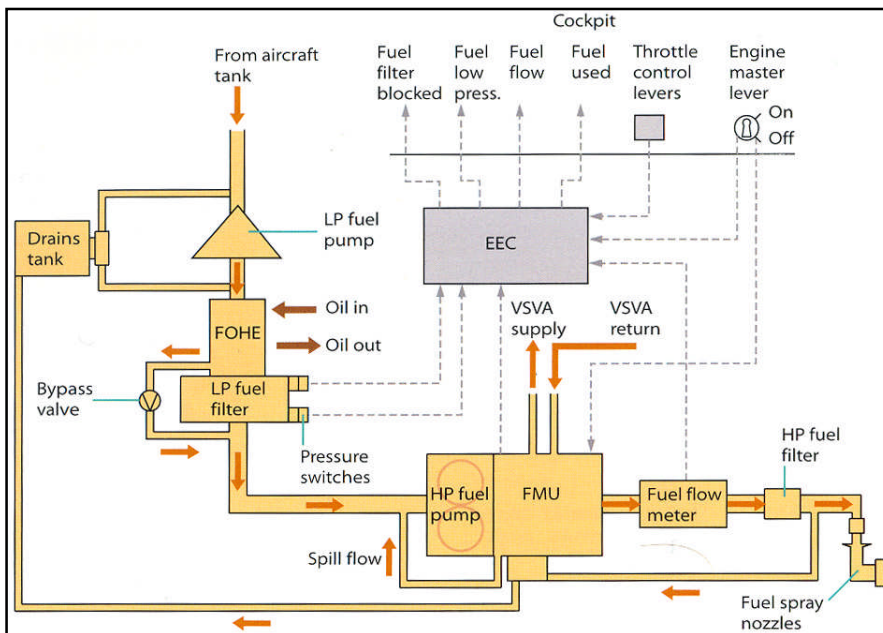


Fig: 3.3.1 Schematic of a Typical Engine Fuel System [29]

Advanced Performance Simulation of Gas Turbine Components and Fluid Thermodynamic Properties

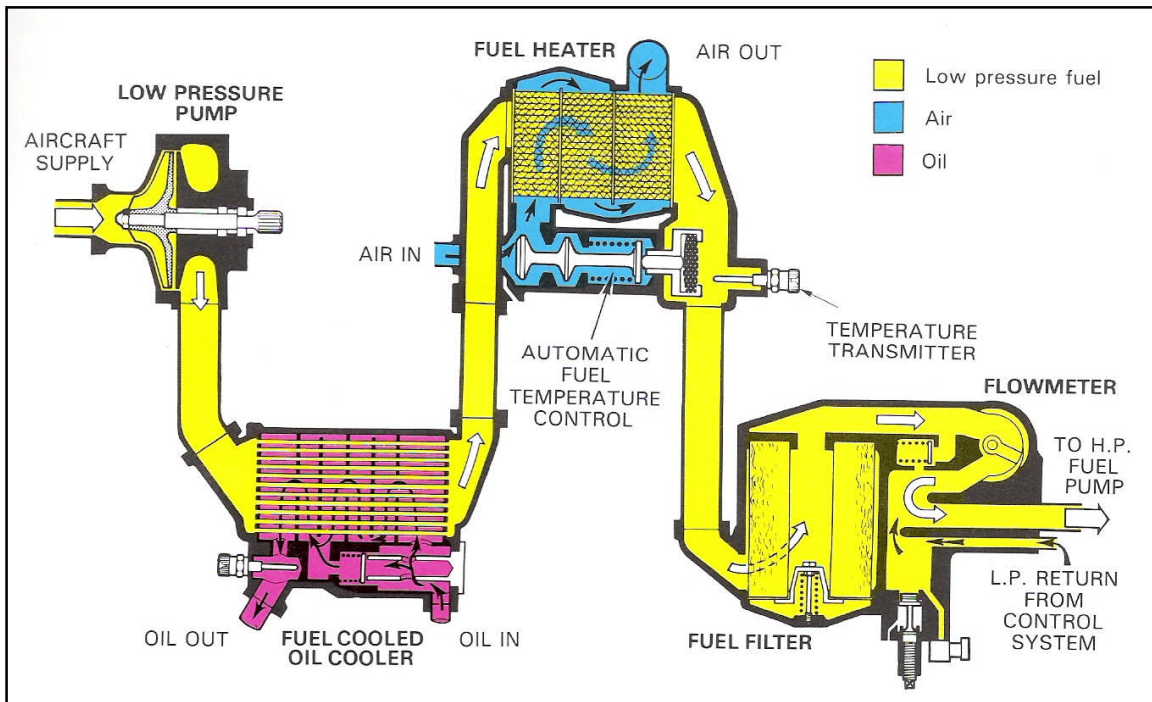


Fig: 3.3.2 Typical Engine LP Fuel System [30]

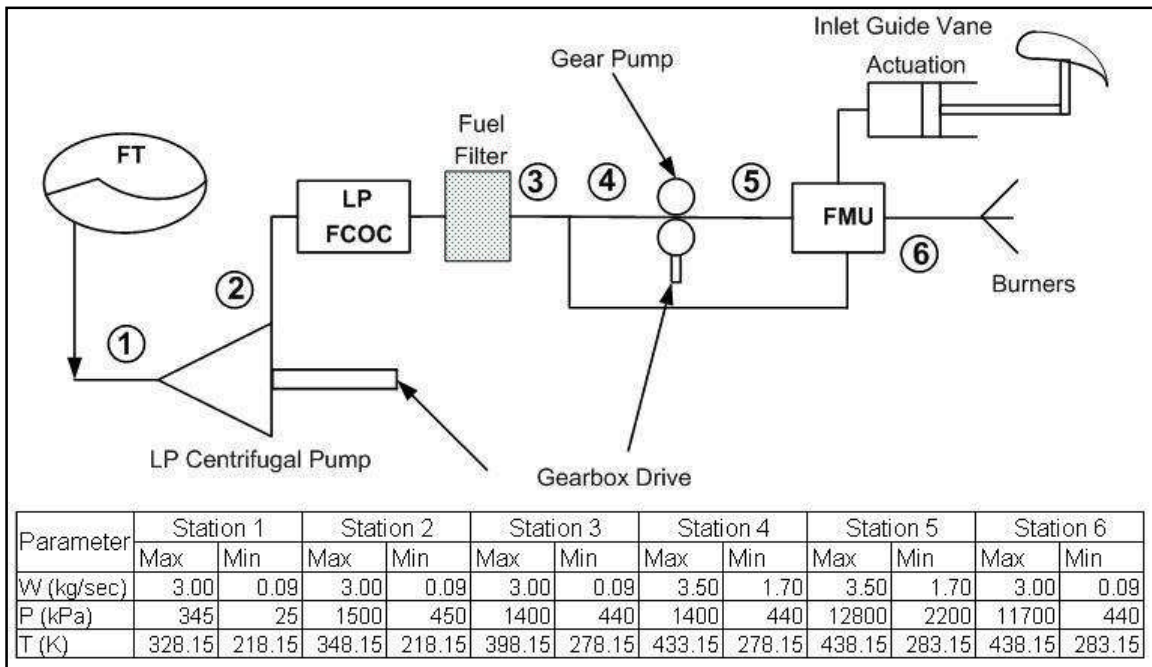


Fig: 3.3.3 Typical Values of Civil Engine Fuel System Parameters [31]

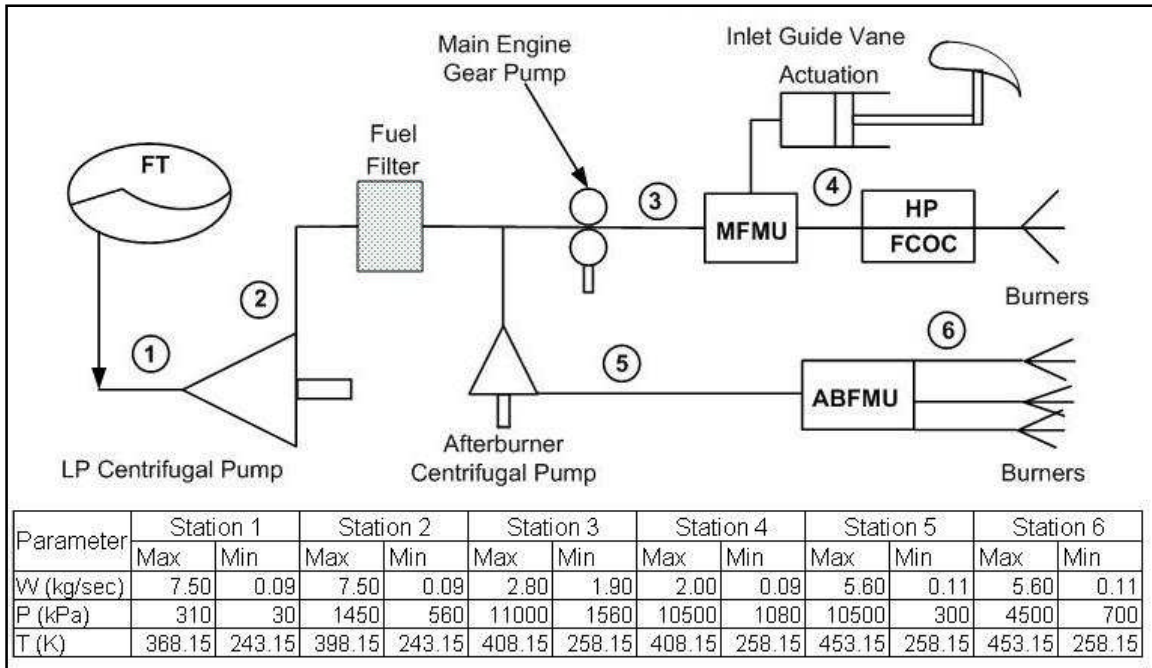


Fig: 3.3.4 Typical Values of Military Engine Fuel System Parameters [31]

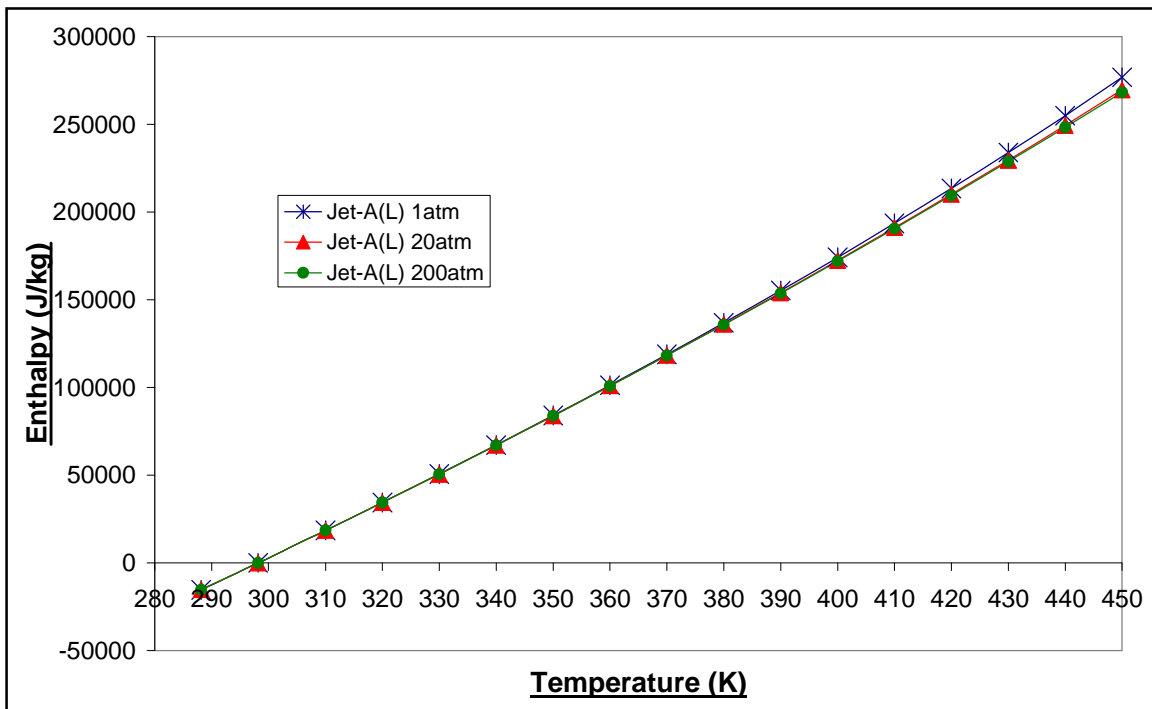


Fig: 3.3.5 Variation of Jet-A₍₀₎ Enthalpy with Temperature and Pressure

Advanced Performance Simulation of Gas Turbine Components and Fluid Thermodynamic Properties

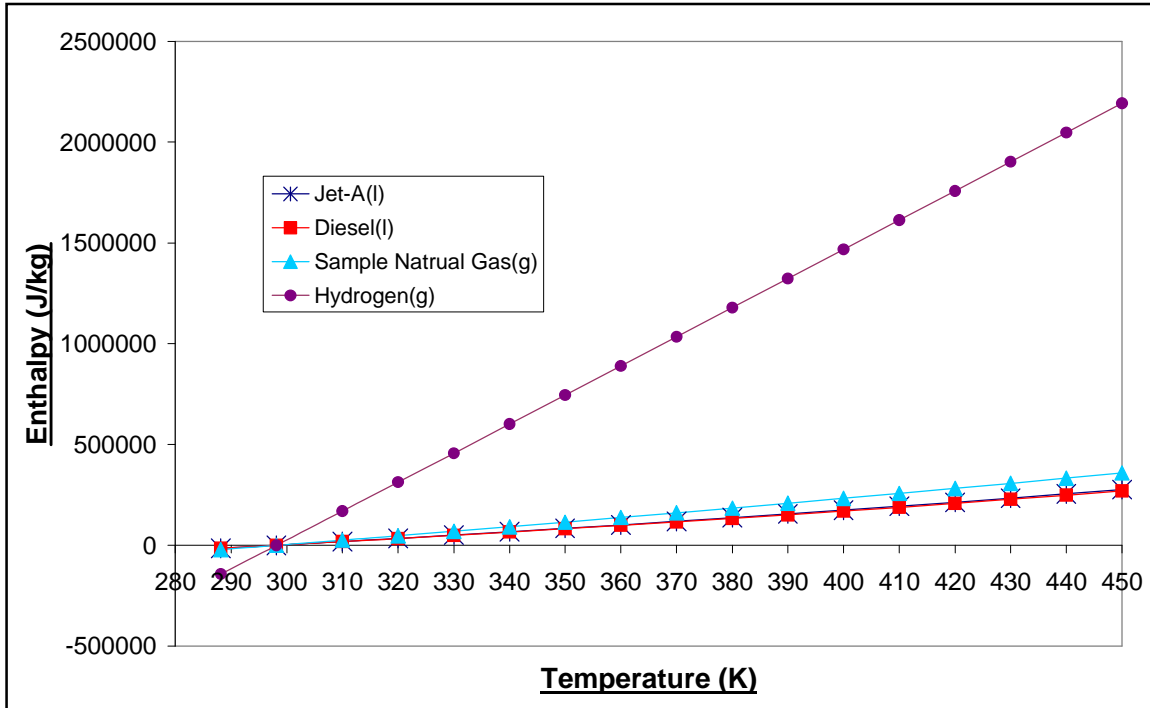


Fig: 3.3.6 Variation of Fuel Enthalpy with Temperature

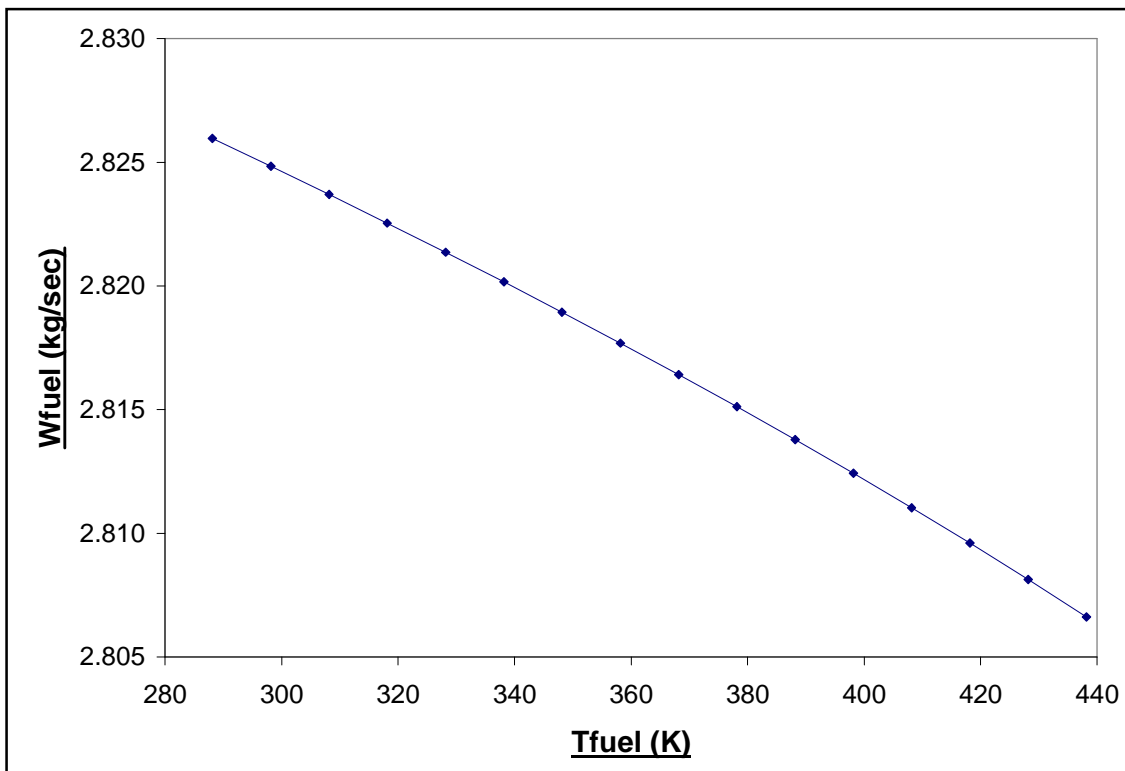


Fig: 3.3.7 Case Study 1: Effect of Fuel Injection Temperature on the Required Fuel Mass Flow Rate for a Given Burner Outlet Total Temperature (Isolated Burner)

Advanced Performance Simulation of Gas Turbine Components and Fluid Thermodynamic Properties

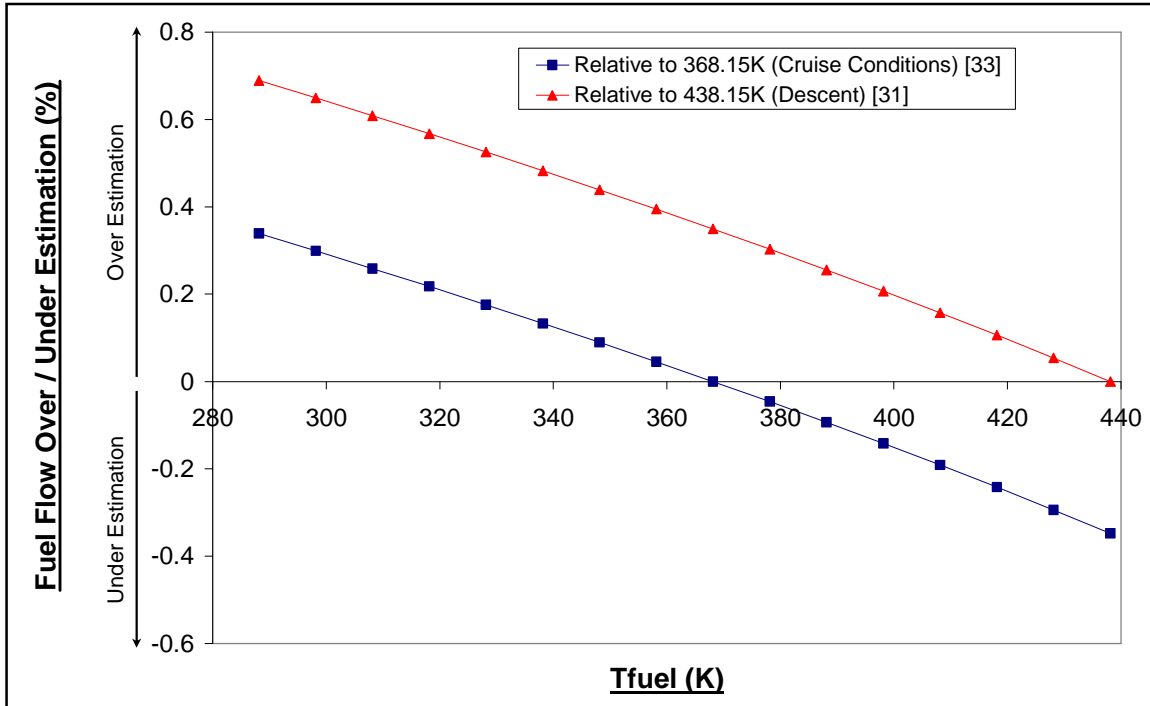


Fig: 3.3.8 Case Study 1: Relative Fuel Flow Over/Under Estimation as a Function of Fuel Injection Temperature (Isolated Burner)

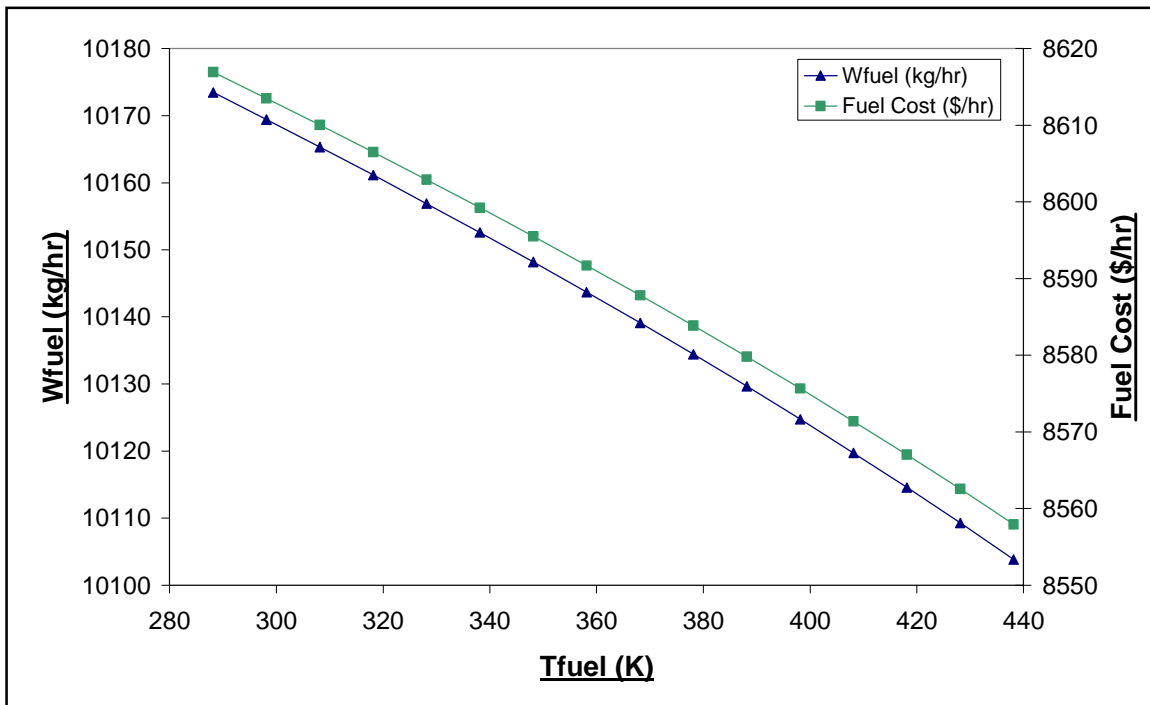


Fig: 3.3.9 Case Study 1: Effect of Fuel Injection Temperature on the Required Fuel Mass Flow Rate and subsequently the Fuel Cost (Isolated Burner)

Advanced Performance Simulation of Gas Turbine Components
and Fluid Thermodynamic Properties

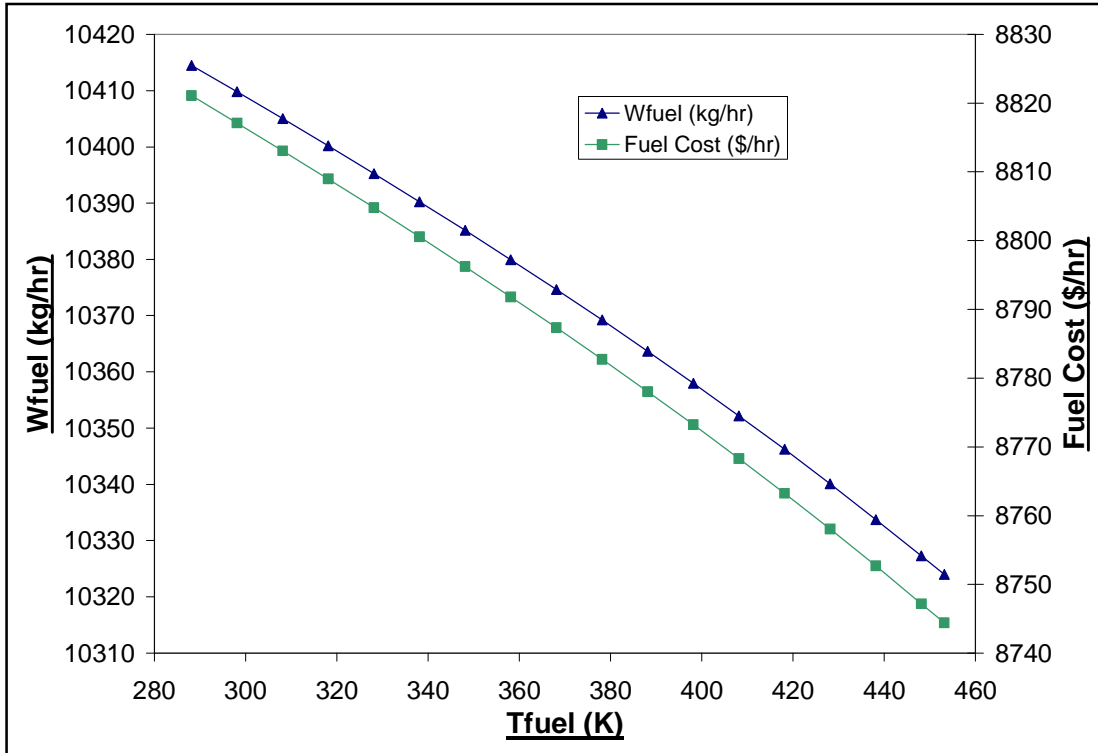


Fig. 3.3.10 Case Study 2: Effect of Fuel Injection Temperature on the Required Fuel Mass Flow Rate and Subsequently the Fuel Cost (Isolated Afterburner)

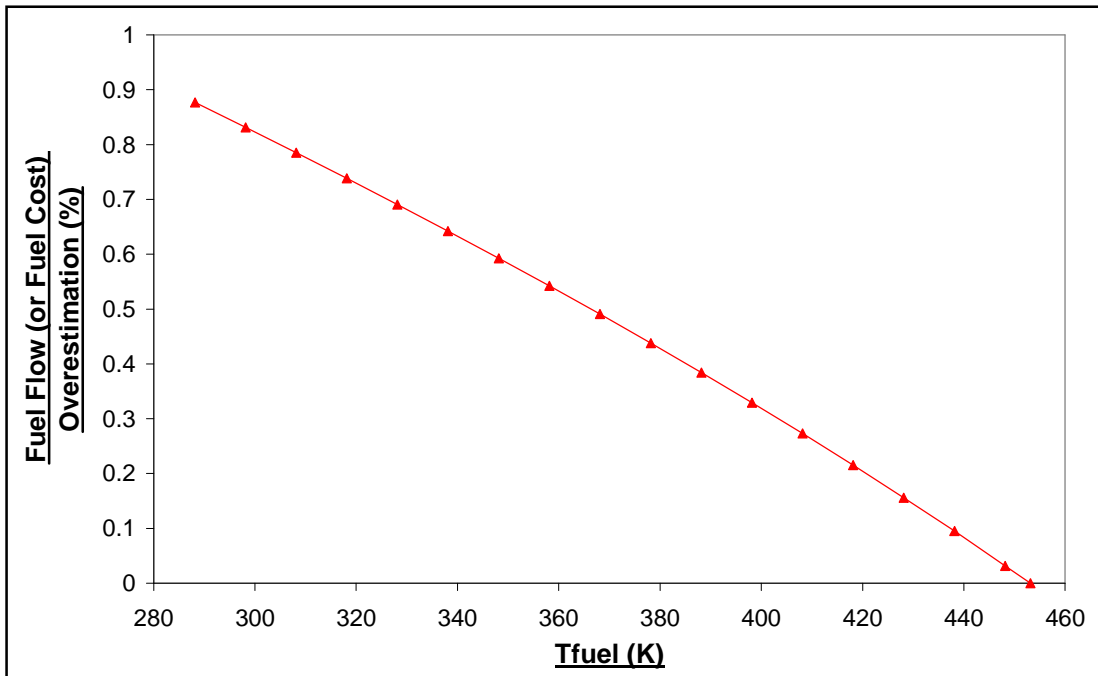


Fig. 3.3.11 Case Study 2: Relative Fuel Flow Over (or Fuel Cost) Estimation as a Function of Fuel Injection Temperature (Isolated Afterburner)

Advanced Performance Simulation of Gas Turbine Components
and Fluid Thermodynamic Properties

Boundary Condition	Case Study 1	Case Study 2	Case Study 3	Case Study 4
Win (kg/s)	15.20	13.60	11.60	6.70
Ttin (K)	600.00	566.00	533.00	439.00
Ptin (Pa)	592000	506000	416000	213000
FARBin (-)	0	0	0	0
FARUin (-)	0	0	0	0
WARin (-)	0	0	0	0
Angin (-)	0	0	0	0
Wfuel (kg/s)	0.33	0.26	0.2	0.09
Tfuel (K)	288.15, 358.15 & 438.15	288.15, 358.15 & 438.15	288.15, 358.15 & 438.15	288.15, 358.15 & 438.15
Pfuel (Pa)	101325	101325	101325	101325
dPqP (-)	0.05	0.05	0.05	0.03
$\eta_{b,c}$	1.00	1.00	1.00	1.00

Fig: 3.4.1 Boundary Conditions for the Presented Case Studies for Isolated Burner Component Testing and Validation

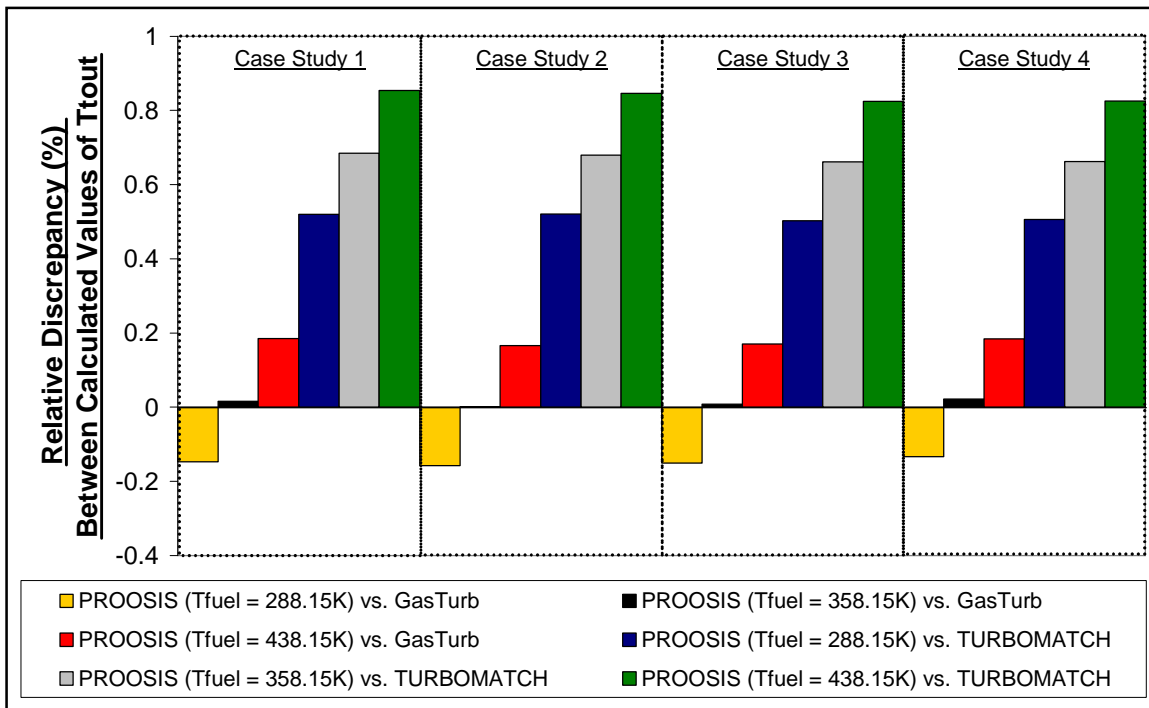


Fig: 3.4.2 Relative Discrepancies for the Calculated Value of T_{out} (Based on the Boundary Conditions in Fig: 3.4.1) Between:

1. PROOSIS and GasTurb (for different values of T_{fuel})
2. PROOSIS and TURBOMATCH (for different values of T_{fuel})

Advanced Performance Simulation of Gas Turbine Components
and Fluid Thermodynamic Properties

Boundary Condition	Case Study	
	Burner Component	Afterburner Component
Win (kg/s)	104.80	76.22
Ttin (K)	928.40	906.30
Ptin (Pa)	4211780	349753
FARBin (-)	0.00	0.016245
FARUin (-)	0.00	0.000055
WARin (-)	0.00	0.00
Angin (-)	0.00	0.00
Tfuel (K)	368.15	388.15
Pfuel (Pa)	101325	101325
dPqP (-)	0.06	0.05
η_b (-)	0.998	0.90
Ttout Range (K)	2200 - 1600	2705 - 1905

Fig: 3.5.1 Boundary Conditions for the Presented Case Studies to Demonstrate the Effects of Dissociation of Isolated Burner Component and Isolated Afterburner Component Performance Simulation

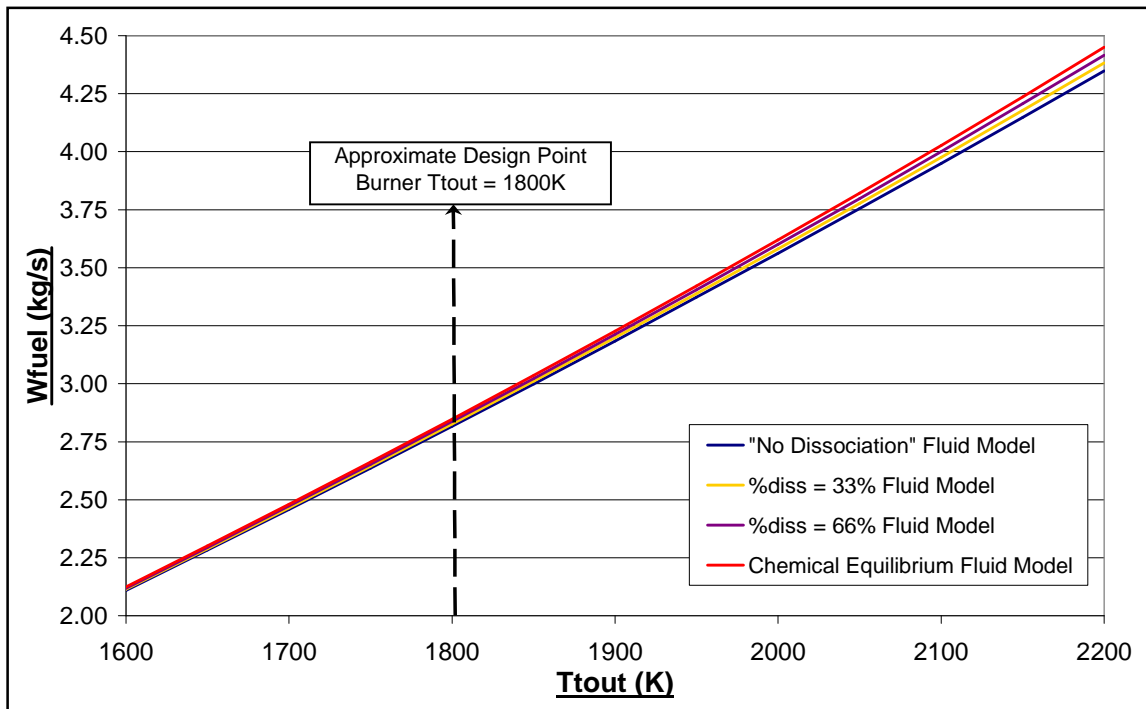


Fig: 3.5.2 Burner Component Case Study: Effects of $\%_{diss}$ on the calculated values of W_{fuel} as a function of T_{tout}

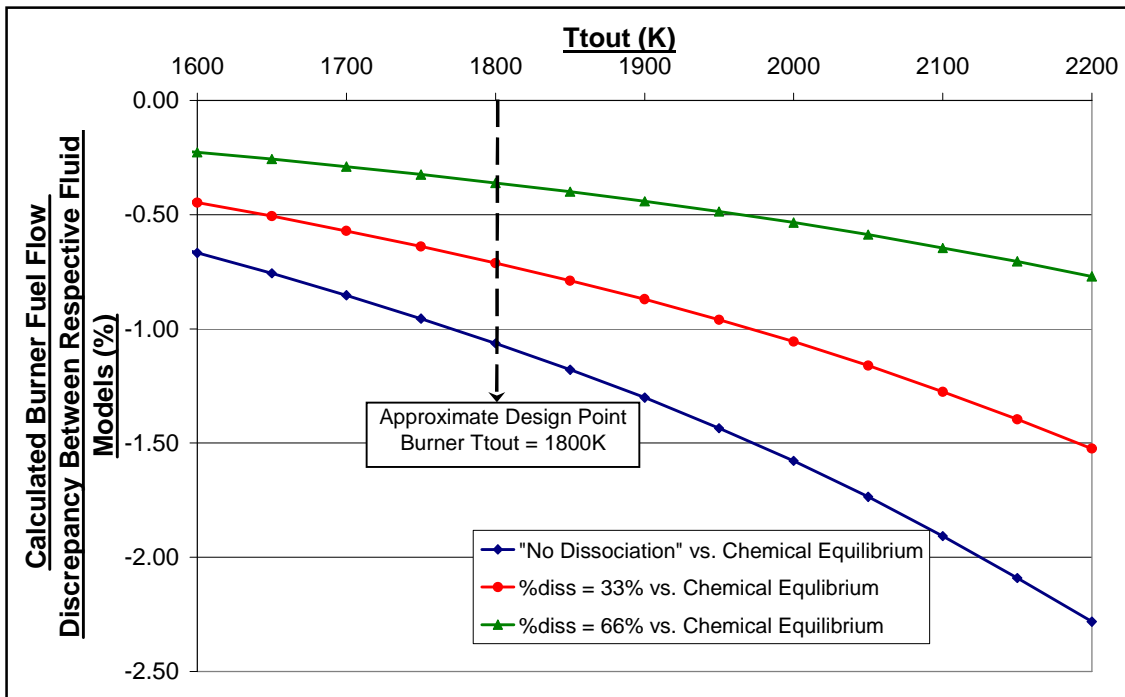


Fig: 3.5.3 Burner Component Case Study:
 Discrepancies for the calculated values of W_{fuel} as a function of T_{tout} between:
 a. The "No Dissociation" and the Chemical Equilibrium Fluid Models
 b. The $\%_{diss} = 33\%$ and the Chemical Equilibrium Fluid Models
 c. The $\%_{diss} = 66\%$ and the Chemical Equilibrium Fluid Models

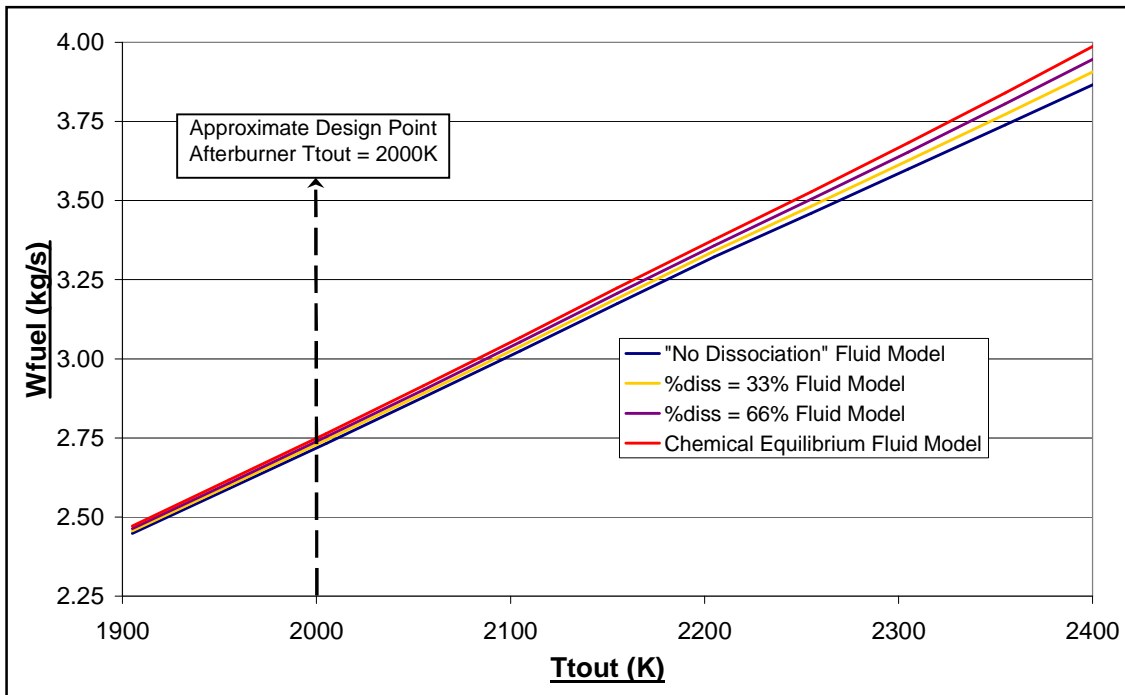


Fig: 3.5.4 Afterburner Component Case Study:
 Effects of $\%_{diss}$ on the calculated values of W_{fuel} as a function of T_{tout}

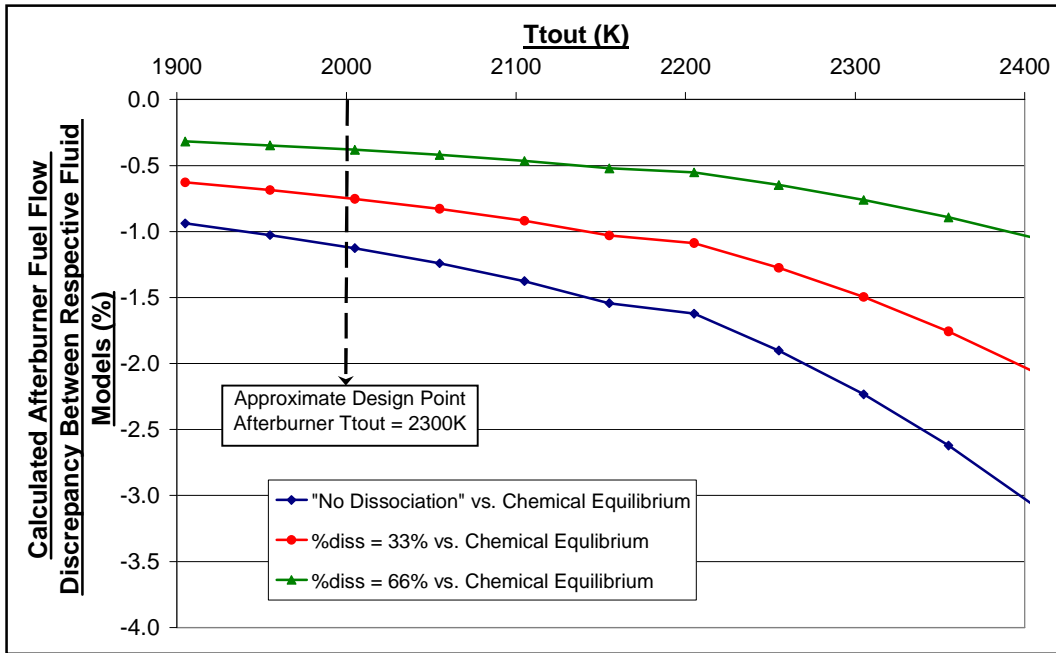


Fig: 3.5.5 Afterburner Component Case Study:
 Discrepancies for the calculated values of W_{fuel} as a function of T_{total} between:
 a. The "No Dissociation" and the Chemical Equilibrium Fluid Models
 b. The $\%_{diss} = 33\%$ and the Chemical Equilibrium Fluid Models
 c. The $\%_{diss} = 66\%$ and the Chemical Equilibrium Fluid Models

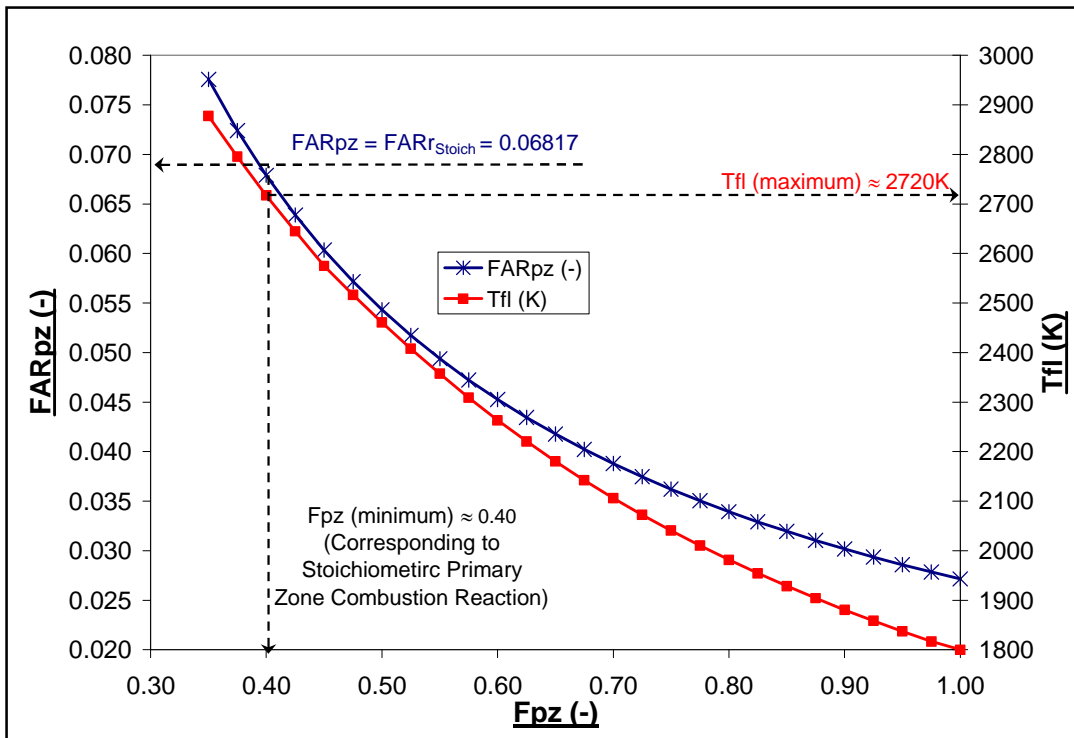


Fig: 3.6.1 Burner_Emissions Component Case Study:
 Effect of F_{pz} on FAR_{pz} and T_{fl} for $T_{total} = 1800K$

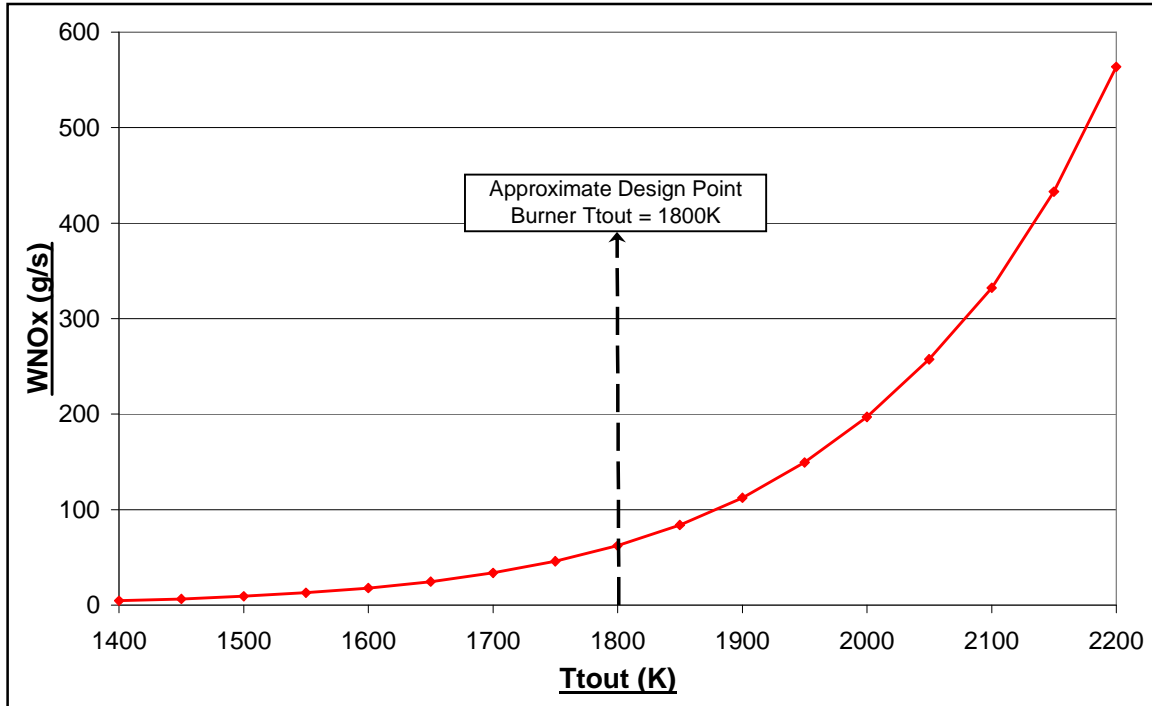


Fig: 3.6.2 Burner_Emissions Component Case Study:
Variation of WNOx as a function of Ttout

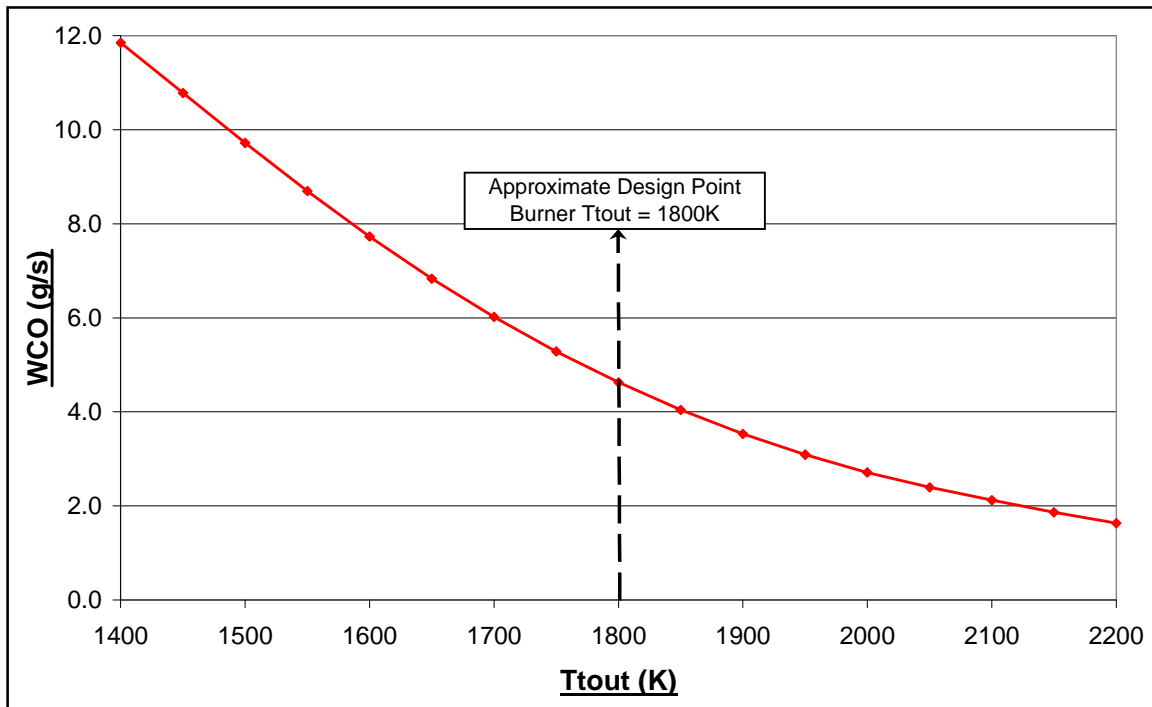


Fig: 3.6.3 Burner_Emissions Component Case Study:
Variation of WCO as a function of Ttout

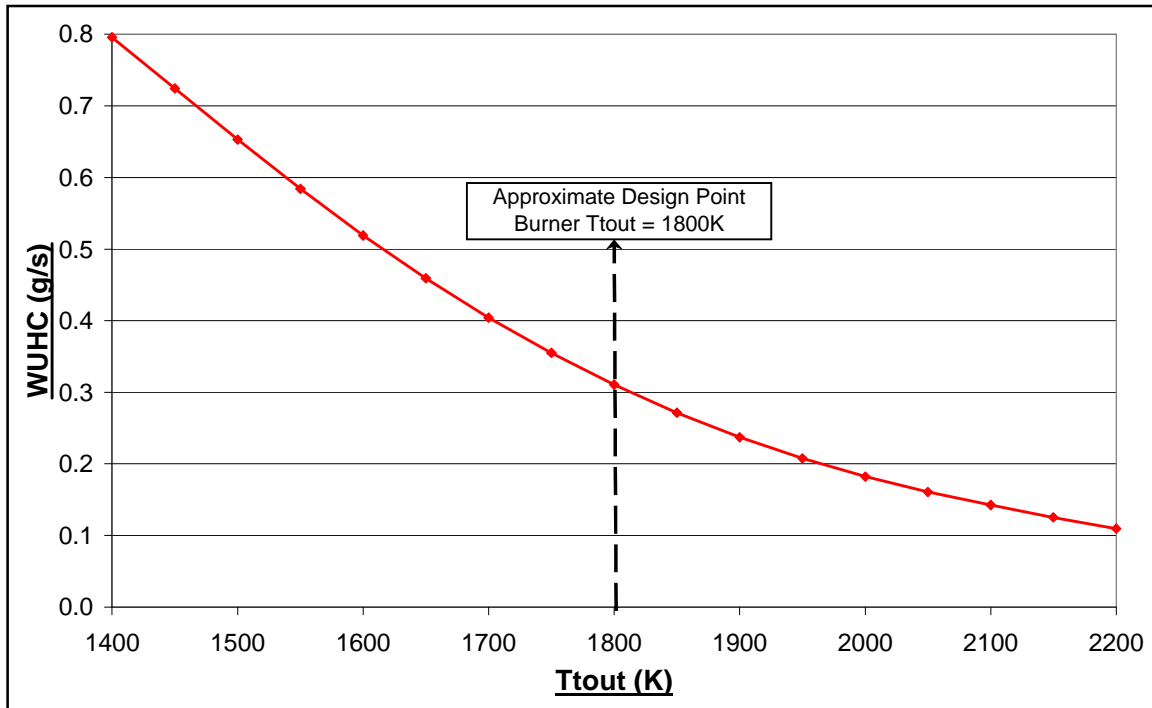


Fig: 3.6.4 Burner_Emissions Component Case Study:
Variation of WUHC as a function of Ttout

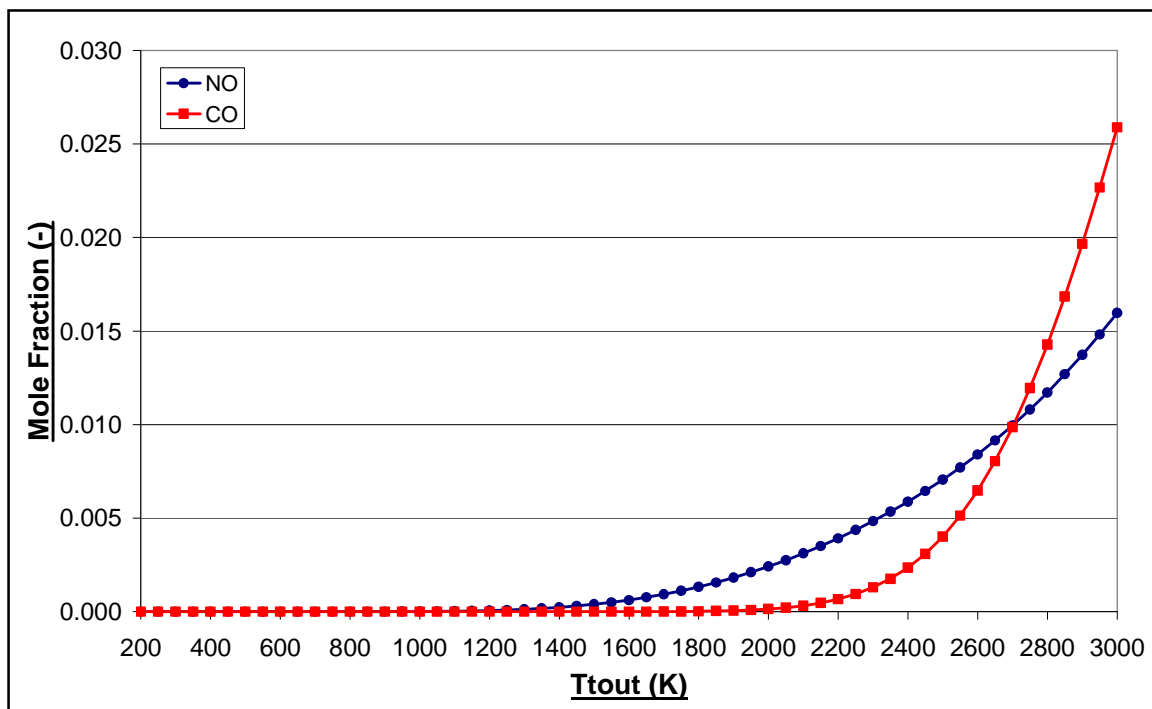


Fig: 3.6.5 Composition of NO and CO present in the Products of the Chemical Equilibrium Combustion of Jet-A as a function of Ttout for FAR_{Bout} = 0.06 and WAR_{out} = 0.10

Chapter 3: References

- [1] SAE, 5th August 2004, "Aerospace Recommended Practice: Gas Turbine Engine Performance Presentation and Nomenclature for Digital Computers Using Object – Oriented Programming", SAE ARP 5571.
- [2] SAE, 1997, "Aircraft Propulsion System Performance Station Designation and Nomenclature", SAE AS 755 C.
- [3] Lefebvre. A. H., 1983, "Gas Turbine Combustion", 1st Edition, New York: Hemisphere Publishing Corporation.
- [4] Singh. R., 2003, "Operational Criteria for Gas Turbine Combustion Systems", Gas Turbine Combustors Course Notes: School of Engineering – Cranfield University.
- [5] Greenhough V.W. and Lefebvre. A. H., 1957, "Some application of Combustion Theory to Gas Turbine Development", Sixth Symposium (international) on Combustion, p.p. 858-869, Reinhold, New York.
- [6] Walsh. P.P. and Fletcher. P., 1998, "Gas Turbine Performance", 2nd Edition, Oxford: Blackwell Science.
- [7] Gordon, S. and McBride, B.J., Oct. 1994, "Computer Program for Calculation of Complex Chemical Equilibrium and Applications: Part I" NASA RP 1311.
- [8] Gordon, S. and McBride, B.J., Jun. 1996, "Computer Program for Calculation of Complex Chemical Equilibrium and Applications: Part II" NASA RP 1311.
- [9] Li, Y. G. and Hales, R. L., Oct. 2003, "Steady and Dynamic Performance and Emissions of a Variable Geometry Combustor in a Gas Turbine Engine", ASME Journal of Engineering for Gas Turbines and Power, Vol.125, pp.961–971.
- [10] Lefebvre, A. H., 1984, "Fuel Effects on Gas Turbine Combustion: Ignition, Stability and Combustion Efficiency", AIAA Journal of Aircraft, 21, No. 11, pp. 887-898.
- [11] Tilston, J., Larkman, J., Plohr, M., Doppelheuer, A., Lischer, T. and Zarzalis N., Aug. 2003, "Future Engine Cycle Prediction and Emissions Study", Final Deliverable Report of CYPRESS Project, G4RD-CT-2000-00383.
- [12] Rizk, N. K. and Mongia, H. C., July 1993, "Semi-analytical Correlations for NO_x, CO and UHC Emissions", ASME Journal of Engineering for Gas Turbines and Power, Vol.115, pp.612-619.
- [13] Held, T. J., Mueller, M. A., Li, S. C., Mongia, H. C., July 2001, "A Data-Driven Model for NO_x, CO and UHC Emissions for a Dry Low Emissions Gas Turbine Combustor" AIAA 2001-3425.

- [14] Mado, J. R. and Roberts, R., Oct. 1974, "A Pollutant Emissions Prediction Model for Gas Turbine Combustors", AIAA-74-1113.
- [15] Cannon, C. M., Smith, C. E., Anand, M. S., July 2003, "LES Predictions of Combustor Emissions in an Aero Gas Turbine Engine" AIAA 2003-4521.
- [16] Rizk, N. K. and Mongia, H. C., July 1993, "Three-Dimensional Gas Turbine Emissions Modelling", ASME Journal of Engineering for Gas Turbines and Power, Vol.115, pp.603-611.
- [17] Alexiou, A. and Mathioudakis, K., (NTUA), 2007, "PROOSIS Standard Component Library: Burner_Emissions Component Specification" VIVACE 2.4.4/NTUA/T/07003.
- [18] Singh. R., 2003, "An Overview: Gas Turbine Generated Pollutants and the Emerging Technology Solutions", Gas Turbine Combustors Course Notes: School of Engineering – Cranfield University.
- [19] Singh. R., 2003, "Control of Pollutant Emissions and Pollutant Generation Processes", Gas Turbine Combustors Course Notes: School of Engineering – Cranfield University.
- [20] Doppelheuer, A. and Lecht, M., 1999, "Influence of Engine Performance on Emission Characteristics", RTO Meeting Proceedings 14 Gas Turbine Engine Combustion, Emissions and Alternative Fuels. RTO-MP-14 AC/323(AVT)TP/10. NATO Research and Technology Organization.
- [21] ICAO Engine Exhaust Emissions Data for the CFM56-5C2 Engine, Official Website, URL: http://www.caa.co.uk/docs/702/1CM010_01102004.pdf
- [22] Saravanamuttoo, H. I. H, Rogers, G. F. C. and Cohen, H., 2001, "Gas Turbine Theory", 5th Edition, Essex: Pearson Education Ltd.
- [23] Tsalavoutas, A., Kelaidis, M., Thoma, N. and Mathioudakis, K., 2007, "Correlations Adaptation for Optimal Emissions Prediction", ASME GT-2007-27060.
- [24] Lefebvre, A. H., June 1984, "Fuel Effects on Gas Turbine Combustion: Linear Temperature Pattern Factor and Pollutant Emissions", AIAA-84-1491.
- [25] Balaal, D. R. and Lefebvre, A. H., 1980, "Flame Propagation in Heterogeneous Mixtures of Fuel Droplets, Fuel Vapour and Air", 18th Symposium (International) on Combustion, p.p.321-328, The Combustion Institute, Pittsburgh.
- [26] ThermoBuild – NASA Online Interactive Tool to Obtain Thermodynamic Data used in NASA Thermodynamic Software, Official Website, URL: <http://cea.grc.nasa.gov>

- [27] Atabak, S., Sept. 2007, "Advanced Performance Simulation of Gas Turbine Burners and Afterburners", MSc Thesis, School of Engineering, Department of Power and Propulsion, Cranfield University.
- [28] Remote Sensing Technique for Aero-engine Emission Certification and Monitoring (AEROTEST Project) Official Website,
URL: <http://www.aerotest-project.net>
- [29] Rolls – Royce plc, 1986, "The Jet Engine", 2nd Edition, Birmingham: Renault Printing Co. Ltd.
- [30] Rolls – Royce plc, 1996, "The Jet Engine", 5th Edition, Birmingham: Renault Printing Co. Ltd.
- [31] Yates, M., 2004, "Engine Fuel Systems", Jet Engine Control Course Notes: School of Engineering – Cranfield University.
- [32] Kirkman, M., 2004, "Engine Control Systems", Jet Engine Control Course Notes: School of Engineering – Cranfield University.
- [33] Darrenogue. B., Jan. 2007, "Impact of Fuel Injection Temperature", VIVACE ECP Internal Memorandum.
- [34] Pachidis, V., 2007, "Gas Turbine Performance Simulation", Simulation and Diagnostics Course Notes: School of Engineering – Cranfield University.
- [35] Gas Turbine Engineering Group, "The TURBOMATCH Scheme", TURBOMATCH, User's Manual, School of Engineering – Cranfield University.
- [36] International Air Transport Association (IATA) Jet Fuel Price Monitor, IATA Official Website,
URL: http://www.iata.org/whatwedo/economics/fuel_monitor/index.htm
- [37] Goodger, E.M., 1975, "Hydrocarbon Fuels", London: Macmillan.
- [38] Bala. A, 2007, "Poly-Dimensional Gas Turbine System Modelling and Simulation", PhD Thesis, School of Engineering – Cranfield University.
- [39] Kurzke, J., 2007, "GasTurb 11 – Gas Turbine Performance Simulation Software", GasTurb Official Website,
URL: <http://www.gasturb.de>
- [40] Sethi, V., 2004, "Water Injection Systems for Aircraft Applications", MSc Thermal Power Engine Systems Symposium 2004, School of Engineering – Cranfield University.

Advanced Performance Simulation of Gas Turbine Components
and Fluid Thermodynamic Properties

[41] Sethi, V., Diara, F., Atabak, S., Jackson, A., Bala, A. and Pilidis, P., 2008, "Advanced Modelling of Fluid Thermodynamic Properties for Gas Turbine Performance Simulation", ASME GT-2008-51126

Chapter 4: Engine Model Performance Simulations

Abstract

The PROOSIS SCLib components, fluid functions and thermodynamic functions can be used to simulate a wide range of engine model configurations ranging from a simple single spool turbojet model to a complex mixed exhaust, multi-spool turbofan with several secondary air systems.

The first part of this chapter describes the generation of a conceptual engine model of a twin spool turbojet with reheat. The design point performance calculation procedure is discussed. Important considerations that are required during the off-design performance simulation for engines with afterburners are discussed. The effects of dissociation on overall engine performance are also analysed. This analysis is one of the major novel contributions to knowledge presented in this thesis.

The second part of this chapter introduces some of the advanced capabilities of PROOSIS including:

1. Test analysis and adaptation
2. "Stand alone" customer deck generation
3. High fidelity component zooming

Chapter 4: Nomenclature

The nomenclature used in this chapter is slightly different from the nomenclature used in other chapters. The nomenclature is based on the “Aerospace Recommended Practice: Gas Turbine Engine Performance Presentation and Nomenclature for Digital Computers Using Object – Oriented Programming.” [38]

X_{in} corresponds to a thermodynamic property at the inlet of a component (where X is the thermodynamic property).

X_{out} corresponds to a thermodynamic property at the outlet of a component (where X is the thermodynamic property).

$F_{in.X}$ corresponds to a main flow port thermodynamic property at the inlet of a component (where X is the main flow port thermodynamic property).

$F_{out.X}$ corresponds to a main flow port thermodynamic property at the outlet of a component (where X is the main flow port thermodynamic property).

$Fu_{in.X}$ corresponds to a fuel port thermodynamic property at the inlet of the Burner or Afterburner component (where X is the fuel port thermodynamic property).

$Me_{in.X}$ corresponds to a mechanical port property at the inlet of a component (where X is the mechanical port property).

$Me_{out.X}$ corresponds to a mechanical port property at the outlet of a component (where X is the mechanical port property).

Each variable is preceded by the component to which it refers.

Symbols

Name	Description	Unit
Aexit	Exit Area	m ²
alt	Altitude	m
Ath	Throat Area	m ²
DhqT	Specific Enthalpy Change	J/kg
dPqP	Fractional Pressure Loss	-
dTamb	Temperature Deviation from ISASLS	K
eff	Isentropic Efficiency	-
FAR _{Stoich}	Stoichiometric Fuel to Air Ratio	-
Fn	Net Thrust	N
heatP.Q	Heat Flux	W
MNf	Flight Mach Number	-
NcRdes	Design Corrected Rotational Speed	-
Nmech	Rotational Speed	rpm
NmechDes	Design Rotational Speed	rpm
Pamb	Ambient Pressure	Pa
PqP	Pressure Recovery	-
PR	Pressure Ratio	-
Pt	Total Pressure	Pa

Advanced Performance Simulation of Gas Turbine Components
and Fluid Thermodynamic Properties

Symbols (contd)

Name	Description	Unit
Pt_th	Throat Total Pressure	Pa
s_adapEff	Isentropic Efficiency Adaptive Scalar	-
s_adapWc	Corrected Mass Flow Rate Adaptive Scalar	-
s_map.Eff	Isentropic Efficiency Map Scaling Factor	-
s_map.PR	Pressure Ratio Map Scaling Factor	-
s_map.Wc	Corrected Mass Flow Rate Map Scaling Factor	-
s_NcRdes	Design Corrected Rotational Speed Map Scaling Factor	-
SFC	Specific Fuel Consumption	g/(kN*s)
Tamb	Ambient Temperature	K
trq	Torque	Nm
Tt	Total Temperature	K
Tt_th	Throat Total Temperature	K
W	Mass Flow Rate	kg/s
Wc	Corrected Mass Flow Rate	kg/s
Wc_th	Throat Corrected Mass Flow Rate	kg/s

Abbreviations

Name	Description	Unit
"33%"	%diss = 33% Fluid Model Combination	-
"66%"	%diss = 66% Fluid Model Combination	-
"CE"	Chemical Equilibrium Fluid Model Combination	-
"CE-66%"	Chemical Equilibrium & %diss = 66% Fluid Model Combination	-
"ND"	No Dissociation Fluid Model Combination	-
ANSYN	Analysis by Synthesis	-
Atm	Atmosphere Component	-
CFD	Computational Fluid Dynamics	-
CondiNozzle	Convergent - Divergent Nozzle	-
CULBR	Engine Model of a Low Bypass Ratio Twin Spool Turbofan	-
CUTSTJ	Engine Model of a Twin Spool Turbojet (No Reheat)	-
CUTSTJR	Engine Model of a Twin Spool Turbojet (With Reheat)	-
DLL	Dynamic Link Library	-
DP	Design Point	-
GUI	Graphical User Interface	-
HPC	High Pressure Compressor	-
HPEnd	High Pressure Shaft End Component	-
HPShaft	High Pressure Shaft	-
HPStart	High Pressure Shaft Start Component	-

Advanced Performance Simulation of Gas Turbine Components
and Fluid Thermodynamic Properties

Abbreviations (contd)

Name	Description	Unit
HPT	High Pressure Turbine	-
IWC	Integrated Workflow Controller	-
LPC	Low Pressure Compressor	-
LPEnd	Low Pressure Shaft End Component	-
LPShaft	Low Pressure Shaft	-
LPStart	Low Pressure Shaft Start Component	-
LPT	Low Pressure Turbine	-
MFT	Map Fitting Tool	-
MTU	MTU Aero Engines	-
NR	Newton Raphson	-
OD	Off-Design	-
SCLib	Standard Components Library	-
USTUTT	University of Stuttgart	-
VIGV	Variable Inlet Guide Vane(s)	-
VSV	Variable Stator Vane(s)	-

4.1: Engine Model Generation and Performance Simulations

4.1.1: Introduction

This section describes the generation of an engine model of a twin spool turbojet with reheat (CUTSTJR), using PROOSIS. A detailed account of the following is presented:

1. Generation of the CUTSTJR schematic (including appropriate DATA switch settings and inputs in each component's attributes editor).
2. The "inverse design" calculation concept and subsequently the need for isolated component performance simulation for each component of the CUTSTJR.
3. The design point simulation of the CUTSTJR engine model.
4. Off-design performance simulations including important considerations necessary for engines with afterburners and convergent – divergent nozzles.
5. The effects of dissociation on performance of the CUTSTJR engine model.

The processes described for the CUTSTJR engine model are representative of the procedure used for any PROOSIS engine model configuration.

4.1.2: CUTSTJR Engine Model: Schematic Generation

The PROOSIS SCLib (standard components library) comprises several components and functions. These components and functions can be used to simulate a wide range of engine configurations ranging from a simple single spool turbojet model to a complex mixed exhaust turbofan with several secondary air systems (bleeds).

Each component and function has been validated by both a SCLib developer (from one of the three partner universities) and an industrial partner who is responsible for the quality control of that particular component or function.

For example:

As discussed in *Section 3.4*, the Burner Component was developed by Cranfield University, validated by Cranfield University using TURBOMATCH^[1] and further validated and tested by the industrial partner MTU using their in-house performance simulation tool (MOPS).

The schematic of the CUTSTJR engine model (Fig: 4.1.1) is created by "dragging and dropping" the various component icons from the SCLib palette window to a blank schematic canvas. A detailed description of PROOSIS engine model schematic generation is presented in [2]. The ports are then appropriately connected as shown in Fig: 4.1.1. Only compatible ports can be connected i.e. a main flow port can only be connected to a main flow port, a secondary air system port can only be connected to a secondary air system port and a mechanical port can only be connected to a mechanical port etc. PROOSIS does not allow the user to connect incompatible ports. A detailed description of PROOSIS port types and the variables contained in each port is presented in [2] and [3]. The main design data of the CUTSTJR engine model is summarised in Fig: 4.1.2.

Once the schematic is generated, the attributes of each component are edited via its attributes editor as shown in Fig: 4.1.3 (based on the design data in Fig: 4.1.2). An example of the attributes editor of the Burner component is shown in Fig: 3.1.3. All PROOSIS components have similar but customised editors. A detailed description of each

component is not provided. However, a detailed specification document of each component as well as the fluid and thermodynamic functions is provided in the references outlined below:

Functions:

- Fluid model and fluid model functions – [4]
- Thermodynamic functions – [5]

NB: Detailed descriptions and analyses of the fluid model and thermodynamic functions are provided in Chapter 2.

Components:

- Atmosphere component – [6]
- Burner / Afterburner component – [7]
- Burner / Afterburner emissions component – [8]
- Casing component – [9]
- Compressor components ((n)bleeds / no bleeds, BETA / MFT maps) – [10]
- Duct components ((n)bleeds / no bleeds) – [11]
- Fan components ((n)bleeds / no bleeds, BETA / MFT maps) – [12]
- Flow splitter components ((n) outlets) – [13]
- Gear component ((n) output shafts) – [14]
- Heat exchangers (regenerators, recuperators, intercoolers) – [15]
- Inlet component – [16]
- Mixer components ((n) inlets) – [17]
- Convergent nozzle component – [18]
- Convergent – Divergent nozzle component – [19]
- Performance monitor components (aero / stationary) – [20]
- Probe components ((n) sensor channels) – [21]
- Propeller component – [22]
- Shaft components (shaft start, shaft end, shaft) – [23]
- Turbine components ((n)re-intros / no re-intros, ZETA / MFT maps) – [24]

NB: Detailed descriptions and analyses of the Burner and Burner_Emissions components are provided in Chapter 3.

Ports:

- SCLib Ports – [25]

These specification documents have been developed in parallel to the source code of each component (or function) as a quality control measure.

Component specification documents provide a detailed description of the following:

1. Component hierarchy
2. Ports and associated port variables
3. Switches and calculation options
4. DATA
5. Calculations (design point and off design)
6. Icons
7. References

Specifications for the fluid and thermodynamic functions provide a detailed description of the following (for each function call):

1. Input variables
2. Output variables
3. Calculations (including any iterations)
4. References

Once the attributes have been edited appropriately, saving and compiling the CUTSTJR schematic automatically generates the source code file for the CUTSTJR engine model.

4.1.3: The “Inverse Design” Calculation Concept

PROOSIS allows the user to use either the conventional design and off-design methodology or the “inverse design” calculation concept. However, based on the discussion which follows, the PROOSIS SCLib has been developed to facilitate only “inverse design” whereby both design point and off-design simulations are based on a single off-design partition (mathematical model) (refer to the “Glossary” section of the thesis).

The conventional design and off-design calculation procedure is described in detail in [26], [27] and [28]. The main drawback of the conventional approach is that each component requires separate algorithms for the design and off-design calculations, thereby increasing the complexity of the system. Additionally, for complex engine models (e.g. detailed models of control systems, secondary air systems, heat transfer effects etc.), the maintainability of two sets of algorithms is complex and cumbersome.

The main advantage of the “inverse design” concept is that only one set of algorithms (off-design) is required. Consequently some of the parameters used to define the design point (in the conventional approach) are not available as boundary conditions (e.g. pressure ratios of compressors and fans, component efficiencies of turbomachinery components, the inlet mass flow rate etc.). However, during a design point simulation, these parameters are specified as dependent variables (target values) in residual equations to determine a series of independent variables. A major drawback of the “inverse design” concept is that an external Newton Raphson (NR) routine is required to solve the residual equations and convergence of this external NR routine is sensitive to the initialisation values used for the independent variables. There are several ways to overcome this problem. One approach is to perform isolated design point performance simulations for each component of the engine model and use the values obtained for the independent variables as initialisation values for the whole engine design point simulation.

A detailed description of the design point simulation of the CUTSTJR is presented below including an example of a required isolated component design point simulation to determine the initialisation values of the independent variables.

CUTSTJR Engine Model: Partition generation

Once the CUTSTJR schematic has been created and the attributes of each component appropriately edited (as described in *Section 4.1.2*), the CUTSTJR off-design

partition is generated using the PROOSIS “Boundary Selection Wizard”. A detailed description of PROOSIS SCLib partition generation is presented in [2] and [3]. For the CUTSTJR engine model, any variables associated with unconnected component inlet ports are specified as boundary conditions. Additionally the off-design partition of the CUTSTJR has two non-linear algebraic loops and the user needs to select appropriate tearing (algebraic) variables for these non-linear boxes. During the simulation (design point or off-design) the user must specify initial values for these tearing variables.

NB: The closer the initialisation values of the tearing variables to the actual values, the more robust and faster the calculation.

The boundary condition variables and tearing variables for the off-design partition of the CUTSTJR engine model are highlighted in Fig: 4.1.4.

NB: Although the Burner outlet total temperature (Burner.F_out.Tt) is not a variable associated to an unconnected inlet port it is still specified as a boundary condition as the Burner injected fuel mass flow rate Fu_in.W is not specified. (Refer to Section 3.1 for the two different partitions which can be generated for the Burner component). The same applies for the Afterburner outlet total temperature (Afterburner.F_out.Tt).

NB: The heat flux across the walls of all the turbomachinery components (LPC.heatP.Q, HPC.heatP.Q, HPT.heatP.Q and LPT.heatP.Q) need to be specified as boundary conditions because the CUTSTJR engine model does not have a casing component.

NB: Although not selected in the “Boundary Selected Wizard”, the shaft speeds (LPEnd.Me_in.Nmech and HPEnd.Me_in.Nmech) are automatically selected as algebraic variables as they are defined as algebraic variables in the turbomachinery and shaft components.

CUTSTJR Engine Model: Design Point Simulation

Once the off-design partition has been generated, it can be used to create “experiments” for any design point, off-design or transient performance simulations.

NB: Transient performance analysis is beyond the scope of the presented research work.

The boundary conditions and initialisation values for the design point simulation of the CUTSTJR engine model are summarised in Fig: 4.1.4. Fig: 4.1.4 also summarises the variables (dependent (target) variables and independent variables) as well as the closure equations required for the external NR iteration.

As discussed earlier, the user must specify fairly accurate initialisation values for the independent variables to ensure convergence of the external NR routine. During the early phase of PROOSIS, the models were extremely sensitive to initialisation values of the independent variables and highly accurate values (a minimum of five decimal places) needed to be specified as discussed in [3]. As PROOSIS developed, the robustness of the NR routine was improved and currently initialisation values of one decimal point suffice and result in convergence for a vast majority of design point simulations. However, as mentioned above, isolated design point component simulation is required to provide a rough indication of the initialisation values to be used for the independent variables during whole engine design point simulation. The isolated design point simulation of the LPC is described as an example.

LPC Isolated Design Point Simulation

The isolated design point simulation of the LPC component is also based on “inverse design”. The boundary conditions and initialisation values for the design point simulation of the isolated LPC component are summarised in Fig: 4.1.5. Fig: 4.1.5 also summarises the variables (dependent (target) variables and independent variables) as well as the closure equations required for the external NR iteration. The simulation yields the values of the LPC pressure ratio, corrected mass flow rate, isentropic efficiency and corrected speed map scaling factors (LPC.s_mapPR_in, LPC.s_mapWC_in, LPC.s_mapEff_in and LPC.s_NcRdes_in respectively). The values obtained are then set as initialisation values of the independent variables for the CUTSTJR engine model DP simulation.

Similarly, isolated DP component simulations of the HPC, HPT, LPT and Condi Nozzle components yield the initialisation values of the remaining independent variables (shown in Fig: 4.1.4) required for the DP simulation of the CUTSTJR engine model. Subsequently the DP simulation of the CUTSTJR engine model can be performed. This yields the accurate values of the independent variables which are then hardcoded in the attributes editor of the appropriate component and are therefore fixed for any further off-design simulations.

4.1.4: CUTSTJR Engine Model: Off-Design Performance Simulation

It is essential for engines with afterburners to be fitted with variable geometry propelling convergent-divergent (conди) nozzles. With the afterburner lit, the nozzle areas (throat and exit) must be carefully controlled both to facilitate complete expansion of the flow (in order to optimise the thrust) and also to avoid compressor surge problems. There are effectively three ways to ensure complete expansion:

1. Changing both the nozzle throat area (ConдиNozzle.Ath) and the nozzle exit area (ConдиNozzle.Aexit).
2. Fixing ConдиNozzle.Ath and only changing ConдиNozzle.Aexit
3. Fixing ConдиNozzle.Aexit and only changing ConдиNozzle.Ath

Following a successful design point (DP) simulation of an engine model in PROOSIS, steady state off-design (OD) simulations (for a majority of engine models) are trivial once the values of the independent variables calculated at design point are hardcoded in the attributes editor of the appropriate component. For the CUTSTJR engine model, the off-design calculations are trivial provided there is no afterburning. However, when running an off-design simulation with afterburning, the nozzle areas need to be suitably modified using one of the three approaches discussed above. The third approach (i.e. Fixing ConдиNozzle.Aexit and only changing ConдиNozzle.Ath) will be used for the analyses which follow.

The case study presented below, highlights two methods to calculate ConдиNozzle.Ath during off-design simulations (with active afterburning). The first method is generally acceptable to a first order. However for fully rigorous calculations, the second method (which was developed and implemented in PROOSIS by the author) should be employed.

Off-Design Case Study 1:

Handle: The Afterburner outlet total temperature (Afterburner.F_out.Tt) was increased from the design point value (1262.3K) (the temperature corresponding to no afterburning) until the total fuel to air ratio (burned + unburned) at the exit of the Afterburner was just below the Stoichiometric fuel to air ratio (Afterburner.F_out.Tt = 2422K) (for Jet-A, FAR_{Stoich} = 0.06817) (Refer to Section 3.5.3).

NB: For this case study it was assumed that for all the off-design simulations the Burner outlet total temperature remained unchanged and was equal to the design point value (1800K).

NB: For this case study the Condi-Nozzle exit area (CondiNozzle.Aexit) was unchanged and was equal to the design point value (0.4170m²).

The two methods used to determine CondiNozzle.Ath are presented below:

Method 1: The " $A_{th} \propto \sqrt{T_{t_th}}$ " method

Since the flow at the throat of the Condi-nozzle is choked, the Condi-Nozzle throat corrected mass flow rate (CondiNozzle.Wc_th) (defined in [Eq. 4.1.1]) remains constant for any off design case regardless of the afterburner outlet total temperature.

$$CondiNozzle.Wc_th = \frac{CondiNozzle.W_th \times \sqrt{CondiNozzle.Tt_th}}{CondiNozzle.Pt_th \times CondiNozzle.Ath} \quad \text{[Eq. 4.1.1]}$$

During afterburning operation, the Afterburner outlet total temperature (Afterburner.F_out.Tt) rises and therefore the Condi-Nozzle inlet total temperature (CondiNozzle.F_in.Tt) and subsequently the Condi-Nozzle throat total temperature (CondiNozzle.Tt_th) also rises. Consequently, the throat area (CondiNozzle.Ath) must also increase to maintain the same value of the throat corrected mass flow rate. From [Eq. 4.1.1] it can be seen that during off-design performance simulations, to a first order, CondiNozzle.Ath can be increased in proportion to the square root of CondiNozzle.Tt_th.

For ease of reference, this method is referred to as the " $A_{th} \propto \sqrt{T_{t_th}}$ " method henceforth.

Method 2: The Fully Rigorous method

The fully rigorous method involves calculating CondiNozzle.Ath afresh for each off-design point using an external Newton Raphson iterative routine. For each off-design point CondiNozzle.Ath is an independent variable, which is calculated iteratively by specifying the design point inlet mass flow rate (Inlet.F_in.W = 200kg/s) as the dependent variable in a suitable closure equation. In order to increase the speed of the external iterations and to improve the robustness of the model with respect to convergence, the initial value of CondiNozzle.Ath is varied in proportion to the square root of Afterburner.F_out.Tt. The reasons for this are justified in the " $A_{th} \propto \sqrt{T_{t_th}}$ " method discussed above.

The case study described above was performed using both methods to determine CondiNozzle.Ath. The discrepancies between the two methods are presented in Fig: 4.1.6 – Fig: 4.1.9.

Fig: 4.1.6 shows a comparison of the variation of CondiNozzle.Ath as a function of Afterburner.F_out.Tt for:

1. The " $Ath \propto \sqrt{Tt_th}$ " method
2. The fully rigorous method

Fig: 4.1.7 shows a comparison of the variation of Inlet.F_in.W as a function of Afterburner.F_out.Tt when using:

1. The " $Ath \propto \sqrt{Tt_th}$ " method
2. The fully rigorous method

Fig: 4.1.8 and Fig: 4.1.9 show the effects of each of the two methods on the working lines of the LPC and HPC respectively.

The main observations and conclusions that can be drawn from Fig: 4.1.6 – Fig: 4.1.9, regarding the two methods are as follows:

1. From Fig: 4.1.6 it can be observed that the discrepancies between the calculated values of CondiNozzle.Ath using the " $Ath \propto \sqrt{Tt_th}$ " method and the fully rigorous method are clearly not negligible especially for off-design calculations "far away" from the design point. For a given Afterburner.F_out.Tt, the " $Ath \propto \sqrt{Tt_th}$ " method calculates a lower value of CondiNozzle.Ath than the fully rigorous method. This implies flow under expansion in the condi-nozzle, which manifests as a reduced inlet mass flow rate as Afterburner.F_out.Tt increases as shown in Fig: 4.1.7.
2. For the presented case study, the Burner outlet total temperature (Burner.F_out.Tt) was kept constant (1800K). Consequently the performance of the engine core should not have changed provided the throat area of the condi-nozzle was varied correctly. Fig: 4.1.8 and Fig: 4.1.9 clearly show that for the fully rigorous method this is true and the operating points on both the LP and HP characteristics remain unchanged for all the off-design simulations. However, when using the " $Ath \propto \sqrt{Tt_th}$ " method the operating points on both characteristics are not fixed as a consequence of under-expansion in the condi-nozzle and the subsequent decrease in the inlet mass flow rate. The low pressure shaft seems to be decelerating with the LP running line moving away from surge while the high pressure shaft seems to be accelerating with the HP running line moving towards surge. The presented errors when using the " $Ath \propto \sqrt{Tt_th}$ " method propagate through the engine performance off-design simulations and adversely affect the accuracy of the calculated overall engine performance parameters i.e. net thrust and specific fuel consumption.

3. Whilst it is evident that the " $Ath \propto \sqrt{Tt_th}$ " method does "adapt" the condi-nozzle, thereby allowing for afterburning without surging the compressors, it is clearly only valid to a first order (especially for Afterburner components with higher values of Afterburner.F_out.Tt and lower efficiencies (≈ 0.90) where the effects of fuel flow are not negligible). The rigorous method, although more "tedious" is clearly more suited (and is therefore the method used) for the investigations regarding the effects of dissociation and liquid fuel sensible enthalpy on the performance of the CUTSTJR engine model. These investigations are presented in Section 4.1.5 and Section 4.1.6 respectively.

4.1.5: CUTSTJR Engine Model: The Effects of Dissociation

Two off-design case studies are presented to demonstrate the effects of dissociation on overall performance of the CUTSTJR engine model.

Off-Design Case Study 2:

Handle: The Burner injected fuel mass flow rate (Burner.Fu_in.W) was reduced from the design point value until the low pressure compressor (LPC) surged and then increased from the design point value until the calculation did not converge.

NB: For this case study it was assumed that there was no afterburning and therefore CondiNozzle.Ath was fixed to the design point value.

NB: For this case study, the effects of the following five "combinations" of fluid models were analysed:

(Refer to *Chapter 2* for a detailed description of the PROOSIS fluid model)

Combination 1: The "no dissociation" fluid model is used for all the components of the CUTSTJR engine model.

Combination 2: The "%diss = 33%" fluid model is used for all the components of the CUTSTJR engine model.

Combination 3: The "%diss = 66%" fluid model is used for all the components of the CUTSTJR engine model.

Combination 4: The chemical equilibrium fluid model is used for all the components of the CUTSTJR engine model.

Combination 5: The chemical equilibrium fluid model is used for the Burner and Afterburner components and the "%diss = 66%" model is used for all the other components of the CUTSTJR engine model.

NB: Combination 5 has been included as it is thought to be the most realistic model from the available combinations, based on the discussion in *Section 2.1.3*.

For ease of reference, combinations 1 – 5 above are henceforth referred to as "ND", "33%", "66%", "CE" and "CE-66%" respectively.

Fig: 4.1.10 and Fig: 4.1.11 show the effects of dissociation on the LPC and HPC running lines respectively. The effects of dissociation on the running lines of both the LPC and HPC are clearly negligible.

Fig: 4.1.12 shows the effects of dissociation on the calculated value of Burner.F_out.Tt as a function of Burner.Fu_in.W. In addition to the results shown for all the fluid models highlighted above, the discrepancies between the "ND" and "CE-66%" cases are also presented. These observations are consistent with the observations made

regarding the effects of dissociation on fluid properties and the effects of dissociation on isolated Burner component performance presented in Chapter 2 and Chapter 3 respectively. For a given Burner.Fu_in.W, the calculated value of Burner.F_out.Tt is lower when dissociation is accounted for. As expected, the higher the “level of dissociation”, the lower the calculated value of Burner.F_out.Tt. Furthermore, as expected, the discrepancies between the calculated value of Burner.F_out.Tt between the “ND” and “CE-66%” fluid models increases as Burner.Fu_in.W increases. This discrepancy in turn manifests as a discrepancy in the calculated net thrust (positive discrepancy) and subsequently the calculated specific fuel consumption (negative discrepancy) as shown in Fig: 4.1.13 and Fig: 4.1.14 respectively.

Appendix 1 provides a detailed summary of the main performance parameters of the CUTSTJR for the following three off-design values of Burner.Fu_in.W:

1. Burner.Fu_in.W = 2.438kg/s (this is the minimum fuel flow rate chosen for the OD analysis and corresponds to an LPC operating point very close to surge).
2. Burner.Fu_in.W = 5.238kg/s (this is the design point fuel flow rate which corresponds to a Burner outlet total temperature of approximately 1800K - depending on the fluid model used).
3. Burner.Fu_in.W = 8.288kg/s (this is the maximum fuel flow rate chosen for the OD analysis beyond which the model does not converge).

The main performance parameters presented for each fuel flow rate include the following:

1. The mass flow rate at the exit of each component
2. The total temperature at the exit of each component
3. The total pressure at the exit of each component
4. The burned fuel to air ratio at the exit of each component
5. The unburned fuel to air ratio at the exit of each component
6. The net thrust
7. The specific fuel consumption

The main observations that can be drawn from Appendix 1 are as follows:

1. For the “Burner.Fu_in.W = 2.438kg/s” case, Burner.F_out.Tt is relatively low (approximately 1507K for the “CE-66%” fluid model combination) for dissociation to have a significant impact. As discussed in *Section 2.1.3*, for temperatures lower than 1800K the effects of dissociation are negligible. The results obtained for Burner.Fu_in.W confirm this. The discrepancies for the calculated values of Burner.F_out.Tt, Fn and SFC between the “ND” and “CE-66%” fluid model combinations are 0.25%, 0.01% and -0.01% respectively and it can safely be deduced that the effects of dissociation on the overall engine performance (Fn and SFC) are negligible for “lower” values of Burner.Fu_in.W due to the corresponding “lower” values of Burner.F_out.Tt.
2. For the “Burner.Fu_in.W = 5.238kg/s” case, Burner.F_out.Tt is approximately 1791K (for the “CE-66%” fluid model combination). For this off-design case the effects of dissociation are more visible due to the higher temperature. The discrepancies for the calculated values of Burner.F_out.Tt, Fn and SFC between the “ND” and “CE-66%” fluid model combinations are 0.46%, 0.23% and -0.23% respectively. Although the

discrepancies are still quite small, the effects of dissociation cannot be neglected for fully rigorous calculations.

3. For the “Burner.Fu_in.W = 8.288kg/s” case, Burner.F_out.Tt is approximately 2023K (for the “CE-66%” fluid model combination). For this off-design case, the effects of dissociation are more significant. The discrepancies for the calculated values of Burner.F_out.Tt, Fn and SFC between the “ND” and “CE-66%” fluid model combinations are 0.80%, 0.43% and -0.43% respectively. Although the discrepancies are still small, they are certainly not negligible for accurate gas turbine performance simulation calculations.

For this case study the effects of dissociation on overall engine performance are relatively modest. However, for the case study presented below (Off-Design Case Study 3), the off-design simulations are based on active reheat and the effects of dissociation on performance are therefore more significant.

Off-Design Case Study 3:

Handle: The Afterburner injected fuel mass flow rate (Afterburner.Fu_in.W) was increased from the design point value (0 kg/s) until the burned fuel to air ratio at the exit of the Afterburner was just below the Stoichiometric fuel to air ratio (for Jet-A, $FAR_{Stoich} = 0.06817$) (Refer to *Section 3.5.3*).

NB: For this case study the Burner outlet total temperature was unchanged and was equal to the design point value (1800K)

NB: For this case study, the effects of the same five “combinations” of fluid models as those used for case study 2 were analysed.

NB: The throat area of the Condi Nozzle (CondiNozzle.Ath) was modified using the “fully rigorous method” described in *Section 4.1.4*.

Appendix 2 provides a detailed summary of the main performance parameters of the CUTSTJR for the following three off-design values of Afterburner.Fu_in.W:

1. Afterburner.Fu_in.W = 0kg/s (this is the design point calculation corresponding to no reheat).
2. Afterburner.Fu_in.W = 4.7kg/s
3. Afterburner.Fu_in.W = 9.2kg/s (this is the maximum fuel flow rate chosen for the OD analysis beyond which Afterburner.F_out.FARB > FAR_{Stoich}).

The main performance parameters presented for each afterburner fuel flow rate include the following:

1. The mass flow rate at the exit of each component
2. The total temperature at the exit of each component
3. The total pressure at the exit of each component
4. The burned fuel to air ratio at the exit of each component
5. The unburned fuel to air ratio at the exit of each component
6. The main Burner fuel flow rate
7. The net thrust
8. The specific fuel consumption

The effects of dissociation on the calculated values of the Afterburner outlet total temperature (Afterburner.F_out.Tt), the net thrust (Fn) and the specific fuel consumption

(SFC), as a function of Afterburner.Fu_in.W are shown in Fig: 4.1.15, Fig: 4.1.16 and Fig: 4.1.17 respectively. As for case study 2, the discrepancies between the “ND” and “CE-66%” cases are also presented on each chart.

The main observations that can be drawn from Appendix 2 and Fig: 4.1.15 – Fig: 4.1.17 are as follows:

1. As mentioned above, the throat area of the Condi Nozzle (CondiNozzle.Ath) was modified using the “fully rigorous method” described in Section 4.1.4. From the results presented in Appendix 2, it is evident that for a given fluid model combination (“ND”, “33%”, “66%”, “CE” or “CE-66%”) the performance of the all the components upstream of the Afterburner component remain unchanged regardless of the value of Afterburner.Fu_in.W. This confirms that CondiNozzle.Ath has been correctly calculated for each off-design point.
2. As shown in Appendix 2, for all the three cases, the Burner injected fuel mass flow rate (Burner.Fu_in.W) required to achieve the design point Burner outlet total temperature (Burner.F_out.Tt = 1800K) increases as the level of dissociation increases (this is consistent with the results presented in Section 3.5). Consequently as the level of dissociation increases, Burner.F_out.W increases.
NB: The Burner.Fu_in.W discrepancies between the different fluid model combinations are the same regardless of the value of Afterburner.Fu_in.W due to the reasons discussed in the point above.
3. For the design point case (Afterburner.Fu_in.W = 0kg/s), the increase in Burner.F_out.W (as the level of dissociation increases) manifests as an increase in Afterburner.F_out.Tt and subsequently an increase in Fn. Although there is an increase in net thrust, the SFC is worse because Burner.Fu_in.W increases as the level of dissociation increases. As shown in Fig: 4.1.15 – Fig: 4.1.17, the discrepancies of the calculated values of Afterburner.F_out.Tt, Fn and SFC between the “ND” and “CE-66%” cases are -0.46%, -0.39% and -0.7% respectively. These discrepancies are not negligible for rigorous performance calculations. For the design point case the discrepancies are clearly only due to the effects of dissociation on the performance simulation of the Burner component.
4. For the “Afterburner.Fu_in.W = 4.7kg/s” case, although there is an increase in Burner.Fu_in.W (and consequently Burner.F_out.W), the value of Afterburner.F_out.Tt actually decreases as the level of dissociation increases. This is because the effects of dissociation in the Afterburner component begin to show. As discussed in Section 3.5, for a fixed fuel flow rate, the Afterburner outlet total temperature decreases as the level of dissociation increases. Although Afterburner.F_out.Tt decreases, Fn still increases as the level of dissociation increases as the effects of a lower Afterburner.F_out.Tt are overwhelmed by a larger Burner.Fu_in.W. As shown in Fig: 4.1.15 – Fig: 4.1.17, the discrepancies of the calculated values of Afterburner.F_out.Tt, Fn and SFC between the “ND” and “CE-66%” cases are 0.13%, -0.17% and -0.41% respectively. The discrepancies are clearly lower than those presented above for the design point calculation. For the “Afterburner.Fu_in.W = 4.7kg/s” case, the discrepancies are due to the effects of dissociation on both the Burner and the Afterburner.

5. The results for the “Afterburner.Fu_in.W = 9.2kg/s” case are similar to those obtained for the “Afterburner.Fu_in.W = 4.7kg/s” case. However the effects of dissociation on the Afterburner component are more prominent due to a higher value of Afterburner.F_out.Tt. Consequently although there is an increase in Burner.Fu_in.W (and consequently Burner.F_out.W), the value of Afterburner.F_out.Tt actually decreases significantly as the level of dissociation increases. As shown in Fig: 4.1.15 – Fig: 4.1.17, the discrepancies of the calculated values of Afterburner.F_out.Tt, Fn and SFC between the “ND” and “CE-66%” cases are 1.40%, 0.17% and -0.57% respectively. For this case it is clear that as the level of dissociation increases, the decrease in Afterburner.F_out.Tt overwhelms the increase in Burner.Fu_in.W and therefore Fn is lower and SFC is therefore worse.

The partition used for this case study was such that Burner.F_out.Tt and Afterburner.Fu_in.W were specified as boundary conditions and Burner.Fu_in.W and Afterburner.F_out.Tt calculated respectively. This is the reason the effects of dissociation seem to be negligible even at high temperatures because as the level of dissociation increases for a fixed value of Burner.F_out.Tt, Burner.Fu_in.W increases while for a fixed value of Afterburner.Fu_in.W, Afterburner.F_out.Tt decreases. The two effects seem to cancel each other out and the discrepancies between Fn and SFC are therefore small.

However, the analysis was extended to the following partition. Burner.Fu_in.W and Afterburner.Fu_in.W were specified as boundary conditions. For fixed values of Burner.Fu_in.W and Afterburner.Fu_in.W (for Burner and Afterburner outlet temperatures greater than 1800K) as the level of dissociation increases, the values of Burner.F_out.Tt and Afterburner.F_out.Tt decrease significantly. Therefore as the level of dissociation increases Fn decreases significantly and SFC therefore worsens considerably as the total fuel flow rate (Afterburner.Fu_in.W + Burner.Fu_in.W) is constant. These discrepancies are certainly not negligible for gas turbine performance simulations.

4.2: Advanced Capabilities of PROOSIS

4.2.1: Introduction

The advanced fluid model developed by the author and described in detail in Chapter 2 provides a robust foundation for several advanced modelling capabilities within PROOSIS including, test analysis, generation of customer decks, multi-dimensional component zooming and distributed computing. Some of these advanced capabilities are briefly introduced in this chapter with references to publications and theses where each of them are described in detail. Detailed descriptions of these capabilities are beyond the scope of the author's research.

4.2.2: Test Analysis

PROOSIS has been developed to facilitate test analysis via a suitable ANSYS (analysis by synthesis) technique. The procedure is summarised in Fig: 4.2.1.

Discrepancies between engine test bed performance and the results obtained from both DP and OD performance simulation models are inevitable. The main sources of these discrepancies are assembly or manufacturer tolerances, amongst others [29]. The test analysis process aims to minimise these discrepancies by calculating a series of appropriate turbo machinery map adaptive scalars and 'calibrating' the performance simulation model based on these scalars. The presented test analysis case study is based on an engine model of a simple twin spool turbojet (CUTSTJ) shown in Fig: 4.2.2.

The test analysis process has four different stages [30].

1. Engine Test (Test Bed):

Performance data (highlighted in red in Fig: 4.2.2) was obtained for four different operating points (fuel flow handle) of the CUTSTJ (courtesy of USTUTT). The mean values of these performance parameters at each of the four operating points were then obtained by filtering the data using a suitable data reduction technique. Data reduction is defined as the transformation of information, usually empirically or experimentally derived, into a corrected, ordered and simplified form [31]. Currently the data reduction technique employed is external to PROOSIS. However, PROOSIS will be developed to comprise internal data reduction algorithms.

2. Tramline Point:

A working line OD simulation of the CUTSTJ "Pre-Test" model (Fig: 4.2.2) was run imposing the same ambient conditions as the actual test bed. The results obtained are very similar to those obtained from the test bed. However, as expected, slight discrepancies do exist. Fig: 4.2.3 is a graph of the low pressure compressor exit total temperature (LPC.F_out.Tt) as a function of the injected fuel mass flow rate (Burner.Fu_in.W) and is an example of the discrepancies between the test data and the pre-test model results, at each of the four operating points. Although not presented, similar discrepancies exist for all the other measured parameters.

3. ANSYN Analysis:

In addition to the conventional scaling factors for corrected mass flow rate and isentropic efficiency (map scalars and scalars for Reynolds and Gamma correction) the PROOSIS turbomachinery components (fans, compressors and turbines) also make allowances for adaptive scalars. For the PROOSIS pre-test model, these scalars are set to unity (i.e. no adaptive scaling).

The CUTSTJ ANSYN simulation calls an external NR routine in a similar manner as described for the design point simulation of the CUTSTJR engine model in *Section 4.1.3*. The boundary conditions and initialisation values for the ANSYN simulation of the CUTSTJ engine model are summarised in Fig: 4.2.4. Fig: 4.2.4 also summarises the variables (dependent (target) variables and independent variables) as well as the closure equations required for the external NR iteration. The independent variables are all the adaptive scalars while the residual/closure equations are the differences between the test bed results and the PROOSIS pre-test model. The PROOSIS ANSYN experiment is a synthesis matching scheme which yields the values of the corrected mass flow rate and isentropic efficiency adaptive scalars for all the turbo machinery components, at each of the four operating points.

The next phase of the ANSYN analysis involves determining the schedule of each adaptive scalar as a function of shaft speed. As shown in Fig: 4.2.5, using the LPC as an example, the corrected mass flow and isentropic efficiency adaptive scalars, obtained at each operating point, are plotted as a function of the LP shaft speed. A linear correlation is then applied to deduce the schedule of each adaptive scalar as a function of the LP shaft speed. Although the correlation applied in this example is linear, any user defined correlation can be applied. The process highlighted above is then repeated for the HPC, HPT and LPT.

4. Referred Case (Post Test Model):

The SCLib turbomachinery components each have several switches with two different calculation options for adders and scalars. The user can either input the value of the scalar or adder as DATA or calculate the value of the scalar or adder via a user defined function. The schedules obtained, from the correlation procedure described above, are hard coded in the source files of the respective turbomachinery components.

The next step is to create the PROOSIS "Post-Test" CUTSTJ model. The post-test model is almost identical to the pre-test model shown in Fig: 4.2.2. The only difference between the two models is the calculation procedure of the turbomachinery adaptive scalars. For the pre-test model, all adaptive scalars are set to unity but for the post-test model the adaptive scalars are a function of shaft speed. Before the post-test model can be compiled and the partition generated, the adaptive scalar calculation switch, for each turbomachinery component, is set to the option which corresponds to the adaptive scalar schedule.

Once the attributes are edited, the post-test model working line simulation is run and the results obtained are compared to the test bed measurements. Fig: 4.2.6 highlights the reduction in discrepancies as a consequence of applying the adaptive scalar schedules using a comparison between LPC.F_out.Tt and Tt21 as an example. As expected the discrepancies between the results from the simulation model and the test bed measurements have been significantly reduced as a consequence of the ANSYN analysis. Similarly, the discrepancies for all the other test parameters included in the simulation and highlighted in Fig: 4.2.2 are also significantly reduced.

Another advantage of the PROOSIS test analysis procedure is the flexibility of either internal or external visualisation of results. The example discussed demonstrates the possibility of linking PROOSIS with external tools (e.g. Microsoft Excel). The same analysis can be easily performed entirely using PROOSIS and the results visualised via a graphical simulation. The results obtained can be carefully analysed by a diagnostics team and amongst other actions, they can be used to correct instrumentation.

The CUTSTJ test analysis discussed above is a crude example to demonstrate the capability of PROOSIS to perform test analysis. The matching scheme used was quite simple. In reality however, the matching scheme is quite complex and should comprise several considerations. This has been discussed in some detail and illustrated using the BR710 engine as an example in ^[30]. The analysis discussed in ^[30], excluding the data reduction process (temporarily), can easily be performed using PROOSIS.

4.2.3: Customer Deck Generation

One of the objectives of PROOSIS is to reduce the time and cost of generating customer decks. Customer decks are aero-thermal, numerical representations of engines which are typically created by engine manufacturers and delivered to airframe manufacturing companies and others. A PROOSIS customer deck is effectively an executable or a DLL which encapsulates a performance simulation.

The structure of a PROOSIS standalone deck (with respect to the deck input and output parameters) is defined by the requirements of the airframe manufacturer. PROOSIS has an inbuilt deck generation wizard which eases the customer deck generation process. Generating a customer deck in PROOSIS based on an OD experiment automatically creates:

1. A DLL, which can be used when connecting PROOSIS engine models to external tools for sub-program mode analysis.
2. An executable file, which (together with the DLL) creates a standalone customer deck application with a GUI.

PROOSIS customer decks can be used to perform several studies of engine OD performance e.g. evaluating the engine performance for the entire flight envelope. An example of a typical PROOSIS standalone customer deck is shown in Fig: 4.2.7.

NB: For both cases, the decks are self contained and it is not necessary for the client to have PROOSIS installed on their machines.

4.2.4: Integrated Aerodynamic Component Zooming

The work described in this section is based on the collaborative effort between the author and A. Bala ^[3]. The presented work is primarily accredited to A. Bala ^[3]. However the author made a significant contribution to the presented investigations, in particular to the 0-D performance simulations. This section provides a brief summary of the work that has been presented in detail in **[3]** and **[32]**.

Gas turbine performance simulation codes have been evolving rapidly and currently comprise a wide range of capabilities. The capabilities available cater for the early stages of preliminary design through to in-service support. Although conventional 0-D cycle codes offer good performance predicting capabilities (steady and non-steady state), they fail to capture complex physical phenomena and detailed component analysis. Furthermore, they do not account for any axial, radial or circumferential resolution of a component. Recently, major improvements in computational speed and power have enabled sophisticated 3-D computational simulation techniques (CFD) for either individual components or group of components to be fully or partially coupled with 0-D performance simulation codes. This integrated performance simulation approach is referred to as “integrated component zooming”. The presented case study involved adapting the integrated component zooming approach to investigate the effects of variable stator vanes (VSV) on the performance of a 0-D engine model of a twin spool, low bypass ratio turbofan with mixed exhausts (CULBR engine model) with 3-D analysis of the first stage (rotor and stator) of the Fan component.

The integrated component zooming approach was achieved via the “Integrated Workflow Controller” (IWC) shown in Fig: 4.2.8. The IWC encapsulates both 0-D and 3-D simulation tools and can therefore automatically perform high-fidelity 3D aerodynamic component zooming in a synchronised and controlled manner. Initially 0-D engine performance simulations for both design point and a number of off-design conditions (e.g. different power settings) were performed using standard, empirically generated component characteristics in order to generate a database of component specific entry and exit boundary conditions.

NB: The analysis described in **[3]**, **[32]** and shown in Fig: 4.2.8 was performed using TURBOMATCH ^[33] & ^[34] (the Cranfield University, in-house gas turbine performance simulation software). However, the same approach is also valid for PROOSIS.

The boundary conditions generated from the initial 0-D off-design simulations were subsequently used for the 3-D CFD analysis of the first stage of the Fan component.

NB: The Fan component model was designed using typical preliminary design techniques and the CFD was performed using the ANSYS commercial CFD simulation package comprising:

- ANSYS BladeGen^[35]
- ANSYS CFX Turbo-Grid^[36]
- ANSYS CFX 10.0^[37]

A detailed analysis of the preliminary design methodology as well as details of the CFD simulations (including the geometry and grid generation are presented in **[3]** and **[32]**.

Each 3-D simulation produced a single averaged component characteristic point for a given boundary condition and power setting. Several CFD runs for a fixed power setting subsequently resulted in a range of characteristic points and joining all these points established a single speed line for the Fan characteristic. Repeating this process for different power settings and slightly modified stage exit boundary conditions yielded “Mini-Map 1”, which corresponds to a VSV setting of 0° . The entire process highlighted above was then repeated to generate “Mini-Map 2” and “Mini-Map 3” corresponding to VSV settings of 10° and 15° respectively.

The three Mini-Maps were then integrated to produce one high fidelity, variable geometry composite map for the first stage of the Fan. This map, referred to as the “Composite Mini-Map”, is shown in Fig: 4.2.9 and Fig: 4.2.10. As shown in Fig: 4.2.9, at lower non-dimensional speeds, the surge line exhibits a “kink”. This kink is a consequence of the absence of an upstream variable inlet guide vane (VIGV). At low speeds and in the absence of an upstream VIGV, it is typical for the forward stages to operate close to stalled conditions while the rear stages operate close to choke. For a given axial velocity and blade speed, the incidence angle can be restored to an optimum value by introducing VIGV, which would reduce forward stage stall thereby smoothing out the “kinked” surge lines. VIGV and VSV are common “part speed crutches” which are often employed to improve the part speed performance of fans and compressors. A turbomachinery map is unique for a given set of flow conditions and geometry. VSV and VIGV are generally rotated about their centroid in order to get them re-staggered. The change in flow angle manifests as an approximately horizontal shift of the turbomachinery characteristic (this can clearly be seen in Fig: 4.2.9). This results in an improved surge margin at part speed and therefore a larger off-design operating range. Although VIGV and VSV are commonly used to improve compressor and fan part speed performance, they are accompanied with a fall in temperature (due to acceleration of the flow) which could possibly give rise to icing during operation in humid conditions. Auxiliary air to prevent ice build up is then necessary. Another disadvantage is the noise that is generated due to VIGV and VSV wake interaction.

The format of the Mini-Maps generated from the CFD simulations are identical to the map format of TURBOMATCH and the “Composite Mini-Map” could therefore be easily added to the TURBOMATCH “maps” folder and used for higher fidelity 0-D performance simulations. The new “Composite Mini-Map” provides a more accurate, physics-based estimation of the performance of the first stage of the fan component and subsequently a better estimation of overall engine off-design performance. A detailed analysis of the high fidelity 0-D overall engine off-design performance simulation is presented in [3] and [32]. Fig: 4.2.10 is a plot of the working line for the 0-D high fidelity simulation discussed above, on the “Composite Mini-Map” and clearly highlights the improved part speed performance (and corresponding larger operating range) associated with increasing the angle of the VSV.

Chapter 4: Figures

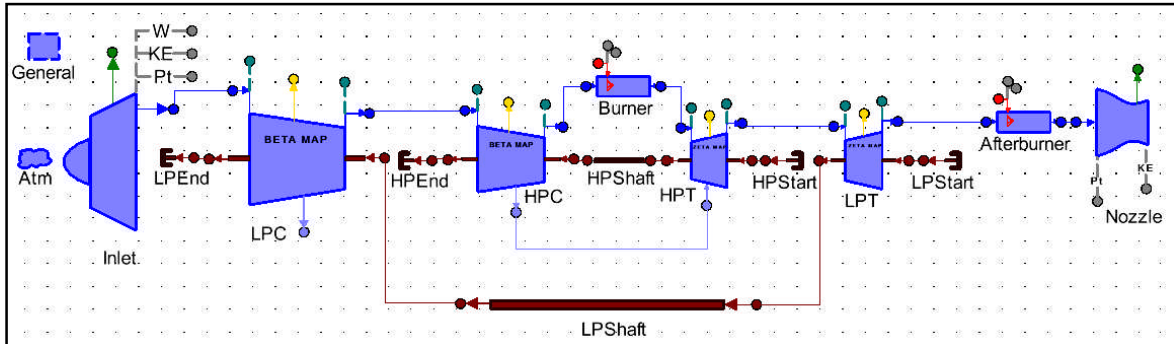


Fig: 4.1.1 CUTSTJR Engine Model Schematic

<u>Design Point Data</u>	<u>Abbreviation</u>	<u>Unit</u>	<u>Value</u>	
Altitude	Atmosphere.alt_in	m	0	(ISASLS)
Flight Mach Number	Atmosphere.MNf_in	-	0	
Inlet Mass Flow Rate	Inlet.Win	kg/s	200	
Intake Pressure Recovery	Inlet.PqP_in	-	1	
LPC Pressure Ratio	LPC.PR	-	7.075	
LPC Efficiency	LPC.eff	-	0.87	
LPC Design Rotational Speed	LPC.NmechDes	rpm	10000	
HPC Pressure Ratio	HPC.PR	-	7.075	
HPC Efficiency	HPC.eff	-	0.87	
HPC Design Rotational Speed	HPC.NmechDes	rpm	12000	
Burner Efficiency	Burner.eff_in	-	0.999	
Burner Fractional Pressure Loss	Burner.dPqP_in	-	0.05	
Burner Outlet Total Temperature	Burner.F_out.Tt	K	1800	
Fuel	-	-	Jet-A	
HPT Isentropic Efficiency	HPT.eff	-	0.89	
HPT Design Rotational Speed	HPT.NmechDes	rpm	12000	
LPT Isentropic Efficiency	LPT.eff	-	0.89	
LPT Design Rotational Speed	LPT.NmechDes	rpm	10000	
Afterburner Efficiency	Afterburner.eff	-	0.9	(No
Afterburner Fractional Pressure Loss	Afterburner.dPqP_in	-	0.05	Reheat
Afterburner Fuel Flow Rate	Afterburner.Fu_in.W	kg/s	0	at DP)

Fig: 4.1.2 Main Design Data of the CUTSTJR Engine Model

Advanced Performance Simulation of Gas Turbine Components
and Fluid Thermodynamic Properties

COMPONENT	SWITCH / DATA	Abbreviation	Unit	Switch Setting / DATA Value
Atmosphere	Fluid Model Selection	Atmosphere.fluid_in	-	"no dissociation"
	Calculation Option	Atmosphere.switchMode	-	"ALDTMN"
	Altitude	Atmosphere.alt_in	m	0
	Flight Mach Number	Atmosphere.MNf_in	-	0
	Ambient Temperature	Atmosphere.Tamb	K	288.15
	Ambient Pressure	Atmosphere.Pamb	Pa	101325
	Temperature Deviation from ISASLS	Atmosphere.dTamb	K	0
All other Atmosphere Component DATA and Switch Settings Set to Default Values				
Inlet	Fluid Model Selection	Inlet.fluid_in	-	"no dissociation"
	Pressure Recovery Option	Inlet.switchRec	-	"INPUT_PqP"
	Inlet Pressure Recovery	Inlet.PqP_in	-	1
All other Inlet Component DATA and Switch Settings Set to Default Values				
LPC	Fluid Model Selection	LPC.fluid_in	-	"no dissociation"
	Design Rotational Speed	LPC.NmechDes	rpm	10000
	Compressor Map Filepath	LPC.Comp_map	-	"@SCLib@/maps/CUSTOM1.xml"
All other LPC Component DATA and Switch Settings Set to Default Values				
HPC	Fluid Model Selection	HPC.fluid_in	-	"no dissociation"
	Design Rotational Speed	HPC.NmechDes	rpm	12000
	Compressor Map Filepath	HPC.Comp_map	-	"@SCLib@/maps/CUSTOM1.xml"
All other HPC Component DATA and Switch Settings Set to Default Values				

Fig: 4.1.3 Switch Settings and DATA for each component of the CUTSTJR Engine Model

Advanced Performance Simulation of Gas Turbine Components
and Fluid Thermodynamic Properties

<u>COMPONENT</u>	<u>SWITCH / DATA</u>	<u>Abbreviation</u>	<u>Unit</u>	<u>Switch Setting / DATA Value</u>
Burner	Fluid Model Selection	Burner.fluid_in	-	"chemical equilibrium"
	Fuel	Burner.Fuel	-	"JetA"
	Fractional Pressure Loss Calculation Option	Burner.switchdPqP	-	"INPUTdPqP"
	Efficiency Calculation Option	Burner.switcheff	-	"INPUTeff"
	Fractional Pressure Loss	Burner.dPqP_in	-	0.05
	Efficiency	Burner.eff_in	-	0.999
	All other Burner Component DATA and Switch Settings Set to Default Values			
HPT	Fluid Model Selection	HPT.fluid_in	-	"chemical equilibrium"
	Design Rotational Speed	HPT.NmechDes	rpm	12000
	Turbine Map Filepath	HPT.Trb_map	-	"@SCLib@/maps/TURB1.xml"
	All other HPT Component DATA and Switch Settings Set to Default Values			
LPT	Fluid Model Selection	LPT.fluid_in	-	"chemical equilibrium"
	Design Rotational Speed	LPT.NmechDes	rpm	10000
	Turbine Map Filepath	LPT.Trb_map	-	"@SCLib@/maps/TURB1.xml"
	All other LPT Component DATA and Switch Settings Set to Default Values			
Afterburner	Fluid Model Selection	Afterburner.fluid_in	-	"chemical equilibrium"
	Fuel	Afterburner.Fuel	-	"JetA"
	Fractional Pressure Loss Calculation Option	Afterburner.switchdPqP	-	"INPUTdPqP"
	Efficiency Calculation Option	Afterburner.switcheff	-	"INPUTeff"
	Fractional Pressure Loss	Afterburner.dPqP_in	-	0.05
	Efficiency	Afterburner.eff_in	-	0.9
	All other Afterburner Component DATA and Switch Settings Set to Default Values			
Condi Nozzle	Fluid Model Selection	CondiNozzle.fluid_in	-	"chemical equilibrium"
	All other Condi Nozzle Component DATA and Switch Settings Set to Default Values			
NB: All DATA and Switch Settings of the Mechanical Shaft Components (Shaft Start, Shaft End and Shaft) Set to Default Values (For both - LP and HP Systems)				

Fig: 4.1.3 (Cont'd) Switch Settings and DATA for each component of the CUTSTJR Engine Model

Advanced Performance Simulation of Gas Turbine Components
and Fluid Thermodynamic Properties

<u>Independent Variables</u>	<u>Corresponding Closure Equations</u> (With Specified Dependent Variables)	<u>Boundary Conditions</u>
LPC.s_mapWc_in = x[1]	fres[1] = (0.70 - LPC.BETA) / LPC.BETA	Afterburner.Fu_in.P = 101325
LPC.s_mapEff_in = x[2]	fres[2] = (0.87 - LPC.eff) / LPC.eff	Afterburner.Fu_in.T = 388.15
LPC.s_NcRdes_in = x[3]	fres[3] = (1.0000 - LPC.NcRdesMap) / LPC.NcRdesMap	Afterburner.F_out.Tt = 2310
LPC.s_mapPR_in = x[4]	fres[4] = (7.075 - LPC.PR) / LPC.PR	Burner.Fu_in.P = 101325
		Burner.Fu_in.T = 358.15
HPC.s_mapWc_in = x[5]	fres[5] = (0.70 - HPC.BETA) / HPC.BETA	Burner.F_out.Tt = 1800
HPC.s_mapEff_in = x[6]	fres[6] = (0.87 - HPC.eff) / HPC.eff	HPC.heatP.Q = 0
HPC.s_NcRdes_in = x[7]	fres[7] = (1.0000 - HPC.NcRdesMap) / HPC.NcRdesMap	HPT.heatP.Q = 0
HPC.s_mapPR_in = x[8]	fres[8] = (7.075 - HPC.PR) / HPC.PR	LPC.heatP.Q = 0
		LPT.heatP.Q = 0
LPT.s_mapWc_in = x[9]	fres[9] = (1.0 - LPT.ZETA) / LPT.ZETA	
LPT.s_mapEff_in = x[10]	fres[10] = (0.89 - LPT.eff) / LPT.eff	
LPT.s_mapNc_in = x[11]	fres[11] = (1.0 - LPT.NcRdesMap) / LPT.NcRdesMap	<u>Tearing Variables</u>
LPT.s_mapDhqT_in = x[12]	fres[12] = (10000 - LPT.Nmech) / LPT.Nmech	LPEnd.Me_in.Nmech = 10000
		HPEnd.Me_in.Nmech = 12000
HPT.s_mapWc_in = x[13]	fres[13] = (1.0 - HPT.ZETA) / HPT.ZETA	Inlet.F_in.WAR = 0
HPT.s_mapEff_in = x[14]	fres[14] = (0.89 - HPT.eff) / HPT.eff	HPC.BETA = 0.7
HPT.s_mapNc_in = x[15]	fres[15] = (1.0 - HPT.NcRdesMap) / HPT.NcRdesMap	HPT.ZETA = 1
HPT.s_mapDhqT_in = x[16]	fres[16] = (12000 - HPT.Nmech) / HPT.Nmech	Inlet.F_in.W = 200
		LPC.BETA = 0.7
CondiNozzle.Ath = x[17]	fres[17] = (200 - Inlet.W_in) / Inlet.W_in	LPT.ZETA = 0.7
CondiNozzle.Aexit = x[18]	fres[18] = (Pamb - CondiNozzle.Ps_out) / CondiNozzle.Ps_out	

Fig: 4.1.4 CUTSTJR Engine Model Partition Generation and DP Simulation Data

Advanced Performance Simulation of Gas Turbine Components
and Fluid Thermodynamic Properties

<u>Independent Variables</u>	<u>Corresponding Closure Equations</u> (With Specified Dependent Variables)	<u>Boundary Conditions</u>
LPC.s_mapWc_in = x[1]	fres[1] = (0.70 - LPC.BETA) / LPC.BETA	LPC.F_in.Ang = 0
LPC.s_mapEff_in = x[2]	fres[2] = (0.87 - LPC.eff) / LPC.eff	LPC.F_in.FARB = 0.
LPC.s_NcRdes_in = x[3]	fres[3] = (1.0000 - LPC.NcRdesMap) / LPC.NcRdesMap	LPC.F_in.FARU = 0.
LPC.s_mapPR_in = x[4]	fres[4] = (7.075 - LPC.PR) / LPC.PR	LPC.F_in.Pt = 101325
		LPC.F_in.Tt = 288.15
		LPC.F_in.W = 200
		LPC.F_in.WAR = 0
		LPC.Me_in.Nmech = 10000.
		LPC.Me_in.inertia = 0
		LPC.Me_in.inertia_tot = 1
		LPC.Me_in.trq = 1
		LPC.heatP.Q = 0
		<u>Tearing Variable</u>
		LPC.BETA = 0.7

Fig: 4.1.5 Isolated LPC Component Partition Generation and DP Simulation Data

NB: The LPC inlet main flow port variables (LPC.F_in.Ang, LPC.F_in.FARB, LPC.F_in.FARU, LPC.F_in.Pt, LPC.F_in.Tt, LPC.F_in.W and LPC.F_in.WAR) need to be specified as boundary conditions for isolated component performance. During whole engine simulation however, these variables are obtained from the immediate upstream component (the Inlet component of the CUTSTJR engine model).

NB: Similarly, the LPC inlet mechanical port variables (LPC.Me_in.Nmech, LPC.Me_in.inertia, LPC.Me_in.Inertia_tot and LPC.Me_in.trq) need to be specified as boundary conditions for isolated component performance. During whole engine simulation however, these variables are obtained from the LP shaft component.

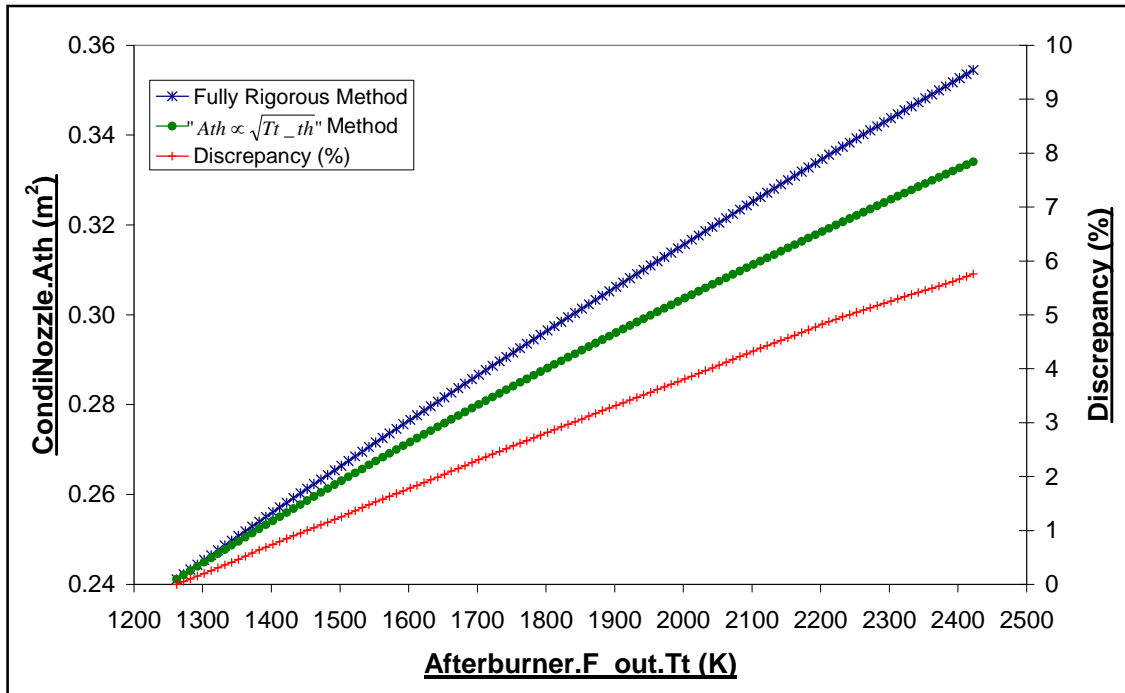


Fig: 4.1.6 CUTSTJR Off-Design Case Study 1:
Variation of CondiNozzle.Ath as function of Afterburner.F_out.Tt -
Comparison between the two methods to determine CondiNozzle.Ath

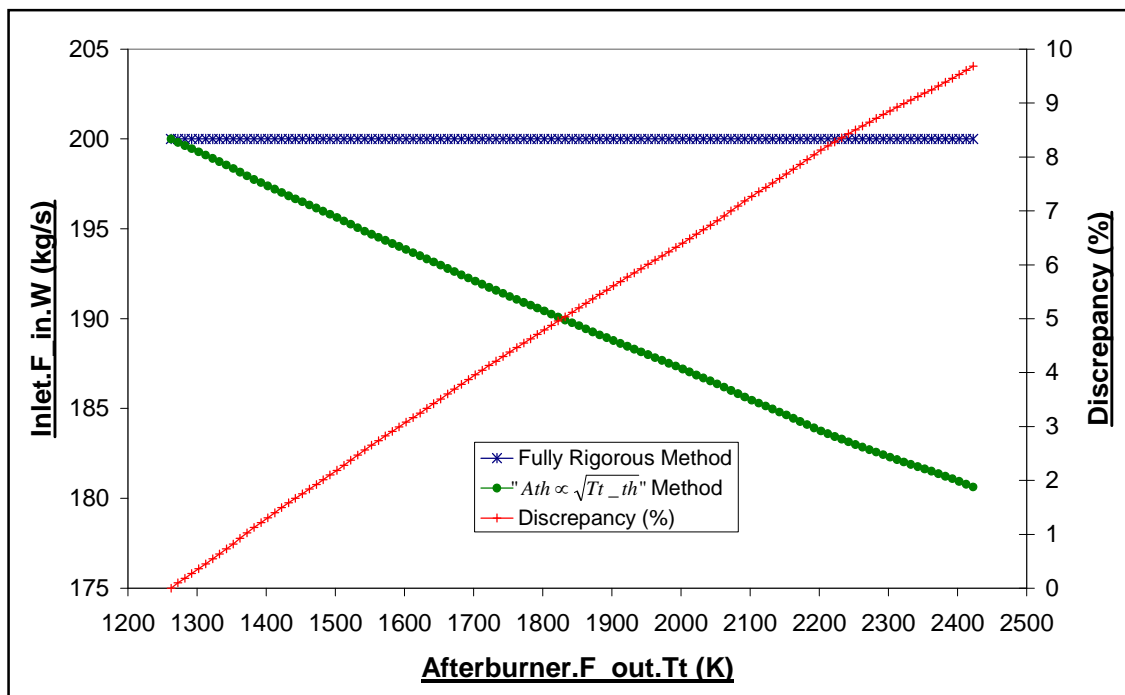


Fig: 4.1.7 CUTSTJR Off-Design Case Study 1:
Variation of Inlet.F_in.W as function of Afterburner.F_out.Tt:
Comparison between the two methods to determine CondiNozzle.Ath

Advanced Performance Simulation of Gas Turbine Components and Fluid Thermodynamic Properties

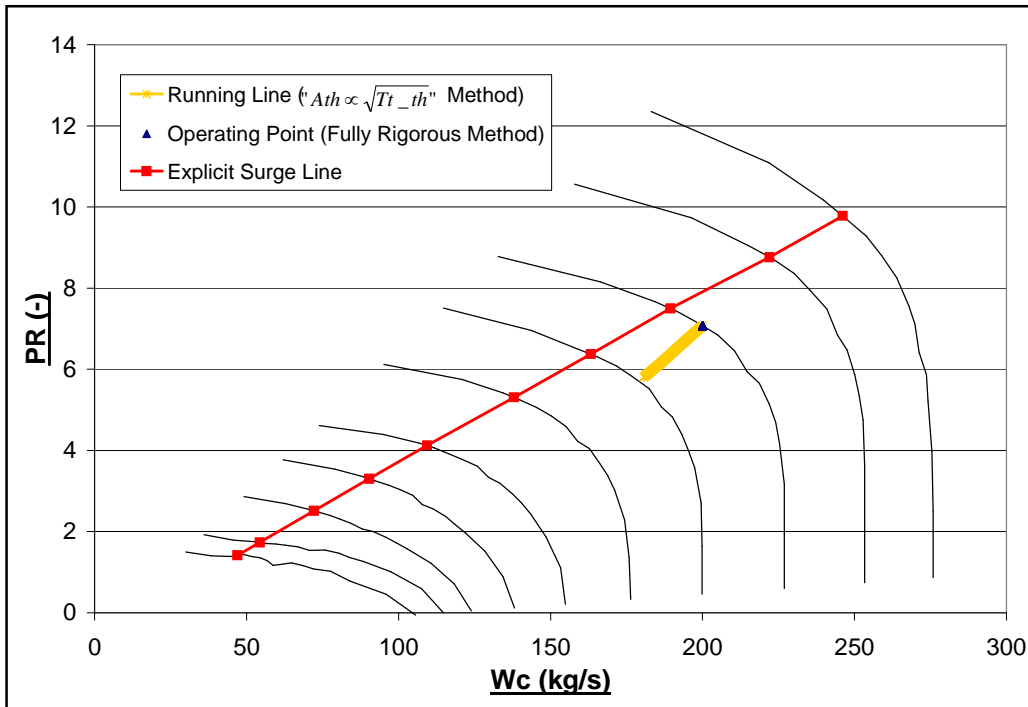


Fig: 4.1.8 CUTSTJR Off-Design Case Study 1:
Low Pressure Compressor (LPC) Map:
Effects of the two methods to determine CondiNozzle.Ath on the LPC Characteristic

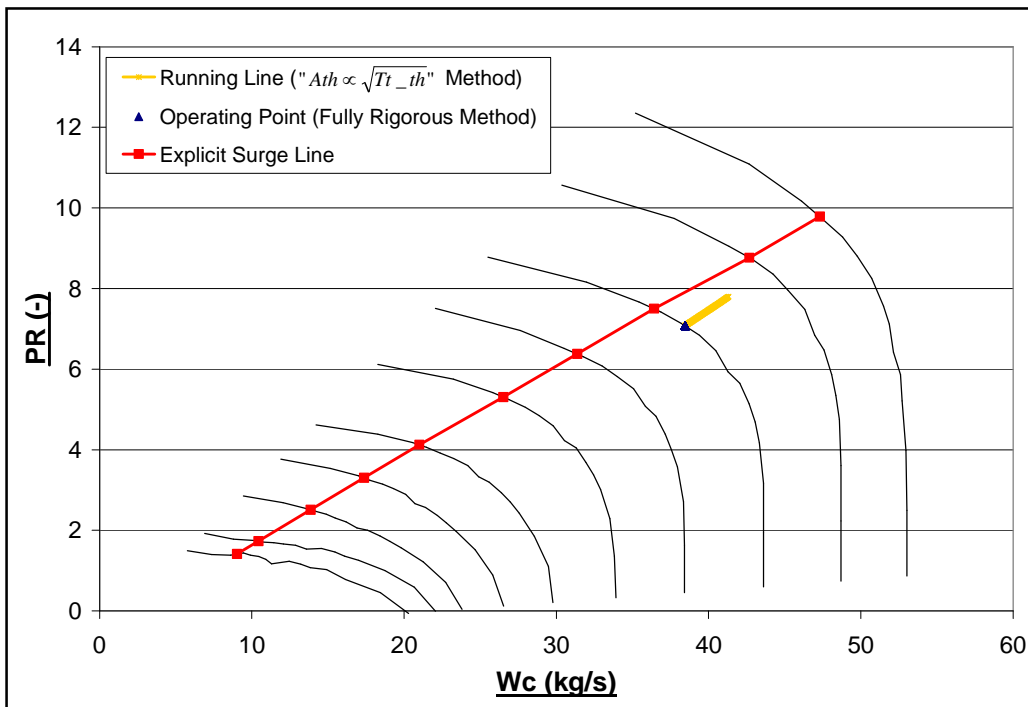


Fig: 4.1.9 CUTSTJR Off-Design Case Study 1:
High Pressure Compressor (HPC) Map:
Effects of the two methods to determine CondiNozzle.Ath on the HPC Characteristic

Advanced Performance Simulation of Gas Turbine Components and Fluid Thermodynamic Properties

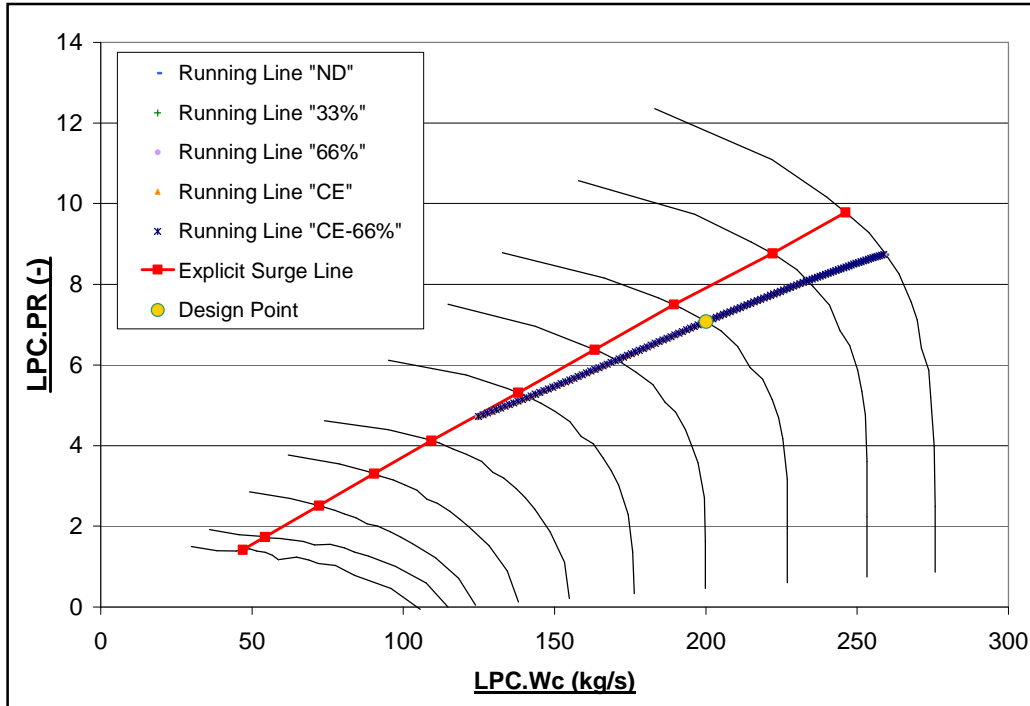


Fig: 4.1.10 CUTSTJR Off-Design Case Study 2:
LPC Compressor Map: Effects of Dissociation on the LPC running line

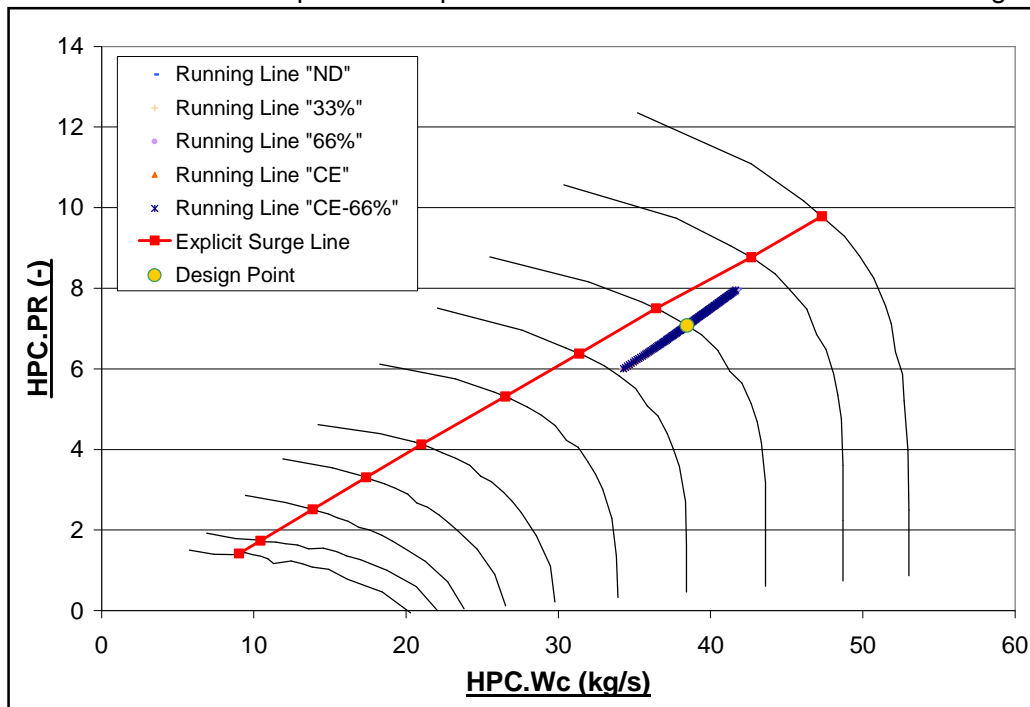


Fig: 4.1.11 CUTSTJR Off-Design Case Study 2:
HPC Compressor Map: Effects of Dissociation on the HPC running line

Advanced Performance Simulation of Gas Turbine Components and Fluid Thermodynamic Properties

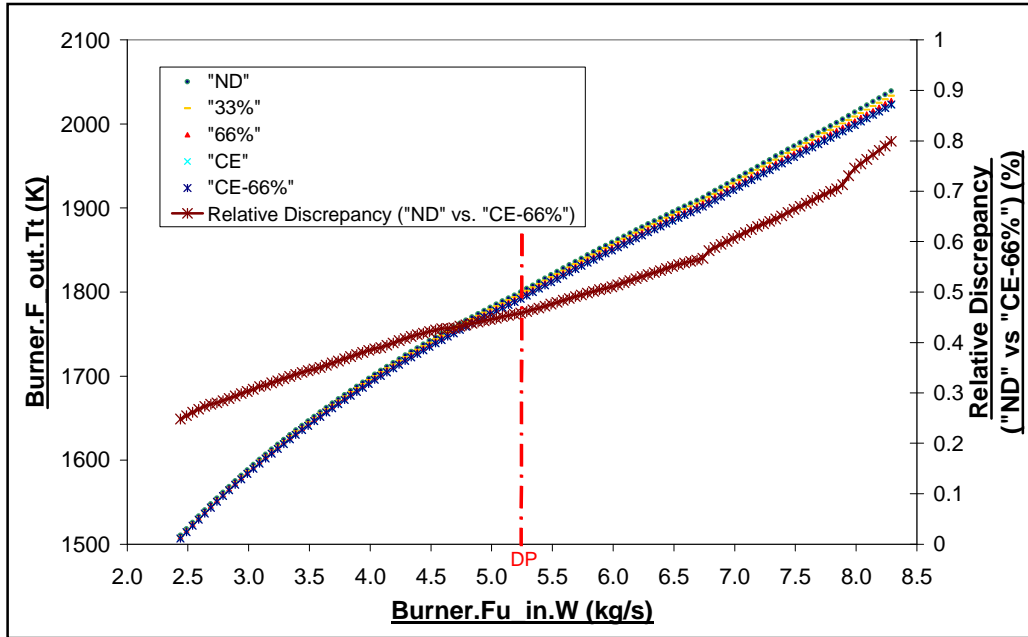


Fig: 4.1.12 CUTSTJR Off-Design Case Study 2: Effects of Dissociation on Burner.F_out.Tt as a function of vs. Burner.Fu_in.W

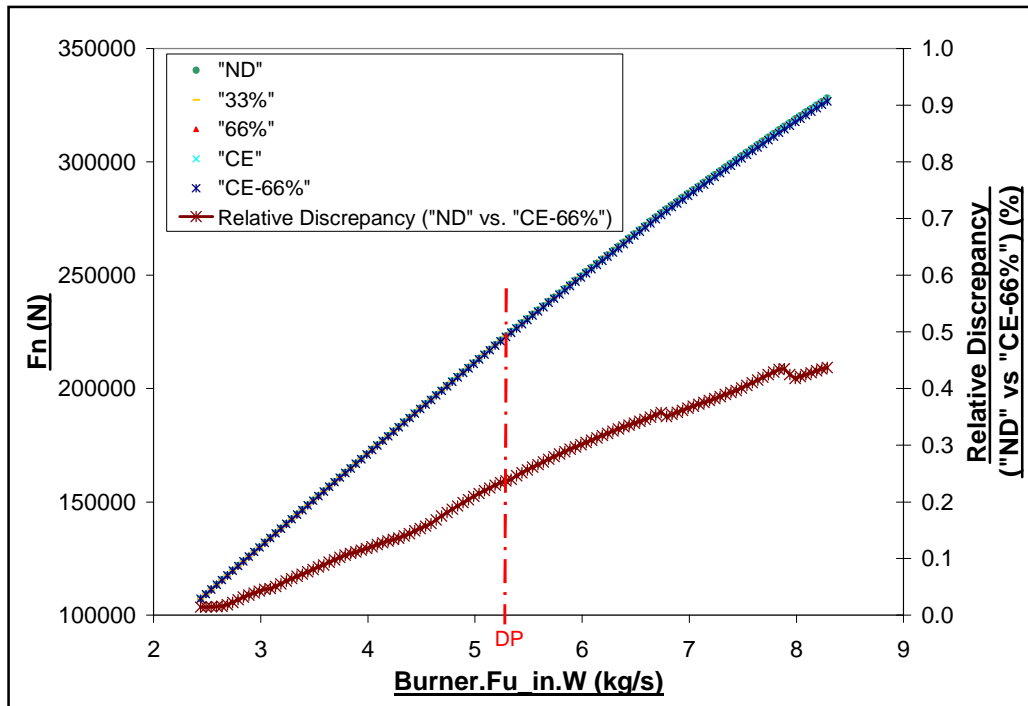


Fig: 4.1.13 CUTSTJR Off-Design Case Study 2: Effects of Dissociation on Fn as a function of Burner.Fu_in.W

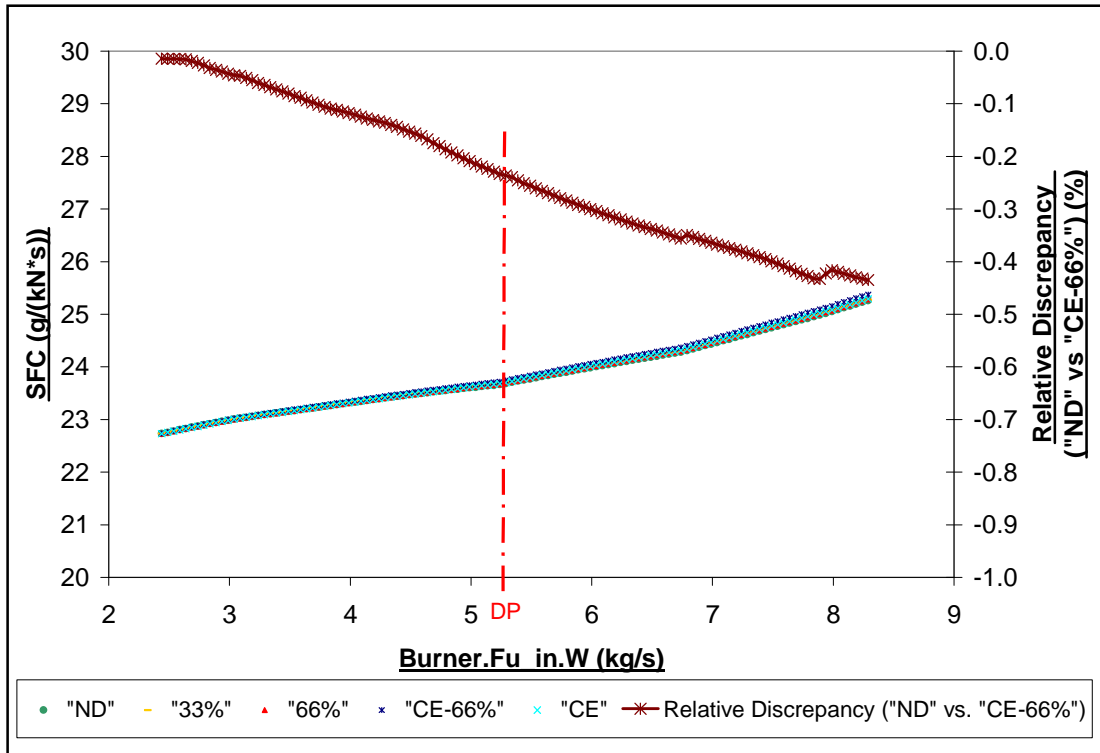


Fig: 4.1.14 CUTSTJR Off-Design Case Study 2:
Effects of Dissociation on SFC as a function of Burner.Fu_in.W

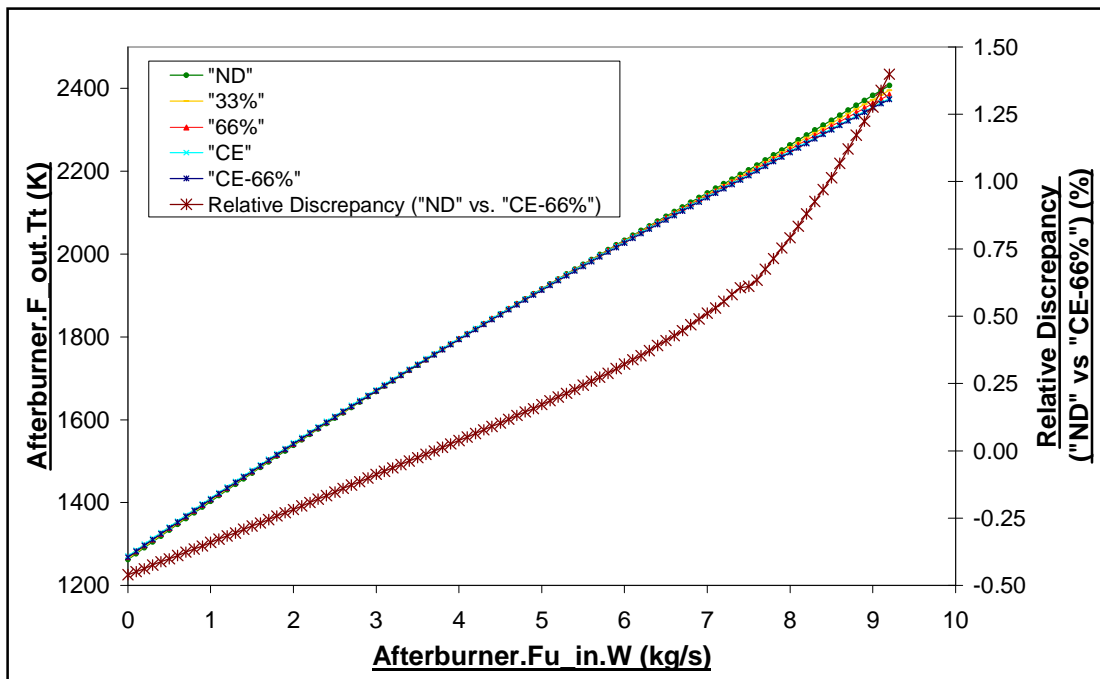


Fig: 4.1.15 CUTSTJR Off-Design Case Study 3:
Effects of Dissociation on Afterburner.F_out.Tt as a function of
Afterburner.Fu_in.W

Advanced Performance Simulation of Gas Turbine Components
and Fluid Thermodynamic Properties

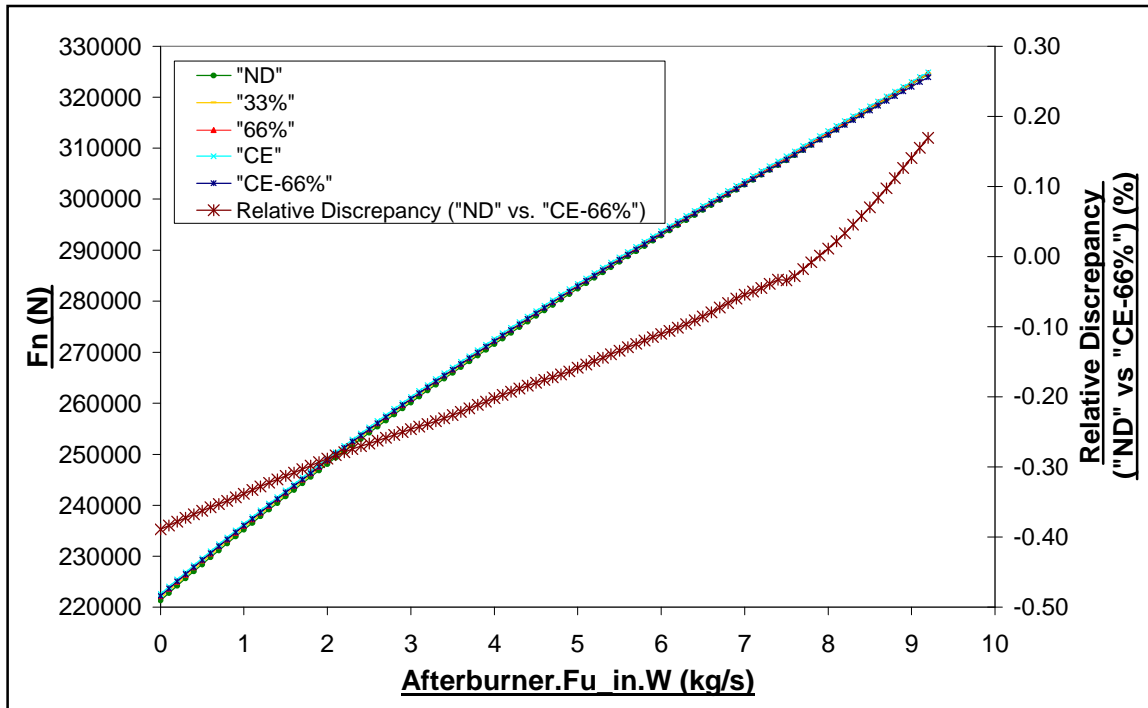


Fig: 4.1.16 CUTSTJR Off-Design Case Study 3:
Effects of Dissociation on Fn as a function of Afterburner.Fu_in.W

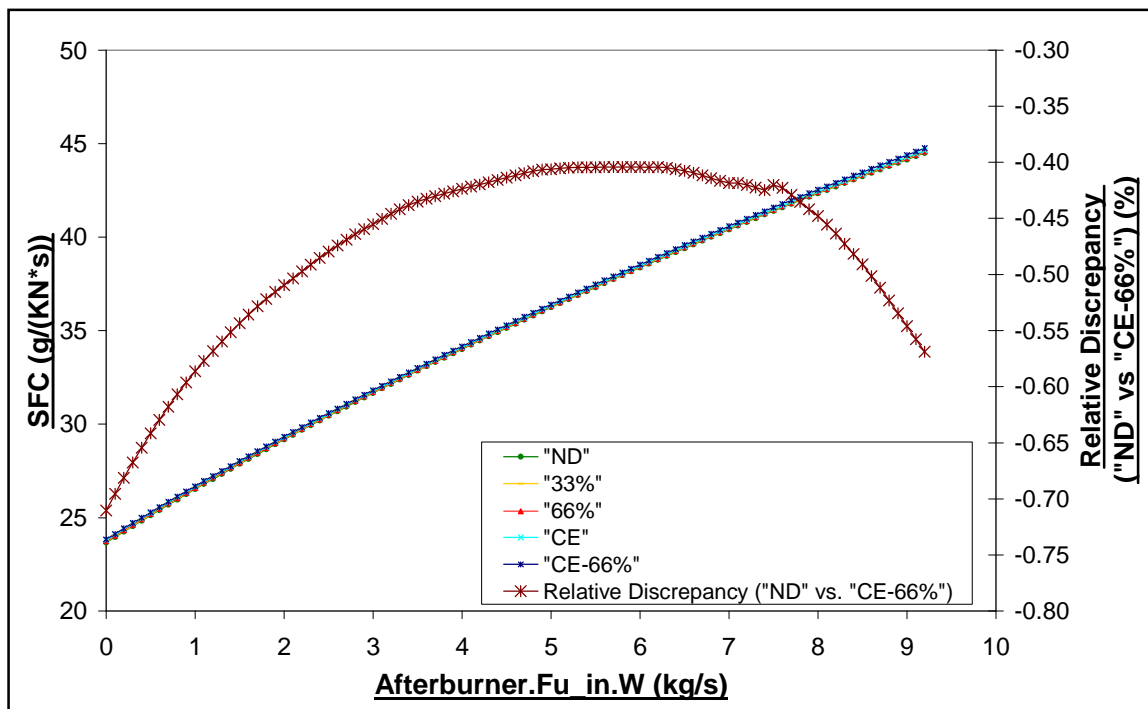


Fig: 4.1.17 CUTSTJR Off-Design Case Study 3:
Effects of Dissociation on SFC as a function of Afterburner.Fu_in.W

Advanced Performance Simulation of Gas Turbine Components and Fluid Thermodynamic Properties

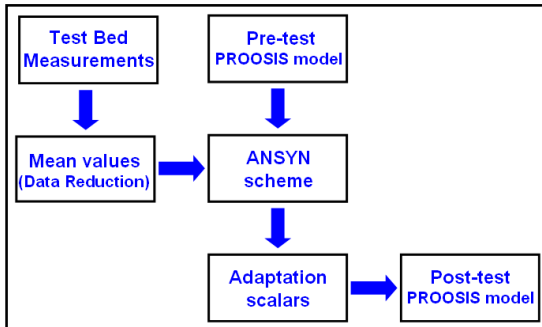


Fig: 4.2.1 PROOSIS Test Analysis Process

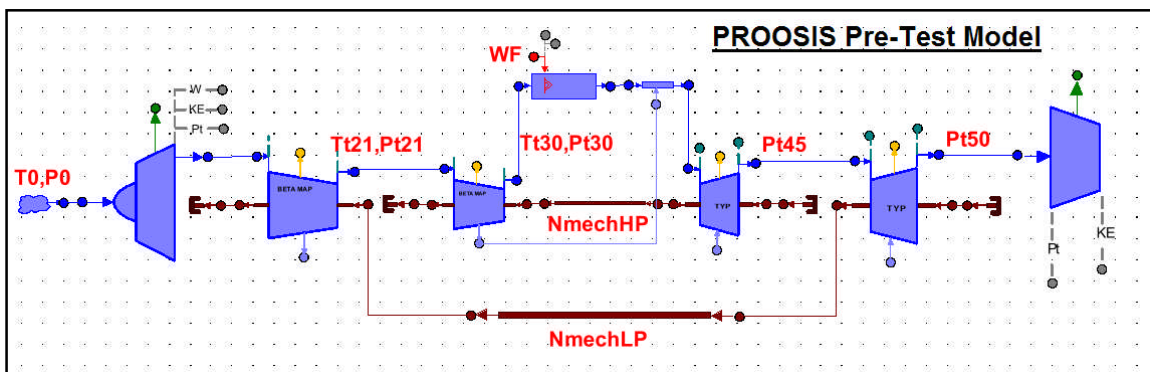


Fig: 4.2.2 CUTSTJ “Pre-Test” Model (Test Bed Measurements in Red)

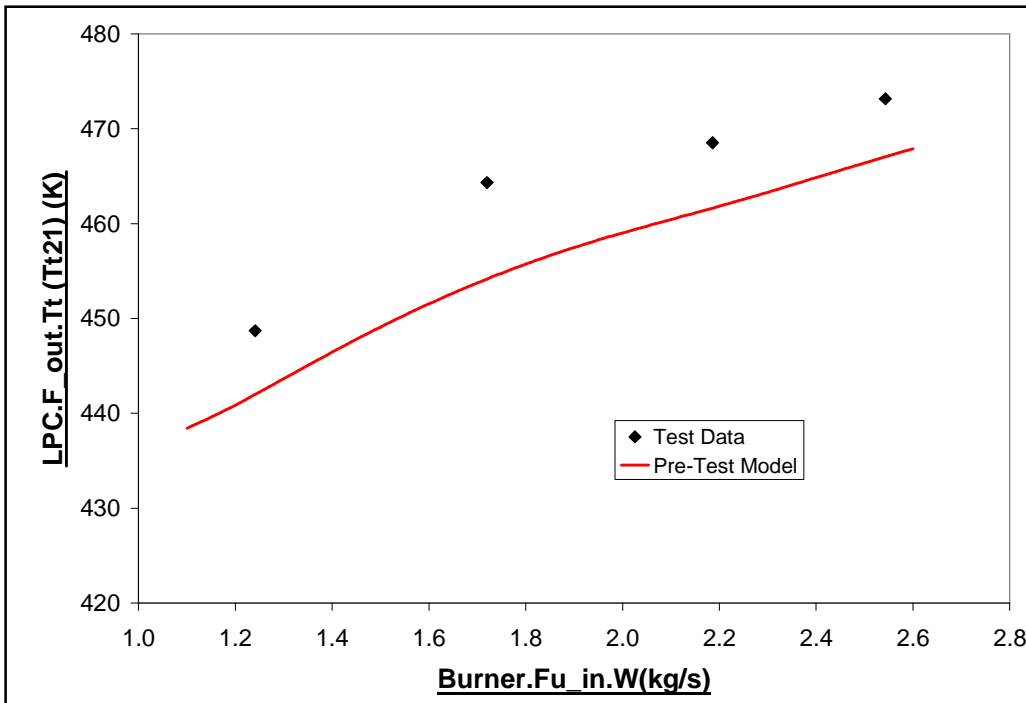


Fig: 4.2.3 CUTSTJ “Pre-Test” Model and Test Data Discrepancies (LPC.F_out.Tt vs. Tt21)

<u>Independent Variables</u>	<u>Corresponding Closure Equations</u> (With Specified Dependent Variables)	<u>Boundary Conditions</u>
LPC.s_adapEff_in = x[1]	fres[1] = (Tt21 - LPC.F_out.Tt) / LPC.F_out.Tt	Burner.Fu_in.P = 101325
LPC.s_adapWc_in = x[2]	fres[2] = (Pt21 - LPC.F_out.Pt) / LPC.F_out.Pt	Burner.Fu_in.T = 358.15
HPC.s_adapEff_in = x[3]	fres[3] = (Tt30 - HPC.F_out.Tt) / HPC.F_out.Tt	Burner.Fu_in.W = 2.16
HPC.s_adapWc_in = x[4]	fres[4] = (Pt30 - HPC.F_out.Pt) / HPC.F_out.Pt	HPC.heatP.Q = 0
HPT.s_adapEff_in = x[5]	fres[5] = (Pt45 - HPT.F_out.Pt) / HPT.F_out.Pt	HPT.heatP.Q = 0
HPT.s_adapWc_in = x[6]	fres[6] = (Pt50 - LPT.F_out.Pt) / LPT.F_out.Pt	LPC.heatP.Q = 0
LPT.s_adapEff_in = x[7]	fres[7] = (NmechLP - LPT.Me_in.Nmech) / LPT.Me_in.Nmech	LPT.heatP.Q = 0
LPT.s_adapWc_in = x[8]	fres[8] = (NmechHP - HPT.Me_in.Nmech) / HPT.Me_in.Nmech	
		<u>Tearing Variables</u>
		LPEnd.Me_in.Nmech = 8500
		HPEnd.Me_in.Nmech = 10000
		Inlet.F_in.WAR = 0
		HPC.BETA = 0.5
		HPT.ZETA = 1
		Inlet.F_in.W = 50
		LPC.BETA = 0.7
		LPT.ZETA = 0.7

Fig: 4.2.4 CUTSTJ ANSYN Simulation Data

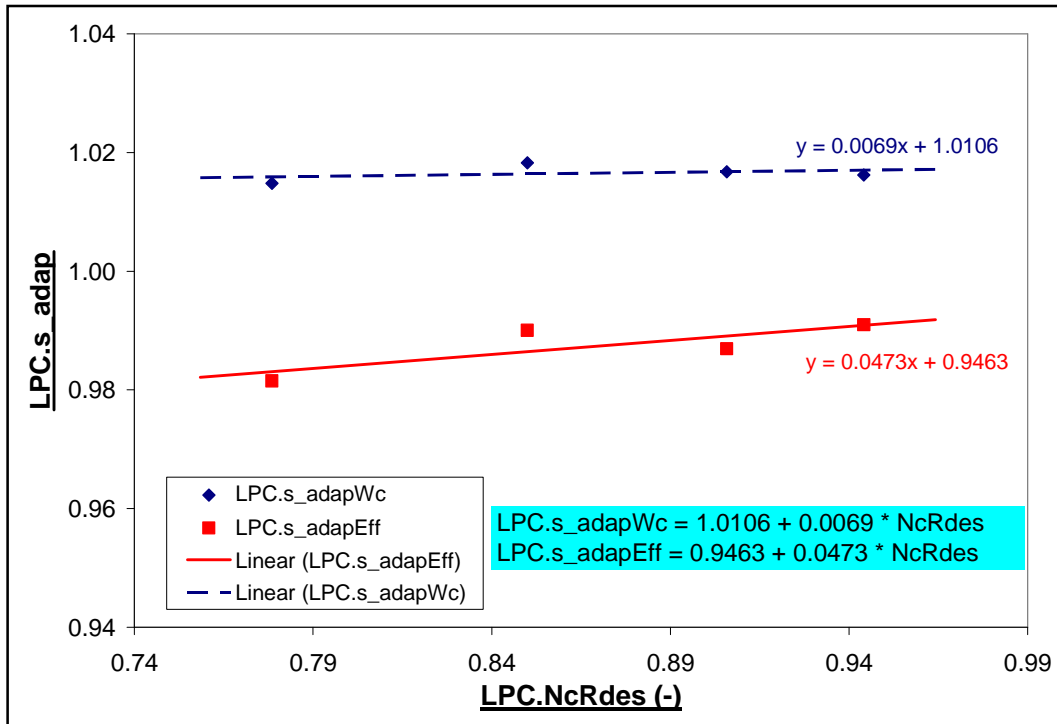


Fig: 4.2.5 CUTSTJ LPC Adaptive Scalar Schedules

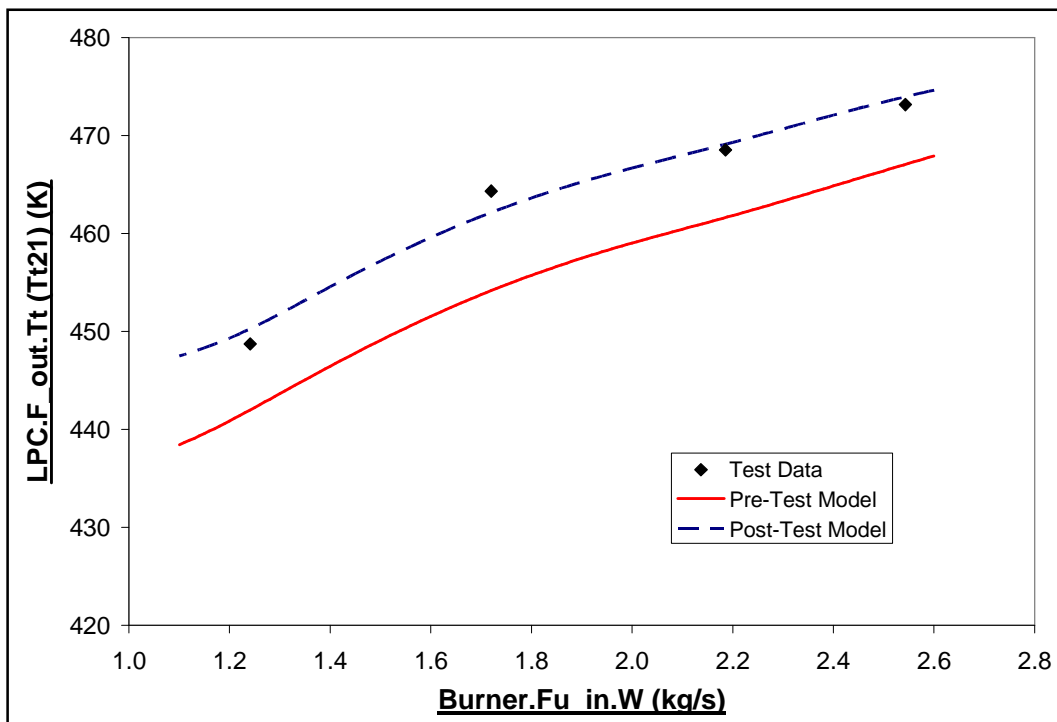


Fig: 4.2.6 CUTSTJ Test Data, Pre-Test Model & Post-Test Model Discrepancies (LPC.F_out.Tt vs. Tt21)

Advanced Performance Simulation of Gas Turbine Components
and Fluid Thermodynamic Properties

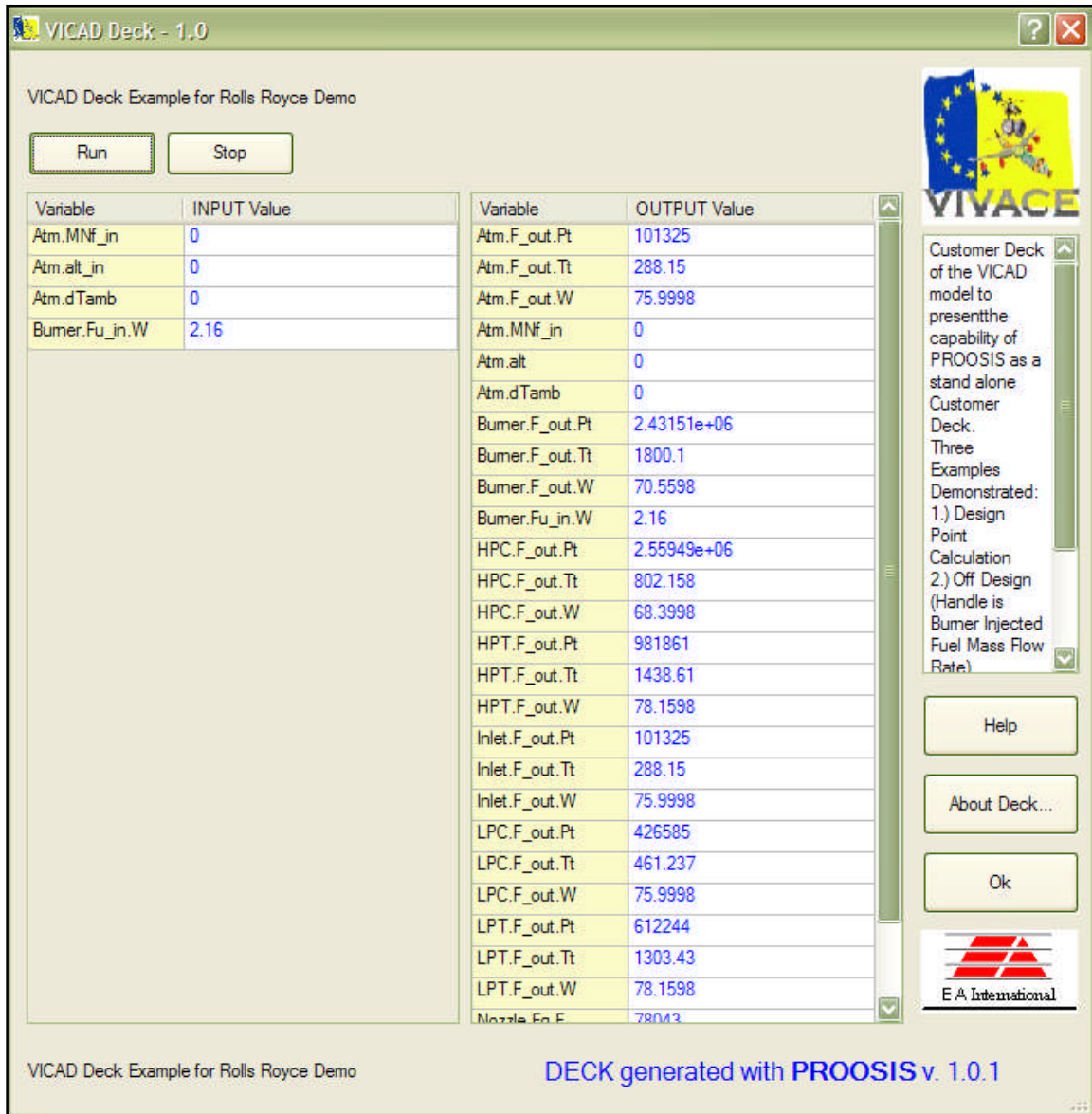


Fig: 4.2.7 Example of a PROOSIS Standalone Customer Deck
(This particular customer deck was used by the author as an example during a PROOSIS demonstration to the Rolls Royce performance team as part of the PROOSIS technology transfer process)

Advanced Performance Simulation of Gas Turbine Components and Fluid Thermodynamic Properties

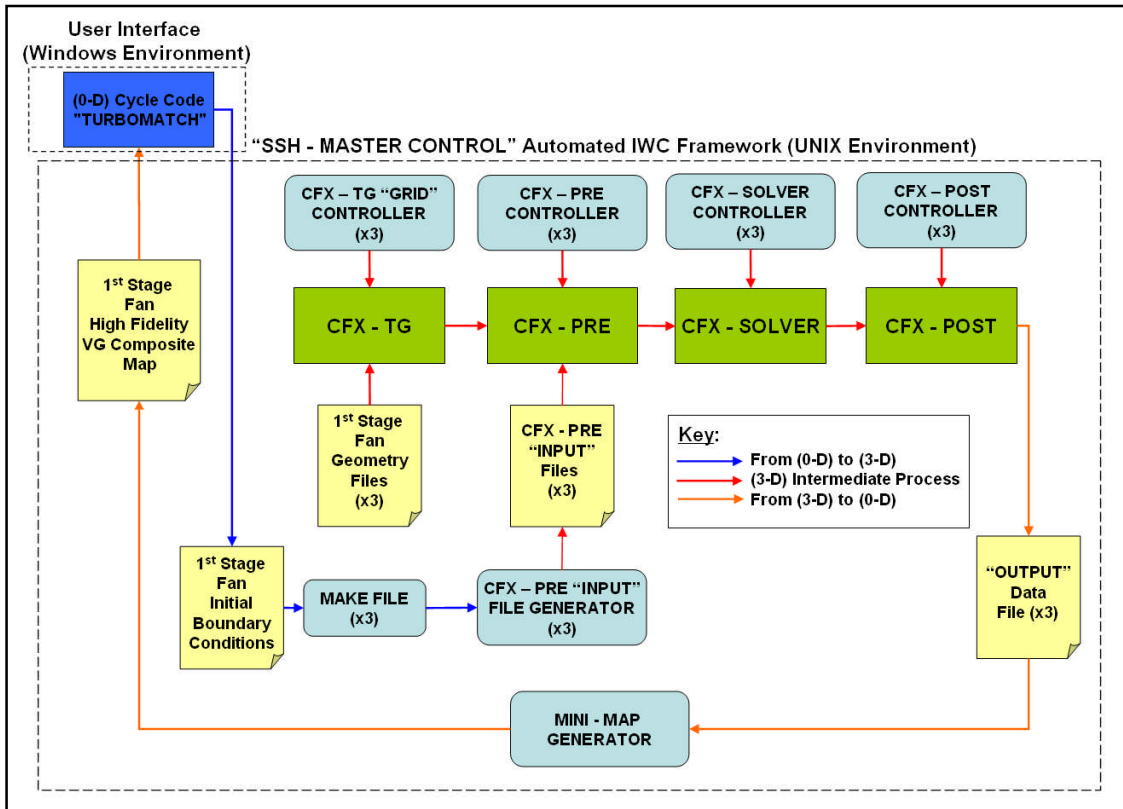


Fig: 4.2.8 Integrated (3D) Aerodynamic Component Zooming Process using an IWC [32]

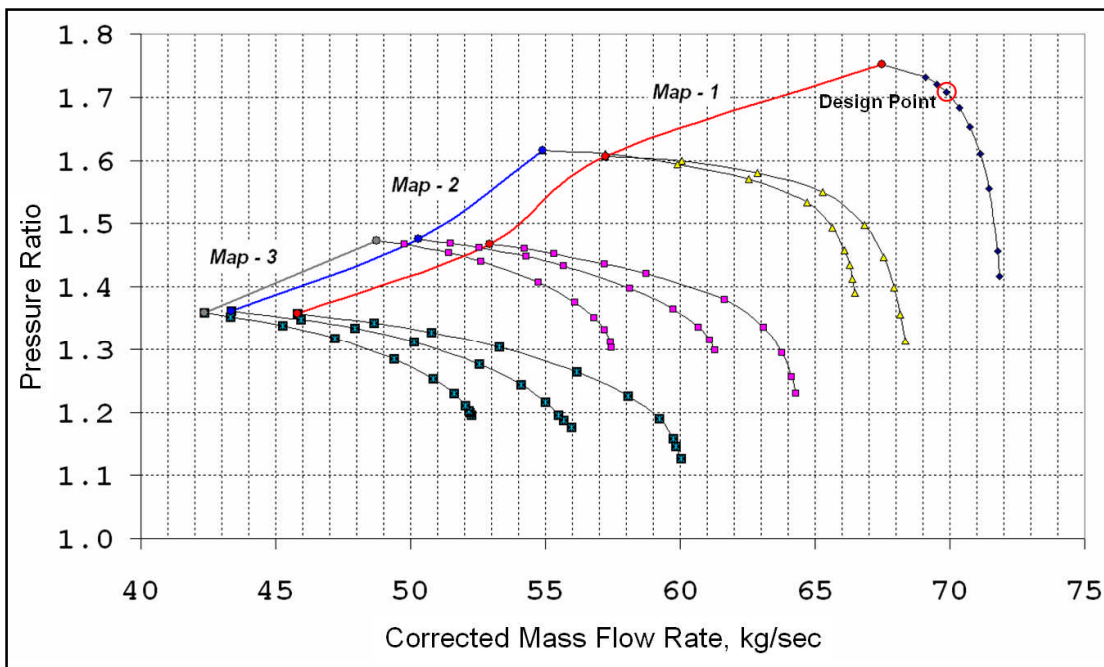


Fig: 4.2.9 Fan Component – First Stage High Fidelity, Variable Geometry Composite Mini-Map (PR vs. W_c) [32]

Advanced Performance Simulation of Gas Turbine Components and Fluid Thermodynamic Properties

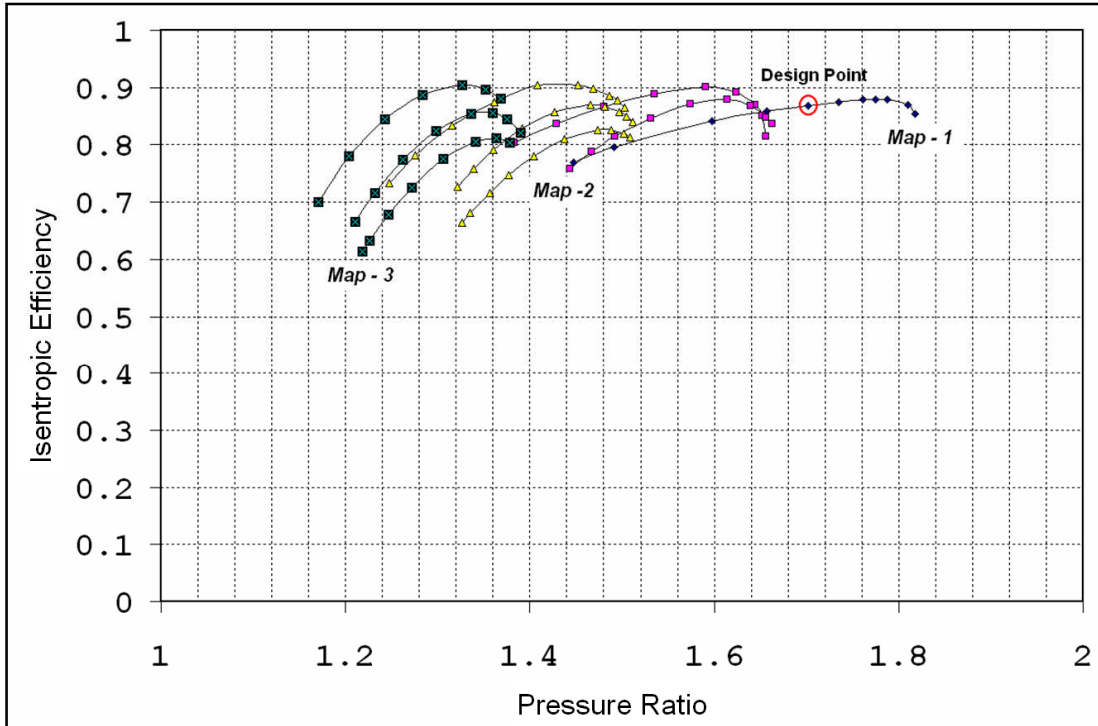


Fig: 4.2.10 Fan Component – First Stage
High Fidelity, Variable Geometry Composite Mini-Map (η vs. PR) ^[32]

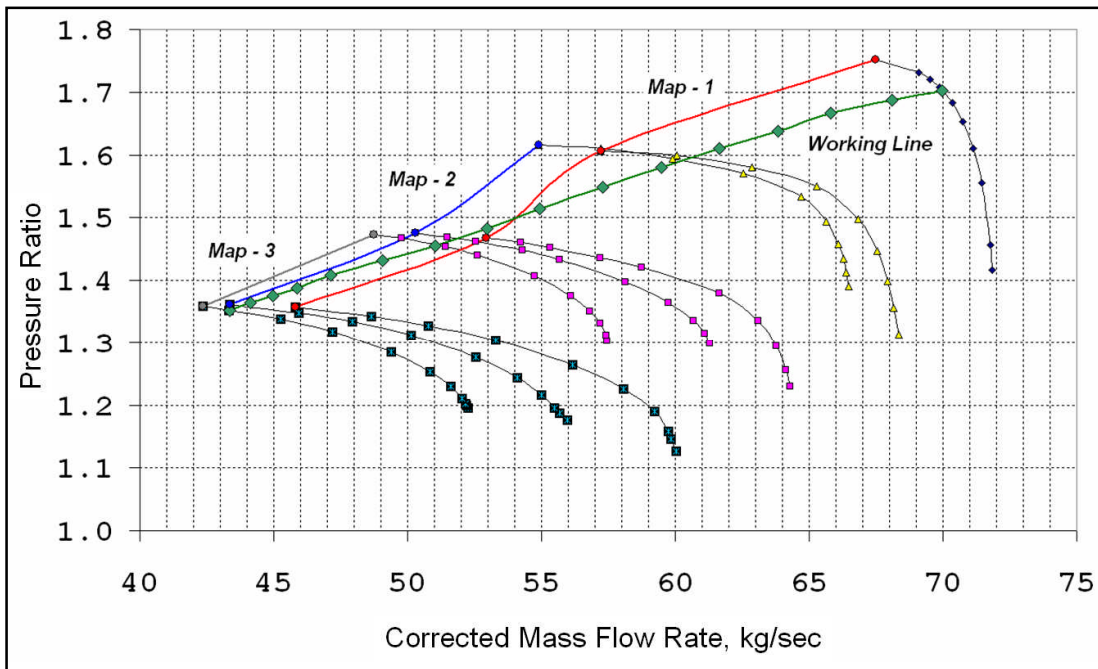


Fig: 4.2.10 Fan Component – First Stage
Working Line for High Fidelity 0-D Off-Design Simulation ^[32]

Chapter 4: Appendix 1
CUTSTJR Off-Design Case Study 2: Detailed Results

Burner.F_in.W = 2.43829754kg/s (Extreme OD Point - Close to LPC Surge)					
Performance Parameter	Fluid Model Combination				
	"ND"	"33%"	"66%"	"CE"	"CE-66%"
Inlet.F_out.FARB(-)	0.00000	0.00000	0.00000	0.00000	0.00000
Inlet.F_out.FARU(-)	0.00000	0.00000	0.00000	0.00000	0.00000
Inlet.F_out.Pt(Pa)	101325	101325	101325	101325	101325
Inlet.F_out.Tt(K)	288.15	288.15	288.15	288.15	288.15
Inlet.F_out.W (kg/s)	123.10	123.15	123.21	123.26	123.37
LPC.F_out.FARB(-)	0.00000	0.00000	0.00000	0.00000	0.00000
LPC.F_out.FARU(-)	0.00000	0.00000	0.00000	0.00000	0.00000
LPC.F_out.Pt(Pa)	474125	473920	473723	473544	474144
LPC.F_out.Tt(K)	482.84	482.77	482.70	482.64	482.82
LPC.F_out.W(kg/sec)	123.10	123.15	123.21	123.26	123.37
HPC.F_out.FARB(-)	0.00000	0.00000	0.00000	0.00000	0.00000
HPC.F_out.FARU(-)	0.00000	0.00000	0.00000	0.00000	0.00000
HPC.F_out.Pt(Pa)	2823937	2824753	2825776	2826618	2830170
HPC.F_out.Tt(K)	836.10	836.11	836.14	836.16	836.45
HPC.F_out.W(kg/sec)	123.10	123.15	123.21	123.26	123.37
Burner.F_out.FARB(-)	0.01979	0.01978	0.01977	0.01976	0.01975
Burner.F_out.FARU(-)	0.00002	0.00002	0.00002	0.00002	0.00002
Burner.F_out.Pt(Pa)	2682740	2683515	2684487	2685287	2688661
Burner.F_out.Tt(K)	1510.54	1509.38	1508.22	1507.06	1506.80
Burner.F_out.W(kg/sec)	125.54	125.59	125.65	125.70	125.80
Burner.Fu_in.W(kg/sec)	2.438	2.438	2.438	2.438	2.438
HPT.F_out.FARB(-)	0.01979	0.01978	0.01977	0.01976	0.01975
HPT.F_out.FARU(-)	0.00002	0.00002	0.00002	0.00002	0.00002
HPT.F_out.Pt(Pa)	903395	902721	902082	901419	901731
HPT.F_out.Tt(K)	1212.55	1212.06	1211.53	1211.05	1209.86
HPT.F_out.W(kg/sec)	125.54	125.59	125.65	125.70	125.80
LPT.F_out.FARB(-)	0.01979	0.01978	0.01977	0.01976	0.01975
LPT.F_out.FARU(-)	0.00002	0.00002	0.00002	0.00002	0.00002
LPT.F_out.Pt(Pa)	448242	447835	447452	447043	446603
LPT.F_out.Tt(K)	1051.83	1051.51	1051.15	1050.82	1049.32
LPT.F_out.W(kg/sec)	125.54	125.59	125.65	125.70	125.80
Afterburner.F_out.FARB(-)	0.01979	0.01978	0.01977	0.01976	0.01975
Afterburner.F_out.FARU(-)	0.00002	0.00002	0.00002	0.00002	0.00002
Afterburner.F_out.Pt(Pa)	425830	425443	425080	424691	424273
Afterburner.F_out.Tt(K)	1051.83	1051.51	1051.15	1050.82	1049.32
Afterburner.F_out.W(kg/sec)	125.54	125.59	125.65	125.70	125.80
Fn(N)	107263	107264	107270	107272	107247
SFC (g/(KN*s))	22.732	22.732	22.730	22.730	22.735

Advanced Performance Simulation of Gas Turbine Components
and Fluid Thermodynamic Properties

Burner.F_in.W = 5.23829754kg/s (Design Point)					
Performance Parameter	Fluid Model Combination				
	"ND"	"33%"	"66%"	"CE"	"CE-66%"
Inlet.F_out.FARB(-)	0.00000	0.00000	0.00000	0.00000	0.00000
Inlet.F_out.FARU(-)	0.00000	0.00000	0.00000	0.00000	0.00000
Inlet.F_out.Pt(Pa)	101325	101325	101325	101325	101325
Inlet.F_out.Tt(K)	288.15	288.15	288.15	288.15	288.15
Inlet.F_out.W (kg/s)	200.00	200.00	200.00	200.00	200.00
LPC.F_out.FARB(-)	0.00000	0.00000	0.00000	0.00000	0.00000
LPC.F_out.FARU(-)	0.00000	0.00000	0.00000	0.00000	0.00000
LPC.F_out.Pt(Pa)	716874	716874	716874	716874	716874
LPC.F_out.Tt(K)	532.91	532.91	532.91	532.91	532.91
LPC.F_out.W(kg/sec)	200.00	200.00	200.00	200.00	200.00
HPC.F_out.FARB(-)	0.00000	0.00000	0.00000	0.00000	0.00000
HPC.F_out.FARU(-)	0.00000	0.00000	0.00000	0.00000	0.00000
HPC.F_out.Pt(Pa)	5071886	5071886	5071886	5071886	5071886
HPC.F_out.Tt(K)	951.03	951.02	951.01	951.01	951.01
HPC.F_out.W(kg/sec)	200.00	200.00	200.00	200.00	200.00
Burner.F_out.FARB(-)	0.02617	0.02617	0.02617	0.02617	0.02617
Burner.F_out.FARU(-)	0.00003	0.00003	0.00003	0.00003	0.00003
Burner.F_out.Pt(Pa)	4818292	4818292	4818292	4818292	4818292
Burner.F_out.Tt(K)	1800.00	1797.24	1794.52	1791.78	1791.79
Burner.F_out.W(kg/sec)	205.24	205.24	205.24	205.24	205.24
Burner.Fu_in.W(kg/sec)	5.238	5.238	5.238	5.238	5.238
HPT.F_out.FARB(-)	0.02617	0.02617	0.02617	0.02617	0.02617
HPT.F_out.FARU(-)	0.00003	0.00003	0.00003	0.00003	0.00003
HPT.F_out.Pt(Pa)	1634276	1632704	1631130	1629564	1628000
HPT.F_out.Tt(K)	1456.00	1455.36	1454.72	1454.07	1451.89
HPT.F_out.W(kg/sec)	205.24	205.24	205.24	205.24	205.24
LPT.F_out.FARB(-)	0.02617	0.02617	0.02617	0.02617	0.02617
LPT.F_out.FARU(-)	0.00003	0.00003	0.00003	0.00003	0.00003
LPT.F_out.Pt(Pa)	806566	805609	804649	803685	801882
LPT.F_out.Tt(K)	1262.30	1262.09	1261.89	1261.68	1258.98
LPT.F_out.W(kg/sec)	205.24	205.24	205.24	205.24	205.24
Afterburner.F_out.FARB(-)	0.02617	0.02617	0.02617	0.02617	0.02617
Afterburner.F_out.FARU(-)	0.00003	0.00003	0.00003	0.00003	0.00003
Afterburner.F_out.Pt (Pa)	766238	765329	764417	763500	761788
Afterburner.F_out.Tt(K)	1262.30	1262.09	1261.89	1261.68	1258.98
Afterburner.F_out.W(kg/sec)	205.24	205.24	205.24	205.24	205.24
Fn(N)	221375	221322	221270	221218	220858
SFC (g/(KN*s))	23.663	23.668	23.674	23.679	23.718

Advanced Performance Simulation of Gas Turbine Components
and Fluid Thermodynamic Properties

Burner.F in.W = 8.28829754kg/s (Extreme OD Point - High Burner Outlet Temperature)					
Performance Parameter	Fluid Model Combination				
	"ND"	"33%"	"66%"	"CE"	"CE-66%"
Inlet.F_out.FARB(-)	0.00000	0.00000	0.00000	0.00000	0.00000
Inlet.F_out.FARU(-)	0.00000	0.00000	0.00000	0.00000	0.00000
Inlet.F_out.Pt(Pa)	101325	101325	101325	101325	101325
Inlet.F_out.Tt(K)	288.15	288.15	288.15	288.15	288.15
Inlet.F_out.W (kg/s)	259.14	259.08	259.02	258.96	258.73
LPC.F_out.FARB(-)	0.00000	0.00000	0.00000	0.00000	0.00000
LPC.F_out.FARU(-)	0.00000	0.00000	0.00000	0.00000	0.00000
LPC.F_out.Pt(Pa)	884754	885434	886218	886916	885588
LPC.F_out.Tt(K)	570.44	570.41	570.41	570.39	570.15
LPC.F_out.W(kg/sec)	259.14	259.08	259.02	258.96	258.73
HPC.F_out.FARB(-)	0.00000	0.00000	0.00000	0.00000	0.00000
HPC.F_out.FARU(-)	0.00000	0.00000	0.00000	0.00000	0.00000
HPC.F_out.Pt(Pa)	7058139	7055609	7053474	7051279	7042326
HPC.F_out.Tt(K)	1041.47	1041.11	1040.77	1040.43	1040.13
HPC.F_out.W(kg/sec)	259.14	259.08	259.02	258.96	258.73
Burner.F_out.FARB(-)	0.03195	0.03196	0.03197	0.03197	0.03200
Burner.F_out.FARU(-)	0.00003	0.00003	0.00003	0.00003	0.00003
Burner.F_out.Pt(Pa)	6705232	6702828	6700800	6698715	6690210
Burner.F_out.Tt(K)	2039.22	2033.53	2028.01	2022.55	2023.05
Burner.F_out.W(kg/sec)	267.43	267.36	267.31	267.25	267.02
Burner.Fu_in.W(kg/sec)	8.288	8.288	8.288	8.288	8.288
HPT.F_out.FARB(-)	0.03195	0.03196	0.03197	0.03197	0.03200
HPT.F_out.FARU(-)	0.00003	0.00003	0.00003	0.00003	0.00003
HPT.F_out.Pt(Pa)	2284825	2282266	2279823	2277306	2271837
HPT.F_out.Tt(K)	1659.00	1657.73	1656.44	1655.15	1651.64
HPT.F_out.W(kg/sec)	267.43	267.36	267.31	267.25	267.02
LPT.F_out.FARB(-)	0.03195	0.03196	0.03197	0.03197	0.03200
LPT.F_out.FARU(-)	0.00003	0.00003	0.00003	0.00003	0.00003
LPT.F_out.Pt(Pa)	1127295	1125849	1124417	1122981	1118790
LPT.F_out.Tt(K)	1442.61	1442.31	1441.97	1441.65	1437.24
LPT.F_out.W(kg/sec)	267.43	267.36	267.31	267.25	267.02
Afterburner.F_out.FARB(-)	0.03195	0.03196	0.03197	0.03197	0.03200
Afterburner.F_out.FARU(-)	0.00003	0.00003	0.00003	0.00003	0.00003
Afterburner.F_out.Pt(Pa)	1070930	1069557	1068196	1066832	1062850
Afterburner.F_out.Tt(K)	1442.61	1442.31	1441.97	1441.65	1437.24
Afterburner.F_out.W(kg/sec)	267.43	267.36	267.31	267.25	267.02
Fn(N)	328079	327949	327830	327702	326652
SFC (g/(KN*s))	25.263	25.273	25.282	25.292	25.373

Chapter 4: Appendix 2
CUTSTJR Off-Design Case Study 3: Detailed Results

Afterburner.Fu_in.W = 0.00 kg/s (No Reheat) (Design Point)					
Performance Parameter	Fluid Model Combination				
	"ND"	"33%"	"66%"	"CE"	"CE-66%"
Inlet.F_out.FARB(-)	0.00000	0.00000	0.00000	0.00000	0.00000
Inlet.F_out.FARU(-)	0.00000	0.00000	0.00000	0.00000	0.00000
Inlet.F_out.Pt(Pa)	101325	101325	101325	101325	101325
Inlet.F_out.Tt(K)	288.15	288.15	288.15	288.15	288.15
Inlet.F_out.W	200.00	200.00	200.00	200.00	200.00
LPC.F_out.FARB(-)	0.00000	0.00000	0.00000	0.00000	0.00000
LPC.F_out.FARU(-)	0.00000	0.00000	0.00000	0.00000	0.00000
LPC.F_out.Pt(Pa)	716874	716874	716874	716874	716874
LPC.F_out.Tt(K)	532.91	532.91	532.91	532.91	532.91
LPC.F_out.W(kg/sec)	200.00	200.00	200.00	200.00	200.00
HPC.F_out.FARB(-)	0.00000	0.00000	0.00000	0.00000	0.00000
HPC.F_out.FARU(-)	0.00000	0.00000	0.00000	0.00000	0.00000
HPC.F_out.Pt(Pa)	5071886	5071886	5071886	5071886	5071886
HPC.F_out.Tt(K)	951.03	951.02	951.01	951.01	951.01
HPC.F_out.W(kg/sec)	200.00	200.00	200.00	200.00	200.00
Burner.F_out.FARB(-)	0.02617	0.02626	0.02636	0.02646	0.02646
Burner.F_out.FARU(-)	0.00003	0.00003	0.00003	0.00003	0.00003
Burner.F_out.Pt(Pa)	4818292	4818292	4818292	4818292	4818292
Burner.F_out.Tt(K)	1800.00	1800.00	1800.00	1800.00	1800.00
Burner.F_out.W(kg/sec)	205.24	205.26	205.28	205.30	205.30
Burner.Fu_in.W	5.238	5.258	5.277	5.296	5.296
HPT.F_out.FARB(-)	0.02617	0.02626	0.02636	0.02646	0.02646
HPT.F_out.FARU(-)	0.00003	0.00003	0.00003	0.00003	0.00003
HPT.F_out.Pt(Pa)	1634276	1636070	1637823	1639644	1638051
HPT.F_out.Tt(K)	1456.00	1458.30	1460.58	1462.90	1460.66
HPT.F_out.W(kg/sec)	205.24	205.26	205.28	205.30	205.30
LPT.F_out.FARB(-)	0.02617	0.02626	0.02636	0.02646	0.02646
LPT.F_out.FARU(-)	0.00003	0.00003	0.00003	0.00003	0.00003
LPT.F_out.Pt(Pa)	806566	808604	810608	812659	810827
LPT.F_out.Tt(K)	1262.30	1265.16	1267.99	1270.90	1268.13
LPT.F_out.W(kg/sec)	205.24	205.26	205.28	205.30	205.30
Afterburner.F_out.FARB(-)	0.02617	0.02626	0.02636	0.02646	0.02646
Afterburner.F_out.FARU(-)	0.00003	0.00003	0.00003	0.00003	0.00003
Afterburner.F_out.Pt(Pa)	766238	768174	770078	772026	770286
Afterburner.F_out.Tt(K)	1262.30	1265.16	1267.99	1270.90	1268.13
Afterburner.F_out.W(kg/sec)	205.24	205.26	205.28	205.30	205.30
Afterburner.Fu_in.W(kg/sec)	0.000	0.000	0.000	0.000	0.000
Fn(N)	221375	221784	222190	222606	222239
SFC (g/(KN*s))	23.663	23.706	23.749	23.793	23.832

Advanced Performance Simulation of Gas Turbine Components
and Fluid Thermodynamic Properties

Afterburner.Fu in.W = 4.70 kg/s					
Performance Parameter	Fluid Model Combination				
	"ND"	"33%"	"66%"	"CE"	"CE-66%"
Inlet.F_out.FARB(-)	0.00000	0.00000	0.00000	0.00000	0.00000
Inlet.F_out.FARU(-)	0.00000	0.00000	0.00000	0.00000	0.00000
Inlet.F_out.Pt(Pa)	101325	101325	101325	101325	101325
Inlet.F_out.Tt(K)	288.15	288.15	288.15	288.15	288.15
Inlet.F_out.W	200.00	200.00	200.00	200.00	200.00
LPC.F_out.FARB(-)	0.00000	0.00000	0.00000	0.00000	0.00000
LPC.F_out.FARU(-)	0.00000	0.00000	0.00000	0.00000	0.00000
LPC.F_out.Pt(Pa)	716874	716874	716874	716874	716874
LPC.F_out.Tt(K)	532.91	532.91	532.91	532.91	532.91
LPC.F_out.W(kg/sec)	200.00	200.00	200.00	200.00	200.00
HPC.F_out.FARB(-)	0.00000	0.00000	0.00000	0.00000	0.00000
HPC.F_out.FARU(-)	0.00000	0.00000	0.00000	0.00000	0.00000
HPC.F_out.Pt(Pa)	5071886	5071886	5071886	5071886	5071886
HPC.F_out.Tt(K)	951.03	951.02	951.01	951.01	951.01
HPC.F_out.W(kg/sec)	200.00	200.00	200.00	200.00	200.00
Burner.F_out.FARB(-)	0.02617	0.02626	0.02636	0.02646	0.02646
Burner.F_out.FARU(-)	0.00003	0.00003	0.00003	0.00003	0.00003
Burner.F_out.Pt(Pa)	4818292	4818292	4818292	4818292	4818292
Burner.F_out.Tt(K)	1800.00	1800.00	1800.00	1800.00	1800.00
Burner.F_out.W(kg/sec)	205.24	205.26	205.28	205.30	205.30
Burner.Fu_in.W	5.238	5.258	5.277	5.296	5.296
HPT.F_out.FARB(-)	0.02617	0.02626	0.02636	0.02646	0.02646
HPT.F_out.FARU(-)	0.00003	0.00003	0.00003	0.00003	0.00003
HPT.F_out.Pt(Pa)	1634276	1636070	1637823	1639644	1638051
HPT.F_out.Tt(K)	1456.00	1458.30	1460.58	1462.90	1460.66
HPT.F_out.W(kg/sec)	205.24	205.26	205.28	205.30	205.30
LPT.F_out.FARB(-)	0.02617	0.02626	0.02636	0.02646	0.02646
LPT.F_out.FARU(-)	0.00003	0.00003	0.00003	0.00003	0.00003
LPT.F_out.Pt(Pa)	806566	808604	810608	812659	810827
LPT.F_out.Tt(K)	1262.30	1265.16	1267.99	1270.90	1268.13
LPT.F_out.W(kg/sec)	205.24	205.26	205.28	205.30	205.30
Afterburner.F_out.FARB(-)	0.04732	0.04741	0.04751	0.04761	0.04761
Afterburner.F_out.FARU(-)	0.00238	0.00238	0.00238	0.00238	0.00238
Afterburner.F_out.Pt(Pa)	766238	768174	770078	772026	770286
Afterburner.F_out.Tt(K)	1879.82	1879.80	1879.79	1879.77	1877.36
Afterburner.F_out.W(kg/sec)	209.94	209.96	209.98	210.00	210.00
Afterburner.Fu_in.W(kg/sec)	4.700	4.700	4.700	4.700	4.700
Fn(N)	279269	279583	279893	280211	279751
SFC (g/(KN*s))	35.587	35.616	35.645	35.675	35.733

Advanced Performance Simulation of Gas Turbine Components
and Fluid Thermodynamic Properties

Afterburner.Fu in.W = 9.2kg/s (Reheat Limit) (Afterburner.F out.FARB < FAR_{Stoich})					
Performance Parameter	Fluid Model Combination				
	"ND"	"33%"	"66%"	"CE"	"CE-66%"
Inlet.F_out.FARB(-)	0.00000	0.00000	0.00000	0.00000	0.00000
Inlet.F_out.FARU(-)	0.00000	0.00000	0.00000	0.00000	0.00000
Inlet.F_out.Pt(Pa)	101325	101325	101325	101325	101325
Inlet.F_out.Tt(K)	288.15	288.15	288.15	288.15	288.15
Inlet.F_out.W	200.00	200.00	200.00	200.00	200.00
LPC.F_out.FARB(-)	0.00000	0.00000	0.00000	0.00000	0.00000
LPC.F_out.FARU(-)	0.00000	0.00000	0.00000	0.00000	0.00000
LPC.F_out.Pt(Pa)	716874	716874	716874	716874	716874
LPC.F_out.Tt(K)	532.91	532.91	532.91	532.91	532.91
LPC.F_out.W(kg/sec)	200.00	200.00	200.00	200.00	200.00
HPC.F_out.FARB(-)	0.00000	0.00000	0.00000	0.00000	0.00000
HPC.F_out.FARU(-)	0.00000	0.00000	0.00000	0.00000	0.00000
HPC.F_out.Pt(Pa)	5071886	5071886	5071886	5071886	5071886
HPC.F_out.Tt(K)	951.03	951.02	951.01	951.01	951.01
HPC.F_out.W(kg/sec)	200.00	200.00	200.00	200.00	200.00
Burner.F_out.FARB(-)	0.02617	0.02626	0.02636	0.02646	0.02646
Burner.F_out.FARU(-)	0.00003	0.00003	0.00003	0.00003	0.00003
Burner.F_out.Pt(Pa)	4818292	4818292	4818292	4818292	4818292
Burner.F_out.Tt(K)	1800.00	1800.00	1800.00	1800.00	1800.00
Burner.F_out.W(kg/sec)	205.24	205.26	205.28	205.30	205.30
Burner.Fu_in.W	5.238	5.258	5.277	5.296	5.296
HPT.F_out.FARB(-)	0.02617	0.02626	0.02636	0.02646	0.02646
HPT.F_out.FARU(-)	0.00003	0.00003	0.00003	0.00003	0.00003
HPT.F_out.Pt(Pa)	1634276	1636070	1637823	1639644	1638051
HPT.F_out.Tt(K)	1456.00	1458.30	1460.58	1462.90	1460.66
HPT.F_out.W(kg/sec)	205.24	205.26	205.28	205.30	205.30
LPT.F_out.FARB(-)	0.02617	0.02626	0.02636	0.02646	0.02646
LPT.F_out.FARU(-)	0.00003	0.00003	0.00003	0.00003	0.00003
LPT.F_out.Pt(Pa)	806566	808604	810608	812659	810827
LPT.F_out.Tt(K)	1262.30	1265.16	1267.99	1270.90	1268.13
LPT.F_out.W(kg/sec)	205.24	205.26	205.28	205.30	205.30
Afterburner.F_out.FARB(-)	0.06757	0.06766	0.06776	0.06786	0.06786
Afterburner.F_out.FARU(-)	0.00463	0.00463	0.00463	0.00463	0.00463
Afterburner.F_out.Pt(Pa)	766238	768174	770078	772026	770286
Afterburner.F_out.Tt(K)	2406.56	2395.29	2385.02	2375.38	2373.37
Afterburner.F_out.W(kg/sec)	214.44	214.46	214.48	214.50	214.50
Afterburner.Fu_in.W(kg/sec)	9.200	9.200	9.200	9.200	9.200
Fn(N)	324465	324602	324738	324880	323917
SFC (g/(KN*s))	44.499	44.539	44.580	44.621	44.753

Chapter 4: References

- [1] Gas Turbine Engineering Group, "The TURBOMATCH Scheme", TURBOMATCH, User's Manual, School of Engineering – Cranfield University.
- [2] Bala, A., Sethi, V., Lo Gatto, E., Pachidis, V. and Pilidis, P., 2007, "PROOSIS – A Collaborative Venture for Gas Turbine Performance Simulation using an Object Oriented Programming Schema" ISABE 2007-1357.
- [3] Bala, A. 2007, "Poly-Dimensional Gas Turbine System Modelling and Simulation", PhD Thesis, School of Engineering – Cranfield University.
- [4] Sethi, V., Jackson, A. and Pilidis, P., (Cranfield University), 2007, "PROOSIS Standard Component Library: Fluid Model Specification" VIVACE 2.4.4/CU/T/06003.
- [5] Sethi, V., Jackson, A. and Pilidis, P., (Cranfield University), 2007, "PROOSIS Standard Component Library: Thermodynamic Functions Specification" VIVACE 2.4.4/CU/T/06004.
- [6] Alexiou, A. and Mathioudakis, K., (NTUA), 2007, "PROOSIS Standard Component Library: Atmosphere Component Specification" VIVACE 2.4.4/NTUA/T/04008.
- [7] Sethi, V., Jackson, A. and Pilidis, P., (Cranfield University), 2007, "PROOSIS Standard Component Library: Burner Component Specification" VIVACE 2.4.4/CU/T/05007.
- [8] Alexiou, A. and Mathioudakis, K., (NTUA), 2007, "PROOSIS Standard Component Library: Burner_Emissions Component Specification" VIVACE 2.4.4/NTUA/T/07003.
- [9] Alexiou, A. and Mathioudakis, K., (NTUA), 2007, "PROOSIS Standard Component Library: Casing Component Specification" VIVACE 2.4.4/NTUA/T/06006.
- [10] Bala, A., Sethi, V. and Jackson, A., (Cranfield University), 2007, "PROOSIS Standard Component Library: Compressor Component Specification" VIVACE 2.4.4/CU/T/04006.
- [11] Sethi, V., Jackson, A. and Pilidis, P., (Cranfield University), 2007, "PROOSIS Standard Component Library: Duct Component Specification" VIVACE 2.4.4/CU/T/05006.
- [12] Bala, A. and Jackson, A., (Cranfield University), 2007, "PROOSIS Standard Component Library: Compressor Component Specification" VIVACE 2.4.4/CU/T/06008.
- [13] Sethi, V., Jackson, A. and Pilidis, P., (Cranfield University), 2007, "PROOSIS Standard Component Library: Flow Splitter Component Specification" VIVACE 2.4.4/CU/T/06005.
- [14] Bretschneider, S., Banzhaf, B. and Staudacher, S. (USTUTT), 2007, "PROOSIS Standard Component Library: Gear Component Specification" VIVACE 2.4.4/USTUTT/T/05004.

- [15] Sethi, V., Jackson, A. and Pilidis, P., (Cranfield University), 2007, "PROOSIS Standard Component Library: Heat Exchanger Components Specification" VIVACE 2.4.4/CU/T/07004.
- [16] Bala, A., Sethi, V. and Jackson, A., (Cranfield University), 2007, "PROOSIS Standard Component Library: Inlet Component Specification" VIVACE 2.4.4/CU/T/04005.
- [17] Banzhaf, B. and Staudacher, S. (USTUTT), 2007, "PROOSIS Standard Component Library: Mixer Component Specification" VIVACE 2.4.4/USTUTT/T/04003.
- [18] Banzhaf, B. and Staudacher, S. (USTUTT), 2007, "PROOSIS Standard Component Library: Convergent Nozzle Component Specification" VIVACE 2.4.4/USTUTT/T/04002.
- [19] Banzhaf, B. and Staudacher, S. (USTUTT), 2007, "PROOSIS Standard Component Library: Convergent - Divergent Nozzle Component Specification" VIVACE 2.4.4/USTUTT/T/04004.
- [20] Alexiou, A. and Mathioudakis, K., (NTUA), 2007, "PROOSIS Standard Component Library: Performance Monitor Component Specification" VIVACE 2.4.4/NTUA/T/06010.
- [21] Alexiou, A. and Mathioudakis, K., (NTUA), 2007, "PROOSIS Standard Component Library: Probe Component Specification" VIVACE 2.4.4/NTUA/T/07002.
- [22] Banzhaf, B. and Staudacher, S. (USTUTT), 2007, "PROOSIS Standard Component Library: Propeller Component Specification" VIVACE 2.4.4/USTUTT/T/05005.
- [23] Bretschneider, S., Banzhaf, B. and Staudacher, S. (USTUTT), 2007, "PROOSIS Standard Component Library: Shaft Component Specification" VIVACE 2.4.4/USTUTT/T/05003.
- [24] Alexiou, A. and Mathioudakis, K., (NTUA), 2007, "PROOSIS Standard Component Library: Turbine Component Specification" VIVACE 2.4.4/NTUA/T/05005.
- [25] Alexiou, A. and Mathioudakis, K., (NTUA), 2007, "PROOSIS Standard Component Library: SCLib Ports Specification" VIVACE 2.4.4/NTUA/T/04007.
- [26] Walsh. P.P. and Fletcher. P., 1998, "Gas Turbine Performance", 2nd Edition, Oxford: Blackwell Science.
- [27] Saravanamuttoo, H. I. H, Rogers, G. F. C. and Cohen, H., 2001, "Gas Turbine Theory", 5th Edition, Essex: Pearson Education Ltd.
- [28] Gronstedt, T., 2000, "Development of methods for analysis and optimisation of jet engine systems", PhD Thesis, Department of Thermo- and Fluid Dynamics, Chalmers University.

- [29] Stamatis, A., Mathioudakis, K., Papailiou, K.D., 1990, "Adaptive Simulation of Gas Turbine Performance", ASME J. of Eng. For Gas Turbines and Power, 112, pp. 168-175.
- [30] Canalias, X., Kopf, F., Sahm, P., 2005, "Generation of Physically Based Analysis Factors to Improve Synthesis Models of Jet Engines", Proceedings of 2005 ASME Turbo Expo, ASME GT2005-68617.
- [31] McGraw Hill Professional Science and Technology Encyclopaedia, 2007, Official Website,
URL: www.answers.com/topic/data-reduction
- [32] Bala, A., Sethi, V., Lo Gatto, E., Pachidis, V. and Pilidis, P., 2007, "Study of VSV Effects on Performance via Integrated Aerodynamic Process" AIAA 2007-5046.
- [33] Pachidis, V., 2007, "Gas Turbine Performance Simulation", Simulation and Diagnostics Course Notes: School of Engineering – Cranfield University.
- [34] Gas Turbine Engineering Group, "The TURBOMATCH Scheme", TURBOMATCH, User's Manual, School of Engineering – Cranfield University.
- [35] ANSYS CFX-BladeGen, User Manual, Version 10.0, 2005.
- [36] ANSYS CFX-TurboGrid, User Manual, Version 10.0, 2005.
- [37] ANSYS CFX-Pre/Solver/Post, User Manual, Version 10.0, 2005.
- [38] SAE, August 2004, "Aerospace Recommended Practice: Gas Turbine Engine Performance Presentation and Nomenclature for Digital Computers Using Object – Oriented Programming" SAE ARP 5571.

Chapter 5: Extended Parametric Representation of Compressor Characteristics

Abstract

This chapter describes the structure and the implementation in PROOSIS of an extended parametric representation of compressor characteristics. The work presented in this chapter is the outcome of a collaborative effort between M. Doussinault (Snecma) and the author. Snecma have introduced “Map Fitting Tool” (MFT) maps to model the off-design performance of all the turbomachinery components (Fans, Compressors and Turbines) within Janus (the in-house gas turbine performance simulation tool developed and used by Snecma). The MFT map methodology, which is based on a concept developed collaboratively by General Electric (GE) and NASA, is presented. The development and implementation of Compressor MFT maps in PROOSIS is discussed. The integration of Compressor_BETA and Compressor_MFT components, with respect to the overall hierarchy structure of the PROOSIS Compressor components is also highlighted. The implementation of MFT maps in PROOSIS and considering the object oriented modelling implications is the author’s contribution to extended parametric representation of compressor characteristics.

Chapter 5: Nomenclature

The nomenclature used in this chapter is slightly different from the nomenclature used in other chapters. The nomenclature is based on the “Aerospace Recommended Practice: Gas Turbine Engine Performance Presentation and Nomenclature for Digital Computers Using Object – Oriented Programming.”^[7] A comprehensive nomenclature guide is provided as the nomenclature used is exhaustive.

X_{in} corresponds to a thermodynamic property at the inlet of the Compressor component (where X is the thermodynamic property).

X_{out} corresponds to a thermodynamic property at the outlet of the Compressor component (where X is the thermodynamic property).

F_{in.X} corresponds to a main flow port thermodynamic property at the inlet of the Compressor component (where X is the main flow port thermodynamic property).

F_{out.X} corresponds to a main flow port thermodynamic property at the outlet of the Compressor component (where X is the main flow port thermodynamic property).

Common Symbols for Compressor Beta and Compressor MFT Calculations

Name	Description	Unit
a_adapEff	Isentropic Efficiency Adaptive Adder	-
a_adapEff_in	Isentropic Efficiency Adaptive Adder (directly input by the user)	-
a_adapWc	Corrected Mass Flow Rate Adaptive Adder	-
a_adapWc_in	Corrected Mass Flow Rate Adaptive Adder (directly input by the user)	-
a_mapEff	Isentropic Efficiency Map Adder	-
a_mapEff_in	Isentropic Efficiency Map Adder (directly input by the user)	-
a_mapWc	Corrected Mass Flow Rate Map Adder	-
a_mapWc_in	Corrected Mass Flow Rate Map Adder (directly input by the user)	-
a_NcRdes	Design Corrected Rotational Speed Adder	-
a_NcRdes_in	Design Corrected Rotational Speed Adder (directly input by the user)	-
Alpha	VIGV or VSV Angle	°
alphaRef	MFT / BETA Map Reference VIGV / VSV angle	°

Advanced Performance Simulation of Gas Turbine Components
and Fluid Thermodynamic Properties

Name	Description	Unit
delta	Non Dimensional Compressor Inlet Total Pressure	-
Δh	Change in Specific Enthalpy	J/kg
eff	Isentropic Efficiency (after applying all corrections)	-
effMap	Isentropic Efficiency (before applying any corrections)	-
f1	MFT / BETA Map Reference Correction Factor For RNI1	-
f2	MFT / BETA Map Reference Correction Factor For RNI2	-
FARBref	MFT / BETA Map Reference Burned Fuel to Air Ratio	-
FARUref	MFT / BETA Map Reference Unburned Fuel to Air Ratio	-
gamRef	MFT / BETA Map Reference Isentropic Coefficient (gamma)	-
gamt_in	Compressor Inlet Isentropic Coefficient (based on total conditions)	-
ht_in	Compressor Inlet Specific Enthalpy (based on total conditions)	J/kg
ht_out	Compressor Outlet Specific Enthalpy (based on total conditions)	J/kg
MNf	Flight Mach Number	-
muRef	MFT / BETA Map Reference Dynamic Viscosity	Ps*s
mut_in	Compressor Inlet Dynamic Viscosity (based on total conditions)	Ps*s
Nc	Compressor Corrected Rotational Speed	rpm
NcRdes	Design Corrected Rotational Speed (before applying any corrections)	-
NcRdesMap	Design Corrected Rotational Speed (after applying all corrections)	-
Nmech	Compressor Rotational Speed	rpm
NmechDes	Compressor Design Rotational Speed	rpm
NmechRef	MFT / BETA Map Reference Rotational Speed	rpm
Pamb	Ambient Pressure	Pa
PR	Pressure Ratio (after applying all corrections) (including the effects of heat flux)	-
PR_cw	Pressure Ratio (after applying all corrections) (excluding the effects of heat flux)	-
Pref	MFT / BETA Map Reference Pressure	Pa
PRmap	Pressure Ratio (before applying any corrections)	-
PRref	MFT / BETA Map Reference Pressure Ratio	-
PRsurge	Surge Pressure Ratio (after applying all corrections)	-

Advanced Performance Simulation of Gas Turbine Components
and Fluid Thermodynamic Properties

Name	Description	Unit
PRsurgeMap	Surge Pressure Ratio (before applying any corrections)	-
Pstd	Standard Pressure	Pa
Pt	Total Pressure	Pa
R_in	Compressor Inlet Gas Constant	J/(kg*K)
RNI	Reynolds Number Index	-
RNI1	MFT / BETA Map Reference Reynolds Number Index 1	-
RNI2	MFT / BETA Map Reference Reynolds Number Index 2	-
Rref	MFT / BETA Map Reference Gas Constant	J/(kg*K)
s_adapEff	Isentropic Efficiency Adaptive Scalar	-
s_adapEff_in	Isentropic Efficiency Adaptive Scalar (directly input by the user)	-
s_adapWc	Corrected Mass Flow Rate Adaptive Scalar	-
s_adapWc_in	Corrected Mass Flow Rate Adaptive Scalar (directly input by the user)	-
s_gamEff	Isentropic Efficiency Scalar for Gamma Correction	-
s_gamEffC	Calculated Isentropic Efficiency Scalar for Gamma Correction	-
s_gamNc	Rotational Speed Scalar for Gamma Correction	-
s_gamNcC	Calculated Rotational Speed Scalar for Gamma Correction	-
s_gamPR	Pressure Ratio Scalar for Gamma Correction	-
s_gamPRc	Calculated Pressure Ratio Scalar for Gamma Correction	-
s_gamWc	Corrected Mass Flow Scalar for Gamma Correction	-
s_gamWcC	Calculated Mass Flow Scalar for Gamma Correction	-
s_mapEff	Isentropic Efficiency Map Scalar	-
s_mapEff_in	Isentropic Efficiency Map Scalar (directly input by the user)	-
s_mapPR	Pressure Ratio Map Scalar	-
s_mapPR_in	Pressure Ratio Map Scalar (directly input by the user)	-
s_mapWc	Corrected Mass Flow Rate Map Scalar	-
s_mapWc_in	Corrected Mass Flow Rate Map Scalar (directly input by the user)	-
s_NcRdes	Design Corrected Rotational Speed Scalar	-
s_NcRdes_in	Design Corrected Rotational Speed Scalar (directly input by the user)	-

Advanced Performance Simulation of Gas Turbine Components
and Fluid Thermodynamic Properties

Name	Description	Unit
s_ReEff	Isentropic Efficiency Scalar for Reynolds Correction	-
s_ReEffC	Calculated Isentropic Efficiency Scalar for Reynolds Correction	-
s_ReWc	Corrected Mass Flow Rate Scalar for Reynolds Correction	-
s_ReWcC	Calculated Corrected Mass Flow Rate Scalar for Reynolds Correction	-
SMpct	Percentage Surge Margin	-
theta	Non Dimensional Compressor Inlet Total Temperature	-
Tref	MFT / BETA Map Reference Temperature	K
Tstd	Standard Temperature	K
Tt	Total Temperature	K
WARref	MFT / BETA Map Reference Water to Air Ratio	-
Wc	Corrected Mass Flow Rate (after applying all corrections)	kg/s
WcMap	Corrected Mass Flow Rate (before applying any corrections)	kg/s

Specific Symbols for Compressor MFT Calculations

Name	Description	Unit
Ae	Compressor Inlet Effective Area	m ²
Aref	MFT Map Reference Inlet Area	m ²
CpRef	MFT Map Reference Specific Heat	J/(kg/K)
effmIMap	Backbone Isentropic Efficiency (before applying any corrections)	-
gh	Work Parameter	(J*s ²)/(kg*m ²)
gh ²	Signed Square Work Parameter	(J ² *s ⁴)/(kg ² *m ⁴)
ghchoke	Work Coefficient For Choked Exit Annulus Flow	(J*s ²)/(kg*m ²)
ghMap	Work Parameter Relative to MFT Map Conditions	(J*s ²)/(kg*m ²)
ghml	Backbone Work Coefficient (after applying s_gh)	(J*s ²)/(kg*m ²)

Advanced Performance Simulation of Gas Turbine Components
and Fluid Thermodynamic Properties

Name	Description	Unit
ghmlMap	Backbone Work Coefficient (before applying s_gh)	$(J*s^2)/(kg*m^2)$
ghr	Work Coefficient (also known as Energy Function)	$(J*s^2)/(kg*m^2)$
ghrls	Isentropic Work Coefficient (also known as Isentropic Energy Function)	$(J*s^2)/(kg*m^2)$
gl	Compressor Aerodynamic Loss	$(J*s^2)/(kg*m^2)$
gld	Difference Between Working Point Loss and Backbone Loss	$(J*s^2)/(kg*m^2)$
glml	Backbone Loss (Minimum Loss) (after applying s_gl)	$(J*s^2)/(kg*m^2)$
glmlMap	Backbone Loss (before applying s_gl)	$(J*s^2)/(kg*m^2)$
MNj	Local Mach Number	-
MNjMap	Intermediate Local Mach Number	-
MNml	Local Backbone Mach Number	-
MNmlMap	Intermediate Local Backbone Mach Number	-
NcRdes_X	Intermediate Design Corrected Rotational Speed	-
NcRdesMFT	Design Corrected Rotational Speed (before applying s_gamNc)	-
rhoRef	MFT Map Reference Density	kg/m ³
s_gh	Work Coefficient Primary Scalar	-
s_gh_in	Work Coefficient Primary Scalar (directly input by the user)	-
s_gl	Loss Primary Scalar	-
s_gl_in	Loss Primary Scalar (directly input by user)	-
s_VqU	Tip Axial to Tangential Velocity Ratio Primary Scalar	-
s_VqU_in	Tip Axial to Tangential Velocity Ratio Primary Scalar (directly input by the user)	-
TRmap	Temperature Ratio Relative to MFT Map Conditions	-

Advanced Performance Simulation of Gas Turbine Components
and Fluid Thermodynamic Properties

Name	Description	Unit
TRmapls	Isentropic Temperature Ratio Relative to MFT Map Conditions	-
Uc _{tip}	Tangential Blade Tip Speed of First Compressor Stage	m/s
Uc _{tip} Des	Design Point Tangential Blade Tip Speed	m/s
Uc _{tip} Map	Tangential Blade Tip Speed Relative to MFT Map Conditions	m/s
Uc _{tip} Ref	MFT Map Reference Tangential Blade Tip Speed	m/s
Vcml	Compressor Inlet Backbone Corrected Velocity	-
VqU _{tip}	Blade Tip Axial to Tangential Velocity Ratio (after applying s_VqU)	-
VqU _{tip} Map	Blade Tip Axial to Tangential Velocity Ratio (before applying s_VqU)	-
Wcml	Backbone Corrected Mass Flow Rate	kg/s

Abbreviations

Name	Description	Unit
BETA	Auxilliary Compressor Map Parameter	-
MFT	Map Fitting Tool	-
ml	Minimum Loss	-
SCLib	Standard Components Library	-
VIGV	Variable Inlet Guide Vane(s)	-
VSV	Variable Stator Vane(s)	-

5.1: PROOSIS CompressorMFT Component Modelling

5.1.1: Introduction

This section describes the modelling of the CompressorMFT component for the PROOSIS Standard Components Library (SCLib). The CompressorMFT Component calculates the compressor off-design performance (isentropic efficiency (eff), corrected mass flow rate (Wc), pressure ratio (excluding effects of heat flux) (PR_{cw}) and percentage surge margin ($SMpct$)) by reading, interpolating and scaling appropriate Map Fitting Tool (MFT) compressor maps. The development of the PROOSIS CompressorMFT component is based on the literature presented in [1], [2], [3], [4] and [5]. A brief summary of this literature is presented in *Section 5.1.2 and Section 5.1.3*.

5.1.2: BETA Line Compressor Maps

The basic thermodynamic variables that define the off-design performance of a gas turbine Compressor are as follows:

1. The Compressor inlet corrected mass flow rate (Wc)
2. The pressure ratio of the compressor (PR)
3. The isentropic efficiency of the compressor (eff)
4. The design corrected rotational speed (after applying all corrections) ($NcRdesMap$)
5. The surge pressure ratio (PR_{surge})

Where:

1. eff is a function of Wc and $NcRdesMap$
2. PR is a function of Wc and $NcRdesMap$
3. PR_{surge} is a function of Wc

The main limitation of this implementation of compressor maps is that at high values of $NcRdesMap$, for low values of PR , the “constant $NcRdesMap$ ” lines become vertical. Hence for a given value of Wc and $NcRdesMap$, there are an infinite number of PR values. Similarly for low values of $NcRdesMap$, the “constant $NcRdesMap$ ” lines become horizontal. Hence there are infinite values of Wc corresponding to fixed values of $NcRdesMap$ and PR . The problem can be solved by introducing a new auxiliary parameter called BETA. BETA serves simply as an array address and avoids the problem of horizontal and vertical portions of “constant $NcRdesMap$ ” lines. A typical Compressor BETA map is shown in Fig: 5.1.1.

Where:

1. Wc is a function of BETA and $NcRdesMap$
2. PR is a function of BETA and $NcRdesMap$
3. eff is a function of BETA and $NcRdesMap$
4. PR_{surge} is a function of Wc

A detailed description of the “inverse design” and off-design performance of the PROOSIS Compressor BETA component is presented in [5] and [6].

NB: The “inverse design” concept including an example of an isolated Compressor BETA “inverse design” simulation is presented in *Section 4.1.3*.

5.1.3: NASA and General Electric Representation of Compressor Maps

NASA and General Electric have collaboratively developed a method called the Map Fitting Tool (MFT) [1], [2] & [3] to provide an extended parametric representation of turbomachinery maps. This approach has been adopted by Snecma to model the off-design performance of all the turbomachinery components (Fans, Compressors and Turbines) within Janus (the in-house gas turbine performance simulation tool developed and used by Snecma). The description in this section is based on [4] which was produced from [1] and served as a guide for the development of Compressor MFT capabilities within PROOSIS.

NB: The nomenclature used in the sections which follow (based on the programming nomenclature used in PROOSIS) is based on the “Aerospace Recommended Practice: Gas Turbine Engine Performance Presentation and Nomenclature for Digital Computers Using Object – Oriented Programming.” [7]

Compressor Component – Fundamental Definitions:

The isentropic efficiency (*eff*) of a Compressor is defined as the ratio of the isentropic specific enthalpy rise to the real enthalpy rise of the compressor as shown in [Eq. 5.1.1].

$$eff = \frac{(\Delta h)_{isentropic}}{(\Delta h)_{real}} \quad \text{[Eq. 5.1.1]}$$

Where: Δh is the difference between the specific enthalpy at Compressor outlet (*ht_out*) and the specific enthalpy at Compressor inlet (*ht_in*) as shown in [Eq. 5.1.2].

$$\Delta h = ht_out - ht_in \quad \text{[Eq. 5.1.2]}$$

The work coefficient or energy function (*ghr*) is defined as shown in [Eq. 5.1.3].

$$ghr = \frac{\Delta h}{0.5 \times U_{c_{tip}}^2} \quad \text{[Eq. 5.1.3]}$$

Where: $U_{c_{tip}}$ is the tangential blade tip speed of the first stage of the Compressor.

The aerodynamic loss of a compressor (*gl*) is defined as shown in [Eq. 5.1.4].

$$gl = ghr_{real} - ghr_{isentropic} = ghr_{isentropic} \times \left(\frac{1}{eff} - 1 \right) \quad \text{[Eq. 5.1.4]}$$

Definition of Losses:

- For a constant value of design corrected rotational speed ($NcRdesMap$), the tangential blade tip speed ($U_{c_{tip}}$) is constant. The corresponding “loss curve”, which is a curve of gl as a function of ghr has a point of minimum loss (ml) as shown in Fig: 5.1.2. At the point of minimum loss:

$$gl = glml \quad \text{[Eq. 5.1.5]}$$

$$ghr = ghml \quad \text{[Eq. 5.1.6]}$$

$$gh = ghr - ghml = 0 \quad \text{[Eq. 5.1.7]}$$

Where: gh is defined as the work parameter

NB: [Eq. 5.1.7] is only true at the point of minimum loss (where $gl = glml$). For all the other points on the loss characteristic $gh \neq 0$.

- For every line of “constant $NcRdesMap$ ” there is a point of minimum loss. The line which joins these minimum loss points is called the “Backbone Line”.
- For every line of “constant $NcRdesMap$ ”, the difference between the loss at any working point and the minimum loss point (gld) is expressed as shown in [Eq. 5.1.8].

$$gld = gl - glml \quad \text{[Eq. 5.1.8]}$$

For a line of “constant $NcRdesMap$ ”, gld increases from 0 with both an increase and a decrease in ghr as can be seen in Fig: 5.1.2.

Description of Flow:

- For any working point, the ratio of the axial velocity to the tangential blade speed (VqU_{tip}) can be defined as a function of $NcRdesMap$ only. On the backbone (where $gh = 0$), the ratio of the axial velocity to tangential blade speed is referred to as $VqU_{tip,ml}$ (as it corresponds to a point of minimum loss).
- The compressor inlet Mach number (MN_j) is a function of gh and $NcRdesMap$. For a line of “constant $NcRdesMap$ ”, $MN_j = 1$ defines the point at which the line becomes vertical.
- The corrected mass flow rate (Wc) and the work parameter (gh) are limited by $ghchoke$ which is the point at which the exit annulus is choked. $ghchoke$ is a function of $NcRdesMap$ only.

Fig: 5.1.3 is a graphic summary of the main flow properties highlighted above, with respect to the choke limits for a given line of “constant $NcRdesMap$ ”.

Comparisons between the characteristics of Compressor BETA maps and Compressor MFT maps are summarised in Fig: 5.1.4. Fig: 5.1.5 provides a visualisation of a typical Compressor MFT map. The black lines are lines of “constant gh” The green line is the “Backbone Line” and corresponds to $gh = 0$ (minimum loss). The working line of the compressor is often close to this line. As shown in Fig: 5.1.5, the lines of “constant gh” are located on efficiency peaks. An example of a typical Compressor MFT map XML format input file is presented in Appendix 1.

5.1.4: CompressorMFT Component Hierarchy

As mentioned in *Chapter 1*, component hierarchy is one of the several benefits of object oriented programming. It reduces code duplication and redundancy thereby improving code maintainability. A detailed description of the PROOSIS SCLib component hierarchy tree is presented in *Chapter 1*. The specific hierarchy of the Compressor component is presented in Fig: 5.1.6. The presented Compressor hierarchy has evolved continuously since its conception and currently comprises a variety of Compressor components which can be customised by the user. A detailed description of the Compressor hierarchical structure is presented in [6].

Based on the hierarchy presented in Fig: 5.1.6, the CompressorBETA and CompressorMFT components have been optimally integrated to ensure that code duplication is kept to a minimum. All the common calculations of the CompressorBETA and CompressorMFT components are contained within the Abstract Components “CompressorBasicMap” and “CompressorSasPMap” (depending on whether the user wishes to simulate a Compressor with no bleeds or with a user defined number of bleeds). These common calculations are highlighted in the sections which follow.

5.2: PROOSIS CompressorMFT Component Calculations

5.2.1: Introduction

Detailed descriptions of the CompressorMFT component calculations are presented in this section. Some of the calculations (e.g. the calculation of common scaling factors) are identical to those for the CompressorBETA component and as mentioned in Section 5.1.4, they are contained within the “CompressorBasicMap” and “CompressornSasPMap” Abstract Components. These common calculations are highlighted with references to the hierarchical structure presented in Fig: 5.1.6.

5.2.2: Definition of W_c

NB: The calculations described in this section are common to both the CompressorBETA and CompressorMFT components and are contained within the “CompressorBasicMap” and “CompressornSasPMap” Abstract Components (Refer to Fig: 5.1.6).

Calculation of theta and delta:

The values of the non dimensional total temperature (theta) and the non dimensional total pressure (delta) are calculated using [Eq. 5.2.1] and [Eq. 5.2.2] respectively.

$$\theta = \frac{F_{in.Tt}}{T_{ref}} \quad \text{[Eq. 5.2.1]}$$

$$\delta = \frac{F_{in.Pt}}{P_{ref}} \quad \text{[Eq. 5.2.2]}$$

Where: T_{ref} is the map (BETA or MFT) reference total temperature
 P_{ref} is the map (BETA or MFT) reference total pressure
 $F_{in.Pt}$ is the Compressor inlet total pressure
 $F_{in.Tt}$ is the Compressor inlet total temperature

NB: In general, $T_{ref} = T_{std} = 288.15K$ and $P_{ref} = P_{std} = 101325Pa$.

Definition of W_c :

The corrected mass flow rate (after applying all scalars and adders) (W_c) is defined as shown in [Eq. 5.2.3].

$$W_c = \frac{F_{in.W} \times \sqrt{\theta}}{\delta} \quad \text{[Eq. 5.2.3]}$$

5.2.3: Calculation of NcRdes

NB: The calculations described in this section are common to both the CompressorBETA and CompressorMFT components and are contained within the “CompressorBasicMap” and “CompressornSasPMap” Abstract Components (Refer to Fig: 5.1.6).

Calculation of Nc:

The corrected rotational speed (Nc) is calculated using [Eq. 5.2.4].

$$Nc = \frac{Nmech}{\sqrt{\theta}} \quad \text{[Eq. 5.2.4]}$$

Where: Nmech is the rotational speed of the Compressor

Calculation of NcRdes:

The design corrected rotational speed (NcRdes) is calculated using [Eq. 5.2.5]

$$NcRdes = \frac{Nc}{NmechDes} \quad \text{[Eq. 5.2.5]}$$

Where: NmechDes is the design rotational speed of the Compressor

NB: NcRdes is the design corrected rotational speed before applying any corrections.

5.2.4: Obtaining Alpha

NB: The calculation described in this section is common to both the CompressorBETA and CompressorMFT components and is contained within the “CompressorBasicMap” and “CompressornSasPMap” Abstract Components (Refer to Fig: 5.1.6).

The value of the variable inlet guide vane (VIGV) angle or variable stator vane (VSV) angle (Alpha) is obtained from a one dimensional table of Alpha vs. Nmech. This table is input by the user as DATA and is based on a user specific “Alpha Law”. The value of Alpha is then obtained using linear interpolation as shown in [Eq. 5.2.6].

$$\text{Alpha} = \text{linearInterp1D}(\text{Alpha_vs_Nmech}, Nmech) \quad \text{[Eq. 5.2.6]}$$

5.2.5: Calculation of the Scalars for Gamma and Reynolds Correction

A detailed description regarding the need for gamma and Reynolds corrections is presented in [6].

NB: The calculations described in this section are common to both the CompressorBETA and CompressorMFT components and are contained within the “CompressorBasicMap” and “CompressornSasPMap” Abstract Components (Refer to Fig: 5.1.6).

Obtaining Rref and gamRef from the Fluid Model:

The values of map reference gas constant (Rref) and the map reference isentropic coefficient (gamRef) are obtained from the fluid model as shown below:

$$\begin{aligned} R_{ref} &= R_FARB(\text{fluid}, T_{ref}, FAR_{Bref}, WAR_{ref}) \\ \text{gamRef} &= \text{gam_T}(\text{fluid}, T_{ref}, FAR_{Bref}, WAR_{ref}) \end{aligned}$$

Where: The values of Tref (the map reference total temperature) FARBref (the map reference burned fuel to air ratio) and WARref (the map reference water to air ratio) are read from the MFT or BETA Compressor map header. (Refer to Appendix 1).

Obtaining all the scalars for gamma correction:

There are three options to obtain the four scalars for gamma correction. The four scalars for gamma correction include:

- Rotational speed scalar for gamma correction (s_gamNc)
- Isentropic efficiency scalar for gamma correction (s_gamEff)
- Pressure ratio scalar for gamma correction (s_gamPR)
- Corrected mass flow rate scalar for gamma correction (s_gamWc)

The three options to obtain each of these scalars are:

1. The value of each scalar is calculated using the following function call. The function is contained within the Compressor_F.el file (which contains all the Compressor specific functions).

$$\text{Corr_gamC}(\text{gamRef}, \text{gamt_in}, R_{ref}, R_{in}, s_{\text{gamNcC}}, s_{\text{gamEffc}}, s_{\text{gamPRc}}, s_{\text{gamWcC}})$$

The inputs for the function Corr_gamC are:

- The map reference isentropic coefficient (gamRef)
- The Compressor inlet isentropic coefficient (based on total properties) (gamt_in)
- The map reference Gas Constant (Rref)
- The Compressor inlet Gas Constant (R_in)

Where: R_{in} and gam_{t_in} are obtained from the Fluid Model as shown below:

$$\begin{aligned} R_{in} &= R_FARB(\text{fluid}, Ts_{in}, F_{in}.FARB, F_{in}.WAR) \\ gam_{t_in} &= gam_T(\text{fluid}, F_{in}.Tt, F_{in}.FARB, F_{in}.WAR) \end{aligned}$$

The outputs of the function `Corr_gamC` are:

- The calculated value of the corrected rotational speed scalar for gamma correction (`s_gamNcC`)
- The calculated value of the isentropic efficiency scalar for gamma correction (`s_gamEffC`)
- The calculated value of the pressure ratio scalar for gamma correction (`s_gamPRc`).
- The calculated value of the corrected mass flow rate scalar for gamma correction (`s_gamWcC`).

Within the function `Corr_gamC`, `s_gamNcC`, `s_gamEffc`, `s_gamPRc` and `s_gamWcC` are calculated using [Eq. 5.2.7], [Eq. 5.2.8], [Eq. 5.2.9] and [Eq. 5.2.10] respectively.

$$s_gamNcC = \sqrt{\frac{gam_{t_in} \times R_{in}}{gam_{ref} \times R_{ref}}} \quad \text{[Eq. 5.2.7]}$$

$$s_gamEffc = 1 \quad \text{[Eq. 5.2.8]}$$

$$s_gamPRc = \frac{gam_{t_in}}{gam_{ref}} \quad \text{[Eq. 5.2.9]}$$

$$s_gamWcC = \sqrt{\frac{gam_{t_in} \times R_{ref}}{gam_{ref} \times R_{in}}} \quad \text{[Eq. 5.2.10]}$$

2. The value of each scalar is not calculated and is simply equal to unity implying no correction.
3. The value of each scalar is calculated using a user defined model.

NB: This option is only recommended for a Level 1 user as the Compressor source files will need to be modified.

Obtaining `muRef` from the fluid model and calculation of RNI:

The value of the map reference dynamic viscosity (`muRef`) is obtained from the fluid model as shown below:

$$muRef = mu_T(\text{fluid}, Tref, FARBref, WARref)$$

Where: The values of Tref (the map reference total temperature) FARBref (the map reference burned fuel to air ratio) and WARref (the map reference water to air ratio) are read from the MFT or BETA Compressor map header. (Refer to Appendix 1).

The Reynolds Number Index (RNI) is calculated using [Eq. 5.11].

$$RNI = \left(\frac{\text{delta}}{\text{theta}} \right) \times \left(\frac{\mu \text{ Re } f}{\text{mut_in}} \right) \quad \text{[Eq. 5.2.11]}$$

Where: mut_in is the Compressor inlet dynamic viscosity (based on total properties) and is obtained from the fluid model as shown below:

$$\text{mut_in} = \mu_T(\text{fluid}, F_in.Tt, F_in.FARB, F_in.WAR)$$

Obtaining all the scalars for Reynolds correction:

There are three options to obtain the two scalars for Reynolds correction. The two scalars for Reynolds correction include:

- Isentropic efficiency scalar for Reynolds correction (s_ReEff)
- Corrected mass flow rate scalar for Reynolds correction (s_ReWc)

The three options to obtain each of these scalars are:

1. The value of each scalar is calculated using the following function call. The function is contained within the Compressor_F.el file (which contains all the Compressor specific functions).

Corr_Rey (RNI, RNI1, f1, RNI2, f2, s_ReEffc, s_ReWcC)

The inputs for the function Corr_Rey are:

- The Reynolds Number Index (RNI)
- The map reference Reynolds Number Index 1 (RNI1)
- The map reference correction factor for Reynolds Number Index 1 (f1)
- The map reference Reynolds Number Index 2 (RNI2)
- The map reference correction factor for Reynolds number index 2 (f2)

The outputs of the function Corr_Rey are:

- The calculated value of the isentropic efficiency scalar for Reynolds correction (s_ReEffC)
- The calculated value of the corrected mass flow rate scalar for Reynolds correction (s_ReWcC)

Within the function *Corr_Rey*, *s_ReEffc* and *s_ReWcC* are calculated using [Eq. 5.2.12] and [Eq. 5.2.13] respectively.

$$s_Re\ Effc = \frac{\{[\log(RNI) - (f1 - f2)] + [\log(RNI1) \times f2] - [\log(RNI2) \times f1]\}}{\left\{\log \frac{RNI1}{RNI2}\right\}} \quad [\text{Eq. 5.2.12}]$$

$$s_Re\ WcC = \sqrt{s_Re\ Effc} \quad [\text{Eq. 5.2.13}]$$

2. The value of each scalar is not calculated and is simply equal to unity implying no correction.
3. The value of each scalar is calculated using a user defined model.

NB: This option is only recommended for a Level 1 user as the Compressor source files will need to be modified.

5.2.6: Calculation of NcRdesMap

NB: Most of the calculations described in this section are common to both the CompressorBETA and CompressorMFT components and are contained within the “CompressorBasicMap” and “CompressornSasPMap” Abstract Components (Refer to Fig: 5.1.6). The only calculation that is specific to CompressorMFT components is the “Calculation of NcRdesMFT” described below.

Obtaining the design corrected rotational speed adder and scalar:

There are two options to obtain the design corrected rotational speed scalar (*s_NcRdes*).

1. The value of the design corrected rotational speed scalar is directly input by the user as DATA in the attributes editor. The nomenclature for the variable representing the design corrected rotational speed scalar directly input by the user is (*s_NcRdes_in*). However, the value of *s_NcRdes* is required and it is calculated as highlighted in [Eq. 5.2.14].

$$s_NcRdes = s_NcRdes_in \quad [\text{Eq. 5.2.14}]$$

2. The value of the design corrected Rotational Speed scalar is calculated using a user defined model.

NB: This option is only recommended for a Level 1 user as the Compressor source files will need to be modified.

There are two options to obtain the design corrected rotational speed adder (*a_NcRdes*).

1. The value of the design corrected Rotational Speed adder is directly input by the user as DATA in the attributes editor. The nomenclature for the variable representing the design corrected Rotational Speed adder directly input by the user is (a_NcRdes_in). However, the value of a_NcRdes is required and it is calculated as highlighted in [Eq. 5.2.15].

$$a_NcRdes = a_NcRdes_in \quad \text{[Eq. 5.2.15]}$$

2. The value of the design corrected rotational speed adder is calculated using a user defined model.

NB: This option is only recommended for a Level 1 user as the Compressor source files will need to be modified.

Calculation of $NcRdes_X$:

The intermediate design corrected Rotational Speed ($NcRdes_X$) is calculated by applying a design corrected Rotational Speed adder and scalar to the design corrected rotational speed ($NcRdes$) as shown in [Eq. 5.2.16].

$$NcRdes_X = \frac{NcRdes - a_NcRdes}{s_NcRdes} \quad \text{[Eq. 5.2.16]}$$

Calculation of $NcRdesMFT$:

There are three options to calculate the design corrected rotational speed (without gamma correction) ($NcRdesMFT$):

1. The value of the design corrected rotational speed (without gamma correction) ($NcRdesMFT$) is equal to the intermediate design corrected rotational speed ($NcRdes_X$) as shown in [Eq. 5.2.17].

$$NcRdesMFT = NcRdes_X \quad \text{[Eq. 5.2.17]}$$

2. The value of the design corrected rotational speed (without gamma correction) ($NcRdesMFT$) is a function of the intermediate design corrected rotational speed ($NcRdes_X$) and the ambient total pressure ($Pamb$).
3. The value of the design corrected rotational speed (without gamma correction) ($NcRdesMFT$) is a function of the intermediate design corrected rotational speed ($NcRdes_X$) and the flight Mach Number (MNf).

NB: Option 2 and Option 3 have not been implemented for the first version of the SCLib.

Calculation of NcRdesMap:

The value of the design corrected rotational speed (including gamma correction) (NcRdesMap) is calculated by applying the rotational speed scalar for gamma correction (s_gamNc) to the design corrected rotational speed (without gamma correction) (NcRdesMFT) as shown in [Eq. 5.2.18].

$$NcRdesMap = \frac{NcRdesMFT}{s_gamNc} \quad \text{[Eq. 5.2.18]}$$

As outlined in Section 5.1.2 and Fig: 5.1.4, NcRdesMap is an argument used for both the BETA and MFT characteristics.

5.2.7: Calculation of ghMap

NB: The calculations described in this section are specific calculations for CompressorMFT components only.

Obtaining the value of ghchoke:

The value of the work coefficient assuming exit annulus choked flow (ghchoke) is obtained from a one dimensional MFT map as shown in [Eq. 5.1.19]. ghchoke is a function of only the design corrected rotational speed (with gamma correction) (NcRdesMap).

$$ghchoke = \text{map.interpd1D}(\text{"ghchoke_vs_NcRdes"}, NcRdesMap) \quad \text{[Eq. 5.2.19]}$$

Where: "ghchoke_vs_NcRdes" is a map of ghchoke as a function of NcRdes. Fig: 5.2.1 is a typical plot of "ghchoke_vs_NcRdes" and is based on the "ghchoke_vs_NcRdes" characteristic of the Compressor MFT map in Appendix 1.

Obtaining the value of ghMap:

The value of the work parameter relative to MFT map conditions (ghMap) is obtained as shown in [Eq. 5.2.20].

$$ghMap = \max(gh, ghchoke) \quad \text{[Eq. 5.2.20]}$$

NB: ghMap cannot be less than ghchoke as shown in Fig: 5.1.3.

NB: The variable "gh" for MFT maps is the equivalent of the variable "BETA" for BETA line maps. Like BETA, gh is also an algebraic variable.

5.2.8: Calculation of effMap

NB: The calculations described in this section are specific calculations for CompressorMFT components only.

Obtaining the value of ghmlMap:

The value of the “Backbone” (minimum loss point) work coefficient (without applying a primary work coefficient scalar) (ghmlMap) is obtained from a one dimensional MFT map as shown in [Eq. 5.2.21]. ghmlMap is a function of only the design corrected rotational speed (with gamma correction) (NcRdesMap).

$$ghmlMap = \text{map.interpd1D}(\text{“ghml_vs_NcRdes”}, \text{NcRdesMap}) \quad \text{[Eq. 5.2.21]}$$

Where: “ghml_vs_NcRdes” is a map of ghml as a function of NcRdes. Fig: 5.2.2 is a typical plot of “ghml_vs_NcRdes” and is based on the “ghml_vs_NcRdes” characteristic of the Compressor MFT map in Appendix 1.

NB: On the “Backbone Line”, for any value of ghml, gh = 0 as outlined in Section 5.1.3.

Obtaining the primary work coefficient scalar:

There are two options to obtain the primary work coefficient scalar (s_gh).

1. The value of the primary work coefficient scalar is directly input by the user as DATA in the attributes editor. The nomenclature for the variable representing the primary work coefficient scalar directly input by the user is (s_gh_in). However, the value of s_gh is required and it is calculated as highlighted in [Eq. 5.2.22].

$$s_gh = s_gh_in \quad \text{[Eq. 5.2.22]}$$

2. The value of the primary work coefficient scalar is calculated using a user defined model.

NB: This option is only recommended for a Level 1 user as the Compressor source files will need to be modified.

The effects of s_gh = 1.05 on a typical Compressor MFT map is shown in Fig: 5.2.3.

Obtaining the value of ghml:

The value of the “Backbone” (minimum loss point) work coefficient (including a primary work Coefficient scalar) (ghml) is calculated by applying the primary work coefficient scalar (s_gh) to the work coefficient at the minimum loss point (without applying a primary work Coefficient scalar) (ghmlMap) as shown in [Eq. 5.2.23].

$$ghml = ghmlMap \times s_gh \quad \text{[Eq. 5.2.23]}$$

Calculation of ghr:

The work coefficient (energy function) (ghr) is the sum of the work coefficient at the minimum loss point (including a primary work coefficient scalar) (ghml) and the work coefficient relative to MFT map conditions (ghMap) as shown in [Eq. 5.2.24].

$$ghr = ghml + ghMap \quad [\text{Eq. 5.2.24}]$$

Calculation of $U_{c_{tip}Map}$:

The first stage tangential blade tip corrected speed (relative to MFT map conditions) ($U_{c_{tip}Map}$) is the product of the design corrected rotational speed (with gamma correction) ($NcRdesMap$) and the first stage tangential blade tip corrected speed at design point ($U_{c_{tip}Des}$) as shown in [Eq. 5.2.25]. The value of $U_{c_{tip}Des}$ is input by the user as DATA in the attributes editor of the CompressorMFT component as shown in Fig: 5.2.4.

$$U_{c_{tip}Map} = NcRdesMap \times U_{c_{tip}Des} \quad [\text{Eq. 5.2.25}]$$

Calculation of TRmap:

The temperature ratio relative to MFT map conditions (TRmap) is calculated assuming constant specific heat. The MFT map reference specific heat ($CpRef$) and consequently the temperature ratio relative to MFT map conditions (TRmap) are calculated using [Eq. 5.2.26] and [Eq. 5.2.27] respectively.

$$CpRef = \frac{(gamRef \times Rref)}{(gamRef - 1)} \quad [\text{Eq. 5.2.26}]$$

$$TRmap = \left[\frac{(U_{c_{tip}Map}^2 \times ghr)}{(2 \times CpRef \times Tref)} \right] + 1 \quad [\text{Eq. 5.2.27}]$$

NB: The “constant specific heats” assumption is just for the purposes of calculating the map parameters. The overall Compressor performance is performed using the same rigorous “specific enthalpy and entropy function” methodology which is used for the CompressorBETA component. A detailed description of this rigorous approach is outlined in [6].

Obtaining the value of $glmlMap$:

The value of the “Backbone” (minimum loss point) loss (without applying a primary work coefficient scalar) ($glmlMap$) is obtained from a one dimensional MFT map as shown in [Eq. 5.2.28]. $glmlMap$ is a function of only the design corrected rotational speed (with gamma correction) ($NcRdesMap$).

$$glmlMap = \text{map.interpd1D}(\text{“glml_vs_NcRdes”}, NcRdesMap) \quad [\text{Eq. 5.2.28}]$$

Where: “glml_vs_NcRdes” is a map of $glml$ as a function of $NcRdes$. Fig: 5.2.5 is a typical plot of “glml_vs_NcRdes” and is based on the “glml_vs_NcRdes” characteristic of the Compressor MFT map in Appendix 1.

Obtaining the primary loss scalar:

There are two options to obtain the primary loss scalar (s_{gl}).

1. The value of the primary loss scalar is directly input by the user as DATA in the attributes editor. The nomenclature for the variable representing the primary loss scalar directly input by the user is (s_{gl_in}). However, the value of s_{gl} is required and it is calculated as highlighted in [Eq. 5.2.29].

$$s_{gl} = s_{gl_in} \quad \text{[Eq. 5.2.29]}$$

2. The value of the primary loss scalar is calculated using a user defined model.

NB: This option is only recommended for a Level 1 user as the Compressor source files will need to be modified.

Obtaining the value of glml:

The value of the “Backbone” (minimum loss point) loss (including a primary scalar) ($glml$) is calculated by applying the primary loss scalar (s_{gl}) and the primary work coefficient scalar (s_{gh}) to the loss at the minimum loss point (without applying level scalars) ($glmlMap$) as shown in [Eq. 5.2.30].

$$glml = glmlMap \times s_{gl} \times s_{gh} \quad \text{[Eq. 5.2.30]}$$

Calculation of gh²:

The signed squared work parameter (gh^2) is the product of the work parameter (gh) and the absolute value of the work parameter ($abs(gh)$) as shown in [Eq. 5.2.31].

$$gh^2 = gh \times abs(gh) \quad \text{[Eq. 5.2.31]}$$

NB: Based on the definition in [Eq. 5.2.31], gh^2 can be negative.

Obtaining the value of gld:

The value of gld , which is the difference in the loss at the working point and the minimum loss point, is obtained from a two dimensional MFT map as shown in [Eq. 5.2.32]. gld is a function of the design corrected rotational speed (with gamma correction) ($NcRdesMap$) and the signed square work parameter (gh^2).

$$gld = map.interpd2D("gld_vs_gh^2_NcRdes", gh^2, NcRdesMap) \quad \text{[Eq. 5.2.32]}$$

Where: “ $gld_vs_gh^2_NcRdes$ ” is a map of gld as a function of gh^2 and $NcRdes$. Fig: 5.2.6 is a typical plot of “ $gld_vs_gh^2_NcRdes$ ” and is based on the “ $gld_vs_gh^2_NcRdes$ ” characteristic of the Compressor MFT map in Appendix 1.

NB: Although the range of gh^2 in the Compressor MFT map in Appendix 1 is $-36 \leq gh^2 \leq 25$ ($(J^2 \cdot s^4) / (kg^2 \cdot m^4)$), Fig: 5.2.6 only displays a range of $-4 \leq gh^2 \leq 4$ ($(J^2 \cdot s^4) / (kg^2 \cdot m^4)$) to ease visualisation of the map.

Calculating the value of ghrIs:

The isentropic work coefficient (energy function) (ghrIs) is calculated using [Eq. 5.2.33].

$$ghrIs = ghr - (glml + gld) \quad \text{[Eq. 5.2.33]}$$

Calculation of effMap:

The value of the isentropic efficiency (without any corrections) (effMap) is calculated using [Eq. 5.2.34].

$$effMap = \frac{ghrIs}{ghr} \quad \text{[Eq. 5.2.34]}$$

NB: For the Compressor MFT components, effMap is obtained from the lengthy process (as described above) by reading and interpolating a variety of MFT characteristics. For the Compressor BETA components, effMap is directly obtained from the effMap characteristic of the BETA line map and is simply a function of BETA and NcRdesMap.

Calculation of effmlMap:

The value of the isentropic efficiency at the minimum loss point / backbone (effmlMap) is calculated using [Eq. 5.2.35].

$$effmlMap = 1 - \left[\frac{(glmlMap \times s - gl)}{(ghmlMap)} \right] \quad \text{[Eq. 5.2.35]}$$

5.2.9: Calculation of the Off-Design Isentropic Efficiency

NB: The calculations described in this section are common to both the CompressorBETA and CompressorMFT components and are contained within the “CompressorBasicMap” and “CompressornSasPMap” Abstract Components (Refer to Fig: 5.1.6).

Obtaining the isentropic efficiency map and adaptive scalars and adders:

There are two options to obtain the isentropic efficiency map scalar (s_mapEff).

1. The value of the isentropic efficiency map scalar is directly input by the user as DATA in the attributes editor. The nomenclature for the variable representing the

isentropic efficiency map scalar directly input by the user is (s_mapEff_in). However, the value of s_mapEff is required and it is calculated as highlighted in [Eq. 5.2.36].

$$s_mapEff = s_mapEff_in \quad \text{[Eq. 5.2.36]}$$

2. The value of the isentropic efficiency map scalar is calculated using a user defined model.

NB: This option is only recommended for a Level 1 user as the Compressor source files will need to be modified.

There are two options to obtain the isentropic efficiency map adder (a_mapEff).

1. The value of the isentropic efficiency map adder is directly input by the user as DATA in the attributes editor. The nomenclature for the variable representing the isentropic efficiency map adder directly input by the user is (a_mapEff_in). However, the value of a_mapEff is required and it is calculated as highlighted in [Eq. 5.2.37].

$$a_mapEff = a_mapEff_in \quad \text{[Eq. 5.2.37]}$$

2. The value of the isentropic efficiency secondary adder is calculated using a user defined model.

NB: This option is only recommended for a Level 1 user as the Compressor source files will need to be modified.

There are two options to obtain the isentropic efficiency adaptive scalar ($s_adapEff$).

1. The value of the isentropic efficiency adaptive scalar is directly input by the user as DATA in the attributes editor. The nomenclature for the variable representing the isentropic efficiency adaptive scalar directly input by the user is ($s_adapEff_in$). However, the value of $s_adapEff$ is required and it is calculated as highlighted in [Eq. 5.2.38].

$$s_adapEff = s_adapEff_in \quad \text{[Eq. 5.2.38]}$$

2. The value of the isentropic efficiency adaptive scalar is calculated using a user defined model.

NB: This option is only recommended for a Level 1 user as the Compressor source files will need to be modified.

There are two options to obtain the isentropic efficiency adaptive adder ($a_adapEff$).

1. The value of the isentropic efficiency adaptive adder is directly input by the user as DATA in the attributes editor. The nomenclature for the variable representing the isentropic efficiency adaptive adder directly input by the user is ($a_adapEff_in$).

However, the value of $a_adapEff$ is required and it is calculated as highlighted in [Eq. 5.2.39].

$$a_adapEff = a_adapEff_in \quad \text{[Eq. 5.2.39]}$$

2. The value of the isentropic coefficient adaptive adder is calculated using a user defined model.

NB: This option is only recommended for a Level 1 user as the Compressor source files will need to be modified.

Adaptive adders and scalars have been incorporated into turbomachinery components to facilitate test analysis. (Refer to *Section 4.2.2* for a test analysis case study).

Calculation of eff:

The off-design isentropic efficiency (eff) is obtained by applying all the isentropic efficiency adders and scalars to the isentropic efficiency (without any corrections) ($effMap$) as shown in [Eq. 5.2.40].

$$eff = (effMap \times s_gamEff \times s_ReEff \times s_mapEff \times s_adapEff) + (a_mapEff + a_adapEff) \quad \text{[Eq. 5.2.40]}$$

5.2.10: Calculation of PRmap

NB: The calculations described in this section are specific calculations for CompressorMFT components only.

Calculation of TRmapIs:

The isentropic temperature ratio relative to MFT map conditions ($TRmapIs$) is calculated as shown [Eq. 5.2.41].

$$TRmapIs = \left[\frac{(Uc_{ip} Map^2 \times ghrIs)}{(2 \times Cp Re f \times Tref)} \right] + 1 \quad \text{[Eq. 5.2.41]}$$

Calculation of PRmap:

The value of pressure ratio (without any corrections) ($PRmap$) is calculated using [Eq. 5.2.42].

$$PRmap = TRmapIs^{\left[\frac{(gamRe f)}{(gamRe f - 1)} \right]} \quad \text{[Eq. 5.2.42]}$$

NB: For the Compressor MFT components, $PRmap$ is obtained from the lengthy process (as described above) by reading and interpolating a variety of MFT characteristics.

For the Compressor BETA components, PRmap is directly obtained from the PRmap characteristic of the BETA line map and is simply a function of BETA and NcRdesMap.

5.2.11: Calculation of the Off-Design Pressure Ratio

NB: The calculations described in this section are common to both the CompressorBETA and CompressorMFT components and are contained within the “CompressorBasicMap” and “CompressornSasPMap” Abstract Components (Refer to Fig: 5.1.6).

Obtaining the pressure ratio map scalar:

There are two options to obtain the pressure ratio map scalar (s_mapPR).

1. The value of the pressure ratio map scalar is directly input by the user as DATA in the attributes editor. The nomenclature for the variable representing the pressure ratio map scalar directly input by the user is (s_mapPR_in). However, the value of s_mapPR is required and it is calculated as highlighted in [Eq. 5.2.43].

$$s_mapPR = s_mapPR_in \quad \text{[Eq. 5.2.43]}$$

2. The value of the pressure ratio map scalar is calculated using a user defined model.

NB: This option is only recommended for a Level 1 user as the Compressor source files will need to be modified.

Calculation of PR_cw:

The off-design compressor pressure ratio (excluding the influence of heat flux) (PR_cw) is obtained by applying all the pressure ratio scalars to the pressure ratio (without any corrections) ($PRmap$) as shown in [Eq. 5.2.44].

$$PR_cw = \left\{ \left[e^{\log(PRmap)} \times s_gamPR \right] - 1 \right\} \times s_mapPR + 1 \quad \text{[Eq. 5.2.44]}$$

A detailed description of the calculation procedure for the off-design compressor pressure ratio (including the influence of heat flux) (PR) is provided in [6].

5.2.12: Calculation of Wcml

NB: The calculations described in this section are specific calculations for CompressorMFT components only.

Obtaining the value of VqU_{tip}Map:

The value of the tip axial to tangential velocity ratio (without applying a primary scalar) ($VqU_{tip}Map$) is obtained from a one dimensional MFT map as shown in [Eq. 5.2.45]. $VqU_{tip}Map$ is a function of only the design corrected rotational speed (with gamma correction) ($NcRdesMap$).

$$VqU_{tip,Map} = \text{map.interpd1D}(\text{"VqU}_{tip_vs_NcRdes"}, NcRdesMap) \quad \text{[Eq. 5.2.45]}$$

Where: "VqU_{tip_vs_NcRdes}" is a map of VqU_{tip} as a function of NcRdes. Fig: 5.2.7 is a typical plot of "VqU_{tip_vs_NcRdes}" and is based on the "VqU_{tip_vs_NcRdes}" characteristic of the Compressor MFT map in Appendix 1.

Obtaining the primary axial to tangential velocity ratio scalar:

There are two options to obtain the primary axial to tangential velocity ratio scalar (s_VqU).

1. The value of the primary axial to tangential velocity ratio scalar is directly input by the user as DATA in the attributes editor. The nomenclature for the variable representing the primary axial to tangential velocity ratio scalar directly input by the user is (s_VqU_in). However, the value of s_VqU is required and it is calculated as highlighted in [Eq. 5.2.46].

$$s_VqU = s_VqU_in \quad \text{[Eq. 5.2.46]}$$

2. The value of the primary axial to tangential velocity ratio scalar is calculated using a user defined model.

NB: This option is only recommended for a Level 1 user as the Compressor source files will need to be modified.

Obtaining the value of VqU_{tip}:

The value of the tip axial to tangential velocity ratio (including a primary scalar) (VqU_{tip}) is calculated by applying the primary axial to tangential velocity ratio scalar (s_VqU) to the tip axial to tangential velocity ratio (without applying a primary axial to tangential velocity ratio scalar) (VqU_{tip,Map}) as shown in [Eq. 5.2.47].

$$VqU_{tip} = VqU_{tip,Map} \times s_VqU \quad \text{[Eq. 5.2.47]}$$

Calculation of Vcml:

The compressor inlet corrected velocity at the minimum loss point / backbone (Vcml) is the product of the corrected blade tip speed (relative to MFT map conditions) (Uc_{tip,Map}) and the axial to tangential velocity ratio (including a level 1 axial to tangential velocity ratio scalar) (VqU_{tip}) as shown in [Eq. 5.2.48].

$$Vcml = Uc_{tip,Map} \times VqU_{tip} \quad \text{[Eq. 5.2.48]}$$

Calculation of Wcml:

The value of the MFT map reference density (ρ_{ref}) is calculated as shown in [Eq. 5.2.49].

$$\rho_{ref} = \frac{Pr_{ef}}{(R_{ref} \times T_{ref})} \quad [\text{Eq. 5.2.49}]$$

The corrected mass flow rate at the minimum loss point / backbone (W_{cml}) is calculated as shown in [Eq. 5.2.50].

$$W_{cml} = A_e \times \rho_{ref} \times V_{cml} \times \left\{ \left[1 - \left(\frac{V_{cml}^2}{2 \times C_{pref} \times T_{ref}} \right) \right]^{\frac{1}{(\gamma_{ref} - 1)}} \right\} \quad [\text{Eq. 5.2.50}]$$

Where: A_e is the compressor inlet effective area and is input by the user as DATA in the attributes editor of the CompressorMFT component as shown in Fig: 5.2.4.

5.2.13: Calculation of WcMap

NB: The calculations described in this section are specific calculations for CompressorMFT components only.

Obtaining the value of MN_j:

The value of the intermediate local Mach Number (MN_{jMap}) is obtained from a two dimensional MFT map as shown in [Eq. 5.2.51]. MN_{jMap} is a function of the design corrected rotational speed (with gamma correction) (NcR_{desMap}) and the work parameter relative to MFT map conditions (gh_{Map}).

$$MN_{jMap} = \text{map.interpd2D}(\text{"MN}_j\text{ vs_gh_NcRdes"}, gh, NcR_{desMap}) \quad [\text{Eq. 5.2.51}]$$

Where: "MN_j vs_gh_NcRdes" is a map of MN_j as a function of gh and NcRdes. Fig: 5.2.8 is a typical plot of "MN_j vs_gh_NcRdes" and is based on the "MN_j vs_gh_NcRdes" characteristic of the Compressor MFT map in Appendix 1.

NB: The tabulated values include values of $MN_j > 1$, to improve extrapolation and subsequently convergence. However, from Fig: 5.1.3, it is clear that MN_j cannot exceed unity.

The local Mach Number (MN_j) is always less than or equal to 1 and is obtained using [Eq. 5.2.52].

$$MN_j = \min(1, MN_{jMap}) \quad [\text{Eq. 5.2.52}]$$

Obtaining the value of MNml:

The value of the intermediate compressor inlet Mach Number at the minimum loss point / “Backbone” (MNmlMap) is obtained from a two dimensional MFT map as shown in [Eq. 5.2.53]. MNmlMap is a function of the design corrected rotational speed (with gamma correction) (NcRdesMap) and the work parameter relative to MFT map conditions (ghMap), which is set to 0 (as gh = 0 on the “Backbone”).

$$MNmlMap = \text{map.interpd2D}(\text{“MNj_vs_gh_NcRdes”}, 0, NcRdesMap) \quad \text{[Eq. 5.2.53]}$$

NB: [Eq. 5.2.53] is similar to [Eq. 5.2.51] the only difference is that gh = 0 for the MNmlMap calculation.

The compressor inlet Mach Number at the minimum loss point / “Backbone” (MNml) is always less than or equal to 1 and is obtained using [Eq. 5.2.54].

$$MNml = \min(1, MNmlMap) \quad \text{[Eq. 5.2.54]}$$

Calculation of WcMap:

The value of the corrected mass flow rate (without any corrections) (WcMap) is calculated using [Eq. 5.2.55].

$$WcMap = Wcml \times \left(\frac{MNj}{MNml} \right) \times \left\{ \frac{1 + \left[\left(\frac{gamRe f - 1}{2} \right) \times MNml^2 \right]}{1 + \left[\left(\frac{gamRe f - 1}{2} \right) \times MNj^2 \right]} \right\}^{\left[\frac{gamRe f + 1}{2 \times (gamRe f - 1)} \right]} \quad \text{[Eq. 5.2.55]}$$

NB: For the Compressor MFT components, WcMap is obtained from the lengthy process (as described above) by reading and interpolating a variety of MFT characteristics. For the Compressor BETA components, WcMap is directly obtained from the WcMap characteristic of the BETA line map and is simply a function of BETA and NcRdesMap.

5.2.14: Calculation of the Off-Design Corrected Mass Flow Rate

NB: The calculations described in this section are common to both the CompressorBETA and CompressorMFT components and are contained within the “CompressorBasicMap” and “CompressorSasPMap” Abstract Components (Refer to Fig: 5.1.6).

Obtaining the corrected mass flow rate map & adaptive scalars & adders:

There are two options to obtain the corrected mass flow rate map scalar (s_{mapWc}).

1. The value of the corrected mass flow rate map scalar is directly input by the user as DATA in the attributes editor. The nomenclature for the variable representing the corrected mass flow rate map scalar directly input by the user is (s_{mapWc_in}). However, the value of s_{mapWc} is required and it is calculated as highlighted in [Eq. 5.2.56].

$$s_{mapWc} = s_{mapWc_in} \quad \text{[Eq. 5.2.56]}$$

2. The value of the corrected mass flow rate map scalar is calculated using a user defined model.

NB: This option is only recommended for a Level 1 user as the Compressor source files will need to be modified.

There are two options to obtain the corrected mass flow rate map adder (a_{mapWc}).

1. The value of the corrected mass flow rate map adder is directly input by the user as DATA in the attributes editor. The nomenclature for the variable representing the corrected mass flow rate map adder directly input by the user is (a_{mapWc_in}). However, the value of a_{mapWc} is required and it is calculated as highlighted in [Eq. 5.2.57].

$$a_{mapWc} = a_{mapWc_in} \quad \text{[Eq. 5.2.57]}$$

2. The value of the corrected mass flow rate map adder is calculated using a user defined model.

NB: This option is only recommended for a Level 1 user as the Compressor source files will need to be modified.

There are two options to obtain the corrected mass flow rate adaptive scalar (s_{adapWc}).

1. The value of the corrected mass flow rate adaptive scalar is directly input by the user as DATA in the attributes editor. The nomenclature for the variable representing the corrected mass flow rate adaptive scalar directly input by the user is (s_{adapWc_in}). However, the value of s_{adapWc} is required and it is calculated as highlighted in [Eq.5.2.58].

$$s_{adapWc} = s_{adapWc_in} \quad \text{[Eq. 5.2.58]}$$

2. The value of the corrected mass flow rate adaptive scalar is calculated using a user defined model.

NB: This option is only recommended for a Level 1 user as the Compressor source files will need to be modified.

There are two options to obtain the corrected mass flow rate adaptive adder (a_adapWc).

1. The value of the corrected mass flow rate adaptive adder is directly input by the user as DATA in the attributes editor. The nomenclature for the variable representing the corrected mass flow rate adaptive adder directly input by the user is (a_adapWc_in). However, the value of a_adapWc is required and it is calculated as highlighted in [Eq.5.2.59].

$$a_adapWc = a_adapWc_in \quad \text{[Eq. 5.2.59]}$$

2. The value of the corrected mass flow rate adaptive adder is calculated using a user defined model.

NB: This option is only recommended for a Level 1 user as the Compressor source files will need to be modified.

Calculation of Wc :

The off-design corrected mass flow rate (Wc) is obtained by applying all corrected mass flow rate adders and scalars to the corrected mass flow rate (without any corrections) ($WcMap$) as shown in [Eq. 5.2.60].

$$IMPL()Wc = \frac{(WcMap \times s_gamWc \times s_ReWc \times s_mapWc \times s_adaptWc) + (a_mapWc + a_adaptWc)}{\quad} \quad \text{[Eq. 5.2.60]}$$

NB: Wc is solved implicitly with gh as the algebraic variable (for MFT maps) and BETA as the algebraic variable for BETA line maps.

5.2.15: Calculation of the Off-Design Compressor Percentage Surge Margin

NB: The calculations described in this section are common to both the CompressorBETA and CompressorMFT components and are contained within the “CompressorBasicMap” and “CompressornSasPMap” Abstract Components (Refer to Fig: 5.1.6).

Obtaining the value of PRsurgeMap:

The value of the surge pressure ratio (without any corrections) (PRsurgeMap) is obtained from a one dimensional map as shown in [Eq. 5.2.61]. PRsurgeMap is a function of the corrected mass flow rate (without any corrections) ($WcMap$) only.

$$PRsurgeMap = \text{map.interpd1D}(\text{“PRsurge_vs_Wc”}, WcMap) \quad \text{[Eq. 5.2.61]}$$

Where: “PRsurge_vs_Wc” is a map of PRsurge as a function of Wc . Both MFT and BETA line maps have a “PRsurge_vs_Wc” characteristic.

Calculation of PRsurge:

The off-design compressor surge pressure ratio (PR_{surge}) is obtained by applying all pressure ratio scalars to the surge pressure ratio (without any corrections) ($PR_{surgeMap}$) as shown in [Eq. 5.2.62].

$$PR_{surge} = \left\{ \left(e^{\log(PR_{surgeMap}) \times s_gamPR} - 1 \right) \times s_mapPR \right\} + 1 \quad \text{[Eq. 5.2.62]}$$

Calculation of SMpct:

The off-design compressor percentage surge margin (SMpct) is calculated using [Eq. 5.2.63].

$$SMpct = 100 \times \left[\frac{(PR_{surge} - PR)}{PR} \right] \quad \text{[Eq. 5.2.63]}$$

Where: PR is the compressor overall pressure ratio (including the influence of heat flux).
NB: If SMpct < 0 a message is displayed indicating the compressor is working beyond the surge line.

Chapter 5: Figures

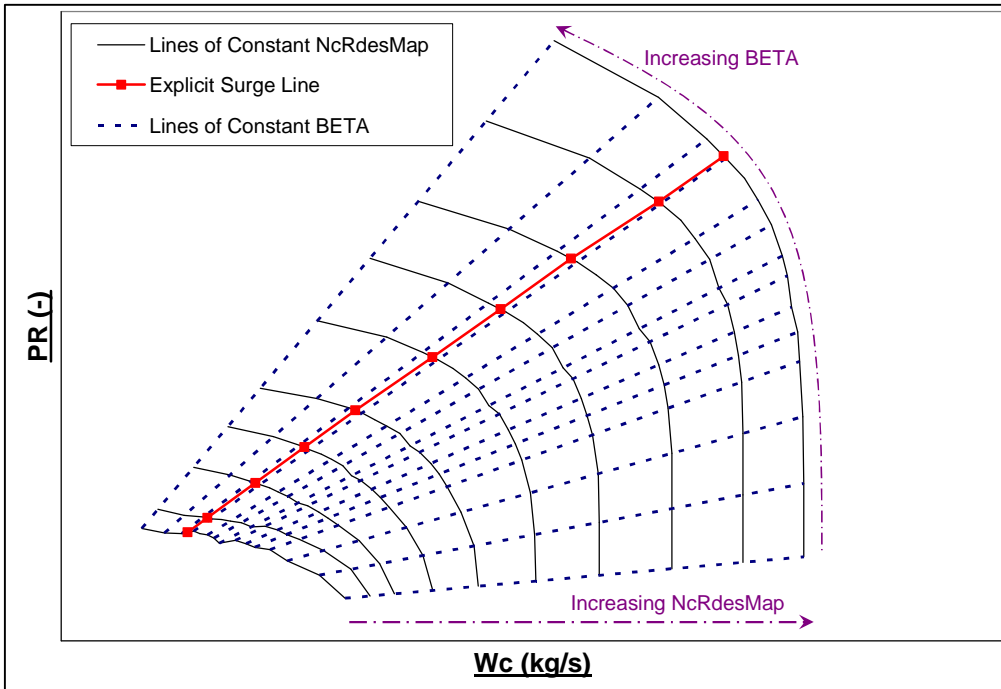


Fig: 5.1.1 Typical Compressor BETA Line Map

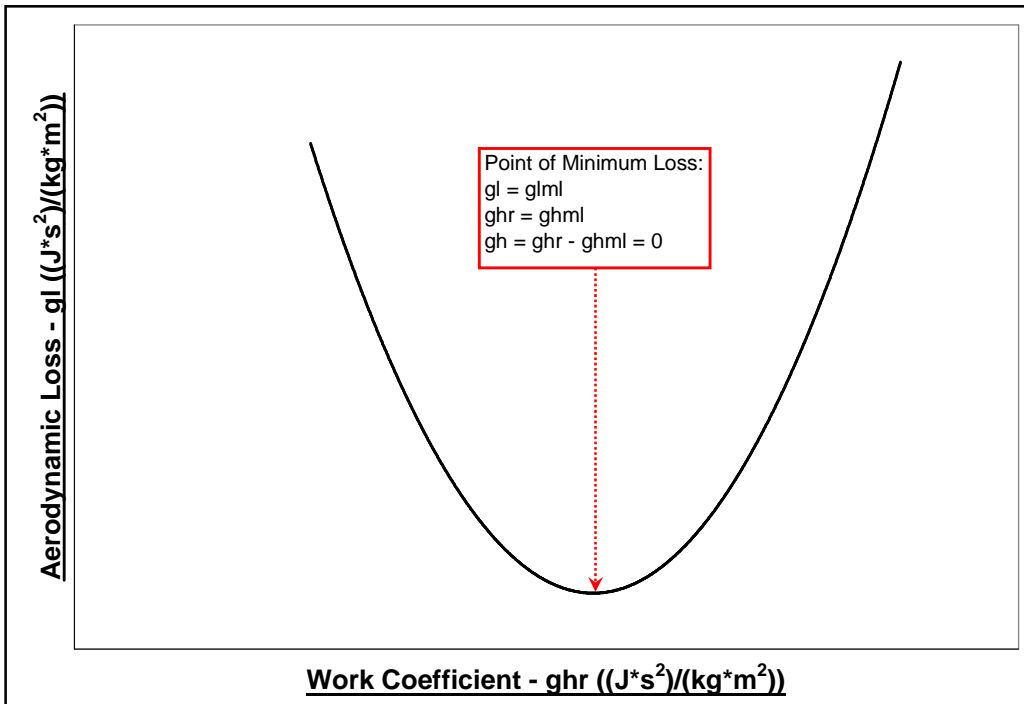


Fig: 5.1.2 Compressor ghr vs. gl Characteristic

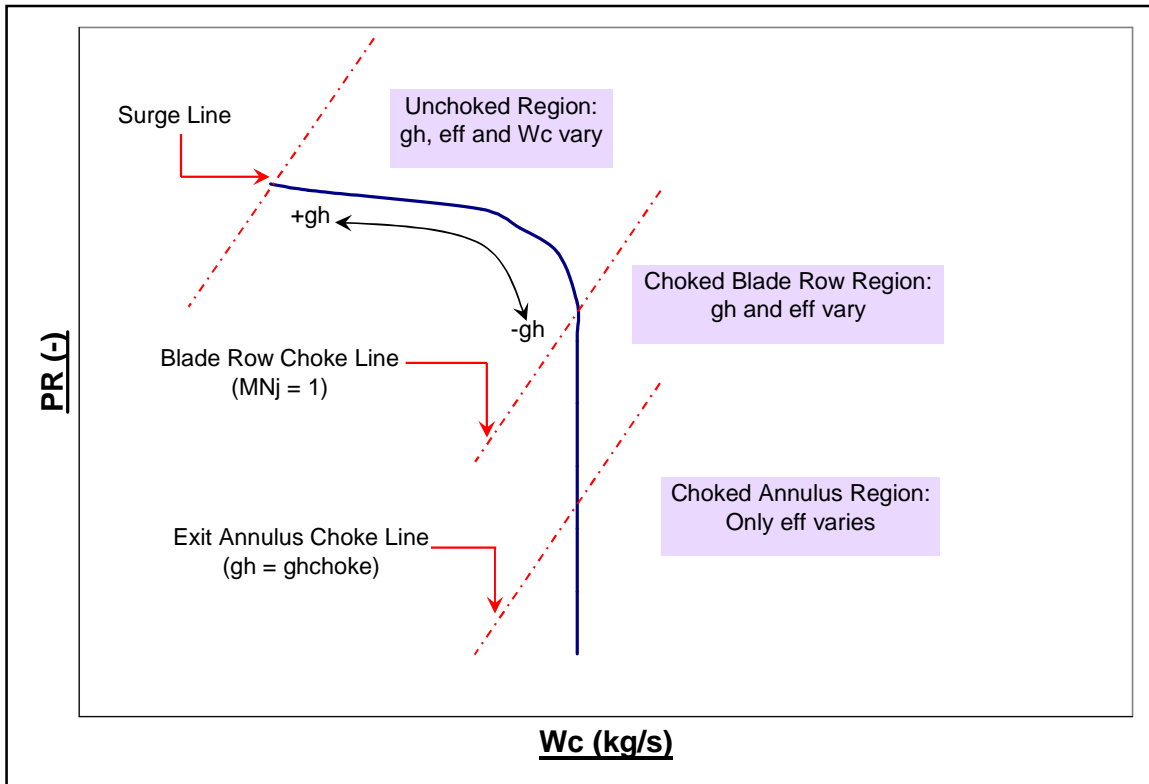


Fig: 5.1.3 Compressor MFT Map Choke Limits

BETA Map Characteristics	MFT Map Characteristics
eff as a function of (BETA & NcRdesMap)	ghchoke as a function of (NcRdesMap)
PR as a function of (BETA & NcRdesMap)	ghml as a function of (NcRdesMap)
PRsurge as a function of (Wc)	gld as a function of (gh ² & NcRdesMap)
Wc as a function of (BETA & NcRdesMap)	glml as a function of (NcRdesMap)
	MNj as a function of (gh and NcRdesMap)
	VqU _{tip} as a function of (NcRdesMap)

Fig: 5.1.4 Comparison between the Characteristics of Compressor BETA & MFT Maps

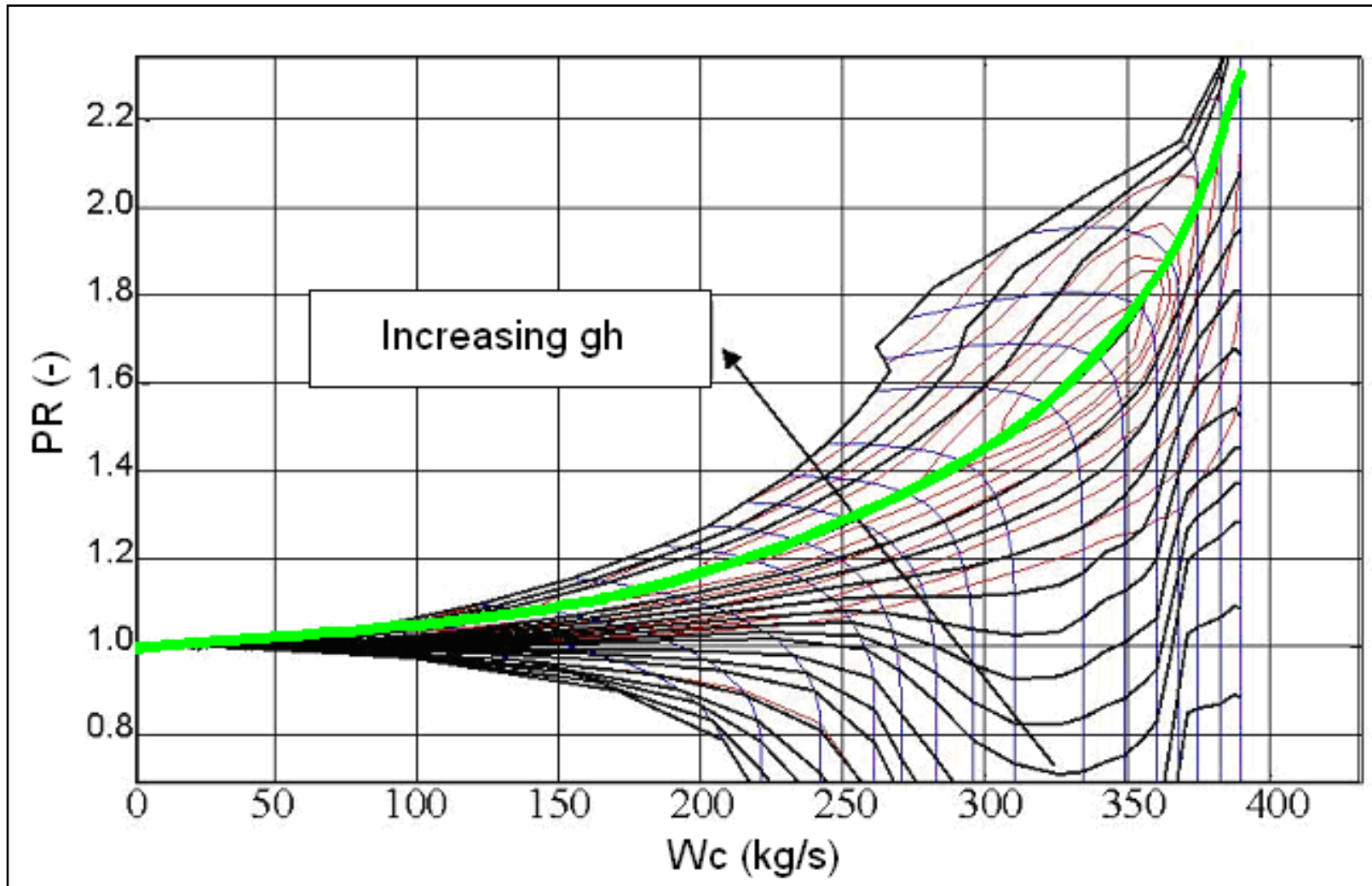


Fig: 5.1.5 Visualisation of a Typical Compressor MFT Map ^[4]

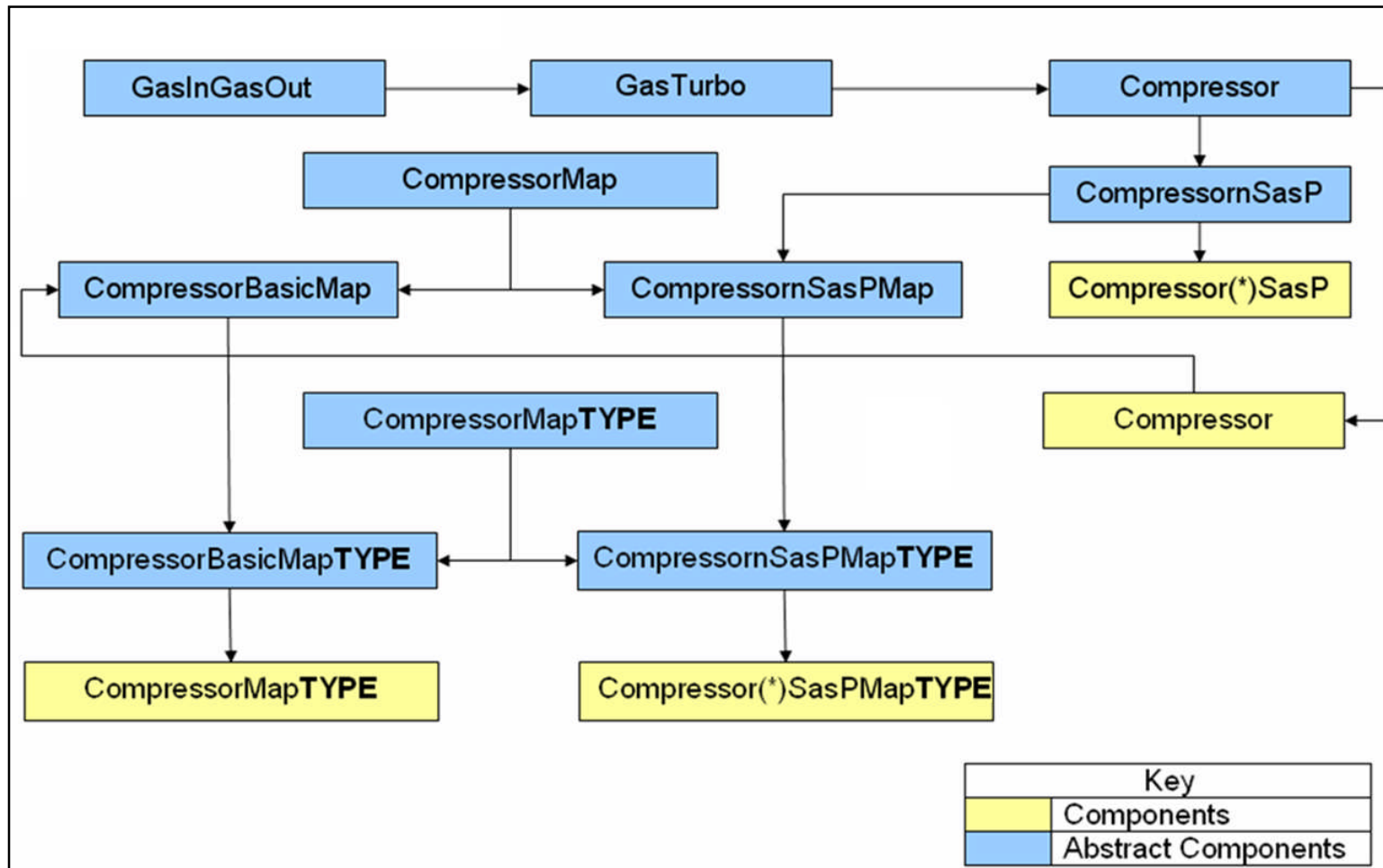


Fig: 5.1.6 CompressorMFT Component Hierarchy

NB: "TYPE" Corresponds to Either "BETA" or "MFT" depending on the type of Compressor map.

For components "Compressor(*)SasP" and "Compressor(*)SasPMapTYPE", (*) is replaced with an integer which corresponds to the number of bleeds the user wishes to simulate.

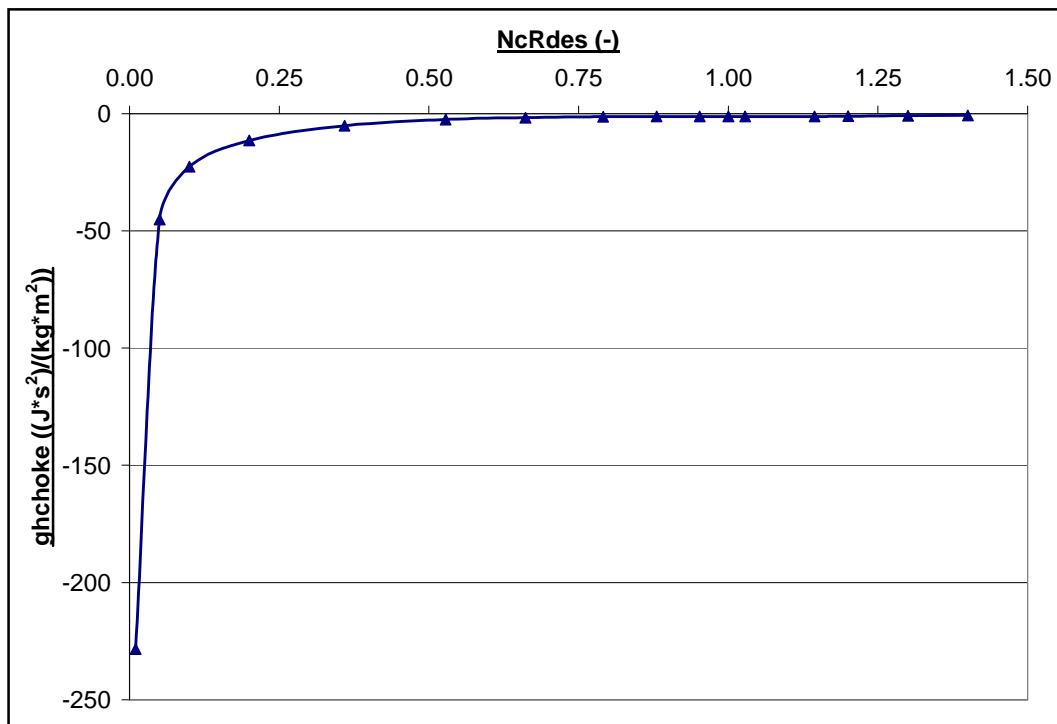


Fig: 5.2.1 “ghchoke_vs_NcRdes” Characteristic

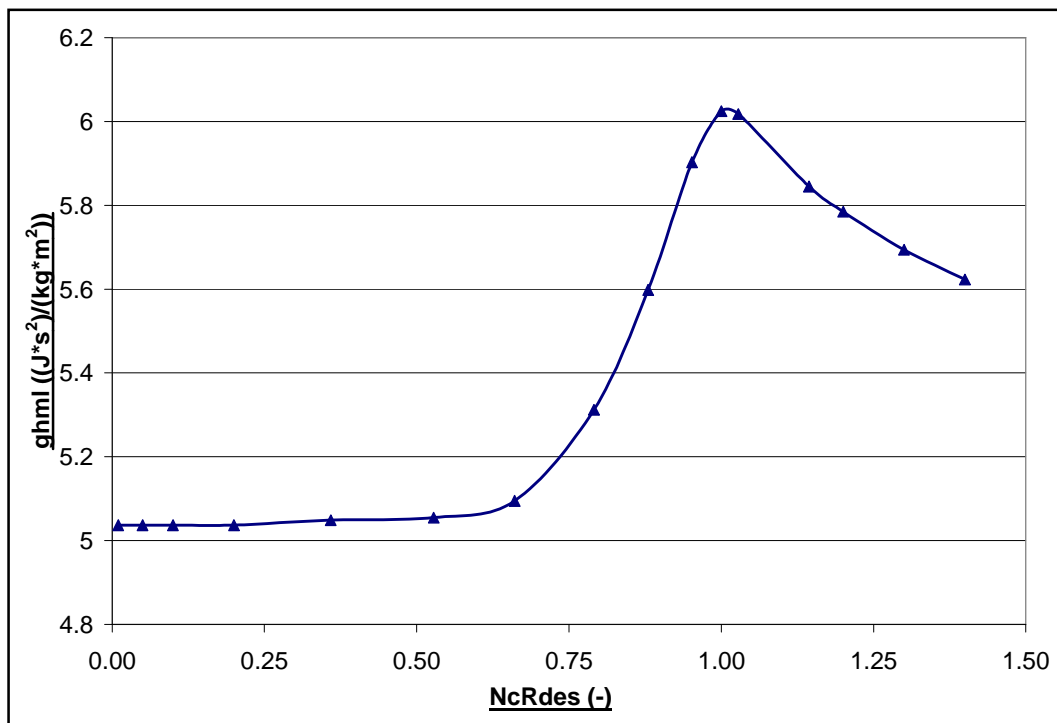


Fig: 5.2.2 “ghml_vs_NcRdes” Characteristic

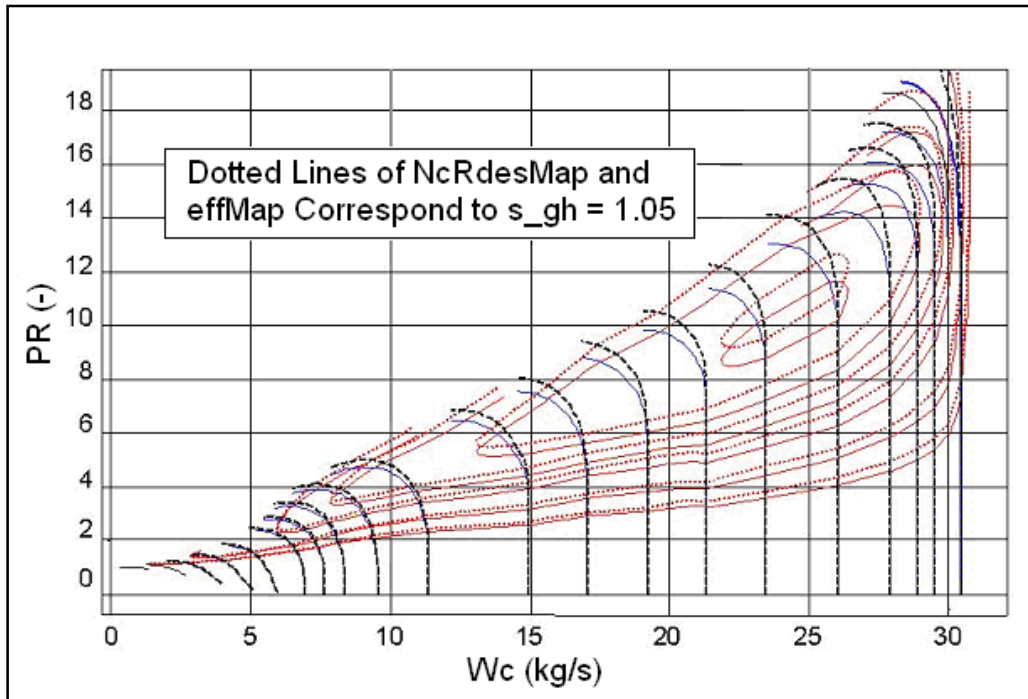


Fig: 5.2.3 Effects of s_{gh} on a typical Compressor MFT map [4]

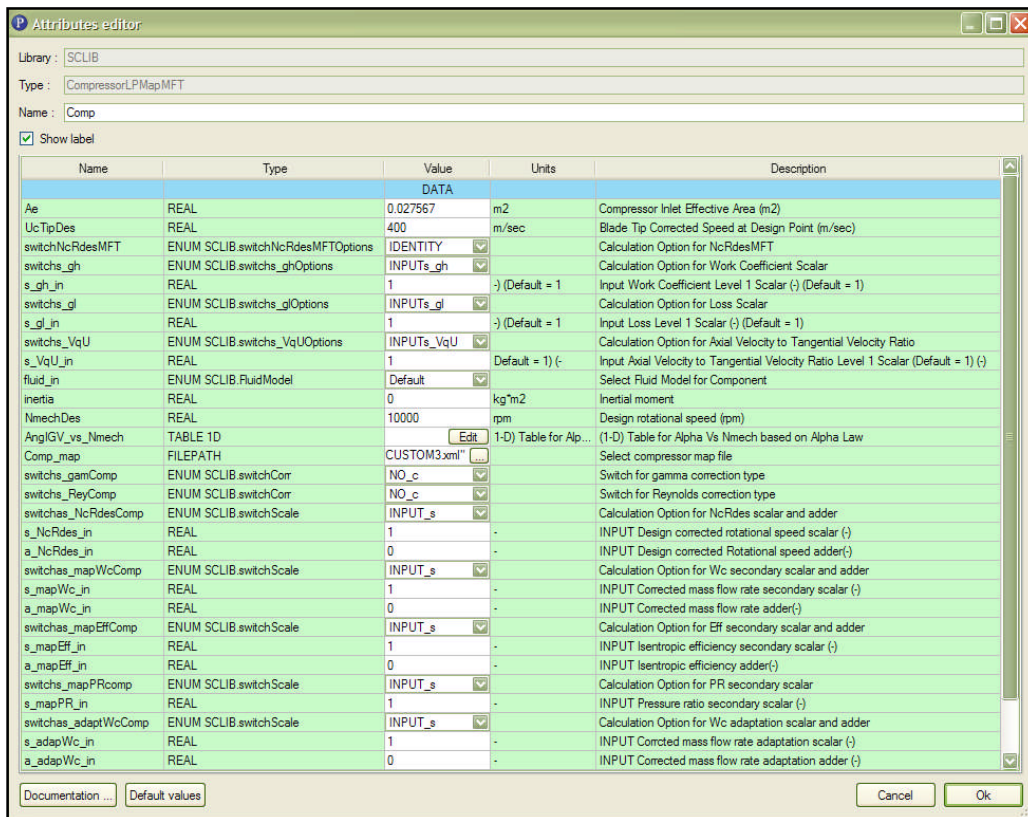


Fig: 5.2.4 CompressorMFT Component Attributes Editor

Advanced Performance Simulation of Gas Turbine Components
and Fluid Thermodynamic Properties

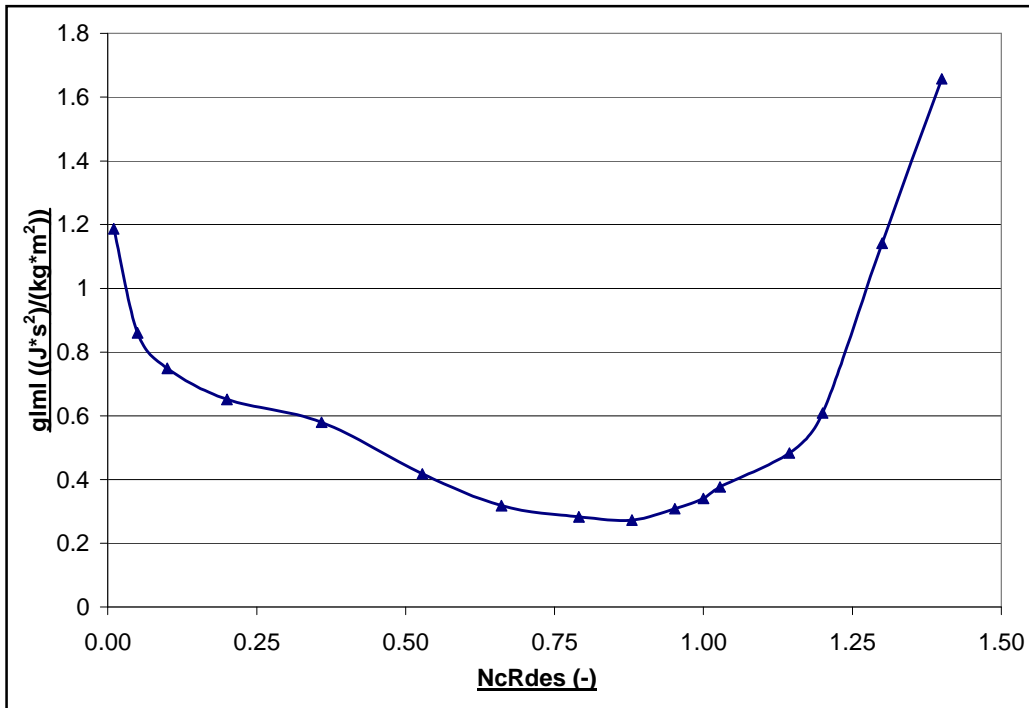


Fig. 5.2.5 "glml_vs_NcRdes" Characteristic

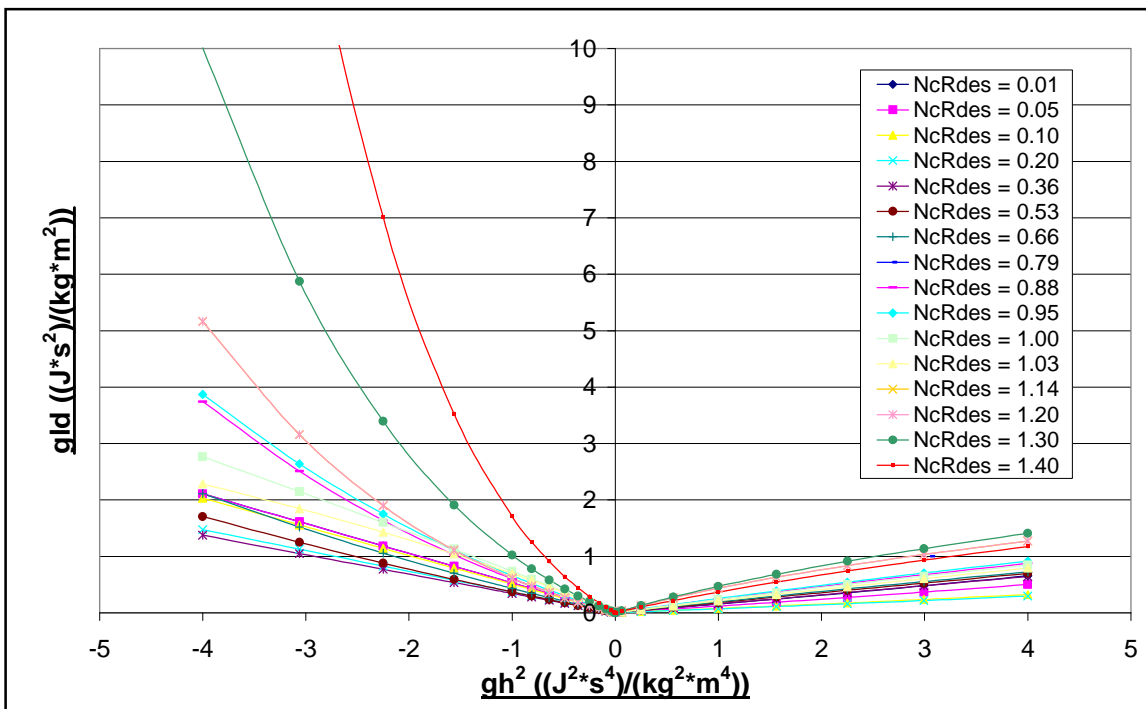


Fig. 5.2.6 "gld_vs_gh²_NcRdes" Characteristic

Advanced Performance Simulation of Gas Turbine Components and Fluid Thermodynamic Properties

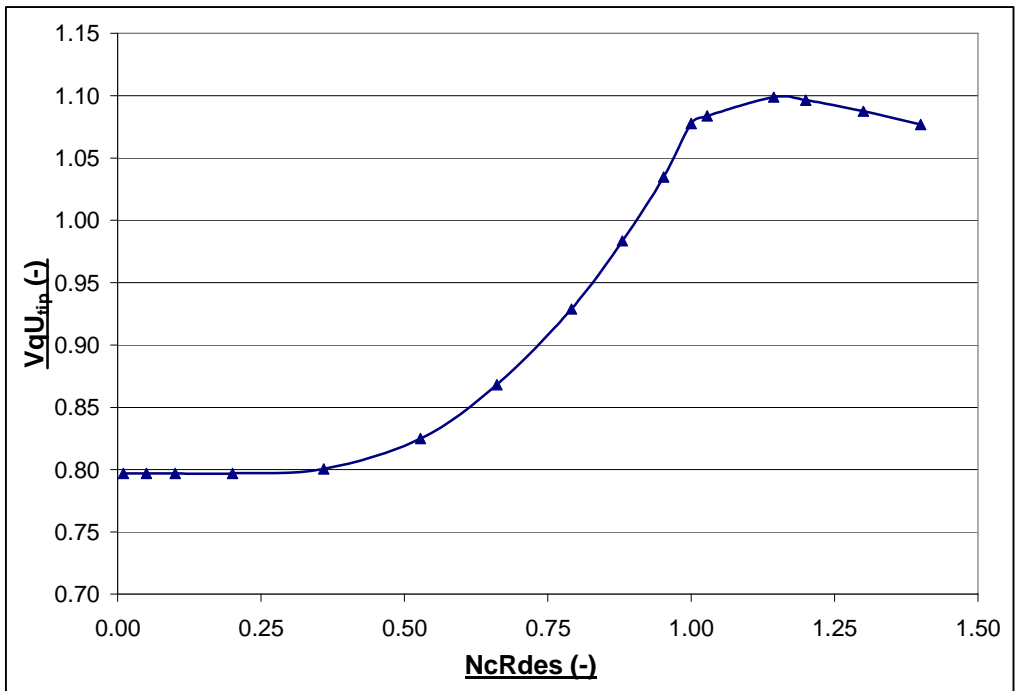


Fig: 5.2.7 “ $VqU_{tip_vs_NcRdes}$ ” Characteristic

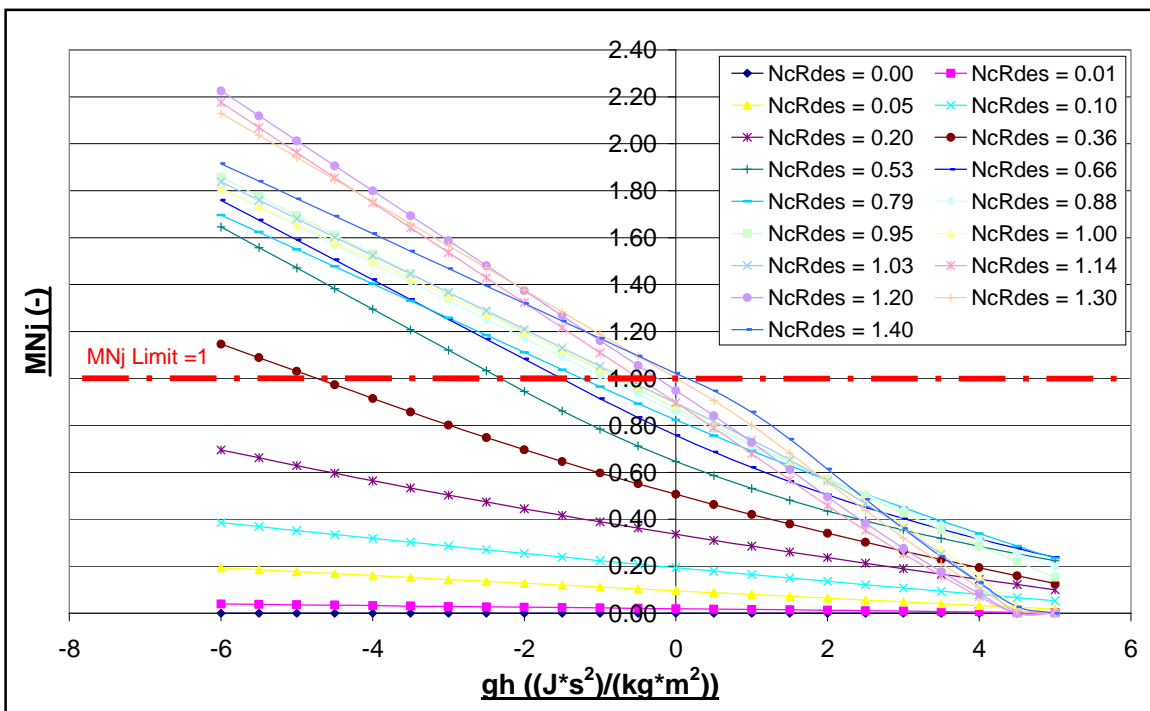


Fig: 5.2.8 “ $MNj_vs_gh_NcRdes$ ” Characteristic
 MNj > 1 values included to improve extrapolation and convergence. However, MNj values cannot exceed 1 as shown in Fig: 5.1.3.

Chapter 5: Appendix 1

Sample PROOSIS CompressorMFT Map

```

<?xml version="1.0" encoding="UTF-8" standalone="no" ?>
- <map version="1.0" type="compressor_mft" name="M_FCO_VICOB" description="VICOB BOOSTER MFT MAP" cdate="20/11/2007"
  mdate="20/11/2007" revision="0.1">
  <var type="REAL" name="RNI1" description="Lower Reynolds Index" value="0.1" />
  <var type="REAL" name="f1" description="Lower Reynolds Correction" value="0.95" />
  <var type="REAL" name="RNI2" description="Upper Reynolds Index" value="1.0" />
  <var type="REAL" name="f2" description="Upper Reynolds Correction" value="1.0" />
  <var type="REAL" name="NmechRef" description="Map Reference rotational speed" value="2663.24134" />
  <var type="REAL" name="PRref" description="Map Reference pressure ratio" value="2.532" />
  <var type="REAL" name="Pref" description="Map Reference total pressure" value="101325.0" />
  <var type="REAL" name="Tref" description="Map Reference total pressure" value="288.15" />
  <var type="REAL" name="Aref" description="Map Reference inlet Area" value="0.62475" />
  <var type="REAL" name="UcTipRef" description="Map Reference Tip speed" value="192.559" />
  <var type="REAL" name="alphaRef" description="Map Reference flow angle" value="0.0" />
  <var type="REAL" name="FARBref" description="Map Reference fuel to air ratio burnt" value="0.0" />
  <var type="REAL" name="FARUref" description="Map Reference fuel to air ratio un-burnt" value="0.0" />
  <var type="REAL" name="WARref" description="Map Reference water to air ratio" value="0.0" />
= <table type="1D" name="ghchoke_vs_NcRdes" description="Output Work Coefficient at Exit Annulus Choked Flow vs Design Point Relative Corrected Rotational
  Speed">
  <interp default="LINEAR" valid="{LINEAR}" />
  <extrap default="LINEAR" valid="{FORBIDDEN, CONSTANT, LINEAR}" />
  <axis1 id="NcRdes" description="Design Point Relative Corrected Rotational Speed (-)" value="{0.10000000E-01, 0.50000000E-01, 0.10000000E+00, 0.20000000E+00,
    0.35900000E+00, 0.52800000E+00, 0.66100000E+00, 0.79100000E+00, 0.88000000E+00, 0.95200000E+00, 0.10000000E+01, 0.10280000E+01, 0.11440000E+01,
    0.12000000E+01, 0.13000000E+01, 0.14000000E+01}" />
  <return id="ghchoke" description="Work Coefficient at Exit Annulus Choked Flow ((J*sec2)/(kg*m2))" value="{-0.22834530E+03,-0.45128630E+02,-
    0.22693940E+02,-0.11424660E+02, -0.51490000E+01,-0.24890000E+01,-0.17300000E+01,-0.13160000E+01, -0.12180000E+01,-0.12225850E+01,-0.12260000E+01,-
    0.12650000E+01, -0.12417160E+01,-0.11021660E+01,-0.98116640E+00,-0.77016640E+00}" />
  </table>
= <table type="1D" name="ghml_vs_NcRdes" description="Output Intermediate Work Coefficient on the Backbone">
  <interp default="LINEAR" valid="{LINEAR}" />
  <extrap default="LINEAR" valid="{FORBIDDEN, CONSTANT, LINEAR}" />

```

Advanced Performance Simulation of Gas Turbine Components and Fluid Thermodynamic Properties

```

<axis1 id="NcRdes" description="Design Point Relative Corrected Rotational Speed (-)" value="{0.1000000E-01, 0.5000000E-01, 0.1000000E+00,
0.2000000E+00, 0.3590000E+00, 0.5280000E+00, 0.6610000E+00, 0.7910000E+00, 0.8800000E+00, 0.9520000E+00, 0.1000000E+01, 0.1028000E+01,
0.1144000E+01, 0.1200000E+01, 0.1300000E+01, 0.1400000D+01}" />
<return id="ghml" description="Intermediate Work Coefficient at minimum loss point ((J*sec2)/(kg*m2))" value="{0.5037000D+01, 0.5037000D+01,
0.5037000D+01, 0.5037000D+01, 0.5049000D+01, 0.5055000D+01, 0.5095000D+01, 0.5312459D+01, 0.5598188D+01, 0.5902585D+01, 0.6024346D+01,
0.6017889D+01, 0.5844550D+01, 0.5785000D+01, 0.5694000D+01, 0.5623000D+01}" />
</table>
= <table type="1D" name="gml_vs_NcRdes" description="Output Intermediate Losses Coefficient on the Backbone" >
<interp default="LINEAR" valid="{LINEAR}" />
<extrap default="LINEAR" valid="{FORBIDDEN, CONSTANT, LINEAR}" />
<axis1 id="NcRdes" description="Design Point Relative Corrected Rotational Speed (-)" value="{0.1000000E-01, 0.5000000E-01, 0.1000000E+00, 0.2000000E+00,
0.3590000E+00, 0.5280000E+00, 0.6610000E+00, 0.7910000E+00, 0.8800000E+00, 0.9520000E+00, 0.1000000E+01, 0.1028000E+01, 0.1144000E+01,
0.1200000E+01, 0.1300000E+01, 0.1400000D+01}" />
<return id="gml" description="Intermediate Losses Coefficient at minimum loss point ((J*sec2)/(kg*m2))" value="{0.1186990E+01, 0.8603058E+00,
0.7489398E+00, 0.6519899E+00, 0.5800000E+00, 0.4182397E+00, 0.3183782E+00, 0.2830222E+00, 0.2732939E+00, 0.3088758E+00, 0.3409348E+00,
0.3769219E+00, 0.4831213E+00, 0.6086221E+00, 0.1142220E+01, 0.1657414E+01}" />
</table>
= <table type="2D" name="gld_vs_gh2_NcRdes" description="Output Losses Delta from Current Point to Backbone" >
<interp default="LINEAR" valid="{LINEAR}" />
<extrap default="LINEAR" valid="{FORBIDDEN, CONSTANT, LINEAR}" />
<axis1 id="gh2" description="Signed Square Work Parameter ((J2*sec4)/(kg2*m4))" value="{-0.3600000E+02,-0.2500000E+02,-0.1600000E+02,-0.1296000E+02,
-0.1225000E+02,-0.1056250E+02,-0.9000000E+01,-0.7562500E+01, -0.6250000E+01,-0.5062500E+01,-0.4000000E+01,-0.3062500E+01, -0.2250000E+01,-
0.1562500E+01,-0.1000000E+01,-0.8099999E+00,-0.6400000E+00,-0.4900000E+00,-0.3600000E+00,-0.2500000E+00,-0.1600000E+00,-0.9000000E-01,-0.4000000E-
01,-0.1000000E-01, -0.2500000E-02, 0.0000000E+00, 0.6250000E-03, 0.2500000E-02, 0.5625000E-02, 0.1000000E-01, 0.6250000E-01, 0.2500000E+00,
0.5625000E+00, 0.1000000E+01, 0.1562500E+01, 0.2250000E+01, 0.2992900E+01, 0.4000000E+01, 0.6250000E+01, 0.7562500E+01, 0.7840000E+01,
0.7952400E+01, 0.8122499E+01, 0.9000000E+01, 0.1225000E+02, 0.1600000E+02, 0.2025000E+02, 0.2500000E+02}" />
<axis2 id="NcRdes" description="Design Point Relative Corrected Rotational Speed (-)" value="{0.1000000E-01, 0.5000000E-01, 0.1000000E+00, 0.2000000E+00,
0.3590000E+00, 0.5280000E+00, 0.6610000E+00, 0.7910000E+00, 0.8800000E+00, 0.9520000E+00, 0.1000000E+01, 0.1028000E+01, 0.1144000E+01,
0.1200000E+01, 0.1300000E+01, 0.1400000D+01}" />
<return id="gld" description="Losses Delta from Current Point to Backbone ((J*sec2)/(kg*m2))" value="{0.1896236E+02, 0.1899366E+02, 0.1840450E+02,
0.1357245E+02, 0.1378126E+02, 0.5975726E+02, 0.1081086E+03, 0.6580489E+03, 0.9592719E+03, 0.6812070E+03, 0.2699315E+02, 0.1011805E+02,
0.9604938E+04, 0.1172649E+05, 0.3601024E+05, 0.8687409E+06}, {0.1316804E+02, 0.1318322E+02, 0.1275483E+02, 0.9350099E+01, 0.9227187E+01,
0.2696110E+02, 0.4387076E+02, 0.1789239E+03, 0.2489648E+03, 0.1957532E+03, 0.1744070E+02, 0.8111552E+01, 0.1471198E+04, 0.1909898E+04,
0.4689603E+04, 0.6472834E+05}, {0.8427404E+01, 0.8433688E+01, 0.8149448E+01, 0.5944865E+01, 0.5730081E+01, 0.1182323E+02, 0.1738900E+02,
0.4829751E+02, 0.6420435E+02, 0.5576132E+02, 0.1072001E+02, 0.6123679E+01, 0.2254340E+03, 0.3107590E+03, 0.6104598E+03, 0.4822539E+04},
{0.6826159E+01, 0.6830310E+01, 0.6597324E+01, 0.4804646E+01, 0.4594096E+01, 0.8377563E+01, 0.1185697E+02, 0.2845725E+02, 0.3716272E+02,
0.3354047E+02, 0.8630460E+01, 0.5335434E+01, 0.1064555E+03, 0.1501554E+03, 0.2699214E+03, 0.1706511E+04}, {0.6452187E+01, 0.6455904E+01,
0.6235070E+01, 0.4539070E+01, 0.4332026E+01, 0.7671224E+01, 0.1075597E+02, 0.2491200E+02, 0.3239058E+02, 0.2951041E+02, 0.8153049E+01,
0.5139214E+01, 0.8824483E+02, 0.1251646E+03, 0.2200814E+03, 0.1316156E+04}, {0.5563348E+01, 0.5566128E+01, 0.5374474E+01, 0.3908958E+01,
0.3714040E+01, 0.6129032E+01, 0.8398433E+01, 0.1782835E+02, 0.2293066E+02, 0.2138169E+02, 0.7032076E+01, 0.4650500E+01, 0.5519745E+02,
0.7935807E+02, 0.1320709E+03, 0.6874947E+03}, {0.4740354E+01, 0.4742388E+01, 0.4578103E+01, 0.3326901E+01, 0.3147944E+01, 0.4861509E+01,
0.6514999E+01, 0.1271367E+02, 0.1617948E+02, 0.1543042E+02, 0.6008520E+01, 0.4165026E+01, 0.3451030E+02, 0.5025720E+02, 0.7919986E+02,
0.3590453E+03}, {0.3983204E+01, 0.3984654E+01, 0.3845850E+01, 0.2792579E+01, 0.2632298E+01, 0.3821108E+01, 0.5012222E+01, 0.9022141E+01,
0.1136327E+02, 0.1107555E+02, 0.5075435E+01, 0.3683862E+01, 0.2155636E+02, 0.3176963E+02, 0.4743839E+02, 0.1874443E+03}, {0.3291896E+01,

```

Advanced Performance Simulation of Gas Turbine Components and Fluid Thermodynamic Properties

0.32928990E+01, 0.31776130E+01, 0.23056970E+01, 0.21657890E+01, 0.29687620E+01, 0.38152870E+01, 0.63594310E+01, 0.79294690E+01, 0.78913210E+01,
0.42269110E+01, 0.32085710E+01, 0.13441180E+02, 0.20024920E+02, 0.28358370E+02, 0.97789990E+02, {0.26664300E+01, 0.26670990E+01, 0.25732980E+01,
0.18659900E+01, 0.17472270E+01, 0.22724290E+01, 0.28643520E+01, 0.44406500E+01, 0.54835600E+01, 0.55658720E+01, 0.34581340E+01, 0.27414230E+01,
0.83541840E+01, 0.12564270E+02, 0.16896740E+02, 0.50949530E+02, {0.21068050E+01, 0.21072320E+01, 0.20328210E+01, 0.14732140E+01, 0.13755460E+01,
0.17058980E+01, 0.21116210E+01, 0.30600610E+01, 0.37493080E+01, 0.38708090E+01, 0.27654920E+01, 0.22856730E+01, 0.51628630E+01, 0.78257490E+01,
0.10012080E+02, 0.26477640E+02, {0.16130200E+01, 0.16132780E+01, 0.15561070E+01, 0.11271540E+01, 0.10497970E+01, 0.12478160E+01, 0.15190070E+01,
0.20691840E+01, 0.25095770E+01, 0.26389880E+01, 0.21467080E+01, 0.18459280E+01, 0.31589630E+01, 0.48173420E+01, 0.58774710E+01, 0.13692650E+02,
{0.11850740E+01, 0.11852200E+01, 0.11430900E+01, 0.82761970E+00, 0.76914750E+00, 0.88089200E+00, 0.10562870E+01, 0.13610070E+01, 0.16373550E+01,
0.17482550E+01, 0.16009850E+01, 0.14285570E+01, 0.18997350E+01, 0.29092230E+01, 0.33957660E+01, 0.70140710E+01, {0.82296690E+00, 0.82304320E+00,
0.79371070E+00, 0.57444600E+00, 0.53287960E+00, 0.59125470E+00, 0.69964400E+00, 0.85862300E+01, 0.10254180E+01, 0.11095880E+01, 0.11291350E+01,
0.10420850E+01, 0.11086800E+01, 0.17019220E+01, 0.19084210E+01, 0.35268050E+01, 0.52669830E+00, 0.52673370E+00, 0.50792170E+00, 0.36749370E+00,
0.34038900E+00, 0.36793800E+00, 0.43053170E+00, 0.50708780E+00, 0.60173230E+00, 0.65849100E+00, 0.73360200E+00, 0.69740580E+00, 0.61353730E+00,
0.94268280E+00, 0.10207580E+01, 0.17086990E+01, {0.42662540E+00, 0.42665040E+00, 0.41140200E+00, 0.29762840E+00, 0.27553630E+00, 0.29520820E+00,
0.34409440E+00, 0.39958370E+00, 0.47309500E+00, 0.51972710E+00, 0.59758870E+00, 0.57409650E+00, 0.47284730E+00, 0.72653790E+00, 0.77710540E+00,
0.12557400E+01, {0.33708670E+00, 0.33710380E+00, 0.32504810E+00, 0.23513380E+00, 0.21758140E+00, 0.23127010E+00, 0.26862630E+00, 0.30798080E+00,
0.36388840E+00, 0.40115480E+00, 0.47469610E+00, 0.46044410E+00, 0.35724600E+00, 0.54885410E+00, 0.58050850E+00, 0.90809970E+00, {0.25808190E+00,
0.25809330E+00, 0.24885800E+00, 0.18000450E+00, 0.16650050E+00, 0.17573640E+00, 0.20348690E+00, 0.23065660E+00, 0.27202170E+00, 0.30081280E+00,
0.36523990E+00, 0.35736420E+00, 0.26286400E+00, 0.40376450E+00, 0.42276980E+00, 0.64220260E+00, {0.18961120E+00, 0.18961840E+00, 0.18283010E+00,
0.13223560E+00, 0.12227260E+00, 0.12827040E+00, 0.14812120E+00, 0.16623640E+00, 0.19572730E+00, 0.21703070E+00, 0.26954200E+00, 0.26576390E+00,
0.18655920E+00, 0.28647850E+00, 0.29731280E+00, 0.44001690E+00, {0.13167440E+00, 0.13167880E+00, 0.12696270E+00, 0.91822860E-01, 0.84879610E-01, 0.88584150E-01,
0.10205580E+00, 0.11357040E+00, 0.13352960E+00, 0.14840530E+00, 0.18791840E+00, 0.18651530E+00, 0.12580390E+00, 0.19312340E+00, 0.19890640E+00,
0.28783090E+00, {0.84271590E-01, 0.84274060E-01, 0.81254770E-01, 0.58762740E-01, 0.54306260E-01, 0.56436970E-01, 0.64895470E-01, 0.71715320E-01, 0.42200400E-01,
0.93780250E-01, 0.12066730E+00, 0.12042720E+00, 0.78596060E-01, 0.12061700E+00, 0.12344780E+00, 0.17532420E+00, {0.47402770E-01, 0.47404010E-01, 0.45705220E-01,
0.33052350E-01, 0.30539970E-01, 0.31633760E-01, 0.36320510E-01, 0.39919160E-01, 0.46836540E-01, 0.52230490E-01, 0.68055190E-01, 0.68214850E-01, 0.43386690E-01,
0.66564950E-01, 0.67790600E-01, 0.94867070E-01, {0.21067890E-01, 0.21068400E-01, 0.20313240E-01, 0.14689390E-01, 0.13571000E-01, 0.14023970E-01, 0.16084450E-01,
0.17609140E-01, 0.20646810E-01, 0.23049060E-01, 0.30305090E-01, 0.30471330E-01, 0.19025210E-01, 0.29182720E-01, 0.29614320E-01, 0.41003240E-01, {0.52669730E-02,
0.52670920E-02, 0.50782820E-02, 0.36722670E-02, 0.33924020E-02, 0.35006770E-02, 0.40124290E-02, 0.43824600E-02, 0.51363990E-02, 0.57376790E-02, 0.75851520E-02,
0.76411790E-02, 0.47180050E-02, 0.72359490E-02, 0.73272040E-02, 0.10079920E-01, {0.13167430E-02, 0.13167720E-02, 0.12695690E-02, 0.91806170E-03, 0.84807880E-03,
0.87483750E-03, 0.10025650E-02, 0.10943790E-02, 0.12825220E-02, 0.14328860E-02, 0.18968470E-02, 0.19117630E-02, 0.11771180E-02, 0.18052700E-02, 0.1870520E-02,
0.25093880E-02, {0.00000000E+00, 0.00000000E+00, 0.00000000E+00, 0.00000000E+00, 0.00000000E+00, 0.00000000E+00, 0.00000000E+00, 0.00000000E+00, 0.00000000E+00,
0.00000000E+00, 0.00000000E+00, 0.00000000E+00, 0.00000000E+00, 0.00000000E+00, 0.00000000E+00, 0.00000000E+00, 0.00000000E+00, 0.00000000E+00, 0.00000000E+00,
0.456675030E-04, 0.42178000E-04, 0.97966720E-04, 0.11258020E-03, 0.12184410E-03, 0.10744750E-03, 0.15747680E-03, 0.16364840E-03, 0.15171040E-03, 0.13503450E-03,
0.32917840E-03, 0.37095170E-03, 0.34032740E-03, 0.25763480E-03, {0.37202520E-03, 0.28504910E-03, 0.18270810E-03, 0.16871940E-03, 0.39187120E-03, 0.45031270E-03,
0.48735770E-03, 0.54815880E-03, 0.62985370E-03, 0.65454220E-03, 0.60679190E-03, 0.54010790E-03, 0.13161080E-02, 0.14831780E-02, 0.13608380E-02, 0.10302730E-02,
{0.83711800E-03, 0.64140730E-03, 0.41112340E-03, 0.37964640E-03, 0.88172630E-03, 0.10131730E-02, 0.10964840E-02, 0.12332410E-02, 0.14169710E-02, 0.14725270E-02,
0.13650950E-02, 0.12151310E-02, 0.29589770E-02, 0.33347970E-02, 0.30601230E-02, 0.23171180E-02, {0.14883620E-02, 0.11403960E-02, 0.73096090E-03, 0.67499610E-03,
0.15675530E-02, 0.18011220E-02, 0.19491290E-02, 0.21921370E-02, 0.25185610E-02, 0.26173470E-02, 0.24263710E-02, 0.21599530E-02, 0.52547800E-02, 0.59226850E-02,
0.54358390E-02, 0.41168440E-02, {0.93136940E-02, 0.71362360E-02, 0.45741190E-02, 0.42239100E-02, 0.98002160E-02, 0.11251410E-01, 0.12168870E-01, 0.13679150E-01,
0.15703870E-01, 0.16322620E-01, 0.15130170E-01, 0.13478910E-01, 0.32430330E-01, 0.36587510E-01, 0.33650980E-01, 0.25547170E-01, {0.37418410E-01, 0.28670320E-01,
0.18376840E-01, 0.16969850E-01, 0.39243900E-01, 0.44926430E-01, 0.48489440E-01, 0.54413300E-01, 0.62297120E-01, 0.64788530E-01, 0.60036600E-01, 0.53625700E-01,
0.12436000E+00, 0.14070410E+00, 0.13029380E+00, 0.99719460E-01, {0.84807620E-01, 0.64980360E-01, 0.41650520E-01, 0.38461610E-01, 0.88460680E-01, 0.10079350E+00,
0.10842080E+00, 0.12134190E+00, 0.13831380E+00, 0.14396210E+00, 0.13334790E+00, 0.11962370E+00, 0.26297330E+00, 0.29851730E+00, 0.27900610E+00,
0.21610060E+00, {0.15231250E+00, 0.11670320E+00, 0.74803360E-01, 0.69076170E-01, 0.15766850E+00, 0.17848610E+00, 0.19111600E+00, 0.21318030E+00,
0.24157700E+00, 0.25166450E+00, 0.23302060E+00, 0.21027070E+00, 0.43424660E+00, 0.49422920E+00, 0.46654290E+00, 0.36654920E+00, {0.24111530E+00,
0.18474470E+00, 0.11841600E+00, 0.10934970E+00, 0.24717600E+00, 0.27752930E+00, 0.29549270E+00, 0.32839740E+00, 0.36950820E+00, 0.38523380E+00,
0.35662230E+00, 0.32416460E+00, 0.62698980E+00, 0.71456210E+00, 0.68090690E+00, 0.54324900E+00, {0.35276870E+00, 0.27029450E+00, 0.17325090E+00,
0.15998620E+00, 0.35738650E+00, 0.39737180E+00, 0.42031570E+00, 0.46539460E+00, 0.51942690E+00, 0.54179520E+00, 0.50160960E+00, 0.45988500E+00,
0.83370410E+00, 0.95012460E+00, 0.91290790E+00, 0.73982170E+00, {0.47733910E+00, 0.36574150E+00, 0.23442970E+00, 0.21648090E+00, 0.47749490E+00,
0.52548720E+00, 0.55208770E+00, 0.60936060E+00, 0.67457680E+00, 0.70367990E+00, 0.65178930E+00, 0.60290830E+00, 0.10322760E+01, 0.11750890E+01,
0.11364250E+01, 0.93416180E+00, {0.65284960E+00, 0.50021920E+00, 0.32062590E+00, 0.29607770E+00, 0.64202830E+00, 0.69707290E+00, 0.72607370E+00,
0.79884090E+00, 0.87531730E+00, 0.91265600E+00, 0.84625850E+00, 0.79184560E+00, 0.12728120E+01, 0.14453170E+01, 0.14066460E+01, 0.11752980E+01,
{0.10735360E+00, 0.82255270E+00, 0.52723230E+00, 0.48686560E+00, 0.10168890E+01, 0.10729090E+01, 0.10982700E+01, 0.12038700E+01, 0.12926100E+01,
0.13441980E+01, 0.12509090E+01, 0.11986780E+01, 0.17341900E+01, 0.19554400E+01, 0.19197550E+01, 0.16510170E+01, {0.13378940E+01, 0.10251060E+01,
0.65706320E+00, 0.60675630E+00, 0.12403060E+01, 0.12880850E+01, 0.13064960E+01, 0.14312940E+01, 0.15206120E+01, 0.15778200E+01, 0.14721410E+01,
0.14290100E+01, 0.19714510E+01, 0.22132800E+01, 0.21799000E+01, 0.19009130E+01, {0.13956350E+01, 0.10693480E+01, 0.68542100E+00, 0.63294900E+00,
0.12879990E+01, 0.13332450E+01, 0.13497900E+01, 0.14787140E+01, 0.15676280E+01, 0.16257760E+01, 0.15177680E+01, 0.14772140E+01, 0.20193950E+01,
0.22650060E+01, 0.22321250E+01, 0.19517800E+01, {0.14192090E+01, 0.10874110E+01, 0.69699860E+00, 0.64363410E+00, 0.13073620E+01, 0.13515060E+01,
0.13672570E+01, 0.14978610E+01, 0.15865630E+01, 0.16450670E+01, 0.15361440E+01, 0.14966950E+01, 0.20386180E+01, 0.22857100E+01, 0.22530310E+01,
0.19722080E+01, {0.14550900E+01, 0.11149030E+01, 0.17462040E+00, 0.65990660E+00, 0.13367160E+01, 0.13791070E+01, 0.13936170E+01, 0.15267740E+01,
0.16151010E+01, 0.16741190E+01, 0.15638410E+01, 0.15261320E+01, 0.20675010E+01, 0.23167800E+01, 0.22844060E+01, 0.20029370E+01, {0.16441550E+01,

Advanced Performance Simulation of Gas Turbine Components and Fluid Thermodynamic Properties

```

0.12597660E+01, 0.80747340E+00, 0.74565060E+00, 0.14891120E+01, 0.15208800E+01, 0.15282430E+01, 0.16747830E+01, 0.17602070E+01, 0.18213760E+01,
0.17046760E+01, 0.16771840E+01, 0.22127820E+01, 0.24723670E+01, 0.24415630E+01, 0.21581280E+01}, {0.24044030E+01, 0.18422750E+01, 0.11808450E+01,
0.10904350E+01, 0.20679040E+01, 0.20381850E+01, 0.20094350E+01, 0.22095970E+01, 0.22717590E+01, 0.23340600E+01, 0.22012030E+01, 0.22280650E+01,
0.27074270E+01, 0.29935250E+01, 0.29682410E+01, 0.26937810E+01}, {0.34070890E+01, 0.26105430E+01, 0.16732820E+01, 0.15451700E+01, 0.27647700E+01,
0.26234400E+01, 0.25374030E+01, 0.28092900E+01, 0.28242810E+01, 0.28759210E+01, 0.27373930E+01, 0.28551460E+01, 0.32181380E+01, 0.35181220E+01,
0.34984510E+01, 0.32576570E+01}, {0.47217990E+01, 0.36178850E+01, 0.23189590E+01, 0.21414120E+01, 0.35937920E+01, 0.32766830E+01, 0.31095200E+01,
0.34770650E+01, 0.34169780E+01, 0.34432520E+01, 0.33122950E+01, 0.35647100E+01, 0.37452810E+01, 0.40459220E+01, 0.40317350E+01, 0.38504880E+01},
{0.64397160E+01, 0.49341680E+01, 0.31626580E+01, 0.29205150E+01, 0.45719340E+01, 0.39992800E+01, 0.37246050E+01, 0.42178230E+01, 0.40504410E+01,
0.40340490E+01, 0.39263240E+01, 0.43650590E+01, 0.42893400E+01, 0.45768650E+01, 0.45679450E+01, 0.44734650E+01}}"/>

```

</table>

```

=<table type="1D" name="VqUt看_vs_NcRdes" description="Output Intermediate Blade Tip Axial to Tangential Velocity Ratio">

```

```

<interp default="LINEAR" valid="{LINEAR}" />

```

```

<extrap default="LINEAR" valid="{FORBIDDEN, CONSTANT, LINEAR}" />

```

```

<axis1 id="NcRdes" description="Design Point Relative Corrected Rotational Speed (-)" value="{0.10000000E-01, 0.50000000E-01, 0.10000000E+00, 0.20000000E+00,
0.35900000E+00, 0.52800000E+00, 0.66100000E+00, 0.79100000E+00, 0.88000000E+00, 0.95200000E+00, 0.10000000E+01, 0.10280000E+01, 0.11440000E+01,
0.12000000E+01, 0.13000000E+01, 0.14000000E+01}" />

```

```

<return id="VqUt看" description="Intermediate Blade Tip Axial to Tangential Velocity Ratio (-)" value="{0.79695520E+00, 0.79698300E+00, 0.79691050E+00,
0.79690120E+00, 0.80043350E+00, 0.82496570E+00, 0.86812570E+00, 0.92875960E+00, 0.98356910E+00, 0.10347140E+01, 0.10776060E+01, 0.10836700E+01,
0.10988690E+01, 0.10964200E+01, 0.10876000E+01, 0.10770000E+01}" />

```

</table>

```

=<table type="2D" name="MNj_vs_gh_NcRdes" description="Output Intermediate Local Mach Number Calculated with static temperature">

```

```

<interp default="LINEAR" valid="{LINEAR}" />

```

```

<extrap default="LINEAR" valid="{FORBIDDEN, CONSTANT, LINEAR}" />

```

```

<axis1 id="gh" description="Signed Square Work Parameter ((J2*sec4)/(kg2*m4))" value="{0.60000000E+01,-0.50000000E+01,-0.40000000E+01,-0.36000000E+01, -
0.35000000E+01,-0.32500000E+01,-0.30000000E+01,-0.27500000E+01, -0.25000000E+01,-0.22500000E+01,-0.20000000E+01,-0.17500000E+01, -0.15000000E+01,-
0.12500000E+01,-0.10000000E+01,-0.90000000E+00, -0.80000000E+00,-0.70000000E+00,-0.60000000E+00,-0.50000000E+00, -0.40000000E+00,-0.30000000E+00,-
0.20000000E+00,-0.10000000E+00,-0.50000000E-01, 0.00000000E+00, 0.25000000E-01, 0.50000000E-01, 0.75000000E-01, 0.10000000E+00, 0.25000000E+00, 0.50000000E+00,
0.75000000E+00, 0.10000000E+01, 0.12500000E+01, 0.15000000E+01, 0.17300000E+01, 0.20000000E+01, 0.25000000E+01, 0.28000000E+01,
0.28200000E+01, 0.28500000E+01, 0.30000000E+01, 0.35000000E+01, 0.40000000E+01, 0.45000000E+01, 0.50000000E+01}" />

```

```

<axis2 id="NcRdes" description="Design Point Relative Corrected Rotational Speed (-)" value="{0.00000000E+00, 0.10000000E-01, 0.50000000E-01, 0.10000000E+00,
0.20000000E+00, 0.35900000E+00, 0.52800000E+00, 0.66100000E+00, 0.79100000E+00, 0.88000000E+00, 0.95200000E+00, 0.10000000E+01, 0.10280000E+01,
0.11440000E+01, 0.12000000E+01, 0.13000000E+01, 0.14000000E+01}" />

```

```

<return id="MNj" description="Intermediate Local Mach Number Calculated with static temperature (-)" value="{0.00000000E+00, 0.38925200E-01,
0.19394530E+00, 0.38608930E+00, 0.69590400E+00, 0.11433750E+01, 0.16436850E+01, 0.17605470E+01, 0.16959300E+01, 0.18098380E+01, 0.18597820E+01,
0.18096950E+01, 0.18317340E+01, 0.21878310E+01, 0.22251210E+01, 0.21292100E+01, 0.19150350E+01}, {0.00000000E+00, 0.35587360E-01, 0.17704920E+00,
0.35190640E+00, 0.62842140E+00, 0.10281420E+01, 0.14685670E+01, 0.15914770E+01, 0.15498000E+01, 0.16503200E+01, 0.16951680E+01, 0.16566370E+01,
0.16755870E+01, 0.19726290E+01, 0.20123610E+01, 0.19412600E+01, 0.17661550E+01}, {0.00000000E+00, 0.32255780E+01, 0.16035670E+00, 0.31866690E+00,
0.56422640E+00, 0.91290820E+00, 0.12934490E+01, 0.14224070E+01, 0.14036700E+01, 0.14908020E+01, 0.15305540E+01, 0.15035790E+01, 0.15194410E+01,
0.17574260E+01, 0.17996020E+01, 0.17533090E+01, 0.16172760E+01}, {0.00000000E+00, 0.30924890E-01, 0.15373450E+00, 0.30562180E+00, 0.53942700E+00,
0.86681470E+00, 0.12234020E+01, 0.13547790E+01, 0.13452180E+01, 0.14269950E+01, 0.14647090E+01, 0.14423560E+01, 0.14569820E+01, 0.16713450E+01,
0.17144980E+01, 0.16781290E+01, 0.15577250E+01}, {0.00000000E+00, 0.30592320E-01, 0.15208380E+00, 0.30238220E+00, 0.53330310E+00, 0.85548960E+00,
0.12058910E+01, 0.13378720E+01, 0.13306050E+01, 0.14110430E+01, 0.14482470E+01, 0.14270500E+01, 0.14413680E+01, 0.16498250E+01, 0.16932220E+01,
0.16593340E+01, 0.15428370E+01}, {0.00000000E+00, 0.29761160E-01, 0.14796510E+00, 0.29432050E+00, 0.51812390E+00, 0.82751880E+00, 0.11621110E+01,
0.12956040E+01, 0.12940720E+01, 0.13711640E+01, 0.14070940E+01, 0.13887860E+01, 0.14023310E+01, 0.15960240E+01, 0.16400320E+01, 0.16123460E+01,
0.15056170E+01}, {0.00000000E+00, 0.28930390E-01, 0.14385810E+00, 0.28631120E+00, 0.50312890E+00, 0.80003000E+00, 0.11183320E+01, 0.12533370E+01,
0.12575400E+01, 0.13312840E+01, 0.13659400E+01, 0.13505210E+01, 0.13632940E+01, 0.15422230E+01, 0.15868430E+01, 0.15653590E+01, 0.14683970E+01},

```

Advanced Performance Simulation of Gas Turbine Components
and Fluid Thermodynamic Properties

{0.00000000E+00, 0.28099990E-01, 0.13976210E+00, 0.27833530E+00, 0.48831440E+00, 0.77302160E+00, 0.10745520E+01, 0.12110690E+01, 0.12210070E+01,
0.12914050E+01, 0.13247870E+01, 0.13122570E+01, 0.13242580E+01, 0.14884230E+01, 0.15336530E+01, 0.15183710E+01, 0.14311770E+01}, {0.00000000E+00, 0.27269970E-
01, 0.13567810E+00, 0.27044640E+00, 0.47367680E+00, 0.74648260E+00, 0.10307730E+01, 0.11688010E+01, 0.11844750E+01, 0.12515250E+01, 0.12836340E+01,
0.12739920E+01, 0.12852210E+01, 0.14346220E+01, 0.14804360E+01, 0.14713830E+01, 0.13939570E+01}, {0.00000000E+00, 0.26440340E-01, 0.13160530E+00,
0.26258990E+00, 0.45921400E+00, 0.72040670E+00, 0.98699360E+00, 0.11265340E+01, 0.11479420E+01, 0.12116460E+01, 0.12424800E+01, 0.12357280E+01,
0.12461850E+01, 0.13808210E+01, 0.14272730E+01, 0.14243960E+01, 0.13567380E+01}, {0.00000000E+00, 0.25611070E-01, 0.12754350E+00, 0.25478160E+00,
0.44492110E+00, 0.69478690E+00, 0.94321420E+00, 0.10842660E+01, 0.11114100E+01, 0.11717660E+01, 0.12013270E+01, 0.11974630E+01, 0.12071480E+01,
0.13270210E+01, 0.13740830E+01, 0.13774080E+01, 0.13195180E+01}, {0.00000000E+00, 0.24782180E-01, 0.12349270E+00, 0.24702140E+00, 0.43079520E+00,
0.66961560E+00, 0.90070480E+00, 0.10419990E+01, 0.10748770E+01, 0.11318870E+01, 0.11601730E+01, 0.11591990E+01, 0.11681110E+01, 0.12732200E+01,
0.13208930E+01, 0.13304200E+01, 0.12822980E+01}, {0.00000000E+00, 0.23953670E-01, 0.11945270E+00, 0.23930820E+00, 0.41683260E+00, 0.64488400E+00,
0.85957500E+00, 0.99973110E+00, 0.10383450E+01, 0.10920070E+01, 0.11190200E+01, 0.11209340E+01, 0.11290750E+01, 0.12194190E+01, 0.12677040E+01,
0.12834330E+01, 0.12450780E+01}, {0.00000000E+00, 0.23125520E-01, 0.11542330E+00, 0.23164130E+00, 0.40303000E+00, 0.62058620E+00, 0.81989780E+00,
0.95746360E+00, 0.10018120E+01, 0.10521280E+01, 0.10778660E+01, 0.10826700E+01, 0.10900380E+01, 0.11656190E+01, 0.12145140E+01, 0.12364450E+01,
0.12078590E+01}, {0.00000000E+00, 0.22297750E-01, 0.11140440E+00, 0.22401980E+00, 0.38938390E+00, 0.59671140E+00, 0.78172870E+00, 0.91519600E+00,
0.96527960E+00, 0.10122490E+01, 0.10367130E+01, 0.10444060E+01, 0.10510020E+01, 0.11118180E+01, 0.11613240E+01, 0.11894580E+01, 0.11706390E+01},
{0.00000000E+00, 0.21966740E-01, 0.10979970E+00, 0.22098360E+00, 0.38396840E+00, 0.58727810E+00, 0.76689100E+00, 0.89861450E+00, 0.95066660E+00,
0.99629670E+00, 0.10202520E+01, 0.10291000E+01, 0.10353870E+01, 0.10902980E+01, 0.11400480E+01, 0.11706630E+01, 0.11557510E+01}, {0.00000000E+00, 0.21635800E-
01, 0.10819670E+00, 0.21795460E+00, 0.37857710E+00, 0.57791040E+00, 0.75230000E+00, 0.88222970E+00, 0.93617060E+00, 0.98034500E+00, 0.10037900E+01,
0.10137940E+01, 0.10197720E+01, 0.10687780E+01, 0.11187720E+01, 0.11518680E+01, 0.11408630E+01}, {0.00000000E+00, 0.21304910E-01, 0.10659530E+00,
0.21493260E+00, 0.37320990E+00, 0.56860800E+00, 0.73795590E+00, 0.86603980E+00, 0.92178370E+00, 0.96453120E+00, 0.98732880E+00, 0.99848820E+00,
0.10041580E+01, 0.10472570E+01, 0.10974960E+01, 0.11330720E+01, 0.11259750E+01}, {0.00000000E+00, 0.20974080E-01, 0.10499560E+00, 0.21191750E+00,
0.36786650E+00, 0.55937010E+00, 0.72385830E+00, 0.85004820E+00, 0.90749970E+00, 0.94883880E+00, 0.97086750E+00, 0.98348240E+00, 0.98542840E+00,
0.10257370E+01, 0.10762200E+01, 0.11142770E+01, 0.11110870E+01}, {0.00000000E+00, 0.20643310E-01, 0.10339750E+00, 0.20890930E+00, 0.36254660E+00,
0.55019610E+00, 0.7100620E+00, 0.83425720E+00, 0.89332970E+00, 0.93327280E+00, 0.9545730E+00, 0.96767600E+00, 0.97292830E+00, 0.10042170E+01,
0.10549440E+01, 0.10954820E+01, 0.10961990E+01}, {0.00000000E+00, 0.20312590E-01, 0.10180090E+00, 0.20590800E+00, 0.35725000E+00, 0.54108550E+00,
0.69639830E+00, 0.81866860E+00, 0.87925950E+00, 0.91782430E+00, 0.93833940E+00, 0.95223880E+00, 0.95740210E+00, 0.98269670E+00, 0.10336680E+01,
0.10766870E+01, 0.10813110E+01}, {0.00000000E+00, 0.19981940E-01, 0.10020600E+00, 0.20291350E+00, 0.35197660E+00, 0.53203760E+00, 0.68303260E+00,
0.80328170E+00, 0.86528870E+00, 0.90248630E+00, 0.92225340E+00, 0.93687910E+00, 0.94196080E+00, 0.96117640E+00, 0.10123920E+01, 0.10578920E+01,
0.10664230E+01}, {0.00000000E+00, 0.19651340E-01, 0.19992570E-01, 0.19992570E-01, 0.34672600E+00, 0.34672600E+00, 0.52305140E+00, 0.78810330E+00,
0.85141590E+00, 0.88726220E+00, 0.90626930E+00, 0.92157070E+00, 0.92656280E+00, 0.93978100E+00, 0.99111640E+00, 0.10390970E+01, 0.10515350E+01},
{0.00000000E+00, 0.19320800E-01, 0.97020920E-01, 0.19694460E+00, 0.34149810E+00, 0.51412730E+00, 0.65701840E+00, 0.77312980E+00, 0.83763870E+00,
0.87214020E+00, 0.89039120E+00, 0.90629260E+00, 0.91119220E+00, 0.91841270E+00, 0.96984050E+00, 0.10203020E+01, 0.10366470E+01}, {0.00000000E+00, 0.19155560E-
01, 0.96225630E-01, 0.19545650E+00, 0.33889260E+00, 0.50968800E+00, 0.65066110E+00, 0.76572020E+00, 0.83078530E+00, 0.86461660E+00, 0.88248500E+00,
0.89866550E+00, 0.90350760E+00, 0.90771900E+00, 0.95923310E+00, 0.10109050E+01, 0.102902030E+01}, {0.00000000E+00, 0.18990320E-01, 0.95430740E-01,
0.19397010E+00, 0.33629270E+00, 0.50526380E+00, 0.64436350E+00, 0.75836210E+00, 0.82395510E+00, 0.85711740E+00, 0.87460010E+00, 0.89103900E+00,
0.89582710E+00, 0.89702210E+00, 0.94865670E+00, 0.10015070E+01, 0.10217600E+01}, {0.00000000E+00, 0.18907710E-01, 0.95033440E-01, 0.19322750E+00,
0.33499480E+00, 0.50305740E+00, 0.64123640E+00, 0.75470240E+00, 0.82054860E+00, 0.85337690E+00, 0.87066540E+00, 0.88722560E+00, 0.89198540E+00,
0.89166610E+00, 0.94336580E+00, 0.99680830E+00, 0.10180380E+01}, {0.00000000E+00, 0.18825110E-01, 0.94636230E-01, 0.19248530E+00, 0.33369830E+00,
0.50085380E+00, 0.63812360E+00, 0.75105550E+00, 0.81714780E+00, 0.84964220E+00, 0.86673580E+00, 0.88341170E+00, 0.88814230E+00, 0.88630470E+00,
0.93807320E+00, 0.99210950E+00, 0.10143150E+01}, {0.00000000E+00, 0.18742500E-01, 0.94239130E-01, 0.19174350E+00, 0.33240320E+00, 0.49865560E+00,
0.63502520E+00, 0.74742160E+00, 0.81375270E+00, 0.84591340E+00, 0.86281110E+00, 0.87959720E+00, 0.88429770E+00, 0.88093750E+00, 0.93277770E+00,
0.98742500E+00, 0.10105940E+01}, {0.00000000E+00, 0.18659900E-01, 0.93842120E-01, 0.91910220E+00, 0.33110940E+00, 0.49646040E+00, 0.63194100E+00,
0.74380050E+00, 0.81036310E+00, 0.84219030E+00, 0.85889140E+00, 0.87578190E+00, 0.88045120E+00, 0.87556370E+00, 0.92747830E+00, 0.98271180E+00,
0.10068720E+01}, {0.00000000E+00, 0.18164380E-01, 0.91462110E-01, 0.18656250E+00, 0.32337570E+00, 0.48336670E+00, 0.61373240E+00, 0.72234440E+00,
0.79014210E+00, 0.81997090E+00, 0.83546910E+00, 0.85285780E+00, 0.85731920E+00, 0.84316220E+00, 0.89553430E+00, 0.95450100E+00, 0.98453970E+00},
{0.00000000E+00, 0.17338800E-01, 0.87503110E-01, 0.17919530E+00, 0.31059410E+00, 0.46183560E+00, 0.58448710E+00, 0.68760850E+00, 0.75687550E+00,
0.78336700E+00, 0.79675890E+00, 0.81442120E+00, 0.81843870E+00, 0.78844020E+00, 0.84135560E+00, 0.90621840E+00, 0.94731990E+00}, {0.00000000E+00, 0.16513570E-
01, 0.83553600E-01, 0.17186740E+00, 0.29794450E+00, 0.44066010E+00, 0.55656470E+00, 0.65413720E+00, 0.72412840E+00, 0.74726250E+00, 0.75840020E+00,
0.77502300E+00, 0.77892720E+00, 0.73283360E+00, 0.78563640E+00, 0.85501680E+00, 0.90512260E+00}, {0.00000000E+00, 0.15688710E-01, 0.79613440E-01,
0.16457820E+00, 0.28542340E+00, 0.41982990E+00, 0.52989760E+00, 0.62190340E+00, 0.69188040E+00, 0.71162070E+00, 0.72033760E+00, 0.73589940E+00,
0.73855690E+00, 0.67661280E+00, 0.72845640E+00, 0.80031640E+00, 0.85644810E+00}, {0.00000000E+00, 0.14864200E-01, 0.75682480E-01, 0.15732680E+00,
0.27302740E+00, 0.39933450E+00, 0.50441670E+00, 0.59087350E+00, 0.66011360E+00, 0.67641570E+00, 0.68254050E+00, 0.69543120E+00, 0.69712600E+00,
0.62020260E+00, 0.67025210E+00, 0.74246980E+00, 0.80159410E+00}, {0.00000000E+00, 0.14040050E-01, 0.71760600E-01, 0.15011240E+00, 0.26075380E+00,
0.37916350E+00, 0.48005280E+00, 0.56100670E+00, 0.62881210E+00, 0.64416280E+00, 0.64499280E+00, 0.65393840E+00, 0.65446040E+00, 0.56405820E+00,
0.61161750E+00, 0.68232970E+00, 0.74191250E+00}, {0.00000000E+00, 0.13282140E-01, 0.68160360E-01, 0.14350710E+00, 0.24956630E+00, 0.36088350E+00,
0.45856690E+00, 0.53451840E+00, 0.60041520E+00, 0.60998290E+00, 0.61067000E+00, 0.61473810E+00, 0.61398630E+00, 0.51299230E+00, 0.55780620E+00,
0.62584820E+00, 0.68415650E+00}, {0.00000000E+00, 0.12392800E-01, 0.63943490E-01, 0.13579080E+00, 0.23655750E+00, 0.33975220E+00, 0.43440890E+00,
0.50458170E+00, 0.56755550E+00, 0.57326320E+00, 0.57065410E+00, 0.56732860E+00, 0.56483610E+00, 0.45411810E+00, 0.49535020E+00, 0.55915360E+00,
0.61453670E+00}, {0.00000000E+00, 0.10746970E-01, 0.56160980E-01, 0.12180850E+00, 0.21280850E+00, 0.30151230E+00, 0.39244560E+00, 0.45224490E+00,
0.50802090E+00, 0.50647350E+00, 0.49740460E+00, 0.47510450E+00, 0.46867420E+00, 0.34904300E+00, 0.38321660E+00, 0.43746400E+00, 0.48520210E+00},

Advanced Performance Simulation of Gas Turbine Components and Fluid Thermodynamic Properties

```
{0.00000000E+00, 0.99245720E-02, 0.52282350E-01, 0.11456700E+00, 0.20109370E+00, 0.28280560E+00, 0.37271750E+00, 0.42748590E+00, 0.47887580E+00,
0.47366500E+00, 0.46123530E+00, 0.42662810E+00, 0.41787580E+00, 0.29867570E+00, 0.32931990E+00, 0.37846770E+00, 0.42191310E+00}, {0.00000000E+00, 0.97595770E-
02, 0.51507620E-01, 0.11316260E+00, 0.19876310E+00, 0.27909600E+00, 0.36886220E+00, 0.42264060E+00, 0.47309520E+00, 0.46715080E+00, 0.45404040E+00,
0.41673090E+00, 0.40748590E+00, 0.28878270E+00, 0.31872970E+00, 0.36685370E+00, 0.40942840E+00}, {0.00000000E+00, 0.96938170E-02, 0.51197820E-01,
0.11260120E+00, 0.19783200E+00, 0.27761510E+00, 0.36732830E+00, 0.42071210E+00, 0.47078730E+00, 0.46454930E+00, 0.45116620E+00, 0.41275280E+00,
0.40330790E+00, 0.28484250E+00, 0.31451160E+00, 0.36222630E+00, 0.40445210E+00}, {0.00000000E+00, 0.95951820E-02, 0.50733220E-01, 0.11175950E+00,
0.19643660E+00, 0.27539690E+00, 0.36503650E+00, 0.41782980E+00, 0.46733150E+00, 0.46065180E+00, 0.44685890E+00, 0.40676470E+00, 0.39701730E+00,
0.27895020E+00, 0.30820380E+00, 0.35530490E+00, 0.39700720E+00}, {0.00000000E+00, 0.91020720E-02, 0.48411970E-01, 0.10755780E+00, 0.18948110E+00,
0.26436150E+00, 0.35373460E+00, 0.40360140E+00, 0.45013450E+00, 0.44124850E+00, 0.42539610E+00, 0.37644300E+00, 0.36513120E+00, 0.24981560E+00,
0.27701320E+00, 0.32105880E+00, 0.36014290E+00}, {0.00000000E+00, 0.74592150E-02, 0.40695350E-01, 0.93633080E-01, 0.16655000E+00, 0.22821760E+00,
0.31784290E+00, 0.35826890E+00, 0.39382700E+00, 0.37758610E+00, 0.35477750E+00, 0.27053100E+00, 0.25336790E+00, 0.15655600E+00, 0.17723560E+00,
0.21139950E+00, 0.24192680E+00}, {0.00000000E+00, 0.58176580E-02, 0.33010040E-01, 0.79828010E-01, 0.14399060E+00, 0.19300120E+00, 0.28443170E+00,
0.31589150E+00, 0.33902790E+00, 0.31547380E+00, 0.28565660E+00, 0.15641670E+00, 0.13235100E+00, 0.68922690E-01, 0.83656870E-01, 0.10862770E+00,
0.13110480E+00}, {0.00000000E+00, 0.41774040E-02, 0.25354930E-01, 0.66136580E-01, 0.12177830E+00, 0.15863440E+00, 0.25320140E+00, 0.27614580E+00,
0.28566050E+00, 0.25487930E+00, 0.21808620E+00, 0.32783270E-01, 0.58194470E-03, 0.00000000E+00, 0.00000000E+00, 0.12274990E-01, 0.27306910E-01},
{0.00000000E+00, 0.25384580E-02, 0.17728950E-01, 0.52552820E-01, 0.99890380E-01, 0.12504140E+00, 0.22389340E+00, 0.23874360E+00, 0.23364210E+00, 0.19574470E+00,
```

```
0.15205870E+00, 0.00000000E+00, 0.00000000E+00, 0.00000000E+00, 0.00000000E+00, 0.00000000E+00, 0.00000000E+00, 0.00000000E+00 }" />
```

```
</table>
```

```
= <table type="1D" name="PRsurge_vs_Wc" description="Output Intermediate Surge Pressure Ratio">
```

```
<interp default="LINEAR" valid="{LINEAR}" />
```

```
<extrap default="LINEAR" valid="{FORBIDDEN, CONSTANT, LINEAR}" />
```

```
<axis1 id="Wc" description="Corrected Mass Flow Rate Relative to Map Conditions (without applying gamma corrections)(kg/sec)" value="{0.00000000E+00,
0.25869479E+02, 0.43790693E+02, 0.61936034E+02, 0.83698126E+02, 0.10128562E+03, 0.11671552E+03, 0.12660410E+03, 0.13038131E+03, 0.14182339E+03}" />
```

```
<return id="PRsurge" description="Intermediate Surge Pressure Ratio (-)" value="{0.10000000E+01, 0.11824670E+01, 0.14341916E+01, 0.17405149E+01,
0.21761867E+01, 0.25826961E+01, 0.29793764E+01, 0.32532911E+01, 0.33619818E+01, 0.37049075E+01}" />
```

```
</table>
```

```
</map>
```


Chapter 5: References

- [1] General Electric Company, March 1984, "Extended Parametric Representation of Compressor Fans and Turbines (Volume 1 – CMGEN User's Manual (Parametric Compressor Generator))" NASA-CR-174645.
- [2] General Electric Company, March 1984, "Extended Parametric Representation of Compressor Fans and Turbines (Volume 2 – Part User's Manual (Parametric Turbine))" NASA-CR-174645.
- [3] General Electric Company, March 1984, "Extended Parametric Representation of Compressor Fans and Turbines (Volume 3 – MODFAN User's Manual (Parametric Modulating Flow Fan))" NASA-CR-174645.
- [4] Doussinault. M, January 2006, "PROOSIS Standard Component Library: MFT Map Specifications" VIVACE 2.4.4/SM/T/05002.
- [5] Bala, A., Sethi, V. and Jackson, A., (Cranfield University), 2007, "PROOSIS Standard Component Library: Compressor Component Specification" VIVACE 2.4.4/CU/T/04006.
- [6] Bala, A. 2007, "Poly-Dimensional Gas Turbine System Modelling and Simulation", PhD Thesis, School of Engineering – Cranfield University.
- [7] SAE, August 2004, "Aerospace Recommended Practice: Gas Turbine Engine Performance Presentation and Nomenclature for Digital Computers Using Object – Oriented Programming" SAE ARP 5571.

Chapter 6: Project Management, Quality Control and Technology Transfer

Abstract

This chapter provides a useful insight into the “evolution of PROOSIS” from the early stages of development until the final delivery of the gas turbine performance simulation software. The structure of the “VIVACE-ECP” collaboration is presented. Additionally a detailed time-line highlighting the evolution of the project is provided, emphasising the author’s contribution to the project. The importance of quality control for the “VIVACE-ECP” and the various tasks performed to maintain it are described. Technology transfer is a fundamental deliverable of a project such as the “VIVACE-ECP” and the chapter concludes with an analysis of the various channels of technology transfer with an emphasis on the author’s contribution.

The author’s project responsibilities included project management. The author was an ambassador for the Cranfield University gas turbine group and the focal point of communication between Cranfield University and the “VIVACE-ECP” partners. This chapter provides an insight into the challenges faced by a PhD researcher, with respect to technical project management, for a typical modern EU collaborative project.

Chapter 6: Nomenclature

Abbreviations

Name	Description	Unit
ACARE	Advisory Council for Aeronautics Research in Europe	-
AIAA	American Institute of Aeronautics and Astronautics	-
ASEE	American Society of Engineering Education	-
ASME	American Society of Mechanical Engineers	-
CEA	Chemical Equilibrium With Applications Software	-
CU	Cranfield University	-
CUHBR	Engine Model of a Three Spool High Bypass Ratio Turbofan With Separate Exhausts	-
CULBR	Engine Model of a Twin Spool Low Bypass Ratio Turbofan With Mixed Exhausts & Reheat	-
CUTSTJ	Engine Model of a Twin Spool Turbojet (No Reheat)	-
DoW	Description of Work	-
EA	Empresarios Agrupados Internacional	-
ECP	European Cycle Program	-
EL	EcosimPro Language	-
EU	European Union	-
FP	Framework Package	-
GUI	Graphical User Interface	-
HPT	High Pressure Turbine	-
IE	IberEspacio	-
ISABE	International Symposium on Air Breathing Engines	-
ITP	Industria de Turbo Propulsores	-
MFT	Map Fitting Tool	-
MTU	MTU Aero Engines	-
NLR	National Aerospace Laboratory	-
NPSS	Numerical Propulsion System Simulation	-
NTUA	National Technical University of Athens	-

Advanced Performance Simulation of Gas Turbine Components
and Fluid Thermodynamic Properties

Name	Description	Unit
OEM(s)	Original Equipment Manufacturer(s)	-
OO	Object Oriented	-
PRI	Priority Level of User Requirement	-
PROOSIS	Propulsion Object Oriented Simulation Software	-
R&D	Research and Development	-
SAE	Society of Automotive Engineers	-
s-A-s	Share A Space Collaborative Platform	-
SCLib	Standard Components Library	-
SELib	Standard Engines Library	-
SN	Snecma Moteurs	-
SNTSTF	Engine Model of a Twin Spool High Bypass Ratio Turbofan With Separate Exhausts	-
SP	Sub-Project	-
SR	Software Requirement(s)	-
SRD	Software Requirements Document	-
SVVP	Software Validation and Verification Test Report Document	-
UC-DEM(s)	User Case Demonstrator(s)	-
UR(s)	User Requirement(s)	-
URD	User Requirements Document	-
USTUTT	Stuttgart University	-
VIVACE	Value Improvement Through a Virtual Aeronautical Collaborative Enterprise	-
WP	Work Package	-

NB: The nomenclature used in the Appendices is consistent with the nomenclature used in Chapters 2 – 5.

6.1: “VIVACE-ECP” Project Structure

6.1.1: Introduction

This section provides a brief description of the “Value Improvement through a Virtual Aeronautical Collaborative Enterprise” (VIVACE) project. The structure of the VIVACE European Cycle Program (“VIVACE-ECP”) work package (WP) is presented and a timeline highlighting the “evolution of PROOSIS” from the early stages of development until the final delivery of the gas turbine performance simulation software is analysed. A detailed analysis of the main project objectives and deliverables, the project structure and channels of communication, the quality control processes and technology transfer is presented. An emphasis is made on the author’s technical and managerial contribution to the project as a whole including management of the Cranfield University team and the contribution made to technology transfer and dissemination.

6.1.2: The VIVACE Project

NB: Parts of this section are quoted directly from the official website of the VIVACE project^[1]

The VIVACE project^[1] was a European Union integrated project within Framework Package 6 (FP-6). The project began in January 2004 and concluded in December 2007. VIVACE set out to address several of the “Vision 2020” objectives that were formulated by the Advisory Council for Aeronautics Research in Europe (ACARE). The main objectives of VIVACE were to achieve a 5% cost reduction in aircraft development and a 5% reduction in the development phase of a new aircraft design combined with a contribution to a 30% reduction in the lead time and 50% reduction in development costs for a new or a derivative gas turbine.^[1]

The structure of the VIVACE project is highlighted in Fig: 6.1.1. VIVACE consisted of the following three technical sub-projects (SP)^[1]:

- Virtual Aircraft (SP1): A specific global product work area that developed the different elements of the aircraft and worked around the products for design, modelling, interfacing and testing.
- Virtual Engine (SP2) A specific global product work area that developed the different engine modules of the aircraft propulsion system and key areas of multidisciplinary optimisation, knowledge management and collaborative enterprises.
- Advanced Capabilities (SP3): A key integrated work area that developed common tools, methodologies and guidelines that were shared amongst the developments in SP1 and SP2 and provided for further integration between them.

The VIVACE project has provided a base which defines the future of European aeronautical collaborative design. More details about the structure and deliverables of each of these sub-projects are presented in [1].

6.1.3: The “VIVACE-ECP” Work Package - PROOSIS

As highlighted in Fig: 6.1.1, the “VIVACE-ECP” was part of the virtual engine sub-project (SP2) and was worth 6.63 million Euros. The main outcome of the “VIVACE-ECP” was the development of a cost effective gas turbine simulation environment called PROOSIS. PROOSIS, which is the Greek word for “propulsion”, is an acronym for “**PR**opulsion **O**bject **O**riented **S**imulation **S**oftware”. PROOSIS was developed by facilitating optimal use of multi-partner gas turbine performance simulation research and development resources and expertise. PROOSIS is a single framework which provides shared standards and methodologies for the European Union (EU) gas turbine community, including original equipment manufacturers (OEMs), industrial companies, universities and research centres.

Advanced gas turbine performance simulation software is becoming increasingly important in design studies, mission analysis, life cycle analysis, performance prediction and diagnostics. The international gas turbine community is worth thirty billion pounds annually. The EU gas turbine community are major contributors to research and development (R&D) of advanced gas turbine engines and cycles for aircraft propulsion as well as land and sea based applications. Currently the United States of America (USA) are Europe’s biggest gas turbine technology competitors. USA engine manufacturers and research institutes including NASA, General Electric, Pratt and Whitney, Georgia Institute of Technology and Massachusetts Institute of Technology amongst others, have collaboratively developed NPSS ^[3] & ^[4] (Numerical Propulsion System Simulation) as part of the EDS ^[5], ^[6] & ^[7] (Environmental Design Space) project. NPSS is a powerful gas turbine simulation tool with several advanced capabilities. Unfortunately, NPSS and the related technologies are broadly unavailable to the European gas turbine community. PROOSIS is effectively the EU’s equivalent to NPSS. PROOSIS encompasses advanced gas turbine simulation technology which provides significant competitive advantages for EU partners in this highly competitive industry. The main advantages of PROOSIS include:

- A reduction in workload in non-competitive areas both internally and externally
- A reduction in development time and costs for all types of gas turbines or propulsion systems
- A common platform for implementing improvements in engine modelling capabilities.

The PROOSIS application framework conforms to an object oriented (OO) programming schema and fulfils the following object oriented criteria:

- Objects
- Object classes
- Data Encapsulation
- Inheritance and Aggregation
- Polymorphism

This application framework provides modularity, maintainability, reusability and extensibility.

PROOSIS is based on the EcosimPro tool ^[8]. PROOSIS is a sophisticated tool which enables the user to generate mathematical models of a physical system and solve the related complex numerical problems within the gas turbine environment. These models are programmed using a high level programming language known as EL. EL has been

fundamentally created with C++ as a base which gives it the programming power and unbeatable robustness of C++ with complete OO capabilities.

PROOSIS caters for the following four levels of users:

Level 1 Users:

- These users are the modellers of basic libraries.
- They need to have a deep knowledge of the physical and mathematical formulation of the models.
- They need to be familiar with the PROOSIS modelling language.
- They need to know how to interact with thermodynamic packages (map files, fluid functions etc).
- They need to understand the final mathematical models in terms of boundary conditions, DATA etc.

Level 2 Users:

- These users create engine configurations based on existing robust libraries (developed by Level 1 Users).
- They do not program, they only drag and drop component icons to the schematic canvas and then they connect and customise the objects.
- They need to know the mathematical implications of connecting components.
- They are responsible for creating the final mathematical partition based on what they expect the boundaries, DATA etc. to be.

Level 3 Users:

- These users run simulation cases based upon robust mathematical models (developed by Level 1 or Level 2 Users).
- They can prepare design and off-design cases and run the simulations.
- They need to debug the non-convergent cases and to understand the log produced by the simulation.
- They can introduce overall conditions (independent variables and dependent conditions).

Level 4 Users:

- These users simply run PROOSIS using a customer deck.
- They use the models in a limited manner, having only a few options to change.
- They do not need to know how to run PROOSIS.
- The Graphical User Interface (GUI) used for the simulation is limited to allow changes in some boundaries and data.
- The customer decks are generated by Level 3 Users with the aid of wizards.

NB: A detailed description of the PROOSIS 0-dimensional code with respect to the programming language as well as the advantages offered by OO programming is presented in [9].

The structure of the “VIVACE-ECP” work package collaboration is shown in Fig: 6.1.2. Fig: 6.1.3 is a timeline which highlights the “evolution of PROOSIS” from the early stages of development until the final delivery of the gas turbine performance simulation

software. The sections which follow provide an in-depth analysis of Fig: 6.1.2 and Fig: 6.1.3 with respect to the project management structure, the main project objectives, quality control and technology transfer with an emphasis on the author's contribution to each.

6.1.4: "VIVACE-ECP": Main Project Objectives and Deliverables

The User Requirements Document (URD):

Development of the PROOSIS URD began before the official launch of the "VIVACE-ECP" in January 2004. The URD comprises several user requirements (URs) which were collectively defined by each partner based on their gas turbine performance and simulation software expertise. Initially, more than 600 URs were collected, however, many of them were redundant and others were extremely low level requirements. Following a rigorous analysis of these URs, the URs were "filtered" and reduced to 257. A detailed description of each of these URs is presented in the PROOSIS User Requirements Document [11], however a short description of the nature of the URs is provided in Fig: 6.1.4. An example of a UR is shown below:

UR-MOD-USE-01: Inexperienced User

PRI-2: An inexperienced user of PROOSIS (typically a student) with a good knowledge of engine modelling should be capable of running an engine model from the engine library within 5 minutes i.e. running an existing engine model changing only input data.

NB: For each UR, a priority level was defined. The priority levels were as follows:

- PRI-1: Mandatory for the first version of PROOSIS (Jan. 2006)
- PRI-2: Mandatory for the final release of PROOSIS (Dec. 2007)
- PRI-3: Mandatory for the final version of the Advanced Capabilities (Dec. 2007)
- PRI-4: Non-Mandatory, yet "nice to have" at the end of the "VIVACE-ECP"

As shown in Fig: 6.1.3, the URD was "frozen" in August 2005 so that there was sufficient time to map these URs into software requirements and implement them within the project time frame. Any URs received after August 2005 were not implemented unless they were fundamental and therefore high priority.

The Software Requirements Document (SRD):

93% of the final URs were mapped to software requirements (SRs) by Empresarios Agrupados Internacional (the core tool developers). Of these, 95% were fully implemented, 2% were partially implemented and 3% were not implemented in PROOSIS. As shown in Fig: 6.1.3, the SRD was "frozen" in December 2005, however the implementation of the SRs continued for the duration of the project. A detailed description of the SRs and their final status is available in the PROOSIS Software Requirements Document [12].

The PROOSIS Standard Components and Standard Engine Libraries (SCLib and SELib):

The PROOSIS standard components library (SCLib) is a common, flexible and shared database comprising a collection of engine components and functions including

fluid and thermodynamic functions. The fundamental purpose of the SCLib is to establish standards for gas turbine performance simulation throughout Europe and has been developed in collaboration with various industrial companies, research centres and universities as highlighted in Fig: 6.1.2.

Essentially the three partner universities (Cranfield University (CU), the National Technical University of Athens (NTUA) and Stuttgart University (USTUTT) were responsible for the development of the PROOSIS SCLib, based on the URs defined by all the partners. The components and functions developed by each university are shown in Fig: 6.1.5. The components and functions fully and partially developed by the author are also highlighted.

Although the SCLib has been robustly modelled (based on the standards and modelling guidelines highlighted in [13]) to enable the simulation of a wide range of engine configurations, it still has a large element of flexibility which allows the user to perform several calculations using user defined algorithms. The flexibility of the SCLib is further enhanced via the implementation of several switches. These switches allow the user to define the way in which several calculations are performed. Examples of switches and the flexibility of calculations are demonstrated in the various case studies presented in *Chapter 3, Chapter 4* and *Chapter 5*.

As discussed in Section 6.1.3, one of the many advantages of the OO modelling approach is the feature of component hierarchy which serves to minimise code duplication and thereby increase the maintainability of the software. The PROOSIS SCLib hierarchy tree was not static and was continuously optimised as the library expanded by rearranging the modules according to the functionality. Each component “inherits” from abstract (parent) components. An abstract component does not represent a physical component. It holds DATA, ports, declarations and methods that are used as a base by components (children) which inherit from it. The final component hierarchy (abstract level) of the PROOSIS SCLib is shown in Fig: 6.1.6. The hierarchy tree of an individual component may have several “branches” as highlighted for the Compressor component in Fig: 5.1.6. This modelling approach aids extensibility of the SCLib.

As shown in Fig: 6.1.3, three versions of the SCLib were developed. The first version was released in February 2006, the second in December 2006 and the final version was delivered in October 2007. At each of these milestones, development of the SCLib was temporarily frozen so that specification documents could be produced (or updated), the engine library could be updated and rigorous testing of the SCLib and SELib could be performed. The SCLib evolved continuously based on the testing and validation of the components and functions both by the developers and by the industrial partners. A detailed account of the SCLib testing procedure is discussed in *Section 6.1.6*, which highlights the various aspects of quality control.

The PROOSIS SCLib components, fluid functions and thermodynamic functions can be used to simulate a wide range of engine model configurations ranging from a simple single spool turbojet model to a complex mixed exhaust, multi-spool turbofan with several secondary air systems. As shown in Fig: 6.1.2, in addition to the PROOSIS SCLib one of the deliverables of the “VIVACE-ECP” was the PROOSIS standard engines library SELib. The PROOSIS SELib comprises engine models with several configurations which

are kept as simple as possible e.g. no Ducts (pressure losses), simple secondary air systems (bleeds and reintroductions) etc. However, the partitions and experiments for these “simple” models are robust and do not require significant modifications as complexity increases provided the basic configurations remain the same. The final version of the PROOSIS SELib, delivered in December 2007, (as shown in Fig: 6.1.3) was developed by the Stuttgart University team. However, development of the SELib was the result of a detailed troubleshooting analysis performed by all partners on the following engine models (most of which were developed by the Cranfield University (CU) team under the technical lead of the author).

NB: The engine models are listed in chronological order starting with the earliest model developed.

1. The CUTSTJ engine model (Fig: 4.2.2):

- This was the first engine modelled using PROOSIS and was developed by the CU team.
- It is an engine model of a simple twin spool turbojet.
- The CUTSTJ served as an extremely useful model for checking component compatibility, identifying software and coding bugs and troubleshooting.
- The CUTSTJ engine model was used as a base model during VIVACE Forum 2 to demonstrate the advanced capabilities of PROOSIS including component zooming, optimisation, stage-stacking, distributed computing, test analysis and customer deck generation.

NB: The CUTSTJ engine model was used in *Section 4.2.2* to demonstrate the ability of PROOSIS to perform test analysis.

2. The SNTSTF engine model (Fig: 6.1.7):

- This engine model was developed by the Snecma team.
- It is a highly representative engine model of a typical twin spool high bypass ratio turbofan engine with separate exhausts.
- Like the CUTSTJ engine model, the SNTSTF engine model also served as a useful model for checking component compatibility, identifying software and coding bugs and troubleshooting.
- The SNTSTF engine model was used as a base model during VIVACE Forum 2 to demonstrate basic capabilities of PROOSIS including isolated component performance simulation, overall engine steady state (design point and off design) and transient performance simulation.

3. The CUHBR engine model (Fig: 6.1.8):

- This engine model was developed solely by the author to assist with the troubleshooting process for the “inverse design” calculations. (Refer to *Section 4.1.3*).
- It is a representative engine model of a typical three spool high bypass ratio turbofan engine with separate exhausts but was modelled using limited data available from the public domain.
- The CUHBR engine model was used as a training aid to introduce Cranfield University MSc students to PROOSIS during a short course provided by the author.

4. The CULBR engine model (Fig: 6.1.9):

- This engine model was developed by the CU team.
- It is a representative engine model of a typical twin spool low bypass ratio military turbofan engine with mixed exhausts and reheat and was modelled using limited data available from the public domain.
- The CULBR engine model was extremely useful for the development of PROOSIS as it addressed several complex modelling issues associated with the Mixer component, Condi-Nozzle adaptation etc.

NB: All subsequent engine models evolved from the detailed analyses which were performed on the CUTSTJ, SNTSTF, CUHBR and CULBR engine models. These engine models are not however, part of the final SELib.

The SELib is the result of a lengthy testing, validation and troubleshooting process and evolved continuously. All engine models were appropriately updated, tested and validated once a version of the SCLib was frozen as shown on the timeline in Fig: 6.1.3. The final PROOSIS SELib, developed by the USTUTT team, comprises the following engine models:

1. Simple turbojet
2. Turbojet with an Afterburner
3. Twin spool turbofan (separate exhausts)
4. Twin spool turbofan (mixed exhausts)
5. Twin spool geared turbofan (separate exhausts)
6. Twin spool turboprop
7. Single spool turboshaft
8. Twin spool turboshaft
9. Single spool turboshaft with a heat exchanger

The Advanced Capabilities Prototype:

For PROOSIS to maintain its value and significant competitive advantages, one of the main deliverables of the "VIVACE-ECP" was to develop user case demonstrators (UC-DEMs) to demonstrate several advanced performance simulation capabilities using PROOSIS. These various user case demonstrators were used to investigate the feasibility and implementation of three advanced capabilities including:

UC-DEM-1: 3-D Compressor aerodynamic zooming ^{[9] & [14]} (TURBOMATCH ^{[20] & [21]})
3-D Compressor aerodynamic zooming (PROOSIS)
1-D Compressor aerodynamic zooming ^[25]
Distributed simulation ^[25]
Fan blade optimisation ^{[26] & [59]}

UC-DEM-2: Turbine aerodynamic zooming
Secondary air system library
Combustor zooming
Secondary air system optimisation

- UC-DEM-3: Definition of slam experiments
Boundary conditions for high pressure turbine (HPT) aerodynamic zooming
HPT aerodynamic zooming (without the effects of tip clearance)
HPT aerodynamic zooming (including the effects of tip clearance)
HPT Thermo-mechanical model preparation
HPT Thermo-mechanical zooming
HPT Multi-disciplinary zooming

A detailed description of all these user case demonstrators and the associated sub-tasks are highlighted in [22] and [23]. The outcome of each of the sub-tasks is presented in the PROOSIS final test report document [24]. The PROOSIS final test report document [24] is described in more detail in *Section 6.1.6*.

Cranfield University's major contribution to the advanced capabilities prototype was within UC-DEM-1 and involved 3-D Compressor aerodynamic zooming. A brief summary of the analyses performed by the Cranfield University team is presented in *Section 4.2.4*. As outlined in *Section 4.2.4*, the 3-D Compressor aerodynamic zooming studies were a collaborative effort between the author and A. Bala [9]. The author made a significant contribution to the study, in particular to the 0-D performance simulation model used for the 3-D Compressor aerodynamic zooming. A detailed account of Cranfield University's contribution to the advanced capabilities prototype is provided in [9] and [14].

As shown in Fig: 6.1.3, the first version of the advanced capabilities prototype was delivered in June 2006. However, following the release of PROOSIS V2.0 β (which was an improved version of PROOSIS with respect to both the quality of the SCLib and robustness of the core tool) the advanced capabilities prototype was updated and the final version was released in December 2007. Intermediate deliverables for the advanced capabilities (not shown on Fig: 6.1.3) included (in chronological order):

- Blueprint description of prototype (NLR – June 2005)
- Description of physical models used (Cranfield University – December 2005)
- Implementation plan (EA Internacional – June 2006)
- First intermediate version of advanced capabilities (NLR – June 2006)
- Initial prototype and test plan (Snecma – December 2006)
- Test results and modification plan (Snecma – June 2007)
- Final prototype and test description (NLR – December 2007)

The PROOSIS Software:

As shown in Fig: 6.1.3, two main intermediate versions of PROOSIS were released (Version 1 – Prototype (May 2006) and Version 2.0 β (June 2007)). Each of these versions reflected:

- Improvements in the quality of the SCLib (new components / functions and improved robustness of existing components)
- Improvements of the core tool robustness and implementation of new features according to the high priority user requirements)

An important point to note is that developments of the SCLib and the core tool were simultaneous. Consequently, the testing process of the SCLib and the tool as a whole was iterative. The main reason was because the universities were responsible for the development of the SCLib while EA Internacional was responsible for the development of the tool and these tasks were independent. Therefore following every release of PROOSIS the whole SCLib had to be retested and cases did arise where the new versions of PROOSIS introduced new bugs that did not exist in earlier versions. These issues were all resolved before the final delivery of PROOSIS V2.0 in December 2007.

6.1.5: “VIVACE-ECP”: Project Structure and Communication

A well defined project structure and good communication is fundamental for any collaborative project particularly for a project like the “VIVACE-ECP”, which had numerous partners involved, as shown in Fig: 6.1.2 (eleven industrial partners, three universities and two research centres). This section describes the project structure with respect to the break down of tasks and the distribution of responsibilities within the “VIVACE-ECP” work package. Additionally the various channels to facilitate effective communication are presented including the use of collaborative platforms, regular project meetings and workshops to address general or specific modelling issues. A well defined project structure and good communication channels largely contributed to the success of the “VIVACE-ECP”

Project Structure:

The project structure and task distribution of the “VIVACE-ECP” is summarised in Fig: 6.1.10. Fig: 6.1.10 should be viewed in parallel with Fig: 6.1.2. Snecma were the work package leaders for the “VIVACE-ECP” (WP 2.4). A brief description of the various tasks within WP 2.4 is provided below.

Task 2.4.1 (“Functional Requirements”) was lead by Snecma and was the task which involved collecting all the user requirements and preparing the URD as discussed in *Section 6.1.4*.

Task 2.4.2 (“Business Case Definition”) was lead by Snecma and involved preparing a business case to demonstrate the capabilities and benefits of PROOSIS to the European Union commissioners. Cranfield University (and therefore also the author) were not involved with this task.

Task 2.4.3 (“Software Specification and Design”) was lead by the software developers EA Internacional and involved creating the architectural design, as well as mapping the URs to SRs as described in *Section 6.1.4*. As with task 2.4.2, Cranfield University (and therefore also the author) were not involved with this task.

Task 2.4.4 (“SCLib and SELib Development”) was lead by MTU and involved development of the standard component and standard engine libraries. Cranfield University (together with the other partner universities) were heavily involved with this task. A detailed outline of the distribution of the responsibilities for the development of the SCLib and SELib is presented in *Section 6.1.4*, with an emphasis on the author’s contribution.

Task 2.4.5 (“Industrial Core Tool Development”) was lead by EA Internacional and involved rigorous testing and validation of PROOSIS to ensure quality control. Each one of the 257 URs was rigorously tested and a test report document was created highlighting the result of each test. The 257 URs were intelligently distributed amongst all “VIVACE-ECP” partners based on the available resources (time and technical) of each partner at the time.

Task 2.4.6 (“Advanced Capabilities Prototype”) was lead by NLR and involved demonstrating several advanced capabilities including high fidelity (1-D and 3-D) component zooming, distributed computing architecture and multidisciplinary optimisation amongst others. A detailed summary of the advanced capabilities prototype is presented in *Section 6.1.4*. As with task 2.4.4, Cranfield University had a major role to play within this task.

Communication - Collaborative Platforms:

Collaborative platforms are becoming increasingly popular in modern EU collaborative projects due to the advantages they offer with respect to secure data sharing and remote team working. Collaborative platforms were, and are still used for several EU collaborative projects within the sixth framework program (FP6). They will also play a major role for several new projects within FP7.

The following two collaborative platforms were used for the “VIVACE-ECP”:

1. Arttic International Management Services ^[27]
2. Eurostep – Share-A-Space (s-A-s) ^[28]

Arttic International Management Service is a leading company which provides consultancy and management services to international R&D partnerships. Arttic specialises in the following five key areas:

1. R&D strategy consultation
2. Proposal preparation
3. Project management
4. Collaborative platforms
5. Training

“Share-A-Space is a software application that supports cost effective management of product data, both across the product life cycle and across system and company borders. Share-A-Space works alongside existing product data management tools and is extremely quick to set up when compared to such tools. Share-A-space can be purchased or just rented for the life of a collaborative project with the project data being archived to a standard file format on project completion.” ^[28]

After determining the relative advantages and disadvantages of both collaborative platforms, the “VIVACE-ECP” partners unanimously decided to use both Share-A-Space and Arttic. Share-A-Space was used for all the standard component library developments including component/function source files, component/function specification documents, component/function approvals and component default partitions and associated experiments. Arttic was used for all other tasks within WP2.4. The minutes of all the “VIVACE-ECP” meetings, the PROOSIS engine models and all other miscellaneous

communication was done via Arttic. Fig: 6.1.11 and Fig: 6.1.12 are screen shots of the Arttic and Share-A-Space collaborative platforms respectively, as used for the “VIVACE-ECP”.

Communication – Regular Project Meetings and Workshops:

As shown in Fig: 6.1.3, “VIVACE-ECP” technical meetings were held at least once every quarter with just a couple of exceptions. These technical meetings provided an excellent opportunity for each partner to present their work progress and address any general modelling issues. They also provided all partners a good opportunity to effectively liaise in order to discuss the structure of the live demonstrations / presentations for the various VIVACE Forums as well as the demonstration of PROOSIS to the Rolls Royce performance team in Derby.

In addition to the regular “VIVACE-ECP” technical meetings, three modelling workshops were organised (two at Cranfield University and one at USTUTT). These workshops were extremely important for establishing modelling standards and compatibility between the components and functions developed by the different universities. They also provided a good opportunity to address any compatibility issues between the SCLib and the core tool and consequently establish optimum modelling techniques to ensure robust modelling of the SCLib (by the universities) and the core tool (by the software developers – EA Internacional).

Additionally, a specific workshop was organised specifically for the author and EA Internacional to investigate an “intelligent” means of implementing the flow continuity model. A summary of the investigation is presented in *Section 2.3.6*.

As discussed in *Chapter 5*, one of the author’s major contributions to the SCLib was the development of an extended parametric representation of compressor characteristics. The development of the Compressor component with MFT (map fitting tool) maps was a collaborative effort between the author and M. Doussinault (Snecma). As shown in Fig: 6.1.3, a specialist “MFT modelling (week long) workshop” was organised at the Snecma plant in Villaroche. This proved to be an extremely successful and optimum (both in terms of the requirements and time) approach to develop the MFT capabilities.

6.1.6: “VIVACE-ECP”: Quality Control

Quality control is an essential part of any project, particularly for large collaborative projects like the “VIVACE-ECP”, which have several partners from various backgrounds. Quality control is also particularly important for the development of a new gas turbine performance simulation software with respect to value, validity, maintainability and extensibility. Brief descriptions of the various quality control processes are highlighted below, particularly for the PROOSIS SCLib.

SCLib Component and Function Specifications:

A detailed breakdown of the distribution of the responsibilities for the development of the PROOSIS SCLib is provided in Fig: 6.1.5. Each SCLib developer was responsible for developing a specification document to describe the performance model of each

component / function developed. All the specification documents produced for the PROOSIS SCLib were uploaded and modified using the s-A-s collaborative platform. The author was primarily responsible for developing the following specification documents:

- Burner / Afterburner component specification document
- Duct component specification document
- Flow splitter component specification document
- Fluid model specification document
- Thermodynamic functions (flow continuity model) specification document
- Heat exchangers (regenerators, recuperators, intercoolers) specification document

NB: The specification document of the Burner /Afterburner component is based on the work presented in *Section 3.1*.

The fluid model and flow continuity model specifications are based on the work presented in *Section 2.1* and *Section 2.3* respectively.

The author also made valuable contributions to the following specification documents which were developed by the Cranfield University team:

- Compressor component specification document
(The author made a major contribution to the description of the PROOSIS Compressor MFT component based on the model presented in *Chapter 5*.)
- Fan component specification document
- Inlet component specification document

NB: The specification document of the Compressor component includes a detailed description of the CompressorMFT component which is based on the work presented in *Section 5.2*.

A typical (component) specification document comprises a comprehensive description of the component with respect to:

1. The component's hierarchical structure
2. The component's ports
3. The various models of the component (e.g. pressure loss models, energy balance models etc)
4. The component's calculations (with detailed descriptions of all equations)
5. The component's specific switches
6. The component's PROOSIS icon(s)
7. Comments regarding the component's current limitations etc.
8. References

The fluid model specification provides a comprehensive description of the following:

1. The various fluid model tables generated using the CEA ^[29] & ^[30] software developed by NASA
2. Graphical plots of the various fluid model properties
3. Definition of input and output variables for the fluid model functions
4. The fluid model calculations (with detailed descriptions of all equations)
5. The fluid model switches and data files.

6. References

The flow continuity model specification provides a comprehensive description of the various thermodynamic functions with respect to:

1. The inputs required and the outputs which are calculated
2. A breakdown of the calculations of each thermodynamic function (with detailed descriptions of all equations)
3. An example of a typical thermodynamic function call
4. References

Since a complete specification document is quite comprehensive and therefore “bulky”, a complete specification has not been included as an appendix. However, Appendix 1, Appendix 2 and Appendix 3 are the table of contents for the Burner component, Fluid model and Flow continuity model specifications respectively. These appendices provide a good indication of the structure of the specification documents for the PROOSIS SCLib. The complete specification documents for all the components and functions highlighted in Fig: 6.1.5 are available from [31] – [52]. All the specification documents were merged into a single document entitled “Physical Modelling Specifications” [53] by H. Gonser (MTU) (who was the task 2.4.4 leader). The “Physical Modelling Specifications” document was revised following revisions of the SCLib and the final version will be provided as a manual to users of PROOSIS V2.0.

Approval of the SCLib Components and Functions by the Industrial Partners:

As discussed in *Section 4.1.2*, each component and function developed for the PROOSIS SCLib was validated by both a SCLib developer (from one of the three partner universities) and an industrial partner who was responsible for the quality control of that particular component or function.

For example:

As discussed in *Section 3.4*, the Burner Component was developed by Cranfield University, validated by Cranfield University using TURBOMATCH [20] & [21] and further validated and tested by the industrial partner MTU using their in-house performance simulation tool (MOPS).

In addition to the distribution of component and function development tasks between the SCLib developers, Fig: 6.1.5 also highlights the industrial partner responsible for testing and validating a particular component or function. Rigorous testing and validation analysis were performed by both SCLib developers and industrial partners (using either their in-house (legacy) or commercially available gas turbine performance simulation software e.g. GasTurb^[56]) following the delivery of a new version of the SCLib. Each industrial partner was responsible for producing a test report for the component or function tested followed by an approval “certificate”. All the test reports, produced by each industrial partner were then merged into a single document entitled “Test Definitions and Reports”^[54].

A typical test report produced by MTU for the Burner component (which was developed by the author) is presented in Appendix 4, as an example.

NB: Appendix 4 has been extracted from [54].

A typical approval “certificate” produced by Snecma, for the thermodynamic functions (which were developed by the author for the flow continuity model) is presented in Appendix 5, as an example.

Following the rigorous testing by the industrial partners, any open issues or problems were addressed by the SCLib developers and resolved before the delivery of the version of the SCLib.

Software Validation and Verification Test Reports:

As discussed in *Section 6.1.5*, and shown in Fig: 6.1.10, task 2.4.5 (“Industrial Core Tool Development”) was lead by EA Internacional and involved rigorous testing and validation of PROOSIS to ensure quality control. Each one of the 257 URs was rigorously tested and a test report document (known as the “Software Validation and Verification Report” (SVVP) [55]) was created highlighting the result of each test. The 257 URs were intelligently distributed amongst all “VIVACE-ECP” partners based on the available resources (time and technical) of each partner at the time.

The URs which the Cranfield University team were responsible for testing (under the technical leadership of the author) are highlighted below:

NB: Refer to Fig: 6.1.4 for the nomenclature used to define the URs.

Refer to *Section 6.1.4* for the definition of the priority levels (PRI) of the URs

The definitions of the URs below, are identical to those in the URD^[11]

UR-MOD-MAT-11: Definition of Tearing Relations inside Components

PRI-1: It should be possible to define tearing variables inside a component (refer to the “Glossary” section of the thesis). These variables are proposed to the user when the mathematical model is created. Only the tearing variables to make the model coherent will be proposed by the boundary selection wizard. However, it will always be possible for the user to select other tearing variables.

UR-MOD-USE-01: Inexperienced User

PRI-2: An inexperienced user of PROOSIS (typically a student) with a good knowledge of engine modelling should be capable of running an engine model from the engine library within 5 minutes i.e. running an existing engine model changing only input data.

UR-LIB-CMP-01: Use of Terminal Components

PRI-1: Unconnected input ports in final models should be connected to “terminal components” to impose boundary conditions. It should not be necessary to connect output ports to end caps (e.g. for shafts or gas paths).

UR-LIB-CMP-14: Dynamic Effects to be Modelled

PRI-2: PROOSIS should incorporate the following dynamics: rotor dynamics, volume dynamics, and heat soakage. To be defined in the SCLib.

UR-ADV-ZOO-01: Zooming Capability

PRI-3: PROOSIS should be capable of zooming. Zooming means using a multi-dimensional code for simulating a component (or a subcomponent, thermodynamic or multi-disciplinary) instead of the usual 0-D representation. Specific ports have to be developed to convert 0D component boundary conditions to multi-dimensional boundaries (1D mean-line, 3D CFD etc) and vice-versa. Component interfaces must use object orientation philosophy.

UR-ADV-ZOO-02: Single Module Zooming

PRI-1: It should be possible to run a single module in zooming mode (component or assembly of components) under given boundary conditions, without modelling the whole engine component.

UR-ADV-ZOO-04: Distortion Modelling

PRI-3: PROOSIS should allow the modelling of non-axisymmetric effects e.g. (inlet distortion, pattern formation at the Turbine inlet, etc.).

UR-ADV-MUL-02: Multidisciplinary Capabilities

PRI-3: PROOSIS should be capable of building multidisciplinary models (e.g. electrics, electronics, mechanics, thermal, thermodynamics, chemicals, fluid-dynamics, emissions, sound, vibration, mechanical behaviour, etc). In particular, heat soakage should be the first step of multi-disciplinary and zooming capabilities.

As an example, the test report for UR-ADV-MUL-02 is provided in Appendix 6. This report is representative of the reports generated for all URs (tested by all the “VIVACE-ECP” partners).

NB: Appendix 6 has been extracted from the Cranfield University specific SVVP test report document (i.e. before all the test reports were merged into the final SVVP test report ^[55]).

A summary of the test results of all the 257 final URs is provided below ^[55].

- Priority level 1: 90% of the URs were implemented, 82% of the tests were successful
- Priority level 2: 68% of the URs were implemented, 47% of the tests were successful
- Priority level 3: 71% of the URs were implemented, 64% of the tests were successful
- Priority level 4: 62% of the URs were implemented, 54% of the tests were successful

6.1.7: “VIVACE-ECP”: Technology Transfer

Technology transfer is a fundamental deliverable of a collaborative project such as the “VIVACE-ECP”. This section highlights the various channels of technology transfer within the “VIVACE-ECP” with an emphasis on the author’s contribution.

VIVACE Forums:

The VIVACE Forums were primarily set-up for the following reasons:

1. The Forums served as a communication channel between all the VIVACE work packages (shown in Fig: 6.1.1). The Forums provided a good opportunity for each work

package to demonstrate their progress (tools developed, analyses performed etc) with respect to milestone deliverables defined for their work package in the VIVACE “Description of Work” (DoW) document.

2. The Forums provided an opportunity for the EU commissioners to ensure each work package was progressing well and the allocated budget was being used effectively. Following their observations, the EU commissioners subsequently “flagged” each work package as follows:
Green Flag: “All clear” (Work progressing well)
Amber Flag: “Proceed with caution” (Some concerns expressed, which needed to be resolved)
Red Flag: “Stop” (Major actions required to resolve fundamental problems)

NB: The “VIVACE-ECP” was a relatively smooth sailing work package, which mostly progressed with green flags with the odd amber flags on rare occasions, when there were slight delays with certain deliverables.

3. The VIVACE Forums were open to the general public (including the press) and provided an excellent opportunity for the VIVACE partners to market the tools and methodologies developed as part of their work package.

As shown in Fig: 6.1.3, three VIVACE Forums were held.

VIVACE Forum 1^[56] was held at the University of Warwick in the United Kingdom (20th – 21st September 2005). A detailed guide of the structure of VIVACE Forum 1 including all the presentations (of all the work packages) is available on the VIVACE Forum 1 official website^[56]. The “VIVACE-ECP” partners used Forum 1 as a platform to introduce PROOSIS to the other VIVACE partners, the European commissioners and the general public. The “VIVACE-ECP” work package demonstration was split into three parts. The first part involved a general presentation of the various capabilities of PROOSIS. The second part involved a live demonstration using the first PROOSIS prototype. The final part involved a presentation (delivered by Cranfield University) regarding the advanced capabilities of PROOSIS. A detailed guide of the structure of VIVACE Forum 1 including all the presentations (of all the work packages) is available on the VIVACE Forum 1 official website^[56].

VIVACE Forum 2^[57] was held at the World Forum Convention Centre in The Hague (24th – 26th October 2006). VIVACE Forum 2 was built around a storyboard with “acts” and “scenes” which reflected the methods and tools developed by the various work packages. A detailed guide of the structure of VIVACE Forum 2 including a detailed breakdown of all “acts” and “scenes” is available on the VIVACE Forum 2 official website^[56]. The “VIVACE-ECP” fell under Act 4 (“Design, Performance, Testing and Simulation Validation”) Scene 1 (“Engine Performance: Integrating the Components”). Between the introduction and conclusion (provided by M. Doussinault (Snecma) and P. Cobas (EA Internacional)), Act 4, Scene 1 comprised six sub-scenes. A brief description of each of these sub-scenes is provided below with an emphasis on the author’s contribution.

Act 4 – Scene 1 – Sub-scene 1 (A4S1S1): “Building a collaborative engine model”
“Actors”: M. Doussinault (Snecma) & V. Sethi (Cranfield University)

When developing a collaborative engine model, an integrator is responsible for the engine architecture while the various partners are responsible for individual components. A4S1S1 included a live demonstration of this. The integrator first created a skeletal model of a twin spool turbojet using a high pressure compressor component with “no-maps”. He then ran a design point simulation of the engine model and sent the results to a partner responsible for developing the high pressure Compressor component accompanied with a work request, using the s-A-s collaborative platform (refer to *Section 6.1.5*).

The partner subsequently performed an isolated design point calculation of a Compressor component (with a new map) using boundary conditions and DATA from the results file provided by the integrator. The partner then customised the Compressor component by hard coding the various map scaling factors obtained from the “inverse-design” simulation (refer to *Section 4.1.3*), before responding to the work request and uploading the customised compressor component with the new map on s-A-s.

The integrator subsequently replaced the high pressure Compressor component (with “no maps”) with the customised Compressor component developed by the partner and added the map file to the SCLib “maps” folder. Finally the integrator ran several steady state (design point and off-design) and transient graphical simulations for the twin spool turbojet model.

Act 4 – Scene 1 – Sub-scene 2 (A4S1S2): “Developing external Libraries”
“Actors”: M. Doussinault (Snecma) & A. Alexiou (NTUA)

For preliminary performance calculations, it is common to keep an engine model as simple as possible. However, for more detailed analyses, a more accurate representation of the model (in particular the secondary air system) is necessary. A4S1S2 included a live demonstration of the development of a secondary air system library which was then integrated in the twin spool turbojet engine model thereby yielding more realistic and accurate results.

Act 4 – Scene 1 – Sub-scene 3 (A4S1S3): “Secondary Air System Optimisation”
“Actors”: M. Doussinault (Snecma) & R. Coelho (Cenaero)

A4S1S3 included a live demonstration of the optimisation of the secondary air system by Cenaero, using their in-house legacy optimisation software MAX^[26] & ^[59].

Act 4 – Scene 1 – Sub-scene 4 (A4S1S4): “Distributed Architecture and Zooming”
“Actors”: O. Kogenhop (NLR) & A. Alexiou (NTUA)

A4S1S4 included a live demonstration of 1-D compressor zooming via a distributed computing network. The distributed computing capability was demonstrated by creating higher fidelity Fan characteristics by remotely executing a proprietary 1-D compressor stage stacking FORTRAN function. The work presented during the live demonstration was based on **[25]**.

Act 4 – Scene 1 – Sub-scene 5 (A4S1S5): “Customer Decks”

“Actors”: V. Sethi (Cranfield University) & A. Alexiou (NTUA)

A4S1S5 included a live demonstration which involved generating a “stand-alone” customer deck (using the PROOSIS deck generation wizard) and using a customer deck in “sub-program” mode. A brief description of the PROOSIS “stand-alone” deck is presented in *Section 4.2.3*.

Act 4 – Scene 1 – Sub-scene 6 (A4S1S6): “Test Analysis”

“Actors”: V. Sethi (Cranfield University) & A. Alexiou (NTUA)

A4S1S6 included a live video (developed by USTUTT) which demonstrated the capability of PROOSIS to perform test analysis via a suitable ANSYN (analysis by synthesis technique). A detailed description of the test analysis capability of PROOSIS is presented in *Section 4.2.2*.

One of the outcomes of the “VIVACE-ECP” Forum 2 demonstrations was that they triggered a conversation between the “VIVACE-ECP” partners and the Rolls Royce performance team. As shown in Fig: 6.1.2 and Fig: 6.1.10 Rolls Royce was the only major European engine manufacturer or OEM (original equipment manufacturer) who did not participate in the “VIVACE-ECP”. The Rolls Royce representative (although not a performance expert) was suitably impressed with PROOSIS and following correspondence between the “VIVACE-ECP” partners and the Rolls Royce performance team, a PROOSIS demonstration was held at the Rolls Royce plant in Derby (February 2006). The demonstration was similar (although significantly more technical) to that delivered during VIVACE forum 2. The author played a significant role both in organising and delivering the demonstration. The response from the Rolls Royce team was encouraging and they expressed an interest in “perhaps” participating in the development of PROOSIS in CRESCENDO which is the sequel to VIVACE and is scheduled to begin in 2009.

VIVACE Forum 3 ^[58] was held at the Diagona Congress Centre in Toulouse (17th – 19th October 2006). VIVACE Forum 3 was less technical than Forum 2 and Forum 1 and was mainly aimed at the European commissioners and the press. Each work package was required to provide a brief summary of their achievements and contribution to the overall VIVACE objectives. As mentioned in *Section 6.1.2*, the main objectives of VIVACE were to achieve a 5% cost reduction in aircraft development and a 5% reduction in the development phase of a new aircraft design combined with a contribution to a 30% reduction in the lead time and 50% reduction in development costs for a new or a derivative gas turbine.^[1] A detailed guide of the structure of VIVACE Forum 3 including all the presentations (of all the work packages) is available on the VIVACE Forum 3 official website ^[58]. Although the “VIVACE-ECP” presentations were similar to those given during Forum 1 and Forum 2, they were far less technical and provided a general overview of the capabilities of PROOSIS. There was however, a “PROOSIS stand” outside the main auditoriums where live demonstrations of PROOSIS were run. A “PROOSIS poster” (developed courtesy of NTUA) was also displayed at the stand. An image of the “PROOSIS poster” is provided in Appendix 7.

Advanced Performance Simulation of Gas Turbine Components and Fluid Thermodynamic Properties

The final deliverable of PROOSIS with respect to technology transfer was the PROOSIS training course, which was hosted by EA Internacional in Madrid (3rd – 5th December 2007). The PROOSIS training course was primarily geared towards the performance simulation teams of the “VIVACE-ECP” partner companies. The main objective of the training was to introduce the various capabilities of PROOSIS to the trainees so that (with practice) they could become proficient users of PROOSIS. The PROOSIS training was delivered by A. Rueda (EA Internacional), A. Alexiou (NTUA), B. Banzhaf (UTUTTT) and the author (Cranfield University) with the aid of live demonstrations, presentations, videos and a comprehensive training manual. The training course contained elements which were suitable for all PROOSIS user levels (refer to *Section 6.1.3*) and covered the following topics, which were delivered in the following order.

- Topic 1: Introduction to PROOSIS
- Topic 2: Basic EL description (components, ports, functions etc.)
- Topic 3: Creation of partitions and experiments
- Topic 4: Standard components library (hierarchy, fluid and thermodynamic functions, design and off-design isolated component simulations)
- Topic 5: Calculation wizards (steady state design and off-design, transient, parametric, sensitivity analysis)
- Topic 6: Standard engines library (engine configurations, design and off-design calculations)
- Topic 7: Customer Decks
- Topic 8: Connection with Microsoft Excel
- Topic 9: Advanced Capabilities (connection to external functions, component zooming and distributed simulations)

In addition to the preparation and delivery of the training material, the author was also responsible for preparing a “PROOSIS training questionnaire” and collecting and analysing the results. The main feedback regarding the quality (content and delivery) of the training and the PROOSIS tool itself is highlighted below:

- A general consensus was that PROOSIS already seems like a very powerful and “complete” tool.
- Trainees suggested making PROOSIS familiarisation a pre-requisite before future training sessions to optimise the benefits from the training.
- It was suggested that future training courses should be split and customised for specific user levels of PROOSIS. Some trainees felt that the exercises were covered too slowly whilst others felt that they were covered too fast. Some trainees felt that the exercises were too simple whilst others suggested they were too complex.
- Possible improvements to PROOSIS which were highlighted by the trainees include:
 1. Improving the wizards
 2. Improving the customer decks
 3. Improving the debugging process and debugging reports
 4. Improving the connections to external tools

5. Improving the test analysis process (catering for data reduction)
6. Improving the partitions editor (boundary selection wizard)
7. Increasing the options for reporting results (including creating a standard output file format)
8. Including nomenclature aliases between PROOSIS object oriented nomenclature and conventional gas turbine nomenclature
9. Allow for “multi-partitions” for each point of a multipoint design (e.g. specifying fuel flow as a boundary for the first point and burner outlet total temperature as a boundary for the next etc.)

6.1.8: Technology Transfer: The Author’s Contribution to Dissemination

In addition to contributing to technology transfer within the “VIVACE-ECP”, the author also made other significant contributions to knowledge and gas turbine performance simulation technology. This section highlights the author’s various conference publications as well as the contribution made to other research projects.

A list of the author’s conference publications is provided below.

Published Papers:

“PROOSIS – A Collaborative Venture for Gas Turbine Performance Simulation using an Object Oriented Programming Schema” ^[10]

Conference: ISABE 2007

Paper Reference: ISABE–2007–1357

Authors: V. Sethi, A. Bala, E. Lo Gatto, V. Pachidis and P. Pilidis

NB: The abstract of this publication is presented in Appendix 8.

“Study of VSV Effects on Performance via an Integrated Aerodynamic Zooming Process” ^[14]

Conference: 43rd AIAA/ASME/SAE/ASEE Joint Propulsion Conference

Paper Reference: AIAA–2007–5046

Authors: A. Bala, V. Sethi, E. Lo Gatto, V. Pachidis and P. Pilidis

NB: The abstract of this publication is presented in Appendix 9.

Paper Accepted for Publication (Final Draft Accepted):

“Advanced Performance Modelling of Fluid Thermodynamic Properties for Gas Turbine Performance Simulation” ^[15]

Conference: ASME Turbo Expo 2008

Paper Reference: ASME GT-2008-51126

Authors: V. Sethi, F. Diara, S. Atabak, A. Jackson and P. Pilidis

NB: The abstract of this publication is presented in Appendix 10.

Contribution to Research Projects:

The author also provided the technical lead for several MSc and visiting student research projects including:

“Implementation of Accurate Gas Properties on Gas Turbine Simulations” [16]

NB: The abstract of this MSc thesis is presented in Appendix 11.

“Development of Accurate Fluid Models for Gas Turbine Performance Calculations” [17]

NB: The abstract of this visiting student’s research report is presented in Appendix 12.

“Advanced Modelling of Fluid and Thermodynamic Functions for Gas Turbine Mixers and Nozzles” [18]

NB: The abstract of this MSc thesis is presented in Appendix 13.

“Advanced Performance Simulation of Gas Turbine Burners and Afterburners” [19]

NB: The abstract of this MSc thesis is presented in Appendix 14.

The author played a vital role in the management of the Cranfield University technical team which primarily comprised the author, a doctoral researcher and the several researchers mentioned above. A complimentary doctoral thesis to this doctoral thesis is highlighted below and the author strongly recommends that (in addition to the theses and reports highlighted above) it should be read in parallel with this thesis.

“Poly-Dimensional Gas Turbine System Modelling and Simulation” [9]

NB: The abstract of this PhD thesis is presented in Appendix 15.

Chapter 6: Figures

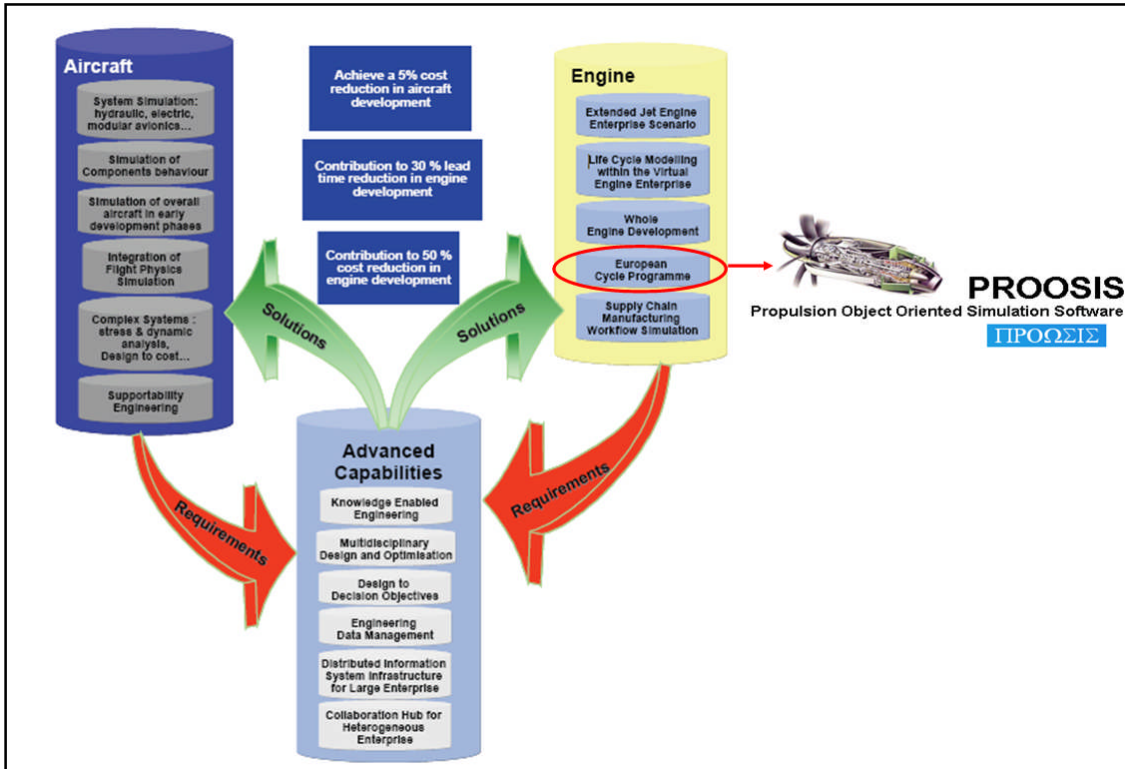


Fig: 6.1.1 Structure of the VIVACE Project [1] & [2]

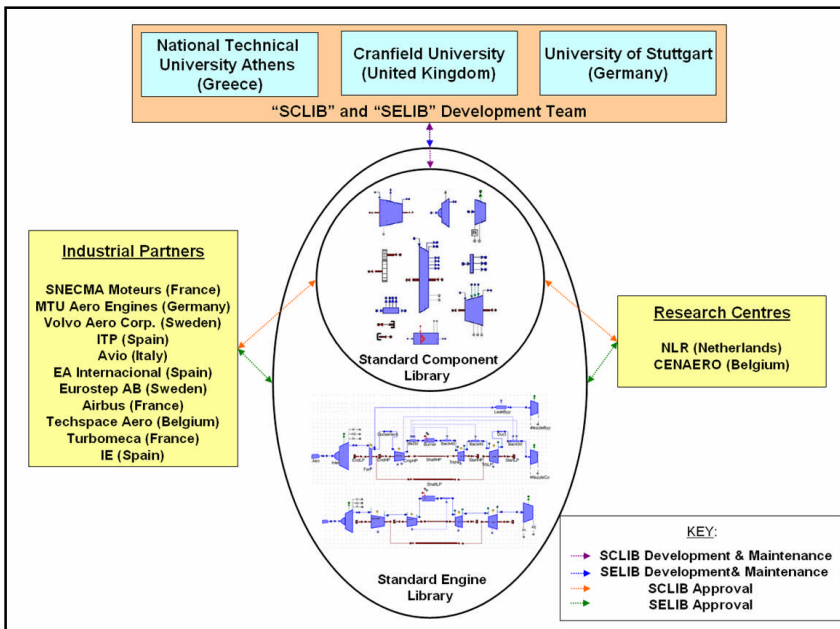


Fig: 6.1.2 Structure of the "VIVACE-ECP" Work Package Collaboration [10]

Advanced Performance Simulation of Gas Turbine Components
and Fluid Thermodynamic Properties

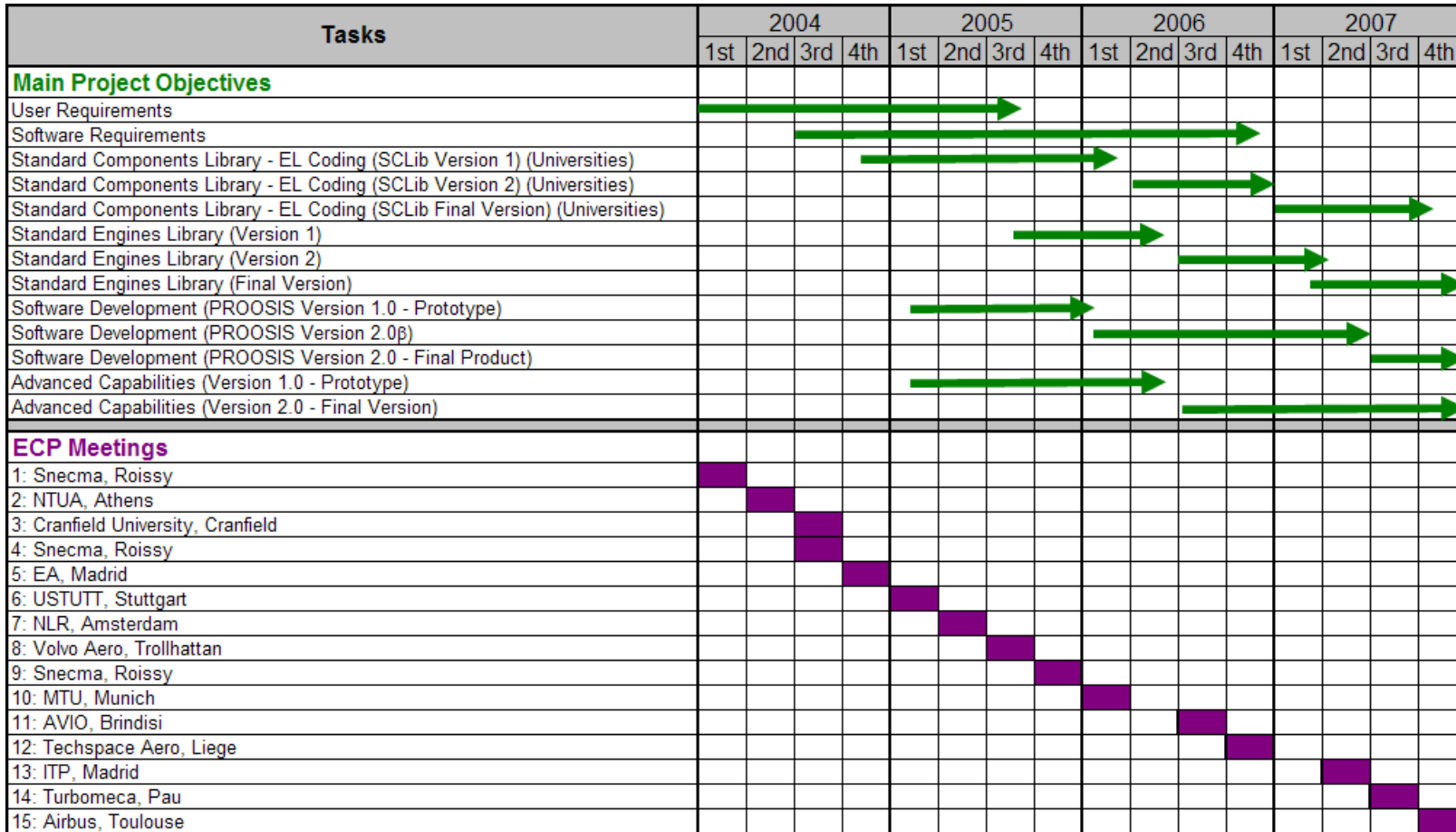


Fig: 6.1.3 Timeline highlighting the “evolution of PROOSIS” within the “VIVACE-ECP” Work Package

Advanced Performance Simulation of Gas Turbine Components
and Fluid Thermodynamic Properties

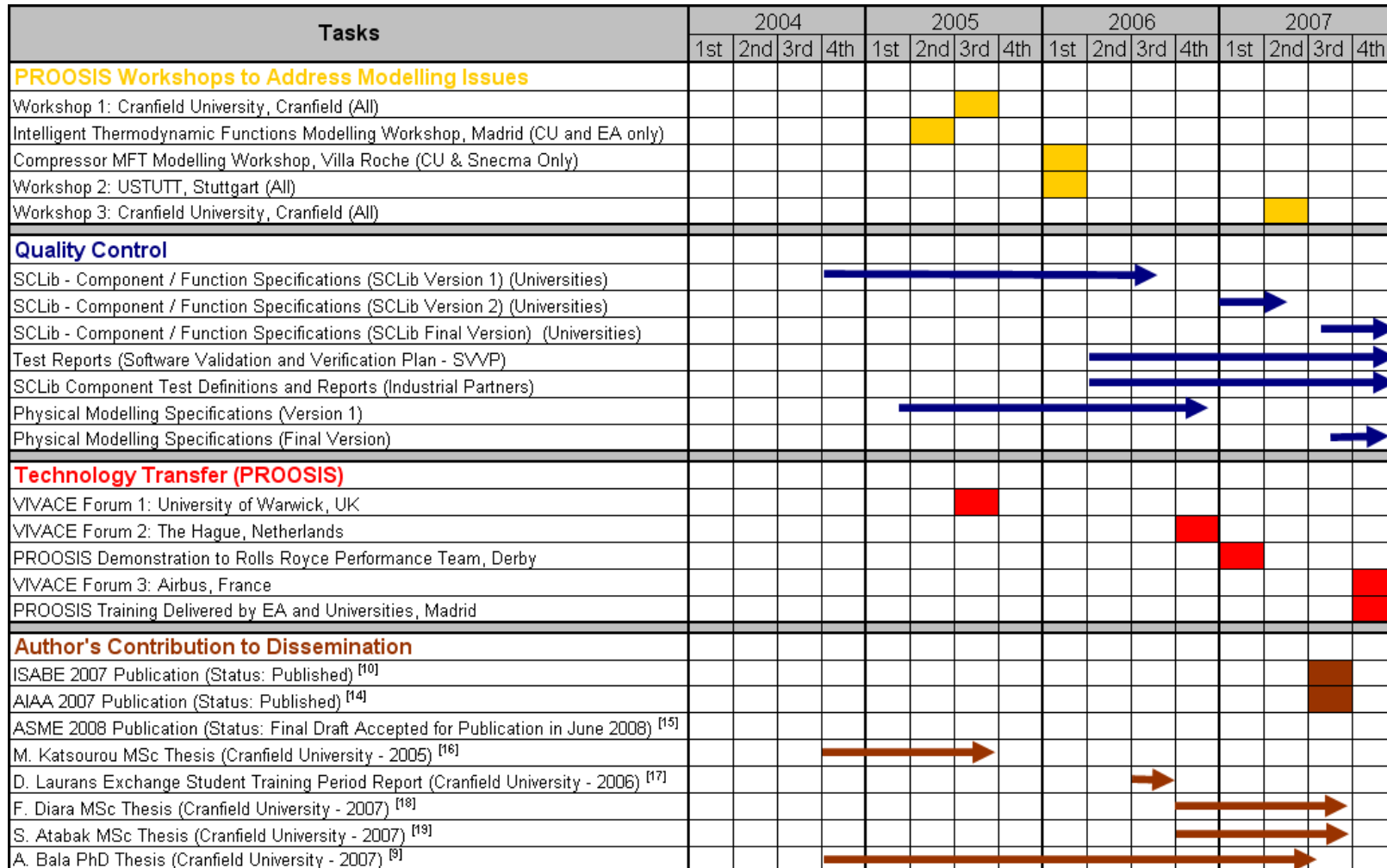


Fig: 6.1.3 (contd.) Timeline highlighting the “evolution of PROOSIS” within the “VIVACE-ECP” Work Package

Advanced Performance Simulation of Gas Turbine Components
and Fluid Thermodynamic Properties

<u>Main Category</u>	<u>Sub-Topic</u>	<u>Description</u>
MOD	MOD-GEN	General modelling (components, ports, functions, maps, libraries etc.)
	MOD-PML	PROOSIS modelling language
	MOD-PPP	Pre and post processing
	MOD-MAT	Mathematical capabilities
	MOD-USE	Ways to use models (experiments, design, off-design etc.)
	MOD-DEB	Debugging and error detection of models
	MOD-USR	General requisites for user management
	MOD-MAN	Management of models
	MOD-CUS	Customer deck generation and external usage of PROOSIS
	GUI	GUI-TED
GUI-GED		Editing of models in graphical format
GUI-GRU		Running graphical simulations
LIB	LIB-FUN	Libraries of functions (Fortran, C, C++ etc.)
	LIB-MAP	Libraries of standard maps
	LIB-POR	Standard ports
	LIB-CMP	Standard components
	LIB-MIS	Miscellaneous
STA	STA-SOF	Software standards
	STA-LIB	PROOSIS library standards
	STA-FIL	Format of files
DOC	DOC-SOF	Software documentation
	DOC-LIB	Documentation of libraries
ADV	ADV-ZOO	Zooming
	ADV-DIS	Distributed calculation, real time, grid computing etc.
	ADV-MUL	Multidisciplinary capabilities
	ADV-OPT	Optimisation
	ADV-CON	Connection with other tools

Fig: 6.1.4 Categorized description of PROOSIS User Requirements

Advanced Performance Simulation of Gas Turbine Components
and Fluid Thermodynamic Properties

<u>Cranfield University</u>		<u>Testing & Validation</u>
Burner / Afterburner component	✓✓	MTU
Compressor components ((n) bleeds / no bleeds, BETA / MFT maps)	✓	Snecma
Duct components ((n) bleeds / no bleeds, BETA / MFT maps)	✓✓	Avio
Fan components ((n) bleeds / no bleeds, BETA / MFT maps)	✓	Snecma
Flow splitter components ((n) outlets)	✓✓	NLR
Fluid model and fluid model functions	✓✓	NLR
Heat exchangers (regenerators, recuperators, intercoolers)	✓✓	NLR
Inlet component	-	MTU
Thermodynamic functions	✓✓	Snecma
<u>National Technical University of Athens</u>		
Atmosphere component	-	NLR
Burner / Afterburner emissions component	-	MTU
Casing component	-	Snecma
Performance monitor components (aero / stationary)	-	Avio
Ports	-	MTU
Probe components ((n) sensor channels)	-	Snecma
Turbine components ((n) re-intros / no re-intros, ZETA / MFT maps)	-	MTU
<u>Stuttgart University</u>		
Gear component ((n) output shafts)	-	AVIO
Mixer components ((n) inlets)	-	ITP
Nozzle components (convergent, condi)	-	ITP
Propeller component	-	Turbomeca
Shaft component (shaft start, shaft end, shaft)	-	Turbomeca
<u>Key</u>		
Components / Functions Fully Developed by The Author	✓✓	
Components / Functions Partially Developed by The Author	✓	
Components / Functions Developed by Colleagues / Other Partners	-	

Fig: 6.1.5: PROOSIS SCLib Component / Function Development Responsibilities

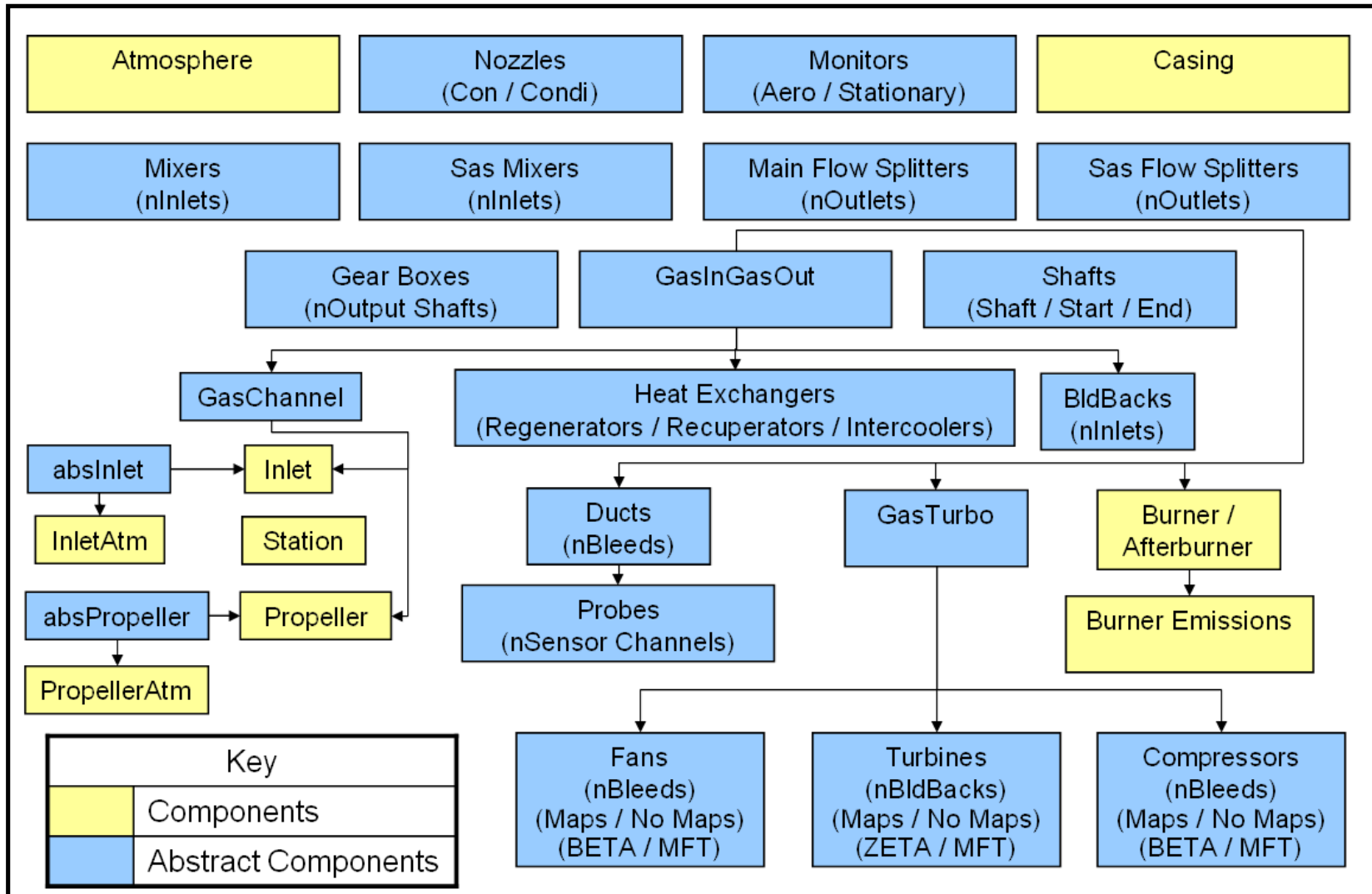


Fig: 6.1.6: SCLib Component Hierarchy (Abstract Level)

Advanced Performance Simulation of Gas Turbine Components and Fluid Thermodynamic Properties

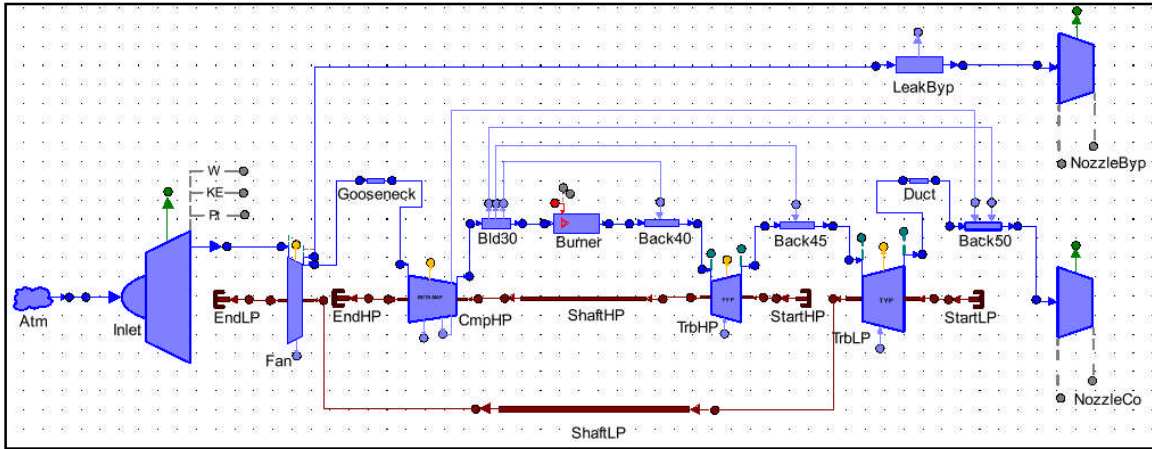


Fig: 6.1.7: SNTSTF Engine Model

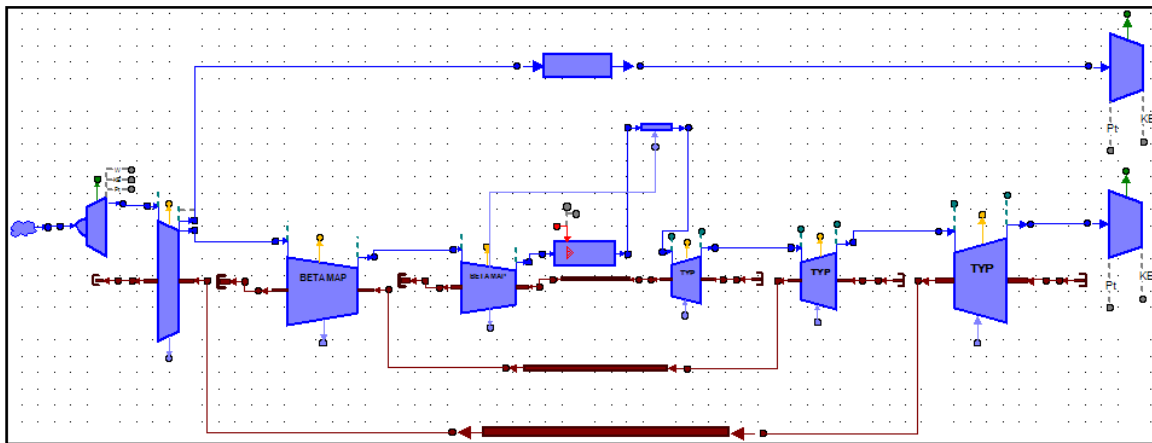


Fig: 6.1.8: CUHBR Engine Model

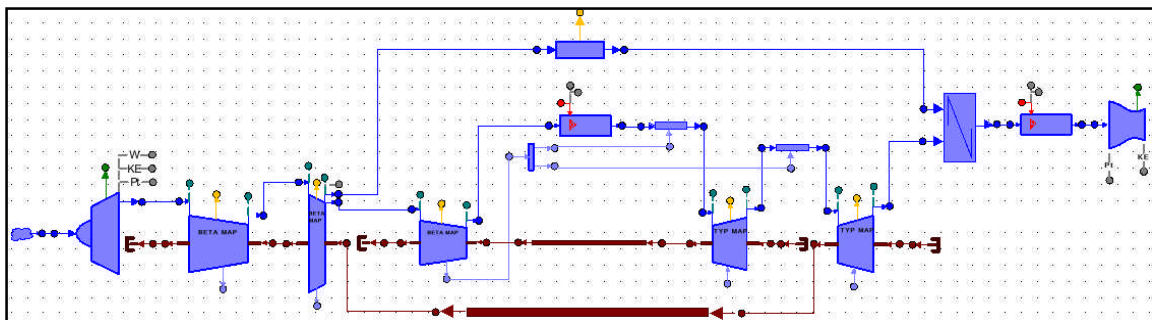


Fig: 6.1.9: CULBR Engine Model

Advanced Performance Simulation of Gas Turbine Components and Fluid Thermodynamic Properties

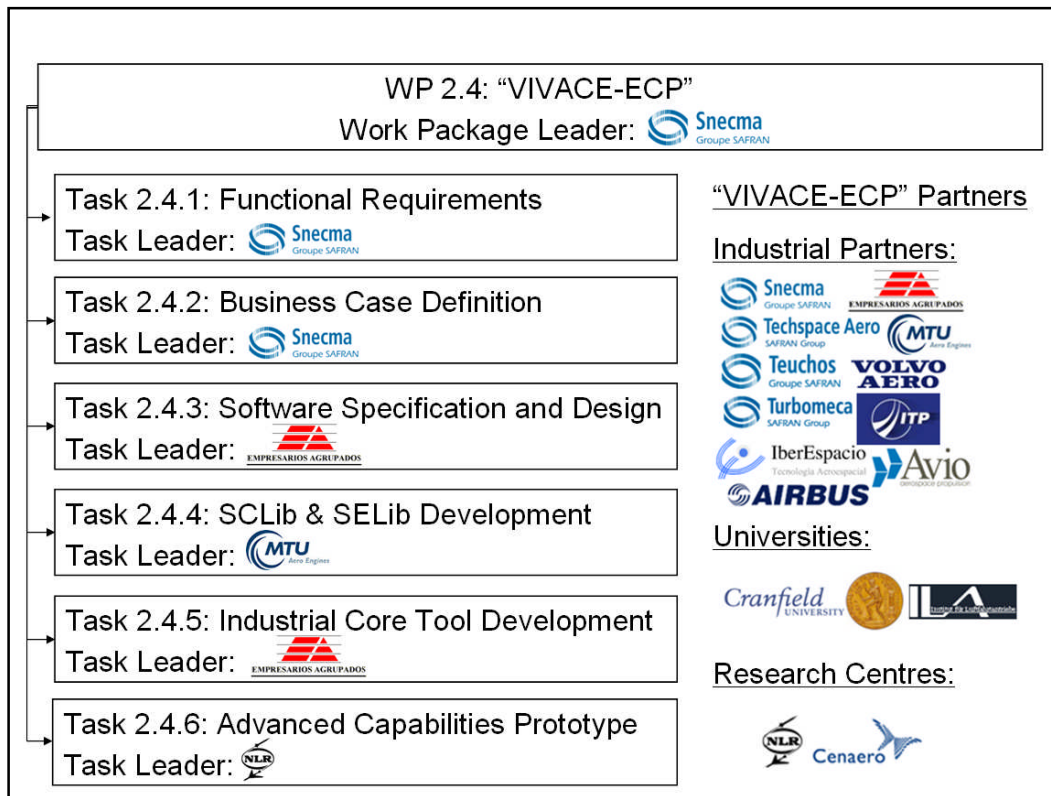


Fig: 6.1.10 Project Structure and Task Distribution of the "VIVACE-ECP" (Logos courtesy of the official websites of the various industrial partners, universities and research institutes)

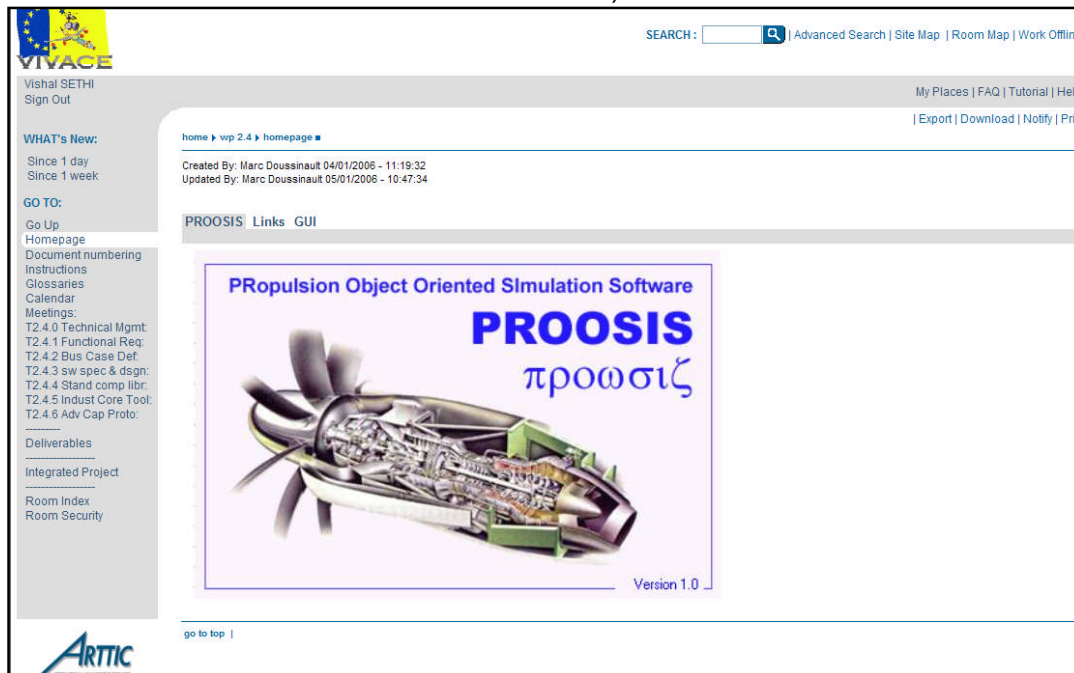


Fig: 6.1.11 Arttic Collaborative Platform for "VIVACE-ECP"

Advanced Performance Simulation of Gas Turbine Components and Fluid Thermodynamic Properties

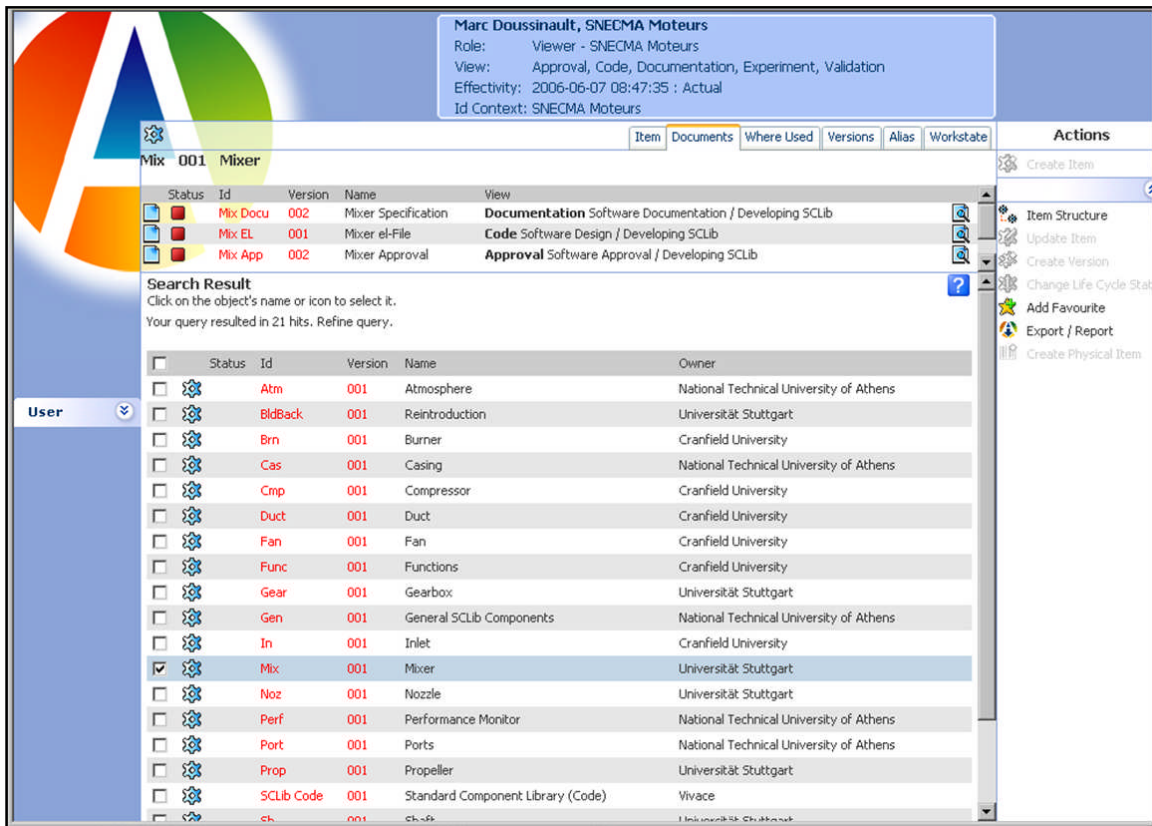


Fig. 6.1.12 Share-A-Space Collaborative Platform for the “VIVACE-ECP” (Image courtesy of a presentation delivered by M. Doussinault (Sneema) at VIVACE Forum 3)

Chapter 6: Appendix 1
SCLib Burner Component Specification Document: Table of Contents

CONTENTS

CONTENTS	3
1: EXECUTIVE SUMMARY	4
2: NOMENCLATURE	5
3: GENERAL DESCRIPTION OF COMPONENT BURNER	7
3.1: Burner Component Hierarchy And Ports Nomenclature	7
3.2: Burner Component Pressure Loss Model	8
3.3: Burner Component Efficiency Model	8
3.4: Burner Component Injected Fuel Type Selection	8
3.5: Combustion Model	9
3.6: Input Parameters For The Burner Component	9
4: CALCULATIONS	11
4.1: References To Other SCLib Components/Functions	11
4.2: Burner Component Outlet Total Pressure Calculation	11
4.3: Burner Component Efficiency Model	13
4.4: Burner Component Combustion Model Calculations	14
4.5: Variables Required For Global Engine Performance Calculation	16
5: BURNER COMPONENT SPECIFIC SWITCHES	18
5.1: Burner Fractional Pressure Loss (dPqP) Calculation Options	18
5.2: Burner Efficiency (eff) Calculation Options	18
5.3: Burner Injected Fuel Type (FUEL) Selection Options	18
6: COMMENTS	19
APPENDIX 1: PROOSIS ICON	21
REFERENCES	21

Chapter 6: Appendix 2
SCLib Fluid Model Specification Document: Table of Contents

CONTENTS

CONTENTS	3
1: EXECUTIVE SUMMARY	4
2: NOMENCLATURE.....	5
3: GENERAL DESCRIPTION OF THE FLUID MODEL.....	6
3.1: Fluid Model Description.....	6
3.2: Fluid Model Tables: Specific Enthalpy	7
3.3: Fluid Model Tables: Entropy Function	8
3.4: Fluid Model Tables: Isentropic Coefficient (Gamma)	8
3.5: Fluid Model Tables: Gas Constant.....	9
3.6: Fluid Model Tables: Dynamic Viscosity	10
3.7: Fluid Model Charts	11
3.8: Definition Of Input and Output Variables	17
4: CALCULATIONS	18
4.1: Fluid Model Calculations	18
5: FLUID MODEL SWITCH AND DATA FILES	19
5.1: Fluid Model Selection Switch	19
5.2: Fluid Model Data Files	19
6: COMMENTS	20
REFERENCES	20

Chapter 6: Appendix 3

SCLib Flow Continuity Model Specification Document: Table of Contents

Contents

CONTENTS	3
1: EXECUTIVE SUMMARY	4
2: NOMENCLATURE	5
3: THERMODYNAMIC FUNCTIONS – GENERAL DESCRIPTION	6
3.1: General Description	6
3.2: Required Inputs And Calculated Outputs	6
4: CALCULATIONS	8
4.1: References To Other Sclib Functions	8
4.2: Thermodynamic Functions - Calculations	8
5: EXAMPLE OF THERMODYNAMIC FUNCTION CALL	16
6: COMMENTS	17
REFERENCES	17

Chapter 6: Appendix 4

Test Definition and Report for the PROOSIS SCLib Burner Component

VIVACE

SCLib: Test Definition and Report

This document is classified as VIVACE Confidential

3.6. BURNER COMPONENT (MTU)

3.6.1. Test Design

The heat addition within this component has to be tested. There is the possibility to choose between two different pressure loss models in the Burner component. Both models have to be tested.

3.6.2. Test Case 1

The first pressure loss model (INPUTdPqP) and the heat addition due to combustion are tested for different points of a working line.

3.6.2.1. INPUT SPECIFICATIONS (DPQP_IN=0.05)

Following steps must be performed to execute the test case:

- Create a new schematic (burner and general component).
- Double click on the schematic. Choose pressure loss model "INPUTdPqP". Specify the following values "dPqP_in=0.05" and "eff_in=1.0".
- Press "OK" and compile the schematic.
- Create a default partition and execute the following experiment:

```
EXPERIMENT exp_1 ON Test_Burner.default_1
```

```
DECLS
```

```
INIT
```

```
BOUNDS
```

```
Burner1.F_in.ANG = 0.0  
Burner1.F_in.FARB = 0.0  
Burner1.F_in.FARU = 0.0  
Burner1.F_in.Pt = 592000.  
Burner1.F_in.Tt = 600.0  
Burner1.F_in.W = 15.2  
Burner1.F_in.WAR = 0.0  
Burner1.Fu_in.P = 101325.0  
Burner1.Fu_in.T = 300.0  
Burner1.Fu_in.W = 0.33
```

```
BODY
```

```
REPORT_LIST("report>All","Burner1.")
```

```
STEADY()
```

```
Burner1.F_in.Pt = 506000.  
Burner1.F_in.Tt = 566.0  
Burner1.F_in.W = 13.6  
Burner1.Fu_in.W = 0.26
```

```
STEADY()
```

```
Burner1.F_in.Pt = 416000.  
Burner1.F_in.Tt = 533.0  
Burner1.F_in.W = 11.6  
Burner1.Fu_in.W = 0.2
```

```
STEADY()
```

```
Burner1.F_in.Pt = 337000.  
Burner1.F_in.Tt = 502.0  
Burner1.F_in.W = 9.8  
Burner1.Fu_in.W = 0.16
```

```
STEADY()
```

```
END EXPERIMENT
```

3.6.2.2. INPUT SPECIFICATIONS (DPQP_IN=0.03)

Following steps must be performed to execute the test case:

- Use the same schematic as in section before.

VIVACE 2.4.4/MTU/T06002

Page: 35/73

© 2007 VIVACE Consortium Members. All rights reserved.

Advanced Performance Simulation of Gas Turbine Components and Fluid Thermodynamic Properties

VIVACE

SCLib: Test Definition and Report

This document is classified as VIVACE Confidential

- Double click on the schematic. Redefine the value "dPqP_in=0.03".
- Press "OK" and compile the schematic.
- Execute the following experiment:

```
EXPERIMENT exp_2 ON Test_Bumer.default_1
DECLS
INIT
BOUNDS
Bumer1.F_in.ANG = 0.0
Bumer1.F_in.FARB = 0.0
Bumer1.F_in.FARU = 0.0
Bumer1.F_in.Pt = 271000.
Bumer1.F_in.Tt = 471.0
Bumer1.F_in.W = 8.2
Bumer1.F_in.WVAR = 0.0
Bumer1.Fu_in.P = 101325.0
Bumer1.Fu_in.T = 300.0
Bumer1.Fu_in.W = 0.12
BODY
REPORT_LIST("reportAll","Bumer1.*")
STEADY()
Bumer1.F_in.Pt = 213000.
Bumer1.F_in.Tt = 439.0
Bumer1.F_in.W = 6.7
Bumer1.Fu_in.W = 0.09
STEADY()
Bumer1.F_in.Pt = 165000.
Bumer1.F_in.Tt = 410.0
Bumer1.F_in.W = 5.4
Bumer1.Fu_in.W = 0.08
STEADY()
Bumer1.F_in.Pt = 129000.
Bumer1.F_in.Tt = 384.0
Bumer1.F_in.W = 4.3
Bumer1.Fu_in.W = 0.07
STEADY()
END EXPERIMENT
```

3.6.3. Test Case 2

The second pressure loss model (CALCULATEDpqp) is tested.

3.6.3.1. INPUT SPECIFICATIONS

Following steps must be performed to execute the test case:

- Use the same schematic as in section before.
- Double click on the schematic. Choose pressure loss model "CALCULATEDpqp". Specify the following values "Kcold=2", "Khot=1", "eff_in=0.99", Ae_in=0,5 and GeoAm=0,5.
- Press "OK" and compile the schematic.
- Execute the following experiment:

```
EXPERIMENT exp_3 ON Test_Bumer.default_1
DECLS
INIT
BOUNDS
Bumer1.F_in.ANG = 0.0
Bumer1.F_in.FARB = 0.0
Bumer1.F_in.FARU = 0.0
Bumer1.F_in.Pt = 3000000.0
Bumer1.F_in.Tt = 700.0
Bumer1.F_in.W = 50.0
```

VIVACE 2.4.4/MTU/T/06002

Page: 36/73

© 2007 VIVACE Consortium Members. All rights reserved.

Advanced Performance Simulation of Gas Turbine Components and Fluid Thermodynamic Properties

VIVACE

SCLib: Test Definition and Report

This document is classified as VIVACE Confidential

```

Bumer1.F_in.WAR = 0.0
Bumer1.Fu_in.P = 5000000.0
Bumer1.Fu_in.T = 300.0
Bumer1.Fu_in.W = 1.0
BODY
REPORT_LIST("reportAll","Bumer1.*")
STEADY()
END EXPERIMENT
    
```

3.6.4. Test Report

The expected results are calculated with GasTurb 10. The expected and the calculated results are shown in the following two tables.

GasTurb 10									
		1	2	3	4	5	6	7	8
P3	[kPa]	592,000	506,000	416,000	337,000	271,000	213,000	165,000	129,000
T3	[K]	600,0	566,0	533,0	502,0	471,0	439,0	410,0	384,0
W3	[kg/s]	15,200	13,600	11,600	9,800	8,200	6,700	5,400	4,300
FAR	[-]	0,02171	0,01912	0,01724	0,01633	0,01463	0,01343	0,01481	0,01628
eff_in	[-]	1,000	1,000	1,000	1,000	1,000	1,000	1,000	1,000
dPqP_in	[-]	0,05	0,05	0,05	0,05	0,03	0,03	0,03	0,03
WF	[kg/s]	0,33	0,26	0,20	0,16	0,12	0,09	0,08	0,07
W4	[kg/s]	15,530	13,860	11,800	9,960	8,320	6,790	5,480	4,370
P4	[kPa]	562,400	480,700	395,200	320,150	262,870	206,610	160,050	125,130
T4	[K]	1371,1	1259,8	1170,1	1113,1	1028,4	958,6	982,2	1011,4

PROOSIS									
		1	2	3	4	5	6	7	8
P3	[kPa]	592,000	506,000	416,000	337,000	271,000	213,000	165,000	129,000
T3	[K]	600,0	566,0	533,0	502,0	471,0	439,0	410,0	384,0
W3	[kg/s]	15,200	13,600	11,600	9,800	8,200	6,700	5,400	4,300
WF	[kg/s]	0,33	0,26	0,20	0,16	0,12	0,09	0,08	0,07
eff_in	[-]	1,000	1,000	1,000	1,000	1,000	1,000	1,000	1,000
dPqP_in	[-]	0,95	0,95	0,95	0,95	0,97	0,97	0,97	0,97
FAR	[-]	0,02171	0,01912	0,01724	0,01633	0,01463	0,01343	0,01481	0,01628
W4	[kg/s]	15,530	13,860	11,800	9,960	8,320	6,790	5,480	4,370
P4	[kPa]	562,400	480,700	395,200	320,150	262,870	206,610	160,050	125,130
T4	[K]	1368,5	1257,3	1167,9	1111,0	1026,6	957,0	980,6	1009,3

It is shown that the pressure loss model within PROOSIS (INPUT dPqP) calculates exactly the same results as expected. There are differences in the exit temperature of the burner. These differences occur because of the different fluid models used in the two programs and a different handling concerning the inlet fuel temperature.

The following table shows the expected and calculated results with the pressure loss model "CALCULATEDPqP".

Advanced Performance Simulation of Gas Turbine Components and Fluid Thermodynamic Properties

VIVACE

SCLib: Test Definition and Report

This document is classified as VIVACE Confidential

PROOSIS		
		1
Am	[m ²]	0,5
rhos	[kg/m ³]	14,929
W3	[kg/s]	50,0
Pt3	[kPa]	3000,00
Tt3	[K]	700,0
Tt4	[K]	1391,7
Kcold	[-]	2,0
Khot	[-]	1,0
dPqP_exp	[-]	0,00033
dPqP	[-]	0,00033
Pt4_exp	[kPa]	2999,0
Pt4	[kPa]	2999,0

The expected and calculated values for dPqP and Pt4 are shown. Both calculated values are exactly the same as expected.

The result of the test cases is that it is no problem creating the schematic, the default partition and the experiments. There are also no problems executing the test cases and the burner component works properly. There are no errors detected.

Chapter 6: Appendix 5

Approval “Certificate” Produced by Snecma for the Flow Continuity Model



This document is classified as VIVACE Confidential

INTERNAL APPROVAL TEMPLATE FOR THE CONTENT OF SOURCE CODE FILES

Date of review:	14/12/07
Reviewer name & organisation:	Doussinault Snecma
File name (.el-file):	SCLib_ThermFuncs.el
Version n°:	4.0

Please answer the questions below and fill in any comments you may have.

Document content	Checked	Answers / comments
Is there a correct header with the following information: Filename, Author, Company, Date and Purpose?	✓	OK
Do all variables use the correct / standard nomenclature (SAE ARP5571)?	✓	OK
Are all variables initialized with a default value?	✓	Yes, when needed.
Exist for all variables a short description, a unit and a range?	✓	OK
Is the code well structured and are all equations commented?	✓	OK
Is the icon defined?	✓	No icon needed
Are there open issues?	✓	NO

Miscellaneous	Space reserved for addition remarks / recommendations
In function where variable "flow" is an output, why is "flow" declared as STRING and not UNUM FlowCase ?	

Advanced Performance Simulation of Gas Turbine Components
and Fluid Thermodynamic Properties

VIVACE

Internal approval template for .el-files

This document is classified as VIVACE Confidential

Issues

N°	Raised by	Date	Issue / question
1	SN	09.01.06	Code description must be improved. Main equations must be commented. A reference to the specification document is not enough.
2	SN	09.01.06	Definition of a unit and if possible a range for all variables.
3	SN	09.01.06	No specification of the function \sqrt{s}_T .
4	SN	09.01.06	Usage of only one of the functions sqrt, sqrt(abs()) and ssqrt.
5	SN	09.01.06	FlowCase should always be the last argument.
6	SN	09.01.06	Sound velocity is sometimes calculated using $ssqrt(\gamma R T_s)$, and sometimes using \sqrt{s}_T function. It should always be calculated the same way.
7	SN	09.01.06	\sqrt{s} and \sqrt{rit} should be defined in the specifications document nomenclature.
8	SN	09.01.06	Inputs and outputs of them_WtPsAe are not defined.
9	SN	28.05.07	For internal loops, the definition of the function to minimize should be relative, not absolute.
10	SN	28.05.07	WtPsAe function is not robust when the solution is nearly sonic. The robustness of this function must be improved, at least physical values should be returned in case of non convergence (today a negative Mach number is returned in case of non convergence)
11	SN	28.05.07	Warning message should be reported when results are out of range. It should be possible to know which component was calling the function when the error occurs.

Answer

N°	Answered by	Date	Issue / question
1	CU	18.01.06	Description improved.
2	CU	18.01.06	Description improved.
3	CU	18.01.06	Defined in the specification document.
4	CU	18.01.06	Now only $ssqrt()$ is used.
5	CU	18.01.06	FlowCase is now always the last argument.
6	CU	18.01.06	Sound velocity is now always calculated using \sqrt{s}_T function.
7	CU	18.01.06	Defined in the specification document.
8	CU	18.01.06	Inputs and outputs of all functions including symbols and units have been clearly outlined.
9-11	MTU	17.12.07	Done

Note: This document should be returned to the Task Leader from task 2.4.4 once completed. It will be held by the Task Leader.

This document may be requested by the Work Package Leader from WP 2.4 to demonstrate that the PROUSIS source code has been internally reviewed.

Chapter 6: Appendix 6

Example of a Typical Test Report for a User Requirement

VIVACE

PROOSIS-SVVP-SHCU

This document is classified as VIVACE Confidential

Test Design TAD-ADV-MUL-CU-001

Description:

Verify multidisciplinary modelling capabilities

Option:

Schematic / Code / Simulation View

Preconditions:

1. SCLIB Burner / Afterburner component
2. The following fluid models stored in the SCLIB "maps" folder.
 - "No dissociation model" – (FluidModel_NoDiss.xml)
 - "Complete dissociation model" – (FluidModel_Diss50atm.xml)

Test Case TAC-ADV-MUL-CU-001-001

Description:

Test one of the various multidisciplinary capabilities of PROOSIS – "Chemicals". Compare the performance of the Afterburner component (using the same boundary conditions) but with the following configurations:

1. Using the "No dissociation" fluid model
2. Using the "Complete dissociation" fluid model

Purpose:

1. To demonstrate the different fluid models available in PROOSIS
2. To demonstrate the effects of dissociation on Afterburner component performance

Preconditions:

1. SCLIB Burner / Afterburner component
2. The following fluid models stored in the SCLIB "maps" folder.
 - "No dissociation model" – (FluidModel_NoDiss.xml)
 - "Complete dissociation model" – (FluidModel_Diss50atm.xml)

Inputs:

Create and simulate Afterburner component experiment using the configurations outlined in the Test Case Description"

Outputs:

The results of the various simulations are viewed using one of the two options:

1. Report File
2. Output window (using write statements)

User Requirements: UR-ADV-MUL – 02 (T6): MULTIDISCIPLINARY CAPABILITY

PRI-3 PROOSIS shall be capable of building multidisciplinary models (e.g. electricals, electronics, mechanics, thermal, thermodynamics, chemicals, fluid dynamics,

VIVACE

PROOSIS-SVVP-SHCU

This document is classified as VIVACE Confidential

emissions.) In particular; heat soakage should be the first step of multi-disciplinary and zooming capabilities.

Comment:

This UR is slightly vague. "Chemicals" is just one of the multidisciplinary capabilities of PROOSIS.

Test Procedure TAP-ADV-ZOO-CU-001-001-001

Description:

Step		Result
1	<p>Create a new schematic of an Afterburner component.</p> <p>Edit the attributes (DATA) as follows:</p> <p>1. fluid_in = "Standard"</p> <p>NB: this corresponds to the "No dissociation" fluid model)</p> <p>2. dPqP_in = "0.05"</p> <p>3. eff_in = "0.90"</p> <p>4. Change the component name to "Afterburner"</p> <p>Leave all other DATA variables with their default values</p> <p>Save and compile the schematic</p>	<p>A new EL source file for the Afterburner component is automatically generated.</p>
2	<p>Choose the "Code View" tab, compile the Afterburner .el source file and select the "Partitions" tab.</p>	<p>The Afterburner component is displayed as a compiled component.</p>
3	<p>Create an off-design partition.</p> <p>Select the following boundary conditions in the "Boundary Selection Wizard" window and then click "Next".</p> <ol style="list-style-type: none"> 1) "Afterburner.F_in.Ang" 2) "Afterburner.F_in.FARB" 3) "Afterburner.F_in.FARU" 4) "Afterburner.F_in.Pt" 5) "Afterburner.F_in.Tt" 6) "Afterburner.F_in.W" 7) "Afterburner.F_in.WAR" 8) "Afterburner.Fu_in.P" 	<p>A new off-design partition is successfully generated.</p>

Advanced Performance Simulation of Gas Turbine Components
and Fluid Thermodynamic Properties


VIVACE

PROOSIS-SVVP-SHCU

This document is classified as VIVACE Confidential

	<p>9) "Afterburner.Fu_in.T" 10) "Afterburner.F_out.Tt" Call the new partition "OffDesign"</p>	
4	<p>Choose the "Simulation View" tab and create a new experiment using the Afterburner.OffDesign partition. Call the new experiment "TestDiss" and click "OK"</p>	<p>A new experiment entitled TestDiss is generated</p>
5	<p>Allocate the following values to each of the boundary conditions: Afterburner.F_in.Ang = 0 Afterburner.F_in.FARB = 0.01831 Afterburner.F_in.FARU = 0 Afterburner.F_in.Pt = 415104.21 Afterburner.F_in.Tt = 985.70 Afterburner.F_in.W = 77.391 Afterburner.F_in.WAR = 0 Afterburner.Fu_in.P = 101325 Afterburner.Fu_in.T = 358 Afterburner.F_out.Tt = 1990 Compile and simulate the experiment.</p>	<p>The results can be either viewed in the report file or in the PROOSIS output window (using the appropriate "write" statements).</p>
6	<p>Repeat Steps 1 - 6 but let fluid_in = "FluidModel_Diss50atm" NB: this corresponds to the "Complete dissociation" fluid model) Compare the results of the two simulations</p>	<p>For this example: To achieve the same Afterburner outlet temperature (Afterburner.F_out.Tt = 1990K), the "No Dissociation" fluid model requires a slightly lower fuel flow (~1.2% lower) than the "Complete Dissociation" model.</p>


Chapter 6: Appendix 7
PROOSIS Poster (developed courtesy of NTUA)



Value Improvement through a Virtual Aeronautical Collaborative Enterprise

PROOSIS: Improving Engine Performance Design and Simulation

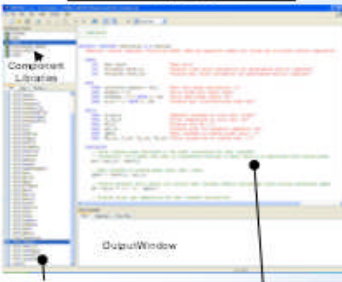
Partners: AIF, AVIO, CEIAERO, CU, EAI, IE, ITP, MTU, NLR, NTUA, SH, TA, TEUCHOS, TM, USTUTT, VAC



PROOSIS is a standalone, multi-platform, object-oriented simulation environment for gas turbine engine performance simulation.

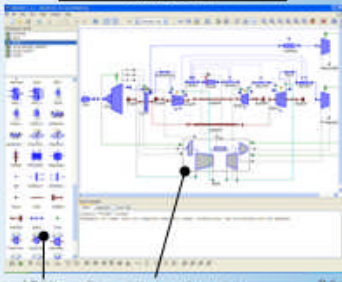
- > It can be used to create, run, manage and share engine models in a modular way using either the standard or custom libraries of engine components.
- > It performs all standard calculations (steady state, transient design, off-design, mono and multi-point real time).
- > It is a set of Analytical capabilities.
- > It can produce different types of Customer Decks (stand-alone, executable, DLL, Excel).
- > It allows connection with external software and tools (FORTRAN, C++, Simulink, thermodynamic libraries, optimization tools, database).
- > It is capable of performing multi-fidelity, multi-discipline and distributed simulation.

Code View



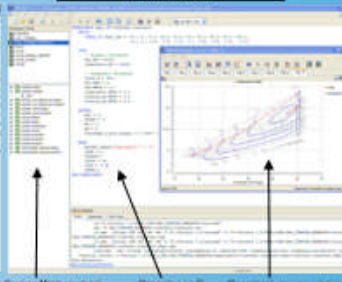
Library DLL Files
Component DLL object-oriented code containing mathematical description of real components

Schema View



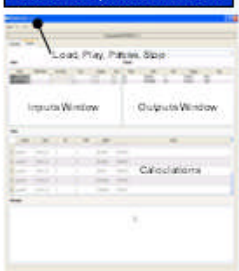
Library Parasets
Drag-and-drop components from parasets to construct engine model. Connect components through appropriate distribution ports

Simulation View




Define engine Mathematical Model and Simulation Cases
Describe in DLL calculation mode or type
Graphical representation of results

Standalone Graphical Customer Deck

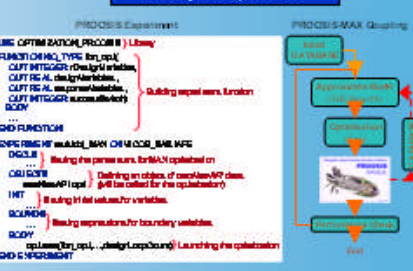


Load, Play, Pause, Stop
Inputs Window
Outputs Window
Calculations

Excel Deck



Multi-Objective Optimization



PROOSIS Experiment
LIB OPTIMIZATION_PROOBSIS Library
FUNCTIONAL_TYPES for opt
CUFFPTGASD: Design variables
CUFFPTCAL: optimization variables
CUFFPTGASD: success criteria
BODY
Building equal area, iteration

PROOSIS-MAX: Grouping
Build the library
Approximate Deck
Optimization
Optimization Deck
Optimization Deck
Exit

Remote & Enterprise

- > Collaborative modeling among geographically dispersed engineers
- > easy and efficient deployment of executable models
- > protection of ownership and IPR
- > reduction of simulation time through load sharing
- > size and complexity of the simulation model may grow irrespective of capability of computing infrastructures
- > reuse of sub models in different simulations

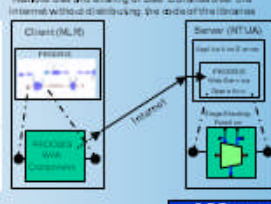
Compressor Zooming via Remote Web Service Interaction between NLR & NTUA

PROOSIS simulation in The Netherlands

Compressor Stage Stacking Calculation in Greece (proprietary code in FORTRAN)

Distributed Simulation

Remote use and sharing of User Libraries over the Internet without distributing the code of the libraries




Client (NLR)
Server (NTUA)

Distributed Simulation developed in a FORTRAN-2

Distributed Multi-disciplinary Design Simulation

- Integrated Multi-disciplinary Simulation Models based on Single Parametric Geometry
- Multi-Level Optimization
- Multi-Objective Optimization (e.g. weight and fatigue life)
- Each element in the optimization tool runs at different locations in Europe (demonstrated at Figure 2)

3-D Component Zooming Automated Workflow Framework



INPUT MINI-MAP DATA
DESIGN GEOMETRIC DATA
CFX BLAD-GEN MODEL
CFX TURBO GRID
CFX 10.0 PRE-SOLVER
CFX 10.0 SOLVER
CFX 10.0 POST
OUTPUT DATA STORAGE FILE
POST SCRIPT MAP GENERATOR
BOUNDARY CONDITIONS INPUT TEXT FILE

DESIGN TOGETHER, GAIN TOGETHER

WWW.VIVACE-EPIC.COM
<http://www.vivace-epic.com>

Chapter 6: Appendix 8

PROOSIS – A Collaborative Venture for Gas Turbine Performance Simulation using an Object Oriented Programming Schema^[10]

Arjun Bala, Vishal Sethi, Enrico Lo Gatto, Vassilios Pachidis and Pericles Pilidis
Department of Power and Propulsion
Cranfield University
Cranfield, Bedfordshire MK43 0AL
United Kingdom

Abstract

This paper describes the development and applications of a modern, interactive gas turbine simulation and modelling environment called “**PROOSIS**” (**PR**opulsion **O**bject **O**riented **S**imulation **S**oftware). PROOSIS has been developed as part of the “**VIVACE-ECP**” (**V**alue **I**mprovement through a **V**irtual **A**eronautical **C**ollaborative **E**nterprise - **E**uropean **C**ycle **P**rogramme) project. The main objective of the “VIVACE-ECP” is to develop a cost effective gas turbine simulation environment that facilitates optimal use of multi-partner GT performance simulation R&D resources and expertise to create a single framework providing shared standards and methodologies for European Universities, Research Centres and manufacturing companies. This paper provides a brief introduction to the collaborative project and discusses several capabilities of PROOSIS including isolated component performance simulation, engine model DP and OD simulation, test analysis and customer deck generation.

Chapter 6: Appendix 9

Study of VSV Effects on Performance via an Integrated Aerodynamic Component Zooming Process^[14]

Arjun Bala, Vishal Sethi, Enrico Lo Gatto, Vassilios Pachidis and Pericles Pilidis
Department of Power and Propulsion
Cranfield University
Cranfield, Bedfordshire MK43 0AL
United Kingdom

Abstract

The work presented in this paper adapts a modern simulation approach of “Integrated Mini-Map based Component Zooming” in order to investigate the effects of variable stator vanes on performance of both, the first stage of a Fan component at (3-D) component level and on overall engine at (0-D) engine system level, during part speed operation. This paper also highlights the structure and operation of the custom developed integrated workflow controller framework. This single algorithmic framework facilitates optimal use of readily available simulation technology at different fidelity levels.

Chapter 6: Appendix 10

Advanced Modeling of Fluid Thermodynamic Properties for Gas Turbine Performance Simulation ^[15]

Vishal Sethi, Fulvio Diara, Sina Atabak,
Anthony Jackson, Arjun Bala and Pericles Pilidis
Department of Power and Propulsion
Cranfield University
Cranfield, Bedfordshire MK43 0AL
United Kingdom

Abstract

This paper describes the structure of an advanced fluid thermodynamic model which has been developed for a novel advanced gas turbine simulation environment called PROOSIS. PROOSIS (PRopulsion Object Oriented Simulation Software) is part of the VIVACE-ECP (Value Improvement through a Virtual Aeronautical Collaborative Enterprise - European Cycle Programme) project. The main objective of the paper is to determine a way to achieve an accurate, robust and reliable fluid model. The results obtained demonstrate that accurate modelling of the working fluid is essential to avoid convergence problems of the thermodynamic functions thereby increasing the accuracy of calculated fluid properties. Additionally, the impact of accurately modelling fuel thermodynamic properties, at the point of the injection, is discussed.

Chapter 6: Appendix 11

Implementation of Accurate Gas Properties on Gas Turbine Simulations ^[16]

Maria Katsourou: MSc Thesis
Department of Power and Propulsion
Cranfield University

Abstract

The aim of the thesis is to provide accurate thermodynamic properties for the products of combustion of kerosene and pure hydrogen and implement them on gas turbine engines for performance simulations. Tables of thermodynamic properties have been produced for a great variety of pressures, fuel to air ratios, water to air ratios and for temperatures up to 3000K using CEA code. Two different fluid models have been created; one accounting for dissociation, which is defined as Reacting Compositions, and the other ignoring any chemical reactions taking place at high temperatures, defined as Frozen Chemistry. Performance calculations have then been carried out assuming variable gas properties throughout the engine's components and comparisons have been made between the two different fluid models. Different cases are also examined referring to the change in fuel and change in the amount of water added in the burner. Comparing the two fluid models, the results show improvement of the engine's thrust when the Equilibrium-Reacting Compositions is adopted compared to Equilibrium-Frozen Chemistry but also an increase in the s.f.c due to the increase of the fuel to air ratio demanded in the burner for the same temperature rise. The use of hydrogen instead of kerosene increases the specific thrust of the engine and improves the s.f.c while water addition boosts the specific thrust of the engine and worsens the s.f.c.

Chapter 6: Appendix 12

Development of Accurate Fluid Models for Gas Turbine Performance Calculations^[17]

Damien Laurans: Visiting Student Technical Report
Department of Power and Propulsion
Cranfield University

Abstract

The aim of this thesis is to provide an accurate way to calculate with CEA software the thermodynamic and transport properties for products of combustion of any fuel. This thesis contains a detailed explanation on how running combustion simulations with any burned fuel to air ratio, unburned fuel to air ratio, water to air ratio, temperature, pressure and dissociation level. The dissociation level assesses the amount of fluid dissociated into a component whereas the other part didn't have the time to reach the dissociation equilibrium. This work is expected to be helpful for the integration of CEA code into PROOSIS, advanced gas turbine performances simulator. Tables of thermodynamic properties of combustion products of Jet-A, Diesel, Natural Gas and Hydrogen have been produced for different values of each parameter listed below. Then the performances of combustor component have been simulated. The influence of each parameter has been thoroughly investigated. It appears that dissociation increases significantly the fuel consumption required to achieve a given temperature increase. The conclusion is that as the working temperature keeps being increased in recent high power engines, the dissociation phenomenon have to be considered in gas turbine simulations.

Chapter 6: Appendix 13

Advanced Modelling of Fluid and Thermodynamic Functions for Gas Turbine Mixers and Nozzles ^[18]

Fulvio Diara: MSc Thesis
Department of Power and Propulsion
Cranfield University

Abstract

For the last four years the European Gas Turbine community (comprising industrial companies, research institutes and universities) has decided to join the VIVACE-ECP project, with the intention of sharing knowledge and experience to develop an advanced gas turbine performance simulation software called PROOSIS. Cranfield University is one of the main institutes involved in this project as a developer of gas turbine component and fluid-thermodynamic models. PROOSIS is a new software which is under development, and it is still affected by some convergence problems that need to be resolved. This document describes the work carried out in order to improve robustness and accuracy of the fluid and thermodynamic functions used in PROOSIS.

Besides this task, strictly connected with software development, a detailed literature research about mixer and nozzle modelling for gas turbine performance simulation is described in this thesis. The modifications introduced in fluid and thermodynamic functions have been tested on both mixer and nozzle components. The results of these tests are reported comparing old and new fluid functions, in order to verify the effective impact of these improvements.

The last objective of the thesis was to build the model of a two-spool military turbofan, in order to verify the effective impact of the fluid function modifications on the whole engine simulation. Because of the convergence problems that still affect PROOSIS this task has revealed some difficulties, which made impossible to realise a proper comparison between PROOSIS and another gas turbine performance simulation code. However, the experience achieved in engine modelling for design point and off-design simulations has been described in this document.

At the end of the whole thesis work a consistent development of fluid and thermodynamic functions has been fulfilled, thereby improving the robustness of PROOSIS. Additionally it has been revealed that there are limitations with directly connecting PROOSIS with a chemical equilibrium code. That needs to be considered during future developments of PROOSIS in VIVACE 2 (CRESCENDO).

Chapter 6: Appendix 14

Advanced Performance Simulation of Gas Turbine Burners and Afterburners^[19]

Sina Atabak: MSc Thesis
Department of Power and Propulsion
Cranfield University

Abstract

Gas turbine engine performance simulations are constantly improving as increased engine technological complexity demands a more complete understanding of dynamic system behavior. Refinements in dynamic system modeling, the evolution of computer languages and improvements of computer hardware and operations have resulted in significant advances in simulation technology.

The work presented within this thesis has been conducted under the flagship of VIVACE-ECP" (Value Improvement through a Virtual Aeronautical Collaborative Enterprise- European Cycle Program) a European union sponsored collaborative project. This project is geared towards the development of an advanced gas turbine performance modeling and simulation platform (PROOSIS) with the ambition of developing a cost effective, reliable and extensible platform which integrates the expertise of various European aeronautical industries, research institutes and universities.

The aim of the thesis is to implement liquid fuel enthalpy in advanced burner and afterburner performance simulation. In particular the effects of fuel temperature changes between the fuel tank and point of injection have been investigated. Liquid fuel sensible enthalpy tables have been generated using the NASA Chemical Equilibrium Application software (CEA) and then integrated with the burner energy balance equation to take into account the rise of fuel enthalpy at the injection point.

Chapter 6: Appendix 15

Poly-Dimensional Gas Turbine System Modelling and Simulation^[9]

Arjun Bala: PhD Thesis
Department of Power and Propulsion
Cranfield University

Abstract

The intense global competition in the commercial aviation and power generation industry is placing a significant pressure on minimizing cost while meeting challenging goals in-terms of performance, efficiency, emissions and reliability. During recent years an opportunity has been identified and is currently being focused on, for reducing the design and development cost by largely replacing the larger scale and expensive hardware based testing, with multi-fidelity and cross-domain predictive simulation platforms. A greater use of such predictive simulations not only save some costs directly associated with hardware design and testing but also enables engine design trade-offs and component interactions, to be studied in detail earlier on before a commitment is made towards the final hardware design. Experts have estimated a reduction of 30 to 40% in development time and cost when such dynamic simulation techniques are implemented. Furthermore, to keep the engine development ongoing, joining forces with various gas turbine industrial manufacturers, research centres and universities especially within the European Union is of utmost importance because tomorrow's advanced engine configurations can no longer be developed with today's simulation tools in the way they are currently used.

The research work, presented within this thesis has been conducted under the flagship of "VIVACE-ECP" (Value Improvement through a Virtual Aeronautical Collaborative Enterprise – European Cycle Program) an European Union sponsored collaborative research project, geared towards the development of an advanced gas turbine performance modeling and simulation platform with cross domain analysis capability. The research work undertaken by the author within the scope of this thesis and the project, fundamentally encompasses around the two distinct aspects; 1) development of a new and modern (0-D) gas turbine performance simulation industrial core tool called as PROOSIS and 2) development in the form of a prototype demonstrator a multi-fidelity simulation technology, fundamentally aiming to reduce engine development cost and time.

The new and modern PROOSIS application framework conforms to an OO programming schema giving the tool features in terms of flexibility, extensibility, robustness, etc. Although, PROOSIS has been envisaged as a long term development process, several of its current capabilities and component modeling philosophies have been discussed in detail.

Poly-Dimensional Gas Turbine System Modelling and Simulation^[9]

Arjun Bala: PhD Thesis
Department of Power and Propulsion
Cranfield University

Abstract (continued)

The prototype (3-D) integrated Aerodynamic Component Zooming Framework makes the optimal use of two different simulation platforms at different fidelity levels, thus allowing for variable complexity analysis to be performed as required. In order to demonstrate the prototype (3-D) integrated Aerodynamic Component Zooming Framework a case-study has been developed. The case study is to study the effect of VSV on a single stage compressor (or fan) during part speed performance and which was successfully completed. The integrated component zooming technique has been performed using a custom developed workflow management tool referred to as "Integrated Workflow Controller" making use of a distributed computing architecture.

The key contribution of the author within the scope the project and the thesis has been the development of the modern object oriented GT (0-D) cycle code PROOSIS framework and the development of the modern (3-D) integrated aerodynamic compressor zooming framework. Within this thesis, full and comprehensive information on the research work undertaken by the author in order to achieve the above discussed goals, along with suitable results have been presented. Also discussed in detail are results generated as a part of the software testing, verification and validation of both 1) PROOSIS and 2) (3-D) Integrated Aerodynamic Component Zooming Framework.

In an effort to reduce engine development cost and time as discussed earlier, the research work undertaken by the author part of the CU team has made an extensive and optimal use of modern, sophisticated and cross domain, numerical simulation technology readily available and affordable, at different fidelity levels. Additionally, the collaborative effort which has been another key aspect of the project in creating a standard and a modern GT simulation framework (with a prototype component zooming capability) for the advanced gas turbine systems in future has also been achieved. This has been possible by mutually sharing the technical expertise between all participating GT industrial manufacturers, research centres and universities within the European Union. It is the author's opinion that both of the above highlighted developments form a strong foundation for future technological developments leading to an even more sophisticated and capable, multi-disciplinary and multi-fidelity simulation environment which will lead to a significant reduction in engine development cost and time.

Chapter 6: References

[¹] VIVACE Project, Official Website,
URL: <http://www.vivaceproject.com/>

[²] PROOSIS, Official Website,
URL: <http://www.proosis.com/>

[³] Lytle, J. K., July 1999, "The Numerical Propulsion System Simulation: A Multidisciplinary Design System for Aerospace Vehicles", NASA/TM-1999-209194.

[⁴] Follen, G., auBuchon, M., April 2000, "Numerical Zooming Between NPSS Engine Simulation and a One-Dimensional High Compressor Analysis Code", NASA/TM-2000-209913.

[⁵] ICAO, February 2006, "Environmental Design Space (EDS) Prototype", Tucson, AZ, US, ICAO CAEP/7-WG2-TG2-6_IP01.

[⁶] ICAO, February 2007, "Environmental Design Space (EDS) Progress", Montreal, ICAO CAEP/7- IP/23.

[⁷] ICAO, February 2007, "Aviation Environmental Design Tool (AEDT) Progress", Montreal, ICAO CAEP/7- IP/24.

[⁸] EA Internacional, 2007, EcosimPro, Official Website,
URL: <http://www.ecosimpro.com/>

[⁹] Bala, A. 2007, "Poly-Dimensional Gas Turbine System Modelling and Simulation", PhD Thesis, School of Engineering – Cranfield University.

[¹⁰] Bala, A., Sethi, V., Lo Gatto, E., Pachidis, V. and Pilidis, P., 2007, "PROOSIS – A Collaborative Venture for Gas Turbine Performance Simulation using an Object Oriented Programming Schema" ISABE 2007-1357.

[¹¹] Doussinault, M., (Snecma), 2005, "ECP-PROOSIS User Requirements Document" VIVACE 2.4.1/SM/T/04005.

[¹²] Garcia, B., (EA Internacional), 2005, "ECP-PROOSIS Software Requirements Document" VIVACE 2.4.3/EA/T/05001.

[¹³] SAE, August 2004, "Aerospace Recommended Practice: Gas Turbine Engine Performance Presentation and Nomenclature for Digital Computers Using Object – Oriented Programming" SAE ARP 5571.

[¹⁴] Bala, A., Sethi, V., Lo Gatto, E., Pachidis, V. and Pilidis, P., 2007, "Study of VSV Effects on Performance via Integrated Aerodynamic Process" AIAA 2007-5046.

- [15] Sethi, V., Diara, F., Atabak, S., Jackson, A., Bala, A. and Pilidis, P., 2008, "Advanced Modelling of Fluid Thermodynamic Properties for Gas Turbine Performance Simulation", ASME GT-2008-51126
- [16] Katsourou, M., Sept. 2005, "Implementation of Accurate Gas Properties on Gas Turbine Simulations", MSc Thesis, School of Engineering, Department of Power and Propulsion, Cranfield University.
- [17] Laurans, D., Sept. 2006, "Development of Accurate Fluid Models for Gas Turbine Performance Calculations", Exchange Student Training Period Report, School of Engineering, Department of Power and Propulsion, Cranfield University.
- [18] Diara, F., Sept. 2007, "Advanced Performance Modelling of Fluid and Thermodynamic Functions for Gas Turbine Mixers and Nozzles", MSc Thesis, School of Engineering, Department of Power and Propulsion, Cranfield University.
- [19] Atabak, S., Sept. 2007, "Advanced Performance Simulation of Gas Turbine Burners and Afterburners", MSc Thesis, School of Engineering, Department of Power and Propulsion, Cranfield University.
- [20] Pachidis, V., 2007, "Gas Turbine Performance Simulation", Simulation and Diagnostics Course Notes: School of Engineering – Cranfield University.
- [21] Gas Turbine Engineering Group, "The TURBOMATCH Scheme", TURBOMATCH, User's Manual, School of Engineering – Cranfield University.
- [22] Pachidis, V. and Jackson, A. J. B., (Cranfield University) December 2005, "PROOSIS Advanced Capabilities: Physical Model Description", VIVACE/2.4.6/T/CU/05002 – Ver. 1.0
- [23] Arendson, P., (NLR) June 2005, "PROOSIS Advanced Capabilities: Blueprint Description of Prototype", VIVACE 2.4.6/NLR/P/05001.
- [24] "VIVACE-ECP" Partners, November 2007, "PROOSIS Test Reports", VIVACE 2.4.3/SN/T/06013.
- [25] Alexiou, A., Baalbergen, E.H., Kogenhop, O, Mathioudakis, K., Arendsen, P., May 2007, "Advanced Capabilities for Gas Turbine Engine Performance Simulation", ASME GT-2007-27086.
- [26] Coelho, R.F., Pierret, S., May 2007, "Optimisation aéromécanique d'aubes de turbomachines dans le cadre du projet européen VIVACE", 8ème Colloque National en Calcul des Structures.
- [27] Arttic International Management Services, Official Website, URL: <http://www.arttic.com/>

- [28] Eurostep – Share-A-Space, Official Website,
URL: <http://www.share-a-space.com/>
- [29] Gordon, S. and McBride, B.J., Oct. 1994, “Computer Program for Calculation of Complex Chemical Equilibrium and Applications: Part I” NASA RP 1311.
- [30] Gordon, S. and McBride, B.J., Jun. 1996, “Computer Program for Calculation of Complex Chemical Equilibrium and Applications: Part II” NASA RP 1311.
- [31] Sethi, V., Jackson, A. and Pilidis, P., (Cranfield University), 2007, “PROOSIS Standard Component Library: Fluid Model Specification” VIVACE 2.4.4/CU/T/06003.
- [32] Sethi, V., Jackson, A. and Pilidis, P., (Cranfield University), 2007, “PROOSIS Standard Component Library: Thermodynamic Functions Specification” VIVACE 2.4.4/CU/T/06004.
- [33] Alexiou, A. and Mathioudakis, K., (NTUA), 2007, “PROOSIS Standard Component Library: Atmosphere Component Specification” VIVACE 2.4.4/NTUA/T/04008.
- [34] Sethi, V., Jackson, A. and Pilidis, P., (Cranfield University), 2007, “PROOSIS Standard Component Library: Burner Component Specification” VIVACE 2.4.4/CU/T/05007.
- [35] Alexiou, A. and Mathioudakis, K., (NTUA), 2007, “PROOSIS Standard Component Library: Burner_Emissions Component Specification” VIVACE 2.4.4/NTUA/T/07003.
- [36] Alexiou, A. and Mathioudakis, K., (NTUA), 2007, “PROOSIS Standard Component Library: Casing Component Specification” VIVACE 2.4.4/NTUA/T/06006.
- [37] Bala, A., Sethi, V. and Jackson, A., (Cranfield University), 2007, “PROOSIS Standard Component Library: Compressor Component Specification” VIVACE 2.4.4/CU/T/04006.
- [38] Sethi, V., Jackson, A. and Pilidis, P., (Cranfield University), 2007, “PROOSIS Standard Component Library: Duct Component Specification” VIVACE 2.4.4/CU/T/05006.
- [39] Bala, A. and Jackson, A., (Cranfield University), 2007, “PROOSIS Standard Component Library: Compressor Component Specification” VIVACE 2.4.4/CU/T/06008.
- [40] Sethi, V., Jackson, A. and Pilidis, P., (Cranfield University), 2007, “PROOSIS Standard Component Library: Flow Splitter Component Specification” VIVACE 2.4.4/CU/T/06005.
- [41] Bretschneider, S., Banzhaf, B. and Staudacher, S. (USTUTT), 2007, “PROOSIS Standard Component Library: Gear Component Specification” VIVACE 2.4.4/USTUTT/T/05004.
- [42] Sethi, V., Jackson, A. and Pilidis, P., (Cranfield University), 2007, “PROOSIS Standard Component Library: Heat Exchanger Components Specification” VIVACE 2.4.4/CU/T/07004.

- [43] Bala, A., Sethi, V. and Jackson, A., (Cranfield University), 2007, "PROOSIS Standard Component Library: Inlet Component Specification" VIVACE 2.4.4/CU/T/04005.
- [44] Banzhaf, B. and Staudacher, S. (USTUTT), 2007, "PROOSIS Standard Component Library: Mixer Component Specification" VIVACE 2.4.4/USTUTT/T/04003.
- [45] Banzhaf, B. and Staudacher, S. (USTUTT), 2007, "PROOSIS Standard Component Library: Convergent Nozzle Component Specification" VIVACE 2.4.4/USTUTT/T/04002.
- [46] Banzhaf, B. and Staudacher, S. (USTUTT), 2007, "PROOSIS Standard Component Library: Convergent - Divergent Nozzle Component Specification" VIVACE 2.4.4/USTUTT/T/04004.
- [47] Alexiou, A. and Mathioudakis, K., (NTUA), 2007, "PROOSIS Standard Component Library: Performance Monitor Component Specification" VIVACE 2.4.4/NTUA/T/06010.
- [48] Alexiou, A. and Mathioudakis, K., (NTUA), 2007, "PROOSIS Standard Component Library: Probe Component Specification" VIVACE 2.4.4/NTUA/T/07002.
- [49] Banzhaf, B. and Staudacher, S. (USTUTT), 2007, "PROOSIS Standard Component Library: Propeller Component Specification" VIVACE 2.4.4/USTUTT/T/05005.
- [50] Bretschneider, S., Banzhaf, B. and Staudacher, S. (USTUTT), 2007, "PROOSIS Standard Component Library: Shaft Component Specification" VIVACE 2.4.4/USTUTT/T/05003.
- [51] Alexiou, A. and Mathioudakis, K., (NTUA), 2007, "PROOSIS Standard Component Library: Turbine Component Specification" VIVACE 2.4.4/NTUA/T/05005.
- [52] Alexiou, A. and Mathioudakis, K., (NTUA), 2007, "PROOSIS Standard Component Library: SCLib Ports Specification" VIVACE 2.4.4/NTUA/T/04007.
- [53] Gonser, H., (MTU), December 2007, "VIVACE-ECP PROOSIS Physical Modelling Specifications" VIVACE 2.4.4/MTU/T/06001.
- [54] Orsini, A. (AVIO), Cordoba, O. (ITP), Gonser, H. (MTU), Kogehop, O. (NLR), Doussinault, M. (Snecma), Pons, B. (Turbomeca), December 2007, "VIVACE-ECP PROOSIS Test Definitions and Reports" VIVACE 2.4.4/MTU/T/06002
- [55] Kurzke, J., 2007, "GasTurb 11 – Gas Turbine Performance Simulation Software", GasTurb Official Website,
URL: <http://www.gasturb.de>
- [56] VIVACE Forum 1, Official Website,
URL: <http://www.vivaceproject.com/content/forum1/forum1.php>

[57] VIVACE Forum 2, Official Website,

URL: <http://www.vivaceproject.com/content/forum2/forum2.php>

[58] VIVACE Forum 3, Official Website,

URL: <http://www.vivaceproject.com/content/forum3/forum3.php>

[59] Coelho, R.F., Pierret, S., Cobas, P. 2006, "Multi-objective Evolutionary Algorithms Applied to Aircraft Engine Design", ICAS 2006 25th Aeronautical Congress of the Aeronautical Sciences.

Chapter 7: General Conclusions and Recommendations for Further Work

7.1: Introduction

The primary objective of this doctoral thesis was to present advanced performance simulation models of gas turbine components and advanced fluid modelling capabilities developed by the author. As discussed in *Chapter 1*, this thesis adopted a “modular” structure. Each chapter is self contained with chapter specific brief abstracts, nomenclature guides, introductions, literature reviews, technical analyses, results, conclusions, appendices and references. The modular structure of this thesis reflects the object oriented nature of PROOSIS. A collection and analysis of the conclusions of each chapter is provided below, including the limitations of the work. Subsequently recommendations are made for further work where appropriate.

NB: The nomenclature used in the analysis of each chapter below is consistent with the nomenclature used in the main chapter.

7.1.1: Chapter 2 Conclusions

The major contribution made by the author to the development of an advanced fluid model with densely populated multi-dimensional fluid model tables, catering for several fuels and accounting for different levels of dissociation has been presented in Chapter 2. Additionally the evolution of a robust flow continuity model which was conceived and developed by the author has been presented. The fluid model and flow continuity model developed by the author are the foundation of the PROOSIS standard components library (SCLib).

The advanced fluid model generated by the author for the PROOSIS standard components library (SCLib) comprises multi-dimensional tables of specific enthalpy, entropy function, isentropic coefficient, Gas constant and dynamic viscosity as functions of temperature, burned fuel to air ratio and water to air ratio. The reasons for choosing multi-dimensional fluid property tables as opposed to polynomial functions have been discussed. The advanced fluid model caters for several fuels including Jet-A, diesel, sample natural gas and hydrogen. The fluid model tables were generated using the NASA CEA software.

Two basic types of fluid models were generated. The first fluid model (the “no dissociation” fluid model) was generated assuming a constant gaseous composition of the products of combustion, while the second fluid model was generated assuming chemical equilibrium of the products of combustion.

Effects of temperature on chemical equilibrium fluid properties:

The analyses below are only valid for temperatures above 1500K (the temperature above which the effects of dissociation begin to become significant). As the temperature increases beyond 1500K the level of dissociation increases and subsequently each of the effects described below is greater.

For a given temperature, FARB and WAR the specific enthalpy and entropy function of the dissociated products of combustion are higher than that of the non dissociated products as the dissociation process is endothermic and therefore heat is absorbed by the dissociated species.

For a given temperature, FARB and WAR, the chemical equilibrium gas constant is also higher because the molecular weight of the dissociated species is lower than that of the non dissociated species. Due to conservation of mass, the total mass of the products of combustion (dissociated or non-dissociated) is constant. However, the total number of moles of dissociated species is higher than that of non dissociated species, which is why the molecular weight of the chemical equilibrium products of combustion is less.

For a given temperature, FARB and WAR, the chemical equilibrium isentropic coefficient is lower than that of the “no dissociation” model. Although the chemical equilibrium C_p is higher, the chemical equilibrium gas constant is proportionally even higher so the term $(C_p - R)$ dominates and γ is therefore lower.

For a given temperature, FARB and WAR, the discrepancy between the chemical equilibrium and “no dissociation” dynamic viscosity is relatively significantly lower than that for the other fluid properties. The chemical equilibrium dynamic viscosity is slightly lower than the “no dissociation” dynamic viscosity.

Effects of pressure on chemical equilibrium fluid properties:

The analyses and charts shown revealed that for temperatures above 1500K, pressure begins to strongly influence the chemical equilibrium fluid properties of both dry air and the products of combustion of Jet-A.

For a given temperature, FARB and WAR, the chemical equilibrium specific enthalpy and entropy function increase as the pressure reduces. The total number of moles of the dissociated species is more than the total number of moles of the non-dissociated species. Since pressure is proportional to the number of moles, LeChatelier's principle dictates that a reduction in pressure will favour dissociation to maintain chemical equilibrium. Since the dissociated species have a higher specific enthalpy and entropy function than the non-dissociated species, it is fair to deduce that the lower the pressure, the greater the level of dissociation, therefore the higher the concentration of the dissociated species and consequently the higher the specific enthalpy and entropy function of the products of combustion (or air). For a temperature of 3000K the maximum discrepancies between the “no dissociation” and chemical equilibrium (at $P=0.02\text{atm}$) specific enthalpies are approximately 40% and 48% for dry air and the products of combustion of Jet-A (FARB=0.02) respectively. Additionally for a temperature of 3000K the maximum discrepancies between the “no dissociation” and chemical equilibrium (at $P=0.02\text{atm}$) entropy functions are approximately 8% and 11% for dry air and the products of combustion of Jet-A (FARB=0.02) respectively.

For a given temperature, FARB and WAR, the chemical equilibrium gas constant increases as the pressure reduces. Since lower pressures favour dissociation, at lower pressures the molecular weight of dissociated products of combustion (or air) is lower and therefore the gas constant is higher. For a temperature of 3000K the maximum

discrepancies between the “no dissociation” and chemical equilibrium (at $P=0.02\text{atm}$) gas constant are approximately 10% and 15% for dry air and the products of combustion of Jet-A ($FARB=0.02$) respectively.

For a given temperature, $FARB$ and WAR , the chemical equilibrium isentropic coefficient reduces as the pressure reduces. As the pressure reduces (consequently increasing the level of dissociation), although C_p increases, the gas constant is proportionally even higher so the term $(C_p - R)$ dominates and γ is therefore lower. This is the general trend. For $P=0.02\text{atm}$, γ actually begins to increase for temperatures greater than approximately 2600K. For these temperatures (for $P=0.02\text{atm}$) it can therefore be deduced that the increase in C_p is proportionally higher than the increase in R therefore γ increases. For a temperature of 3000K the maximum discrepancies between the “no dissociation” and chemical equilibrium (at $P=0.02\text{atm}$) isentropic coefficients are approximately (-)12% and (-)11% for dry air and the products of combustion of Jet-A ($FARB=0.02$) respectively.

For a given temperature, $FARB$ and WAR , the chemical equilibrium dynamic viscosity increases as the pressure reduces. The discrepancy however is negligible.

It can clearly be deduced that for higher temperatures ($>1500\text{K}$), the effects of pressure on all the fluid properties (except dynamic viscosity) cannot be ignored.

In addition to the effects of temperature and pressure on the chemical equilibrium fluid properties, the effects of $FARB$, $FARU$ and WAR were also analysed, in detail, in Chapter 2. However, these effects are secondary relative to the effects of temperature and pressure.

The main limitations of the advanced fluid model are summarised below:

Limitation 1: Theoretically dissociation should cease following subsequent cooling of the products of combustion which should consequently return to the non-dissociated species. In practice however, due to local chilling of the reactions due to turbulence and/or contact with the cooler walls of the Burner, as well as insufficient residence times of the working fluid in components downstream of the Burner, some dissociated species may still be present, in components downstream of the Burner (e.g. Turbines, Core Nozzle etc). This gives rise to the need of a third fluid model which is an intermediate fluid model that lies between the two extreme cases (no dissociation and chemical equilibrium) and is effectively a function of the “dissociation percentage” ($\%_{\text{diss}}$). Generating an accurate fluid model of this type is not easy as the compositions of the species present in the products of combustion will need to be determined experimentally using techniques such as chemical absorption or adsorption, infrared radiation or paramagnetism. Although this third fluid model has not been implemented in PROOSIS, a simple model (external to PROOSIS) was developed by the author to determine the effects of $\%_{\text{diss}}$ on fluid properties and consequently isolated Burner component and overall engine performance.

Limitation 2:

Currently, PROOSIS only supports a maximum of 3D tables (T , $FARB$ and WAR) and therefore the fluid model tables do not account for the effects of pressure. This is acceptable for the “no dissociation” model. Pressure heavily influences the level of dissociation. The chemical equilibrium fluid model has been generated for only one

pressure (50atm). Currently the chemical equilibrium fluid model is only used for Burner and Afterburner simulations while the “no dissociation” model is used for all other components. Based on the limitation, this model is fairly accurate for Burner and Afterburner component simulations as Burner pressures of >50atm are unlikely to be encountered even for modern and conceptual high pressure ratio engines. Although the default chemical equilibrium fluid model is based on a pressure of 50atm, it can easily be replaced by different user defined models which have been generated for more appropriate pressures. Although not implemented in PROOSIS, the effects of pressure on dissociation (with respect to fluid properties) and isolated component performance are discussed.

The second part of Chapter 2 involved a discussion about the evolution of a robust flow continuity model which was conceived and developed by the author for the PROOSIS SCLib. The flow continuity model of the PROOSIS SCLib comprises twelve thermodynamic functions to calculate the unknown local flow properties, at any point (inlet, outlet or intermediate) of any component provided one of a set of twelve compatible input options is satisfied. Additionally the flow continuity model comprises three auxiliary functions which are required for the calculations contained within the twelve main thermodynamic functions. The flow continuity model presented in Chapter 2 is valid for all the PROOSIS fuels, provided robust fluid models for dry air and the products of combustion of each of these fuels are available. An accurate and robust flow continuity model, such as that developed for the PROOSIS SCLib, is particularly important to ensure global convergence of isolated component as well as engine model simulations. Detailed descriptions of both the main and auxiliary thermodynamic functions have been provided with respect to the required inputs, the calculated outputs and the calculation procedure. The author developed the thermodynamic functions based on a fully rigorous approach using changes in specific enthalpy and entropy function between total and static properties as opposed to using the simplified (“constant C_p ” and “constant γ ”) methodology.

The flow continuity model analysis also includes a detailed study, undertaken by the author (and a colleague), to improve the convergence of the thermodynamic functions close to sonic conditions. Following a detailed analysis which involved creating several hybrid fluid models, it was deduced that the problems with convergence were attributed to the accuracy of the values of entropy function obtained from the fluid model. The following two methods, which could yield improved results, were investigated.

The first method involved reducing the tabulated temperature intervals of the entropy function fluid tables from 50K to 10K. The results obtained clearly suggested that reducing the temperature intervals resulted in significantly improved solutions. However, there was still a small region of non-convergence very close to sonic conditions.

The second method involved using “logarithmic interpolation” for temperature for the entropy function tables. For the purposes of this analysis “logarithmic interpolation” actually referred to linear interpolation of $\ln(T)$ (as opposed to linear interpolation of T). The solutions obtained were extremely accurate and the region of non-convergence very close to sonic conditions was completely eliminated.

Recommendations for Further Work:

The main limitations of the PROOSIS fluid model are presented above and solving these limitations is a good starting point for further work.

From the observations presented above, it is clear that accounting for the effects of pressure is fundamental for a chemical equilibrium fluid model. Including pressure as an additional argument for the fluid model functions will require each of the thermodynamic functions to be updated as a new iterative loop will need to be introduced for pressure. The new fluid model and thermodynamic functions could then be used to repeat the calculations outlined in Chapter 3 and Chapter 4 to provide a more realistic representation of the effects of dissociation both on isolated component and overall engine performance.

The simple “%diss” model developed by the author is a good starting point to determine the effects of the level of dissociation on fluid properties and subsequently gas turbine performance. This model could be developed further by performing high fidelity combustor analyses thereby providing a more realistic indication of the products of combustion and consequently a more realistic calculation of fluid properties.

Although not presented in this thesis, the author has already had a brief “brainstorming session” with some colleagues including “VIVACE-ECP” partners regarding the possibility of directly connecting PROOSIS to the NASA CEA software thereby eliminating the need for multi-dimensional fluid tables. Theoretically this seems like a good solution as it would yield extremely accurate fluid properties. Although a few problems have been conceived, these problems seem trivial and could be easily resolved. Due to time constraints of the project, this idea could not be pursued further but it is definitely a thought for the future.

Chapter 2 concluded with a brief description of an idea which was conceived by the author which involved an “intelligent” means of implementing the flow continuity model. The main objective was to develop a model which would:

1. Automatically detect which inputs are available.
2. Check to see if at least one of the twelve compatible input sets is satisfied.
3. Automatically perform all the relevant series of calculations corresponding to the compatible input option to obtain all the local thermodynamic properties.

After exploring several options to implement the “intelligent” flow continuity model and following the advice from the software developers (Empresarios Agrupados – (EA), Abstract Component THERM was developed. The intention was that every component of the PROOSIS SCLib would inherit from Abstract Component THERM. Consequently, any flow property required at the inlet or outlet of any component would be readily available. In addition to fulfilling the three main objectives highlighted above, Abstract Component THERM seemed to offer another significant advantage arising from the object oriented nature of the PROOSIS software. As opposed to the conventional means of implementing the main thermodynamic functions, within Abstract Component THERM, all the equations could just be listed once for the input of the component and once for the output and in a random order. The equations would then be automatically rearranged based on the known variables (as opposed to the relatively more sequential programming that is required for

the conventional approach). Abstract Component THERM consequently introduces an element of intelligence which serves to minimise the need for skilled user resource.

Despite the several foreseeable advantages, implementing Abstract Component THERM in PROOSIS proved to be unsuccessful mainly due to limitations of the solver and the object oriented programming approach of PROOSIS. These limitations are discussed in *Section 2.3.6*. Based on these problems and due to time constraints, the PROOSIS partners collaboratively decided to abandon the idea of developing an “intelligent” means to implement the thermodynamic functions and decided to stick to the conventional, more robust approach. However, research into an intelligent means for implementing the thermodynamic functions with a view to minimise skilled user resource whilst minimizing modelling complexity and retaining robustness of the flow continuity model is definitely a thought for future developments.

7.1.2: Chapter 3 Conclusions

Chapter 3 presented several advanced considerations which are important for accurate performance simulations of gas turbine combustion systems. The performance simulation model of the PROOSIS Burner component has been presented with detailed descriptions of the pressure loss, efficiency and energy balance models. A component which calculates Burner emissions (inheriting from the main Burner component) was also introduced. The effects of liquid fuel sensible enthalpy on isolated Burner and Afterburner performance have been discussed. The results of the validation of the PROOSIS Burner component against well established (industry standard approved) gas turbine performance simulation software are presented. The chapter concludes with several isolated Burner and Afterburner simulation case studies which analyse:

1. The effects of dissociation on isolated Burner and Afterburner performance.
2. The limitations of the Burner_Emissions component.

The effects of liquid fuel sensible enthalpy:

As a consequence of global fuel cost escalation and increased stringent engine emission regulations, fuel conservation is a high priority for engineers (airframe and engine) as well as Airline companies. Reliable fuel consumption estimations are fundamental in order to achieve the engine performance and emissions targets defined in a contractual agreement between Airline companies and engine manufacturers. The energy balance equation of the PROOSIS Burner component was developed based on significant input from several industrial partners (including both airframe and engine manufacturers) from the “VIVACE-ECP” consortium and includes a term which accounts for the sensible enthalpy of the fuel. The sensible enthalpy of the fuel is the change in enthalpy of the liquid fuel (Jet-A_(l) or Diesel_(l)) or the gaseous fuel (Sample Natural Gas_(g) or Hydrogen_(g)) corresponding to the difference in the temperature of the fuel in the fuel tank ($T_{Ref} = 288.15K$) (which is also the reference temperature at which the fuel LHV is defined) and the temperature of the fuel at the point of Burner injection (T_{fuel}).

A detailed justification for including the liquid fuel sensible enthalpy in the energy balance of the Burner component was provided with the aid of two case studies; a Burner component case study and an Afterburner case study.

The isolated Burner component used for the first case study is based on the Burner component of an engine model of a typical three spool, high bypass turbofan engine (with separate exhausts) while the isolated Afterburner component used in the second case study is based on the Afterburner component of an engine model of a two spool low bypass turbofan engine (with mixed exhausts and reheat).

For the Burner component case study it was observed that as a consequence of neglecting the fuel sensible enthalpy (i.e. by keeping $T_{fuel} = 288.15K$) the fuel flow was over estimated by $\approx 0.35\%$ and $\approx 0.70\%$ for cruise conditions and descent respectively. A simple cost calculation demonstrated that as a consequence of neglecting the fuel sensible enthalpy, the fuel cost was overestimated by $\approx 29\$/hr$ and $\approx 59\$/hr$ for cruise conditions and descent respectively.

For the Afterburner component case study, it was observed that as a consequence of neglecting the fuel sensible enthalpy (i.e. by keeping $T_{fuel} = 288.15K$) the fuel flow and fuel cost were overestimated by a maximum of $\approx 91kg/hr$ and $\approx 77\$/hr$ respectively during descent ($T_{fuel} = 453.15$).

Based on the results of these two case studies (and several other case studies which have not been presented) it is evident that, including (or neglecting) the liquid fuel sensible enthalpy can be negligible for calculations of the main engine DP performance parameters (thrust and SFC). However, as suggested by the isolated component performance simulations, for several long range flights the cumulative effect of the fuel weight and subsequent cost penalty cannot be neglected by an airframe engineer especially for aircraft with afterburners for thrust augmentation.

Burner component testing and validation:

As part of the PROOSIS testing and validation process, the Burner component (like all other components) was rigorously tested by both the author and an industrial partner over a wide range of boundary conditions and DATA including:

- A range of Burner inlet conditions (W_{in} , T_{in} and P_{in})
- A range of Burner fractional pressure losses (dP_{qP}) and efficiencies (η_b)
- A range of Burner fuel injection temperatures (T_{fuel})

In particular the Burner component pressure loss model and, more importantly, the Burner energy balance model were tested. The results were validated using GasTurb and TURBOMATCH.

The main conclusions that were drawn for the calculated value of T_{tout} (regardless of the values of the boundary conditions (W_{in} , T_{in} , P_{in} , FAR_{Bin} , FAR_{Uin} , WAR_{in} , Ang_{in} , P_{fuel} , W_{fuel} , dP_{qP} and η_b) are:

1. The maximum discrepancy between GasTurb and PROOSIS never exceeds a magnitude of 0.3% regardless of the value of T_{fuel} .
2. The discrepancy between GasTurb and PROOSIS for $T_{fuel} = 358.15K$ never exceeds 0.1%. Since the discrepancy between GasTurb and PROOSIS is negative for $T_{fuel} = 288.15K$ and positive for $T_{fuel} = 438.15$, it appears that GasTurb also accounts for the sensible enthalpy of the liquid fuel. Although GasTurb does not allow the user to

change the value of T_{fuel} , it seems to use a default value of T_{fuel} very close to 358.15K. It can fairly be deduced that if GasTurb did allow the user to change the value of T_{fuel} , the results for all simulations would be very consistent with the results obtained for the PROOSIS Burner component.

3. The discrepancy between TURBOMATCH and PROOSIS is greater. The results obtained suggest that TURBOMATCH does not account for the sensible enthalpy of the liquid fuel. Consequently the discrepancy between TURBOMATCH and PROOSIS increases as T_{fuel} increases. Developing the TURBOMATCH Burner “brick” to cater for liquid fuel sensible enthalpy is a strong recommendation for the future.

Despite the relatively high discrepancies between TURBOMATCH and PROOSIS, the results obtained from the validation tests (over a wide range of boundary conditions) using GasTurb are sufficient to confirm that the PROOSIS Burner component combustion model is robust. The values of FAR_{Bout} , FAR_{Uout} , WAR_{out} , W_{out} and Ang_{out} between all three gas turbine performance simulation software were identical (for the partition where the Burner injected fuel mass flow rate was specified).

Additionally, for all the simulations GasTurb, PROOSIS and TURBOMATCH all yielded identical results for P_{tout} for specified values of P_{tin} and dP_{qP} thereby validating the PROOSIS Burner component pressure loss model.

Although not presented the Afterburner validation tests proved equally successful, thereby suggesting that the PROOSIS Burner component can also be used to simulate a gas turbine Afterburner.

The effects of dissociation:

The effects of dissociation on isolated Burner and Afterburner component simulations were presented, with the aid of two case studies. The isolated Burner component simulations were based on the Burner component of a typical three spool high bypass ratio turbofan engine with separate exhausts (CUHBR engine model) while the isolated Afterburner component simulations were based on the Afterburner component of a typical two spool low bypass ratio turbofan engine with mixed exhausts and reheat (CULBR engine model). The boundary conditions used for each case study were taken from existing TURBOMATCH engine models.

For the Burner component case study a range of $1600K \leq T_{tout} \leq 2200K$ was investigated. Although for the CUHBR engine the design point Burner outlet total temperature is $\approx 1800K$, it is highly likely that, with advances in turbine materials technology, Burner outlet temperatures of future military engines (for which emission regulations are not as stringent as for civil engines) may exceed 2200K. The presented case study therefore provided an insight into the effects of dissociation on the performance of not only an existing Burner component but also Burner components with higher Burner outlet temperatures which may be developed in the future. The main observations that were made are as follows:

Advanced Performance Simulation of Gas Turbine Components and Fluid Thermodynamic Properties

1. The design point ($T_{tout} = 1800K$) W_{fuel} discrepancy, between the “no dissociation” fluid model and chemical equilibrium fluid model simulations was approximately 1.1%. This is not negligible for gas turbine performance simulation calculations.
2. As expected, the W_{fuel} discrepancy between the “no dissociation” fluid model and the chemical equilibrium fluid model simulations increased significantly with an increase in T_{tout} . For $T_{tout} = 2200K$, the discrepancy was approximately 2.3% and certainly not negligible.
3. For a given value of T_{tout} , the discrepancy between the chemical equilibrium fluid model ($\%_{diss} = 100\%$) increased as $\%_{diss}$ decreased.

For the Afterburner component case study a range of $1900K \leq T_{tout} \leq 2400K$ was investigated. An upper temperature limit of 2400K was chosen for T_{tout} as this is the temperature which corresponds to a calculated value of W_{fuel} required for Stoichiometric combustion (for the presented case study). Beyond this temperature, the combustion reaction would be fuel rich and therefore the calculation would be inaccurate as the PROOSIS fluid models do not currently cater for fuel rich mixtures. As for the Burner component case study, existing material restrictions were ignored. For the CULBR engine model, the design point Afterburner T_{tout} is approximately 2000K (to achieve the rated “wet” thrust). The main observations that were made are as follows:

1. The design point ($T_{tout} = 2000K$) W_{fuel} discrepancy, between the “no dissociation” fluid model and chemical equilibrium fluid model simulations was approximately 1.1%. This is not negligible for gas turbine performance simulation calculations.
2. As expected, the W_{fuel} discrepancy between the “no dissociation” fluid model and the chemical equilibrium fluid model simulations increased significantly with an increase in T_{tout} . For $T_{tout} = 2400K$, this discrepancy was approximately 3% and certainly not negligible.
3. For a given value of T_{tout} , the discrepancy between the chemical equilibrium fluid model ($\%_{diss} = 100\%$) increases as $\%_{diss}$ decreases.

Burner Emissions component testing and limitations:

Chapter 3 concluded with an isolated Burner_Emissions component case study. The presented case study revealed several limitations of emissions correlations available in the public domain. The isolated Burner_Emissions component simulations were based on the Burner component of a typical three spool high bypass ratio turbofan engine with separate exhausts (CUHBR engine model). The main observations that were made are as follows:

1. As expected, the rate of NO_x emissions (W_{NO_x}) increases with an increase in T_{tout} . The higher the temperature, the higher the level of dissociation and therefore the higher the concentration of NO_x .
NB: With respect to A. Lefebvre’s NO_x emissions model, as T_{tout} increases, W_{fuel} increases and therefore FAR_r also increases. Consequently, for a fixed value of F_{pz} , FAR_{pz} also increases. For fixed values of all the Burner inlet port variables

(Win, P_{tin}, T_{tin}, FAR_{Bin}, FAR_{Uin}, WAR_{in} and Ang_{in}) and fixed values of η_b and LHV, an increase in FAR_{pz} implies an increase in h_{tpz} and consequently a higher value of T_{fl}. A higher value of T_{fl} implies a higher value of EINO_x and subsequently a higher value of WNO_x.

2. The rate of CO (WCO) and UHC (WUHC) emissions initially decrease with an increase in T_{tout}. As expected, higher values of T_{tout} favour complete combustion and consequently less CO and UHC are present as T_{tout} increases. This however, is only true for temperatures where dissociation does not occur. At higher temperatures, which favour dissociation, an increase in T_{tout} should result in an increase in CO and UHC. Therefore, as T_{tout} increases, WCO and WUHC should decrease (until $\approx 1900\text{K}$) and then increase. A limitation with the emissions correlations for CO and UHC is that they calculate EICO and EIUHC on the basis of combustion “completeness” only and do not account for the effects of dissociation. Therefore it can be deduced that the correlations are only valid for temperatures less than 1900K where the effects of dissociation on CO and UHC emissions are negligible.

Recommendations for Further Work:

One approach to rectify the limitation with existing emissions correlations (discussed above) could be to directly connect a chemical equilibrium software (e.g. CEA) to PROOSIS so that at any point an accurate calculation of the exact chemical equilibrium composition corresponding to a specific T_{tout}, W_{out} and FAR_{out} (including the concentration of NO_x, CO and UHC) could be readily available. This would eliminate the need for emissions correlations. It was however observed that the CEA chemical equilibrium calculations do not account for combustion “completeness” which is a function of several factors like Burner efficiency, primary zone residence time, inadequate mixing of fuel and air and quenching of post flame products of combustion. Clearly these factors cannot be implemented in chemical equilibrium software such as CEA as they are specific to gas turbine applications only. Therefore although the NO calculations of the CEA software are accurate, correction factors would need to be applied to the CO results. Currently the emissions correlations available in the public domain only cater for relatively modest values of T_{tout}. It is the author’s view that engine rig tests should be extended to cater for higher values of T_{tout} so that the correlations account for the effects of dissociation thereby yielding accurate results for a broader range of T_{tout}.

NB: It is highly likely that such correlations have already been developed by industrial companies (for their in-house legacy gas turbine performance simulation software) but have not been published in the public domain.

The analyses with respect to the effects of dissociation on isolated Burner and Afterburner component simulations should be repeated with the modified fluid model which does account for the effects of pressure on fluid properties (refer to Section 7.2). This would yield more accurate results. The same applies for the engine model simulations described in Chapter 4 and highlighted below.

7.1.3: Chapter 4 Conclusions

The first part of chapter 4 described the generation of an engine model of a twin spool turbojet with reheat (CUTSTJR), using PROOSIS. A detailed account of the following was presented:

1. Generation of the CUTSTJR schematic (including appropriate DATA switch settings and inputs in each component's attributes editor).
2. The "inverse design" calculation concept and subsequently the need for isolated component performance simulation for each component of the CUTSTJR.
3. The design point simulation of the CUTSTJR engine model.
4. Off-design performance simulations including important considerations necessary for engines with afterburners and convergent – divergent nozzles.
5. The effects of dissociation on performance of the CUTSTJR engine model.

The second part of this chapter introduced some of the advanced capabilities of PROOSIS including:

1. Test analysis and adaptation
2. "Stand alone" customer deck generation
3. High fidelity component zooming

It is essential for engines with afterburners to be fitted with variable geometry propelling convergent-divergent (con-di) nozzles. With the afterburner lit, the nozzle areas (throat and exit) must be carefully controlled both to facilitate complete expansion of the flow (in order to optimise the thrust) and also to avoid compressor surge problems. There are effectively three ways to ensure complete expansion:

1. Changing both the nozzle throat area (CondiNozzle.Ath) and the nozzle exit area (CondiNozzle.Aexit).
2. Fixing CondiNozzle.Ath and only changing CondiNozzle.Aexit
3. Fixing CondiNozzle.Aexit and only changing CondiNozzle.Ath

A case study was presented describing two methods to calculate CondiNozzle.Ath (for a fixed value of CondiNozzle.Aexit) during off-design simulations (with active afterburning). The first method involved simply varying CondiNozzle.Ath proportionally to square root of CondiNozzle.Tt_th. This method was deemed to be acceptable to a first order only. However, for fully rigorous calculations, the second method (which was developed and implemented in PROOSIS by the author) should be employed. The rigorous method involved calculating CondiNozzle.Ath afresh for each off-design point using an external Newton Raphson iterative routine. For each off-design point CondiNozzle.Ath was an independent variable, which was calculated iteratively by specifying the design point inlet mass flow rate (Inlet.F_in.W = 200kg/s) as the dependent variable in a suitable closure equation.

The effects of dissociation on overall engine performance:

Two off-design case studies were presented to demonstrate the effects of dissociation on overall performance of the CUTSTJR engine model. The first case study was based on dry operation (no reheat) while the second case study was assumed active afterburning.

For the “dry operation” case study, the Burner injected fuel mass flow rate (Burner.Fu_in.W) was reduced from the design point value until the low pressure compressor (LPC) surged and then increased from the design point value until the calculation did not converge. The main observations and conclusions from this case study are summarised below.

NB: Refer to Section 4.1.5 for the definitions of the various fluid model combinations which are used in the analyses below.

1. For the “Burner.Fu_in.W = 2.438kg/s” case, Burner.F_out.Tt was relatively low (approximately 1507K for the “CE-66%” fluid model combination) for dissociation to have a significant impact. The discrepancies for the calculated values of Burner.F_out.Tt, Fn and SFC between the “ND” and “CE-66%” fluid model combinations were 0.25%, 0.01% and -0.01% respectively and it can safely be deduced that the effects of dissociation on the overall engine performance (Fn and SFC) are negligible for “lower” values of Burner.Fu_in.W due to the corresponding “lower” values of Burner.F_out.Tt.
2. For the “Burner.Fu_in.W = 5.238kg/s” case, Burner.F_out.Tt is approximately 1791K (for the “CE-66%” fluid model combination). For this off-design case the effects of dissociation were more visible due to the higher temperature. The discrepancies for the calculated values of Burner.F_out.Tt, Fn and SFC between the “ND” and “CE-66%” fluid model combinations were 0.46%, 0.23% and -0.23% respectively. Although the discrepancies are still quite small, the effects of dissociation cannot be neglected for fully rigorous calculations.
3. For the “Burner.Fu_in.W = 8.288kg/s” case, Burner.F_out.Tt is approximately 2023K (for the “CE-66%” fluid model combination). For this off-design case, the effects of dissociation were more significant. The discrepancies for the calculated values of Burner.F_out.Tt, Fn and SFC between the “ND” and “CE-66%” fluid model combinations were 0.80%, 0.43% and -0.43% respectively. Although the discrepancies are still small, they are certainly not negligible for accurate gas turbine performance simulation calculations.

For “dry operation” case study, the effects of dissociation on overall engine performance were relatively modest.

For the “active afterburner” case study, The Afterburner injected fuel mass flow rate (Afterburner.Fu_in.W) was increased from the design point value (0 kg/s) until the burned fuel to air ratio at the exit of the Afterburner was just below the Stoichiometric fuel to air ratio.

NB: For this case study the Burner outlet total temperature was unchanged and was equal to the design point value (1800K).

NB: The throat area of the Condi Nozzle (CondiNozzle.Ath) was modified using the “fully rigorous method”

The main observations and conclusions from this case study are summarised below.

1. For all the tested cases, the Burner injected fuel mass flow rate (Burner.Fu_in.W) required to achieve the design point Burner outlet total temperature (Burner.F_out.Tt =

1800K) increased as the level of dissociation increased. Consequently as the level of dissociation increased, Burner.F_out.W increased.

2. For the design point case (Afterburner.Fu_in.W = 0kg/s), the increase in Burner.F_out.W (as the level of dissociation increased) manifested as an increase in Afterburner.F_out.Tt and subsequently an increase in Fn. Although there was an increase in net thrust, the SFC was worse because Burner.Fu_in.W increased as the level of dissociation increased. The discrepancies of the calculated values of Afterburner.F_out.Tt, Fn and SFC between the “ND” and “CE-66%” cases were -0.46%, -0.39% and -0.7% respectively. These discrepancies are not negligible for rigorous performance calculations. For the design point case the discrepancies were clearly only due to the effects of dissociation on the performance simulation of the Burner component.
3. For the “Afterburner.Fu_in.W = 4.7kg/s” case, although there was an increase in Burner.Fu_in.W (and consequently Burner.F_out.W), the value of Afterburner.F_out.Tt actually decreased as the level of dissociation increases. This is because the effects of dissociation in the Afterburner component began to show. As discussed in Section 3.5, for a fixed fuel flow rate, the Afterburner outlet total temperature decreased as the level of dissociation increased. Although Afterburner.F_out.Tt decreased, Fn still increased as the level of dissociation increased as the effects of a lower Afterburner.F_out.Tt were overwhelmed by a larger Burner.Fu_in.W. The discrepancies of the calculated values of Afterburner.F_out.Tt, Fn and SFC between the “ND” and “CE-66%” cases were 0.13%, -0.17% and -0.41% respectively. The discrepancies are clearly lower than those presented above for the design point calculation. For the “Afterburner.Fu_in.W = 4.7kg/s” case, the discrepancies were due to the effects of dissociation on both the Burner and the Afterburner.
4. The results for the “Afterburner.Fu_in.W = 9.2kg/s” case are similar to those obtained for the “Afterburner.Fu_in.W = 4.7kg/s” case. However the effects of dissociation on the Afterburner component were more prominent due to a higher value of Afterburner.F_out.Tt. Consequently although there was an increase in Burner.Fu_in.W (and consequently Burner.F_out.W), the value of Afterburner.F_out.Tt actually decreased significantly as the level of dissociation increased. The discrepancies of the calculated values of Afterburner.F_out.Tt, Fn and SFC between the “ND” and “CE-66%” cases were 1.40%, 0.17% and -0.57% respectively. For this case it was clear that as the level of dissociation increased, the decrease in Afterburner.F_out.Tt overwhelmed the increase in Burner.Fu_in.W and therefore Fn was lower and SFC was therefore worse.

The partition used for this case study was such that Burner.F_out.Tt and Afterburner.Fu_in.W were specified as boundary conditions and Burner.Fu_in.W and Afterburner.F_out.Tt calculated respectively. This is the reason the effects of dissociation seem to be negligible even at high temperatures because as the level of dissociation increases for a fixed value of Burner.F_out.Tt, Burner.Fu_in.W increases while for a fixed value of Afterburner.Fu_in.W, Afterburner.F_out.Tt decreases. The two effects seem to cancel each other out and the discrepancies between Fn and SFC are therefore small.

However, the analysis was extended to the following partition. Burner.Fu_in.W and Afterburner.Fu_in.W were specified as boundary conditions. For fixed values of Burner.Fu_in.W and Afterburner.Fu_in.W (for Burner and Afterburner outlet temperatures greater than 1800K) as the level of dissociation increased, the values of Burner.F_out.Tt and Afterburner.F_out.Tt decreased significantly. Therefore as the level of dissociation increased Fn decreased significantly and SFC therefore worsened considerably as the total fuel flow rate (Afterburner.Fu_in.W + Burner.Fu_in.W) was constant. These discrepancies are certainly not negligible for gas turbine performance simulations.

Chapter 4 concluded with an introduction of some of the advanced capabilities of PROOSIS including:

1. Test analysis and adaptation
2. "Stand alone" customer deck generation
3. High fidelity component zooming

7.1.4: Chapter 5 Conclusions

The structure and the implementation in PROOSIS of an extended parametric representation of compressor characteristics was presented in Chapter 5. The development and implementation of Compressor MFT maps in PROOSIS was discussed. The integration of Compressor_BETA and Compressor_MFT components, with respect to the overall hierarchy structure of the PROOSIS Compressor components is also highlighted. The implementation of MFT maps in PROOSIS and considering the object oriented modelling implications is the author's contribution to extended parametric representation of compressor characteristics.

NASA and General Electric have collaboratively developed a method called the Map Fitting Tool (MFT) which provides an extended parametric representation of turbomachinery maps. This approach has been adopted by Snecma to model the off-design performance of all the turbomachinery components (Fans, Compressors and Turbines) within Janus (the in-house gas turbine performance simulation tool developed and used by Snecma). Chapter 5 was a descriptive chapter which thoroughly described the implementation of the CompressorMFT component, by the author, in PROOSIS.

Recommendations for further work:

Due to confidentiality constraints, testing of the CompressorMFT component was limited to simply ensuring the off-design equations were robust. An analysis of the design point calculation of the CompressorMFT, using the "inverse design" methodology was beyond the scope of the author's research.

Recommendations for further work include testing and validation of the "inverse design" point simulations of the CompressorMFT components. An additional recommendation is extending the MFT map methodology to cater for other turbomachinery components i.e. Fans and Turbines and rigorously testing the "inverse design" point simulations of these components.

NB: A lot of this work has already been implemented in PROOSIS by Snecma however there is still a lot of information not available in the public domain.

7.1.5: Chapter 6 Conclusions

The author's project responsibilities included project management. The author was an ambassador for the Cranfield University gas turbine group and the focal point of communication between Cranfield University and the "VIVACE-ECP" partners. Chapter 6, the penultimate chapter, provided an insight into the challenges faced by a PhD researcher, with respect to technical project management, for a modern EU collaborative project.

The structure of the VIVACE European Cycle Program ("VIVACE-ECP") work package (WP) was presented and a timeline highlighting the "evolution of PROOSIS" from the early stages of development until the final delivery of the gas turbine performance simulation software was analysed. A detailed analysis of the main project objectives and deliverables, the project structure and channels of communication, the quality control processes and technology transfer was presented. An emphasis was made on the author's technical and managerial contribution to the project as a whole including management of the Cranfield University team and the contribution made to technology transfer and dissemination.

The author played a vital leadership role in the management of the Cranfield University technical team which primarily comprised the author, a doctoral researcher and several MSc researchers. Chapter 6 concluded with references and abstracts for all the author's publications as well as the various theses (MSc and doctoral) to which the author made significant contributions.

GLOSSARY

This glossary describes some of the PROOSIS modelling terminology used in the thesis. A complete guide is available in the “PROOSIS User Manual”. This manual describes the modelling language used by PROOSIS with a detailed description of the syntax and terminology used. The reference of the user manual is provided below:

Arroyo, J. C. (EA Internacional), “PROOSIS User Manual V1.0” VIVACE 2.4.5/EAI/T/07002-1.0

Ports:

Ports are connectors. They establish the contact between objects. Ports carry no redundant information. The standard component library has twelve ports. Each port is uniquely defined by the variables it contains.

Partition:

A partition is a mathematical model of a component. PROOSIS always provides a default partition for each component. PROOSIS can make different partitions depending on Boundary Conditions and Breaks in Linear and Non – Linear Algebraic loops. For engine model simulations, partitions are not defined at component level but by the default partition for the whole engine calculation.

Non Linear Box:

This is a non linear iterative loop. An initial value for a given variable is guessed. This variable is defined as the ‘tearing variable’. The value of the tearing variable is changed using a Newton Raphson iterative procedure until all the equations in the non linear box are satisfied. The values of all the variables in the non linear box corresponding to the converged solution of the tearing variable are then carried forward for any further calculations.

Attributes Editor:

Each component of the standard components library has a set of attributes (DATA or switch settings) which may be changed. The attributes editor of a component is accessed by simply “double clicking” on the component icon in an engine schematic. The component attributes are graphically displayed in a table containing the following:

- A header file with the following information:
 1. The library from which the component is taken (automatically specified)
 2. The component type (automatically specified)
 3. The component name (user specified)
- Identification of the various attributes
- Value or switch setting of the attribute
- The unit of a DATA attribute
- A description of the attribute

Additionally, the attributes editor has a link to the component documentation.